

Photoinitiated Polymerization

August 11, 2012 | <http://pubs.acs.org>
Publication Date: March 3, 2003 | doi: 10.1021/bk-2003-0847.fw001

ACS SYMPOSIUM SERIES **847**

Photoinitiated Polymerization

Kevin D. Belfield, Editor
University of Central Florida

James V. Crivello, Editor
Rensselaer Polytechnic Institute



American Chemical Society, Washington, DC



Library of Congress Cataloging-in-Publication Data

Photoinitiated polymerization / Kevin D. Belfield, editor, James V. Crivello, editor.

p. cm.—(ACS symposium series ; 847)

Includes bibliographical references and index.

ISBN 0-8412-3813-8

1. Photopolymerization. 2. Radiation curing.

I. Belfield, Kevin, 1960- II. Crivello, James V., 1940- III. Series.

QD716. P5P45 2003
668.9'2—dc21

2002038528

The paper used in this publication meets the minimum requirements of American National Standard for Information Sciences—Permanence of Paper for Printed Library Materials, ANSI Z39.48-1984.

Copyright © 2003 American Chemical Society

Distributed by Oxford University Press

All Rights Reserved. Reprographic copying beyond that permitted by Sections 107 or 108 of the U.S. Copyright Act is allowed for internal use only, provided that a per-chapter fee of \$24.75 plus \$0.75 per page is paid to the Copyright Clearance Center, Inc., 222 Rosewood Drive, Danvers, MA 01923, USA. Republication or reproduction for sale of pages in this book is permitted only under license from ACS. Direct these and other permission requests to ACS Copyright Office, Publications Division, 1155 16th St., N.W., Washington, DC 20036.

The citation of trade names and/or names of manufacturers in this publication is not to be construed as an endorsement or as approval by ACS of the commercial products or services referenced herein; nor should the mere reference herein to any drawing, specification, chemical process, or other data be regarded as a license or as a conveyance of any right or permission to the holder, reader, or any other person or corporation, to manufacture, reproduce, use, or sell any patented invention or copyrighted work that may in any way be related thereto. Registered names, trademarks, etc., used in this publication, even without specific indication thereof, are not to be considered unprotected by law.

PRINTED IN THE UNITED STATES OF AMERICA

**American Chemical Society
Library**

1155 16th St., N.W.

Washington, D.C. 20036

In Photoinitiated Polymerization / Kevin D. Belfield, K., et al.;
ACS Symposium Series; American Chemical Society: Washington, DC, 2003.

Foreword

The ACS Symposium Series was first published in 1974 to provide a mechanism for publishing symposia quickly in book form. The purpose of the series is to publish timely, comprehensive books developed from ACS sponsored symposia based on current scientific research. Occasionally, books are developed from symposia sponsored by other organizations when the topic is of keen interest to the chemistry audience.

Before agreeing to publish a book, the proposed table of contents is reviewed for appropriate and comprehensive coverage and for interest to the audience. Some papers may be excluded to better focus the book; others may be added to provide comprehensiveness. When appropriate, overview or introductory chapters are added. Drafts of chapters are peer-reviewed prior to final acceptance or rejection, and manuscripts are prepared in camera-ready format.

As a rule, only original research papers and original review papers are included in the volumes. Verbatim reproductions of previously published papers are not accepted.

ACS Books Department

Preface

The field of photoinitiated polymerizations is one whose current and future importance can be hardly overstated. It is already a vital and exciting area of polymer chemistry from both an academic as well as an industrial perspective. Advances in this field are being driven by the rapid adoption of the technology of photoinitiated polymerizations, known generally as UV-curing, by industry for a myriad of uses. These uses encompass both high-volume applications such as coatings, adhesives, and printing inks as well as advanced high technology uses such as microelectronic encapsulation, photo- and stereolithography and holographic data storage media. With an annual market for UV-curable systems of more than one billion dollars and an annual growth rate of 15%, photopolymerizations is one of the few really exciting expanding areas of polymer technology. As the commercial interest and applications in photopolymerizations have developed, a parallel, synergistic increase in the involvement of the research activity within the academic community has also taken place. The work is both interdisciplinary and international in its character with a great deal of cooperative research activity progressing among various countries of the developed world.

Interest has also grown with the realization that UV-curing has the potential to make major inroads on the resolution of the seemingly intractable problem of environmental impact of the coatings and printing inks industries through the reduction and even elimination of volatile organic solvents. As current thermally based application systems wear out in these industries they are increasingly being replaced by photocuring systems. Advances in UV-curing chemistry have steadily increased the performance characteristics of these materials such that they are now essentially competitive with traditional thermally cured solvent-based systems in all respects. At the same time, the increase productivity resulting from high rates of application and cure of UV-curable materials has provided added economic incentives for the adoption of these materials. Indicative of the interest of industry in the field of UV-curing is the growth of trade associations such as RadTech that serve it. In its

inception in 1986, this association consisted of a few member companies, most of them supply oriented. The first RadTech Conference was attended by 100–150 participants. In contrast, the most recent North American meeting in April 2002 had 2800 registrants. Further, the organization has expanded to include parallel organizations in Europe and Asia.

Although the RadTech organization is primarily oriented toward dissemination of developments in photopolymerization technology targeted toward the end user, a parallel growth in scientific meetings aimed at the basic researcher has also taken place. In April 1995, the first two-day American Chemical Society (ACS)-sponsored symposium exclusively dedicated to the topic of photopolymerizations was organized. This symposium was quickly followed by another ACS Symposium in March 1996 on the same topic. The high level of interest generated by these symposia as well as the general perception that the field had progressed very rapidly in the intervening five years led to the decision that another symposium on this topic should be organized. Accordingly, a symposium entitled *Advances in Photoinitiated Polymerizations* was scheduled and held at the August 2001 ACS Meeting in Chicago, Illinois under the joint sponsorship of the Divisions of Polymer Chemistry, Inc. and Polymer Materials: Science and Engineering, Inc. The three-day symposium included 60 oral and poster papers representing contributions from workers from 12 countries. The symposium provided a nice balance of research and development interests including 42 papers from academic institutions and 18 contributions from industry. This book contains selected expanded papers taken from the symposium. A brief perusal of the table of contents reveals the breadth of the current research efforts in this area and reveals some of the excitement that pervades this field. The book is divided into five major sections. Free radical photopolymerizations still command most of the interest and activity within the field and these photopolymerizations are the subject of the first section. This is followed by a chapter dedicated to kinetic studies of the mechanism of free radical polymerizations. The next section contains chapters on cationic photopolymerizations that are rapidly advancing to take their place with free radical polymerizations in many industrial applications. The next section is devoted to recent developments in novel photopolymerization chemistry. This section contains chapters describing new photobase generators, developments in monomers, oligomers and

templated polymerizations of liquid crystal polymers. A fifth section contains chapters in which new and emerging applications for photopolymerizations are described.

Kevin D. Belfield

Department of Chemistry
University of Central Florida
Orlando, FL 32816–2366

James V. Crivello

Department of Chemistry
Rensselaer Polytechnic Institute
110 8th Street
Troy, NJ 12180–3590

Photoinitiated Polymerization

August 11, 2012 | <http://pubs.acs.org>
Publication Date: March 3, 2003 | doi: 10.1021/bk-2003-0847.pr001

Chapter 1

***N*-Vinylamides and Reduction of Oxygen Inhibition in Photopolymerization of Simple Acrylate Formulations**

Chris W. Miller¹, C. E. Hoyle², S. Jönsson³, C. Nason², T. Y. Lee²,
W. F. Kuang², and K. Viswanathan⁴

¹UCB Chemicals Corporation, 2000 Lake Park Drive, Smyrna, GA 30080

²School of Polymers and High Performance Materials, The University of
Southern Mississippi, Box 10076 Southern Station, Hattiesburg, MS 39406

³Fusion UV-Curing Systems, 910 Clopper Road,
Gaithersburg, MD 20878–1357

⁴Becker-Acroma, Inc., Brantford, Ontario, Canada

Cyclic *N*-vinylamides were found to increase the maximum relative rates of photopolymerization of hexanedioldiacrylate formulations at low light intensities under nitrogen and dramatically under air, while acyclic *N*-vinylamides and cyclic *N*-alkylamides were found to have much smaller, though still significant, effects in air. The combination of the cyclic aliphatic amide and *N*-vinylamide functionalities generally resulted in the maximum benefit for reduction of oxygen inhibition resulting in rapid rates of polymerization in air at low light intensities. While the complete mechanistic explanation of the rate enhancement is still unclear, several possible mechanistic pathways are discussed.

Introduction

Molecular oxygen exists at ambient conditions as a diatomic molecule with a triplet diradical electronic ground state (1,2). Due to its triplet and radical characteristics, oxygen has high chemical reactivity towards radicals and towards molecules in their excited triplet states. Thus, free-radical photopolymerizations can be inhibited significantly by ambient molecular oxygen, especially under curing conditions such as very low film thickness, low light

intensity, or low cure dosage. Several mechanisms are responsible for inhibition including quenching of photoinitiators and scavenging of initiator and polymer radicals. These reactions result in decreased rates of initiation, increased rates of termination, and inclusion of oxygenated species in the surface layers of the cured films. The efficiency of the quenching and radical scavenging reactions depends upon the concentrations of oxygen, radicals, and double bonds. A discussion of the kinetics of free-radical polymerization and competing reactions in the context of oxygen inhibition was given in a previous report (3). A number of techniques have been utilized to combat oxygen inhibition, including use of high intensity lamps/high cure dosages (4-8), inert atmospheres/sandwiching materials (9,10), and additives such as amines, which have been shown to consume oxygen by a photo-oxidation process (4,11-17). In our initial studies (3,18) we confirmed earlier reports (19,20) that NVP dramatically increases the relative rates of acrylate polymerization in air at low light intensities and that a reversible complexation occurs between oxygen and NVP as observed in the UV absorption spectrum (21). In the current work, we have extended our study to include other cyclic and acyclic N-vinylamides and N-alkylamides and to inquiries into the chemical phenomena involved in the observed rate effects.

Experimental Results

Conditions and Compounds

Photo-differential scanning calorimetry (Photo-DSC) was performed on a Perkin-Elmer DSC-7 modified with quartz windows and a medium pressure mercury lamp. Samples were typically 2 - 3 μ L injected into specially crimped aluminum sample pans giving a film thickness of approximately 250 μ m. Real-time Fourier-transform infrared spectroscopy (RTFTIR) was performed on a Bruker FTIR/FTR system modified with a nitrogen-cooled MCT detector and a shuttered xenon lamp. The RTFTIR samples were sandwiched between two salt plates to simulate polymerization under inert atmospheres and placed on the surface of a single salt plate to allow curing in air. Ultraviolet-visible spectroscopy was performed on a Cary 500 UV-visible/NIR spectrophotometer by Varian using standard 1cm quartz sample cells. Unless specifically noted otherwise, all samples for Photo-DSC and RTFTIR were formulated to contain 1 weight-percent 2,2-dimethoxy-2-phenylacetophenone (DMPA) as photoinitiator. All monomers were obtained from Aldrich Chemical Company with the exceptions of 1,6-hexanedioldiacrylate (HDDA), which was also obtained from UCB Chemicals Corporation, and N-vinylformamide (NVF), which was obtained from Air Products Corporation. All monomers were used as received, and polymerization inhibitors were not removed. Names, structures, and acronyms of N-substituted amides used in this study are given in Figure 1.

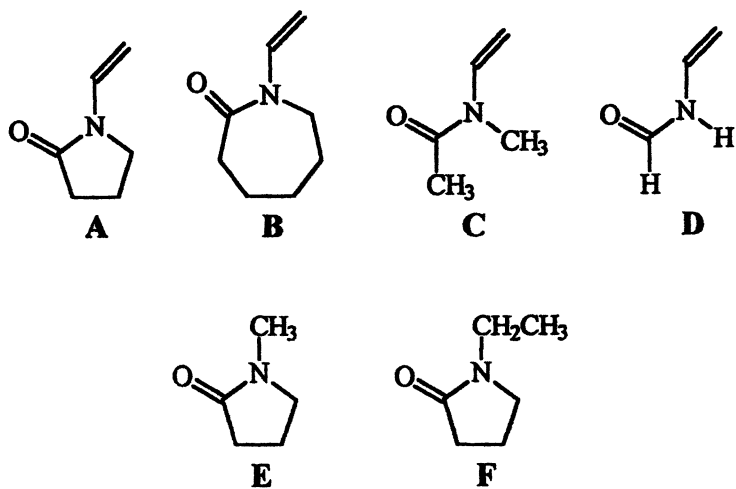


Figure 1. N-vinylamides and N-alkylamides used in this study: (A) N-vinylpyrrolidinone (NVP), (B) N-vinylcaprolactam (NVCL), (C) N-methyl-N-vinylacetamide (NMNVA), (D) N-vinylformamide (NVF), (E) N-methylpyrrolidinone (NMP), (F) N-ethylpyrrolidinone (NEP).

Photo-DSC Results

Formulations were prepared based upon HDDA incorporating various weight percentages of NVP, NVCL, NMNVA, and NVF. NVCL was insoluble in HDDA at ambient conditions at weight percentages above 60%. Samples were polymerized at 25°C in nitrogen and air atmospheres, with on-sample light intensities of 0.32 and 3.1 mW/cm², respectively, and the exotherms recorded. Figures 2 and 3 show the normalized exotherm peak maxima (which are directly related to the relative maximum rates of polymerization) for the formulations in nitrogen and air, respectively. The data were normalized by dividing each data set by its respective exotherm peak maximum at 0% additive to provide a direct basis for comparison by adjusting for small variances in light intensity, photoinitiator concentration, and other parameters that varied slightly from sample to sample within and between data sets. However, while trends may be compared, the values from nitrogen and air should not be compared directly due to the ten-fold difference in light intensity.

The exotherm peak maxima data in nitrogen (Figure 2) show a slight increase in the maximum relative rates of polymerization over the range of 5-60% amide for the NVP and NVCL formulations. In contrast, the data for NMNVA, a linear analogue, shows a linear decrease in the relative maximum rates with increasing amide percentage. The peak maxima data from air (Figure 3) is more striking, showing a dramatic increase in the maximum relative rates of polymerization as a function of increasing NVP percentage up to a maximum effect between 60-80% NVP, followed by a decrease. NVCL also shows a significant increasing effect up to the limit of solubility, though not as dramatically as NVP. NMNVA shows a small, though still significant increase. We note that the polymerization efficiency of the N-vinylamides without HDDA is very low in nitrogen and in air. As expected, the polymerization efficiency of HDDA without amide is quite high in nitrogen and negligible in air at these light intensities. Thus, the 20% increase in the maximum rate of polymerization of HDDA in nitrogen with the addition of only 10% NVP or NVCL is quite significant. The relatively small difference in heat of polymerization of the N-vinylamides compared to the acrylate does not account for the observed rate effects.

A similar experiment was performed using NVP, NMP, NEP, and decane as additives in HDDA in air with on-sample light intensity of 1.4 mW/cm². The data for the NVP set was similar to that described above. Interestingly, the exotherm data for NMP and NEP, which are non-polymerizable N-alkylamides, showed an increase in the relative maximum rates of polymerization with increasing amide content, with the magnitude of the effect roughly equivalent to that observed with NMNVA in the previous data set. The decane data set showed only the typical dilution effect as expected. We note that for the N-alkylamides, the concentration of polymerizable double

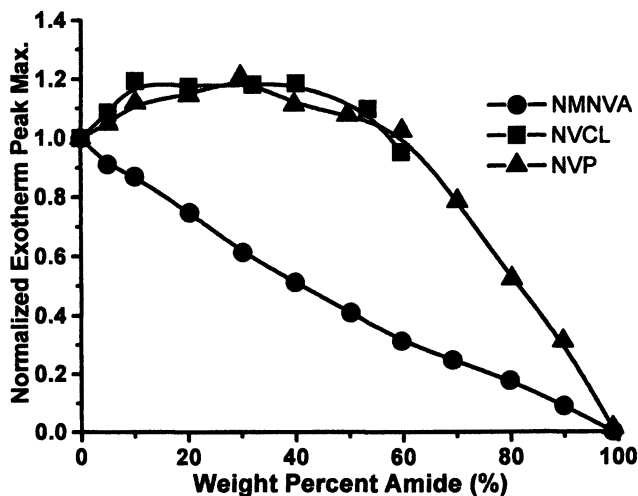


Figure 2. Photo-DSC data for N-vinylamide/HDDA formulations polymerized in nitrogen.
(Reproduced with permission from Polym. Prepr. 2001, 42(2), 811–812. Copyright 2001 Chris W. Miller.)

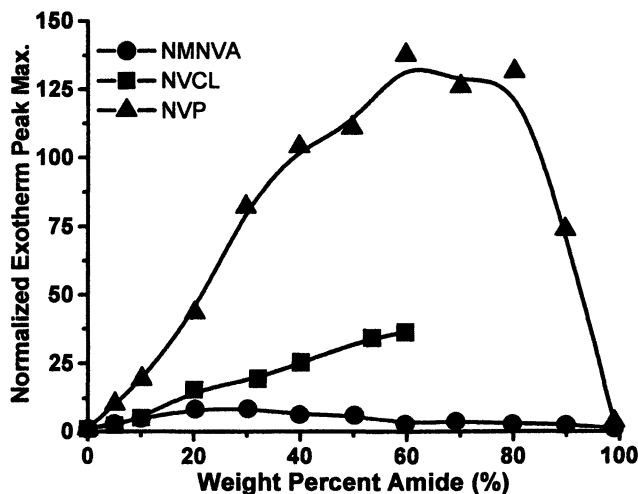


Figure 3. Photo-DSC data for N-vinylamide/HDDA formulations polymerized in air.
(Reproduced with permission from Polym. Prepr. 2001, 42(2), 811–812. Copyright 2001 Chris W. Miller.)

bonds decreases much more significantly with increasing amide concentration than with the N-vinylamides, thus, the observed rate enhancement is likely somewhat understated. These data confirm observations for N-alkylamides with acrylates reported by Kloosterboer (19).

The NVF data sets were omitted from Figures 2 and 3 due to the propensity of NVF to undergo Michael addition reactions with acrylates (22), which changed the effective concentrations of NVF in the formulations. Evidence of this reaction in our studies was formation of a white precipitate in NVF/HDDA formulations upon standing at room temperature. Several formulations were tested despite the precipitate formation, and rate enhancement in air was observed similar to that observed with NVP.

RTFTIR Results

Preliminary RTFTIR analysis was performed on NVP/HDDA formulations polymerized at room temperature with an on-sample light intensity of 11mW/cm^2 (xenon lamp source). Salt plate laminates were used to simulate nitrogen conditions, while air runs were performed on a single salt plate. The double bonds of the HDDA and NVP were monitored simultaneously at 806cm^{-1} and 870cm^{-1} , respectively. Representative percent conversion versus time plots for formulations with 10% and 60% NVP are shown in Figures 4 and 5, respectively. Final percent conversions in nitrogen and air versus weight percent NVP for HDDA and NVP are given in Figures 6 and 7, respectively.

Polymerizations conducted in the salt plate laminate consistently gave HDDA conversions of ~90% for all formulations, with final HDDA conversion reached essentially within the first 10-15 seconds. NVP conversion in the laminate was ~60% over the range of 5-70% NVP, with essentially final conversion reached typically within the first 30 seconds over that same range. Polymerization of the NVP-only sample was quite slow with a final conversion of only ~20%. These data are consistent with the Photo-DSC data that show rapid polymerization over a wide range of NVP percentages in nitrogen.

Polymerizations conducted in air gave very low conversion of NVP and HDDA at NVP percentages lower than 30%. At NVP contents of 10-20%, the conversion of NVP was higher than that of HDDA, while at NVP contents > 40%, the conversion of HDDA was significantly higher than that of NVP. The percent conversion of NVP was consistently 30-40% over the range 10-90% NVP content. HDDA percent conversion increased dramatically with increasing NVP content over the range 10-60% NVP, reaching a peak conversion (~90%) equivalent to that observed in the laminate runs over the range 60-90% NVP content, which corresponds well to the maximum relative rates of polymerization observed via Photo-DSC over a similar NVP content range. In contrast to the runs in laminate where maximum HDDA conversion was reached within the first 15s, the conversion of HDDA in air continued to increase

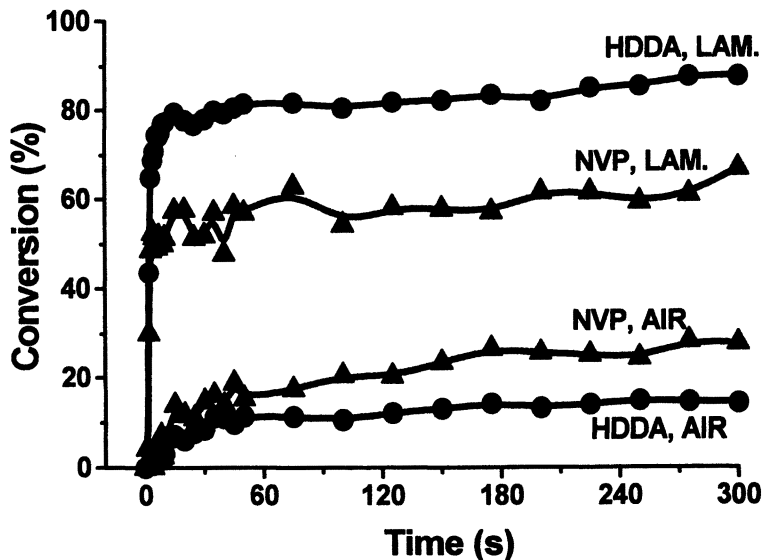


Figure 4. RTFTIR conversion versus time plots for 10% NVP in HDDA in laminate and air.

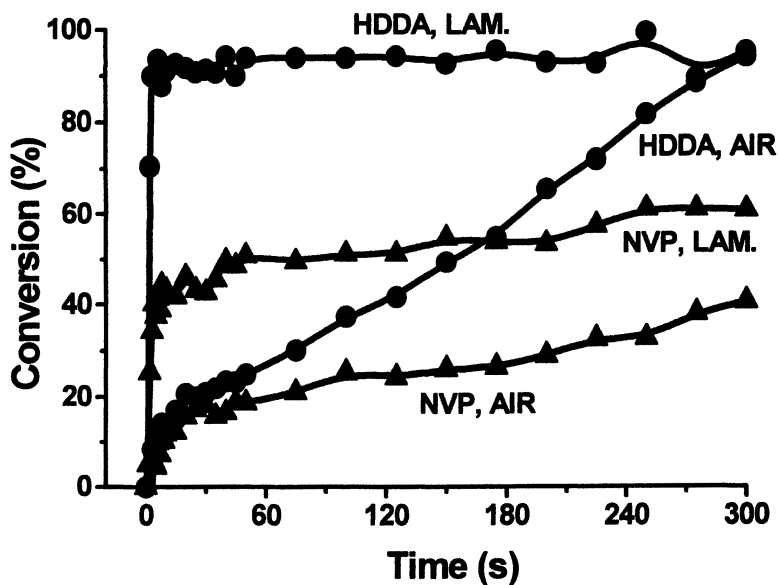


Figure 5. RTFTIR conversion versus time plots for 60% NVP in HDDA in laminate and air.

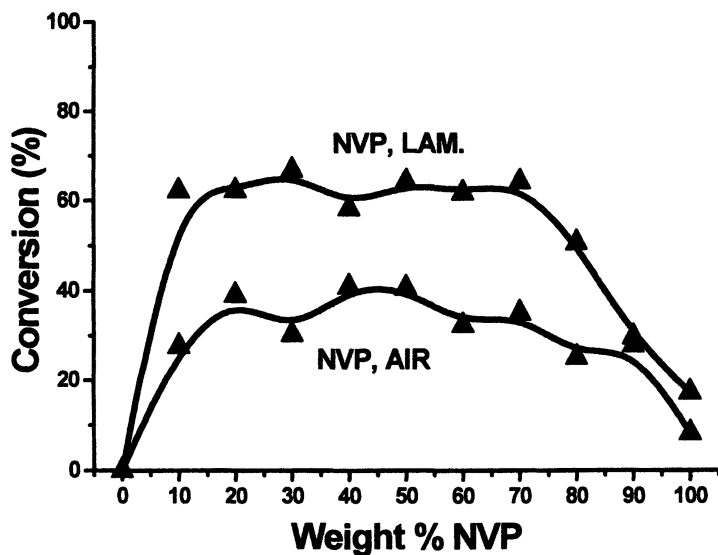


Figure 6. RTFTIR conversion of NVP versus weight percent NVP in HDDA in laminate and air.

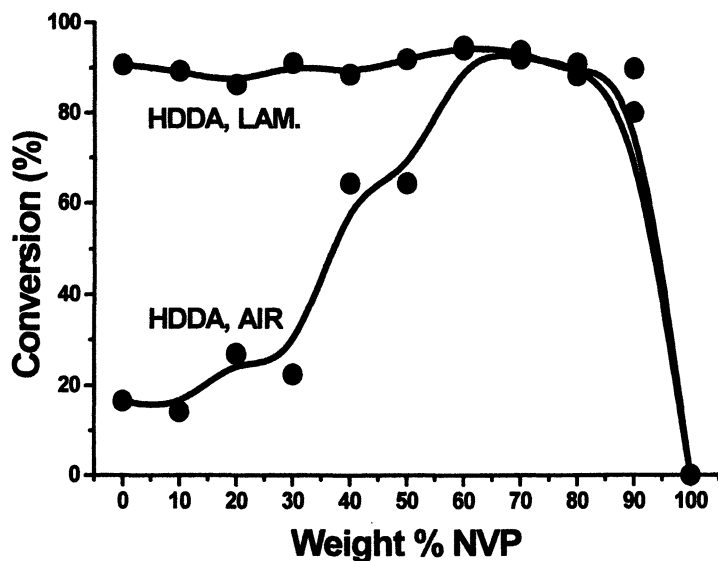


Figure 7. RTFTIR conversion of HDDA versus weight percent NVP in HDDA in laminate and air.

significantly (by a factor of 1.7-3) between 50-300s. As shown in Figure 5, HDDA conversion increased linearly from 20% at 30s to 90% at 300s during polymerization of the 60% NVP formulation. Over the same range, the NVP conversion only increased from ~18% to ~38%.

UV-Visible Spectroscopic Results

Based upon our previous work with maleimides and donor/acceptor chemistry, we considered the possibility that a weak charge-transfer interaction might occur between the relatively electron rich double bonds of the N-vinylamides and the relatively weakly electron poor acrylate double bonds, leading to an enhancement in the rate of polymerization and decreased sensitivity to oxygen inhibition. Generally if a strong ground-state charge-transfer complex is formed in a donor-acceptor system, a shift in the UV-visible absorption bands to lower energy is expected. To explore this possibility, we performed UV-absorption spectral analysis of NVP with HDDA. We found no conclusive evidence for the existence of a ground-state charge-transfer interaction between NVP and HDDA, in agreement with spectroscopic data reported by Ors *et al.* (20) for NVP with isobornylacrylate where no spectral shift was observed.

An interesting report by Takeishi and Tao (21) noted a reversible shift in the UV-visible absorption spectrum of NVP to lower energy when an NVP solution was purged with oxygen compared to the same solution when purged with nitrogen. We repeated this experiment, confirming their observations. In order to determine if the purported complex is dependent upon the presence of the vinyl group, i.e. to partially explain the difference in the oxygen inhibition reduction of NVP versus NMP we observed by Photo-DSC, we measured the UV-visible absorption spectrum of NMP in air, bubbled with nitrogen, and bubbled with oxygen. The resulting spectra show that a reversible oxygen complex similar to that reported (21) for NVP is observed for NMP. This suggests that the complex with oxygen in these compounds is not dependant on the presence of the vinyl group.

Discussion

Kinetically, when a monofunctional vinyl monomer is added to a difunctional vinyl monomer formulation, the rate of polymerization should decrease with increasing monofunctional content, as we previously observed for hexylacrylate with HDDA, and hexylmethacrylate with hexanedioldimethacrylate (18) in nitrogen, and dramatically in air. The reason for this is a decrease in the local concentration of polymerizable double bonds as the monofunctional content is increased. Also, while increasing monofunctional content might be expected to increase final conversion due to delay in the onset

of vitrification, it should also decrease the maximum rate of polymerization for the same reason.

In contrast to this intuition, NVP shows a tremendous enhancement in overall polymerization efficiency in air in HDDA/NVP formulations at low light intensities over a wide range of NVP contents in the formulations, as confirmed by the relative rate and percent conversion data from the Photo-DSC and RTFTIR experiments. Similar results were obtained for NVCL and NVF in Photo-DSC experiments, but have not been confirmed by RTFTIR. A linear N-vinylamide, NMNVA, showed very little rate enhancement in air, in contrast to NVP and NVCL, which are cyclic compounds. Interestingly, Photo-DSC experiments with N-alkylamides, which are not polymerizable by free-radical reactions, showed a small but significant enhancement in the maximum relative rates of polymerization of HDDA formulations, of the same magnitude as the enhancements observed with NMNVA. These observations suggest that both the N-vinyl and the cyclic amide functionalities contribute to the rate enhancement, and that the combination of the two functionalities in NVP and NVCL results in a dramatic synergism.

The lack of a shift in the UV-visible absorption spectra of NVP in combination with acrylates does not exclude the possibility of a weak charge-transfer association between NVP (strong donor) and the acrylate (weak acceptor), though a strong ground-state association is unlikely; nor does it preclude the possibility of formation of a charge-transfer complex between the acrylate and the vinylamide. However, we do not believe that a vinylamide/acrylate ground-state or excited-state complex is responsible for the observed rate enhancement because 1) NMNVA shows a much smaller effect than NVP or NVCL and 2) NMP and NEP show small, though significant rate enhancement effects without the N-vinyl substituent. The reversible UV-absorption spectral shifts observed for NVP and NMP upon alternately sparging with nitrogen and oxygen suggest interaction between molecular oxygen and the amides. Excitation of such a complex or formation of an exciplex (excited state complex with no bound ground state association), might, as Takeishi and Tao suggest (21), lead to an unstable intermediate that might decay into species that could contribute to initiation of polymerization. One hypothesis suggests that in the exciplex or unstable intermediate, electron or hydrogen transfer (or both) might occur producing radicals. For example, a hydrogen peroxide radical (which might initiate polymerization, though slowly) and a pyrrolidonyl radical (with the radical located on the ring carbon alpha to the nitrogen, which could likely initiate polymerization similarly to aminyl radicals) might be formed from decay of an oxygen/NVP exciplex. Differences observed in the magnitude of the oxygen inhibition effects for the various cyclic and acyclic N-vinylamides and N-alkylamides then might be rationalized based upon differences in their respective oxidation potentials and/or differences in the abstractability of hydrogen atoms on the different structures.

Another possible explanation of the decreased oxygen inhibition in N-substituted amide/acrylate formulations is an oxygen consumption process similar to that described for amines (4,11-17). For NVP or NVCL, hydrogen atom abstraction would likely occur on the ring carbon alpha to the nitrogen, followed by consumption of dissolved oxygen through coupling of the pyrrolidonyl radical with an oxygen molecule. The N-vinyl group would be left intact (as observed in the low NVP conversions in the RTFTIR experiments). In the cases of NMP and NEP, the abstractable ring hydrogens on the carbon alpha to the nitrogen are present for the oxygen consumption reaction, though the hydrogen atom abstractability may be decreased through decreased resonance stabilization of the incipient pyrrolidonyl radical. Decreased oxygen inhibition effects for NMVA might be explained by a significantly lower abstractability of the hydrogen atoms on the N-methyl group compared to those on the methylene carbon alpha to the nitrogen on NVP, thereby reducing the efficiency of the oxygen consumption chain mechanism. Observations by RTFTIR that in nitrogen, the maximum conversion of NVP is 60% does not exclude the possibility that some NVP is linked into the polymer matrix through a hydrogen abstraction process. The quite low conversion of NVP in air may explain the high conversion of acrylate obtained late in the reaction, since liquid monomer will plasticize the network and allow diffusion of oligomeric radicals to consume double bonds. However, the low conversion of NVP is in contrast to the rapid overall rates of polymerization observed in air via Photo-DSC.

Conclusions

Our results confirm that N-vinylpyrrolidinone and N-vinylcaprolactam show dramatic rate-enhancement effects when used as additives in HDDA at low light intensities in oxygen-containing atmospheres. N-vinylformamide exhibits similar effects, though Michael addition of NVF to the acrylate is a competing reaction. Acyclic N-vinylamides and cyclic N-alkylamides also show beneficial rate effects in HDDA in air, though to a much smaller extent. The combination of the N-vinyl functionality with the cyclic amide functionality appears to provide the maximum benefit for reduction of oxygen inhibition by N-substituted amides in photopolymerization of HDDA in air at low light intensities. RTFTIR shows that in laminate conditions, NVP conversion was typically only ~60%, while HDDA conversion was quite rapid and was typically 90% over the full range of NVP contents. In air, NVP conversion was typically 30-40%, with HDDA conversion approaching 90% as the NVP content approached 60-80%. Thus, a significant quantity of NVP may be left in the final films at the end of the polymerization reaction under these conditions.

The complex array of interactions that results in the dramatic increase in the efficiency of acrylate photopolymerization in air in the presence of NVP, NVCL, and NVF has not yet been clearly elucidated. Several mechanisms may

synergistically contribute to the observed rate effects including 1) oxygen consumption through photo-oxidation of the N-substituted amides in processes similar to photo-oxidation of amines, and 2) formation of excited state charge-transfer complexes (or exiplexes) between oxygen and the N-substituted amides that decay producing radicals capable of initiation and/or consumption of oxygen.

Acknowledgements

Support for this research was provided by Becker-Acroma, Fusion UV-Curing Systems, DSM Desotech, and UCB Chemicals. The authors further acknowledge contributions from the following students and collaborators: Danning Yang, Robert Kess, Tatsuya Iijima, Jim Owens, and Loo-Teck Ng.

References

1. Turro, N.J. *Modern Molecular Photochemistry*; Univ. Sci. Books: Mill Valley, CA, 1991.
2. Horspool, W., D. Armesto. *Organic Photochemistry: A Comprehensive Treatment*; Ellis Horwood Limited: New York, 1992.
3. C. W. Miller, S. Jönsson, C. E. Hoyle, D. Yang, W. F. Kuang, R. Kess, T. Iijima, C. Nason, L.-T. Ng. *Technical Proceedings. Radtech 2000, Baltimore, MD. 2000*, 754.
4. Decker, C., and A.D. Jenkins. *Macromolecules*. **1985**, *18*, 1241.
5. Decker, C. *Polym. International*. **1998**, *42*, 133.
6. Wight, F.R. *J. Polym. Sci: Polym. Lett. Ed*. **1978**, *16*, 127.
7. Müller, U. *J. Macromol. Sci., Pure Appl. Chem*. **1996**, *32* (4), 523.
8. Odian, G. *Principles of Polymerization*; 3rd edition, Wiley Interscience: New York, 1991.
9. Bolon, D.A., and K.K. Webb. *J. Appl. Polym. Sci*. **1978**, *22*, 2543.
10. Decker, C., and K. Moussa. *Macromolecules*. **1989**, *22*, 4455.
11. *Radiation Curing in Polymer Science and Technology. Volume III: Polymerisation Mechanisms*; Fouassier, J.P., Rabek, J.F., Eds. Elsevier Applied Science: London, 1993.
12. *Chemistry & Technology of UV & EB Formulation for Coatings, Inks & Paints. Volume 2: Prepolymers and Reactive Diluents for UV and EB Curable Formulations*. Oldring, P.K.T., Ed., SITA Technology: London, 1991.
13. Cohen, S.G., A.Parola, and G.H. Parsons. *Chem. Rev*. **1973**, *73*(2), 141.
14. Bartholomew, R.F., and R.S. Davidson. *J. Chem. Soc. (C)*. **1971**, 2342.
15. Bartholomew, R.F., and R.S. Davidson. *J. Chem. Soc. (C)*. **1971**, 2347.
16. Schaefer, F.C., and W.D. Zimmerman. *J. Org. Chem*. **1970**, *35*(7), 2165.

17. Bartholomew, R.F., D.R.G. Brimage, and R.S. Davidson. *J.Chem. Soc. (C)*. **1971**, 3482.
18. Miller, C. W., R. Kess, T. Iijima, C. E. Hoyle. *Poly. Prep.* **1997**, 38(1), 258.
19. Kloosterboer, J.G., G.J.M. Lippits. *J. Rad. Curing. II*, **1984**, 10.
20. Crosslinked Polymers: Chemistry, Properties and Applications. Dickie,R., Labana, S.S., Bauer, R.S., Eds. American Chemical Society, 1988.
21. Takeishi, J., G.-Y. Tao. *J. Polym. Sci: Pt. C. Polym. Lett.* **1989**, 27, 301.
22. Pinschmidt, R.K. Jr., W.L. Renz, W.E. Carroll, K. Yacoub, J. Drescher, A.F. Nordquist, N. Chen. *J. Macromol. Sci., Pure Appl. Chem.* **1997**, A34(10), 1885.

Chapter 2

Spectroscopic Investigation of Three-Component Initiator Systems

Kathryn Sirovatka Padon^{1,2}, Dongkwan Kim¹,
Mohamed El-Maazawi¹, and Alec B. Scranton¹

¹Department of Chemical and Biochemical Engineering, University of Iowa,
125 Chemistry Building, Iowa City, IA 52242

²Current address: Kimberly-Clark Corporation, 2100 Winchester Road,
Neenah, WI 54956

In this contribution, photodifferential scanning calorimetry (DSC) and *in situ* time-resolved steady state fluorescence spectroscopy are used to study the initiation mechanism of the three-component systems: 1) methylene blue/N-methyl-diethanolamine/diphenyliodonium chloride (MB/MDEA/DPI), 2) eosin Y/MDEA/DPI (EY/MDEA/DPI), and 3) eosin Y, spirit soluble/MDEA/DPI (EYss/MDEA/DPI). Kinetic studies reveal that the photopolymerization behavior for eosin dyes is quite similar to that observed for methylene blue. The fastest polymerization rate is obtained when all three components are present, the next fastest with the dye/amine pair, and the slowest with the dye/iodonium pair. In the MB/MDEA/DPI system, it is concluded that the primary photochemical reaction involves electron transfer from the amine to the dye.

We suggest that the iodonium salt reacts with the resulting dye-based radical (which is active only for termination) to generate the original dye and simultaneously produce a phenyl radical that is active in initiation. Moreover, oxygen is found to quench the triplet state of the dye leading to retardation of the reaction. In the eosin/MDEA/DPI system, experimental results showed that the two eosin dyes function quite similarly in the three component system eosin/MDEA/DPI. We propose a sequence of steps in which the dye is rapidly oxidized by DPI in a reaction that is not highly efficient at producing initiating radicals. However, the dye may also be reduced by MDEA producing active initiating amine radicals. Another active radical may be produced if the reduced dye radical is further reduced to its leuco form by an additional molecule of amine. Additionally, the reduction of the bleached dye radical (formed via reaction with DPI) by the amine has a two fold effect. First it regenerates the original eosin dye, and second, it produces an active amine radical in place of the less active dye radical. Dual cell UV-visible absorption spectroscopy yielded no evidence for the formation of a ground state complex between the eosin dyes and the iodonium salt.

Introduction

Free radical photoinitiators, which produce active centers upon absorption of light, have traditionally been built around the benzoyl chromophore, which absorbs light in the ultraviolet (UV) region of the spectrum. Some common classes of these photoinitiators include benzoin ethers, dialkoxyacetophenones, hydroxy alkyl ketones, benzoyl oxime esters, amino ketones, and morpholino ketones. When illuminated with UV light, these photoinitiators produce active centers efficiently by the well-known α -cleavage process. However, the traditional α -cleavage initiators have some important limitations. For example, ultraviolet light is undesirable for applications such as photopolymer master printing plates (1-3) and photopolymerizations in biological systems (4,5). The widespread availability and low cost of visible light sources has made visible initiating systems very attractive for use in photopolymer plates. In addition, for biological applications such as dental composites and bone cements, visible light is preferable due to the damaging effects of UV radiation.

Until recently, the need for visible light radical photoinitiators has been addressed primarily by using bimolecular initiator systems. In these systems, active radicals are generally produced via electron transfer and subsequent proton transfer from an amine to a photo-excited molecule. Using this approach, the system can be tailored to a specific wavelength range by choice of the light-absorbing species. In the last decade, three-component photoinitiation systems have emerged as an improvement over two-component electron transfer initiating systems. Like the two component systems, the three-component initiators include a light absorbing moiety which is typically a dye and an electron donor which is almost always an amine. The third component is usually an iodonium salt. Three-component systems are extremely flexible since a wide variety of dyes may be used. As in the two-component systems, the selection of the dye determines the active wavelength; classes of dyes that have been reported for three-component systems include ketones, xanthenes, thioxanthenes, xanthonones, thioxanthonones, coumarins, ketocoumarins, thiazines, and merocyanines. These three-component systems have consistently been found to be faster, more efficient, and more sensitive than their two-component counterparts (2,6-14). In addition to the advantages of enhanced cure rate and higher sensitivity mentioned above, three component systems have some other significant features which make them quite interesting. For example, a single combination of electron donor and iodonium salt can be used with a variety of different dyes thereby providing tremendous flexibility in selection of the initiating wavelength. In addition, with proper selection of the components the same initiating systems may be effective for initiation of cationic polymerizations as well as radical polymerizations (15).

In this contribution we report a series of spectroscopic studies of three different three-component radical photoinitiator systems. The first system consists of a methylene blue dye (MB), N-methyldiethanolamine (MDEA) as the electron donor component, and diphenyliodonium chloride (DPI) as the third component. Diphenyliodonium chloride and N-methyldiethanolamine were chosen because they are essentially standard constituents in three-component systems. Methylene blue, however, has not been well studied and was selected due to its unique characteristics. For example, since methylene blue is a cationic dye, electrostatic repulsion precludes direct reaction with the iodonium cation. Furthermore, the entire class of cationic dyes has not been well studied in three-component systems. Finally, methylene blue is of extremely low toxicity, making it an appealing choice for biological applications of three-component systems. The second system we investigated consisted of the *neutral* dye Eosin Y (spirit soluble), N-methyldiethanolamine, and diphenyliodonium chloride. The third system was eosin Y (doubly charged anionic dye), N-methyldiethanolamine, and diphenyliodonium chloride. The amine and iodonium components are identical to those in the previous study, and are relatively

standard constituent choices in three-component systems because their efficacy is well-demonstrated. The use of the eosin Y dyes provided some interesting comparisons to the system containing methylene blue.

Experimental

Materials

As in previous publications (16-18), the monomer 2-hydroxyethyl-methacrylate was obtained from Aldrich. It was treated with DeHibit (from Polysciences) to remove hydroquinone inhibitor and filtered prior to use. Methylene blue and Eosin Y were obtained from Aldrich, and N-methyl-diethanolamine (MDEA) and diphenyliodonium chloride (DPI) were obtained from Fluka, and were used as received.

Photo-differential scanning calorimetry

By continuously monitoring the heat flow from the reacting sample, differential scanning calorimetry (DSC) provides a complete polymerization exotherm which yields both instantaneous reaction rate and conversion data. Photo-DSC was conducted using a Hewlett-Packard DSC 7 modified in-house for photo-experiments. The light source was a 200 W Oriel mercury-xenon lamp. The beam was passed through a water filter outfitted with a thermostatted recirculating jacket to reduce infrared radiation and limit sample heating. A glass cover on the DSC sample block was used to eliminate any ultraviolet-induced photoinitiation. The total radiant power incident on the sample was 63 mW/cm^2 , as measured by graphite disc absorption. This measurement includes all visible region light, not all of which can be absorbed by the methylene blue photosensitive component. Comparison of the lamp's spectral characteristics with the absorbance profile of the methylene blue dye reveals that only about 6% of this total radiant intensity can be absorbed by the dye, for an effective incident power of approximately 4 mW/cm^2 . This low light intensity was used in order to produce a relatively slow reaction rate that can be accurately monitored using DSC. A nitrogen purge, flowing at approximately $25 \text{ cm}^3/\text{min}$, was used in the DSC to eliminate oxygen inhibition of the polymerization. Samples were degassed for a minimum of five minutes prior to illumination. The heat flow data collected by the DSC can be easily converted to the polymerization rate data reported in this contribution using the heat of polymerization, which is 49.8 kJ/mol for HEMA.

DSC Dark-Cure Experiments

The DSC apparatus, described above, was used to obtain dark polymerization exotherms for samples that contained 0.00010 M methylene blue and 0.013 M MDEA in ethylene glycol dimethacrylate (EGDMA)/HEMA 8:1 mass ratio at various DPI concentrations between 0 and 5 mM. Each sample was illuminated for 2 minutes then the light was shuttered. The decay in the heat flow was then recorded until the curve was flat at 0 W/g. All experiments were performed at a temperature of 25°C and light intensity $I_a = 0.3 \text{ mW/cm}^2$.

Time-resolved steady state fluorescence

The experimental details for the *in situ* time-resolved steady state fluorescence monitoring studies have been described previously (16-18). Fluorescence may be used to characterize the dye concentration as a function of time because the fluorescence signal decays as the dye is consumed in the initiation reaction. Most studies were carried out in a thin film geometry using a custom-made sample cell that allowed both temperature control and a controlled atmosphere. Typically, fifty complete fluorescence spectra in the wavelength range 700-850 nm were taken at time intervals chosen to capture the entire decay of the methylene blue or Eosin fluorescence. To investigate the effect of oxygen, some studies were performed using a capillary cell which consists of a 1 mm diameter capillary tube held perpendicular to the laser beam.

Dual-cell UV-visible absorption spectroscopy

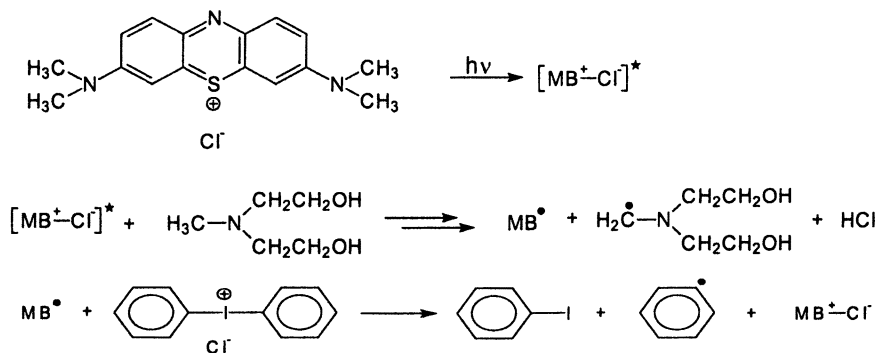
Ultraviolet-visible absorption spectroscopy was used to investigate the possible formation of ground state complexes in all of the three component initiator systems in this study. The experimental protocol was as follows: Solutions of each component were prepared in methanol. For each pair of components, a reference scan was carried out using two cuvettes sandwiched together, each containing one of the components. The samples were then mixed and placed in a 2.0 cm pathlength cuvette, and the difference between the resulting absorbance spectrum and that obtained with the sandwiched cuvettes was obtained. In this way, any signal observed in the sample can be attributed to the effect of mixing the two components.

Results and Discussion

Methylene blue, N-methyldiethanolamine and diphenyliodonium chloride system

The photo-DSC data illustrated that each component plays an important role in the photopolymerization reaction (16). The maximum rate was observed when all three components were present (maximum rate 0.019 mol/L/s observed at 10.5 min). The two component system containing MDEA and MB exhibits the second fastest reaction rate (maximum rate 0.011 mol/L/s observed at 18 min), while a two-component system containing DPI and MB exhibits a relatively slow reaction (maximum rate 0.005 mol/L/s observed at 26 min). Next, a more detailed series of studies on the three-component system was performed to investigate the effects of the concentrations of DPI and MDEA on the observed polymerization rate. With the concentrations of MB and DPI held constant, as the MDEA concentration is increased from zero to 0.051 molar, the maximum polymerization rate was observed to increase from 0.005 to 0.024 mol/L/s. Similarly, the reaction rate also increases dramatically with increasing DPI concentration. With the concentrations of MB and MDEA held constant, as the DPI concentration is increased from zero to 0.0049 molar, the maximum polymerization rate was observed to increase from 0.010 to 0.025 mol/L/s. Therefore, these kinetic studies based upon photo-differential scanning calorimetry revealed a significant increase in polymerization rate with increasing concentration of either the amine or the iodonium salt. However, the laser-induced fluorescence experiments show that while increasing the amine concentration dramatically increases the rate of dye fluorescence decay, increasing the DPI concentration actually slows consumption of the dye (16).

Based upon the experimental trends described above, we concluded that the primary photochemical reaction involves electron transfer/proton transfer from the amine to the dye. We suggest that the iodonium salt reacts with the resulting dye-based radical (which is active only for termination) to regenerate the original dye and simultaneously produce a phenyl radical (active in initiation) derived from the diphenyliodonium salt as shown in scheme I. The role of the iodonium salt proposed in scheme I has two primary implications: First, since the DPI serves to regenerate the methylene blue, it will reduce the rate at which the dye is consumed in the photoinitiation reaction (consistent with the fluorescence observations described above); Second, since the DPI consumes the methylene blue radical (which is active for termination but not for initiation) an increase in the DPI concentration should lead to a decrease in the rate of termination. In this way, DPI can enhance the polymerization rate by two distinct effects.



Scheme I: Major reaction steps for the three component system MB/MDEA/DPI

To test the effect of DPI on the rate of termination, dark cure studies were performed using differential scanning calorimetry. The dark-cure results shown in Figure 1 illustrate that DPI does indeed affect the rate of termination. Samples with higher DPI concentrations exhibit greater and more persistent levels of dark cure than samples with lower DPI concentration. These results suggest that termination is reduced in the samples with higher DPI concentration. Furthermore, as shown in Figure 1, the initial rate when the dark cure experiment begins (at time = 0 seconds) is higher for samples with higher DPI concentrations. This is a natural effect of the increase in photopolymerization rate with increasing DPI concentration. However, the observed effect on the termination step cannot be attributed to hindered diffusion of growing chains arising from a higher degree of crosslinking for the samples with higher DPI concentrations because the overall conversion is quite low for these samples (the sample with the highest DPI concentration reaches only 7% of its final conversion during the first two minutes of exposure). For this reason, variation in degree of crosslinking is expected to be minimal and should not significantly affect the termination step. Hence, the primary cause of the variation in the rate of termination illustrated in Figure 1 is the consumption of terminating MB radicals via reaction with DPI.

A series of studies were also performed to characterize the influence of oxygen on the rate of consumption of the methylene blue dye (17). Oxygen quenches the triplet state of the dye, leading to retardation of the reaction. We use time-resolved steady state fluorescence monitoring to observe the methylene blue concentration *in-situ* in both a constant-oxygen environment and a capillary

tube cell as the dye is consumed via photoreaction. In the capillary tube cell, we observed a retardation period (attributed to the presence of oxygen) followed by rapid exponential decay of the methylene blue fluorescence after the oxygen was depleted. Based on the impact of the amine and iodonium concentrations on the fluorescence intensity and the duration of the retardation period, our proposed mechanism includes an oxygen-scavenging pathway in which the tertiary amine radicals formed in the primary photochemical process consume the oxygen via a cyclic reaction mechanism.

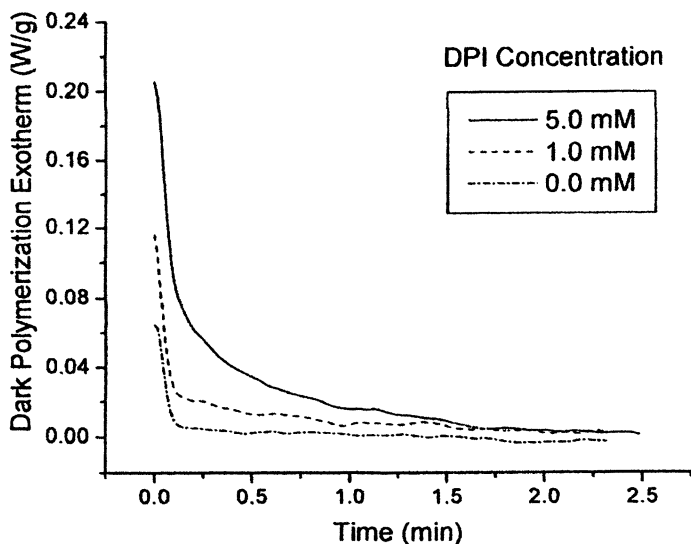


Figure 1: Dark polymerization exotherms for various DPI concentrations. Increasing DPI slows termination of the polymerization reaction. $[MB] = 0.00010\text{ M}$, $[MDEA] = 0.013\text{ M}$ in EGDMA/HEMA 8:1 mass ratio. $T = 25^\circ\text{C}$, $I_a = 0.3\text{ mW/cm}^2$. Each curve is the average of three replicate trials.

Eosin Y, N-methyldiethanolamine and diphenyliodonium chloride system

The dyes eosin Y (EY) and eosin Y, spirit soluble (EYss) (*18*) were chosen as model anionic and neutral dyes with charges of -2 and 0, respectively. In contrast to the cationic methylene blue dye, the eosin dyes are able to react directly with both the amine and the iodonium components. Although the EY/DPI reaction is expected to proceed more vigorously than the EYss/DPI reaction because of the possible electrostatic attraction between the negatively

charged EY dye moiety and the positively charged iodonium ion, experimental results showed that the two dyes function quite similarly in the three component system eosin/MDEA/DPI.

For both of the eosin dyes, kinetic studies based upon photo-differential scanning calorimetry reveal that the fastest polymerization occurs when all three components are present, the next fastest with the dye/amine pair, and the slowest with the dye/iodonium pair. However, the laser-induced fluorescence experiments show that the pairwise reaction between eosin and iodonium bleaches the dye much more rapidly than does the reaction between eosin and amine. In this system, we concluded that although direct eosin/amine reaction can produce active radicals, in the three-component system this reaction is largely overshadowed by the eosin/iodonium reaction, which does not produce active radicals as effectively. We propose that the amine reduces the oxidized dye radical formed in the eosin/iodonium reaction back to its original state and simultaneously produces an active initiating amine-based radical. Due to the difference in the pairwise reaction rates for eosin/amine and eosin/iodonium, it seems likely that this regeneration reaction is the primary source of active radicals in the three-component eosin/amine/iodonium system.

Although, as indicated above, EY and EYss were found to react similarly in the eosin/MDEA/DPI three component system, direct reaction between DPI and EY appears to be somewhat more efficient than that between DPI and EYss. The rate of photocuring for the two-component EYss/DPI pair is significantly slower than that for the EY/DPI pair. This is most likely due to increased initiation efficiency of the radicals generated rather than a significant difference in the rate of the EY/DPI reaction, since the decay profiles for the EY/DPI and EYss/DPI pairs are essentially identical within experimental errors, as shown in Figure 2. (The characteristic decay constants determined from the exponential fit are also equal within experimental errors).

The experimental results described above are not inconsistent with the formation of a ground-state complex between eosin dye and the iodonium salt. In fact, Fouassier and Chesneau (19) report the formation of a ground state complex between a singly charged eosin dye and diphenyliodonium complex under certain conditions. For our two eosin dyes (which are anionically double charged and neutral, respectively) we performed studies using dual-cell UV-visible absorption spectroscopy to seek evidence for the formation of a ground state complex. In these studies, for each of the eosin dyes, the visible absorption spectrum was unchanged by the addition of DPI. Therefore, while the DSC evidence suggests that the EY/DPI produces faster photocuring than EYss/DPI, it seems unlikely that this difference is due to ground-state pre-association of the negatively charged EY dye moiety and the positively charged DPI. Instead, it is likely that difference is due to an enhanced initiation efficiency of the radicals produced from the EY/DPI reaction as compared to the EYss/DPI pair. This

difference may be attributable to the dye charge. After being oxidized by DPI, the charge on EY is reduced from -2 to -1 . However, the charge on the EYss dye moiety changes from neutral to $+1$. MDEA has a dipole moment due to the lone electron pair on the central nitrogen atom. This region of high electron density will experience a greater attraction to the positively charged EYss radical than the negatively charged EY radical.

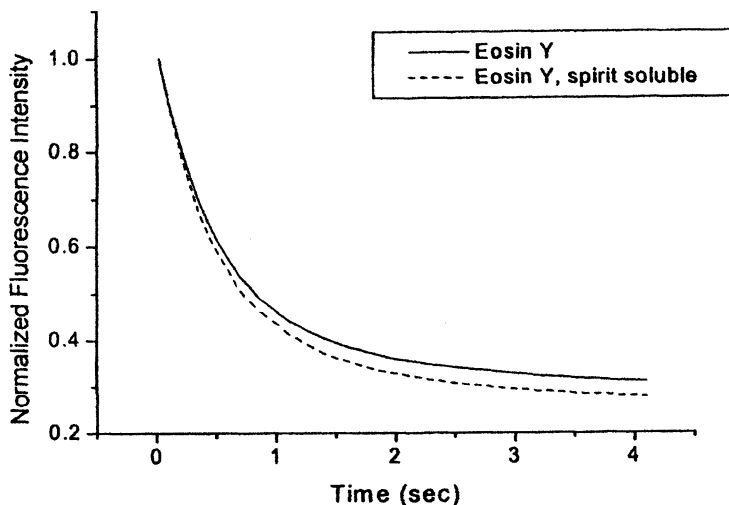


Figure 2: Comparison of Eosin Y and Eosin Y, spirit soluble photobleaching by DPI. $[EY] = [EYss] = 0.0010$ M, $[DPI] = 0.001$ M, all in HEMA, $T = 25$ °C, $I_a = 50$ mW/cm². No MDEA is present. Each curve represents the average of three trials

Conclusions

We have presented experimental characterization of three different three component initiator systems. The three-component system comprised of methylene blue, MDEA, and DPI appears to proceed by a mechanism involving electron transfer/proton transfer from the amine to the dye as the primary photochemical reaction. Interaction between the dye and the iodonium salt is precluded by charge repulsion. The iodonium salt is an electron acceptor, acting to re-oxidize the neutral dye radical back to its original state and allowing it to re-enter the primary photochemical process. This reaction simultaneously generates phenyl radicals that can serve as initiating radicals. Therefore, the

iodonium has a double role: to regenerate the methylene blue and to replace the inactive, terminating dye radical with an active, initiating radical. Based on the impact of the amine and iodonium concentrations on the fluorescence intensity and the duration of the oxygen-induced retardation period, the reaction scheme includes an oxygen-scavenging pathway in which the tertiary amine radicals formed in the primary photochemical process consume the oxygen via a cyclic reaction mechanism.

The three-component systems comprised of neutral or anionically doubly charged eosin Y dyes, MDEA, and DPI appear to produce active radical centers by an electron transfer/proton transfer reaction from the amine to photoexcited dye, and/or to dye that has been reduced by the iodonium. The eosin may be oxidized by the DPI to produce an eosin radical, which may be in turn reduced by an amine back to the original state. This reaction has a twofold effect: first, it regenerates the original eosin dye, and second, it produces an active amine radical in place of the presumably less active dye radical. Because of the difference in reaction rates for the pairwise reactions, this dark amine-mediated dye regeneration reaction may be the primary source of active radicals in the three-component system. No spectroscopic evidence for the formation of ground state complexes between the eosin dyes and the iodonium salt was observed.

Acknowledgements

This material is based upon work supported under a National Science Foundation Graduate Fellowship. (KSP) The authors also acknowledge the assistance of Dr. Ruiping Huang in developing and setting up the thin film fluorescence monitoring experiments. This work was partially supported by the IUCRC Center for Fundamentals and Applications of Photopolymerization.

References

1. Kawabata, M., and Takimoto, Y., *J. Photopolym. Sci. Tech.*, **1990**, *3*, 147.
2. Fouassier, J. P.; Ruhlmann, D.; Graff, B.; Takimoto, Y.; Kawabata, M.; Harada, M. *J. Imaging Sci. and Tech.*, **1993**, *37*, 208.
3. Erddalane, A.; Fouassier, J. P.; Morlet-Savary, F.; Takimoto, Y. *J. Polymer Sci., A: Polym. Chem.*, **1996**, *34*, 633.
4. Anseth, K. S., Svaldi, D. C., Laurencin, C. T., and Langer, R., *Photopolymerization: Fundamentals and Applications*, A. B. Scranton, C. N. Bowman, and R. W. Peiffer (eds.), American Chemical Society, Washington DC: *189*, 1997.

5. Kucybala, Z., Pietrzak, M., Paczkowski, J., Lindén, L.-Å., and Rabek, J., *Polymer*, **1996**, *37*, 4585.
6. Oxman, J. D.; Ubel III, A.; Larson, E. G., *Minnesota Mining and Manufacturing Company* **1988**, U.S. Patent 4,735,632.
7. Padon, K. S.; Scranton, A. B. In *Recent Research Developments in Polymer Science*, vol. 3; Pandalai, S. G., Ed.; Transworld Research Network, p 369, 1999.
8. Palazzotto, M. C.; Ubel III, F. A.; Oxman, J. D.; Ali, M. Z. *Minnesota Mining and Manufacturing Company* **1996**, U.S. Patent 5,545,676.
9. Oxman, J. D.; Ubel III, F. A.; Larson, E. G. *Minnesota Mining and Manufacturing Company* **1989**, U.S. Patent 4,828,583.
10. Palazzotto, M. C.; Ubel III, F. A.; Oxman, J. D.; Ali, M. Z. *3M Innovative Properties Company* **2000**, U.S. Patent 6,017,660.
11. Fouassier, J. P.; Ruhlmann, D.; Takimoto, Y.; Harada, M.; Kawabata, M. *J. Polymer Sci. A: Polym. Chem.* **1993**, *31*, 2245.
12. Fouassier J. P.; Wu, S. K. *J. Appl. Polym. Sci.*, **1992**, *44*, 1779.
13. Fouassier J. P.; Erddalane, A.; Morlet-Savary, F. *Macromolecule.*, **1994**, *27*, 3349.
14. Fouassier J. P.; Morlet-Savary, F.; Yamashita K.; Imahashi S. *J. Appl. Polym. Sci.* **1996**, *62*, 1877.
15. Bi, Y.; and Neckers, D.C. *Macromolecules*, **1994**, *27*, 3683.
16. Padon K. S.; Scranton, A. B. *J. Polymer Sci. A: Polym. Chem.* **2000**, *38*, 2057.
17. Padon K. S.; Scranton, A. B. *J. Polymer Sci. A: Polym. Chem.* **2000**, *38*, 3336.
18. Padon K. S.; Scranton, A. B. *J. Polymer Sci. A: Polym. Chem.* **2001**, *39*, 715.
19. Fouassier J. P.; Chesneau E. *Macromol. Chem.* **1991**, *192*, 1307.

Chapter 3

A Mechanistic Description of the Sensitized N-Substituted Maleimide Initiated Photopolymerization of an Acrylate Monomer

**Chau K. Nguyen¹, T. Brian Cavitt¹, Charles E. Hoyle¹,
Viswanathan Kalyanaraman², and Sonny Jönsson³**

¹School of Polymers and High Performance Materials, Department of Polymer Science, University of Southern Mississippi, 2609 West 4th Street, Hattiesburg, MS 39406

²Becker-Acroma, Hattiesburg, MS 39406

³Fusion UV-Curing Systems, Inc., 910 Clopper Road, Gaithersburg, MD 20878-1357

N-substituted maleimides have been investigated for their use as photoinitiators for free-radical polymerization. The mechanism of initiation in the presence of sensitizers and cointiators is postulated to involve chemical and energy transfer sensitization processes. Photo-DSC and laser-flash photolysis results provide photophysical data supporting the proposed mechanisms.

Ultraviolet (UV) curing in the 1990s has experienced rapid development with the advent of new technologies (1). UV-curable resins usually consist of three major components: (1) functionalized oligomers, (2) mono and multifunctional monomers and (3) a photoinitiator (free-radical or cationic) to absorb the output of an appropriate light source and produce species capable of initiating polymerization. Free-radical photoinitiators can be classified into two basic categories: Type I, those that undergo unimolecular fragmentation (Norrish Type I, α -cleavage), and Type II, those that undergo bimolecular abstraction from a source of labile hydrogens (2). The first produces radicals by photocleavage. Examples of Type I photoinitiators include aromatic carbonyl compounds such as derivatives of acetophenone that undergo Norrish Type I fragmentation to form initiating radicals, *e. g.*, 2,2-dimethoxy-2-phenylacetophenone (DMPA). Abstraction type photoinitiators are typically diaromatic ketones such as thioxanthenes and benzophenone derivatives. Upon irradiation and absorption of a photon, benzophenone (or thioxanthone) ultimately forms the triplet state in high yield. In the presence of transferable hydrogen sources (such as amines, ethers, or alcohols) a reaction from the benzophenone triplet state produces two radicals (Figure 1) by a direct hydrogen transfer process (alcohols, ethers) or an electron/proton transfer process (tertiary amines).

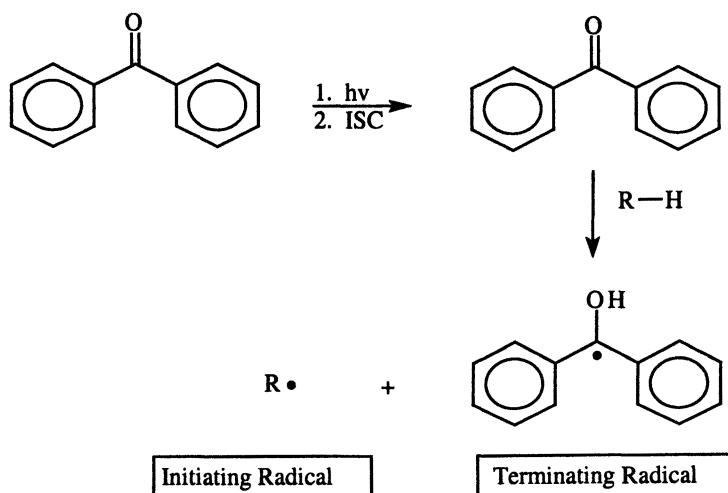


Figure 1. Reaction pathways for benzophenone photolysis.

The two radicals depicted in Figure 1 are the semipinacol radical and a radical centered on the hydrogen donor source. The semipinacol radical does not efficiently initiate polymerization, but rather couples with other radicals in the system. This radical-radical termination process severely reduces the overall polymerization rate. The radical formed on the hydrogen donor source adds to monomer and initiates polymerization. The low rates characteristic of abstraction type photoinitiating systems compared to cleavage type photoinitiators is unfortunate in view of the low cost and ease of synthesis of diaromatic ketones.

Aromatic maleimides have been used extensively in polymer chemistry as crosslinkers for engineering thermoplastics, and for some three decades, it has also been shown that maleimides can be used to initiate photopolymerizations (3-7). Recently, the practical viability of using maleimides as efficient photoinitiators has been addressed (8-11). In the presence of an amine cointiator, the mechanism involves an electron-transfer/proton-transfer to give a radical centered on the amine and a succinimidyl radical, both of which are capable of initiating polymerization (Figure 2). Ground state maleimides can then participate in free-radical homopolymerization (in the case of a neat maleimide sample) or copolymerization (in the case of having a primary monomer such as an acrylate present) depending upon the monomer composition. The maleimide is thus consumed by the very free-radical polymerization process that it initiates.

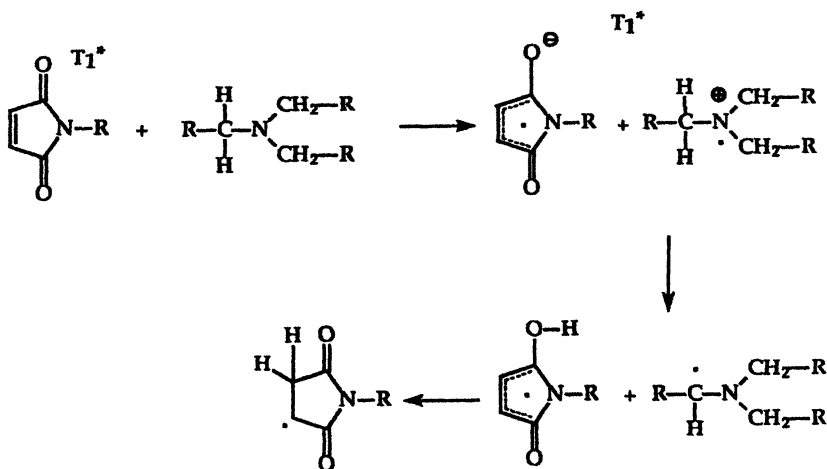


Figure 2. Electron/proton transfer mechanism for maleimide/amine.

Unfortunately, due to a variety of reasons including the low yields of intersystem crossing to produce triplet state maleimides, the efficiency of initiation by

maleimides in the absence of a triplet sensitizer is low as reported by DeSchryver et al. (12).

Recently, we reported that if an appropriate diaromatic ketone sensitizer is added (such as benzophenone or a substituted thioxanthone), the polymerization rate of multifunctional acrylates in the presence of an amine/maleimide system is greatly enhanced (13). Moreover, the rate of polymerization, when the three component initiating system is used, is much greater than that obtained with a sensitizer/amine mixture alone. Thus, the combination of a sensitizer, an amine and a maleimide presents a unique and efficient photoinitiator system that alleviates the problems associated with the low rates inherent to either the sensitizer/amine or the maleimide/amine initiator systems. A previously proposed mechanism for the three component photoinitiator involves triplet-triplet energy transfer from the sensitizer (diaromatic ketone) to the maleimide, which then undergoes an electron-transfer/proton-transfer reaction with an amine (Figure 3). Herein, we will present evidence to suggest that a *chemical sensitization* process involving production and subsequent oxidation of a semipinacol type radical in the presence of a maleimide can also take place to generate two radicals capable of initiating radical polymerization.

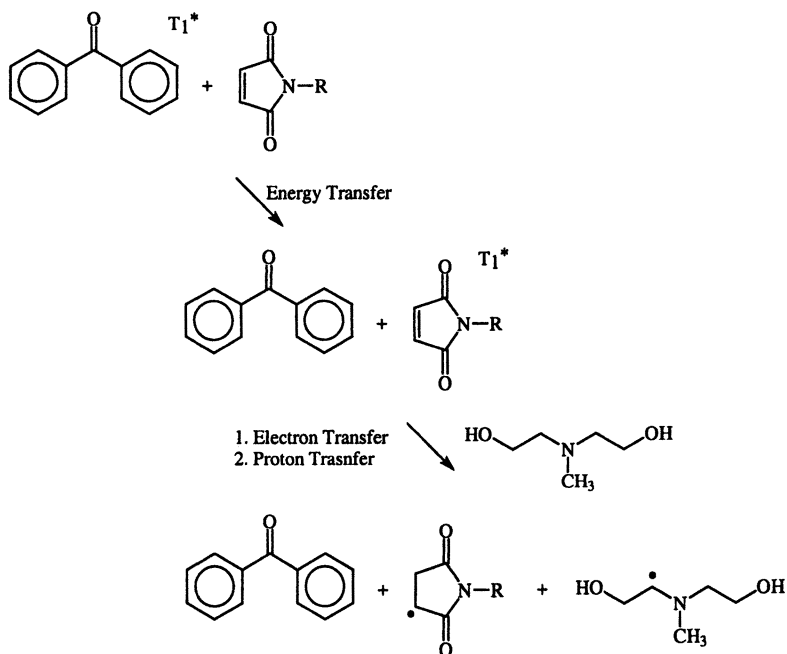


Figure 3. Energy transfer mechanism.

Experimental

N-methylmaleimide, benzanthrone, fluorenone, benzophenone and 4-benzoylbiphenyl were purchased from Aldrich Chemical Company and further purified by sublimation. *N*-methyl-*N,N*-diethanolamine was also purchased from Aldrich and used without further purification. Isopropylthioxanthone was obtained from Albemarle Corporation and used without further purification. 1,6-Hexanedioldiacrylate was donated by UCB Chemicals Corporation. The sensitizers used in this experiment are presented in Table I, along with their respective triplet energies and acronyms (14).

Table I. Triplet Sensitizers

<i>Sensitizer</i>	<i>Triplet Energy</i>
Benzophenone (BP)	69
Triphenylene (TP)	66
Isopropylthioxanthone (ITX) ^a	64
Phenanthrene (PHT)	62
4-Benzoylbiphenyl (BBP)	61
Fluorenone (FLR)	50
Benzanthrone (BZT)	45
Anthracene (ANT)	42
Perylene (PRY)	36

NOTE: The units of the triplet energies are in kilocalories per mole

^a Determined in our lab via phosphorescence at 77 K (1:1 ethanol/methylene chloride glass)

Photo-Differential Scanning Calorimetry (Photo-DSC) was performed using a Perkin-Elmer DSC 7 modified to accommodate quartz windows. The sample cell was purged with nitrogen. The lamp source was a Canrad Hanovia medium-pressure mercury lamp from Ace Glass: specific spectral bands were isolated by the use of band-pass filters at 313 nm and 365 nm. The samples (2 μ L) were injected into specially crimped aluminum sample pans with corresponding film thicknesses of \sim 180-200 μ m. Data were recorded and processed on a PC.

Laser flash photolysis transients and lifetime quenching data were obtained using a system based on an excitation source of a Continuum Surelite Nd-YAG

laser, and the UV-visible emission/absorption was monitored with a xenon probe and data acquisition/analysis system from Applied Photophysics. The main output wavelength of the laser at 1064 nm is converted with frequency quadrupling or tripling crystals to 266 nm or 355 nm. The monitoring system was used in the absorption mode, with a pulsed xenon lamp generating a monitoring beam. The intensity was then monitored by a photomultiplier tube connected to a Phillips digital oscilloscope.

Results and Discussion

In order to define the effect that sensitizers have on the photopolymerization of a typical multifunctional acrylate, photo-DSC results are presented first. Laser flash photolysis results will then be presented and discussed in order to provide a mechanistic rationale for the polymerization observations.

Photo-DSC Exotherms

Photoexotherms in Figure 4 show a marked rate enhancement for polymerization of 1,6-hexanedioldiacrylate (HDDA) when an amine and maleimide in low concentration is mixed with traditional diaromatic ketone sensitizers such as benzophenone (BP) or isopropylthioxanthone (ITX) (8-11). In this initial screening investigation, we have also included sensitizers with varying triplet energies and excited state configurations to determine any dependence of sensitization on energy level and sensitizer type. All of the sensitizers used have high quantum yields for intersystem crossing to the triplet upon direct excitation: some are diaromatic ketones and some are polycyclic aromatics. In each case, the concentrations of the sensitizers were normalized to have the same absorbance at the excitation wavelength of 313 nm as a sample with 1.0 wt% DMPA. Each sample included 0.1 wt% *N*-methylmaleimide (MMI) and 1.0 wt% *N*-methyl-*N,N*-diethanolamine (MDEA) with the corresponding concentration of sensitizer. Returning to an analysis of the results in Figure 4, it is obvious that the HDDA polymerization with the DMPA photoinitiator does not exhibit an exotherm that is much greater than that obtained for HDDA with the three diaromatic ketones ITX, 4-benzoylbiphenyl (BBP) or BP in combination with MMI/MDEA.

Importantly, as shown in previous publications, the rates achieved with these three component sensitizer/maleimide/amine mixtures are far greater than can be

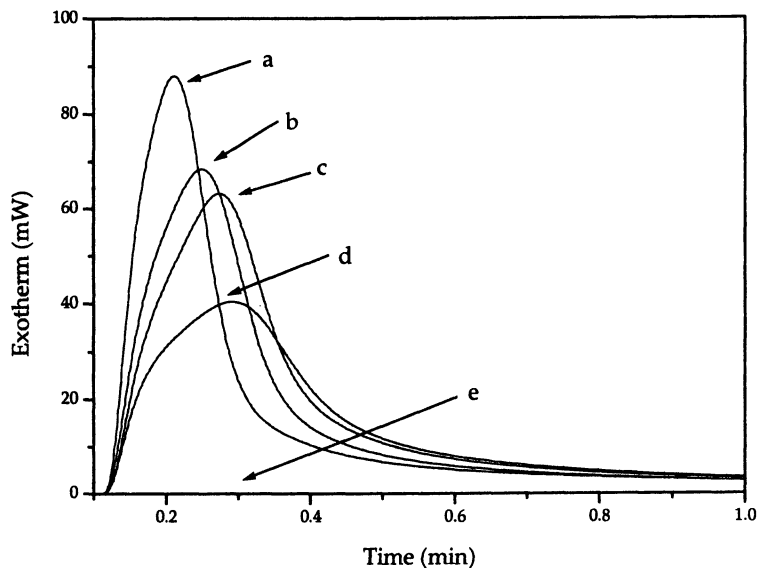


Figure 4. Photo-DSC exotherms for nitrogen purged HDDA initiated by sensitized 0.1 wt% MMI in the presence of 1.0 wt% MDEA. Sensitizer absorbance adjusted to equal absorbance of 1.0 wt% DMPA. Light intensity was 0.52 mW/cm² at 313 nm. (a) DMPA (b) ITX/MDEA/MMI (c) BBP/MDEA/MMI (d) BP/MDEA/MMI (e) TP/MDEA/MMI, PRY/MDEA/MMI, PHT/MDA/MMI and ANT/MDEA/MMI.

achieved with either of the two component sensitizer/amine or maleimide/amine systems alone at 313 nm, where both the maleimide and the sensitizer absorb (8-11). Probably one of the most interesting aspects of the photo-DSC exotherms in Figure 4 is the low (essentially non-existent) exotherms recorded for HDDA polymerization when the sensitizer was a polycyclic aromatic, i. e., triphenylene (TP), perylene (PRY), phenanthrene (PHT), or anthracene (ANT). While ANT and PRY with very low triplet energies might not be expected to sensitize the triplet state of MMI, it would be expected that TRY and PHT with triplet energies equivalent to or greater than BBP should also sensitize formation of the maleimide triplet state (in a later section the triplet energy of MMI will be shown

to be ~ 56 kcal/mol). However, both TRY and PHT have very long singlet lifetimes which will be quenched by MDEA at the concentration used, thereby preventing formation of their respective triplet states. BP, ITX and BBP all have very short singlet lifetimes which cannot be quenched by MDEA.

Next, we confirm that results equivalent to that in Figure 4 can be obtained upon excitation at wavelengths longer than 313 nm. Accordingly, Figure 5 presents results for excitation at 365 nm with concentrations adjusted so that the absorbing chromophore in each system is equivalent to the absorption of 1 wt% DMPA. In the case of the sensitizer/amine/maleimide mixtures, excitation at 365 nm ensures that there is little competitive interference in the absorption of light by the maleimide.

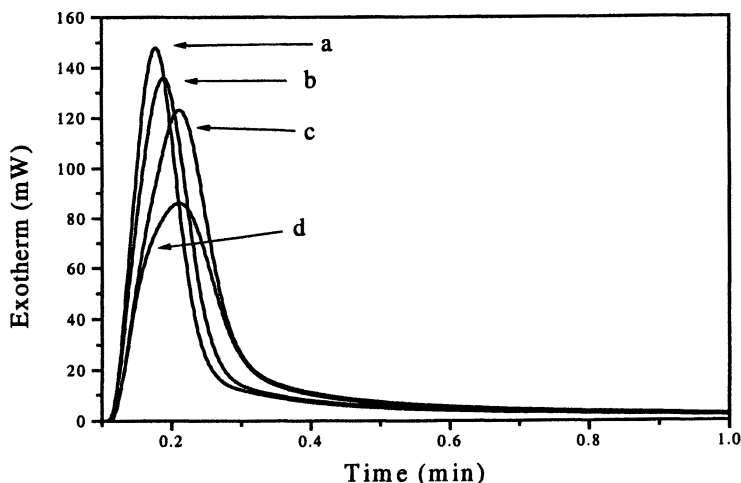


Figure 5. Photo-DSC exotherms for HDDA initiated by sensitized 0.1 wt% MMI in the presence of 1.0 wt% MDEA. For each sample sensitizer absorbance adjusted to equal absorbance of 1.0 wt% DMPA. Light intensity was 0.75 mW/cm^2 at 365 nm. All samples were thoroughly nitrogen purged. (a) DMPA (b) ITX/MDEA/MMI (c) BBP/MDEA/MMI (d) BP/MDEA/MMI.

The photo-DSC results in Figure 5 were obtained with the band-pass isolated 365-nm line of the medium pressure mercury lamp. [Since the molar extinction coefficient of MMI at 365 nm is around $60 \text{ L mol}^{-1} \text{ cm}^{-1}$, and since its concentration is relatively low (0.1 wt% in each sample), it does not

competitively absorb light]. As with the results at 313 nm, the highest HDDA polymerization exotherm was recorded for the sample with the DMPA initiator. Interestingly, the HDDA maximum exotherm rate with the three component ITX/MDEA/MMI photoinitiator mixture approaches that for the HDDA sample with the DMPA photoinitiator. The HDDA polymerization rates with the BBP/MDEA/MMI and BP/MDEA/MMI systems are not quite as efficient as DMPA.

Having established that equivalent results to those obtained using 313 nm light can be obtained at 365 nm, we present results in Figure 6 that highlights the use of sensitizers with very low triplet energies. If the energy transfer mechanism depicted in Figure 3 was the only method for sensitization in the maleimide based three component systems, then it would be expected that use of sensitizers with very low triplet energies (50 kcal/mol or less) would not lead to efficient initiation.

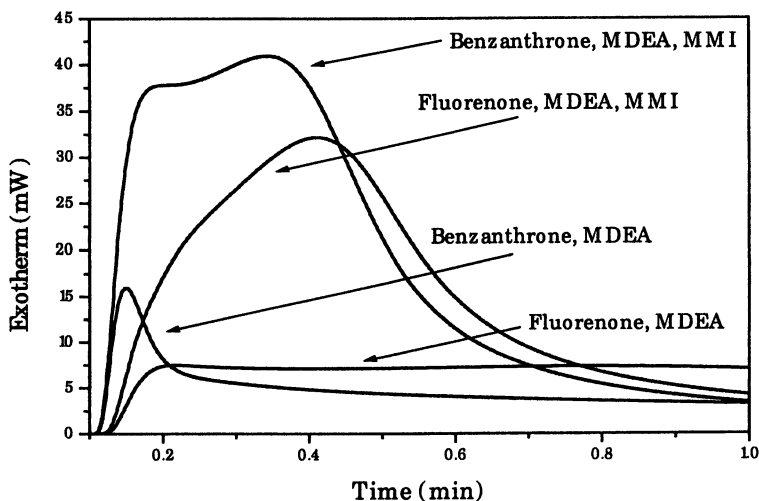


Figure 6. Photo-DSC exotherms for HDDA polymerization initiated by sensitized 0.1 wt% MMI in the presence of 1.0 wt% MDEA. Sensitizer absorbance adjusted to equal absorbance of 1.0 wt% DMPA. Light intensity was 1.61 mW/cm² at 365 nm. All samples were thoroughly nitrogen purged. (a) BZT/MDEA/MMI (b) FLR/MDEA/MMI (c) BZT/MDEA (d) FLR/MDEA.

The results in Figure 6 using FLR ($E_T = 50$ kcal/mol) and BZT ($E_T = 45$ kcal/mol) clearly show that even compounds with low energy triplets are capable

of sensitizing the MMI/MDEA combination (though not by conventional triplet sensitization). Based upon these results, it appears as though the magnitude of the triplet energy is not the sole sufficient factor or the only factor in the sensitization process. What does appear to be essential is the structure of the sensitizer (i. e., it needs to be a diaromatic ketone). In the next section, data is presented that provides a basis for a mechanism to account for the polymerization results in Figures 4-6.

Laser Flash Photolysis

To establish a mechanism for the sensitizer effect and confirm from basic photochemical/photophysical principals a rationale for the results in Figures 4-6, laser flash photolysis data were recorded. First, the maleimide triplet energy must be determined to confirm in which cases energy transfer sensitization may occur. Second, critical quenching rate constants involving the sensitizer and each of the components in the system must be measured to suggest a viable mechanism for the role of the sensitizer and each component in the mixture. The absorption spectrum of the excited state triplet of MMI has a peak maximum near 340 nm. The rate constant for quenching of the excited triplet state of a molecule (in this case either MMI or the sensitizer) may be calculated according to the Stern-Volmer Equation 1,

$$\tau_0/\tau = 1 + k_q \tau [Q] \quad \text{Eq. 1}$$

where

τ_0 is the triplet lifetime in the absence of quencher

τ is the triplet lifetime at a given quencher concentration

k_q is the rate constant for triplet quenching

$[Q]$ is the concentration of the quencher

Table II summarizes rate constants for quenching the MMI triplet by MDEA, as well as each sensitizer triplet by MMI and MDEA. From the rate constants in Table II for quenching of each sensitizer by MMI (and additional constants not shown) the triplet energy of MMI was estimated to be ~ 56 kcal/mol. We note that BP, ITX, and BBP are all readily quenched by MMI at close to diffusion controlled rates, while the triplet states of FLR and BZT are not quenched by MMI to any appreciable extent. Hence, FLR and BZT cannot efficiently sensitize via an energy transfer process formation of the triplet state of MMI, thus ruling out the mechanism in Figure 3 for the generation of radical

species responsible for initiating the polymerization of HDDA in Figure 6. The triplet states of BP, BBP, ITX, FLR and BZT, however, are all readily quenched by MDEA at high rates indicative of an efficient electron/proton transfer process.

Table II. Laser flash quenching constants in acetonitrile solution

<i>Compound/Quencher</i>	<i>k_q (L mol⁻¹ sec⁻¹)</i>
MMI/MDEA	4.3 x 10 ⁹
BP/MDEA	1.1 x 10 ⁹
BP/MMI	5.7 x 10 ⁹
BBP/MDEA	1.6 x 10 ⁸
BBP/MMI	1.4 x 10 ⁹
ITX/MDEA	1.8 x 10 ⁹
ITX/MMI	6.8 x 10 ⁹
FLR/MDEA	2.5 x 10 ⁸
FLR/MMI	No quenching
BZT/MDEA	8.8 x 10 ⁷
BZT/MMI	No quenching
BP ketyl radical/MMI	3.7 x 10 ⁷

Based upon the triplet quenching results in Table II, we suggest that the scheme in Figure 7 may be operative and in certain cases help account for the exotherm results in Figures 4-6. For example, when using a diaromatic ketone sensitizer such as BZT (50 kcal/mol) or FLR (45 kcal/mol) with a triplet energy below that of MMI (56 kcal/mol) there is no observable quenching of the triplet state, and hence the mechanism in Figure 3 does not contribute to initiation of HDDA polymerization in Figure 6. As for BP, ITX and BBP, their triplet energies are all greater than that of MMI. Even though the rate constants for quenching of these sensitizers by MMI are calculated to be anywhere from ~2.5 to 10 times that of quenching by MDEA, the MDEA is in almost ten fold excess in the samples polymerized in Figures 4 and 5. Hence, MDEA would account for a substantial portion of the quenching of the sensitizer. Thus, it might be expected that the initiation process of an amine/maleimide system where the triplet energy of the sensitizer is greater than that of the maleimide would proceed to initiate polymerization according to the mechanisms depicted in both Figures 3 and 7, the contribution of each depending upon the relative energy transfer and electron transfer rates of each process.

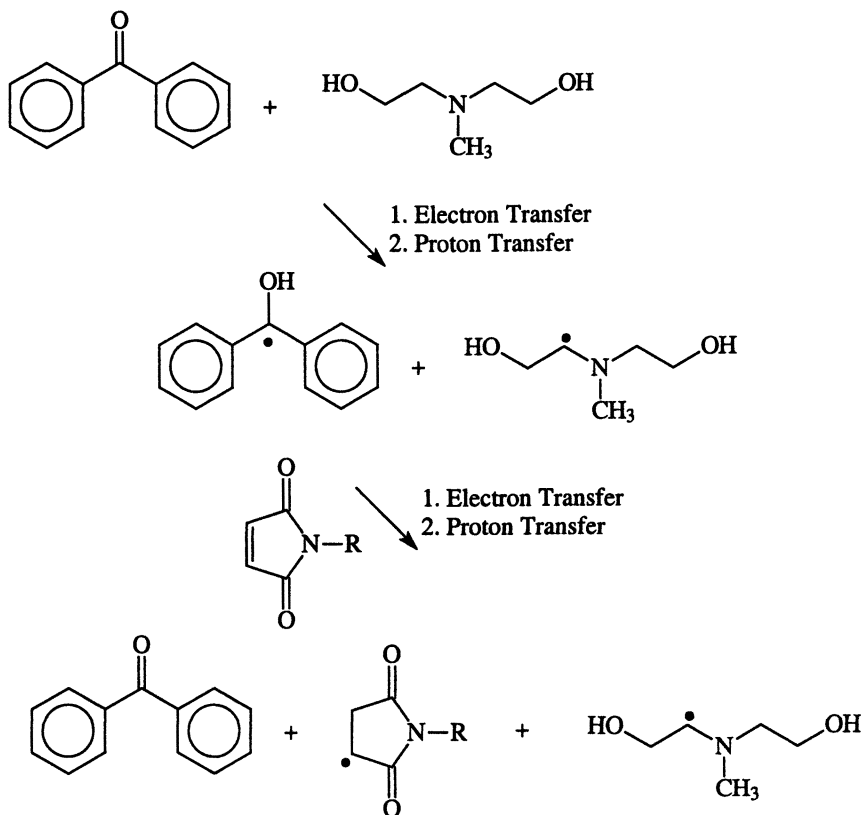


Figure 7. Semipinacol reduction mechanism.

Evidence for the mechanism in Figure 7 is obtained from the quenching rate constant for the semipinacol radical (derived from BP triplet and MDEA) by MMI of $3.7 \times 10^7 \text{ L mol}^{-1} \text{ sec}^{-1}$. This rate constant, indicative of electron transfer (although a little slower than for the electron transfer process involved in quenching of BP, BBP, or ITX by MDEA) is consistent with the scheme in Figure 7. In principal, the semipinacol radical could react with another radical. However, since the radical concentration would be several orders of magnitude lower than the MMI concentration, the chemical sensitization process involving the electron/proton transfer sequence of reactions in Figure 7 would be favored. Interestingly, in both the energy sensitization process depicted in Figure 3 and the chemical sensitization process depicted in Figure 7, two initiating radicals

are produced and the semipinacol radical is rendered inoperative (in Figure 3 it never forms and in Figure 7 it is converted back to the diaromatic ketone). No doubt the exact contribution of each pathway is determined by the lifetimes of the triplet sensitizers and relevant competing quenching rate constants for each step involved.

Conclusions

A chemical sensitization process was found to be operative for diaromatic ketone/maleimide/amine photoinitiator systems. In the presence of a sensitizer with a triplet energy above that of MMI and where higher concentrations of MMI would be employed, both an energy and a chemical sensitization process are probably operative: we project that chemical sensitization is more prevalent at lower MMI concentrations (i.e. 0.1 wt% as used in this paper). In systems where the sensitizer has a triplet energy less than that of the maleimide, the chemical sensitization process probably takes place exclusively.

Acknowledgements

The authors would like to acknowledge Albemarle Corporation and Fusion UV-Curing Systems for support of this research.

References

1. Fouassier, J.P, *Photoinitiation, Photopolymerization and Photocuring*; Verlag: New York, NY, 1995.
2. *Radiation Curing: Science and Technology*; Pappas, S.P., Ed.; Plenum Press: New York, NY, 1992.
3. Yamada, M.; Takase, I.; Kouto, N. *Polym. Lett.* **1968**, *6*, 883.
4. Wipfelder, E.; Huesinger, H. *J. Polym. Lett.* **1978**, *16*, 1779.
5. Zott, H.; Huesinger, H. *Europ. Polym. J.* **1978**, *14*, 89.
6. Ayscough, P.B.; English, T.; Lambert, G.; Elliot A.J. *J. Chem. Soc., Faraday Trans. 1* **1978**, *73*, 1303.
7. Aida, H.; Takase, I.; Nozi, T. *Makromol. Chem.* **1989**, *190*, 2821.
8. Hoyle, C.E.; Kalyanaraman, V.; Clark, S.C.; Miller, C.W.; Nguyen, C.K.; Jönsson, S.; Shao, L. *Macromolecules* **1999**, *32*, 2793.
9. Clark, S.C.; Hoyle, C.E.; Jönsson, E.S.; Morel, F. and Decker, C. *RadTech North America Proceedings* **1998**, 177-181.

10. Miller, C.W.; Hoyle, C.E.; Jönsson, E.S.; Hasselgren, C.; Haraldsson, T.; Shao, L. *RadTech North America Proceedings* **1998**, 182-188.
11. Nguyen, C.K.; Johnson, A.T.; Kalyanaraman, V.; Cole, M.C.; Cavitt, T.B.; Hoyle, C.E.; Jönsson, E.S.; Pappas, S.P.; Miller, C.W.; Shao, L. *RadTech North America Proceedings* **2000**, 197-210.
12. Put, J.; DeSchryver, F.C. *J. Am. Chem. Soc.* **1973**, *95*, 1, 137.
13. Monroe, B.; Weiner, S.A. *J. Am. Chem. Soc.* **1969**, *91*, 450.
14. Murov, S. L.; Carmichael, I. and Hug, G. L. *Handbook of Photochemistry*. Marcel Dekker, New York, **1993**.

Chapter 4

Photoinitiation of Acrylates via Sensitized Phthalimide Derivatives

**T. Brian Cavitt¹, Brian Phillips¹, Charles E. Hoyle¹,
Chau K. Nguyen¹, Viswanathan Kalyanaraman²,
and Sonny Jönsson³**

¹School of Polymers and High Performance Materials, Department of Polymer Science, University of Southern Mississippi, 2609 West 4th Street, Hattiesburg, MS 39406

²Becker-Acroma, Hattiesburg, MS 39406

³Fusion UV-Curing Systems, Inc., 910 Clopper Road, Gaithersburg, MD 20878-1357

When isopropylthioxanthone is used as a coinitiator for substituted N-phenylphthalimide photoinitiators, rapid rates of acrylate polymerization are attained if a tertiary amine is present as a hydrogen source. N-Phenylphthalimide with electron withdrawing substituents on the N-phenyl ring in the presence of a combination of isopropylthioxanthone and N-methyl-N,N-diethanolamine results in an increase in the maximum rate of polymerization of 1,6-hexanedioldiacrylate by a factor of as much as twice that attained when only the coinitiator and N-methyl-N,N-diethanolamine are present.

Introduction

As the EPA stipulates increasingly stringent regulations for coatings usage, industry has been forced to develop more “environmentally friendly” coatings (1). This has promoted steady growth in the UV-curable market over the last twenty years yielding novel technologies compliant to government regulations and consumer demand (1). Each of the major components of a UV-curable coating, monomers, reactive diluents, additives, and photoinitiators, have thus been investigated in detail to further the growth in this market.

Being a vital component in photocurable formulations, photoinitiating systems are the subject of particularly extensive research. Most of this research has focused on *Type I* photoinitiators, which undergo an alpha cleavage process to form two radical species. An example of a *Type I* photoinitiator is 2,2-dimethoxy-2-phenylacetophenone (DMPA), which undergoes cleavage alpha to the carbonyl to form a benzoyl radical and a tertiary carbon-centered radical. The benzoyl radical can subsequently initiate polymerization or abstract a hydrogen to form benzaldehyde. The second radical species rearranges to form methylbenzoate and a highly reactive methyl radical as an initiating species.

Type II photoinitiators are a second class of photoinitiators and are based on compounds whose triplet excited states are reduced by a labile hydrogen transfer process thereby producing an initiating radical. *Type II* photoinitiators are exemplified by the traditional benzophenone/*N*-methyl-*N,N*-diethanolamine system where a hydrogen is transferred to the triplet excited state of benzophenone from the amine via an electron/proton transfer mechanism to yield a carbon-centered radical adjacent to the nitrogen capable of initiation and the semipinacol radical serving only to terminate propagating species.

Recent work on new *Type II* photoinitiators has produced a system involving a maleimide or maleic anhydride, a tertiary amine such as *N*-methyl-*N,N*-diethanolamine, and a sensitizer (2, 3). Depending on the sensitizer and maleimide chosen for the initiating system, the resulting rate of polymerization can rival that of DMPA. The initiation process is probably based on a dual initiating mechanism involving an electron/proton transfer from the ketyl radical to the maleimide (*e.g.* chemical sensitization) and triplet energy transfer from the sensitizer to the maleimide. Phthalimide derivatives have electron affinities and reduction potentials that are comparable to those of maleimides, suggesting their use in three component photoinitiator systems (Table I). In this paper, phthalimide derivatives are evaluated for their viability in three component photoinitiators of acrylate polymerization.

Table I. Electron affinities and reduction potentials of several electron acceptors

	<i>Electron Affinity</i> (4)	<i>Reduction Potential</i> (5)
Maleimide	1.16	---
N-Methylmaleimide	1.12	---
N-Phenylmaleimide	1.36	---
Phthalimide	1.01	-1.45
N-Phenylphthalimide	1.16	-1.31

NOTE: The units for electron affinity and reduction potential are electron volts and volts, respectively.

Experimental

Materials

N-methyl-N,N-diethanolamine (MDEA), N-phenylphthalimide (PPI), 4-aminophthalonitrile, and 4-aminoveratrole were obtained from the Aldrich Chemical Company. UCB provided 1,6-hexanedioldiacrylate (HDDA). The Albemarle Corporation supplied isopropylthioxanthone. The Stepan Company furnished the phthalic anhydride used in the synthesis of N-(3,4-dimethoxyphenyl) phthalimide, denoted DMPPI, and N-(3,4-dicyanophenyl) phthalimide, denoted DCPPI. Synthesis of DMPPI and DCPPI proceeded as given in the literature (6).

Photo-Differential Scanning Calorimetry

Exotherms were measured on a Perkin-Elmer Differential Scanning Calorimeter 7 modified to accommodate a Canrad-Hanovia medium pressure mercury lamp source from Ace Glass. Light intensities were measured at the sample pans via a black body absorber. A mechanical shutter was placed between the light source and the sample chamber to provide control of exposure time. Sample pans were specially crimped and injected with 2 μ L samples, giving a film thickness on the order of 200 μ m (about 8 mils).

Phosphorescence

Phosphorescence studies performed on a Spex Fluorolog 2 fluorimeter were used to estimate the triplet energies of the phthalimides for comparison to the sensitizers. An ethanol/methylene chloride glass (77 K) was used to observe phthalimide phosphorescence at 77 K. The triplet energies were taken as the energy corresponding to the phosphorescence intensity being 10% of the maximum peak intensity where no defined peak was discernable.

Laser Flash Photolysis

Laser flash photolysis lifetime quenching data were obtained by using a system based upon a Continuum Nd-YAG laser as the excitation source and a pulsed xenon probe and data acquisition/analysis system from Applied Photophysics. The ultimate time resolution of the laser flash instrument was approximately 15-20 ns. Each sample was purged with nitrogen for fifteen minutes in the sealed quartz cell. The excitation wavelength was 355 nm where only the sensitizer appreciably absorbed. The analysis wavelength was 630 nm for isopropylthioxanthone.

Results and Discussion

Photo-Differential Scanning Calorimetry (Photo-DSC)

In the past, we have used several diaryl ketone sensitizers with maleimides in the presence of tertiary amines to initiate acrylate polymerization. Three of these diaryl ketones, benzophenone, 4-benzoylbiphenyl and isopropylthioxanthone, were studied in great detail (2,3). All of these sensitizers were also investigated in conjunction with various phthalimides in the presence of an amine. In all of these investigations, systems that incorporated isopropylthioxanthone (ITX) gave higher polymerization rates than benzophenone or 4-benzoylbiphenyl. Selected results are highlighted herein for several N-phenylphthalimides. The trends found for ITX are also found when benzophenone and 4-benzoylbiphenyl are used, although the rates are slower with the latter two sensitizers.

In Figure 1, results for the photopolymerization of 1,6-hexanedioldiacrylate (HDDA) in the presence of several N-phenylphthalimide derivatives and an ITX/MDEA mixture were compared to the standard ITX/MDEA initiating

system. The results are as expected and show that the phthalimides with electron withdrawing substituents [i.e. N-(3,4-dicyanophenyl) phthalimide – DCPPI and N-(3-trifluoromethylphenyl phthalimide – CF3PPI)] yield the fastest rates of initiation as exemplified by the peak maxima. The N-phenylphthalimide substituted with an electron donating group [i.e. N-(3-methoxy phenyl) phthalimide – MPPI] as well as unsubstituted N-phenylphthalimide (PPI) resulted in only moderate rate increases compared to those achieved with ITX/MDEA alone. The results in Figure 1 certainly demonstrate that there is a correlation between the electron affinity of the phthalimide and its ability to initiate polymerization in the presence of an ITX/MDEA combination.

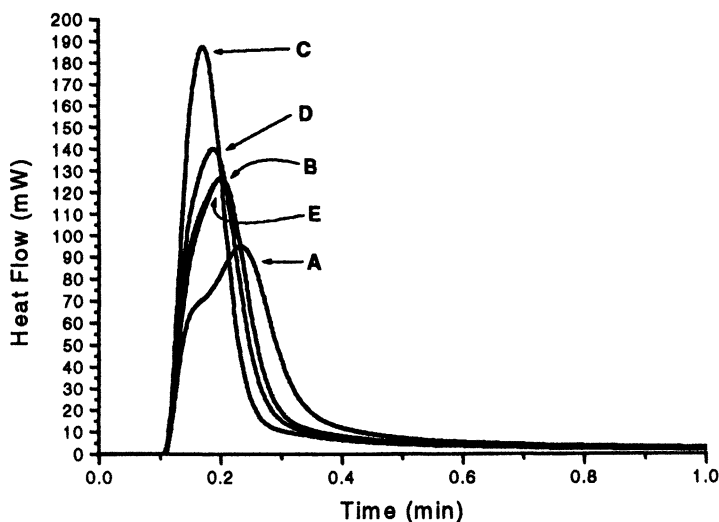


Figure 1. Photo-DSC exotherms of Phthalimide/ITX/MDEA in nitrogen purged HDDA. $I_0=64.31 \text{ mW cm}^{-2}$. Full arc of medium pressure mercury lamp. A is 0.028wt% ITX, 1wt% MDEA; B is 0.1wt% PPI, 0.028wt% ITX, 1wt% MDEA; C is 0.1wt% DCPPI, 0.028wt% ITX, 1wt% MDEA; D is 0.1wt% CF3PPI, 0.028% by weight ITX, 1wt% MDEA; E is 0.1wt% MPPI, 0.028wt% ITX, 1wt% MDEA.

Next we present results that describe the effect that the phthalimide concentration has on the rate of polymerization. This investigation is prompted

by the effect that maleimide concentration has on the rate of acrylate photopolymerization where due to self quenching/inhibition reactions a maximum rate is achieved at only 0.1 wt% maleimide. Although we have measured results for several N-substituted phthalimides with increasing concentration, only results for PPI are presented herein for demonstration purposes. The effect of PPI concentration on the exotherm for HDDA polymerization with ITX as the sensitizer and MDEA as coinitiator is shown in Figure 2. At these higher concentrations of PPI, the rates are even greater than recorded when 0.1 wt% PPI was used (Figure 1). The rate increases even up to a concentration of 1 wt% phthalimide. This dichotomy between phthalimides and maleimides (increased maleimide concentration greater than 0.1 wt% results in a decrease in the polymerization rate) holds true for each of the other phthalimides in this present investigation (although as already mentioned, only results for PPI are given here). Apparently, the high self-quenching and polymerization inhibition characteristic of maleimides are not operative for sensitized phthalimides.

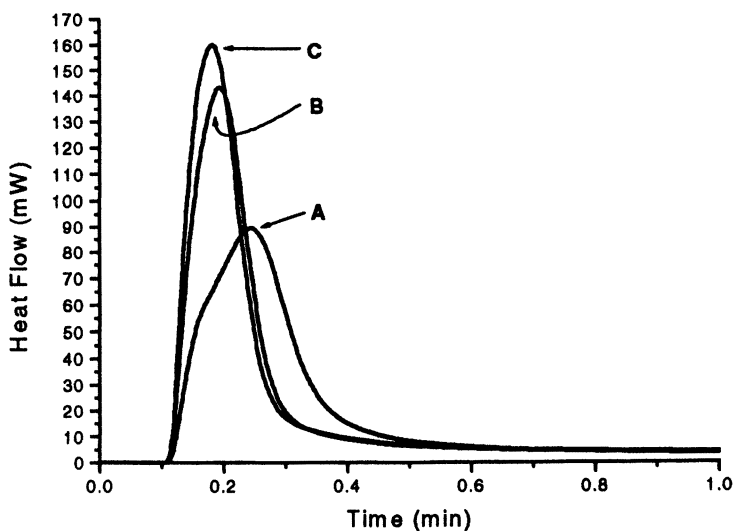


Figure 2. Photo-DSC exotherms of PPI/ITX/MDEA in nitrogen purged HDDA. $I_0=69.52 \text{ mW cm}^{-2}$. Full arc of a medium pressure mercury lamp. A is 0.028wt% ITX, 1wt% MDEA; B is 0.5wt% PPI, 0.028wt% ITX, 1wt% MDEA; C is 1wt% PPI, 0.028wt% ITX, 1wt% MDEA.

Recalling the exotherm results in Figure 1, there is an indication that an electron donating group substituted on the phenyl ring does not result in an enhancement in the polymerization rate. It might be expected that two electron donating groups would result in a reduction in the ability of a phthalimide/ITX/amine system to initiate acrylate polymerization, since as will be shown in the next few sections the initiation is thought to involve an electron transfer process to the N-arylphthalimide molecule. In Figure 3, the results for a phthalimide/ITX/MDEA system where the phthalimide is N-(3,4-dimethoxyphenyl) phthalimide (DMPPI) clearly show that introduction of a second methoxy donating group on the phthalimide ring results in a system that exhibits little appreciable increase in polymerization rate over that achieved with the basic ITX/MDEA initiating system alone. From these results it is clear that the methoxy substituents decrease the ability of DMPPI to participate in the electron/proton transfer process that forms radicals capable of initiating polymerization.

In order to interpret the results in Figures 1-3, we next present photophysical results for the phosphorescence and transient spectra of three of the phthalimides in this investigation with significantly different electron affinities. The electron affinities decrease in the order: DCPPI > PPI > DMPPI.

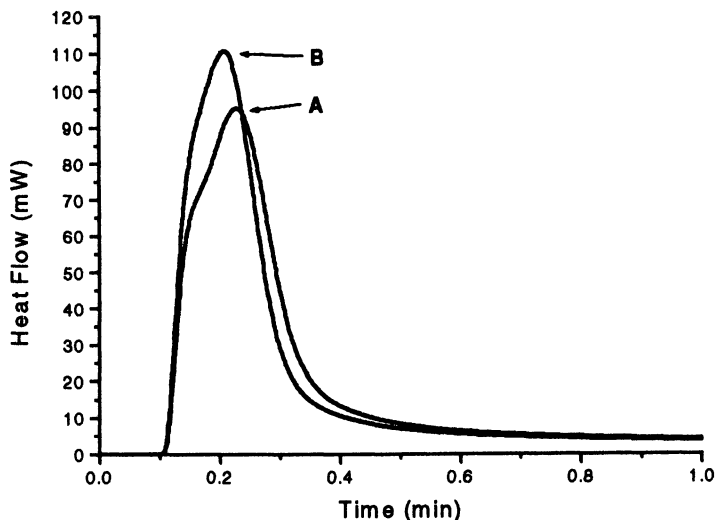


Figure 3. Photo-DSC exotherms of DMPPI/ITX/MDEA in nitrogen purged HDDA. $I_0=61.21 \text{ mW cm}^{-2}$. Full arc of a medium pressure mercury lamp. A is 0.028% by weight ITX, 1% by weight MDEA, HDDA; B is 0.1% by weight DMPPI, 0.028% by weight ITX, 1% by weight MDEA, HDDA.

American Chemical Society
Library

1155 16th St., N.W.

In Photoinitiated Polymerization; Belfield, K., et al.;
ACS Symposium Series; American Chemical Society: Washington, DC, 2003.

Phosphorescence of Substituted N-Phenylphthalimide Derivatives.

The triplet energies of DMPPI, PPI, DCPPI were determined using low temperature phosphorescence as 61.1 kcal/mol, 67.6 kcal/mol, and 68.6 kcal/mol, respectively. From these data, it is obvious that efficient photosensitization of DCPPI and PPI by classical energy transfer from ITX ($E_T=64$ kcal/mol as determined in our lab via phosphorescence at 77 K in a 1:1 ethanol/methylene chloride glass) is not feasible, suggesting that another process is responsible for enhancing the polymerization rate of phthalimides in the presence of ITX and an amine. Before proposing an exact mechanism, laser flash photolysis results are presented for DMPPI, PPI, and DCPPI.

Laser Flash Photolysis

Laser flash photolysis was used to determine the extent of the interaction of the phthalimide derivatives with the excited triplet state of ITX. The lifetime decay of the ITX triplet state monitored at 630 nm was determined at increasing concentrations of the phthalimide derivative in order to calculate the quenching constant, k_q , of ITX ($E_T=64$ kcal/mol) by the phthalimide (Table II).

Table II. Quenching constants of ITX by phthalimide derivatives

<i>Sensitizer</i>	<i>Quencher</i>	k_q ($M^{-1} s^{-1}$)
ITX	DCPPI	$< 10^7$ †
ITX	PPI	7.48×10^7
ITX	DMPPI	3.66×10^9

† Limited by solubility in solvent.

Comparing quenching constants previously acquired for the quenching of ITX by MDEA ($1.8 \times 10^9 M^{-1} s^{-1}$) to those obtained for the quenching of ITX by the phthalimide derivatives, the kinetically preferred reaction is the electron/proton transfer reaction between ITX and MDEA for the two phthalimide derivatives (PPI and DCPPI) with triplet energies greater than that of ITX (7). Only in the case of DMPPI with a triplet energy markedly less than that of ITX is energy transfer efficient.

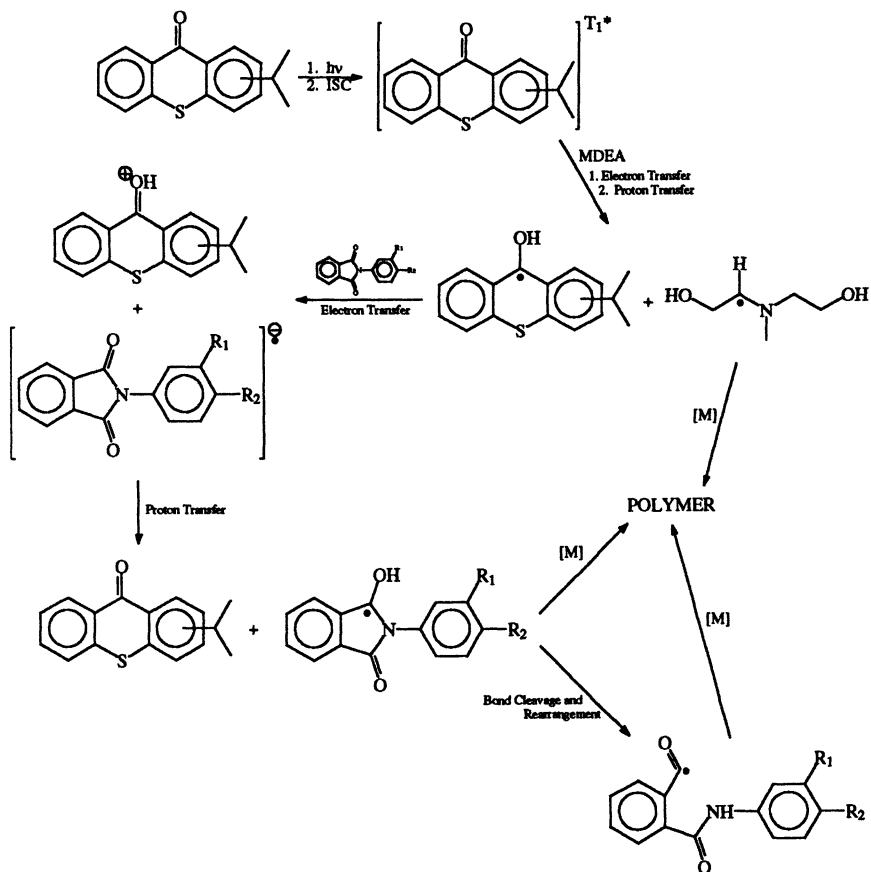


Figure 4. Proposed photoinitiation mechanism involving phthalimide derivatives and ITX.

Proposed Initiation Mechanism

Based on the information acquired via photo-DSC, phosphorescence, and laser flash photolysis, an initiation mechanism can be proposed (Figure 4).

In the mechanism proposed in Figure 4, the sensitizer (ITX) is promoted by absorption of a photon of light to an excited singlet state that subsequently undergoes intersystem crossing to the excited triplet state of ITX. The ITX triplet state then preferentially reacts with the amine via an electron/proton transfer to form a carbon-centered radical on the amine and the corresponding

ketyl radical. The ketyl radical will be formed in high yield in cases where the phthalimides have higher triplet energies than ITX (~64 kcal/mol) such as in the cases of PPI and DCPPI which have triplet energies greater than 64 kcal/mol (see Table II). The radical centered on the amine can initiate polymerization, whereas the ketyl radical can either terminate propagating polymer chains or interact with the phthalimide via an electron/proton transfer to give ground state ITX and the phthalimidyl radical. In the case of DCPPI, which has a relatively favorable electron affinity, the latter occurs readily. It has been reported that phthalimidyl radicals can add to double bonds, which in the present case would lead to acrylate polymerization. As shown in Figure 4, it is also possible that the phthalimidyl radical may form the benzoyl radical followed by reaction with an acrylate to initiate polymerization.

The mechanism in Figure 4 is certainly consistent with the high polymerization rate recorded in Figure 2 for DCPPI, which is electron deficient and would thus be susceptible to reduction by the ketyl radical formed from ITX and MDEA. The lower rate achieved when PPI is used no doubt results from a lower electron affinity than DCPPI. The low enhancement in the overall rate of polymerization for DMPPI/ITX/MDEA compared to ITX/MDEA may be due to a combination of factors. First, since as shown in Table II, DMPPI can readily quench the triplet state of ITX by energy transfer and thus prohibit the formation of the ITX ketyl radical, the efficiency of the resulting electron transfer process will be reduced. Furthermore, an electron/proton transfer process involving the excited triplet state of DMPPI and MDEA would not be favorable due to the reduced electron affinity of DMPPI resulting from the two dimethoxy substituents. Likewise, any ketyl radical which did form from the ITX triplet and MDEA would not readily undergo an electron/proton transfer reaction to the electron rich DMPPI. All of this is consistent with the low polymerization rates noted for HDDA in the presence of the ITX/DMPPI/MDEA mixture as shown in Figure 3.

Conclusions

Electron withdrawing groups assist a facile electron/proton transfer between the ketyl radical of ITX and a phthalimide derivative yielding an enhancement in the polymerization rate, whereas electron donating groups diminish the phthalimide's ability to act as an efficient electron acceptor. Comparison of the triplet energies of ITX and the phthalimide derivatives demonstrate that energy transfer between ITX and DCPPI should be inefficient and thus not a factor in initiating the polymerization. The proposed mechanism (e.g. chemical sensitization) involving the electron/proton transfer

between the ketyl radical of ITX and the phthalimide derivative is supported by laser flash photolysis data.

Acknowledgements

The authors would like to acknowledge Albemarle Corporation and Fusion UV-Curing Systems for support of this research.

References

1. Roffey, C. *Photogeneration of Reactive Species for UV Curing*; John Wiley and Sons: New York, 1997.
2. Hoyle, C.E.; Viswanathan, K.; Clark, S.C.; Miller, C.W.; Nguyen, C.K.; Jönsson, S.; Shao, L. *Macromolecules* **1999**, *32*, 2793.
3. Cavitt, T. B.; Hoyle, C. E.; Nguyen, C. K.; Viswanathan, K.; Jönsson, S. *RadTech 2000 Proceedings* **2000**, 785.
4. Paul, G.; Kebarle, P. *J. Am. Chem. Soc.* **1989**, *111*, 464.
5. Leedy, D. W.; Muck, D. L. *J. Amer. Chem. Soc.* **1971**, *93* (17), 4264.
6. Anzures, E. T. *Photodegradation of Aromatic Polyimides*; University of Southern Mississippi: Hattiesburg, MS, 1991.
7. Nguyen, C. K.; Johnson, A. T.; Viswanathan, K.; Cole, M. C.; Cavitt, T. B.; Hoyle, C. E.; Jonsson, S.; Miller, C. W.; Pappas, S. P.; and Shao, L. *RadTech 2000 Proceedings* **2000**, 196.

Chapter 5

Photoinitiated Polymerization of Selected Thiol-ene Systems

**Charles E. Hoyle¹, M. Cole¹, M. Bachemin¹, W. Kuang¹,
Viswanathan Kalyanaraman², and Sonny Jönsson²**

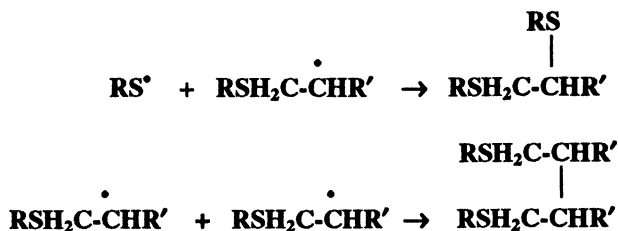
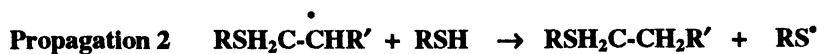
¹School of Polymers and High Performance Materials, Department of Polymer Science, University of Southern Mississippi, 2609 West 4th Street, Hattiesburg, MS 39406

²Fusion UV-Curing Systems, Inc., 910 Clopper Road, Gaithersburg, MD 20878–1357

Thiol-ene based photocurable systems exhibit very rapid rates of polymerization in nitrogen that are comparable to those achieved with traditional nitrogen saturated acrylates. In the presence of air, rates of thiol-ene copolymerization are much greater than are attained by traditional multifunctional acrylates. Even in the absence of an added photoinitiator, rapid copolymerization (thiol-acrylate) and homopolymerization (acrylate) rates of a multifunctional thiol and a difunctional acrylate are recorded in air.

Introduction

Details of the photolysis of a mixture of a difunctional thiol and a difunctional ene to produce a linear polymer were published in the late 1940s (1). In that early report, in which no photoinitiator was used, the polymerization probably proceeded via a free-radical polymerization process initiated by a primary sulfur-hydrogen bond cleavage to yield a thiyl and a hydrogen atom radical pair. In the mid 1970s, Morgan and Ketley (2,3) showed that equimolar mixtures of multifunctional thiols and multifunctional enes with benzophenone as a hydrogen abstracting type photoinitiator formed crosslinked networks characterized by high functional group conversion upon exposure to a high intensity lamp source. It was this benzophenone initiated photocuring that was the heart of the early thiol-ene commercial systems. The polymerization was proposed (2) to involve a two step sequence: the first proposed step is the addition of a thiyl radical into the ene to generate a carbon centered radical, and the second step involves a subsequent hydrogen abstraction by the carbon centered radical produced in the first step. A general kinetic depiction for free-radical curing of thiol-enes built around this two step propagation process is shown in Scheme I.



Scheme I. General thiol-ene photopolymerization process.

It is important to note from Scheme I that after the generation of an initial thiyl radical species the thiol-ene propagation basically involves a free-radical addition step (propagation 1) followed by a chain transfer step (propagation 2) that produces addition of a thiol (RSH) across a carbon-carbon double bond.

Simply put, the thiol acts like a chain transfer agent that limits the chain propagation to a single step. A high molecular weight crosslinked polymer network is only produced when monomers with functionality of three or greater are used. In the thiol-ene free-radical polymerization, the gel point (the point at which an infinite network is produced) is predicted to occur (2,4) according to the standard Eq. 1 for gelation by a step growth mechanism,

$$\alpha = [1/r(f_{\text{thiol}}-1)(f_{\text{ene}}-1)]^{1/2} \quad \text{Eq.1}$$

where α is the fractional conversion required to attain an infinite gel network, r is the stoichiometric thiol/ene molar functionality ratio, f_{thiol} is the functionality of the thiol, and f_{ene} is the functionality of the ene.

The gel formation for thiol-enes according to Eq. 1 is quite different from polymerization of multifunctional acrylate monomers where microgelation, which results in a heterogeneous polymerization medium and reaction diffusion controlled termination kinetics, occurs in the early stages of polymerization. Basically, the thiol-ene step growth polymerization proceeds to relatively high conversion in a medium that has quite a low viscosity before gelation. According to Jacobine (4), this allows the shrinkage which accompanies free-radical polymerization to take place in a homogeneous medium of low viscosity and low gel content. Hence, the shrinkage in a thiol-ene polymerization does not result in delamination of films to the same extent as occurs with traditional acrylate free-radical polymerization where shrinkage occurs during/after the crosslinked network has begun to form extensively. Literature reports (4) indicate little oxygen inhibition of the free-radical polymerization of thiol-enes since the peroxy radicals that are formed by reaction of oxygen with the carbon centered radicals readily abstract a hydrogen from a thiol to continue the free-radical chain process: oxygen inhibition occurs with acrylate based radical polymerization processes since there is only one propagation step (reaction of a carbon centered radical chain end with the double bond of a monomer) and no facile hydrogen abstraction process as occurs in the second propagation step in Scheme I.

A particularly interesting and important aspect of the polymerization process outlined in Scheme I is the wide variation in ene structures which can participate in thiol-ene polymerization. Both in a review article by Jacobine (4) and a crucial paper by Morgan and Ketley (2) relative rates are reported for the addition of thiols to a several enes including simple alkenes (such as 1-heptene, 2-pentene, and 1,6-hexadiene), allyl ethers, vinyl acetate, alkyl vinyl ethers, conjugated dienes, styrene, and even acrylates. Work in other labs, including ours, indicates that virtually any monomer with an ene functionality will participate in a radical polymerization process with thiols. This, of course, makes thiol-ene chemistry very versatile since coating resins that contain one or more of the ene monomer types can be readily formulated from a wide

variety of monomers which impart different physical properties into the final cured films.

In summary, there has been a large body of information published in the past dealing with thiol-ene photopolymerization: most of it during the late 1970s and early 1980s as chronicled in great detail in a review in 1993 (4). The polymerization process and the subsequent polymers produced offer many advantages including fast rates, low oxygen inhibition during curing, low film shrinkage, and flexible films with good adhesion. The versatility of thiol-ene photocuring warrants consideration in solving some of today's most pressing problems in the industry dealing with polymerization in air and cure of thin/thick films.

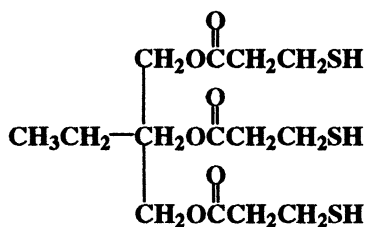
In this paper, we present recent results from our laboratory that clearly point out the salient features of thiol-ene photoinitiated polymerization. In addition to illustrating the kinetic rates for thiol-ene polymerization in air and nitrogen systems, we give quantitative results that show how oxygen inhibition in traditional acrylate systems can be reduced by incorporation of thiol concentrations that are less than stoichiometric. The results reported herein are inspired by the tremendous effort in this field by Ketley and Morgan in the 1970s. Hopefully quantitative examples presented herein of previously defined thiol-ene systems and polymerization characteristics will inspire new practitioners in the field to consider this *old technology* and its relevance to photocuring today and in the future.

Experimental

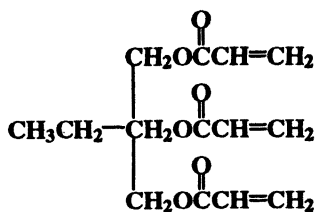
All monomers used were either obtained from Aldrich Chemical Co. or UCB. The photo-DSC and real-time infrared (RTIR) measurements were obtained using either a 450-Watt medium pressure mercury lamp or a high pressure 75-Watt xenon lamp, respectively. The photo-DSC exotherms were recorded on a modified Perkin-Elmer 7 while the real-time infrared results were recorded on a modified Bruker 88 IR spectrometer.

Results and Discussion

Results in this section will be presented in order to illustrate the features of thiol-ene photopolymerization that make it attractive as an alternative to traditional photocurable systems based strictly upon acrylates and mixtures of acrylates. As indicated in the Introduction Section, the free-radical chain reaction involved in the photopolymerization of thiol-ene mixtures has been reported in the literature to be a rapid process that is relatively uninhibited by the presence of oxygen. Herein, we will illustrate that the polymerization is indeed rapid by a direct comparison with acrylate polymerization in the

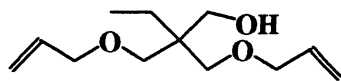
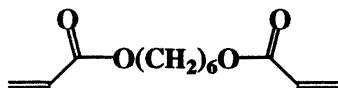
Trimethylolpropane tris(β -mercaptopropionate)

1,6-Hexanedithiol

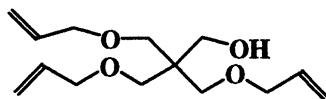


1,6-hexanedioldiacrylate (HDDA)

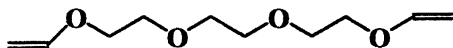
Trimethylolpropanetriacrylate (TMPTA)



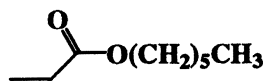
Trimethylolpropane diallyl ether



Pentaerythritol triallyl ether



Triethyleneglycol divinylether



Hexyl acrylate

presence and absence of oxygen. Examples will be drawn from a variety of thiol-ene combinations to illustrate the diversity of combinations which are encompassed by thiol-ene chemistry. Before proceeding it is important to point out that strict copolymerization involving addition of a thiol group across a carbon-carbon double bond does not always occur when the ene is capable of homopolymerization itself. In those cases, *i. e.*, where the ene is capable of independent free-radical polymerization, there can actually be two simultaneous polymerization processes involving both the thiol-ene step growth mechanism (as illustrated in Scheme I) and conventional chain growth polymerization kinetics. Such copolymerization processes are quite interesting as will be described herein. The structures of the monomers used in this investigation are given below to serve as a reference throughout the paper.

Thiol-Ene Polymerization Rate in Nitrogen Compared to Acrylate

Figure 1 shows photo-DSC exotherms for the photopolymerization of a typical thiol-ene combination consisting of 1,6-hexanedithiol and trimethylolpropane diallyl ether with 1 wt% of a typical photoinitiator, 1,1-dimethoxyphenylacetophenone (DMPA), added to initiate the free-radical step-growth polymerization process. Since a linear polymer that is not crosslinked is formed, the exotherm results are compared to the photopolymerization of hexylacrylate which also gives a linear acrylate polymer upon polymerization in the presence of the same photoinitiator. The results in Figure 1 clearly show that this particular thiol-ene polymerization in nitrogen is inherently faster than the acrylate polymerization and certainly illustrates that the basic thiol-ene polymerization (in a nitrogen atmosphere) competes quite favorably with acrylate polymerization. We note that we have chosen to use a particular alkyl dithiol and a difunctional allyl ether as representative of thiol-ene polymerization rates for comparison with the monofunctional acrylate. Different rates would be obtained if different enes or thiols were used. For instance, substantially faster rates would be obtained if the difunctional allyl ether were replaced with a difunctional vinyl ether with electron rich double bonds. Concomitantly, lower rates would be obtained with a difunctional unsaturated ester which is both electron deficient and sterically hindered.

Thiol-Ene Polymerization Rates In Air Compared to Acrylates

Photoexotherms in Figures 2 and 3 show that the photopolymerization of typical multifunctional acrylates 1,6-hexanedioldiacrylate (HDDA) and trimethylolpropane triacrylate (TMPTA) with 1 wt % DMPA photoinitiator is greatly inhibited in air compared to nitrogen.

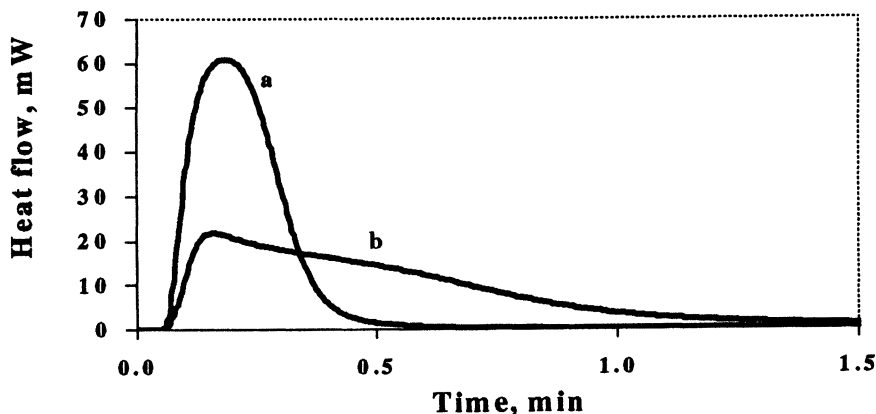


Figure 1. Photo-DSC exotherms for the photopolymerization of (a) a 1:1 molar mixture of 1,6-hexanedithiol and trimethylolpropane diallyl ether, and (b) hexylacrylate: both initiated with 1 wt% DMPA. Light intensity from medium pressure mercury lamp was 1.0 mW/cm².

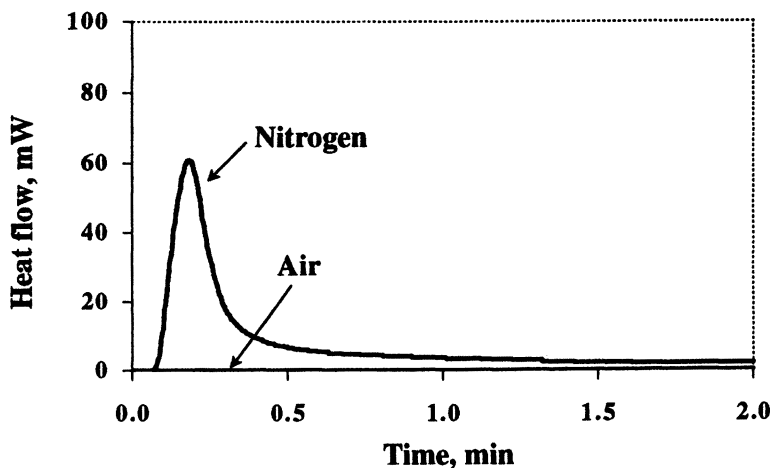


Figure 2. Photo-DSC exotherms of HDDA with 1 wt% DMPA initiated with a medium pressure mercury lamp with intensity of 1.0 mW/cm² in air/nitrogen.

In contrast to the acrylate results, Figure 4 shows that the photopolymerization exotherm of a 1:1 molar mixture of trimethylolpropane tris (β -mercaptopropionate) and pentaerythritol triallyl ether with the same concentration of photoinitiator and light intensity is only marginally diminished in the presence of oxygen. As indicated in previous literature dealing with thiol/acrylate photopolymerization (5), such a result is most likely a consequence of the hydrogen abstraction from a thiol group by peroxy

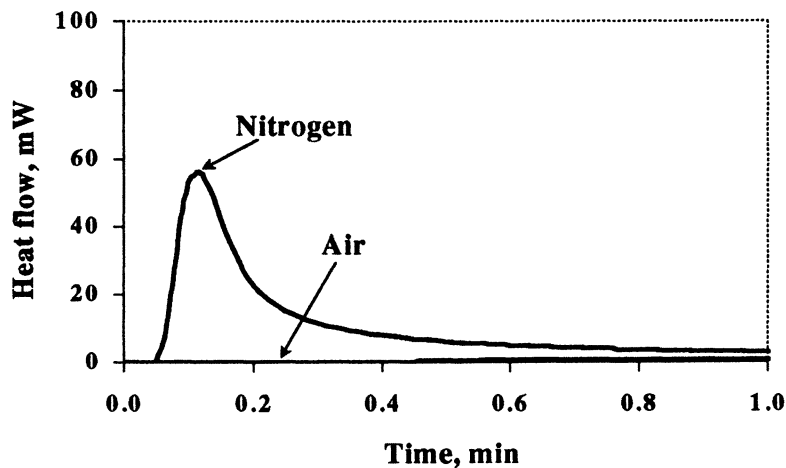


Figure 3. Photo-DSC exotherms of TMPTA with 1 wt% DMPA initiated with medium pressure mercury lamp with intensity of 1.0 mW/cm^2 in air/nitrogen.

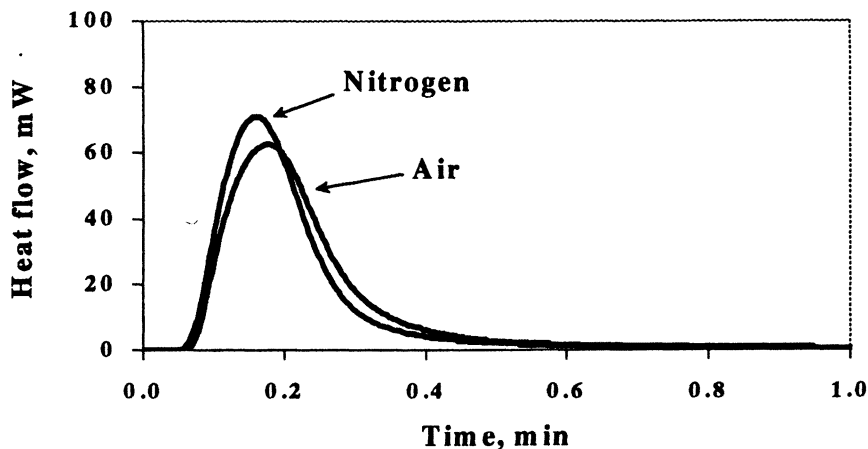
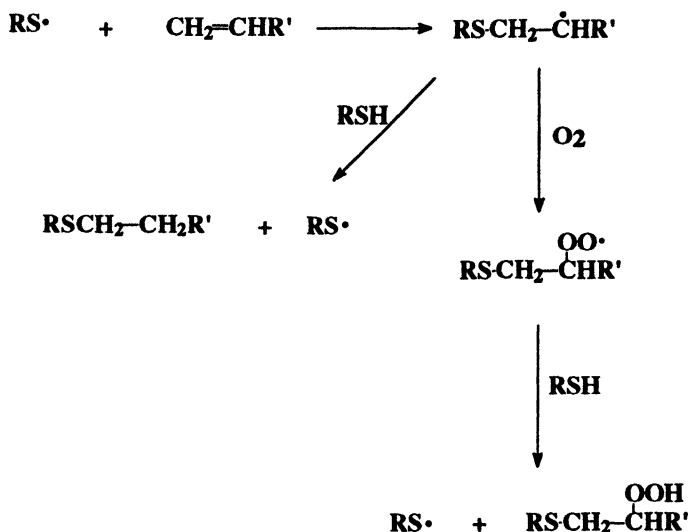


Figure 4. Photo-DSC exotherms of 1:1 molar mixtures of trimethylolpropane tris (β -mercaptopropionate) and pentaerythritol triallyl ether in air and nitrogen initiated by medium pressure mercury lamp with intensity of 1.0 mW/cm^2 .

radicals (see Scheme II) to generate a hydrogen peroxide and a thiyl radical which feeds back into the radical chain process described in Scheme I. In other words, the peroxy terminating radical does not lead to chain termination as found in traditional acrylate radical polymerizations.

Addition of Multifunctional Thiols to Multifunctional Acrylates: With and Without added Cleavage Type Photoinitiator

Varying amounts of trimethylolpropane tris(β -mercaptopropionate) were added to HDDA and the photopolymerizations conducted in air. In Figure 5, exotherms for HDDA polymerization in air with 0, 5, and 50 mole percent of the trithiol are shown for the case where 0.1 wt% DMPA is used as the photoinitiator. Surprisingly, addition of only 5 mol% of trimethylolpropane tris (β -mercaptopropionate) results in a large acceleration of the polymerization compared to the case for HDDA with only the photoinitiator present. Apparently, addition of only a small amount of the thiol greatly enhances the polymerization rate of HDDA in the presence of air in accordance with the oxygen scavenging Scheme II (5).



Scheme II. Basic oxygen scavenging mechanism for thiol-enes.

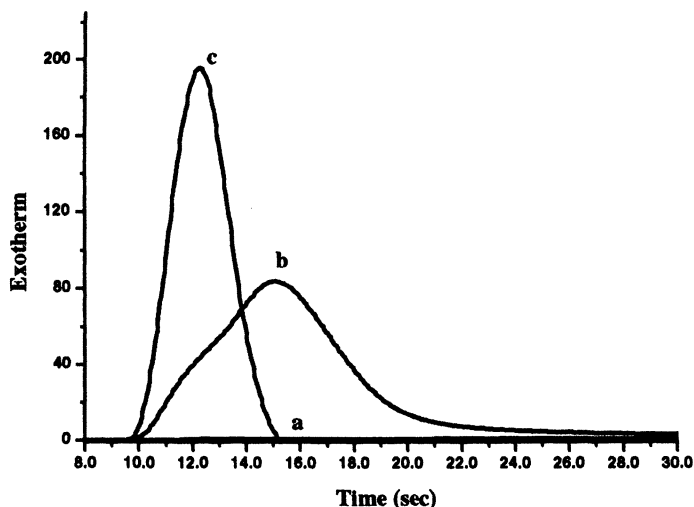


Figure 5. Photo-DSC exotherms of HDDA with 0.1 wt%DMPA with increasing concentration of trimethylolpropane tris(β -mercaptopropionate) in air initiated by a medium pressure mercury lamp with intensity of 60 mW/cm²: (a) HDDA; (b) 5:95 Trithiol:HDDA; (c) 50:50 Trithiol:HDDA.

As exemplified by the RTIR results in Figure 6, a 50:50 molar trimethylolpropane tris(β -mercaptopropionate) and pentaerythritol triallyl ether mixture readily copolymerizes without the need for an added photoinitiator. Photo-DSC exotherm results (not given herein) also show the same relative rapid polymerization for this system in air and nitrogen saturated samples in the absence of an added photoinitiator. The self-initiated process (see reference 4 and references listed therein) probably occurs via direct excitation of the thiol to cleave the sulfur hydrogen bond and generate hydrogen and thiyl radicals capable of initiating the free-radical chain process. Although the rate of HDDA polymerization is substantial in air saturated systems with added thiol (Figure 7), there is still a discernable difference between the rate of polymerization of mixtures of trimethylolpropane tris (β -mercaptopropionate) and HDDA in air versus nitrogen purged samples with no added photoinitiator present. For example, in Figure 8 for a 25:75 trimethylolpropane tris (β -mercaptopropionate) and HDDA mixture, the exotherm rate is substantially reduced in the presence of oxygen.

Although, as pointed out already, the acrylate polymerization exhibits much less oxygen inhibition in the presence of the thiol (see Scheme II) than acrylate polymerization in air with no thiol added. [Incidentally, an interesting aspect of the thiol mixtures with multifunctional enes without added photoinitiator is the enhanced photostability in simulated outdoor weathering tests].

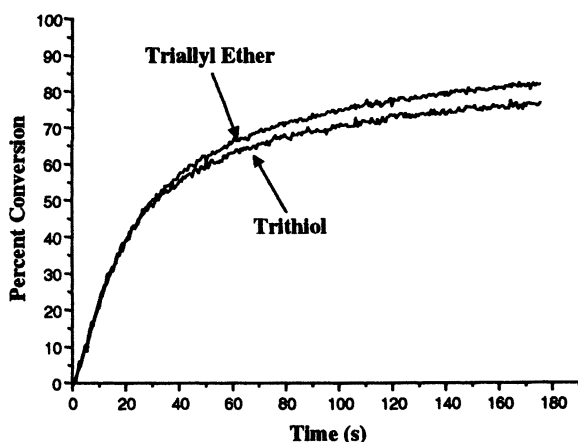


Figure 6. Percent allyl ether and thiol conversion from RT-IR analysis as function of exposure time in a 50:50 trimethylolpropane tris (β -mercaptopropionate)/pentaerythritol triallyl ether molar mixture sandwiched between salt plates with no added photoinitiator.

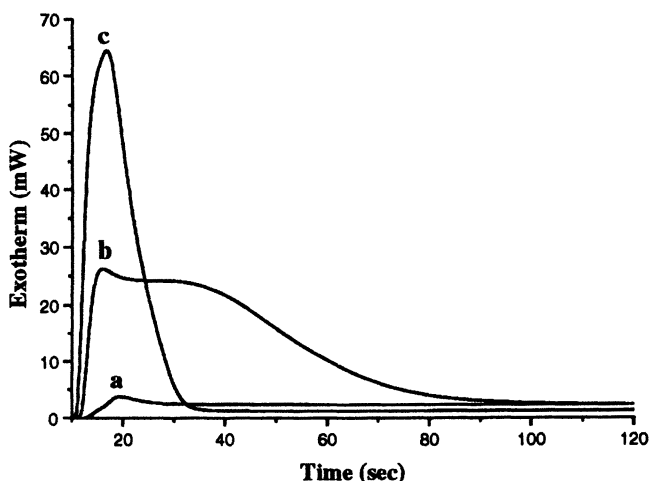


Figure 7. Photo-DSC exotherms of HDDA with added trithiol (concentration as indicated) initiated by output of medium pressure mercury lamp with intensity of 60 mW/cm^2 in air: (a) HDDA with 0.1wt% DMPA; (b) 30:70 Trithiol:HDDA with no initiator; (c) 50:50 Trithiol:HDDA with no initiator.

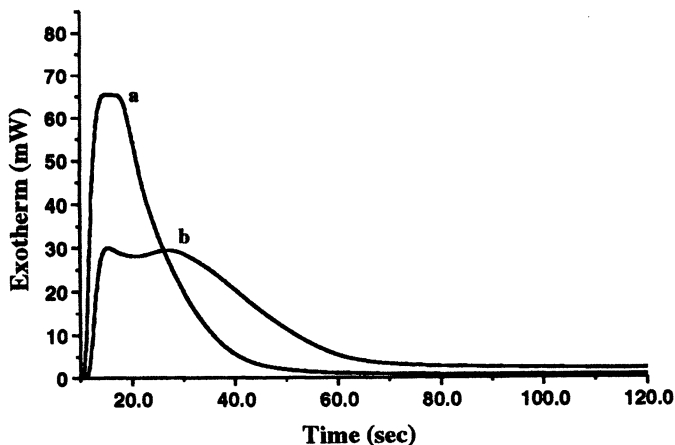


Figure 8. Photo-DSC exotherms of 25:75 trimethylolpropane tris (β -mercaptopropionate)/HDDA mixture initiated by output of medium pressure mercury lamp with intensity of 60 mW/cm^2 in (a) nitrogen and (b) air.

In contrast to the results in Figure 8 for the thiol/HDDA mixture, photopolymerization of a 25:75 molar mixture of trimethylolpropane tris (β -mercaptopropionate) and triethyleneglycol divinylether experiences relatively little reduction in the exotherm rate in air compared to nitrogen (Figure 9). As determined by RTIR (not shown herein), there is essentially no vinyl ether group homopolymerization and oxygen does not quench the thiol/vinyl ether copolymerization to an appreciable extent.

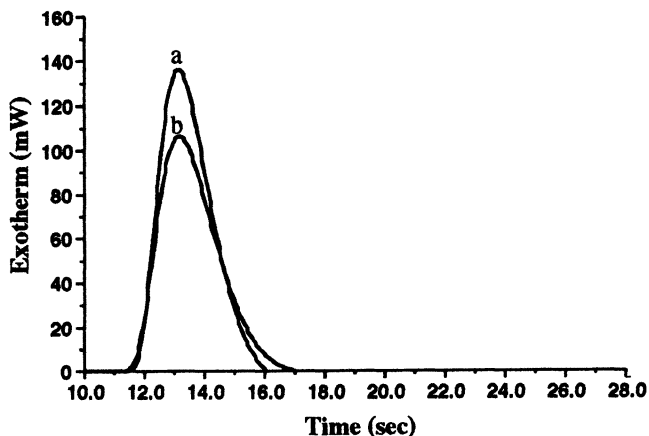


Figure 9. Photo-DSC exotherms of a 25:75 trimethylolpropane tris (β -mercaptopropionate) mixture with triethyleneglycol divinylether initiated by output of medium pressure mercury lamp with intensity of 60 mW/cm^2 in (a) nitrogen and (b) air.

Practical Examples of Thiol-Ene Photocuring

Before concluding, several practical examples from our lab that illustrate how thiol-ene photopolymerization can be used to extend the field of photocuring to new areas are briefly mentioned. First, thick optically clear samples of up to several centimeters thick were made by using various combinations of multifunctional acrylates, multifunctional triallyl ethers and a triallyltriazine with trimethylolpropane tris (β -mercaptopropionate). The trithiol/acrylate formed a very flexible elastic material with excellent energy storage while the trithiol/triallyltriazine formed a hard glass. Second, we found that a tetrafunctional thiol and a trifunctional vinyl ether sample (about 200 microns thick) with a small concentration of photoinitiator cured in air upon exposure to sunlight to give a highly crosslinked network in a few seconds. Third, we found that several thiol-ene mixtures with low concentrations of photoinitiator photocured in air to give highly crosslinked thin films (on the order of 1 micron) with relatively small total light intensities. Details of these practical systems will be forthcoming in future publications.

Conclusions

Thiol-ene photopolymerization with/without added photoinitiator proceeds rapidly in both nitrogen and air. The results herein provide quantitative comparisons for the rapid polymerization of both stoichiometric and non-stoichiometric acrylate/thiol mixtures and a vinyl ether/thiol mixture in air and nitrogen. The acrylate/thiol mixtures are more susceptible to oxygen inhibition probably due, at least in part, to selective oxygen inhibition of the acrylate homopolymerization.

References

1. Marvel, C. S.; Chambers, R. R. *J. Am. Chem. Soc.* **1948**, *70*, 993.
2. Morgan, C. R.; Magnotta, F.; Ketley, A. D. *J. Polym. Sci.: Polym. Chem. Ed.* **1977**, *15*, 627.
3. Morgan, C.R.; Ketley, A. D. *J. Polym. Sci.: Polym. Lett. Ed.* **1978**, *16*, 75.
4. Jacobine, A. T. In *Polymerization Mechanisms*; Fouassier, J. P.; Rabek, J. F., Eds.; Radiation Curing in Polymer Science and Technology; Elsevier Science Publishers Ltd.; New York, **1993**, pp. 219-268.
5. Gush, D. P.; Ketley, A. D. *Mod. Paint. Coat.* **1978**, *68*, 61.

Chapter 6

Allyl Ethers in the Thiol-ene Reaction

**Ingemar Carlsson, Adrian Harden, Stefan Lundmark, Ana Manea,
Nicola Rehnberg*, and Lennart Svensson**

Perstorp Specialty Chemicals AB, S-284 80 Perstorp, Sweden

Characteristics of polyol mercaptoalkanoates, polyol allyl ethers and coatings produced thereof are reported. The viscosities of examined thiols are in the range of 110-410 mPas (23 °C) and the density of functional groups 4–8 mmol/g. The corresponding data for the studied polyol allyl ethers are 3-240 mPas (23 °C) and 7.5–13.3 mmol/g, respectively. Formulations of these components were made and photocured as thin films (100 µm wet, glass plates) using benzophenone as initiator. The coatings were characterized with respect to methyl ethyl ketone resistance (generally > 200 single rubs), pendulum hardness (typical value 140 Ks), contact angle (44-70°), glass transition temperature (-39-2 °C), and thermogravimetric infra red analysis. The latter indicated the thiol-ene coatings to be of good thermal stability (typically 4% weight loss at 300 °C).

Introduction

In the presence of free-radical initiators, thiols (RSH) add to double bonds by a free-radical mechanism and the orientation is anti-Markovnikov. The reaction has been known since the beginning of the last century (1) and basic mechanistic studies were undertaken in the 1930's. The photo-induced polymerization has been reviewed excellently (2). Thiol-ene polymerizations proceed by a step growth addition mechanism that is propagated by a chain-transfer process which is in contrast to the chain mechanism of photopolymerization of e.g., acrylate or epoxy monomers, Figure 1.

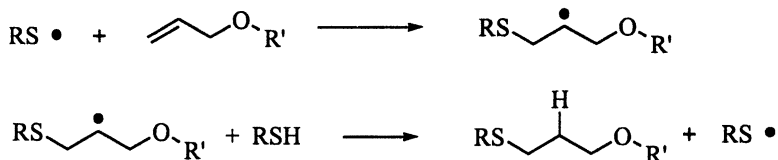


Figure 1. The propagation steps of the thiol-ene reaction.

In further contrast to acrylate polymerization, the thiol-ene reaction is based on a stoichiometric relation between the reacting components, the thiol and the ene. Another feature of the thiol-ene reaction is that both the thiol and the ene must have a functionality of ≥ 2 for polymer formation. At least one of them has to have a functionality of >2 for the production of cross-linked thermoset materials on polymerization.

A most important feature of the thiol-ene reaction is that it does not suffer from oxygen inhibition. High cure speeds and good adhesion to many different substrates are yet other attractive properties. Furthermore, it has been found that UV irradiation of thiol-ene systems in the absence of an added photoinitiator yield colorless films with excellent resistance to UV light exposure, within reasonable cure times (3). A historical disadvantage of the thiol-ene reaction, that has held back the exploitation of this valuable reaction, has been the smell of the mercapto component (4). Commercially available multifunctional thiols of high molecular weight from professional producers are, however, nowadays not associated with pungent odor. After cure, no smell, besides photoinitiator or their fragmentation products can be scented.

The reactivity of alkenes towards thiyl (RS \cdot) radicals has been shown to decrease in the order of bicyclo[2.2.1]heptenes > vinyl ethers > allyl ethers > n-alkenes > acrylates (4). Bicyclo[2.2.1]heptene derivatives have been reported to react up to 30 times as fast as allyl ethers (5). Our study shows, however, that the reactivity of allyl ethers might be adequate for many practical purposes. Allyl ethers of polyols e. g., trimethylolpropane diallyl ether (TMPDE) and pentaerythritol triallyl ether (APE), are in their own right interesting as low

viscous diluents and as starting materials for the synthesis of allyl oligomers by, for example, esterification.

In a study of the reactivity of 1-heptene towards some thiols, the following order was found; 3-mercaptopropanoate > mercaptoacetate > 1-pentanethiol (6).

The Components

The Ene

The allyl ethers in this study are derived from the polyols trimethylolpropane (TMP) and pentaerythritol (penta), Figure 2. APE is a commercial product whereas the other enes are experimental. Traditionally, APE is used as crosslinker in various acrylic systems like thickeners and emulsion paint. Other uses of polyol allyl ethers include raw materials for unsaturated polyesters for coatings and putty to prevent oxygen inhibition on cure, and as a linker between polysiloxanes and other polymers.

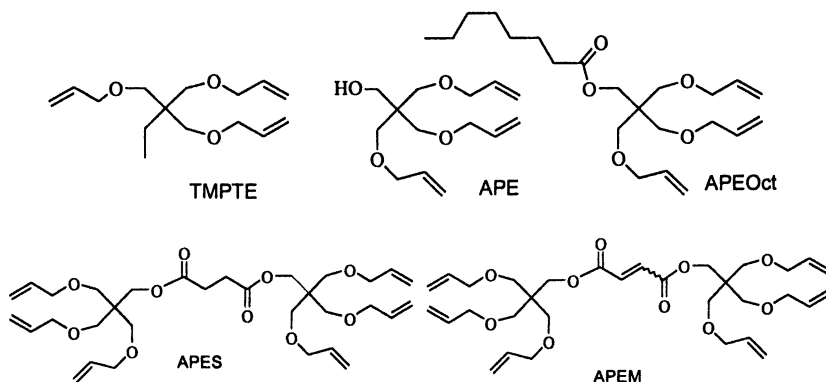


Figure 2. Structures of evaluated allyl derivatives.

APE is an easily handled liquid with a high flash point (146 °C) and low vapor pressure (<1 Pa). The oral LD₅₀ value is high (> 5g/kg rat) but eyes, respiratory system and skin should be protected (Xi, R36/37/38).

The materials have been selected to represent differences with respect to functionality, expressed as number of functional groups per molecule and as mmol reactive group per gram, and polarity, Table I. The functional density is fairly high, in comparison with components for UV acrylate coatings, e.g.,

Table I. Ene characteristics

<i>Components</i>	<i>viscosity/mPas (23 °C)</i>	<i>allyl density/ (mmol/g)</i>	<i>Mw/ (g/mol)</i>	<i>refractive index (20 °C)</i>
TMPTE	3	11.6	259	1.464
APE	20	13.3	226	1.465
APEOct	30	7.76	382	
APES	106	9.85	609	
APEM	240	9.46	634	

Allyl density and Mw are calculated from iodometric data.

oligomers 2-4 mmol acrylate/g, and monomers (e.g., 2-phenoxyethyl acrylate = 5 mmol acrylate/g, TPGDA = 7.5 mmol acrylate /g).

The Thiols

The thiols in this study are mercaptocarboxylic acid esters of TMP, penta, and their respective ethoxylate and propoxylate, Figure 3. The non alkoxyated esters are commercial materials and used as crosslinking or chain transfer agents for polymethacrylates to adjust molecular weight, as curing agent for epoxy resins, and in unsaturated systems with natural or butyl rubber.

All thiols are characterized by low odor and high flash point, e.g., 195 °C for trimethylolpropane tris(mercaptoacetate) (TMPMA3). The oral LD₅₀ for TMPMA3 is 1 g/kg (rat). It should be handled carefully as it is labeled "harmful if swallowed" (Xn, R22). Pentaerythritol tetrakis(3-mercapto propionate) (Penta3MP4) is classified as a potential skin sensitizer (Xi, R43).

The thiols, like the enes, in this study have been selected to represent different properties such as polarity and functional density, Table II.

Table II. Thiol characteristics

<i>Components</i>	<i>viscosity/mPas (23 °C)</i>	<i>SH density/ (mmol/g)</i>	<i>Mw/ (g/mol)</i>	<i>refractive index (20 °C)</i>
TMPMA3	110	8.3	360	1.528
TMP3MP3	140	7,5	402	1.516
TP703MP3	190	4.1	725	1.493
Penta3MP4	410	8.2	488	1.531
PS853MP4	340	3.9	1026	1.483

Mercapto density and Mw are calculated from iodometric data.

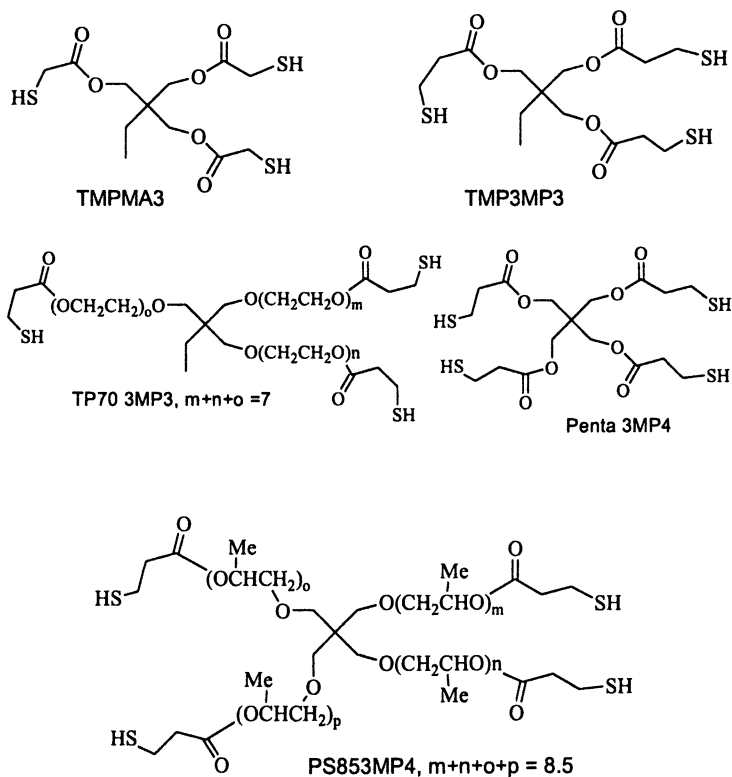


Figure 3. Structures of thiols evaluated.

Characterization of Cured Films

All films were characterized by methyl ethyl ketone resistance which was found to be good, >200 manual single rubs, unless otherwise stated.

Allyl Ethers in Formulations with TMP3MP3

Coated glass plates were prepared and cured, see experimental, based on formulations of equimolar quantities (ene/S_H = 1) of allyl ethers and trimethylolpropane tris(3-mercaptopropanoate) (TMP3MP3). The Koenig hardness and glass transition temperature (T_g) show an inverse relation, Figure 4. The hardest film is formed by the pentaerythritol triallyl ether octanoate (APEOct) derived formulation which also has the lowest T_g. In the other end of the property spectrum, we find bis(pentaerythritol triallyl ether) maleate (APEM) with high T_g and low hardness. Seemingly, T_g increases with increasing functionality, which is to be expected. The rationale for the reverse order of Koenig hardness is less obvious. Despite the high functional density of the monomers, the T_g values are rather low, around zero and below.

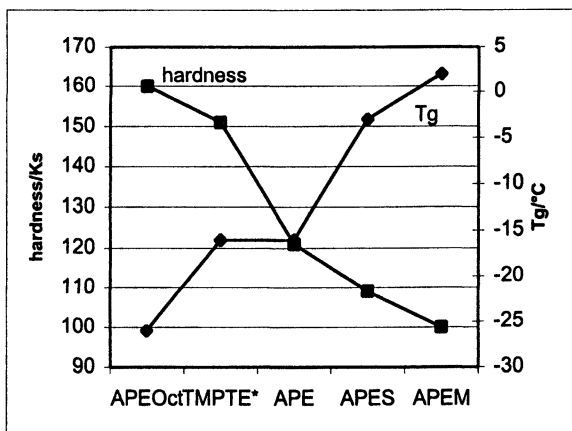


Figure 4. Koenig hardness and glass transition temperature (T_g) of thiol-ene coatings. Hardness and T_g measured 1d after cure. *TMPTE is examined as a mixture (4.6/1) with APE as TMPTE is not compatible with TMP3MP3.

The polarity of the above films were measured as the advancing contact angle of a water drop, Table III. The trend is intuitively correct with high values for the lipophilic octanoate APEOct and low value for the triallyl alcohol APE.

The MEK resistance of the APEOct derived film was only 179 single rubs.

Table III. Contact angle

<i>Components</i>	<i>contact angle/°</i>
APEOct	70
TMPTE*	62
APES	59
APEM	57
APE	49

*TMPTE is examined as a mixture (4.6/1) with APE as TMPTE is not compatible with TMP3MP3. Measurements were made 1 day after cure.

Thiols in Formulations with APE

In the next set of tests, different thiols were evaluated against APE, Table IV. Interestingly, the films formed from TMPMA3 and trimethylolpropane tris(3-mercaptopropanoate) (TMP3MP3) do not differ very much in properties. According to the literature (6), mercaptoacetates are less reactive than 3-mercaptopropanoates but obviously this is not reflected in differences of the examined properties. In contrast to these two thiols, Penta3MP4 gives films with higher glass transition temperature, most likely, a consequence of the higher crosslink density.

The films of the two alkoxyate derived 3-mercaptopropanoates are characterized by the lowest T_g of the studied compounds. This can be understood by considering the high flexibility conferred by the ethylene oxide and propylene oxide chains. In addition, formulations of these two high molecular weight derivatives will be of low crosslink density due to high equivalent weight.

Table IV. Coating characteristics of formulations based on thiols and APE

<i>Components</i>	<i>Contact angle/°</i>	<i>Hardness/Ks</i>	<i>Tg/°C</i>	<i>fraction</i>
	<i>1 day</i>	<i>2 h</i>	<i>1 day</i>	<i>thiol/weight %</i>
TMPMA3	47	113	-13	62
TMP3MP3	49	133	-16	64
TP703MP3	44	99	-39	76
Penta3MP4	46	119	0	62
PS853MP4	56	135	-26	77

Times relate to time between cure and measurement.

Non-stoichiometric Formulations

Thiol-ene compositions are generally formulated to stoichiometric equivalence of thiol and ene, although the ene to a low degree might homopolymerize and the thiols may oxidize to disulfides during cure, thus contributing to the polymer formation. To be a practically useful reaction, coating properties of cured films should not deteriorate seriously if perfect stoichiometry is not reached on formulation. In Table V, the contact angle, Koenig hardness, and glass transition temperature of polymer films prepared from formulations of varying molar ratios of TMP3MP3 and APE are shown. Clearly, within the interval SH/ene = 0.87 – 1.15, no significant property changes are seen.

Table V, Coating characteristics of non-stoichiometric formulations

SH/ene	contact angle/°	hardness/Ks	Tg/°C
	1 day	2 h	1 day
0.87	53	123	-15
1	49	133	-16
1.15	53	121	-22

Times relate to time between cure and measurement.

Thermal stability of Thiol-ene Coatings

In the thiol-ene reaction of 3-mercaptopropanoates, a 3-(alkylthio)propanoate is formed. *A priori*, this structural element is thermally unstable and may revert to components on heating by a reverse Michael addition. Moreover, imbalanced formulations or films with residual reactive groups could be anticipated to be of low thermal stability. Hypothetically, the mercaptofunction could be oxidized to sulfur acids that might catalyze pyrolysis and unreacted allyl ethers, that readily form peroxides, could initiate a radical break down. By thermogravimetric analysis of films from stoichiometrically and non-stoichiometrically formulated films none of the above fears were corroborated. All examined films showed good thermal stability with only a slight weight loss, 4%, at temperatures up to 300 °C, Figure 5.

Even aging of films up to one month, thus giving time for autooxidation, did not result in decreased thermal stability.

With few exemptions, neither Tg nor contact angle changed during one month of aging but frequently Koenig hardness decreased.

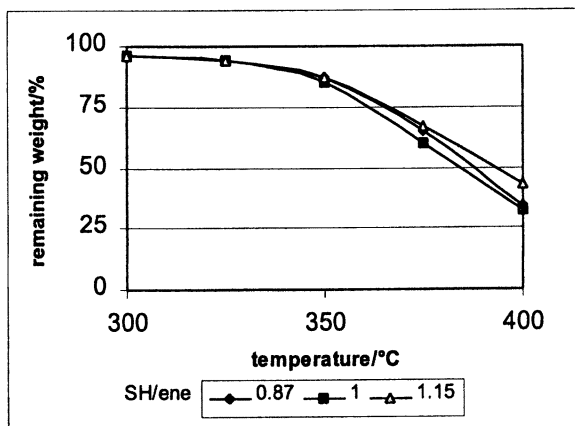


Figure 5. Thermogravimetric analysis of films with various stoichiometric ratios of TMP3MP3 and APE. Measured one day after cure.

On TGA analysis in air or nitrogen, the components carbon dioxide, carbonyl sulfide, and carbon disulfide were detected by FTIR at the maximum decomposition temperature, approx. 400-450 °C. In the gas stream leaving the air purged sample, sulfur dioxide was also detected.

Conclusions

We have presented a study on photoinitiated polymerizations of thiol-ene compositions. The thiols in our study are esters of mercaptocarboxylic acids and polyols and the enes are allyl ethers of polyols. The photo thiol-allyl reaction is rapid and initiated by benzophenone, a type II initiator. No synergist is needed.

Allyl ethers are of low toxicity and beneficial components in thiol-ene formulations as they offer low viscosity and produce films of good solvent resistance and high thermal stability.

By varying the polarity of the formulating components, surfaces with different contact angles are produced. Hydroxyl groups and ethylene oxide chains tend to reduce the contact angle.

Furthermore, ethylene and propylene oxide chains reduce Tg.

Experimental

Instrumentation

TGA-FTIR – Polymer Labs TGA 1000 equipped with BioRad heated cell and connected to BioRad FTS-40 IR., FTIR – Nicolet Protégé 460 FTIR,

DMTA – Netzsch DMA 242, belt cure machine – Wallace Knight UV 80W/cm 20 m/min, Brookfield DV-II or Plate cone CAP 1000 viscometer. Contact angle determination - First Ten Ångström FTÅ 200 instrument.

Materials

Commercially available materials, APE (pentaerythritol triallyl ether, Perstorp Specialty Chemicals), Penta3MP4 (pentaerythritol tetrakis(3-mercaptopropanoate), Bruno Bock Chemische Fabrik, Germany, gratefully acknowledged for having provided their materials free of charge), TMP3MP3 (trimethylolpropane tris(3-mercaptopropanoate), Bruno Bock), TMPMA3 (trimethylolpropane tris(mercaptopropanoate), Bruno Bock), and benzophenone (Aldrich) were used as received. Experimental products, TMPTE (trimethylolpropane triallyl ether, Perstorp Specialty Chemicals), TP703MP3 (trimethylolpropane ethoxylate tris(3-mercaptopropanoate), Perstorp Specialty Chemicals), PS853MP4 (pentaerythritol propoxylate tetrakis(3-mercaptopropanoate), Perstorp Specialty Chemicals). The functionality (mmol reactive group/g) of the allyl and mercapto derivatives were established by iodometric techniques. All formulation ratios are expressed as “% w/w”.

Typical Ester Synthesis

Synthesis of Bis(APE) Maleate, (APEM)

APE (660 g, 2.80 mol), maleic anhydride (124 g, 1.26 mol), pTsOH (1.57 g), hydroquinone (0.78 g) and toluene (39 g) were mixed together under nitrogen and heated (160-170 °C) with stirring in an apparatus equipped with a Dean-Stark trap until no more water was formed. After neutralisation with calcium hydroxide, the toluene was removed and the residue filtered and used as such.

APE succinate (APES) and APE octanoate were analogously synthesized from APE and succinic anhydride and octanoic acid, respectively.

Formulation, Curing, and Contact Angle

Unless otherwise stated, all formulations were made stoichiometric with respect to thiols and enes. Blending of components were made under nitrogen to

reduce risk of spontaneous polymerization. Benzophenone was used as initiator (2 w/w %). Neither stabiliser nor synergists were used. Coating films were prepared on glass using a 100 μm applicator. Films were examined after 4 passages under the lamp (nominally 880 mJ/cm^2).

Contact angle measurements of water droplets were determined when the drop was at rest on the surface. An average of 16 determinations taken 3-18 s after application was used. No particular spreading was observed in this interval. Four determinations were performed on every sample.

References

1. Posner T., *Ber.*, **1905**, *38*, 646.
2. Jacobine A. F., Radiation Curing in Polymer Science and Technology, ed. Fouassier J. P., Rabek J. F., Elsevier Applied Science, **1993**, *3*, 219.
3. Cole M. C., Bachemin M., Nguyen C. K., Viswanathan K., Hoyle C. E., Jönsson S., and Hall H. K Jr., RadTech 2000, Proceedings, April 9-12, 21.
4. Davidson S., Exploring the Science, Technology and Applications of U.V. and E.B Curing, Sita Technology limited, London, 1999, 43.
5. Jacobine A. F., Glaser D. M., and Nakos S. T., Radiation Curing of Polymeric Materials, ACS Symposium Series 417, ACS, Washington, D.C., 1990.
6. Morgan C. R., Magnotta F., and Ketley A. D., *J. Polym. Sci. Polym. Chem. Edn.*, **1977**, *15*, 627.

Chapter 7

Mechanistic Aspects of Maleimide–Donor Photocopolymerizations

S. Jönsson¹, D. Yang², K. Viswanathan², E. Shier², K. Lindgren¹,
K. D. Belfield³, and C. E. Hoyle²

¹Fusion UV-Curing Systems, Inc., 910 Clopper Road,
Gaithersburg, MD 20878–1357

²School of Polymers and High Performance Materials, Department of
Polymer Science, University of Southern Mississippi, 2609 West 4th Street,
Hattiesburg, MS 39406–0076

³Department of Chemistry, University of Central Florida, 4000 Central
Florida Boulevard, Orlando, FL 32819

The relative rates in the alternating copolymerization of a difunctional maleimide and conventional alkenyl ether have been investigated and compared to the exomethylene aryl(alkyl)dioxolane, 4-methylene-2-phenyl-1,3-dioxolane, using real-time infrared (RTIR) spectroscopy. The mechanistic differences in propagation between the two donors have been examined and evaluated by laser flash photolysis. It is shown that structural modifications which increase the electron density in the vinylic C=C bond produce higher rates of copolymerization. Copolymerization studies indicate that the relative extent of ring opening decreases with increasing temperature.

Introduction

Photo-induced, free-radical polymerizations of donor/acceptor (D/A) type monomer combinations such as maleimides with vinyl ethers represent a potential alternative to widely used acrylate resins (1). It has been shown that, in maleimide/vinyl ether mixtures, the copolymerization proceeds rapidly upon UV exposure to attain high conversion in the presence or absence of oxygen via a free radical process (1-3). A unique advantage of such photo-induced polymerizations is that they do not require the addition of a photoinitiator, since the maleimide acts as both an efficient photoinitiator and a comonomer (1-5). The problems of residual photoinitiator can thus be avoided. Unfortunately, during typical vinyl polymerizations, shrinkages in volume as high as 20% can occur (6-10). Due to stringent requirements in many coating technologies, efforts have been made to find systems that undergo little or no volume changes upon polymerization (11-13). The ring opening polymerization of several cyclic monomers has been reported to occur with little shrinkage in volume, or volume expansion in a limited number of instances (14-16). Cationic ring-opening polymerizations of spiro-orthocarbonate, spiro-orthoester and dioxolane type monomers have been fully studied since the 1980's (17). Among them, exomethylenic dioxolanes (DOX), such as 4-methylene-2-aryl(alkyl)-1,3-dioxolanes (M_{Ar}(R)DOX), have recently received a lot of attention. Both thermal- and photo-initiated free-radical polymerizations of DOXs have been reported (11). Polymers produced through photo-induced processes were shown to consist of higher percentages of ring opening units compared to thermally induced processes, possibly due to a temperature effect.

In a significant report, Davidson used real-time infrared (RTIR) spectroscopy to monitor the photoinitiated polymerization of DOX monomers via either a cationic or a free-radical mechanism, and the free-radical polymerization of DOX was shown to be quite a slow process (13). Recently, Belfield and coworkers studied photoinitiated cationic homo- and copolymerizations of DOX with several acyclic and cyclic monomers, such as vinyl ethers and spiro-furans, by using either sulfonium or iodonium salts as photoinitiators (8). ¹H-NMR and FT-IR spectral analysis confirmed the ring-opening reactions of DOX monomers. Cationic polymerizations of vinyl dioxolane monomers, even though they usually exhibit relatively rapid rates of polymerization, display higher sensitivity to moisture and temperature as compared to vinyl ethers and epoxy based materials. Unfortunately, free-radical polymerization of this type of monomer has been found to be very inefficient. Herein, we report on a relatively rapid copolymerization of electron donor/acceptor systems involving a difunctional maleimide acceptor monomer and either an aromatic DOX donor monomer or a vinyl ether donor monomer. The effect of temperature on the ring opening of the DOX monomer was

measured, and the polymerization rate dependence on the electron donating ability of the donor monomer was evaluated.

Experimental

Materials

Q-Bond was obtained from Loctite, and was used as received. Solvents for the laser transient studies were obtained from Burdick and Jackson and used as received. All donor monomers used were purchased from Aldrich. The dioxolanes were synthesized according to literature methods (8). All other chemicals were procured and used as described previously (1-5).

Laser Flash Photolysis

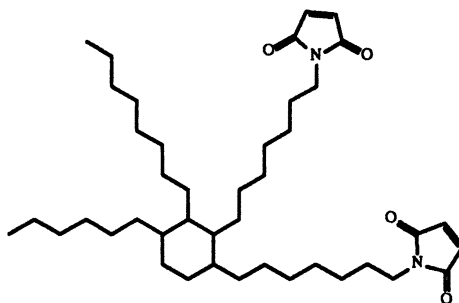
A nanosecond Continuum Surelite Nd-YAG laser was used for the pulsed excitation. A pulsed xenon lamp unit from Applied Photophysics served as the probe beam. A Philips digital oscilloscope was used to collect the transient decay from the output of a photomultiplier tube after the probe beam passed through a high throughput monochromator. Kinetic decay processes were fit to standard exponential decay curves for a first order decay process.

RTIR: Real-Time Infrared Spectroscopy

A stoichiometric 1:1 molar mixture of donor/acceptor monomers was sandwiched between two NaCl salt plates to suppress oxygen diffusion. The sample was placed horizontally in a Bruker IFS-88 FTIR spectroscopy optical bench. A high-pressure mercury xenon lamp from Science Tech was used as the light source. The light intensity was measured by a radiometer (Int. Light IL - 390). The rate of polymerization was followed *in situ* by recording the disappearance of the characteristic IR absorption bands for each monomer type under continuous UV irradiation. The 1649-1603 cm^{-1} band for vinyl ethers, the 843-808 cm^{-1} band for maleimides and the 803 cm^{-1} (C=C) and 973 cm^{-1} (ether ring) bands in the dioxolane were used for recording the rate of disappearance.

Results and Discussion

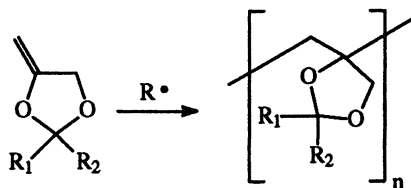
Herein we present RTIR results for the photopolymerization of 1:1 molar mixtures of the difunctional maleimide monomer Q-Bond and both a monofunctional vinyl ether monomer and a monofunctional phenyldioxolane. The polymerization rates are compared, and the copolymerization mechanisms for each system are discussed based upon laser flash photolysis analysis, proton NMR measurements and electron density calculations.



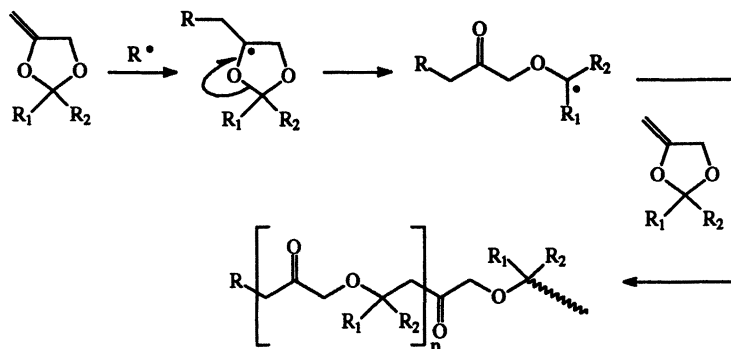
Q-Bond

RTIR Polymerization Results

The percent conversion versus exposure time plots are shown in Figure 1 for the photopolymerization of mixtures of Q-Bond and dodecyl vinyl ether (DDVE) or Q-Bond and 4-methylene-2-phenyl-1,3-dioxolane (MPDOX). First we present results for the Q-Bond/DDVE polymerization. We have already shown that the photoinitiated polymerization process in maleimide/vinyl ether mixtures proceeds by the combination of a free-radical homopolymerization (maleimide-maleimide) and a dominating free-radical copolymerization (maleimide-vinyl ether) process. As shown in Schemes I and II, dioxolanes have the potential of participating in free-radical polymerization or copolymerization processes by either a direct addition across the vinyl double bond (Scheme I) or via ring opening (Scheme II).



Scheme I. 1,2-addition reaction of MPDOX.



Scheme II. Ring-opening reaction of MPDOX.

In order to determine which of the two schemes is operative in the current case, we first consider the RTIR results in Figure 1 and note that the MPDOX conversions for the 803 cm^{-1} ($\text{C}=\text{C}$) and the 973 cm^{-1} (ether ring) groups are very nearly the same over the total exposure time (only at much higher conversions obtained at very long exposure times is there a slight measurable difference in conversions of the ene and ether ring). These results show that the ring-opening mechanism in Scheme II, which according to literature reports (11) can readily occur, is operative under the conditions of the experiment (room temperature). Having established that the ring-opening polymerization occurs for MPDOX, we next turn to consideration of the rates and conversions attained for maleimide functional groups. The higher rates for maleimide conversion and higher overall conversions compared to the vinyl ether or dioxolane double bond conversions in Figure 1 are a result of maleimide participation in both homopolymerization (with itself) and copolymerization with the vinyl ether or dioxolane double bonds. Finally, and perhaps most important for the present

investigation, we note in Figure 1 the higher rates and ultimate conversions for the maleimide and dioxolane functional groups in the case of the photopolymerization of the Q-Bond/MPDOX mixture versus the Q-Bond/DDVE mixture. Apparently, the MPDOX not only ring opens upon copolymerization (according to Scheme II), but it also has the highest copolymerization rate with the N-alkylmaleimide groups of Q-Bond.

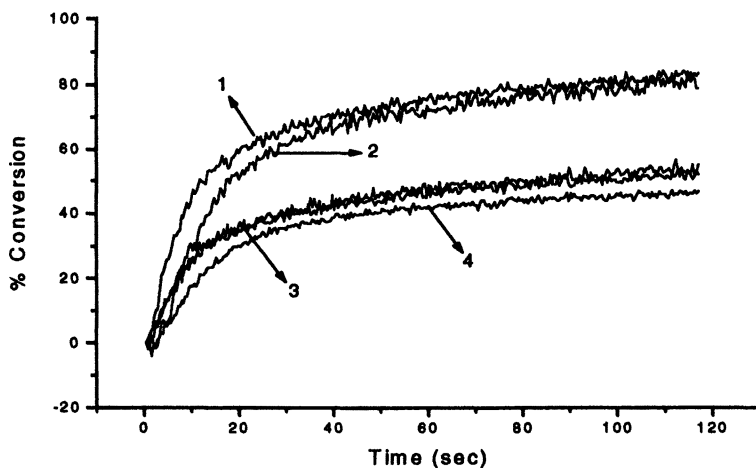
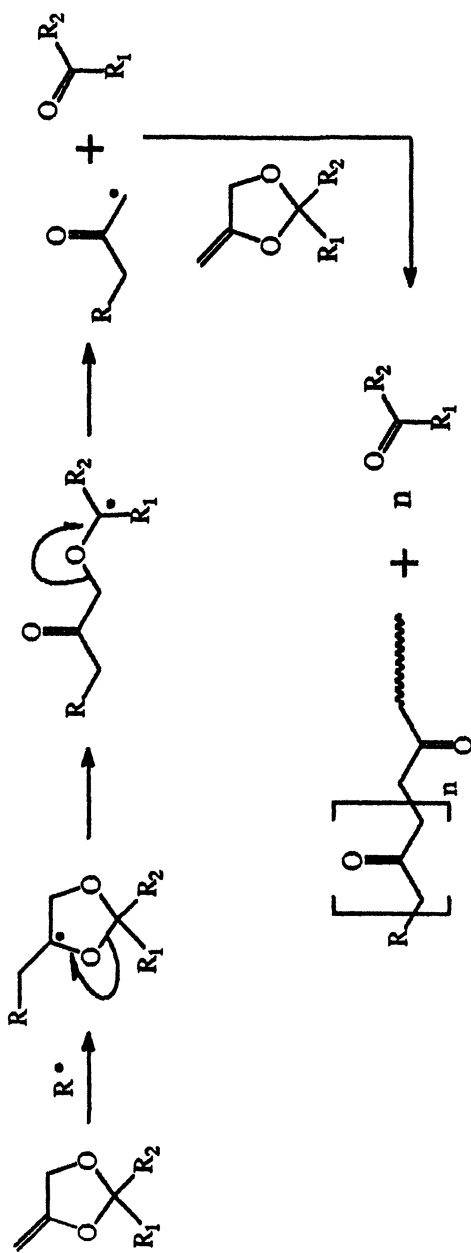


Figure 1. RT-FTIR recordings of copolymerization of 1:1 molar mixtures of Q-Bond/MPDOX and Q-Bond/DDVE using a high-pressure Hg lamp. Light intensity $\approx 190 \text{ mW/cm}^2$. Mixtures were sandwiched between two NaCl plates. (1) Conv. of MI in Q-Bond/MPDOX mixture, (2) Conv. of MI in Q-Bond/DDVE mixture, (3) Conv. of MPDOX (803 cm^{-1} and 973 cm^{-1}) in Q-Bond/MPDOX mixture, (4) Conv. of DDVE in Q-Bond/DDVE mixture.

We make one final note about the photopolymerization results in Figure 1. According to a careful analysis of the IR spectrum of the Q-Bond/MPDOX mixture polymerization, we did not observe the ring-opening elimination reaction that has been reported for the 2,2-disubstituted dioxolane polymerization process depicted in Scheme III.

One particularly interesting and intriguing aspect of the ring-opening photoinitiated copolymerizations of dioxolanes is the expected promotion of substrate adhesion of coatings due to the reduced film shrinkage resulting from the ring opening mechanism defined in Scheme II. In view of this technical advantage expected for the ring opening process, it is important to determine the effect of the polymerization temperature on the ring opening of the MPDOX monomer, since there are choices of processing temperatures for photocurable materials. Figure 2 shows results obtained for the ratio of the ring opening to vinyl polymerization of MPDOX during the photopolymerization of a 50:50 mixture of Q-Bond and MPDOX exposed to a medium-pressure mercury lamp



Scheme III. Ring-opening/elimination reaction of MPDOX.

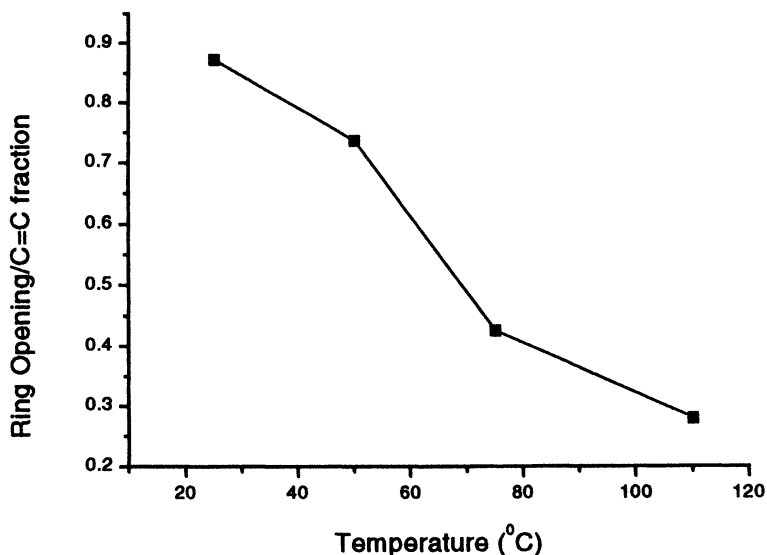


Figure 2. Relative ratio of ring-opening and 1,2-addition reaction in the copolymerization of Q-Bond/MPDOX as a function of temperature. High-pressure Hg light source. Light intensity $\approx 200 \text{ mW/cm}^2$. NaCl sandwich.

for long exposure times in order to attain high conversion in each case at a series of temperatures. As observed from the plot of Figure 2, almost complete ring opening takes place at room temperature, while at 110 °C it is reduced to less than 30% relative to the vinyl C=C conversion. The decrease in the relative amount of ring opening of MPDOX as a function of temperature is due to the increased stability of the α -ether substituted benzylic radical at lower temperatures compared to the initially formed vinylic radical (see Schemes I and II). The ring opening is enhanced at lower temperatures since at higher temperatures the rate of radical addition to the vinylic C=C competes with the rate of the radical rearrangement reaction that promotes ring opening.

In the next two sections we try to answer two questions associated with the rate results in this section. First, how does the MPDOX monomer participate in the photoinitiation process, and second, how can the faster polymerization rate when using MPDOX versus DDVE be explained. Laser flash photolysis and NMR/electron density calculations are used to answer these two questions.

Laser Flash Photolysis

Quenching rate constants (k_q) derived from laser flash analysis in dilute solution of the triplet state N-methylmaleimide (MMI) by a variety of quenching species are given in Table I. These results illustrate that quenching by DDVE

and MPDOX is as efficient as for the tertiary amine N-methyl-N,N-diethanolamine (MDEA). The quenching of MMI triplet by MDEA has previously been shown to proceed by an electron/proton transfer process (7,9), while quenching of MMI by a direct hydrogen abstraction process using isopropyl alcohol (IPA) or tetrahydrofuran (THF) proceeds much slower (by ≈ 2 orders of magnitude). Because of the large quenching rate constants, we conclude that both DDVE and MPDOX quench the MMI triplet state by an electron/proton transfer process.

Table I. Laser Flash quenching rate constants for MMI Triplet State

Quencher	k_q ($M^{-1}s^{-1}$)	Process
IPA	$7 \cdot 10^6$	Direct H - Abstraction
THF	$7 \cdot 10^6$	Direct H - Abstraction
MDEA	$5 \cdot 10^9$	e- / H+ Transfer
DDVE	$6 \cdot 10^9$	e- / H+ Transfer
MPDOX	$4 \cdot 10^9$	e- / H+ Transfer

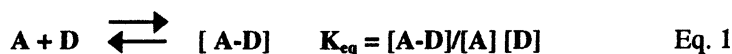
Since electron transfer processes are in general even more favorable for singlet state quenching than triplet state quenching, the results in Table I further suggest that both DDVE and MPDOX will quench the maleimide singlet state at rate constants greater than $\sim 5 \times 10^9 M^{-1}s^{-1}$. As the lifetime of singlet state N-alkyl maleimides (MI_s^*) is about 2 ns, it is reasonable to assume that in neat 50:50 molar maleimide/DDVE or maleimide/MPDOX mixtures the maleimide singlet will be completely quenched by an electron/proton transfer process from DDVE or MPDOX as depicted in the sequence of steps in Scheme IV for MPDOX. The low rate constants for direct hydrogen abstraction from either MPDOX (two alternative mechanisms depicted in Scheme IV) or DDVE (scheme not shown for DDVE quenching) would probably be no greater than $\sim 10^7 M^{-1}s^{-1}$ (based upon the results for IPA and THF), and hence would not account for the high quenching rate constants ($4\text{--}6 \times 10^9 M^{-1}s^{-1}$) actually measured (Table I).

¹H-NMR and C=C Electron Density Modelling (HMO)

In this section, using NMR measurements and electron density calculations, we will characterize the electron donor properties of the dioxolane versus the vinyl ether group and thereby provide a plausible explanation for the variation in the polymerization rate of the Q-Bond/MPDOX and Q-Bond/DDVE mixture observed in Figure 1. We first note that the exomethylene C=C bond in

the MPDOX monomer resembles an “allyl ether”, an “ α -alkyl-substituted vinyl ether” and a “vinyl ether” moiety. As a result, MPDOX is expected to be a better electron donor than the simple DDVE. Hence, MPDOX should be capable of forming a charge-transfer (CT) complex with the highly electron deficient MI acceptor type monomer.

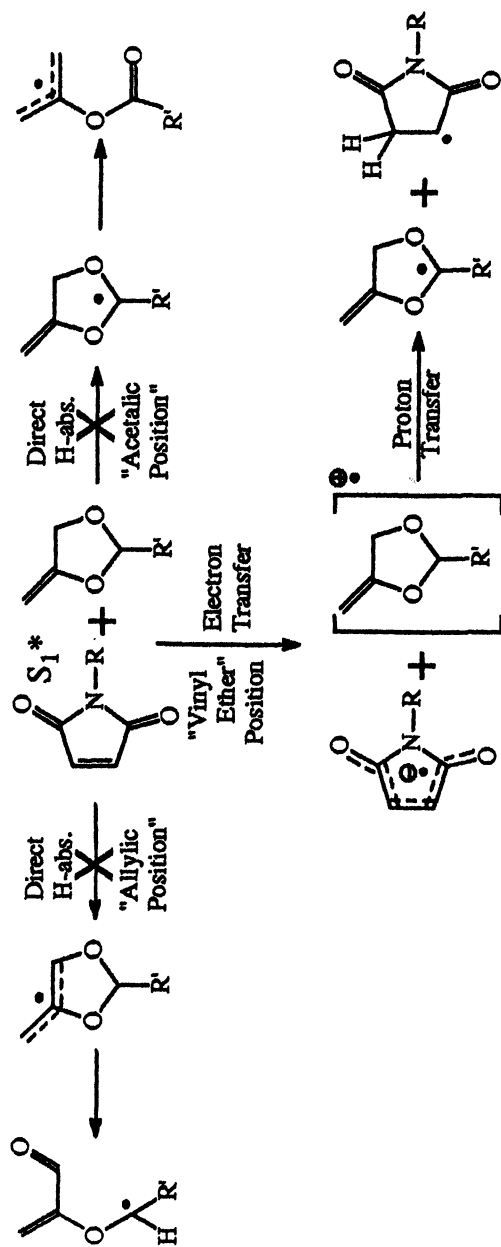
The equilibrium constant K_{eq} of a CT complex [A-D] formed between a donor, D, and an acceptor, A, as shown in Eq.1, is dictated by the strength of the interaction between the electron donor (D) and the electron acceptor (A).



$^1\text{H-NMR}$ spectroscopy can be utilized to characterize CT complexes between acceptors and donors using the Hanna-Ashbough equation (Eq. 2) to calculate K_{eq} from $^1\text{H-NMR}$ shifts,

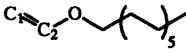
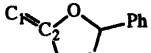
$$1/\Delta C_s = 1/(K_{eq} \Delta C_{s, \infty} [D]) + 1/\Delta C_{s, \infty} \quad \text{Eq.2}$$

where ΔC_s is the difference between the chemical shifts of the uncomplexed and the complexed forms, and $\Delta C_{s, \infty}$ is the difference between the chemical shifts of the acceptor protons in a pure complex and in a noncomplexing medium. By plotting $1/\Delta C_s$ versus $1/[D]$, K_{eq} can be calculated from the slope. Figure 3 shows a typical $1/\Delta C_s$ plot versus $1/[D]$, for a maleimide/MPDOX combination where *N-tert*-butylmaleimide (t-BMI) was used as the maleimide: essentially, any aliphatic maleimide would give equivalent results. A similar plot was made for a t-BMI/DDVE system and the results for the equilibrium constants calculated from the slopes are given in Table II. As seen, the maleimide/MPDOX complex has a much higher equilibrium constant than the maleimide/DDVE system reflecting the enhanced electron donor properties of MPDOX compared to DDVE. The enhanced electron donor properties of MPDOX are also reflected in simple HMO (Hückel Molecular Orbital) calculations of the electron density differences for the C=C bond in DDVE and MPDOX. The resulting electron density calculations given in Table II corroborate the NMR measurements. The higher overall electron density and the greater separated charge distributions in the C=C bond of MPDOX compared to DDVE support the almost 4 times higher K_{eq} for MPDOX. In the past we postulated (5) that the propagation step in the free-radical copolymerization of maleimides and vinyl ethers proceeds by addition of the radical chain end to the CT complex. Therefore, it is reasonable to project that the maleimide/dioxolane polymerization proceeds similarly, and that the higher rate for the Q-Bond/MPDOX polymerization versus the Q-Bond/DDVE as shown in Figure 1 results from the higher concentration of the CT complex (and presumably stronger complex formation).



Scheme IV. Quenching of MI* by MPDOX.

Table II. The equilibrium constants, K_{eq} , for t-BMI/DDVE and t-BMI/MPDOX pairs and corresponding electron density distributions.

Donor Monomer	$K_{eq} (M^{-1})$	$\Sigma_{charge} C1/C2$	$HOMO_{charge} C1/C2$	Π -bond Order
	0.043	$\frac{-0.1341}{+0.0617}$	$\frac{-0.5297}{+0.3044}$	C1=C2 0.9585
	0.168	$\frac{-0.1452}{+0.0642}$	$\frac{-0.5377}{+0.2853}$	C1=C2 0.9396

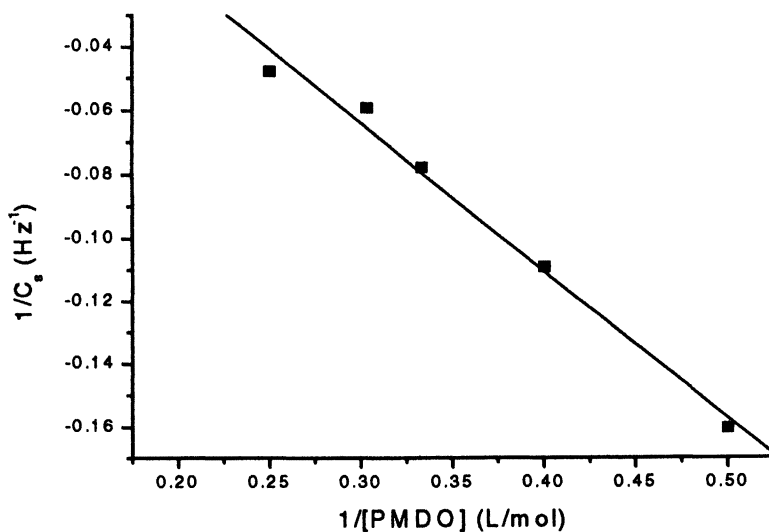


Figure 3. Hanna-Ashbough plot for 2-phenyl-4-methylene-1,3-dioxolane (MPDOX)/t-BMI system. The chemical shift was recorded for the proton on the double bonds of t-BMI near 6.5 ppm.

Conclusions

The aryl dioxolane monomer 4-methylene-2-phenyl-1,3-dioxolane (MPDOX) has been shown to copolymerize with a difunctional maleimide via both ring opening and simple addition across the vinylic (C=C) double bond when exposed to light in the absence of a photoinitiator. An electron/proton transfer involving the maleimide singlet state and the dioxolane results in the production of radical initiators. For the dioxolane monomer used in this investigation (MPDOX) at room temperature, essentially only ring opening occurs, while both processes occur at higher temperatures. There is an enhanced rate measured for photopolymerization of the maleimide/dioxolane combination versus a maleimide/vinyl ether mixture. The increased electron density in the vinylic C=C bond of the dioxolane was proposed as a plausible explanation for this rate enhancement.

Acknowledgments

The support of Fusion UV Systems and Becker-Acroma AB is gratefully acknowledged.

References

1. Hoyle, C. E.; Clark, S. C.; Jönsson, S.; Shimose, M. *Polymer* **1997**, *38*, 5695.
2. Clark, S. C.; Hoyle, C. E.; Jönsson, S. *Polym. Prep.* **1996**, *37* (2), 348.
3. Jönsson, S.; Sundell, P.-E.; Shimose, M.; Clark, S. C.; Miller, C. W.; Morel, F.; Decker, C.; Hoyle, C. E. *Nuc. Inst. Met. Phys. Res. B*, **1997**, *131*, 276.
4. Hoyle, C. E.; Clark, S. C.; Jönsson, S.; Shimose, M. *Poly. Commun.* **1998**, *38*, 5695.
5. Decker, C.; Morel, F.; Jönsson, S.; Hoyle, C. E. *PRA, Conf. Proc.* **1998**, (4) 1-24.
6. Clark, S. C.; Hoyle, C. E.; Viswanathan, K.; Miller, C. W.; Jönsson, S.; Morel, F.; Decker, C. *PRA, Conf. Proc.* **1998**, (5) 1-11.
7. Viswanathan, K.; Clark, S. C.; Miller, C. W.; Hoyle, C. E.; Jönsson, S.; Shao, L. *Polym. Prep.* **1988**, *39* (2), 644.
8. Belfield, K. D.; Abdelrazzaq, F. B. *J. Polym. Sci., Part A, Polym. Chem.* **1997**, *35*, 2207.
9. Sonntag, J.; Beckert, D.; Knolle, W.; Mehnert, R. *J. Radiat. Phys. Chem.* **1998**, *29*, 8.
10. Put, J.; DeSchryver, F. C. *J. Am. Chem. Soc.* **1973**, *95* (1), 137.
11. Pan, C. Y.; Wu, Z.; Bailey, W. J. *J. Polym. Sci., Part C: Polymer Letters* **1987**, *25*, 243.

12. Decker, C.; Bianchi, C.; Jönsson, S.; Hoyle, C. *RadTech 99 Berlin, Conf. Proc.* **1999**, 447.
13. Davidson, R. S.; Howgate, G. J.; Lester, F. H. A.; Mead, C. J. *RadTech 99 Berlin, Conf. Proc.* **1999**, 483.
14. Bailey, W. J. *J. Macromol. Sci., Chem.* **1975**, *9*, 849.
15. Sanda, F.; Takata, T.; Endo, T. *J. Polym. Sci., Part A, Polym. Chem.* **1994**, *32*, 2517.
16. Belfield, K. D.; Zhang, G. *Polym. Prep.* **1996**, *37*, 537.
17. See, e.g., *Expanding Monomers: Synthesis, Characterization, and Applications*; Sathir, R. K.; Luck, R. M., Eds.; CRC Press, Inc.: Boca Raton, FL, 1992.

Chapter 8

Photoinitiated Cross-Linking Polymerization of Monomer Blends

Christian Decker

Département de Photochimie Générale (UMR-CNRS N°7525), Ecole
Nationale Supérieure de Chimie de Mulhouse, Université de
Haute-Alsace - 3, rue Werner, 68200 Mulhouse, France

Introduction

The photoinitiated polymerization of multifunctional monomers is one of the most effective methods for producing rapidly tridimensional polymer networks and transform quasi-instantly a liquid resin into a solid and insoluble material (1-5). In most applications of this UV-curing technology a single type of monomers and telechelic oligomers is being used, mainly acrylates or epoxides which undergo polymerization by a radical or cationic-type mechanism, respectively. For some particular applications, the photopolymerization of monomer blends may provide some additional advantages, as it is an easy way to produce interpenetrating polymer networks (IPN) or crosslinked copolymers which may combine the properties of the two homopolymer networks (6-9). In the case of IPNs, photoinitiation is a unique method to generate separately each polymer network in a sequential timing (1) by a proper selection of the two photoinitiators and the radiation wavelength. A distinct feature of photoinitiation lies in the high polymerization rates which can be reached under intense illumination, together with the advantage of a solvent-free formulation curable at ambient temperature. The photocrosslinking of monomer blends is likely to find a number of industrial applications, in particular to achieve a fast drying of varnishes and printing inks, a quick setting of adhesives and composite materials and a selective insolubilization of photoresists in microlithography.

The objective of this work was to study the light-induced crosslinking-polymerization of various monomer blends, focusing our attention mainly on the kinetic aspect of these ultrafast reactions. In this respect, infrared spectroscopy proved to be a technique particularly well suited because it allows

one to monitor in real time the disappearance of each one of the monomers undergoing polymerization and to record directly the monomer conversion *versus* time curves in a timescale as short as 1 s. The important kinetic parameters can thus be determined, in particular the actual polymerization rate and the final cure extent, a quantity which governs the physico-chemical characteristics of the crosslinked polymer formed.

Experimental

The following monomers and functionalized oligomers have been used in this study:

- acrylate monomers, like hexanedioldiacrylate, HDDA, and a diacrylate derivative of bisphenol A, BPDA (Ebecryl 150), both from UCB Chemicals.
- epoxy monomers, like a bicycloaliphatic diepoxide, BCDE (Araldite CY-179) from Ciba Specialty Chemicals, or epoxidized polyisoprene (EPI).
- vinyl ether monomers, like the divinylether of triethyleneglycol (DVE-3) from ISP
- vinyl functionalized polymers, like polybutadiene in thermoplastic block copolymers (Kraton SBS) from Shell.

The photoinitiators used are generating upon UV-exposure either free radicals (Darocur 1173, Lucirin TPO, Irgacure 819, from Ciba Specialty Chemicals and isopropyl thioxanthone, ITX) or protonic acid (a triarylsulfonium salt TAS, Cyracure 6990 from Union Carbide, or a PF₆ diaryliodonium salt DAI from Ciba Specialty Chemicals).

The liquid resin was applied onto a transparent polypropylene film or onto a silicon wafer at a thickness ranging typically between 10 and 30 μm. The curing was performed in the presence of air by UV-irradiation of the sample placed either in the compartment of an IR spectrophotometer (light intensity between 20 and 100 mW cm⁻²), or on the belt of a UV-line operated at a web speed between 5 and 60 m/min. The maximum light intensity received by the irradiated sample passing under the lamp was measured by radiometry (International Light IL-390) to be on the order of 500 mW cm⁻². All the experiments have been carried at ambient temperature.

The disappearance of each one of the functional groups of the monomer blend, was monitored continuously by real-time infrared (RTIR) spectroscopy, by selecting the proper wavenumber of the IR detection, at 795 cm⁻¹ for the epoxy ring, at 1411 cm⁻¹ for the acrylate double bond and at 1635 cm⁻¹ for the vinyl ether and vinyl double bonds. Conversion *versus* time curves can be readily obtained from the value of the IR absorbance, initially (A₀) and after a given exposure (A_t), by plotting the ratio 1-A_t/A₀ as a function of the exposure time. With the FTIR spectrophotometer used (Bruker IFS 66), up to 50 spectra can be recorded each second, thus allowing an accurate monitoring of fast

proceeding reactions. From the maximum slope of the conversion *versus* time curves recorded, the formulation reactivity, ratio of the rate of polymerization (R_p) to the monomer concentration $[M_0]$, was evaluated for each monomer. The amount of unreacted functionalities in the UV-cured polymer was determined from the value of the final conversion reached at the end of the UV exposure.

To evaluate the extent of the crosslinking reaction, the fraction of the polymer which has become insoluble in chloroform after a certain UV exposure was measured, as well as the swelling ratio defined as the amount of chloroform retained by the crosslinked polymer ($W_{\text{solvent}} / W_{\text{dry polymer}}$). The hardness of the UV-cured polymer was evaluated by monitoring the damping of the oscillations of a pendulum placed onto a glass plate coated with a 30 μm thick film. Persoz values are expressed in seconds and are typically ranging from 30 s for soft elastomeric materials up to 400 s for very hard and glassy polymers.

UV-curing of acrylate / epoxide blends

Multifunctional acrylate and epoxy monomers, as well as telechelic oligomers end-capped with these functional groups, are widely used in today's UV-curable resins (4). By mixing these two types of monomers which polymerize by different mechanisms, interpenetrating polymer networks will be formed upon UV-irradiation in the presence of both radical and cationic-type photoinitiators. With the particular monomer blend selected, a 1/1 mixture by weight of Araldite CY-179 (BCDE) and Ebecryl 150 (BPDA), phase separation did not occur, neither before of after UV-curing.

In the kinetic analysis of the polymerization of the epoxide by infrared spectroscopy, we encountered a problem due to the overlap of the epoxy ring IR band at 795 cm^{-1} by the acrylate double bond IR band centered at 810 cm^{-1} (Figure 1). It was yet possible to overcome this difficulty by monitoring at 1082 cm^{-1} the build-up of the ether bond which is formed upon the ring-opening polymerization of the epoxide. In the neat epoxide, the intensity of the ether band was found to increase linearly with the monomer conversion, measured from the decrease of the epoxy band at 795 cm^{-1} . Since this relationship is expected to remain valid in the monomer mixture, we were able to evaluate accurately the epoxy conversion in the BCDE/BPDA blend from the increase of the IR absorbance at 1082 cm^{-1} .

Figure 2 shows the polymerization profiles of the epoxy and acrylate monomers upon UV exposure of a 1/1 BCDE/BPDA blend containing both types of photoinitiators : $[\text{DAI}] = 2\text{ wt\%}$ and $[\text{Darocur 1173}] = 2\text{ wt\%}$. As expected, the polymerization of the diacrylate proceeds faster and more extensively than the polymerization of the diepoxide because of a higher value of the propagation rate constant. It should be noted that a nearly complete

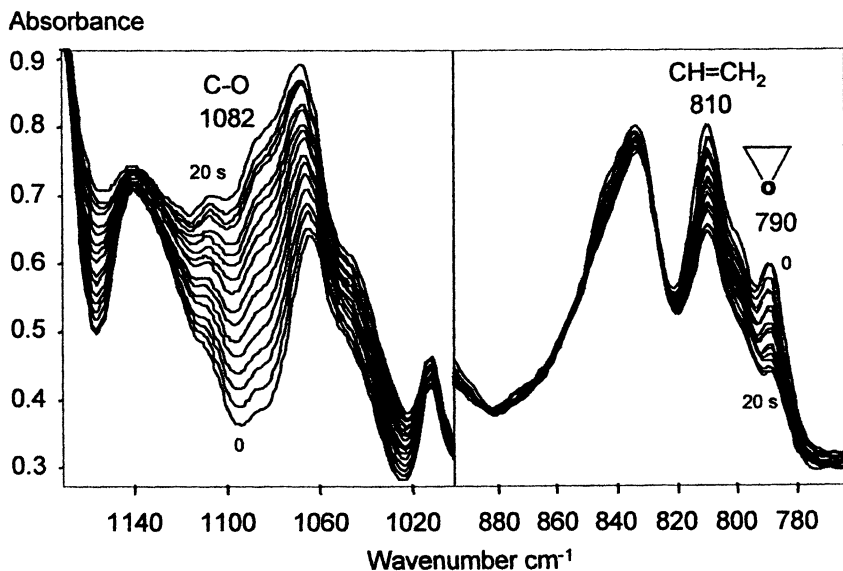


Fig.1 Variation of the infrared spectrum of an acrylate / epoxide monomer blend (BPDA / BCDE) upon UV exposure. [DAI] = 2 wt%. $I = 60 \text{ mW.cm}^{-2}$

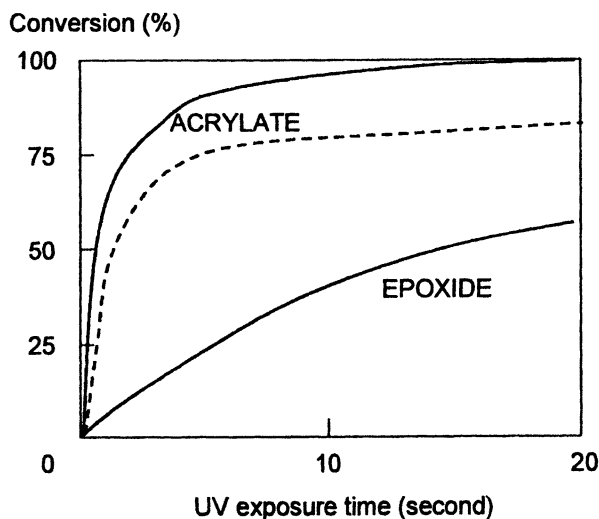


Fig.2 Photopolymerization of a BPDA / BCDE blend in the presence of air. [Darocur 1173] = 2 wt% ; [DAI] : 2 wt%. Light intensity : 60 mW.cm^{-2} . Film thickness : $10 \mu\text{m}$. — neat BPDA.

polymerization of the acrylate double bond was achieved after a 20 s UV-irradiation of the monomer mixture, while the conversion value was levelling off at 85% in the neat BPDA monomer (Figure 2). This behavior can be accounted for by considering that the less reactive epoxy co-monomer acts as a plasticizer during the early polymerization of the acrylate monomer : 80% conversion of the acrylate after 3 s, compared to only 15% conversion of the epoxide which is still liquid at that stage.

The polymerization of the diepoxide is hardly affected by the previous buildup of the acrylate polymer network and reaches 50% conversion after a 20 s UV exposure. It should yet be noted that the remaining epoxy groups continue to react slowly upon storage of the sample in the dark because of the living character of cationic polymerization. The polymerization of the epoxide was found to be somewhat enhanced in the presence of air. This behavior was attributed to some catalytic effect of the atmosphere humidity (35%) which favors chain transfer reactions involving the hydroxyl groups of water (10). As expected, an increase of the light intensity is speeding up the polymerization of both monomers. By working with an industrial type UV-line, a tack-free coating was already obtained after a single pass under the high intensity mercury lamp (500 mW cm^{-2}) at a web speed of 10 m/min, which corresponds to an exposure time of 0.5 second.

The cationic polymerization of the epoxide can be substantially accelerated by the addition of a photosensitizer like isopropylthioxanthone. ITX absorbs more effectively the UV-radiation of the mercury lamp than DAI does, and it generates protonic acid by a redox reaction with the iodonium salt (3). Moreover, it produces free radicals by a photoinduced hydrogen transfer reaction with a H-donor molecule. With the ITX+DAI combination of photoinitiators, the epoxy monomer was found to polymerize half as fast as the acrylate monomer (9). Similar polymerization profiles were recorded in the presence of air and in O_2 diffusion-free conditions (lamine), thus showing the beneficial effect of the epoxide polymerization on the O_2 inhibitory effect in the acrylate polymerization.

The accelerated polymerization of the epoxide in the presence of a photosensitizer is generally attributed to an increase of the initiation rate due to a faster photolysis and decomposition of the diaryliodonium salt. This could be demonstrated by monitoring the disappearance of the DAI photoinitiator by infrared spectroscopy, upon UV-irradiation of the BCDE monomer. This PF_6 iodonium salt was indeed found to exhibit a distinct IR band centered at 844 cm^{-1} , which disappears upon UV exposure. It is clearly apparent from the RTIR curves recorded for the DAI decay and the epoxy conversion (Figure 3), that the two processes are strongly correlated, in both the unsensitized and the ITX sensitized resins. Actually, a linear relationship was found to exist between the polymerization rate of the epoxide and the loss rate of the diaryliodonium photoinitiator.

The crosslinking polymerization of the two monomers leads to a rapid insolubilization of the UV exposed resin, with formation of tight polymer networks, as shown by the low value of the swelling ratio (0.4). A tack-free coating was obtained after a 1 s exposure to intense UV light (0.5 s for the ITX sensitized sample). The polymer film continued to harden upon further exposure to reach Persoz values on the order of 350 s, nearly as high as mineral glass (400 s). In spite of its great hardness, this acrylate/epoxide IPN was found to be more flexible than the epoxy homopolymer, most probably because of the presence of the acrylate network

Similar results have been obtained by UV-irradiation of a mixture of an epoxidized polyisoprene (EPI) and a diacrylate (HDDA) in the presence of both a radical photoinitiator (Lucirin TPO) and a cationic photoinitiator (Cyracure 6990). The ring-opening cationic polymerization of the epoxy groups proceeds nearly as fast as the polymerization of the acrylate double bonds (Figure 4), because of the plasticizing effect of the liquid monomer (20 wt%) introduced in EPI ; it increases markedly the molecular mobility and leads to a more complete cure than in the neat EPI. Here the two interpenetrating polymer networks are bound together by copolymerization of the acrylate double bonds of HDDA and the isoprene double bonds which are still present in the partly epoxidized polyisoprene (8). Owing to their performance regarding both processing and properties, UV-cured acrylate/epoxide polymers are expected to find their main applications as fast-drying protective coatings and for the manufacture of composite materials and optical components at ambient temperature.

UV-curing of acrylate/vinyl ether blends

Vinyl ethers (VE) do not undergo homopolymerization when they are exposed to UV radiation in the presence of a radical-type photoinitiator because of the high electronic density of the VE double bond which prevents its attack by VE radicals. These monomers can however undergo a radical-type copolymerization when they are associated to an acrylate co-monomer (11). Unlike VE radicals, acrylate radicals react with both vinyl ether and acrylate double bonds, which leads to the formation of a copolymer network containing isolated vinyl ether units.

Vinyl ether monomers are very effective in reducing the viscosity of telechelic acrylate oligomers, requiring typically half the amount of the homologous acrylate reactive diluents. An additional advantage of vinyl ether monomers lies in their lower odor and irritancy than acrylate monomers. By increasing the molecular mobility, vinyl ethers provide both faster and more complete curing of multifunctional acrylate monomers. However, since acrylate radicals are twice as reactive toward the acrylate double bond as toward the

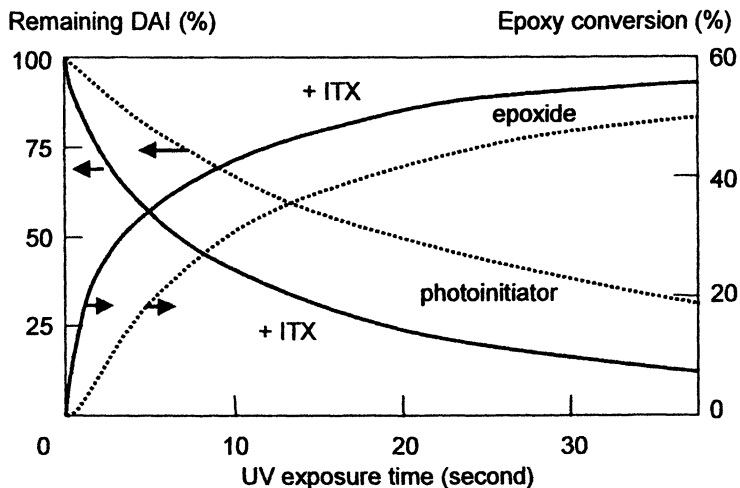


Fig.3 Decay of the iodonium photoinitiator and polymerization of the epoxy monomer upon UV-irradiation of BCDE with and without photosensitizer. [ITX] = 0.5 wt%; [DAI] = 2 wt%; light intensity = $60 \text{ mW}\cdot\text{cm}^{-2}$.

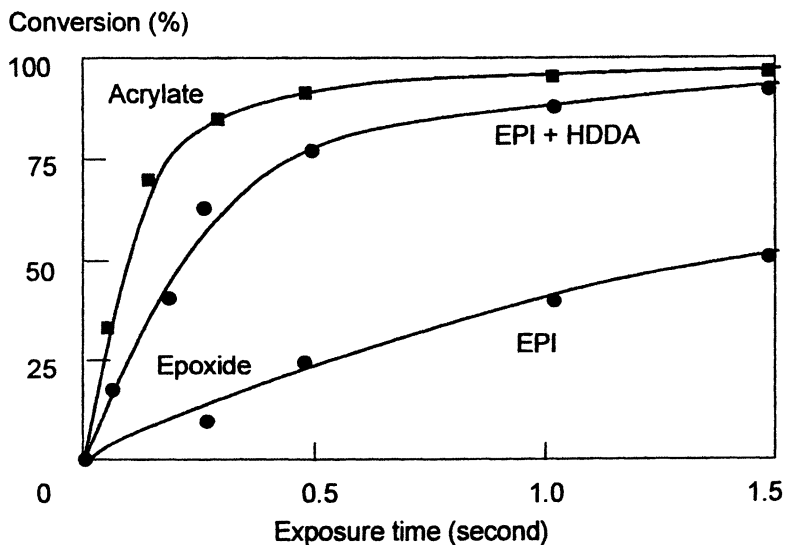


Fig.4 Influence of a diacrylate monomer on the photocrosslinking of an epoxidized polyisoprene. [HDDA] = 20 wt%; [Lucirin TPO] = 1 wt%; [Cyracure 6990] = 2 wt%. Light intensity = $600 \text{ mW}\cdot\text{cm}^{-2}$

vinyl ether double bond, the UV-cured copolymer contains a relatively large amount of unreacted VE double bonds. The latter can not react further because there are no acrylate double bonds available anymore (the unreacted acrylate double bonds are trapped in the polymer network).

In order to achieve a more complete polymerization of the monomer blend, it is necessary to introduce a second photoinitiator (TAS or DAI) to promote the cationic polymerization of the vinyl ether monomer. However, because arylium salts undergo a fast photolysis, there was still an appreciable amount (~ 20%) of residual VE unsaturation in the UV-cured polymer. We have been able to overcome this difficulty by performing the UV-irradiation in a sequential timing. The first exposure with filtered light ($\lambda > 350$ nm) induces only the photocleavage of the radical-type photoinitiator (Lucirin TPO), which initiates the radical copolymerization of the two monomers. The second exposure to unfiltered light induces the decomposition of the onium salt to generate the protonic acid which initiates the cationic polymerization of the unreacted VE double bonds. Figure 5 shows the polymerization profiles recorded by RTIR spectroscopy for a polyurethane-acrylate / DVE-3 mixture which was fully cured by this two step irradiation process. The properties of the polymer material obtained, depend mainly on the chemical structure of the acrylate oligomer selected, since the amount of VE monomer used as reactive diluent can be lowered typically below 20 wt%.

UV-curing of vinyl ether / epoxide

Vinyl ethers are known to polymerize rapidly by a cationic mechanism in the presence of photogenerated protonic acid (12). When they are associated to epoxides, they can speed up the polymerization of these less reactive monomers and lead to a more complete cure. The product formed upon UV-exposure of a VE/epoxide blend can be either a crosslinked copolymer or two interpenetrating polymer networks, depending whether these monomers undergo crosspropagation or not. Because of complex interactions between vinyl ethers and epoxides, copolymerization was not considered to take place in appreciable amount upon UV-exposure of a mixture of these monomers (13).

However, when we exposed to UV-radiation an equimolar blend of BCDE and DVE-3, two monomers widely used in UV-radiation curing, in the presence of a triarylsulfonium salt, the polymerization profiles of the vinyl ether and the epoxide were found to be very similar (Figure 6), which argues in favor of a copolymerization process. An alternating copolymer network could be formed by a crosspropagation mechanism, the VE carbocation reacting preferentially with the epoxy ring, while the oxonium ion would react preferentially with the VE double bond :

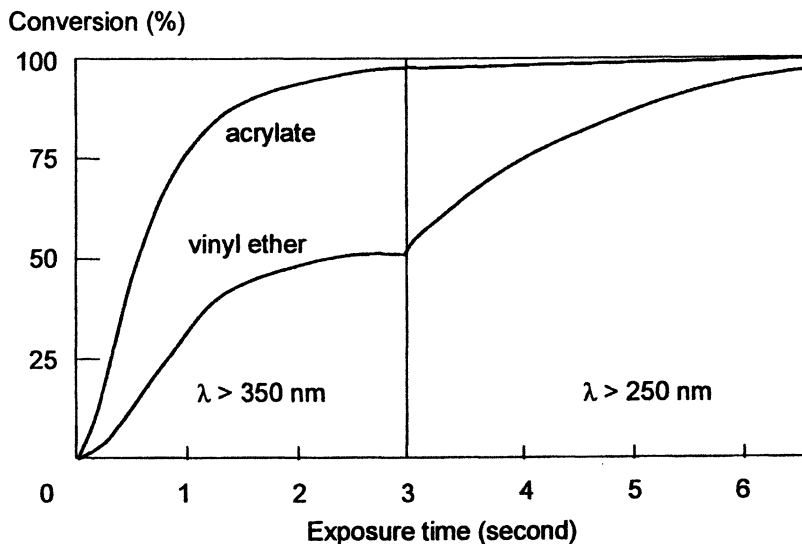


Fig.5 Sequential polymerization of a polyurethane-acrylate / divinyl ether mixture exposed successively to filtered and unfiltered UV radiation Ebecryl 284 / DVE-3 = 2 / 1 molar ; [Lucirin TPO] = 1 wt% ; [Cyracure 6990] = 2 wt% ; Light intensity = 50 mW.cm⁻².

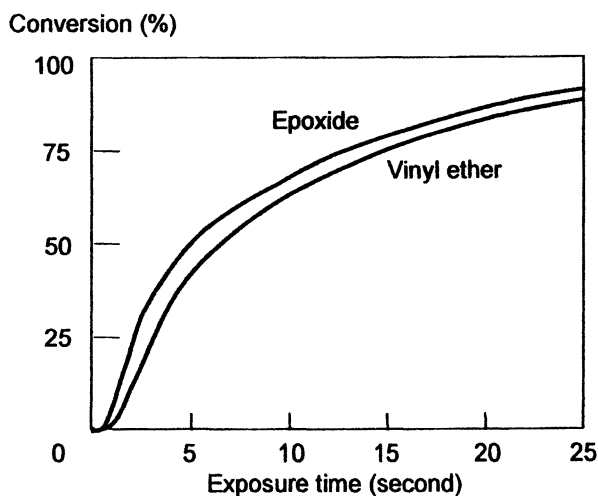
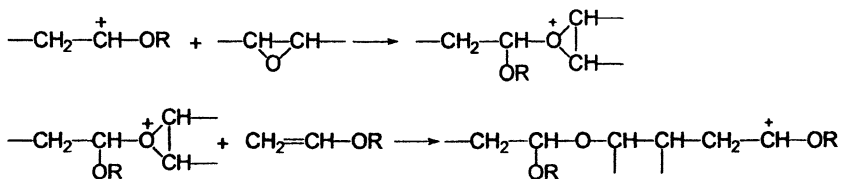


Fig.6 Photopolymerization of a vinyl ether / epoxide blend. [DVE-3] / [BCDE] = 1 molar . [Cyracure UVI-6990] = 4 wt%. Light intensity = 20 mW.cm⁻².



An interesting observation was made by repeating this photopolymerization experiment in the presence of an excess of vinyl ether ([VE] / [Epoxy] = 2 molar). Here again similar polymerization curves were recorded for the two monomers until half of the epoxide had polymerized, as shown in Figure 7. This means that relatively small amounts of epoxides are sufficient to suppress the cationic homopolymerization of the vinyl ether, which is known to proceed very efficiently in the neat monomer. It is only once the epoxy ring concentration has been cut by more than half (a 3 fold excess of VE) that the amount of VE polymerized becomes superior to the amount of epoxide polymerized. But, surprisingly, the homopolymerization of the vinyl ether, quantified by the difference between the two curves of Figure 7, is still proceeding much slower under those circumstances than in the neat DVE-3.

These kinetic results strongly suggest that the epoxy ring of BCDE and the vinyl ether double bond of DVE-3 are undergoing alternating copolymerization. Experimental evidence in favor of such a mechanism has been recently obtained by Kostanski et al. (14) who observed a single T_g for the UV-cured blend. They also showed that a monofunctional VE monomer is totally incorporated into the polymer network, necessarily by copolymerization with the diepoxide.

UV-curing of acrylate and vinyl monomer blends

Photoinitiated crosslinking polymerization may also proceed by a radical mechanism in the case of acrylate and vinyl double bonds, like for example upon UV-irradiation of a polybutadiene plasticized with a diacrylate monomer (15). It proved to be an effective way to speed up the curing reaction and increase the crosslink density in a triblock styrene-butadiene-styrene (SBS) thermoplastic elastomer containing a large amount of vinyl double bonds (59%) produced by 1-2 polymerization of butadiene. This boosting effect is due to both the plasticizing effect of the liquid acrylate monomer which increases the molecular mobility in the elastomeric phase, and to a greater reactivity of vinyl radicals towards the acrylate double bond (copolymerization) than toward the vinyl double bond (homopolymerization). Copolymerization occurs mainly in the very early stage of the UV exposure, about 70% of the acrylate double bonds being consumed within the first 0.2 s. Upon further exposure, vinyl double bonds disappear mainly by homopolymerization, pretty much like in neat SBS. The additional crosslinks are causing a substantial increase of the

polymer hardness but, because of the elastomeric character of the polybutadiene chains, the UV-cured film still maintains a high flexibility (zero-T-bend), thus making this UV-cured polymer well suited for protective coating applications, specially on flexible substrates.

A similar behavior was observed in another type of thermoplastic elastomer, acrylonitrile/butadiene/acrylonitrile (ABA), where the polybutadiene chain contains mainly 2-butene double bonds (97%) formed by the 1-4 polymerization (16). The addition of a triacrylate monomer ([TMPTA] = 20 wt%) was found to accelerate considerably the insolubilization process, as shown in Figure 8. It also leads to the formation of a more tightly crosslinked copolymer, as shown by the drastic decrease of the swelling ratio : a drop from a value of 10 for the neat ABA polymer UV-irradiated for 1 s to a value of 0.8 for the sample containing TMPTA. A similar but less pronounced effect was found by using a diacrylate ([HDDA] = 20 wt%) as reactive plasticizer. It should be noted that the addition of these acrylate monomers (20 wt%) had no major effect on the hardness of the UV-cured rubber which remained soft and flexible, even after extensive UV-exposure (Persoz hardness value between 50 and 70 s). The elastomeric character, in particular the impact resistance and the adhesives properties (tackiness), was thus retained in the photocrosslinked ABA copolymer, thus making it well suited for adhesives and safety glass applications.

Conclusion

The photoinitiated polymerization of blends of multifunctional monomers is an effective method to produce polymer networks with well designed properties. Depending on the polymerization mechanism and on the kind of photoinitiator selected (radical or cationic-type), a variety of network architectures can be generated by combination of different types of monomers. By acting on the proportions of the two monomers one can finely adjust the properties of the UV-cured polymer and make it well suited for the considered application.

Under intense illumination, the crosslinking polymerization of the various monomer blends occurs within a fraction of a second to generate insoluble polymer material. Such ultrafast reaction is best followed by real-time infrared spectroscopy, a technique that records directly conversion *versus* time curves for each one of the two types of monomers. Their intrinsic reactivity can thus be determined accurately, as well as the amount of unreacted monomer in the UV-cured polymer.

Because of its process facility (short UV-irradiation of a solvent-free formulation at ambient temperature) and the broad range of product performance, the UV-curing of monomer blends is expected to attract attention

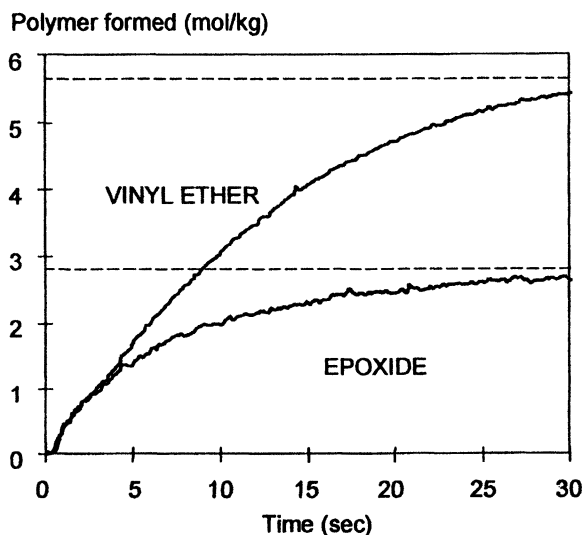


Fig.7 Photoinitiated cationic polymerization of an epoxy monomer in (BCDE) in the presence of an excess of divinyl ether. $[DVE-3]/[BCDE]=2$ molar. $[Cyracure\ 6990]=4$ wt%. Light intensity = $20\text{ mW}\cdot\text{cm}^{-2}$.

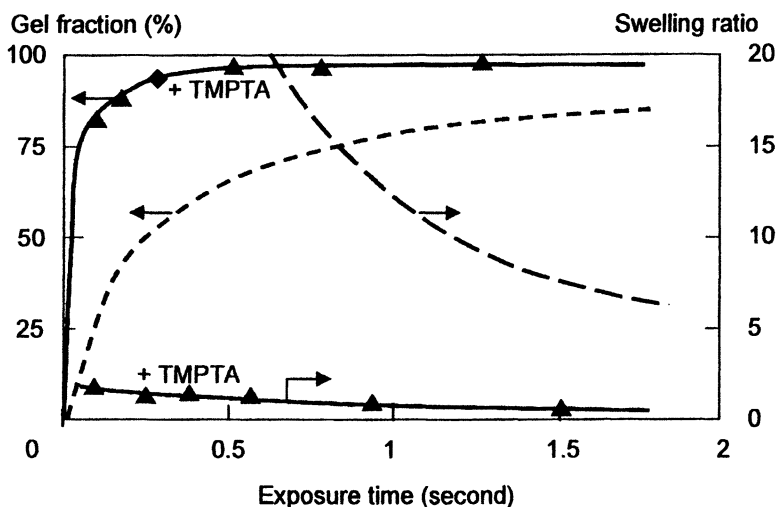


Fig.8 Influence of a triacrylate monomer on the photoinduced insolubilization of an acrylonitrile – butadiene thermoplastic elastomer. $[TMPTA]=20$ wt% ; $[Irgacure\ 819]=3$ wt%. Light intensity = $600\text{ mW}\cdot\text{cm}^{-2}$. --- neat ABA rubber.

in an ever-growing number of industrial sectors, in particular to achieve a fast drying of protective coatings and adhesives, and a rapid manufacturing of composite materials, microcircuits and printing plates.

Acknowledgements

The authors wishes to thank his co-workers at the Polymer Photochemistry Laboratory, Drs. Danielle Decker, Trieu Nguyen Thi Viet and Khalid Zahouily. He also acknowledges the financial support from Ciba Specialty Chemicals (Basle-Switzerland) and the Centre National de la Recherche Scientifique (France).

References

1. Decker C., *Progr.Polym.Sci.* **1996**, *21*, 593
2. Roffey C., *Photogeneration of Reactive Species for UV-Curing*, Wiley, New York **1997**
3. Crivello J.V., *J.Polym.Sci., Polym.Chem.* **1999**, *37*, 4241
4. Davidson R.S., *Exploring the Science Technology and Applications of UV and EB Curing*, SITA Technology London **1999**
5. Andrzejewska E., *Progr.Polym.Sci.* **2001**, *26*, 605
6. Timpe H.J., Strehmel B., *Angew. Makromol. Chem.* **1990**, *178*, 131
7. Moussa K., Decker C., *J.Polym.Sci., Polym.Chem.*, **1993**, *31*, 2633
8. Decker C., Le Xuan H., Nguyen Thi Viet T., *J.Polym.Sci., Polym.Chem.Ed.* **1996**, *34*, 1771
9. Decker C., Nguyen Thi Viet T., Decker D., Weber-Koehl E., *Polymer* **2001**, *42*, 5531
10. Decker C., Nguyen Thi Viet T., Pham Thi H., *Polym. Intern.*, **2001**, *50*, 986
11. Decker C., Decker D., *J.Macromol.Sci.* **1997**, *A34*, 605
12. Lapin S.C., in *Radiation Curing Science and Technology*, Pappas S.P. Ed., Plenum Press, New York, **1992** p.241
13. Rajaraman S.K., Moweeers, Crivello J.V., *J.Polym.Sci.Polym.Chem.Ed.* **1999**, *37*, 4007
14. Kim Y.M., Kostanski L.K., Mac Gregor J.F., *Polymer* (in press)
15. Decker C., Nguyen Thi Viet T., *Macromol.Chem.Phys.* **1999**, *200*, 358
16. Decker C., Nguyen Thi Viet T., *J. Appl.Polym.Sci.*, **2001**, *82*, 2204

Chapter 9

Synthesis and Photochemistry of Monodisperse Oligomeric–Polymeric Photoinitiators

Zhiqiang Liu¹, Matthias Weber¹, Nicholas J. Turro^{1,2,*},
and Ben O'Shaughnessy²

Departments of ¹Chemistry and ²Chemical Engineering,
Columbia University, 3000 Broadway, MC 3119, New York, NY 10027

Monodisperse polystyrene with a photoinitiator end group was prepared using living free radical polymerization. Nanosecond pulsed laser irradiation was used to generate the oligomeric/polymeric radicals, and the relaxation time constants of the electron spin polarized signal were measured using Time-Resolved Fourier-Transform EPR (TR FT EPR). The preliminary results demonstrate the applicability of this method in the direct experimental study of the properties of the oligomeric/polymeric radicals. This method is expected to allow the study of the chain length dependence of free radical polymerization kinetics with improved accuracy and a larger range of concentration and chain length.

Introduction

Free radical polymerization (FRP) is an important method for the industrial preparation of polymers. Typically, the thermal or photochemical decomposition of initiators produces radicals, which can attack monomers and start the growth of polymer chains. In addition to the propagation process in which the chain extends by one monomer unit, the active chains can lose activity and become

dead chains through recombination, disproportionation and chain transfer processes.

It is of significant academic and industrial importance to study the details of all of these competing reactions in a systematically varied environment in order to achieve a thorough understanding of the FRP process. The kinetic details depend on many factors including the polymer chain length and concentration. A number of research groups have reported studies of the initiation steps of FRP and their dependence on a series of factors, e.g. solvent viscosity using typical spectroscopic methods.¹ Recent progress in the determination of propagation rate coefficients was made primarily by Pulsed-Laser Polymerization-Size Exclusion Chromatography (PLP-SEC).² Measurements of termination rate coefficients have been focused mainly on the Single-Pulse Pulsed-Laser Polymerization (SP-PLP) method.³ These methods have provided invaluable insights into the kinetics of FRP, but they are typically based on the time evolution of monomer conversion or product molecular weight distribution analysis and, therefore, do not offer *direct* information on the identity and molecular weight distributions of oligomeric/polymeric radicals. The oligomeric/polymeric systems analyzed were primarily of low conversion. Additionally, in the PLP experiments, time and molecular weight averaged values were obtained during the measurements, and the lack of control on monodispersity of the macro radicals was problematic especially at high conversion.

Our interests focus on the *direct* spectroscopic measurements of the properties of macro radicals with controlled monodispersity, especially the dependence on chain length and environment in the entangled region characterized by a high concentration of long chains. The dynamic properties of polymeric systems in the entangled region display a dramatically different relationship to the chain length compared to the systems below the entanglement threshold.⁴ Although the entanglement effects on the properties of macro radicals have received considerable theoretical treatment, experimental results have been largely unavailable.⁵

The difficulty in the preparation of large quantities (ca. at millimole scale) of monodisperse polymer samples with suitable photoinitiator groups as end labels using conventional ionic or free radical mechanisms has been one of the limiting factors. These samples can be prepared using the living free radical polymerization (LFRP) methods developed in the past decade.^{6,7} LFRP combines the advantage of living anionic polymerization in the excellent control of monodispersity of the polymer samples and the advantage of conventional free radical polymerization in the ease of operation and tolerance toward a large variety of functionalized end groups. It has been shown that polystyrenes^{6,7} and poly(alkyl methacrylates) with a large variety of end labels and a low polydispersity index ($PDI < 1.5$) can be prepared using LFRP.

EPR has been used in the study of initiation rate coefficients in steady state situations, and has provided valuable information about the reactivity difference among different radicals produced from a single photoinitiator.⁸ Time-Resolved

Continuous-Wave EPR (TR CW EPR) was also reported in the direct determination of initiation rate coefficients for small radicals by measuring the decay of the EPR signal of the primary radical when one vinyl monomer is added.⁹ The primary radicals were produced by photolysis of photoinitiator molecules using nanosecond laser pulse. This method enjoys the advantage of acquisition of direct information on radical structure, enhanced signal to noise ratio by CIDEP and microsecond time resolution. The production of secondary radicals by addition of primary radicals to alkenes was directly observed for small molecules using TR CW EPR.^{10,11}

In this chapter, we extended the TR EPR measurements to the oligomeric/polymeric system and directly studied the properties of the polarized electron spin signal of the macro radicals generated by the photolysis of oligomer/polymer bearing photoinitiator groups as end labels.

Experimental

Materials: Ethylbenzene was purchased from Lancaster. Di-tert-butylperoxide, 2,2,6,6-tetramethyl-1-piperidinyloxy (TEMPO), 4-carboxy-TEMPO were purchased from Aldrich. Tetrahydrofuran (THF, HPLC grade) and tert-butyl acrylate were purchased from Acros. 2-Hydroxy-1-[4-(2-hydroxyethoxy)-phenyl]-2-methyl-propan-1-one, **3** (Figure 1) and 2-hydroxy-2-methyl-1-phenyl-propan-1-one, **7** (Scheme 1) were received as gifts from Ciba Specialty Chemicals. All reagents were used as received.

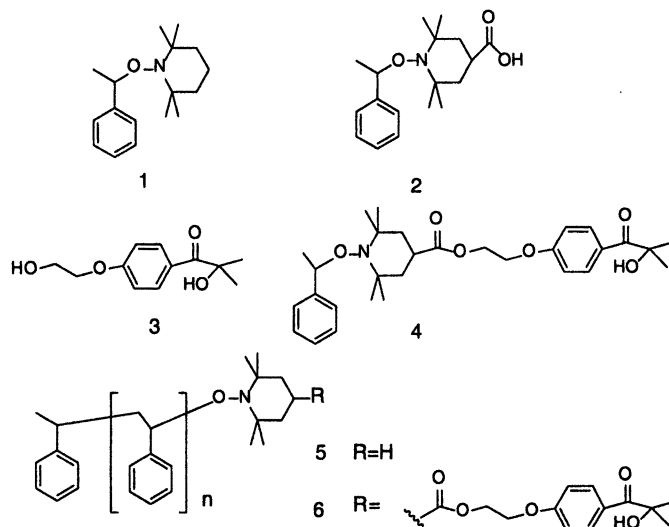


Figure 1. Structures of molecules related to the preparation of end-labeled and non-labeled polystyrenes using nitroxide mediated LFRP.

Instrumentation: ^1H -NMR and ^{13}C -NMR spectra were acquired on a Bruker NMR spectrometer at 400MHz and 100MHz, respectively, using CDCl_3 (TMS) or acetone- d_6 as solvent.

The gel permeation chromatography method was previously described.¹²

Two-pulse electron spin echo (ESE) experiments were performed on a TR FT EPR instrument which was described earlier,¹³ consisting of a Bruker ESP 300/380 pulsed FT EPR spectrometer. Excitation was performed with a Quanta-Ray INDI 50-10 Nd:YAG laser ($\lambda = 355$ nm, 7 ns, 10 Hz, 40 mJ/pulse). A coaxial quartz flow cell with a diameter of 3 mm was used in combination with a syringe pump (flow rate of 1.5 ml/min). Solutions of the photoinitiators (2 mM, absorbance at 355 nm \approx 0.03) were freshly prepared and deoxygenated by bubbling with argon for at least 30 minutes. Experiments were carried out at room temperature in THF. The spectra were recorded by a laser pulse - t - 90° - τ - 180° - τ - echo sequence with $t = 400$ ns and $\tau = 96$ ns at different field position (16 positions with a distance of 1.0 mT were used) in combination with an eight phase cycling in order to suppress unwanted signals. Relaxation times were obtained by measuring the EPR signal intensity of the radical as a function of either t with fixed $\tau = 96$ ns (for T_1) or τ with fixed $t = 400$ ns (for T_M). Typically, 7 to 12 different time positions were used to describe the exponential behavior.

Synthesis:

1 was prepared by a photochemical method following a published procedure with some modifications.¹⁴ To 150ml of ethylbenzene in a Pyrex tube was added TEMPO (2.70g, 17.4 mmol) and di-tert-butylperoxide (10g, 68 mmol). The mixture was placed in a Rayonet photochemical reactor equipped with 16 Rayonet lamps (350 nm) and photolyzed in the reactor under argon atmosphere while stirring. After 22 hours, the red color of TEMPO disappeared and a pale yellow color was present. The solution was washed three times with 10% $\text{Na}_2\text{S}_2\text{O}_3 \cdot 5\text{H}_2\text{O}$ aqueous solution, then washed twice with 60 ml 1N HCl, 60 ml H_2O , 60 ml saturated NaCl solution, and dried over anhydrous MgSO_4 . Ethylbenzene was then removed by vacuum distillation. Flash column chromatography was carried out using silica gel, eluting with hexane/ethyl acetate in increasing polarity from 1:0 to 15:1 (v/v). 2.53g (9.67 mmol) product was obtained as white crystals in 56% yield.

2 was prepared in the same manner as **1**, using 4-carboxy-TEMPO instead of TEMPO. The reaction mixture, initially a slurry, was turned into a clear solution at the completion of the reaction within 22 hours. The product was purified by column chromatography eluting with methylene chloride/methanol (50:1 to 20:1 v/v) and obtained as a white solid in 51% yield.

4 was prepared following a published procedure for room temperature esterification¹⁵ from **2** and **3**, using anhydrous ether as solvent, and purified by column chromatography eluting with hexane/ethyl acetate (20:1 to 4:1 v/v). The product was obtained as a colorless and viscous oil in 86% yield.

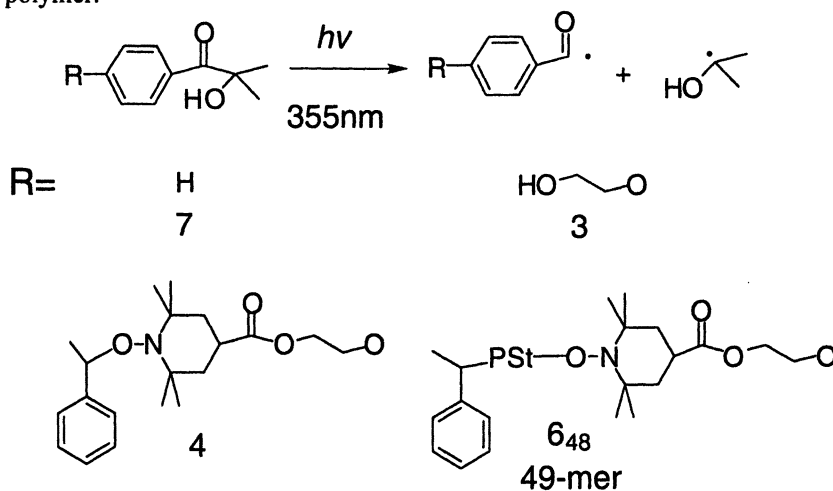
5, **6** were prepared following a published procedure of nitroxide mediated LFRP.⁶ Polymers of different molecular weight can be prepared by varying the

ratio of initiator to monomer and/or the reaction time. The product was purified by dissolving in a minimum amount of THF and precipitating with a large amount of methanol. The dissolving-precipitating cycle was performed 3 times, after which the sample was dried under vacuum.

^1H - and ^{13}C -NMR were used to characterize all the products, and gel permeation chromatography was used to characterize the polymer products.

Results and Discussion

The preparation of monodisperse polystyrene **5** has been well documented.^{6,7} They are prepared as polymers of different molecular weight for control experiments and to adjust viscosity of the solution of the labeled polymer.



Scheme 1. Photochemical generation of (substituted) benzoyl radicals and ketyl radicals.

The monodisperse polystyrene **6**, with a photoinitiator as an end label, has been prepared by an end group exchange method.¹⁶ In this report, it was prepared in a direct manner, i.e., performing the polymerization using end-labeled initiator, **4**. The advantage of this direct route is the removal of the postpolymerization treatment step and a higher degree of labeling. A sample of 49-mer **6**₄₈ ($n=48$ in **Figure 1**) with $M_n=5558$ (GPC) can be prepared in an argon atmosphere at 125°C within 13 hours, with a polydispersity index at 1.19. The low polydispersity index is an indication of the living nature of the polymerization process. The average number of pendent phenyl groups per end label can be measured using ^1H -NMR, via the ratio of integral of signal from aromatic protons to that from methylenic protons on the end label (using

acetone- d_6 as solvent to prevent interference of residual CHCl_3 from CDCl_3 in the aromatic region). The fact that the degree of polymerization of **55** from NMR analysis is very close to the that of **49** from GPC analysis demonstrates the high degree of labeling.

The photoinitiator **3** was chosen as the end label, because the two radicals, produced by photochemical α -cleavage of the parent structure (**Scheme 1**), exhibit strong electron spin polarization (ESP) of the benzoyl and ketyl, drastically enhancing the signal to noise ratio in TR EPR measurements.^{1f,17} **Figure 2** shows the resulting ESE spectra 400 ns after laser excitation of **7,3,4,6₄₈**. By measuring the phase memory time T_M and the spin-lattice relaxation time T_1 of the radicals by TR FT EPR, we can examine the influence of different chain length on the properties of the radicals. Since the addition reaction of benzoyl and ketyl radicals, produced from initiator decomposition, to a vinyl monomer is faster than the decay of ESP of the initial radicals, the ESP can be transferred to the adduct radical, rendering TR FT EPR a powerful technique for studying the adduct radicals.^{10,11} By varying the chain length of the polymer, to which the adduct radical is attached, the influence of chain length can also be monitored.

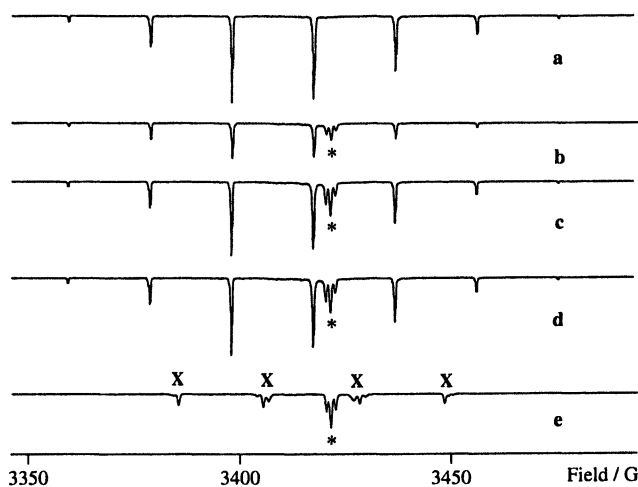


Figure 2. TR FT EPR of the four photoinitiators **7,3,4,6₄₈** (corresponding to **a-d**) and of **6₄₈** in the presence of 0.56 M tert-butyl acrylate (**e**). Asterisks correspond to (substituted) benzoyl radicals, "X" to the adduct radicals and EPR signals without a sign to ketyl radicals. (Reproduced with permission from Polym. Prepr. 2001, 42(2), 771–772. Copyright 2001 Zhiqiang Liu.)

As a preliminary result, the T_M (phase memory time) and T_1 (spin-lattice relaxation time) of the (substituted) benzoyl radicals and ketyl radicals were

measured. The data obtained from 4 different photoinitiators, in the order of increasing molecular weight, were compared (Table 1). The ketyl radical, which is not attached to any chains in all the four structures, is not expected to show any difference in T_M and T_I values in the experiment, unless other effects, such as viscosity, become significant. The insensitivity of T_M of the ketyl radical to different chain length on the benzoyl chain was confirmed by the experiments. Despite the large difference in the chain length in going from 7 to 6_{48} , no clear trend in the T_I of the (substituted) benzoyl radical was observed. In contrast, the T_M value of the (substituted) benzoyl radical increased significantly as the chain length on the para position of the benzoyl radical increased from small substituents in 3 and 4 to a 49-mer polystyrene chain in 6_{48} . Spectrum e in Figure 2 was obtained by photolyzing 6_{48} with tert-butyl acrylate in THF. The ESP signal of adduct radical could be observed while the signal from ketyl radical disappeared. This clearly demonstrated the use of ESP for the study of adduct radicals.

Table 1. T_M and T_I of the (substituted) benzoyl radicals and ketyl radicals generated from different structures, measured by TR-FT EPR.

	7	3	4	6_{48}
T_M (benzoyl) / ns	-	333(14)	361 (21)	456(12)
T_M (ketyl) / ns	878(23)	838(41)	816 (60)	879(34)
T_I (benzoyl) / ns	-	477(19)	492 (20)	521(12)
T_I (ketyl) / ns	981(13)	1025(45)	1051(20)	111 (25)

Source: Reproduced with permission from *Polym. Prepr.* **2001**, 42(2), 771–772. Copyright 2001 Zhiqiang Liu.

However, care must be exercised in the interpretation of the results due to their preliminary nature. It is also possible that the longer relaxation times in the 49-mer solution are due to increased viscosity. Investigations are underway in this research group to study oligomeric/polymeric photoinitiators of different chain length, effect of the addition of dead polymer to the solution to control viscosity, control experiments with small photoinitiators in dead polymer solution of comparable viscosity, the rate of addition of (substituted) benzoyl radicals to monomers and its dependence on the chain length and the presence of dead polymer, and the termination kinetics of oligomeric/polymeric radicals.

Conclusions

Preliminary results show that monodisperse polystyrene with photoinitiator groups as end labels can be prepared by the nitroxide mediated living free radical polymerization. T_M and T_I relaxation can be measured for the (substituted) benzoyl and ketyl radicals produced photochemically from the

initiators with different chain length. Electron spin polarization can also be used to study the macro adduct radicals, which are produced by the addition of photochemically generated radical to a vinyl monomer.

Acknowledgement

The authors thank the National Science Foundation (Grants CHE-98-12676 and CHE-01-10655) for support of this research. The work was supported in part by the MRSEC Program of the National Science Foundation under Award DMR-98-09687.

References

1. Fischer, H.; Radom, L. *Angew. Chem. Int. Ed.* **2001**, *40*, 1340.
2. a) Van Herk, A. M. *Macromol. Theory Simul.* **2000**, *9*, 433. b) Olaj, O. F.; Vana, P.; Zoder, M. *Macromolecules* **2002**, *35*, 1208.
3. Buback, M.; Busch, M.; Kowollik, C. *Macromol. Theory Simul.* **2000**, *9*, 442.
4. Doi, M.; Edwards, S. F. *The Theory of Polymer Dynamics*; Clarendon Press: Oxford, 1986.
5. Karatekin, E. Ph. D. Thesis. Columbia University, NY, 1999.
6. a) Hawker, C. J. *Acc. Chem. Res.* **1997**, *30*, 373. b) Hawker, C. J.; Barclay, G. G.; Orellana, A.; Dao, J.; Devonport, W. *Macromolecules* **1996**, *29*, 5245.
7. Patten, T. E.; Matyjaszewski, K. *Acc. Chem. Res.* **1999**, *32*, 895.
8. Kamachi, M. In *Controlled Radical Polymerization*; Matyjaszewski, K., Ed.; ACS Symposium Series No. 685, American Chemical Society: Washington, D.C. 1998, 145.
9. Kajiwara, A.; Konishi, Y.; Morishima, Y.; Schnabel, W.; Kuwata, K.; Kamachi, M. *Macromolecules* **1993**, *26*, 1656.
10. Ohara, K.; Murai, H.; Kuwata, K. *Bull. Chem. Soc. Jpn.* **1992**, *65*, 1672.
11. Karatekin, E.; O'Shaughnessy, B.; Turro, N. J. *Macromolecules* **1998**, *31*, 7992.
12. Karatekin, E.; Landis, M.; Lem, G.; O'Shaughnessy, B.; Turro, N. J. *Macromolecules*, **2001**, *34*, 8187.
13. Koptug, I. V.; Bossmann, S. H.; Turro, N. J. *J. Am. Chem. Soc.* **1996**, *118*, 1435.
14. Hu, S.; Malpert, J. H.; Yang, X.; Neckers, D. C. *Polymer* **2000**, *41*, 445.
15. Hassner, A.; Alexanian, V. *Tetrahedron Lett.* **1978**, *46*, 4475.
16. Turro, N. J.; Lem, G.; Zavarine, I. S. *Macromolecules* **2000**, *33*, 9782.
17. Jockusch, S.; Landis, M. S.; Freiermuth, B.; Turro, N. J. *Macromolecules* **2001**, *34*, 1619.

Chapter 10

Kinetics of Photopolymerization of Acrylate Coatings

Igor V. Khudyakov¹, Michael B. Purvis¹, and Nicholas J. Turro^{2,*}

¹Alcatel Telecommunications Cable, 2512 Penny Road,
Claremont, NC 28610

²Department of Chemistry, Columbia University, 3000 Broadway,
New York, NY 10027

Kinetics of free radical polymerization (FRP) of acrylate coatings was studied by photoDSC and real-time IR. Kinetic treatment of polymerization of acrylates in bulk and of acrylate coatings is critically analyzed. Experiments on postpolymerization of two commercial coatings ran by photoDSC allow an estimation of dimensionless ratio of parameters $2k_t/k_p$ at different conversions. It was determined that the ratio $2k_t/[k_p(1-\xi)]$, where ξ is acrylate conversion, weakly depends upon ξ within an experimental error of its determination. The latter conclusion is in accordance with a popular concept of “reaction diffusion” (Schultz, 1956) as a main mechanism of FRP of multifunctional acrylates. A different performance of the studied coatings under short UV-irradiation was discussed. An effective mode of cure of the coatings with a short exposure to light was suggested.

Different mono- and multifunctional acrylate monomers and acrylate oligomers (or macromonomers) are widely used in UV-curable coatings (1-3). UV-cure of acrylates is a free radical photopolymerization (FRP), and kinetics of this process is of academic and of practical interest. A natural intention of manufacturers of articles with polyacrylate coatings to increase productivity results in a demand to run polymerization faster and faster. That stimulates an additional interest to kinetics of photopolymerization.

Kinetic treatment of photopolymerization is usually started with the expression given in eq 1 for a chain free radical reaction with bimolecular chain termination in a quasi-stationary regime (1-3):

$$v_t (M/s) = \sqrt{w_{in}} \frac{k_p}{\sqrt{2k_t}} [M], \quad (1)$$

where v_t is a time- dependent rate of polymerization (disappearance of acrylate groups), k_p ($2k_t$) is a rate constant ($M^1.s^{-1}$) of chain propagation (bimolecular chain termination), $[M]$, is a concentration of a monomer (M), here a concentration of acrylate groups, w_{in} (M/s) is the rate of chain initiation. There are two other useful kinetic expressions for postpolymerization, i.e., polymerization after termination of initiation (4):

$$[M]_t / v_t - [M]_0 / v_0 = (2k_t / k_p) \tau \quad (2)$$

$$[M]_t = \frac{[M]_0}{(1 + 2k_t [R_n]_0 \tau)^{2k_t/k_p}} \quad (3)$$

Here a subscript "o" stands for the initial moment when postpolymerization is observed; $[R_n]_0$ is the initial concentration of macroradicals.

Eq 1 is successfully applied for such liquid-phase chain reactions as oxidation of hydrocarbons, kinetics of FRP of vinyl monomers in diluted solutions, and some others. It is known, that polymerization of acrylates in a bulk (or neat acrylates) is accompanied by dramatic changes of the reagents and the media (2,3,5,6). In the case of multifunctional acrylates a network is formed with pending non-reacted acrylates. Viscous liquid of monomers (oligomers) is quickly converted into polymer, into elastomer or even into a hard polyacrylate in the course of photopolymerization (3,5,6). Evidently a formal kinetic treatment (eqs 1-3) is applicable only for an initial stage of cure under such circumstances if at all. Very limited application of formal kinetics to photopolymerization compels researchers to more or less convincing qualitative explanation of changes in a system under irradiation. The following concepts are widely used in the current literature under discussion of photopolymerization: time/conversion/radical length – dependent k_p and $2k_t$; entanglements of macroradicals; cure is a photocrosslinking of a multifunctional monomer; cross-

link density M_c ; free volume; intramolecular chain transfer, backbiting mechanism; branching; cyclization; gel or Norrish-Trommsdorff-Smith effect (1939); autoacceleration, autodeceleration; reaction diffusion (Schultz, 1956); postpolymerization, dark polymerization; trapped macroradicals, linear termination; microgelation; vitrification; final conversion $\xi < 1.0$; polymerization below or above T_g of a forming polymer; 3D-network formation, network structure; volume shrinkage, volume relaxation; 3D-network formation, network structure; polychromatic or dispersive kinetics at high degrees of polymerization. Photopolymerization was successfully described in a number of cases as an autocatalytic reaction (3,6).

Certainly, the list above does not aim to be complete, and an order of concepts or notions is arbitrary. A detailed discussion of the concepts one can find in a current literature; we refer the reader to recent review articles (3,5) and to publications (2, 7-11). Eqs 1-3 do not account for a chain transfer to monomer (solvent, polymer), reaction with molecular oxygen and impurities. (The latter result in an appearance of induction period.) These phenomena can play a role in FRP of acrylates in a bulk and acrylate coatings as well.

There are a number of successful simulations of kinetics of polymerization of monofunctional vinyl monomers in a bulk; these works are mainly based on a dependence of diffusivity and/or reactivity at a high conversion ξ on the free volume of a system, cf., e.g. refs (7,8).

It is known that kinetics of reactions in solid polymers and in a solid state is controlled by other principles rather than kinetics in a liquid state, cf., e.g. refs (12,13). These principles are related to a polychromatic kinetics, where the same chemical species have a certain distribution of their reactivates, and these principles may be applied to polymerization at high ξ .

Conversion Dependent Parameters k_p and $2k_t$

The present status of polymer science and kinetics does not allow practically useful description kinetics of polymerization of multifunctional acrylates and acrylate coatings. At the same time, as it was mentioned above, there is a demand for analysis of rates and efficiency (final conversion) of cure. A coating is cured when $\xi = 1.0$. A possible approach to kinetics of polymerization of multifunctional acrylates and acrylate coatings is still to use eqs 1,2 with conversion-dependent parameters k_p and $2k_t(2,3,9,14,15)^a$. It is

^a A constant, which is in fact a variable, is an oxymoron. In such a cases a term "reaction coefficient" is sometimes used instead of "rate constant". However, "reaction coefficient" is often used in the sense of "rate constant" in particular in a gas phase kinetics (16). Certainly, one might use a term "specific reaction rate", but that term had been suggested by S. Arrhenius in the sense of "rate constant" already (17). In this paper we use term "parameter" k_p or $2k_t$.

hard to justify this approach. The possible logic can be that a free radical polymerization in a complex acrylate system still consists of three main steps: initiation, propagation and (bimolecular) termination, and one ascribes parameters w_{in} , k_p , and $2k_t$ to characterize these steps, respectively. During certain conversion k_p and $2k_t$ are (or are considered) more or less ξ independent. Both k_p and $2k_t$ decrease with ξ increase, usually a ratio $2k_t/k_p$ also decreases with ξ increase (2, 14, 15). One can expect that at $\xi \approx 1.0$, $2k_t$ and k_p become close to each other (2, 14, 15). Close values of parameters k_p and $2k_t$ mean that both propagation and termination are controlled by the same type of diffusion in a supposedly “highly crosslinked” media. Schultz (18) advanced a concept of “reaction diffusion” or “residual diffusion.” Reaction diffusion means that at a high degree of polymerization termination occurs not as a result of a mutual diffusion of macroradicals with a subsequent reaction, but radicals move as a result of propagation, and $2k_t \sim k_p[M]$ or $2k_t \approx R_D \cdot k_p [M]$ (3, 7, 8, 10, 18). The proportionality coefficient R_D has dimension of M^{-1} , and R_D is constant during the rest of polymerization or at least weakly depend upon ξ . In other words, one can expect at high ξ that a dimensionless value

$$2k_t / [k_p(1 - \xi)] \approx \text{const} \quad (4)$$

for a given system at a given temperature. For monofunctional vinyl monomers (so called “linear systems”) an onset of reaction diffusion control may be expected at $\xi > 0.8$, cf., e.g., ref. (10). For multifunctional monomers and acrylate coatings one can expect an onset of reaction diffusion at low ξ due to a formation of a polymer network (3).

Efforts were devoted to an experimental verification of reaction diffusion (eq 3) as a main mechanism of polymerization of multifunctional acrylates (3). It is tempting in photoDSC experiments to get individual values of k_p and $2k_t$ using eqs 1,2. However, eq 1 has an additional unknown value w_{in} . In order to get w_{in} one needs to estimate an absorbed light I_{abs} (einstein/M.s), to know quantum yield of formation of free radicals ϕ_{diss} and a cage escape value e .^b Eq 5 holds true for a case of photodissociation of an initiator into two reactive free radicals:

$$w_{in} = 2I_{abs} \phi_{diss} e = 2I_{abs} f, \quad (5)$$

^b We consider a rather common case of a photoinitiator, which is a benzoyl derivative, and it dissociates into a pair of reactive free radicals in a triplet state. Such photoinitiators are known under trade name of Irgacure[®] or Darocur[®].

where f is often called a photoinitiator efficiency. f is a cage escape e in the case of thermoinitiation. A value of ϕ_{dias} usually weakly depends upon media changes or upon ξ , whereas I_{abs} and e depend upon ξ . First, an initiator is usually consumed during photopolymerization. Second, in a viscous media triplet-singlet evolution of a photogenerated pair of radicals takes place, and e becomes less than 1.0. Experimental evidence for the last statement is an observation of magnetic field effect according to hyperfine coupling mechanism under photopolymerization of acrylates (19,20). The value of e or f changes with ξ (8,21-25). It was stated in a number of publications that f dramatically decreases with ξ increase (21-23). Thus, it is impossible to lump f or f^- with a rate parameter k_p or $2k_t$ as a coefficient because both f and a parameter k_p (or $2k_t$) change with ξ , cf. an approach in ref. 26.

We believe that one can verify eq 4 without estimating individual k_p and $2k_t$. In fact, experiments on postpolymerization allow computation of the ratio $2k_t/k_p$ (eq 2). One can use an average conversion corresponding to the obtained $2k_t/k_p$ and that way calculates ratio of eq 4. In the present work we have studied photopolymerization not of an individual acrylate monomer (oligomer) but of two model commercial coatings. The goal of the work was to verify eq 4 and to study a dependence of efficiency of cure upon UV-light intensity and duration of irradiation of coatings.

Experimental Section

Materials

We have used commercially available UV-curable acrylate coatings for optical fiber of DSM Company (Elgin, IL), namely 0D1-67 (primary "soft" coating) and 0D2-55 (secondary "hard" coating). Coatings were used as received. Composition of coatings includes difunctional and monofunctional acrylates and photoinitiators. We name the coatings "primary" and "secondary" below. Glass transition temperature is -5 and 63 °C for the primary and for the secondary coating, respectively (27). Cured primary coating is an elastomer.

PhotoDSC Experiments

We used Perkin-Elmer photoDSC DPA-7, a regime of fast sample rate. Electronic system of a device practically immediately respond to a heat flow, time resolution is ca. 50 ms. The full light of Osram Hg 150 W lamp was used as the light source. Experiments with DSC device were done in a usual way (3,14,15). A goal of experiments was to get a dimensionless ratio $2k_t/k_p$ at

different ξ . It was done exactly the same way as described in ref. (14,15). At least five experiments on prolong irradiation (minutes) were performed with one coating under the same conditions, and the average values of total heat released Q_{tot} , J/g were obtained. Prolong irradiation was used in order to measure the total heat Q_0 (joules) which is directly proportional to the initial concentration of acrylates $[M]_0$ (3, 14,15). PhotoDSC trace presents a rate of polymerization $\nu = dQ(t)/dt$ (watt), which is directly proportional to a rate of polymerization $d[M]/dt$. Integration of photoDSC trace allows to get a kinetic curve $Q = Q(t)$. A calculated ratio of $Q(t)/[dQ(t)/dt] = [M]_0/\nu_t$ (second), cf. eq 2. A slope of a plot $[M]_0/\nu_t$ vs. t for postpolymerization is a dimensionless ratio $2k_t/k_p$. Ascending portions of a curve $Q(t)/[dQ(t)/dt]$ vs. t were fit to a linear law. Observed under a pulsed irradiation a dependence $Q = Q(t)$ was a descending stepped curve. Duration of each pulse was $\tau_{\text{irr}} = 0.6$ s. Polymerization initiated by such a pulse lasts more than 10 s, and it is in fact postpolymerization. A small amount of heat evolved during a short pulse can be safely ignored in calculations, and time is a dark time. We measured each middle point between each two steps on a curve $Q = Q(t)$ and we calculated ξ which corresponded to the middle point. These middle ξ -values correspond to each obtained in postpolymerization experiment $2k_t/k_p$.

Light intensity (radiant excitation) was measured as described in ref. (15). We used IgorPro software for an analysis of kinetic data obtained in this work.

Real Time IR Experiments

RT FTIR experiments were performed with Nicolet 870 spectrometer of Perkin Elmer (ATR regime, rapid scan). A disappearance of twisting vibration of acrylate group at *ca.* 810 cm^{-1} was monitored. A spectral resolution was 8 cm^{-1} which gives 46 spectra (points in a kinetic curve) per 1s, whereas DSC samples 20 points per 1 s. Determination error in kinetic RT IR experiments is essentially larger than that in DSC experiments. We covered a diamond crystal with coating with a thickness of ~ 0.4 mm. Samples were flushed with nitrogen before and during irradiation. All experiments with DSC (cf. above) and IR were performed at 40°C . We used the focused with a quartz lens full light of Lightingcure 200 UV light source (Hamamatsu). Light came through an Oriel shutter 7940. Light source allows the variation of light intensity, and a range of intensities used in this work was 3 to 100 mW/cm^2 . In order to irradiate a sample for a short time by one or by several light pulses a shutter of UV-source or an Oriel shutter was used. The shutter driver allows pulses with a minimum duration of a pulse of 2 ms and a minimum duration between pulses $\Delta \geq 1$ ms. Start up accessory triggered simultaneously IR and the shutter. Kinetic IR traces obtained and presented in this work demonstrate a good reproducibility despite a moderate S/N ratio.

PhotoDSC Results

Irradiation of coatings during several min result in a total heat $Q_{\text{tot}} = 150 \pm 10$ J/g for the primary and 200 ± 10 J/g for the secondary coating. These values were used in the calculation of Q_0 , J for these two coatings, cf. the Experimental section.

Figures 1,2 present experimental data obtained during pulsed irradiation of coatings.

Data of Figures 1,2 allowed to get estimations of $2k_t/k_p$ (cf. the Experimental section). These values $2k_t/k_p$ decrease with conversion as expected (3,4,14,15). Figure 3 presents a dependence of the calculated ratio

$2k_t/[k_p(1-\xi)]$ vs. ξ . It follows from the data of Figure 3 that the measured ratio does not vary more than several times during polymerization. We may conclude, that eq 4 is more or less valid, and it processes a certain predictive power.

Experiments with RT IR

Polymerization and Postpolymerization

Irradiation of coatings with pulses (10-200 ms) of light of high intensity ($50-100$ mW/cm²) allowed us to monitor postpolymerization by RT IR till a partial or complete cure. Short irradiation can result in a negligible or in a very low conversion during the time of irradiation τ_{irr} and to a large final conversion up till $\xi = 1.0$. Postpolymerization plays an important role in cure of coatings. Evidently, the higher intensity I , the shorter τ_{irr} in order to cure coatings ($\xi = 1.0$). We have noticed that in order to cure the primary coating it is necessary to have $E = I \cdot \tau_{\text{irr}} = 5-10$ mJ/cm², whereas in order to cure the secondary coating the same value is $20-25$ mJ/cm². An increase of light intensity resulted in acceleration of cure.

Initiation of Polymerization: One Long or Two Short Pulses?

In practice the cure of coatings, especially coatings for optical fiber, takes place not by one short irradiation but by two or more short irradiation. An interesting and an important for practice question is: Which is a better way to cure coatings: by two short pulses with one or another delay Δ between them or by one long pulse with a duration equal to sum of duration of two short pulses?

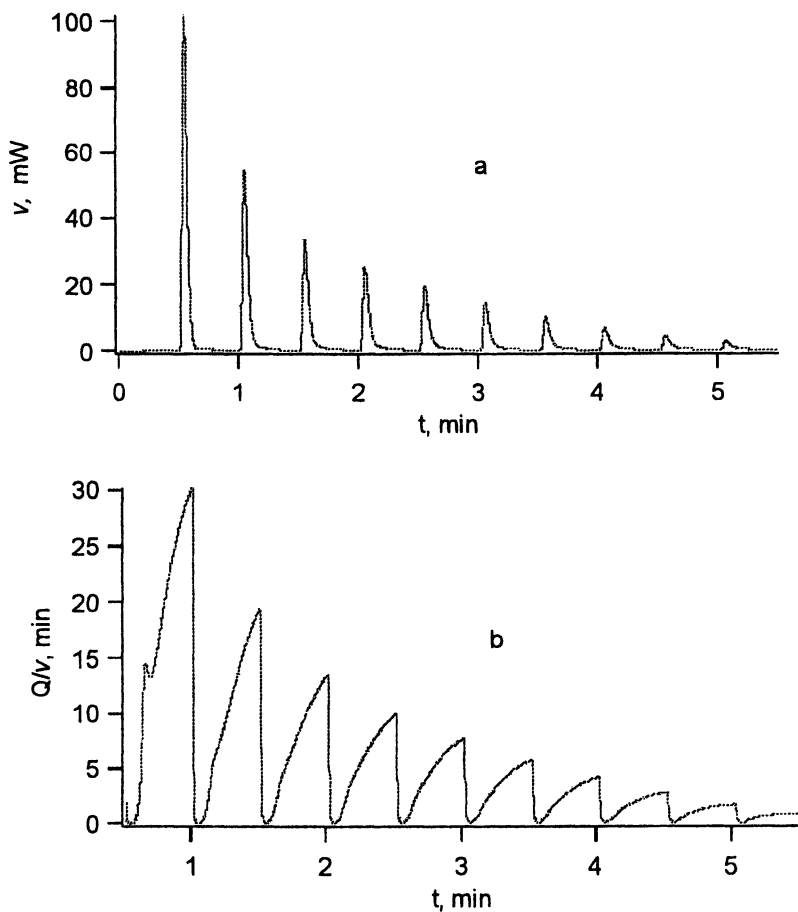


Figure 1. PhotoDSC trace obtained during polymerization of the primary coating with a light of intensity 10 mW/cm^2 (a); calculated ratio Q/v vs. time of polymerization (b).

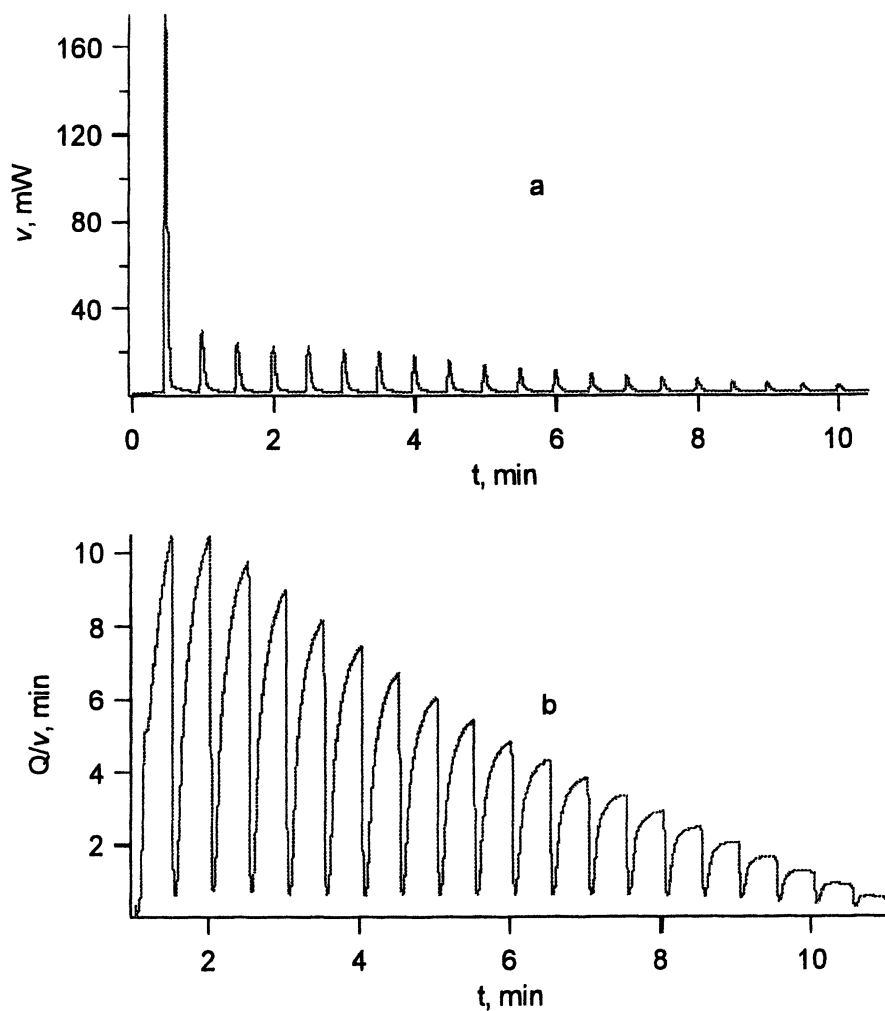


Figure 2. PhotoDSC trace obtained during polymerization of the secondary coating with a light of intensity 10 mW/cm^2 (a); calculated ratio Q/v vs. time of polymerization (b).

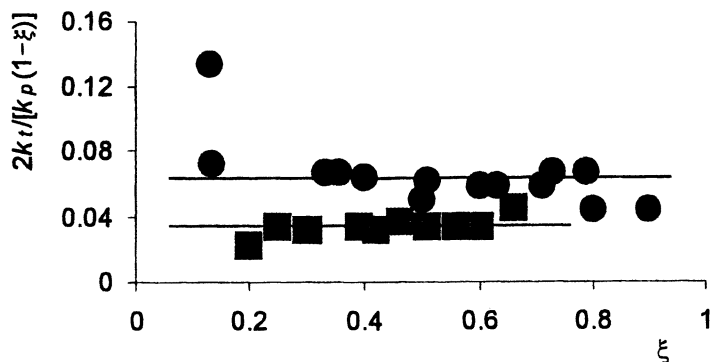


Figure 3. Dependencies of $2k_t/[k_p(1-\xi)]$ vs. ξ for the primary coating (circles) and for the secondary coating (squares).

This way the total exposure of coating to light is the same. We will try to get an answer below.

We use a symbol ξ_1 to define a conversion during the first pulse, ξ_Δ stands for an additional conversion during postpolymerization between the two irradiation, ξ_2 stands for an additional conversion during the second irradiation, ξ_{2p} stands for an additional conversion during postpolymerization till the termination of a reaction, ξ_{12} stands for a conversion during irradiation with one long pulse, ξ_{12p} stands for an additional conversion during postpolymerization after a long pulse till the termination of a reaction.

Figure 4 shows a typical relative position of kinetic traces pertinent to polymerization by one pulse and by two pulses. Experiments with primary coating led to an expected result: two pulses lead to higher conversion than one due to an additional conversion (ξ_Δ) by postpolymerization between two pulses:

$$\xi_1 + \xi_\Delta + \xi_2 + \xi_{p2} \geq \xi_{12} + \xi_{12p} \quad (6)$$

We have found in experiments with primary coatings that $\xi_1 \approx \xi_2$ and $\xi_1 + \xi_2 \approx \xi_{12}$. Further, $\xi_\Delta \approx \xi_{p2} \approx \xi_{12p}$, and eq 6 can be simplified as:

$$\xi_\Delta + \xi_{p2} \geq \xi_{12p} \quad (6a)$$

Thus, a higher ξ can be achieved in the course of two irradiation pulses rather than by one. *Two postpolymerization is better than one, and the larger is Δ , the larger is a beneficial effect of two irradiation.* We have noticed a difference in two ways of irradiation delay between pulses $\Delta > 150$ ms.

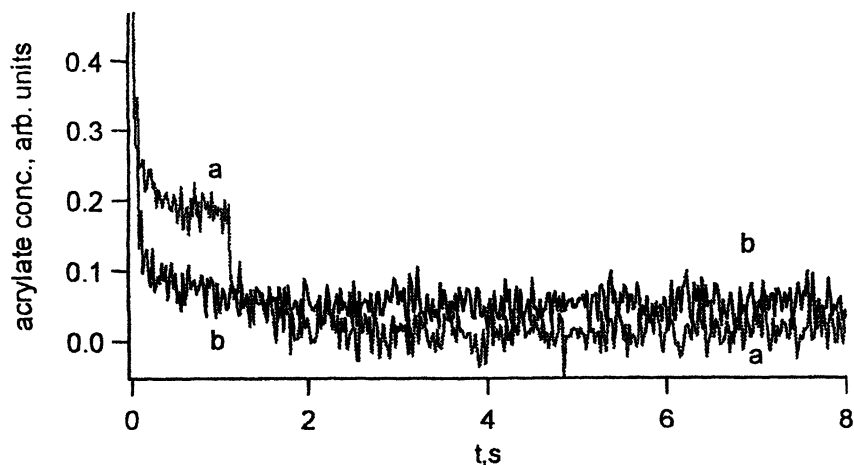


Figure 4. Kinetics of cure of the primary coating under irradiation during: a) two times by 50 ms with a delay between pulses of 1s; b) a pulse of 100 ms (330 mW/cm²). Initial absorption in these experiments is ~0.45.

On the contrary, for the secondary coating we have found that:

$$\xi_1 + \xi_{\Delta} + \xi_2 + \xi_{p2} \leq \xi_{12} + \xi_{12p} \quad (7)$$

cf. Figure 5.^c The second pulse in experiments of Figures 4,5 starts after the same conversion $\xi_1 + \xi_{\Delta} \approx 0.6$. For secondary coating $\xi_2 \ll \xi_1$, and at relatively large Δ of seconds, $\xi_2 \approx 0$. Further, $\xi_{12} \approx 2\xi_1$, $\xi_{\Delta} \approx \xi_{12p}$, and eq 7 can be simplified as:

$$\xi_{p2} \leq \xi_1 \quad (7a)$$

An experimental fulfillment of eqs 7,7a is not evident upfront. We have noticed a difference in two ways of irradiation delay between pulses $\Delta > 250$ ms. As in experiments with the primary coating, the larger is Δ the larger is a difference in a rate of cure and in a conversion. We conclude that *for the secondary coating there are no benefits of irradiation in two pulses: polymerization occurs slower and there is no gain in a conversion.*

^cA study of "tails" of kinetic curves obtained under different conditions demonstrated that ξ after irradiation with one long pulse is larger or equal within an experimental error to ξ achieved after an initiation by two pulses.

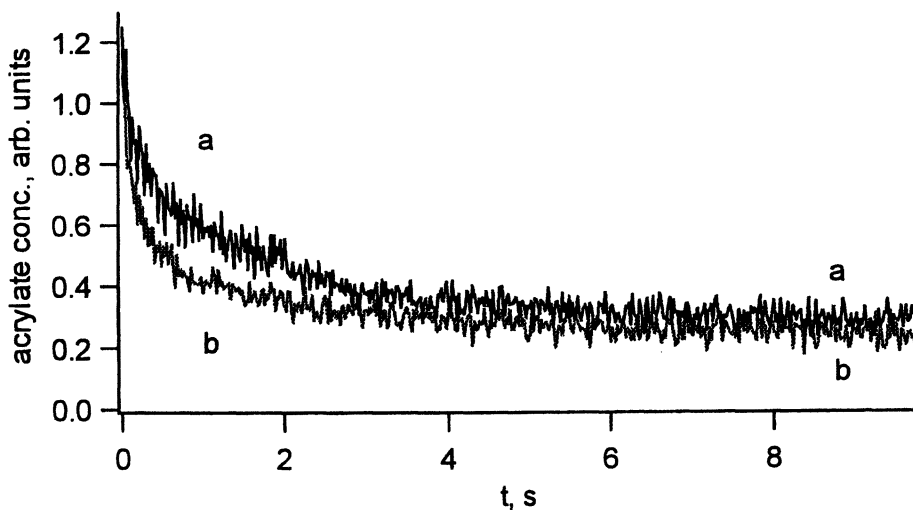


Figure 5. Kinetics of cure of the secondary coating under irradiation during: a) two times by 50 ms with a delay between pulses of 2 s; b) a pulse of 100 ms (330 mW/cm^2). Initial absorption in these experiments is ~ 1.2 .

Comparison of Figures 1 and 2 demonstrate, that the secondary coating yields much less in a successive irradiation than the primary. A difference in behavior of two coatings can be understood, if we take into account that the temperature of cure is essentially higher than T_g of primary coating and it is lower than T_g of the secondary coating, cf. the Experimental section. Partial polymerization of primary and a formation of movable polymer chains does not much prevent further polymerization, whereas a formation of a polymer chains with a reduced molecular movement below T_g in the secondary coating essentially prevents further polymerization. That is why the secondary coating is less prone to an additional polymerization under high conversion. A difference in a performance of the primary and secondary coatings becomes evidently more profound at high conversion.

Conclusions

We have briefly discussed problems related to polymerization of monomers/oligomers in the bulk, and we have studied kinetics of cure of two model coatings with photoDSC and real-time FTIR. These are multifunctional acrylate coatings (“primary” and “secondary”) with essentially different properties. The primary coating has a lower concentration of acrylates, and are composed of oligomer(s) of higher MW, and much lower T_g than the secondary

coating. The main goal of this work was to verify the applicability of reaction diffusion concepts to cure of acrylate coatings without resolution to individual parameters $2k_t$ and k_p . We may conclude that reaction diffusion concept is applicable to photopolymerization of multifunctional acrylate and acrylate coatings (Figure 3). One can make semi-quantitative prediction of kinetics of postpolymerization at different ξ knowing an average value of $2k_t/[k_p(1-\xi)]$. An onset of reaction diffusion control occurs at the initial stage of polymerization of the studied coatings, i.e., at $\xi \geq 0.1-0.2$.

It is possible to ascribe a certain energy of light (E , mJ/cm^2) directed to a surface of a thin coating film required for its cure. In the case of short irradiation (10-200 ms in our experimental conditions) a conversion during irradiation can be very low, and the rest of cure up till $\xi = 1.0$ occurs as postpolymerization.

We have studied kinetics of cure of coatings by two short pulses and by one long pulse. In our experiments the primary coating was cured at a temperature higher than T_g , and cure by two pulses is preferable, and it results in a larger ξ than a cure by one pulse. In experiments with secondary coating ran at temperature below T_g we did not observe any benefits of cure in two pulses.

Acknowledgments

The author at Columbia University is grateful to NSF for financial support of this work (grant NSF-CHE 98-12676). This work was supported in part by the MRSEC Program of the National Science Foundation under award No. DMR-9809687.

References

1. Fouassier, J.-P. *Photoinitiation, Photopolymerization, Photocuring: Fundamentals and Applications*; Hanser: Munich, 1995.
2. Decker, C. *Polym. Int.* **1998**, *45*, 133.
3. Andrzejewska, E. *Prog. Polym. Sci.*, **2001**, *26*, 605.
4. Tryson, G.R.; Shultz, A.R. *J. Polym. Sci., Polym. Phys. Ed.*, **1979**, *17*, 2059.
5. Dušek, K., *Polymer Gels and Networks*, **1996**, *4*, 383.
6. Khudyakov, I. V.; Legg, J.C.; Purvis, M. B.; Overton, B. J. *Ind. Eng. Chem. Res.*, **1999**, *38*, 3353.
7. Zhu, S.; Hamielec, A. *Makromol. Chem., Macromol. Symp.* **1992**, *63*, 135.
8. Zhu, S.; Hamielec, A. *Macromol.* **1989**, *22*, 3093.
9. Beuermann, S.; Buback, M. In *Controlled Radical Polymerization*; Matyjaszewski, K., Ed.; ACS Symposium Series **685**; American Chemical Society: Washington, DC, 1998, pp 84-103.
10. Litvinenko, G.I.; Kaminsky, V.A. *Prog. Reaction Kinetics*, **1994**, *19*, 139.

11. Decker, C. *Europ. Polym. J.* **1995**, *31*, 1155.
12. Emanuel, N.M.; Buchachenko, A.L. *Chemical Physics of Polymer Degradation and Stabilization*; VNU Science Press: Utrecht, The Netherlands, 1987.
13. Caspar, J.V.; Khudyakov, I.V.; Turro, N.J.; Weed, G.C. *Macromol.* **1995**, *28*, 636.
14. Williams, R. M.; Khudyakov, I. V.; Purvis, M. B.; Overton, B.J; Turro, N. J. *J. Phys. Chem. B*, **2000**, *104*, 10437.
15. Khudyakov, I. V. Fox, W.S.; Purvis, M. B. *Ind. Eng. Chem. Res.*, **2001**, *40*, 3092.
16. Pilling, M.J.; Seakins, P.W. *Reaction Kinetics*; Oxford University Press: Oxford, 1997.
17. Logan, S.R. *Fundamentals of Chemical Kinetics*; Longman: Harlow Essex, 1998, cf. p. 4.
18. Schultz, G.V. *Z. Phys. Chem. (Munich)* **1956**, *8*, 290.
19. Khudyakov, I. V.; Legg, J.C.; Purvis, M. B.; Overton, B. J. *SPIE Proc.*, **1999**, *3848*, 151.
20. Khudyakov, I.V.; Nergis, A.; Jockusch, S.; Turro, N.J. *Macromol. Symposia Proc.*, in press.
21. Faldi, A.; Tirrell, M.; Lodge, T.P.; von Meerwall, E. *Macromol.* **1994**, *27*, 4184.
22. Russell, G.T.; Napper, D.H.; Gilbert, R.G. *Macromol.* **1988**, *21*, 2141.
23. Wen, M.; McCormick, A.V. *Macromol.* **2000**, *33*, 9247.
24. Vedeneev, A.A.; Lavrik, N.L.; Khudyakov, I.V. *Izvestia Akad. Nauk. Ser. Khim.* **1992**, 2053.
25. Vedeneev, A.A.; Lavrik, N.L.; Khudyakov, I.V. *Izvestia Akad. Nauk. Ser. Khim.* **1992**, 2059.
26. Anseth, K.S.; Kline, L.M.; Walker, T.A.; Anderson, K.J.; Bowman, C.N. *Macromol.* **1995**, *28*, 2491.
27. Ferguson, H.; Cooper, T., unpublished results, 2001.

Chapter 11

Effect of Preorganization Due to Hydrogen Bonding on the Rate of Photoinitiated Acrylate Polymerization

Johan F. G. A. Jansen*, Aylvin A. Dias, Marko Dorschu,
and Betty Coussens

DSM Research, P.O. Box 18, 6160 MD Geleen, The Netherlands

*Corresponding author: email: johan-fga.jansen@dsm.com

The maximum rate of photo-initiated polymerization of acrylates is strongly influenced by the ability to form hydrogen bonds. In cases where the hydrogen bonds are in the vicinity of the acrylate moiety higher maximum rates of photo-initiated polymerization are observed. Pre-organization via hydrogen bonding is the mechanism by which this rate enhancement occurs as further proven by the following observations. There is a critical distance beyond which the propensity to form hydrogen bonds does not result in a rate enhancement. Temperature dependent RT-FTIR profiling demonstrated that in cases where hydrogen bonds are present anti-Arrhenius behavior is found. An increased amount of iso-tactic triads were found in the polyacrylates based on monomers capable of hydrogen bonding.

Introduction

Photo-initiated polymerization of methacrylates and acrylates, being one of the most efficient processes for the rapid production of polymeric materials with well-defined properties, is widely employed especially in the coatings area focused on decorative and protective coatings, stereolithography, dental restorative fillers and the preparation of contact lenses (1,2).

In terms of improving the reactivity of the whole system, generally the photo-initiator (or mixtures thereof) has been adapted for obtaining higher reaction rates, which is by far the easiest method. The kinetics of the photo-initiated acrylate polymerization, which is a bulk polymerization has received less attention. Although photo-DSC (3) was already employed for the first time in 1979 by Tryson and Schultz in order to monitor in real-time acrylate conversions, based on their enthalpy, true real-time kinetic data could only be obtained after the pioneering work of C. Decker who developed Real-Time InfraRed spectroscopy (RT-IR) in which the assumed acrylate enthalpy was eliminated (4).

Currently both techniques are well established and employed frequently (5) although new techniques are also emerging. Moreover, based on these kinetic results a wide variety of models has evolved (6) for instance bi-molecular termination combined with reaction diffusion control (7), mono-molecular termination in the glassy region (8), primary radical termination (9), chain length dependent termination (10), random-walk for heterogeneity (11), and primary cyclization (12) have all been proposed in order to describe cure profiles and network topology. However, none of the proposed models is capable of fully describing the kinetic profiles.

The elucidation of different acrylate reactivities especially in relation to their molecular structure, however, received almost no attention. Andrzejewska et al. reported a hetero-atom effect (13). Guymon et al. found rate enhancements in liquid crystalline phases (14). Whereas Decker et al reported about new acrylates with a very high intrinsic reactivity (15). Although no explanation was given on a molecular level for the observed high intrinsic reactivities, the work of C. Decker triggered our research to evaluate different acrylates reactivities in terms of hydrogen bonding capability, being one of natures dominating organizational tools. The results are presented in this paper.

Results and Discussion

In Figure 1 some of the fast reacting monomers initially prepared by C. Decker are shown.

Although we can offer no explanation for the high reactivity of the oxazolidone and cyclic carbonate functional acrylate yet, the urethane ethyl acrylates suggest however, that the high reactivity of the urethanes could be attributed to hydrogen bonding. In order to test this concept, we performed some

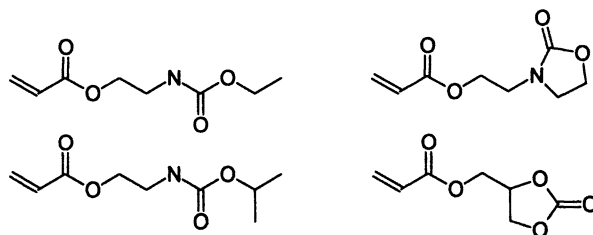


Figure 1. Some of the reactive monomers prepared by C. Decker

initial work with undecyl amide N-ethyl-acrylate, being capable of hydrogen bonding and pentyl amide N-methyl N-ethyl-acrylate as non hydrogen bonding control compound. Employing Real Time Fourier Transform Infra Red spectroscopy (RT-FTIR) we determined the maximum rate of polymerization of these compounds (16). In good agreement with our expectations, based on the requirement of hydrogen bonding for high rates of polymerization, were the maximum rates of polymerization (undecyl amide N-ethyl-acrylate 9 mol/l sec; pentyl amide N-methyl N-ethyl-acrylate 1.9 mol/l sec). These encouraging initial results triggered us to systematically vary the nature of the moiety capable of hydrogen bonding i.e. amides (17), urethane, "inverted urethanes" and ureas and determine the consequences on reactivity. Analogous esters and carbonates were prepared and evaluated as control compounds which possess no capability for hydrogen bonding. The synthesis of these compounds is depicted in Figure 2.

Although the preparation of the amide ethyl-acrylates via the oxazoline route is very facile, purification of the end products however is very difficult due to the fact that during the synthesis approximately 1% of the corresponding ester ethyl-acrylamides are formed. As we were unable to remove this by product by either chromatography or distillation we abandoned this facile synthetic methodology. In order to obtain the compounds with purities exceeding 99% (based on GC) we performed all the synthesis via the acid chloride, chloroformate or isocyanate routes. All the syntheses gave the crude compounds in yields between 70 and 90%. Most of the urea ethyl acrylates (except ethyl urea ethyl-acrylate) were solids at room temperature. As a consequence, the rates of polymerization of the ureas were determined at 50°C when all the samples were in their liquid state. In Table I the maximum rates of polymerization are shown.

It is evident from Table I that all the monomers capable of forming hydrogen bonds exhibit 3-6 times higher polymerization rates when compared with their non-hydrogen bonding analogues, demonstrating that hydrogen bonding plays an important role in these polymerizations. The explanation for these higher rates of polymerization is that the hydrogen bonding of the acrylates facilitates a kind of pre-organization that forces the acrylate double bonds in close vicinity of each other, and consequently enhances the rate of

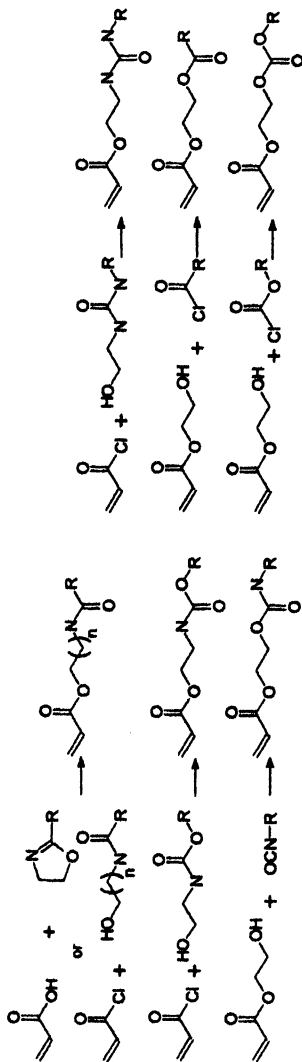


Figure 2. Synthetic routes to various acrylates

Table I. Maximum Rates (mol/l sec) of Photo-Initiated Polymerization of Monomers Capable of Hydrogen Bonding and their Counterparts, Measured by RT-FTIR using a Transflection Cell at Room-Temperature Employing a Light Intensity of 135mW/cm² (medium pressure mercury lamp)

$R=$	C_2H_5	C_4H_9	C_6H_{13}	C_8H_{17}
	23.5	19.1	13.6	9.3
	16.1	9.7	5	4.5
	15.9	15.2	14.5	14.0
	25.2	-	-	-
	22.2*	18.2*	18.0*	17.9*
	4.4	3.8	3.5	3.2
	6.5	5.7	5.5	5.4

*Measured at 50°C due to their melting points

polymerization. However, an explanation based on pre-organisation via hydrogen bonding has several consequences:

- There should be a critical distance between the acrylate group and the hydrogen bonding moiety beyond which there is no effect on the cure speed.
- In contrast to normal Arrhenius type behavior, lower maximum rates of polymerization should be found at elevated temperatures.
- The tacticity of the polymer formed should be altered as the monomers are organized towards each other.

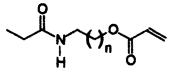
The effect on tacticity is also the final discriminator between inter- and intra-molecular hydrogen bonding. Only when inter-molecular hydrogen bonding is present, an effect on tacticity can be expected (18).

Effect of Bridge Length

A consequence of pre-organization is that when the hydrogen bonding moiety is put at a larger distance from the reactive acrylate group, there will be a critical distance beyond which the pre-organization, due to the hydrogen bonding will have little or no effect on the rate of polymerization. In order to evaluate this effect, we prepared several ethyl amide N-alkyl-acrylates in which the alkyl chain was varied in length i.e. from ethyl to hexyl. The results of the RT-FTIR study are shown in Table II.

The rates of photo-initiated polymerization of these ethyl amid N-alkyl-acrylates are gradually reduced going from ethyl to pentyl. The ethyl amide N-hexyl-acrylate exhibits a rate of polymerization similar to the monomers not capable of forming hydrogen bonds i.e. ester and carbonate acrylates, re-enforcing the pre-organization via hydrogen bonding theory.

Table II: Effect of Bridge Length on the Maximum Rates (mol/l sec) of Photo-Initiated Polymerization of Monomers Capable of Hydrogen Bonding, as Measured by RT-FTIR

$n=$	1	2	3	4	5
	23.5	21.8	18.5	16.8	5.0

Effect of Temperature

Generally, if reactions are performed at higher temperatures, higher rates are observed, this is the so called Arrhenius behavior. However, if the high rate of polymerization is mainly due to pre-organization via hydrogen bonding, the rate will be reduced at higher temperatures, as it is well known that the level of hydrogen bonding is reduced at elevated temperatures. Therefore, we studied the cure behavior of undecyl amide N-ethyl-acrylate, at elevated temperatures. We chose this monomer in order to avoid any problems related to volatility. The results are shown in Table 3 and Figure III.

Table III: Effect of Temperature on the Polymerization rate of Undecyl amide N-ethyl-acrylate

<i>Temp</i> ^o C	30	40	50	60	70	80	90
<i>Rate</i>	9	9.6	9.5	9	8.2	7.3	6.0

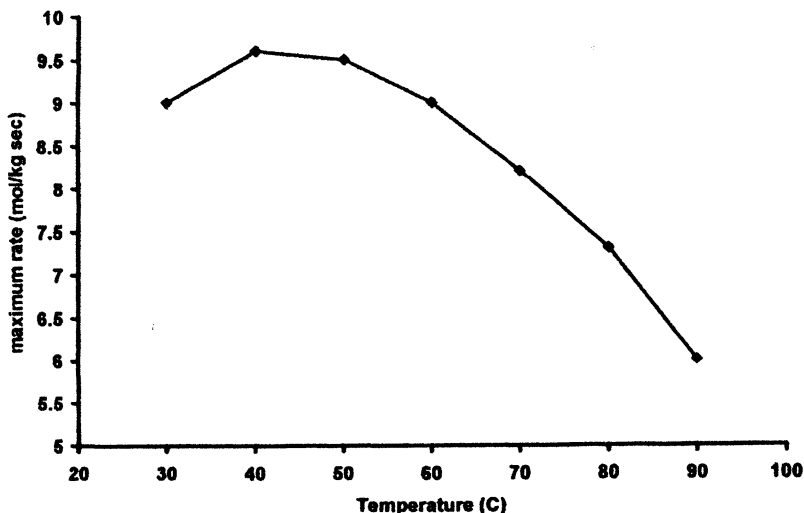


Figure 3. Effect of temperature on the maximum polymerization rate of undecyl amide *N*-ethyl-acrylate

As we are employing RT-FTIR we can monitor the amide shifts simultaneously. The amide II bond shifts from 1546 cm^{-1} at 30°C to 1539 cm^{-1} at 90°C and the N-H shifts from 3312 cm^{-1} at 30°C to 3325 cm^{-1} at 90°C . Both shifts are indicative of the fact that the amount of hydrogen bonding is reduced at higher temperatures. Both shifts are shown in figure 4.

The reduction in polymerization rate, due to the elevated temperature, especially combined with the observed IR-shifts, provides strong additional evidence for the validity of the pre-organization via hydrogen bonding theory. It should be noted that in case of urethanes, we were only able to observe a shift towards non-hydrogen bonding at higher temperatures in the urethane N-H. Unfortunately, additional evidence based on other urethane absorptions could not be obtained due to overlapping signals.

We also did not see any shift in the acrylate carbonyl, which would be the case if the hydrogen bonding was an intra-molecular process towards the acrylate carbonyl. However, as this shift could be obscured by non-bonding acrylate carbonyls this result only suggest that the hydrogen bonding occurs in an inter-molecular fashion.

Effect on Tacticity

Finally one can wonder about the impact of such a pre-organization phenomena on the tacticity of the resultant polymer formed. Assuming that the

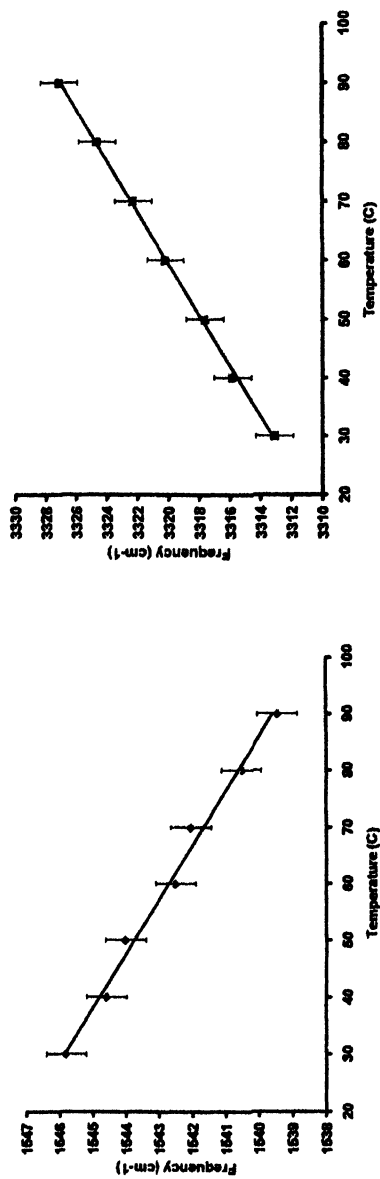


Figure 4. Effect of temperature on the IR shifts of the amid moiety

complete polymerization would occur via an organized structure, mainly isotactic polyacrylate would be formed. The formation of such an iso-tactic polyacrylate is depicted in figure 5. Whereas, generally in the case of polyacrylates prepared radically, predominantly syndio-tactic material would be produced.

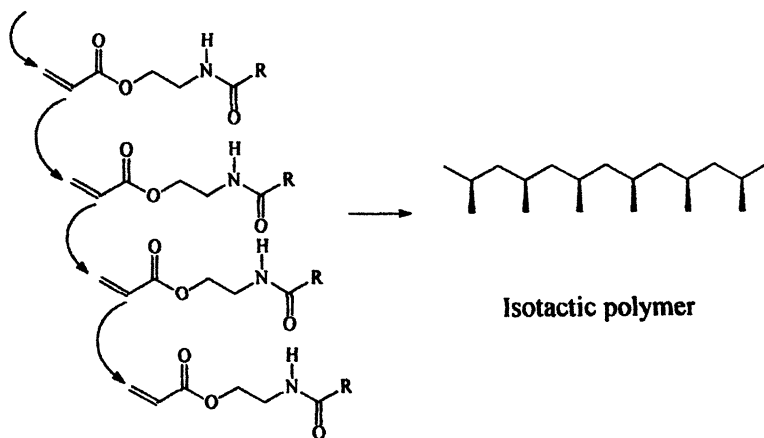


Figure 5. Proposed mechanism by which pre-organisation via hydrogen bonding could lead to the formation of isotactic polymer.

Although, it is very unlikely that in the case of pre-organization via hydrogen bonding all monomers would be organized, one could expect an enhancement in the amount of isotactic polymer formed when pre-organisation plays a dominant role. In general the tacticity can be better determined if methacrylates are used. Therefore, we performed these experiments with undecyl amid N-ethyl-methacrylate as monomer capable of hydrogen bonding, pentyl amid N-methyl N-ethyl-methacrylate as control compound and lauryl methacrylate as reference sample. The results are shown in Table IV.

The tacticity of poly-(lauryl methacrylate) produced via photo-initiated polymerization is identical to poly-(lauryl methacrylate) prepared with thermal initiators like AIBN (19). The tacticity of poly-(pentyl amide N-methyl N-ethyl methacrylate) is the same as for poly-(lauryl methacrylate) (within the errors of the measurements). This indicates that an amide moiety as such does not alter the tacticity of the polymer. Although in the case of poly-(undecyl amide N-ethyl methacrylate) no pure isotactic polymer is formed, the enhancement of the amount of isotactic triads is significant. This strongly suggests that pre-organization via hydrogen bonding plays a role in how the acrylates are oriented towards each other during the polymerization. Moreover, this offers the evidence that the hydrogen bonding is indeed occurring in an inter-molecular fashion.

Table IV. Tacticity Data based on ^{13}C -NMR of Poly-Methacrylates formed by Photo-Initiated Polymerization

<i>Tacticity</i>	<i>Undecyl amide N-ethyl-methacrylate</i>	<i>pentyl amide N-methyl N-ethyl-methacrylate</i>	<i>lauryl methacrylate</i>
Syndio-tactic (%)	58	65	65
a-tactic (%)	28	33	31
Iso-tactic (%)	14	2	4

Conclusion

In conclusion we have demonstrated that the maximum rate of photo-initiated polymerization of acrylates is strongly influenced by the ability to form hydrogen bonds. Pre-organization via hydrogen bonding is the proposed mechanism on a molecular level via which this rate enhancement occurs as further proven by the following findings. There is a critical distance above which the ability to form hydrogen bonds does not result in a rate enhancement. So the mere presence of a hydrogen bonding moiety in the molecule is not sufficient. Temperature dependent RT-FTIR profiling demonstrated that in case hydrogen bonds are present anti-Arrhenius behavior is found i.e. lower rates at higher temperatures in contrast to the observed and expected Arrhenius behavior of lauryl acrylate. And finally an increased amount of isotactic triads are found in the polyacrylates based on monomers capable of hydrogen bonding compared to polyacrylates in which the monomers are not capable of hydrogen bonding.

Acknowledgement

The management of DSM Research, DSM Coating Resins and DSM Desotech are kindly acknowledged for their permission to publish this work

Experimental section

Most of the syntheses are rather straight-forward organic procedures, therefore, only one example is given. All the chemicals are used as obtained from Aldrich or other sources, except THF, which was distilled over Na/benzophenone, and pyridine, which was freshly distilled prior to use. The

RT-FTIR setup is described in detail elsewhere (16). A medium pressure mercury lamp was used as source of irradiation resulting in an intensity of 135 mW/cm² at the sample, as measured with a Solatel Sola-scope 1. It should be noted that in contrast to most published RT-FTIR measurements the samples were not measured as laminates but under an inert atmosphere. Nitrogen was purged for at least 5 min before any RT-FTIR measurement. All RT-FTIR measurements were performed in triplicate including one with a purge time of 15 minutes. As the results were identical to those obtained with a 5 min purge, it was concluded that 5 min purging was sufficient for removing the oxygen. All RT-FTIR measurements were performed employing 1 weight % Irgacure 184 (2-hydroxy-cyclohexyl phenyl ketone, HCPK, Ciba) as the photo-initiator. Curing the methacrylate samples for the determination of the tacticity was performed under nitrogen employing a Fusion curing rig equipped with F600 D bulbs. The tacticity was determined by ¹³C-NMR using a Bruker ARX 400 in DMSO-d₆ at 80°C

Synthesis of ethyl-O-urethane-N-ethyl acrylate:

To a stirred cooled solution at 0 °C, purged with dry air, of 14.22g (107 mmol) N-2-hydroxy ethyl-O-ethyl urethane and 8.45g (107 mmol) pyridine in 300ml THF, was slowly added 10.1g (112 mmol, 1.05 eq) acryloyl chloride whilst maintaining the temperature below 5 °C. After the addition was complete the reaction mixture was allowed to warm slowly to room temperature and was stirred at room temperature for an additional 6 hours.

Work-up: The pyridinium salt was filtered off, followed by a quick wash with 20ml water, 0.1N hydrochloric acid, saturated NaHCO₃ solution and brine (in case the separation was tedious diethyl ether was added). After drying over Na₂SO₄. The THF was removed in vacuo yielding 6.1 g (33mmol, 31 %) ethyl-O-urethane-N-ethyl acrylate as crude product with a purity based on NMR of 97%.

Preferred alternative work-up: The pyridinium salt was filtered off, followed by removal of the THF at a vacuum of 10 mBar, yielding 18,2 g (97mmol, 90%) crude product with a purity based on NMR of 85%.

Distillation procedure: 1 gram of the crude product was used to determine the boiling point of the acrylate by slowly raising the temperature at a vacuum of 2 mBar until all remaining THF, pyridine and acryloyl chloride was distilled off. At 135°C the boiling temperature remained constant for approximately 10 min before the acrylate started to polymerize in the distillation flask due to the prolonged heating. Next 15 g of the remaining crude product was distilled by quickly raising the temperature to 150°C, taking a large first run, followed by the product. As soon as any polymerization was noticed or suspected the distillation was stopped yielding 9 g product, which still contained some trace impurities presumably due to the stabilizer used in the acryloyl chloride. In order to obtain pure product, i.e. no other signals detected on GC, the distillation had to be repeated three times after which only 2 gram (10% yield) of pure ethyl-O-urethane-N-ethyl acrylate was obtained.

¹H-NMR (CDCl₃, 200MHz): δ (ppm) 6.44 (dd; 1H; J=17.22; J=1.48), 6.15 (dd; 1H; J=10.33; J=17.22), 5.88 (dd; 1H; J=10.33; J=1.48), 5.72 (s br; 1H; NH), 4.23 (m; 4H), 3.21 (quintet; 2H; J=6.77), 1.14 (t; 3H; J=6.85); ¹³C-NMR (CDCl₃, 50MHz): δ (ppm) 166.7 (s), 157.0 (s), 132.0 (t), 128.8 (d), 63.6 (t), 63.0 (t), 36.5 (t), 15.8 (q); IR (neat): abs. cm⁻¹, 3345 (N-H), 1728 (C=O), 1534 (N-H def), 810 (C=C-H).

All liquid compounds were distilled at least three times before they were obtained in a pure form, except the ureas, which were recrystallized three times. In case a bulb-to-bulb distillation is used approximately 5 distillations are required, however the overall yields are significantly higher as lower temperatures are employed (for ethyl-O-urethane-N-ethyl acrylate 23% overall yield).

References and Notes:

1. a) Nie, J.; Rabek, J. F.; Linden, L.-A. *Polym. Int.* **1999**, *48*, 129.; b) Narayanan, V.; Scranton, A. B. *Trends in Polym. Sci.* **1997**, *5*, 415.; c) Lovell, L. G.; Stansbury, J. W.; Syrpes, D. C.; Bowman, C. N. *Macromolecules* **1999**, *32*, 3913. and references cited therein.
2. Kloosterboer, J. G. *Adv. Polym. Sci.* **1988**, *84*, 1.
3. Tryson G.R. , Schultz A.R, *J. Polym. Sci., Polym. Phys. Edn.* **1979**, *17*, 2059.
4. See for instance: Decker C., Elzaouk B., Decker D., *J. Macromol Sci; Pure Appl. Chem.* **1996**, *A33*, 173. and references cited therein.
5. a) Doornkamp, A. T.; Tan, Y. Y. *Polym. Commun.* **1990**, *31*, 362.; b) Lecamp, L.; Youssef, B.; Bunel, C.; Lebaudy, P. *Polymer* **1999**, *40*, 1403.; c) Khudyakov, I. V.; Legg, J. C.; Purvis, M. M.; Overton, B. J. *Ind. Eng. Chem. Res.* **1999**, *38*, 3353.; d) Selli, E.; Bellobono, I. R. in "Radiation Curing in Polymer Science and Technology", Fouassier, J. P.; Rabek J. F. eds, Elsevier , London, volume 3, p1. e) Decker, C.; Masson, F.; Bianchi, C. *Polym. Prepr.* **2001**, *42*, 304.; f) Decker, C.; Alzaouk, B.; Decker, D. *J. Macromol. Sci. A Pure Appl. Chem.* **1996**, *A33*, 173.; g) Yamada, B.; Azukizawa, M.; Yamazoe, H.; Hill, D. J. T.; Pomery, P. J. *Polymer*, **2000**, *41*, 5611.; h) Seno, M.; Fukui, T.; Hirano, T.; Sato, T. *J. Polym. Sci., A Polym. Chem.* **2000**, *38*, 4264.; i) Doetschman, D. C.; Mehlenbach, R. C.; Cywar, D. *Macromolecules* **1996**, *29*, 1807.
6. Panke, D. *Macromol. Theory Simul.* **1995**, *4*, 759.
7. Anseth, K. S.; Bowman, C. N. *Polym. React. Eng.* **1993**, *1*, 499.; b) Anseth, K. S.; Wang, C. M.; Bowman, C. N. *Macromolecules* **1994**, *27*, 650.
8. Wen, M.; McCormick, A. V. *Macromolecules* **2000**, *33*, 9247.
9. Goodner, M. D.; Bowman, C. N. *Macromolecules* **1999**, *32*, 6552.
10. Berchtholt, K. A. ; Lovell, L. G.; Nie, J.; Hacıoglu, B.; Bowman, C. N. *Polymer* **2001**, *42*, 4925
11. Hutchinson, J. B.; Anseth, K. S. *Polymer Preprints* **2000**, *41*, 1326.

12. Elliot, J. E., Bowman, C. N. *Macromolecules* **1999**, *32*, 8621.
13. Andrzejewska, E.; Andrzejewski, M. *J. Polym. Sci. A, Polym. Chem.* **1998**, *36*, 665.
14. a) Guymon, C. A.; Hoggan, E. N.; Clark, N. A.; Rieker, T. P. Walba, D. M.; Bowman, C. N. *Science* **1997**, *275*, 57 ; b) Guymon, C. A.; Bowman, C. N. *Macromolecules* **1997**, *30*, 5271
15. Decker, C.; Moussa, K. *Makromol. Chem. Rapid Commun.* **1990**, *11*, 159.
16. For a detailed description about the RT-FTIR equipment used see: Dias A.A., Hartwig H., Jansen J.F.G.A., *Surface Coatings International, JOCCA*, **2000**, *83*, 382.
17. Some data about amid ester acrylates, see for instance Jansen J.F.G.A. WO patent 98/33855, 1998 and Jansen J.F.G.A. European Patent 0970977A1 1997.
18. Based on molecular modeling using Insight II with AM1 as semi-empirical force field it was calculated that the intra-molecular hydrogen bonding structures posses a higher energy level compared to their inter-molecular hydrogen bonding analogues, reducing the possibility that the effect on the rate is caused by intra-molecular hydrogen bonding.
- 19 Pham,Q.-T.; Petiaud, R.; Waton, H.; Llauro, M.-F.; *Proton and Carbon NMR spectra of Polymers*; J. Wiley & Sons: New York, 1984; vol 3. and references cited.

Chapter 12

Photoinitiator Triplet States and Photoinitiating Radical–Monomer Interactions: Investigation through Time-Resolved Photothermal Techniques

Xavier Allonas, Jacques Lalevée, and Jean-Pierre Fouassier

Département de Photochimie Générale, CNRS UMR 7525,
Ecole Nationale Supérieure de Chimie de Mulhouse, 3 rue Alfred Werner,
68093 Mulhouse, France

This paper provides a general presentation of photothermal methods for the study of kinetic or thermodynamic properties of photopolymerization processes. It was shown that photoacoustic (PAS) and thermal lensing (TLS) spectroscopies allow the determination of the triplet quantum yields and energy levels of photoinitiators. Beyond the possibility to determine easily and accurately bond dissociation energies of coinitiators, providing important information on their reactivity, the application of PAS was extended for the first time to the study of the initiation step. A specific data treatment was developed to determine the rate constant and the enthalpy of the addition reaction of a radical onto a monomer unit.

Introduction

In photoinduced polymerization reactions, the photochemical reactivity of the photoinitiator plays a deciding role towards the practical efficiency of the process, which is a very important point for industrial applications in the UV curing area (1-2). More precisely, the characteristics of the excited states as well as the processes involved in these excited states and in the intermediate species generated through secondary reactions will have a strong influence on the ability of a molecule to be a good candidate as a photoinitiator.

For many years, time resolved absorption spectroscopy (TRAS) has been routinely used for the investigation of the excited state processes of photoinitiators (1-2), although a severe pitfall is that the transients must absorb the light to be optically detected.

The aim of this paper is to underline some advantages of time-resolved thermal lens (TLS) and photoacoustic (PAS) spectroscopies, that can circumvent some limitations of TRAS. Measurement of the heat produced in the medium from the non-radiative processes (that results in a change of the refractive index and the generation of acoustic waves) can provide important kinetic and thermodynamic information on the system studied. TLS and PAS give access to triplet quantum yields, triplet energy levels, lifetimes, rate constants of interaction, enthalpies of radical formation and bond dissociation energy of amines (3-5). Several recent examples are briefly recalled in this paper showing the efficiency of these techniques for the investigation of triplet states and radicals reactivity. The study of the photoinitiation step of a radical polymerization reaction is shown to be possible by PAS and a specific data treatment is developed for this purpose. Through several examples, it is evidenced that both enthalpy and rate constant of initiation can be measured.

Experimental

An optical parametric oscillator device pumped by a nanosecond Nd:YAG laser operating at 10 Hz allows the production of any wavelength between 225 nm and 1600 nm with an energy about 10 mJ (4). A solution of 2-hydroxybenzophenone (BPOH) in acetonitrile was used as calorimetric standard (5) and also as chemical attenuator to decrease the incident pulse energy in the range 0.5 to 100 μ J. The optical density of the samples was about 0.1 for TLS and 0.2 for PAS at the excitation wavelength. Oxygen was removed by bubbling argon for 15 minutes. Experimental setups for TLS and PAS have been fully described elsewhere (3-4).

Triplet states studied by photothermal techniques

Excitation of absorbing species in solution results in the creation of excited states that are doomed to deactivate or to react. Photophysical deactivations occurring through non-radiative processes and exothermic photochemical reactions release heat in solution. The subsequent temperature jump causes a variation of pressure ΔP , leading to the generation of acoustic waves, and a variation of the solvent refractive index Δn that can be probed by a continuous wave laser. Therefore, the amplitude and the time evolution of the signal is intimately related to the kinetics of the heat deposited in the media and to the experimental setup. Roughly, the heat deposited can be considered as fast when arising within few nanoseconds or slow if it corresponds to microsecond processes (Figure 1).

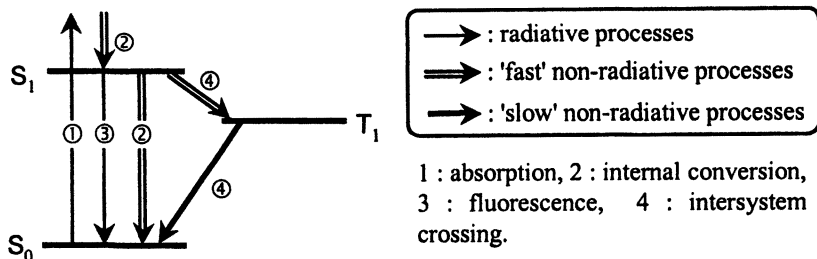


Figure 1. Separation between fast and slow heat deposit processes.

With the typical experimental setups described here, internal conversion and intersystem crossing to the triplet state are considered to be fast processes. In contrast, the deactivation of the triplet state to the ground state is considered as a slow process. In the following, fluorescence and phosphorescence will be neglected for the systems studied.

PAS methodology

Figure 2 shows typical signals obtained by PAS in the case of BPOH and the bifunctional photoinitiator Esacure 1001 (Lamberti Spa., eq 1) in acetonitrile and under argon. As can be seen, the amplitude of the acoustic wave corresponding to Esacure 1001 (S_{PI}) was found lower than that of BPOH (S_{BPOH}). The latter is known to release the whole excitation energy in solution in less than 1 ns, and therefore was used as a calorimetric reference (5). On the contrary, Esacure 1001 gave rise to a triplet state that deactivated slowly in solution, and therefore the fast heat deposition resulted in a lower acoustic wave.

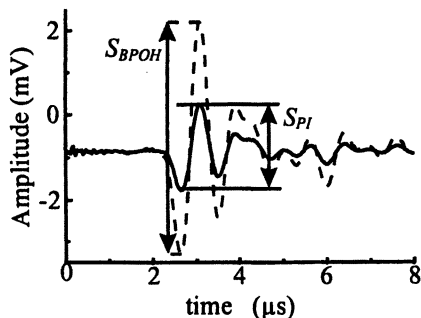
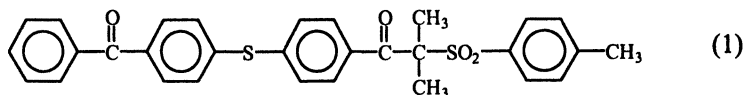


Figure 2. Typical PAS signal obtained in the case of BPOH and Esacure 1001 in argon saturated acetonitrile solution.

The amplitude of the acoustic waves are related to the photophysical parameters of the triplet state through the following expression:

$$\phi_T \cdot E_T = h\nu \cdot \left(1 - \frac{S_{PI}}{S_{BPOH}}\right) \quad (2)$$

where E_T and ϕ_T stands respectively for the energy level and the quantum yield of triplet state (corresponding generally to the quantum yield of intersystem crossing). In order to avoid biphotonic absorption, photothermal experiments are performed at very low pump intensity. Therefore, the most accurate $\phi_T \cdot E_T$ value is deduced by extrapolation at zero pump intensity. If E_T is known, ϕ_T can be easily deduced. A value of $\phi_T = 0.78 \pm 0.02$ was found for Esacure 1001, in good agreement with the literature (6).

TLS methodology

The analysis of the thermal lens signal obtained under direct excitation of the sample can also allows the determination of the ϕ_T values of photoinitiators. Figure 3 shows a typical signal obtained in the case of camphorquinone in acetonitrile.

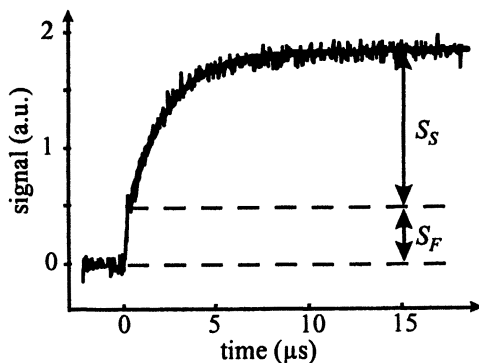


Figure 3. TLS signal obtained for camphorquinone in argon saturated acetonitrile solution and best first-order fit.

The time-dependence of the signal rise $S(t)$ can be fitted with a first-order kinetics: $S(t) = S_F + S_S (1 - \exp(-t/\tau))$, where S_F is the fast heat release and S_S stands for the slow heat deposition, *i.e.* the triplet state deactivation. From the results of the fits one can derive the lifetime of the excited state and the ratio S_S/S_T (with $S_T = S_F + S_S$). In the case of triplet formation, and if no fluorescence nor subsequent photoreaction occurs, eq 2 can be written as:

$$\phi_T = \frac{S_S}{S_T} \cdot \frac{h\nu}{E_T} \quad (3)$$

As for PAS measurements, TLS experiments were carried out at low pump intensity, and the most accurate ϕ_T value was derived from eq 3 using the extrapolated S_S/S_T ratio at zero pump energy. Under excitation at 466 nm, the ϕ_T of camphorquinone was found to be unity, in accordance with the literature (7).

Reactivity of Radicals

One of the most promising capabilities of photothermal techniques is to provide thermodynamic and kinetic information on secondary species such as radicals or dark consecutive reactions. This could be very useful in the study of the reactivity of the initiating radicals, by determining the bond dissociation energy (BDE) of the coinitiators or by measuring directly the rate constant of interaction with monomer units.

Bond dissociation energy of coinitiators

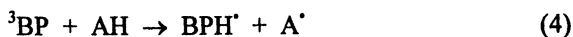
The C-H bond cleavage of a coinitiator leading to the production of radicals represents one of the first steps of photoinitiation processes when aromatic ketones are used as photoinitiators (1-2). Therefore, the measurement of the bond dissociation energy (BDE) is useful in order to compare the relative reactivity of radicals. Amines are extensively used as coinitiators in UV curing so a better knowledge of their reactivity is important. Their α C-H bond dissociation energies have been the subject of intensive experimental and theoretical studies for more than 20 years. Despite the different experimental methods used, the published values of amine α C-H BDEs have a large degree of variability (8,9). Both TLS and PAS allows the determination of the BDEs (4): indeed, the value obtained for triethylamine by TLS matches quite well that determined by PAS (91.5 kcal/mol found by TLS instead of 91.2 kcal/mol obtained by PAS) as well as the value from the literature (9).

Rate constant of interaction between radicals and monomers

The mechanism of radical addition to monomers is a subject of great interest. Indeed, in basic chemistry, it represents a fundamental bond forming process, while in the polymer field, the addition of radical to double-bond in the initiation step is probably one of the most important reactions. Consequently, factors controlling these reactions have been the subject of experimental and theoretical works. Due to their low extinction coefficients at wavelengths higher than 300 nm, aminoalkyl radicals are difficult to detect by classical TRAS. Different experimental methods have been used to solve this problem : ESR (10), CIDNP (11), and optical detection of the radical adduct (12). In this part, a new approach for the determination of the rate constants of photoinitiation k_i based on photoacoustic spectroscopy, is presented.

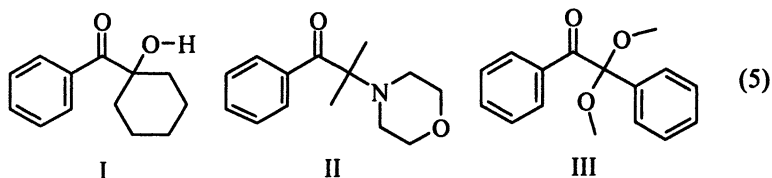
Efficient production of radical can be obtained by using the two following methods :

1/ Photoreduction of benzophenone (BP) by amine (AH) according to the following reaction:



It is well known that this reaction produces a large amount of corresponding aminoalkyl radicals (A^{\cdot}).

2/ Direct cleavage of photoinitiator which can undergo a Norrish type I cleavage. Compounds I to III (eq 5) are expected to produce respectively benzoyl/ketyl, benzoyl/aminoalkyl or benzoyl/dimethoxybenzyl pairs of radicals (R^{\cdot}).



Both processes produce initiating radicals that can react with monomers (M):



where ΔH_r is the enthalpy accompanying the reaction and k_i the rate constant of initiation.

Interaction A' /monomer

Adding various amounts of monomer into a solution of benzophenone/amine results in a decrease of the radical lifetimes and the release in the media of the corresponding heat of reaction, as depicted on Figure 4. The fast heat released was probed by PAS for different amounts of monomers.

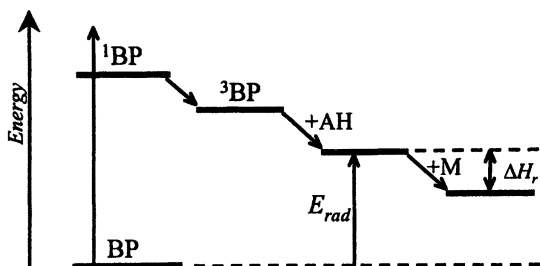


Figure 4. Schematic representation of the energy diagram for the different processes.

Considering that $A-M'$ is a long-lived species (12) and that BPH' does not react efficiently with M (13), the variation of the fast PAS signal with the monomer concentration should allow the measurement of ΔH_r and the extraction of k_i . Indeed, the heat $H(t)$ released at a time t is given by the following relationship :

$$H(t) = hv - \phi_{rad} \cdot E_{rad} - \phi_{rad} \cdot \Delta H_r \left(1 - \exp\left(-\frac{t}{\tau}\right) \right) \quad (7)$$

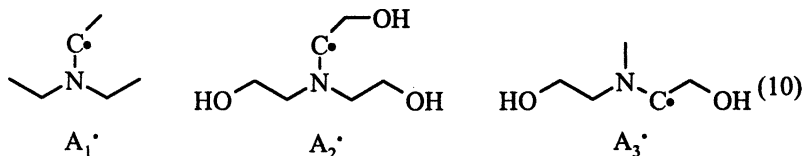
$\phi_{rad} \cdot E_{rad}$ represents the energy stored in the radicals (BPH[•] and A[•]) preceding the addition of monomer, and τ is the lifetime of the initiating radical A[•]. In fact, only the heat $H(t)$ released during the time resolution τ_{tr} of the experimental setup is detected and corresponds to the fast signal S_F , normalized for one photon absorbed and measured at very low pump intensity. However, the volume change associated with the reaction (ΔV_r) can give rise to a fast signal (5), and therefore must be taken into account together with the enthalpy of reaction ΔH_r . This leads to an apparent enthalpy of reaction ΔH_r^{app} . In the following discussion we will consider the term $\Delta H_r' = \phi_{rad} \cdot \Delta H_r^{app}$. The quantities $\phi_{rad} \cdot E_{rad}$ and $\Delta H_r'$ can be extracted from PAS experiments (Figure 5a). Therefore, one can obtain (for $H(\tau_{tr})$):

$$S_F = hv - \phi_{rad} \cdot E_{rad} - \Delta H_r' \left(1 - \exp\left(-\frac{\tau_{tr}}{\tau}\right) \right) \quad (8)$$

Using the Stern-Volmer relationship to express the lifetime of A[•] at a given concentration leads to the expression of the rate constant of quenching k_i :

$$\ln \left(\underbrace{\frac{S_F - hv + \phi_{rad} \cdot E_{rad} + \Delta H_r'}{\Delta H_r'}}_{f(S_F)} \right) = -\tau_{tr} \cdot \left(\frac{1}{\tau_0} + k_i \cdot [M] \right) \quad (9)$$

Therefore, the slope of eq 9 as a function of monomer concentration represents $-k_i \cdot \tau_{tr}$. In Figure 5, the typical evolution of S_F for the quenching of aminoalkyl radicals of triethanolamine by butyl methacrylate is shown. A growth of S_F can be noted, which corresponds to the deactivation of A[•] by M. Obviously, when the lifetime of A[•] is shorter than τ_{tr} , the increase of M concentration does not lead to any increase of S_F and the corresponding data must be eliminated from the treatment. The different aminoalkyl radicals studied are shown below:



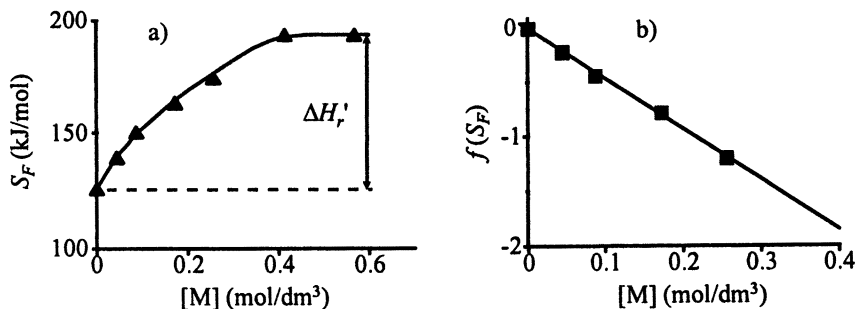


Figure 5. a) Evolution of S_F for different concentration of monomer and b) example of data treatment (system BP/triethanolamine/butyl methacrylate).

Two different monomers are used : butyl acrylate and butyl methacrylate. From the results gathered in Table I, one can notice the very high nucleophilic character of the aminoalkyl radicals studied. In all cases, high rate constants of interaction about $3 \times 10^7 \text{ M}^{-1} \text{ s}^{-1}$ were found. Moreover, the comparison of reactivity of aminoalkyl radicals from triethylamine, methyldiethanolamine and triethanolamine gives valuable information: the very similar rate constants of quenching observed show that the substituents affect very slightly the reactivity of these aminoalkyl radicals. It will be seen below that the volume change during this reaction can be neglected, allowing the evaluation of ΔH_r . The corresponding values of ΔH_r differs notably from butyl acrylate to butyl methacrylate, a fact already observed for different radicals (10).

Table I. Rate constant k_i and enthalpy of reaction ΔH_r for addition of different radicals A_1^\bullet on butyl acrylate and butyl methacrylate.

Radicals	butylacrylate		butylmethacrylate	
	k_i ($10^7 \text{ M}^{-1} \text{ s}^{-1}$)	ΔH_r (kJ/mol)	k_i ($10^7 \text{ M}^{-1} \text{ s}^{-1}$)	ΔH_r (kJ/mol)
A_1^\bullet	3.0	-38	3.5	-80
A_2^\bullet	3.5	-36	4.0	-75
A_3^\bullet	3.0	-31	2.5	-67

Interaction R' /monomer

The same kind of treatment can be applied to the study of the interaction between acrylate monomers and R' produced by direct photocleavage. Using the photoinitiators I to III, the following radicals (eq 11) can be formed and the corresponding results are reported in Table II:

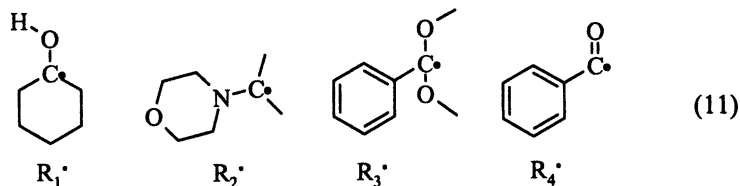


Table II. Rate constant k_i and enthalpy of reaction ΔH_r for addition of different R' radicals on butyl acrylate and butyl methacrylate.

Radicals	butyl acrylate		butyl methacrylate	
	k_i ($10^{-7} M^{-1} s^{-1}$)	$\phi_{rad} \cdot \Delta H_r$ (kJ/mol)	k_i ($10^{-7} M^{-1} s^{-1}$)	$\phi_{rad} \cdot \Delta H_r$ (kJ/mol)
R_1^\bullet	2.5 (1.1 ^a)	-80 ^b	-	-
R_2^\bullet	4.0 (2.9 ^a)	-33 ^b	-	-
R_3^\bullet	-	-	< 0.5	-
R_4^\bullet	-	-	< 0.5	-

a: Values in brackets from (15).

b: Until recently it was assumed that the quantum yield of dissociation was unity. A very recent paper suggests that closely related compounds exhibits lower ϕ_{rad} (14).

From this table it can be seen that k_i is low for the radicals R_3^\bullet and R_4^\bullet formed from compound III. This agrees very well with the observed low rate constants for benzoyl radical (13) and for dimethoxybenzyl radical (16). Therefore, the PAS analysis of the results obtained with compounds I and II were not affected by the presence of R_4^\bullet , due to the 10 fold higher reactivity of R_1^\bullet and R_2^\bullet compared to that of R_4^\bullet . Rate constants of quenching for these radicals can be compared to the results found in the literature, obtained by indirect laser method (15). For both kind of systems, very similar values were

obtained which give confidence to our treatment. In these experiments the contribution of a possible volume change during the reaction should be considered in the determination of ΔH_r . Indeed, the measured signal $\Delta H_r'$ contains both the energetic ΔH_r and volumic ΔV_r contributions. However, The enthalpy of reaction for radical R_2' , for which ΔV_r is negligible (17), is very similar to that of the other aminoalkyl radicals studied. Therefore, the neglect of volume change ΔV_r seems valid, allowing the evaluation of ΔH_r .

For all the radicals A' and R' studied here (except R_3' and R_4'), the rate constants of interaction k_i with monomer were about $3 \cdot 10^7 \text{ M}^{-1} \text{ s}^{-1}$, a value that corresponds to the maximum observed for the addition of tertiary radicals on double bonds (18). This can be ascribed to the exothermicity of the reactions and to the high nucleophilic character of the radicals that react with acrylate monomers exhibiting high electron affinities. In such case, the contribution of a partial electron transfer from radical to alkene can decrease the energy of the transition state, greatly enhancing the reactivity.

Conclusion

The fact that both kinetics and thermodynamics information can be obtained from photothermal techniques made them very promising in the field of photopolymerization studies. As most of the photochemical reactions are exothermic, heat is released in the media and photothermal methods can be applied. Triplet quantum yields and energy levels are easily measured, as well as bond dissociation energies of coiniciators. More interestingly, a new data treatment sheds some light on the thermodynamics and the dynamics of the photoinitiating process. Forthcoming papers will present results obtained on a large variety of photoinitiators.

Financial support from EC (BRPRCT 98064) for the development of the techniques is fully acknowledged

References

- 1 Fouassier, J.P. *Photoinitiation Photopolymerization and Photocuring*, Hanser Publishers, 1995
- 2 Neckers, D.C. *UV and EB at the Millenium*, Sita Technology: London, 1999
- 3 Allonas, X.; Ley, C.; Bibaut, C.; Jacques, P.; Fouassier, J.P. *Chem. Phys. Lett.* **2000**, *322*, 483.
- 4 Lalevée, J.; Allonas, X.; Fouassier, J.P. *Polym. Preprints* **2001**, *42*, 805.

- 5 Braslavsky, S.E.; Heibel, G.E. *Chem. Rev.* **1992**, *92*, 1381.
- 6 Allonas, X.; Grotzinger, C.; Lalevée, J.; Fouassier, J.P.; Visconti, M. *Eur. Polym. J.* **2000**, *37*, 897.
- 7 Romani, A.; Favaro, G.; Masetti, F. *J. Lumines.* **1995**, *63*, 183.
- 8 Nazran, A.S.; Griller, D. *J. Am. Chem. Soc.* **1983**, *105*, 1970.
- 9 Dombrowski, G.W.; Dinnocenzo, J.P.; Farid, S.; Goodman, J.L.; Gould, I.R. *J. Org. Chem.* **1999**, *64*, 427.
- 10 Walbiner, M.; Wu, J.Q.; Fischer, H. *Helv. Chim. Acta* **1995**, *78*, 910.
- 11 Batchelor, S.N.; Fischer, H. *J. Phys. Chem.* **1996**, *100*, 9794.
- 12 Martschke, R.; Farley, R.D.; Fischer, H. *Helv. Chim. Acta* **1997**, *80*, 1363.
- 13 Schnabel, W. *In Lasers in Polymer Science and Technology: Applications*; Fouassier, J.P.; Rabek, J.F., Eds.; CRC, Boca Raton, 1991; Vol. 2, p 95.
- 14 Jockusch, S.; Landis, M.S.; Freiermuth, B.; Turro, N.J. *Macromolecules* **2001**, *34*, 1619.
- 15 Jockusch, S.; Turro, N.J. *J. Am. Chem. Soc.* **1999**, *121*, 3921.
- 16 Hany, R.; Fischer, H. *Proc. XIIIth IUPAC on Photochemistry*, Coventry, **1990**, 90.
- 17 Wayner, D.D.M.; Luszytk, E.; Pagé, D.; Ingold, K.U.; Mulder, P.; Laarhoven, L.J.J.; Aldrich, H.S. *J. Am. Chem. Soc.* **1995**, *117*, 8737.
- 18 Fischer, H.; Radom, L. *Angew. Chem. Int. Ed.* **2001**, *40*, 1340.

Chapter 13

Oxygen Inhibition Effect on Surface Properties of UV-Curable Acrylate Coatings

H. Cao¹, E. Currie², M. Tilley¹, and Y. C. Jean³

¹DSM Desotech Inc., 1122 St. Charles Street, Elgin, IL 60120

²DSM Research, P.O. Box 18, 6160 MD, Geleen, Netherlands

³University of Missouri at Kansas City, Kansas City, MO 64110

Abstract

In past studies the oxygen inhibition effect on the UV curing of polymer coatings has been extensively studied with the focus on oxygen inhibition mechanism and photocuring kinetics. In this study, several advanced surface characterization techniques have been applied to investigate the influences of the presence of oxygen during UV curing on the network structure and surface properties of acrylate coatings. The surface techniques employed in this study include slow beam positron annihilation spectroscopy, ESCA, microthermal analysis and nanoindentation. O₂ inhibition is found to significantly affect the top one micron surface layer of the coatings in terms of network structure and physical properties. The experimental results are in agreement with the proposed O₂ inhibition mechanism.

Introduction

UV-curable coatings are becoming increasingly important in the photo-electronics industry. A major branch in this area is the application of UV-curable coating, ink and matrix materials in optical fiber systems. Fibers are packaged in fiber optic cables using different structural designs. A so-called ribbon is one of the most popular designs to bond several fibers together. As shown in Figure 1, a number of coated fibers are aligned in parallel and encapsulated by a UV-curable polymer matrix to form a flat ribbon structure. In typical ribbon cable designs, multiple ribbons are tightly packed in a ribbon stack. During the cable installation and handling processes, any mechanical stresses induced in the ribbon stack may cause deterioration of fiber optical performance. The surface condition of ribbons is a critical factor that determines the mechanical stresses arising from ribbon-ribbon interactions. In this paper the matrix coating, consisting of a glassy UV-curable acrylate coating, is studied with the focus on the effect of oxygen inhibition on coating surface properties.

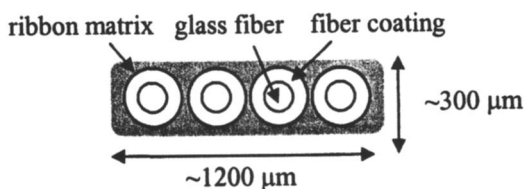


Figure 1. Illustration of a 4-fiber ribbon structure.

Oxygen is a known inhibitor of photopolymerization processes in acrylates. The effects of oxygen on the UV curing of polymer coatings have been extensively studied in terms of oxygen inhibition mechanism, kinetics of photopolymerization in the presence of O_2 , and methods to eliminate O_2 inhibition. (1-3) However, little has been done to characterize the effects of O_2 inhibition on a polymer network structure and its mechanical properties. One reason might be that O_2 inhibition in polymer coatings is limited to a thin surface layer and the requirement of surface analysis raises the level of difficulty to examine the problem.

In this paper we apply several advanced surface characterization techniques to investigate the influence of the presence of oxygen during the curing on the matrix structure and its effect on the surface properties. The surface techniques employed in this study include slow beam positron annihilation spectroscopy (PAS), ESCA, microthermal analysis (micro-TA) and nanoindentation.

Materials & Methods

In this study, two UV-curable urethane-acrylate matrix coatings with different compositions, denominated as matrix A and B were investigated. A 6 inches long D-type UV cure lamp with the power of 500 W/in followed by a 10 inches long H-type lamp with the power of 600 W/in were applied in the OFC21 ribbon machine purchased from Nextrom (Nextrom, Finland). 100% of the D lamp power and 60% of the H lamp power were set as the standard condition to cure the ribbon matrix. The curing process was performed either under the condition of N₂ purging at both lamps (N₂/N₂), or air in the first lamp and N₂ at the second lamp (air/N₂). The ribbon line speed was 400 m/min. The ribbons in this study are 12-fiber ribbons. The cross section dimension is 3000 μm x 300 μm with ~ 25 μm matrix layer each on top and bottom sides of the fiber array.

PAS is a special nuclear analytical technique for material characterization. In the polymer field, PAS has been employed as a unique probe for analyzing free volume size, intensity and distribution, as γ-rays emitted by positron-electron annihilation contain information on the local electronic structure and defect properties of materials at atomic level.⁽⁴⁾ One of the PAS methods, i.e. Doppler broadening of energy spectrum (DBES) technique was employed to measure the broadening of the e⁺-e⁻ annihilation γ-ray energy signal centered at 511 keV. A S-parameter, defined as the ratio of integrated counts in the predefined central area to the total counts, is employed to describe the energy broadening. Since the positron energy in the annihilation pair is almost zero (thermalized), the Doppler broadening of the energy spectrum directly correlates with the momentum distribution of the electrons in the material. Any chemical change or physical structural change in the material could affect this energy distribution peak characterized by the S value. The slow positron beam used in this study had incident energy ranging from 0 to 30 keV with the resolution of 0.1 keV. A detailed description of the instrument can be found elsewhere. ⁽⁵⁾ Slow positron DBES technique is expected to give depth profile information on chemical/physical properties at the surface of the ribbon matrices.

ESCA (electron spectroscopy chemical analysis), also known as XPS (X-ray photo-electron spectroscopy), is a surface-specific scattering technique capable of collecting information on the chemical composition of the first few atomic layers of a surface. In short, when a surface is irradiated with soft X-ray photons, electrons from the inner shells of the atomic constituents are ejected with a characteristic kinetic energy. The electrons are accelerated through a vacuum towards a detector. The photoelectron intensity is then measured as a function of the initial kinetic energy, which results in a chemical fingerprint of the polymeric surface. The limitations of ESCA are mainly related to its limited in-depth resolution (up to 10 nm) and its lateral resolution (a few μm at best). The measurements were performed on a Leybold MAX 200 foto-electron

spectrometer with a vacuum pressure of less than 10^{-8} mbar. More information on ESCA can be found elsewhere. (6)

Micro-TA is a novel technology developed in recent years, which combines surface thermal analysis with atomic force microscopy (AFM). In micro-TA instrument, the regular AFM silicon nitride probe is replaced with a silver-coated platinum wire, a so-called Wollaston wire that acts as a miniature heater and temperature sensor. This enables the micro-TA to measure thermal conductivity and thermal diffusivity of the surface layer along with the topographical image. A detailed description of the micro-TA method can be found in literature. (7) In this study, μ TA 2990 (TA Instruments) was used for thermal analysis of the ribbon surface. The probe was held stationary over a specific area on the sample surface and heated at a very fast rate (25°C/s) in this study. As an analogy to the conventional TMA, micro-TMA measures probe displacement in the Z-axis caused by expansion of the local surface during heating. A thermally induced transition is indicated by a change of slope of the probe displacement curve versus the temperature. Because of the nature of very fast and localized heating by the probe, only a very thin top layer ($< 0.1 \mu\text{m}$) of the coating is heated and thus the surface T_g of the matrix coatings was measured.

Nano-indentation is a relatively new technique with which the mechanical properties of e.g. polymeric coatings can be characterized on the sub-micron level. For a general review on microhardness tests on polymers we refer the reader to the book of Calleja and Fakirov. (8) Nano-indentation measurements were performed on ribbon samples by Micromaterials Ltd on the NanoTest 600. In these tests a Berkovich diamond indenter with the same ratio of projected area to depth as a Vickers indenter was pressed with a prescribed force ($1 \sim 5 \text{ mN}$) into the matrix and the normal displacement was recorded. The indentations were carried out using a load- partial unload approach, i.e. the loading process was stopped, held at the peak load for 30 seconds, reversed to 30% of the intermittent peak load and continued at the next load. At the highest force (5 mN) the indentation depth (an indication of the degree of plastic deformation) did not exceed $2 \mu\text{m}$, which entails that solely the mechanical properties of the matrix were examined.

Results

PAS:

Figures 2 and 3 show the results of the S-parameter versus positron incident energy for the ribbon samples A and B under N_2/N_2 or air/ N_2 curing conditions.

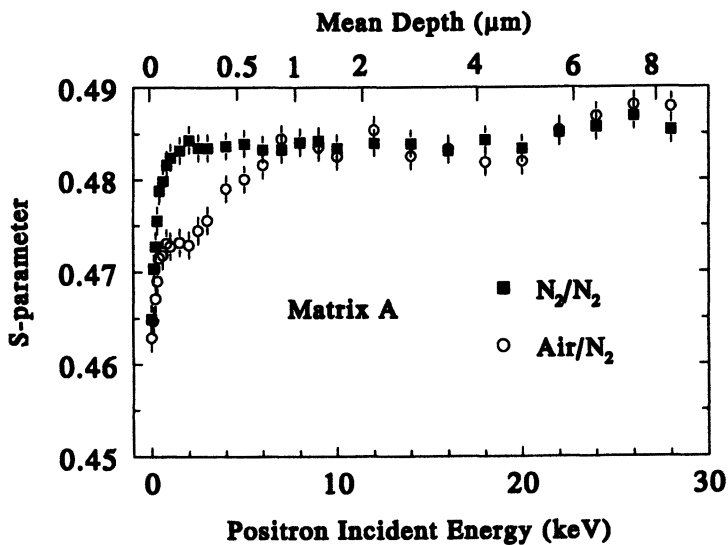


Figure 2. *S*-parameter depth profile of matrix A.

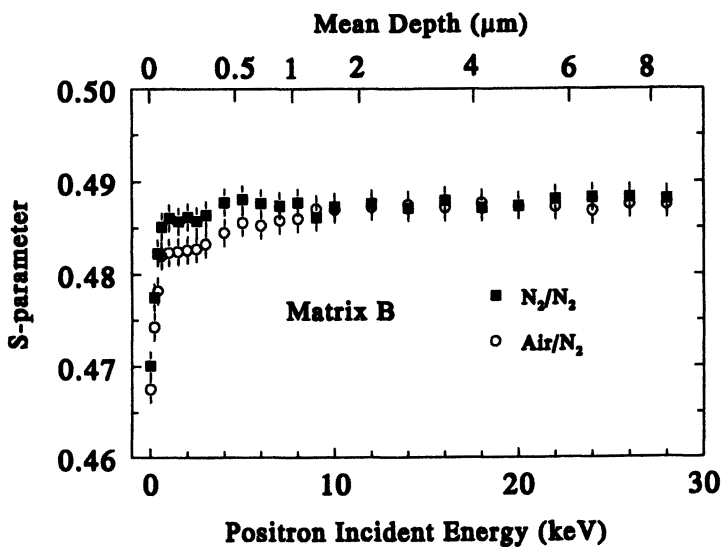


Figure 3. *S*-parameter depth profile of matrix B.

The mean implantation depth of positrons as a function of incident energy is calculated and labeled on the top x-axis. A sharp decrease of the S-parameter near the polymer surface is an intrinsic feature of slow positron depth profile caused by the backscattering of positrons into the vacuum. In the case of ribbons cured under N_2/N_2 , constant S-parameter depth profiles are observed, which indicates spatial chemical and physical homogeneity in those ribbon matrices. In the case of ribbons cured under air/ N_2 conditions, a surface effect is clearly observed when compared with the corresponding ribbons cured under N_2/N_2 . Matrix A in air/ N_2 shows a dramatic decrease of S-parameter at a surface depth of $\sim 1 \mu\text{m}$ thickness, whereas matrix B cured under air/ N_2 only has a slight decrease of S-parameter at the surface layer. The difference spectra ΔS is plotted vs. incident energy and implantation depth in Figure 4. If the decrease due to the backscattering at surface is omitted, ΔS depth profiles can be fitted by exponential decay curves as shown in Figure 4. This trend strongly indicates that the O_2 effect is maximal at surface and diminishes gradually with depth. The mechanism of O_2 effects on structure and properties of surface layer will be addressed in the next section.

ESCA:

The results of quantitative element concentrations analyzed by ESCA showed surface concentrations of elemental oxygen are 22.2%, 23.5% for matrix A, 21.0%, 23.3% for matrix B cured under N_2/N_2 and air/ N_2 respectively. It appears that ribbons cured under air/ N_2 have larger concentrations of O on the surface than the same type of ribbon cured under N_2/N_2 .

Micro-TA:

Surface T_g results measured by micro-TMA are shown in Figures 5 and 6. In contrast to conventional TMA, the micro-TMA sensor displacement curve shows a decrease of expansion slope immediately after passing T_g . It is caused by the probe dipping into the coating when the material becomes soft at T_g . In Figure 5 a trend of decreasing surface T_g is observed for matrix A cured under air/ N_2 , while the surface T_g of matrix B is independent of the atmosphere during curing.

Nano-indentation:

Nano-indentation tests were performed on matrices A and B, both cured in the presence of oxygen and without, for increasing load. The results for 1 and 5

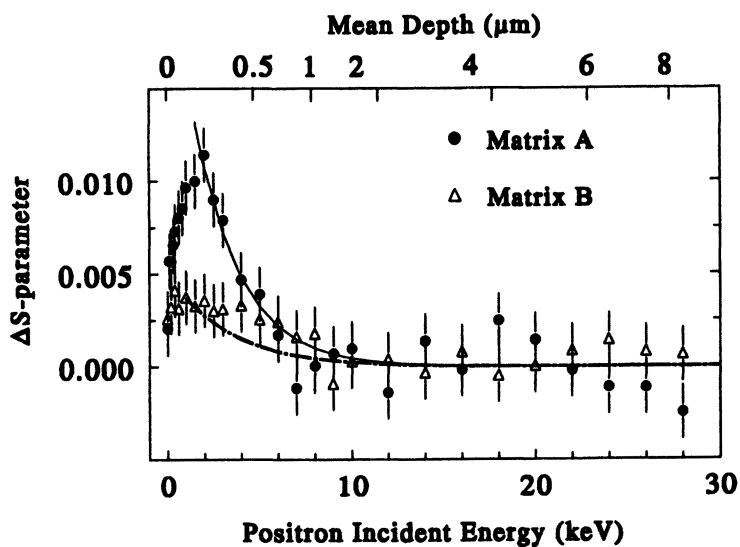


Figure 4. ΔS -parameter depth profile of matrices A and B.

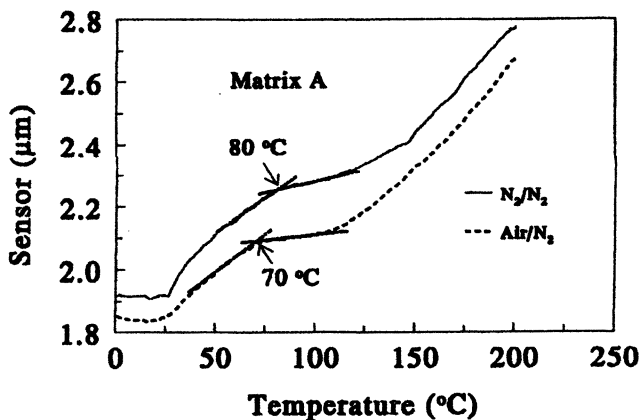


Figure 5. Micro-TMA thermogram of matrix A.

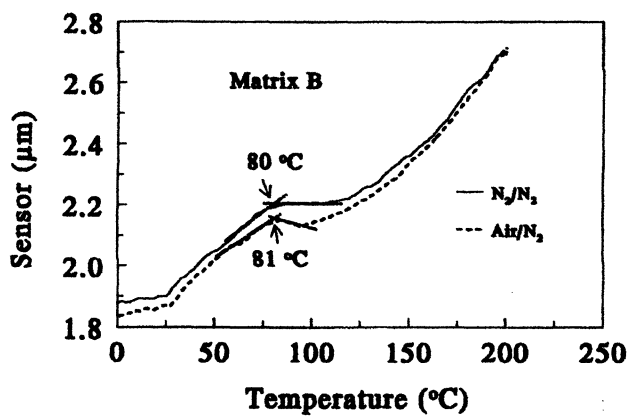


Figure 6. Micro-TMA thermogram of matrix B.

mN, averaged over 9 indentations, are shown in Table 1. The mechanical properties, i.e. hardness and modulus of matrix A are found to decrease significantly when O₂ is present during curing, whereas those of matrix B are insensitive to O₂. This finding is in agreement with PAS and micro-TA results, which all indicate matrices B is relatively insensitive to O₂ compared with A.

Table 1. Nanoindentation results for matrices A and B

<i>Sample</i>	<i>Load (mN)</i>	<i>Depth (nm)</i>	<i>Hardness (MPa)</i>	<i>Modulus (MPa)</i>
A, N ₂ /N ₂	1	589	103.2	1927
	5	1554	83.0	1508
A, air/N ₂	1	670	81.4	1630
	5	1806	62.0	1251
B, N ₂ /N ₂	1	464	155.2	2917
	5	1284	122.5	2249
B, air/N ₂	1	463	161.6	2998
	5	1266	126.4	2336

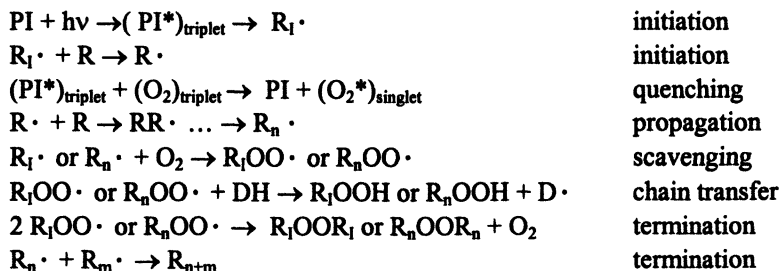
In Table 1 it can be seen that the hardness and modulus decrease with increasing load, i.e. increasing depth of penetration. It is tempting to attribute this to a variation in network structure, for instance a lower cross-link density. However, this decrease in modulus has been observed for other coatings as well, and is believed to result from tip geometry effects. (9)

Discussion

Oxygen inhibition of free radical polymerization is a major concern in UV curing technology. The presence of O₂ during curing usually has negative impacts on the curing process and coating properties, such as a decrease of the polymerization rate, an undercured surface and decrease of solvent resistance. However, in the ribbon curing process, the special two-lamp design with the constant condition of N₂ purging in the second lamp assured complete curing of the ribbon matrices even when the surface layer might be undercured resulting from air exposure in the first lamp. The degree of curing in terms of percent reacted acrylate unsaturation measured by FTIR is 95% for matrix A both N₂/N₂ and air/N₂ samples. However, the surface properties, as characterized by PAS, ESCA, micro-TA and nano-indentation techniques, strongly indicate that the O₂

exposure in the first lamp had permanent influences on the polymer network structure.

O₂ inhibits free radical polymerization through two pathways. (2) First, an oxygen molecule can quench the active triplet state of the photoinitiator and be excited to a singlet state itself. The second path is scavenging of the photoinitiator and polymer radicals through oxidation with the yield of peroxy radicals. The overall chain reactions of photopolymerization with the presence of O₂ is schematically shown below:



where R₁·, R and DH represent photoinitiator radical fragment, acrylic monomer or oligomer and a hydrogen donor molecule respectively. The quenching of PI* and scavenging of PI radicals (R₁·) lead to the decrease of polymerization rate. The scavenging of growing radicals by oxidation, on the other hand, prohibits further propagation of the polymer chains and terminates the chains at a short length. As peroxy radicals, like oxygen molecules, are relatively more stable the propagation activity is much less than the acrylate radicals. The only way that peroxy radicals can continue the chain reactions is by acting as chain transfer agent and undergo H abstraction with a hydrogen donor producing an active radical D·. The hydroperoxide products decompose under UV light to form active ·OH and oxy radical RO·, which can then further participate in the chain reactions. This chain transfer reaction is the mechanism using strong H donor such as tertiary amines to suppress the O₂ effect. No strong H donor is present in the acrylate formulation. As a result, strong O₂ inhibition is expected and the overall effects is proposed to be short chain fragments, a loose network structure and reduced crosslink density. The surface T_g decrease detected by micro-TA and surface modulus decrease measured by nano-indentation provide strong experimental evidence for the proposed mechanism.

The sensitivity to O₂ inhibition among the two formulations could vary due to the different O₂ solubility and diffusivity as well as presence of active species such as hydrogen donor. However, using such arguments the lower O₂ sensitivity of matrix B compared to matrix A cannot be explained, since the backbones of these two acrylate coatings are similar. Our speculation is that an additive in formulation B not present in A is possibly responsible for the O₂ insensitivity,

i.e. a HALS (hindered amine light stabilizer). HALS was added for long term stability of coatings under weathering. Considering the important role of the peroxy radical in O_2 inhibition mechanism and the HALS's function as peroxy radical trapping agent, it is expected that the HALS compound could also influence O_2 inhibition during UV curing. In the photopolymerization process in the presence of O_2 , the peroxy radicals which are readily formed from oxidation reactions, tend not to further propagate the chain reaction because of their stable nature. HALS can however quickly react with $ROO\cdot$ and form peroxide $ROOR$. The intensive heat produced during UV curing and the high dose of UV light may excite the peroxide and decompose it into two oxy radicals $RO\cdot$. Oxy radicals are very active species and they readily react with acrylate and undergo chain propagation. By converting the stable peroxy radical via the HALS into active oxy radicals, the O_2 scavenging effect is expected to be suppressed. The O concentration increases about the same level in matrix B as in matrix A as shown in ESCA results. This is not contradictory with the proposed mechanism. The radicals do react with diffusing O_2 from air but the chain propagation and network formation is not retarded due to the possible role of HALS in suppressing O_2 inhibition during curing. Further investigation is needed to confirm HALS' role in O_2 inhibition.

Evidently, before the curing takes place, O_2 is predissolved in the liquid coating at an equilibrium level, typically below 90 ppm in a viscous organic liquid. (3) However, the observed surface effects are not related to the predissolved O_2 . As O_2 is more mobile than the acrylate monomers, a large fraction of radicals initially reacts with the predissolved O_2 . This leads to fast consumption and depletion of the predissolved O_2 in the liquid coating. Only when the surface is exposed to oxygen during curing can the reacted O_2 be substantially replenished by the O_2 diffusing into the surface layer. A direct experimental evidence for this is the O concentration increase for ribbons cured under air/ N_2 detected by ESCA surface element analysis.

The surface layer thickness affected by O_2 inhibition is controlled by the O_2 diffusion length. According to diffusion theory, the penetration depth L is calculated by the equation $L = \sqrt{6D\Delta t}$ where D is oxygen molecule diffusion coefficient and t is the O_2 exposure time during curing. (3) The O_2 diffusion coefficient is in the range of $10^{-6} \sim 10^{-5}$ cm^2/s in liquid and $10^{-8} \sim 10^{-7}$ in polymeric solids. (2) The exposure time is estimated to be 0.05 s in the ribbon line. Evidently, the exact value of diffusion length can not be predicted because of the very rapid conversion of the liquid coating into solid but it is estimated to be in the level of $0.1 \mu m \sim 10 \mu m$. The $1 \mu m$ surface layer affected by O_2 from PAS depth profile results is therefore in the right range. In past studies the surface layer affected by the O_2 inhibition is usually reported to be in the order of $100 \mu m$. (10) The much thinner surface layer in this case is due to the unique nature of very fast curing process from the 400 m/min ribbon line speed.

The trend of exponential decay of ΔS -parameter as shown in Figure 4 is believed to be caused by the O_2 concentration gradient near the surface. It agrees with the diffusion theory that the concentration of diffused O_2 has an exponential depth profile. (10) Similar S-parameter decrease near surfaces was also observed in polymeric coatings with photodegradation caused by weathering. (11) Positrons entering the material exist in two fundamental states: free positron or bound state of a positron and an electron, known as positronium (Ps). Positronium annihilation attributes to the narrowest part of the energy distribution peak. Materials with larger percentage of positronium formation have sharper energy distribution, thus larger S-parameter. The oxidation products, such as hydroperoxides, carbonyl groups from the further dissociation of hydroperoxide and some caged radicals may act as Ps inhibitors and decrease Ps formation which will lead to S-parameter reduction.

Conclusions

Four advanced surface characterization techniques were applied to measure surface properties of ribbon matrices cured under N_2/N_2 or air/ N_2 conditions. Oxygen presence during UV curing was found to result in a S-parameter decrease in a surface layer of 1 μm in the PAS study, oxygen content increase detected by ESCA, surface T_g decrease from micro-TA and a decrease of the surface modulus from nano-indentation experiments. These results are in agreement with the proposed O_2 inhibition mechanism. The different O_2 sensitivity of acrylate coatings with comparable formulations was explained by the possible role of HALS in suppressing O_2 inhibition through trapping peroxy radicals.

Acknowledgement

The authors would like to express their gratitude to Dr. G. Slough at TA Instruments for micro-TA measurement. We would like to thank Dr. E. Murphy and E. Zahora for the support of this work. Valuable discussions with Dr. V. V. Krongauz is also gratefully acknowledged.

References

1. Decker, C.; Jenkins, A. D. *Macromolecules* **1985**, *18*, 1241.

2. Kunz, M.; Strobel, R.; Gysau, D. *RadTech Proceedings 1996*, Vol. 1, p 278.
3. Krongauz, V. V.; Chawla C. P.; Woodman, R.K. *RadTech Proceedings 2000*, p 260.
4. *Positron and Positronium Chemistry*; Schrader, D.M.; Jean, Y.C., Eds.; Elsevier: New York, 1988.
5. Zhang, R.; Cao, H.; Chen, H. M.; Mallon, P.; Sandreczki, T. C.; Richardson, J. R.; Jean, Y. C.; Nielsen, B.; Suzuki, R.; Ohdaira, T. *Radiation Physics and Chemistry 2000*, 58, 639.
6. *Surface Characterization of Advanced Polymers*; Sabbatini, L; Zambonin, P. G., Eds.; VCH: New York, 1993.
7. Hammiche, A.; Reading M.; Pollock H. M.; Hourston, D. J. *Rev. Sci. Instr.* **1996**, 67, 4268.
8. Calleja Baltá, F. J. B; Fakirov, S. *Microhardness of Polymers*; Cambridge Un. Press: Cambridge, 2000.
9. Andrei, D.C.; Keddie, J. L.; Hay, J. N.; Yeates, S. G.; Briscoe, B. J.; Parsonage, D. J. *Coatings Tech.* **2001**, 73, 65.
10. Wallin, M.; Glover, P. M.; Hellgren, A. C.; Keddie, J. L.; McDonald, P. J. *Macromolecules* **2000**, 33, 8443.
11. Cao, H.; Yuan, J. P.; Zhang, R.; Huang, C. M.; He, Y.; Sandreczki, T.; Jean, Y. C. *Macromolecules*, **1999**, 32(18), 5925.

Chapter 14

Oxygen and Radical Photopolymerization in Films

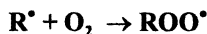
Vadim V. Krongauz^{1,*}, Chander P. Chawla¹, and Juliette Dupre²

¹DSM Desotech Inc., 1122 St. Charles Street, Elgin, IL 60120

²Ecole Nationale Supérieure de Chimie de Mulhouse, Université de Haute-Alsace-3, rue Werner, 68200 Mulhouse, France

Introduction

Radical photopolymerization kinetics is sensitive to the presence of oxygen that reacts with radicals forming peroxides that do not promote chain growth [1].



In solvent-free coatings consisting of oligomer, initiator and additives dissolved in a polymerizable monomer (reactive diluent), the presence of oxygen leads to decrease in reaction rate and a spatial anisotropy of polymer yield [2-6].

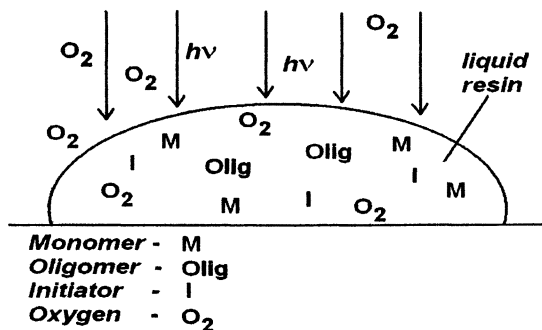


Figure 1. A diagram of anisotropic photopolymerization of a coating

Photopolymerizing resins are rarely degassed prior to exposure to light, and therefore contain, up to 10^{-3}M dissolved oxygen [1]. Special efforts are required to achieve high speed and uniformity of cure in oxygen presence.

One-sided illumination results in photopolymerization anisotropy. Intensity of excitation light decreases with the distance from the illuminated surface exponentially in accordance with Lambert-Beer's law. In optically thin, 1-10 μm thick films light may be reflected from substrate, adding to the complexity.

Assuming bi-radical chain termination mechanism, the square root of the total average photopolymerization rate $\langle R^{1/2} \rangle_{av}$ dependence on the distance from the illuminated surface, L , can be described by the equation (1) [1, 7]:

$$\langle R^{1/2} \rangle_{av} = (4I_0/L^2\epsilon c)^{1/2}[1 - \exp(-\epsilon cL/2)] \quad (1)$$

where I_0 is the incident light intensity at the surface, c is the concentration of the absorbing species, and ϵ is the total extinction coefficient (Fig. 2).

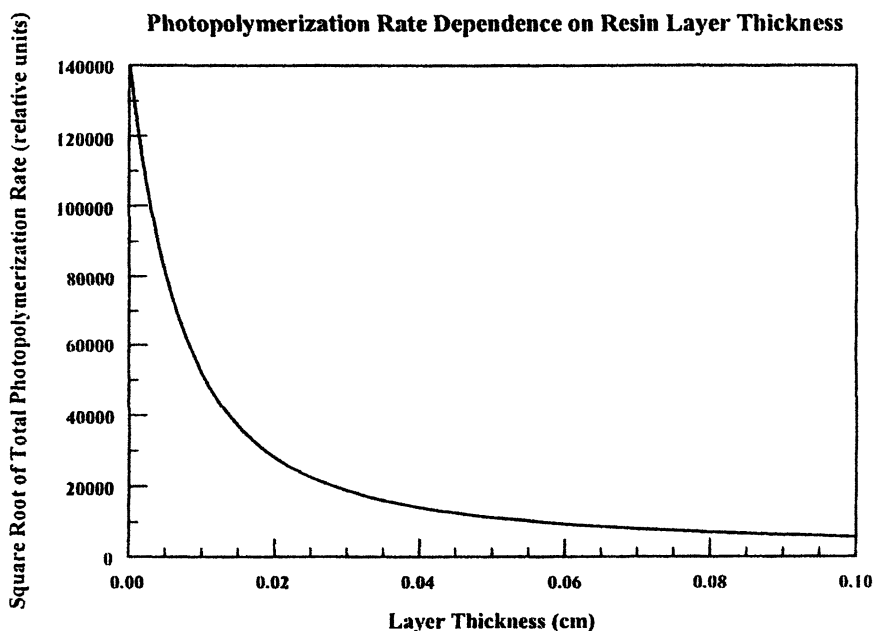


Figure 2. Computed photopolymerization rate dependence on resin layer thickness; polymerization rate is assumed proportional to a square root of light intensity [1, 7]; $I_0 = 2.5 \times 10^{-8}$ Einsteins, extinction coefficient, $\epsilon = 10^6 \text{cm}^3 (\text{mol cm})^{-1}$ were used.

The anisotropy of photopolymerization in films is amplified by the uptake of oxygen from surrounding atmosphere and the diffusion of dissolved oxygen and monomer towards illuminated surface. Diffusion of reagents to illuminated

surface is stipulated by their higher consumption in the regions where radical production is higher, that is, 1-10 μm from the illuminated surface [2-6].

Various techniques are used to reduce the detrimental effects of oxygen on radical photopolymerization in films. These include the use of a protective cover or inert gas flow over the resin film surface, preventing oxygen influx during photopolymerization. Amines may be added, since they react with oxygen, yielding radicals capable of continuing the chain polymerization [8].

We revisited oxygen inhibition of radical photopolymerization in solvent-free acrylate compositions. We compared effectiveness of resin degassing by different inert gases and considered the effects of resin viscosity. We also detected cure rate increase in the presence of small amounts of aromatic thiols. This increase could be attributed to oxygen binding and radicals rejuvenation by thiols [9, 10].

Experimental

Hexanediol diacrylate (HDODA), and isobornyl acrylate (IBOA) reactive diluents, and urethane acrylate oligomers CN963J75, CN963B80 were used (Sartomer). 2,2-Dimethoxy-2-phenylacetophenone (Irgacure[®] 651) or 1-Hydroxycyclohexyl phenyl ketone (Irgacure[®] 184) photoinitiators (Ciba), were used at 0%, 1% or 3% by weight. 2-Benzoxazolethiol (BOT) and 2-benzothiazolethiol (BTT) (Aldrich) were used at levels 0.01 to 5%.

A Perkin-Elmer DSC-7, with 100W high pressure Hg lamp was used at 30°C. Light was attenuated by a neutral density filter (OD=0.1) to yield a light intensity of 62.9 mJ/cm² without a filter, and 7.1 mJ/cm² with a filter. Flow rate of He or N₂ (Air Products) was 24.0 ml/min[15]. Fourier transformed infrared spectroscopy (FTIR) was used to monitor polymerization at the acrylate double bond absorption maximum at 810cm⁻¹ (Nicolet FTIR). For FTIR the resin was placed on a NaCl crystal (oxygen-rich environment) or between two NaCl crystals (oxygen-free environment). The resin side open to air was exposed to UV light (22 mJ/cm²), while the IR absorption was recorded. Dependence of shear modulus of resin on time of UV-exposure was monitored using a Stress Tech (Reologica) instrument.

Results and Discussion

The results of Tryson and Schultz [7] confirmed by us [10] showed the dependence of acrylates photo-polymerization enthalpy on sample size (Fig. 3). The data are only in qualitative agreement with equation (1) (Fig. 2) [7]. We

attempted to explain this [10]. No oxygen reactions were considered in eq. (1) derivation, yet residual oxygen is present in the resins even after nitrogen purge. Unidirectional illumination leads to higher oxygen consumption at the surface depleting oxygen in the depth of an optically thick film. Polymerization in the absence of oxygen is less exothermic as is evident from the experimental data (Fig. 4) and from a simple Hess's cycle estimates presented below [10]

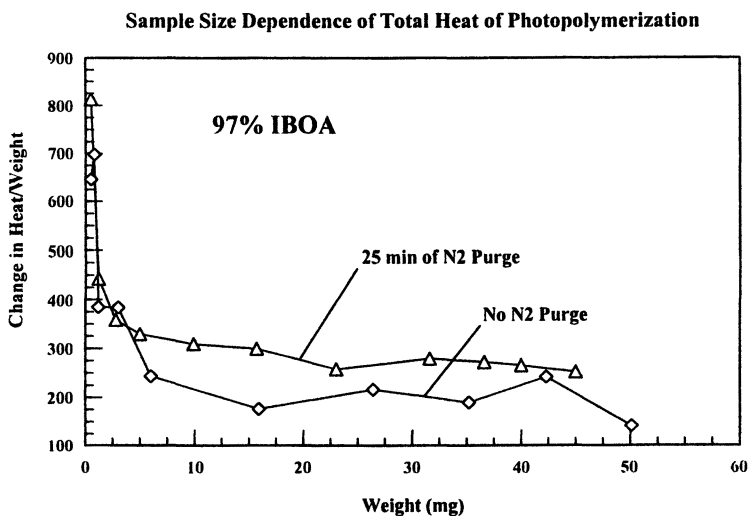
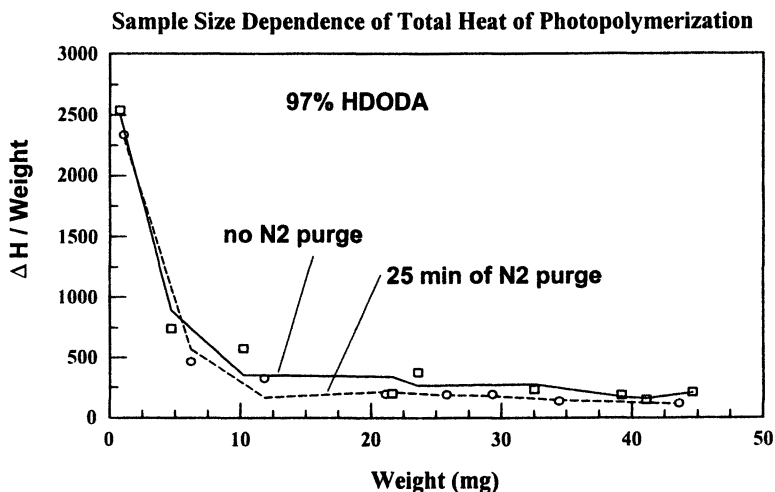
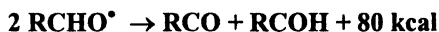
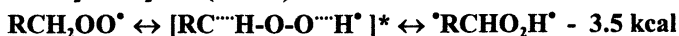
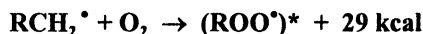
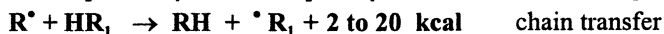
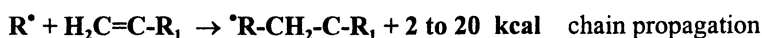


Figure 3 Sample weight dependence of total heat of polymerization

In the presence of oxygen



In the absence of oxygen, the chain propagation and termination reactions, such as listed below, are noticeably less exothermic.



Thus, dissolved oxygen raises the specific total enthalpy of photopolymerization even higher in larger samples, than is predicted by the equation (1) (Fig. 3, 2).

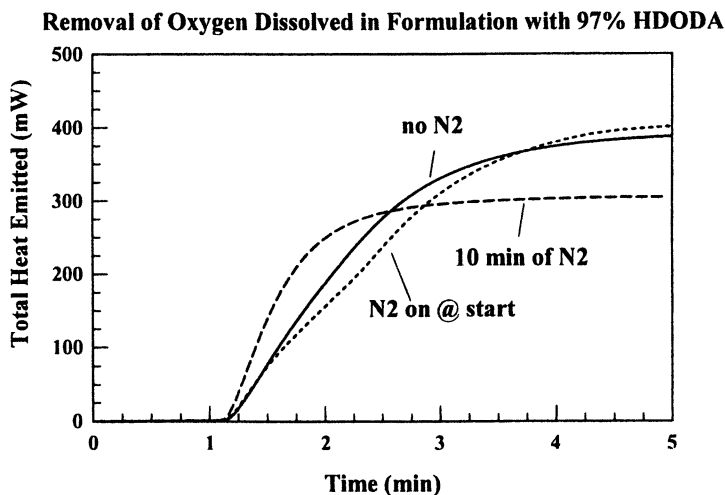


Figure 4. Integral heat emission dependence on nitrogen purge time

Nitrogen purging does not remove oxygen from acrylated compositions efficiently [10]. Kinetics of heat evolution during photopolymerization indicated

that oxygen removal by helium is more effective than by nitrogen at short times of degassing. If degassing is prolonged, nitrogen is more effective (Fig. 5).

Helium is less polar and less soluble in resins, but it diffuses faster than nitrogen. It may be concluded that inert gas diffusivity is dominant factor when the resin degassing time is short. To achieve higher photopolymerization rate at short light exposure, He should be used to purge oxygen from the resin.

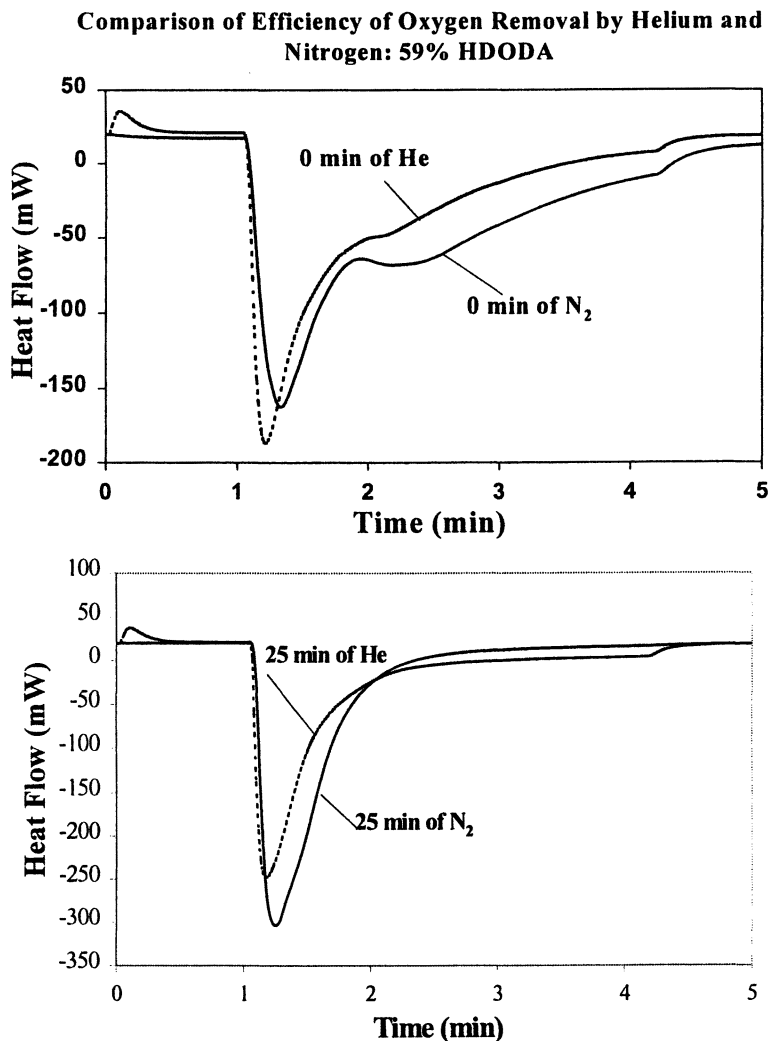


Figure 5. Efficiency of oxygen removal from 200 cps resin by He, and N₂

Photopolymerization and oxygen inhibition kinetics are diffusion controlled [1]. Thus, the differences in oxygen effects on the radical photopolymerization in resins of different viscosity were observed. Kinetics of acrylate photoconversion in the resin films opened to air and protected from oxygen by two NaCl substrates vary in resins with different viscosities (Fig. 6).

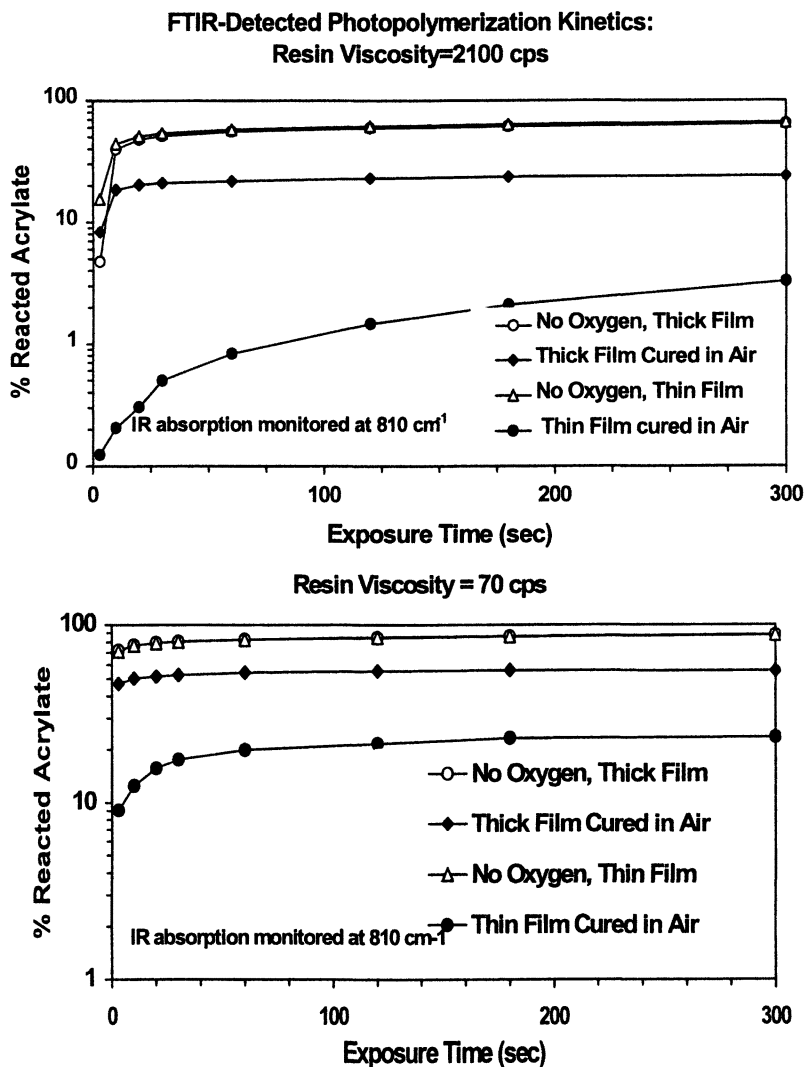


Figure 6. Cure kinetics dependence on layer thickness, films opened to air or cured between NaCl windows. Viscosity 70, 2100 cps, UV intensity 22 mJ/cm^2

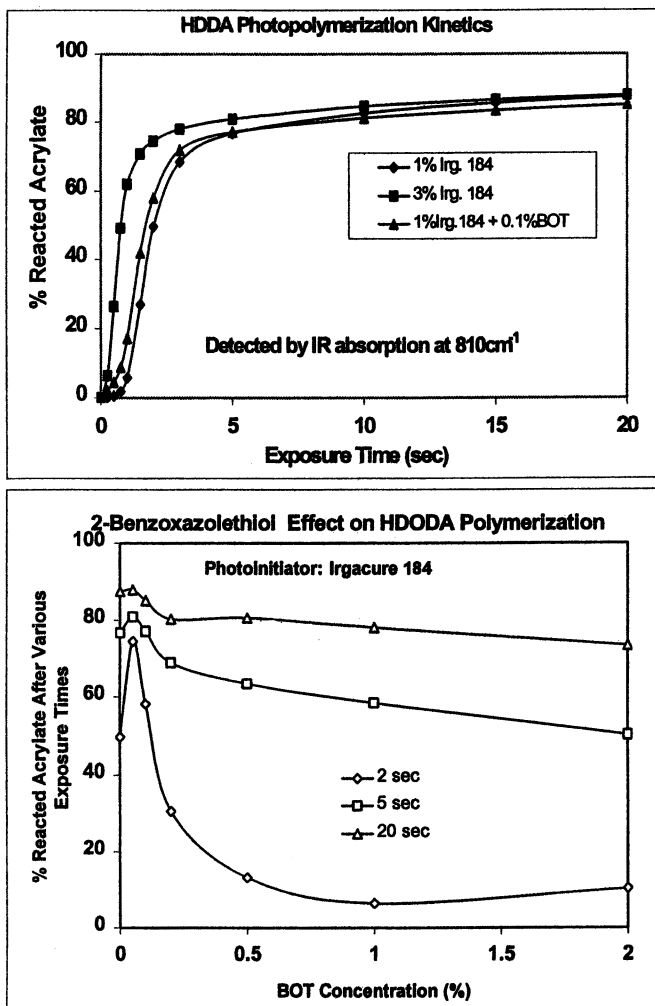
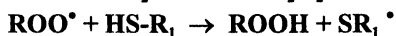
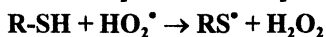
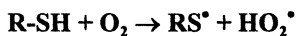


Figure 7. FTIR detected photoconversion of acrylate double bond in HDODA solutions of Irgacure 184 in the presence of 2-benzoxazolethiol

Mercaptans were reported to react with oxygen forming radicals capable of initiating acrylate polymerization [8-10].



The effects of aromatic thiols on the photopolymerization kinetics were studied by FTIR in the resins deposited between two NaCl windows, and thus, protected from oxygen uptake during photopolymerization. At low concentrations all aromatic thiols studied accelerated the photopolymerization (Fig. 7). At a higher concentration of thiols the chain-transfer and termination ability becomes detrimental to the chain growth. At low concentrations, the oxygen binding and "rejuvenation" of peroxy-radicals may be most influential process. Thiols may act as an oxygen removal pump. We confirmed that aromatic thiols form charge-transfer complexes with the photoinitiator. Formation of charge-transfer complexes could further accelerate photopolymerization complimenting the "oxygen pump" effect [10].

In the presence of oxygen growing polymer chains are terminated more frequently. Thus, the crosslink density is lower, vitrification of resin is delayed, and the shear modulus of the formed polymer is lower (film is "softer"). Since polymerization is controlled by monomer diffusion, the polymerization rate close to vitrification point is faster in softer films with lower crosslink density. Therefore, the rate of photopolymerization in the final stages is higher when polymerization is conducted in oxygen (Fig. 8).

The addition of chain-transfer agents and oxygen scavengers, such as thiols, alters kinetics of polymer network formation, and consequently, rheology of the polymer (Fig. 8). Alteration occurs because thiols terminate chain-growth by chain-transfer, further delaying vitrification and yet, initiate growth of the chain terminated by oxygen (Fig. 7). The mechanism and kinetics are interesting, however a detailed discussion of combination effects of thiols and oxygen on photopolymerization kinetics at the late stages of photopolymerization is outside the scope of the present review. The increase in rate of polymerization close to vitrification point in the presence of oxygen was confirmed for all cases by photo-DSC measurements as well.

Conclusion

We presented a brief review of our work on oxygen effects on photopolymerization in films up to 100 μ m thick. The inherent anisotropy of photopolymerization leads to an interesting dependence of oxygen effects on sample thickness and molecular diffusion rates in resin. The "thickness" is defined by light intensity, resin extinction coefficient and the rate of reactants diffusion [3-6]. Diffusion control of photopolymerization leads to oxygen and thiol effects that can be termed, "secondary." That is, the formation of "softer," less crosslinked polymers in the presence of oxygen, leads to higher rate of photopolymerization close to the vitrification point.

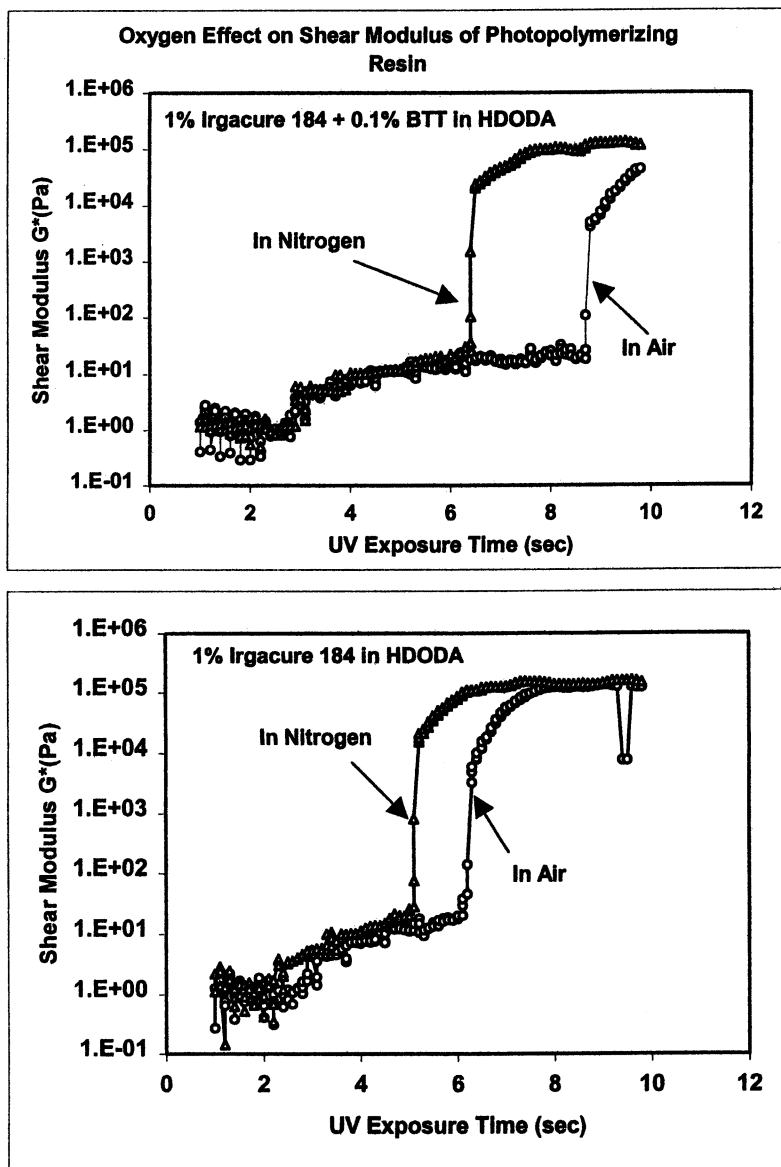


Figure 8. Kinetics of mechanical properties change as a function of time of exposure of photopolymerizing resin to UV radiation. In the presence of oxygen photopolymerization close to vitrification point is faster than in nitrogen.

Acceleration of photopolymerization rate in the presence of small amounts of aromatic thiols was observed. This was attributed to peroxy-radical "rejuvenation" in the presence of thiol.

Oxygen effects on photopolymerization kinetics outlined above are in agreement with previously published experimental and theoretical data [1-12]. It may be beneficial to use more direct methods of radical monitoring such as real-time electron spin resonance and time-resolved spectroscopy, to further study the mechanism of oxygen effects on photopolymerization in films.

Acknowledgement

We would like to thank Dr. Robert Johnson for monitoring the kinetics of the shear modulus change during photopolymerization.

References

1. Kh. S. Bagdasar'yan, "Theory of Free-Radical Polymerization", Israel Program for Scientific Translation, Jerusalem (1968).
2. V. V. Krongauz and R. M. Yohannan, *Mol. Cryst. Liquid Cryst.*, 183, (1990), 495.
3. V. V. Krongauz, E. R. Schmelzer, and R. M. Yohannan, *Polymer*, 32(9), (1991), 1654
4. V. V. Krongauz, and E. R. Schmelzer, *SPIE Proceedings, Photopolymer Device Phys., Chem. and Applicat.*, San Diego, USA, V. 1559, (1991), 354
5. V. V. Krongauz, and E. R. Schmelzer, *Polymer*, 33(9), (1992), 1893
6. V. V. Krongauz in V. V. Krongauz, and A. D. Trifunac, Edtrs., "Processes in Photoreactive Polymers," Chapman & Hall, New York, London, Sydney, etc., (1995), 185, and references therein.
7. G. R. Tryson and A. R. Shultz, *J. Polym. Sci.*, 17, (1979), 2059
8. R. S. Davidson in J. P. Fouassier and J. F. Rabek Edtrs., "Radiation Curing in Polymer Science and Technology-Volume III. Polymerization Mechanism," Elsevier Applied Science, London, New York, (1993), 153
9. M. S. Kharasch, W. Nudenberg, G. J. Mantell, *J. Org. Chem.* 16 (1951) 524
10. V. V. Krongauz, C. P. Chawla, *RadTech Asia Conference Proceedings*, Kunming, China, 15-19 May, (2001), 168
11. V. V. Krongauz and C. P. Chawla, *RadTech North America Conference Proceedings*, Baltimore, MD, (2000), 260.
12. V. V. Krongauz and C. Chawla, *RadTech Report*, September/October, (2001), 34

Chapter 15

Synergistic Free Radical Effects in Photoinitiated Cationic Polymerization

James V. Crivello

New York Center for Polymer Synthesis, Rensselaer Polytechnic Institute,
110 8th Street, Troy, NY 12180

Aryl free radicals produced by the photolysis of an onium salt photoinitiator can be used to accelerate the rates of photoinitiated cationic vinyl and ring-opening polymerizations. Secondary radical species generated by reaction of aryl radicals through hydrogen abstraction or by addition to double bonds of the monomer are oxidized to cations by onium salts. Fragmentation of the reduced onium salt produces radical species that participate in a non-photochemical chain process the generates additional cations. The increased number of initiating cationic species accounts for the observed acceleration effect.

Introduction

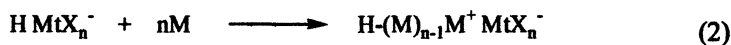
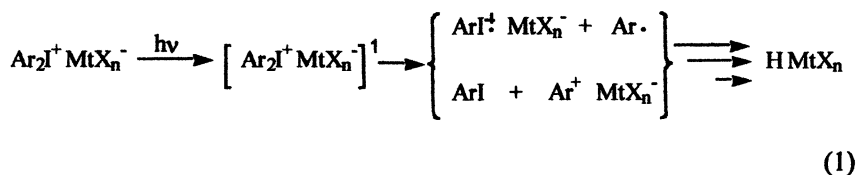
The commercial applications of photoinitiated cationic polymerizations have undergone rapid and broad-based growth in the past several years as this technology has gained widespread acceptance. As a result, there is currently considerable interest in the continued development of this field to discover new classes of photoinitiators, increase photosensitivity and to expand the range of monomers and reactive oligomers to which this chemistry may be applied. The ultimate motive, as always, is to improve the economics of photoinitiated cationic polymerization in commercial applications by further increasing the rates of polymerization of various monomer systems. This paper describes several methods of increasing the rates of cationic photopolymerizations through the use of synergistic reactions with free radical species.

Experimental

Monomers used in this study were obtained from commercial sources or were prepared as previously described.¹ The synthesis of the cationic onium salt photoinitiators used in this work has been described in publications from this laboratory.² The FT-RTIR apparatus and method employed for monitoring the photopolymerizations has already been reported.¹

Results and Discussion

The most common photoinitiators in use for cationic polymerizations are onium salts, such as diaryliodonium and triarylsulfonium salts. The proposed mechanism for their photolysis and initiation of cationic polymerization is shown in Scheme 1 as exemplified for diaryliodonium salts.³



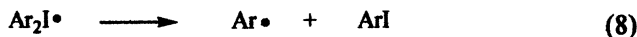
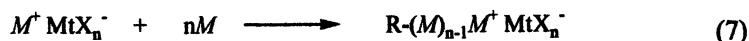
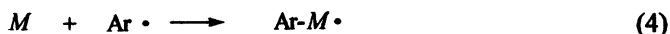
Scheme 1

As illustrated in Scheme 1, during the photolysis of a diaryliodonium salt (eq. 1), cations, radicals and cation-radicals are produced. Further reactions of the highly reactive positively charged species result in the formation of a strong protonic acid, HMtX_n . This latter acid directly initiates the polymerization of a wide variety of vinyl and heterocyclic monomers (eq. 2). Timpe⁴ and Müller, *et al.*⁵ have shown that the rate of a photoinitiated cationic polymerization can be expressed by equation 3 which is directly related to the number of initiating and propagating centers, R^+ and P^+ .

$$R_p = -d[M]/dt = k_p[M][P^+] + k_i[M][R^+] \quad (3)$$

Where the concentration of active cationic centers, $[P^+ + R^+] = \Phi_R \cdot I_{\text{abs}}/kt$ and Φ_R and I_{abs} are respectively, the quantum yield and the amount of light absorbed by the photoinitiator. For a specific monomer at a given light intensity, the rate of polymerization is a fixed quantity determined by the number of initiating and propagating cationic species generated by photolysis of the onium salt. This suggested to us that one should consider alternative means by which the number of cationic species in a photopolymerization mixture can be increased.

Usually, as shown in Scheme 1, the fact that aryl free radicals are also generated by the photolysis of onium salts is ignored since these species react further to form products that are of little consequence for the cationic polymerization. However, as depicted in Scheme 2, if such primary aryl free radicals react with a monomer (M) by addition (eq. 4) or hydrogen abstraction (eq. 5), the secondary free radical species formed may react with an onium salt by a redox reaction to give cations (eq. 6).

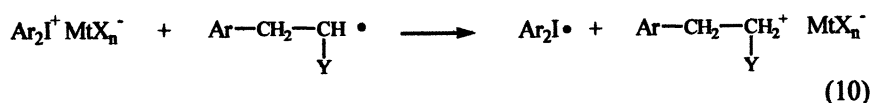
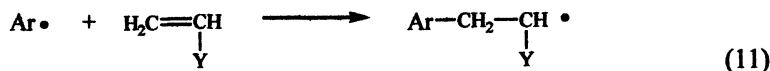


Scheme 2

The above mechanism involves a three-step radical chain process in which aryl radicals are converted to oxidizable radicals ($M \cdot$) that interact with the onium salt. Thereafter, the cations (M^+) generated by this process initiate polymerization (eq. 7), while the reduced onium salt undergoes irreversible

decomposition to regenerate aryl radicals (eq. 8). The overall consequence is that there is an amplification of the photolysis in terms of the number of initiating cationic species generated. Previously, Ledwith, et al.⁶ and Jönsson et al.⁷ have observed that various types of onium salts are capable of oxidizing certain free radicals.

As noted above, oxidizable free radicals can be generated from the addition of primary aryl radicals to vinyl double bonds as depicted in Scheme 3.



Scheme 3

When Y is an electron-donating group or a group that can provide resonance stabilization, the radical that is formed is easily oxidized to the corresponding cation. In this paper, examples in which both types of monomers are employed for the generation of cations will be presented.

Alkyl vinyl ethers are examples of monomers that provide readily abstractable hydrogen atoms and also undergo addition reactions. For these reasons, vinyl ether monomers are very reactive in onium salt photoinitiated cationic polymerizations.⁸ Shown in Figure 1 is a Fourier transform real-time (FT-RTIR) study of the cationic photopolymerization of triethyleneglycol divinyl ether with (4-decyloxyphenyl)phenyliodonium SbF_6^- (IOC10) in the presence and absence of nitrobenzene as a free radical retarder. In the presence of the retarder, the rate of the polymerization is markedly reduced and there is a long induction period before the polymerization proceeds. Similar results were obtained when the photoinitiated cationic polymerizations of vinyl ethers were carried out in the presence of oxygen instead of nitrogen.

Epoxide monomers can be deliberately designed to undergo facile hydrogen abstraction reactions. We have recently shown⁹ that epoxide monomers that incorporate benzylic ethers show extraordinarily high rates of cationic photopolymerization as compared with model compounds that do not contain these groups. This is illustrated in Figure 2. The same methodology can be extended to prepare still other types of monomers. For example, in Figure 3 is shown the photopolymerization of two recently prepared¹⁰ epoxide monomers that bear acetal groups in which the tertiary acetal hydrogens are readily abstractable. Both the radicals and the cations that are formed by hydrogen abstraction and oxidation of these monomers are stabilized by the presence of the flanking oxygen atoms.

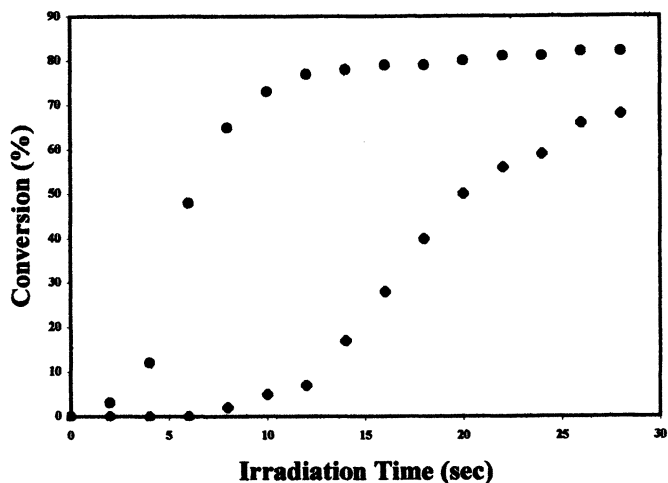


Figure 1. Photopolymerization of triethyleneglycol divinyl ether with 1.0 mol% IOC10 alone (●) and in the presence of 4.0 mol% nitrobenzene (◆).

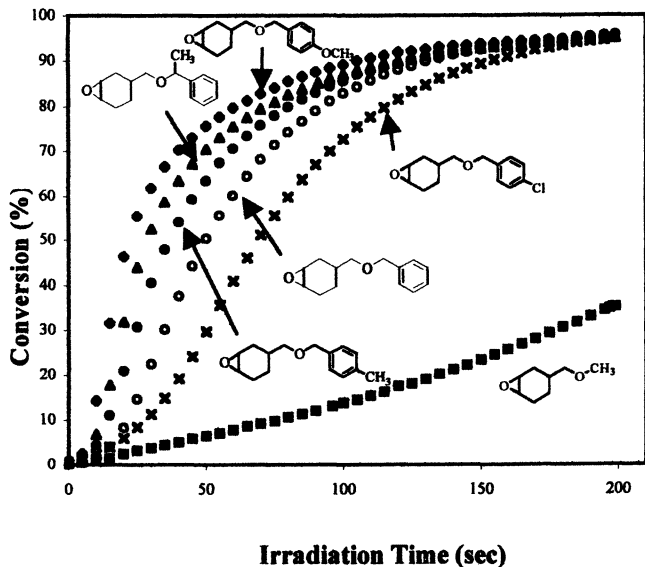


Figure 2. Comparison of the cationic photopolymerizations of various benzyl ether containing epoxy monomers, 1.0 % IOC10; light intensity 200 mJ/cm² min).

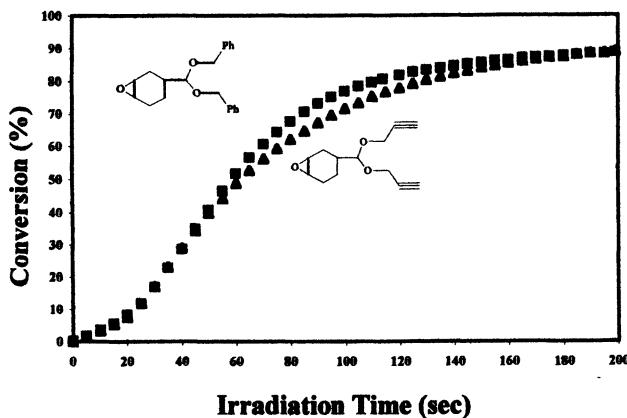


Figure 3. FT-RTIR study of the cationic photopolymerization of two epoxy acetal monomers. (light intensity $192 \text{ mJ/cm}^2 \text{ min}$; 1.0 % IOC10).

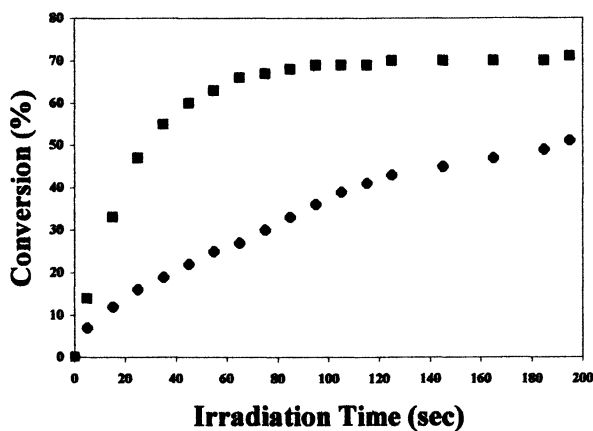


Figure 4. Photopolymerization of 3,4-epoxycyclohexylmethyl 3',4'-epoxycyclohexanecarboxylate alone (◆) in the presence of 2 equivalents of *n*-butyl vinyl ether (■) 1.0 mol% IOC10.

The ability of vinyl ethers to undergo hydrogen abstraction and addition to afford radicals that can induce the decomposition of onium salt photoinitiators was also employed for the acceleration of the ring-opening polymerizations of heterocyclic monomers. An example of this can be seen in Figure 4 in which the polymerization of bicycloaliphatic epoxide monomer, 3,4-epoxycyclohexylmethyl 3',4'-epoxycyclohexanecarboxylate, was carried out in the presence and absence of *n*-butyl vinyl ether. The rate of polymerization of the epoxide monomer is greatly accelerated in the presence of the vinyl ether monomer.

In contrast to vinyl ethers that do not undergo free radical homopolymerization, *N*-vinylcarbazole (NVK) readily polymerizes by a free radical mechanism. Moreover, this monomer is also interesting for two additional reasons. The terminal radical of a growing poly(*N*-vinylcarbazole) chain is readily oxidized to a resonance stabilized cation. In addition, the carbazole group is also a photosensitizer for onium salt photolysis.¹¹ Cationic ring-opening polymerizations of epoxides are markedly accelerated in the presence of NVK.¹² Shown in Figure 5 is a typical result for the polymerization of cyclohexene oxide in the presence and absence of NVK.

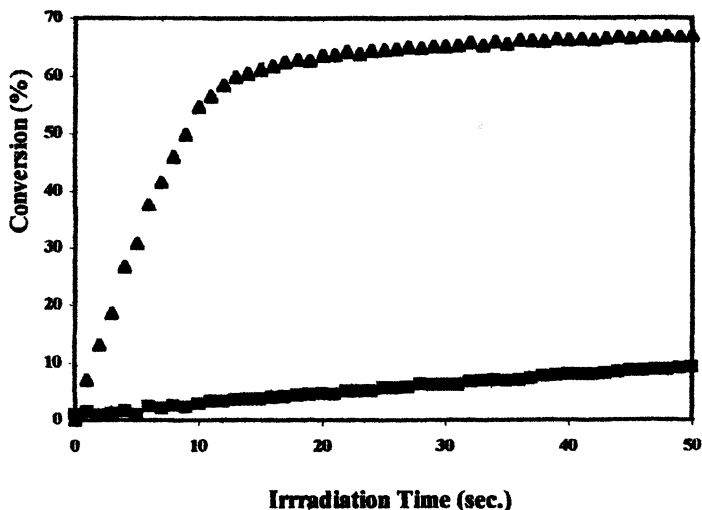


Figure 5. Photopolymerization of cyclohexene oxide with 0.01 mol% IOC10 alone (■) and in the presence of 29.0 mol% NVK (▲).

Despite the very low irradiation intensity (138 mJ/cm²/min) used in this experiment, there is a dramatic acceleration of the rate of polymerization of the

epoxide in the presence of NVK. In addition, the conversion of the epoxide to polymer is also greatly increased.

Epoxide monomers can also be purposefully designed to take advantage of the synergistic interaction of free radicals in their cationic ring-opening polymerizations. For example, in Figure 6 is shown a comparison of two epoxide monomers. Under the same photopolymerization conditions, the monomer bearing an allyl group shows a considerably higher reactivity than the corresponding monomer without a double bond. The allyl group can participate in the synergistic reaction both by providing labile allylic hydrogens for abstraction as well as through radical addition to the double bond.

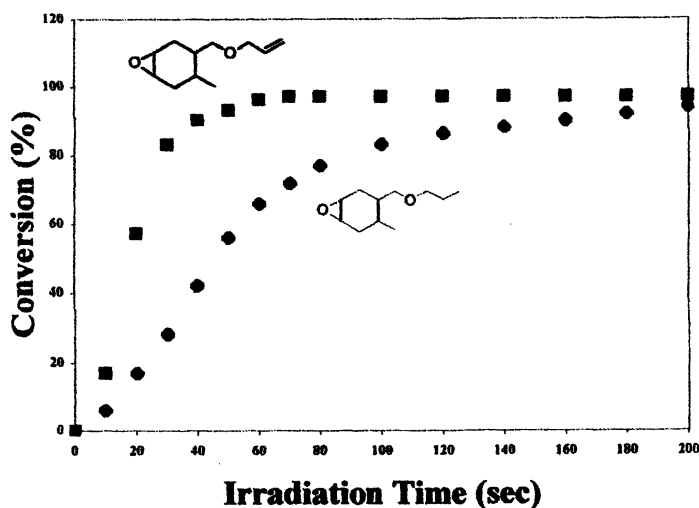


Figure 6. Comparison of the photopolymerizations of two epoxy monomers in the presence of 1.0 mol% IOC10.

Conclusions

In this paper, we have described a number of systems that illustrate how one can take advantage of the fact that the photolysis of onium salts generates aryl radicals to accelerate photoinitiated cationic polymerizations. This is achieved through the conversion of the initially formed aryl radicals to secondary radical species that can subsequently undergo oxidation in the presence of an onium salt photoinitiator by a non-photochemical process to give cations. Four examples were given in which the secondary radical species were produced by either hydrogen abstraction or by addition of the primary radicals to a vinyl carbon-carbon double bond. The resulting radical chain induced

decomposition of the onium salt makes this process especially efficient and has the overall result of substantially increasing the rate of cationic polymerization.

We anticipate that the novel methodology described in this paper will be particularly useful in accelerating photoinitiated cationic polymerizations that are employed in high speed coating, printing ink and adhesive applications.

References

1. Rajaraman S.K., Mowers W.A., Crivello J.V. *J. Polym. Sci., Part A: Polym. Chem. Ed.*, **1999**, *37*, 4007.
2. Crivello J.V., Lee J.L. *J. Polym. Sci., Part A: Polym Chem. Ed.* **1989**, *27*, 3951.
3. Crivello J.V. In: *Photoinitiators for Free Radical Cationic and Anionic Photopolymerization*, 2nd ed. Bradley G., Ed. Wiley New York, 1998, p. 329.
4. Timpe H.J. In: *Radiation Curing in Polymer Science and Technology, Vol. 11*, J.-P. Fouassier and J.E. Rabek, editors, Elsevier Applied Science, London, 1993, p. 535.
5. Müller U., Kunze A., Decker C., Herzig C., Weis J. *J. Macromol. Sci., Pure and Appl. Chem.*, **1997**, *A34(9)* 1515.
6. Abdoul-Rasoul F.A.M., Ledwith A., Yagci Y. *Polymer*, **1978**, *19*, 1219.
7. Jönsson, S.; Sundell, P.-E.; Skolling, O.; Williamson, S.E.; Hoyle, C.E. *Aspects of Photoinitiation, Radcure Coat. Inks*, **1993**, *79*, 81.
8. Mowers, W.A.; Rajaraman, S.K.; Liu, S.; Crivello, J.V. *Proc. RadTech 2000 Meeting*, Baltimore MD, Apr. 11-15, **2000**, p. 45; *RadTech Report*, **2000**, *March April*, 34.
9. Crivello J.V., Acosta Ortiz R. *J. Polym. Sci.: Part A: Polym. Chem. Ed.* **2001**, *39*, 2385.
10. Crivello J.V., Acosta Ortiz R. *J. Polym. Sci.: Part A: Polym. Chem. Ed.*, publication in press.
11. Chen Y., Yamamura T., Igarashi, K. *J. Polym.Sci., Part A: Polym Chem. Ed.*, **2000**, *38*, 90.
12. Hua Y., Crivello J.V. *J. Polym. Sci., Part A: Polym. Chem. Ed.*, **2000**, *38*, 3697.

Chapter 16

Initiation of Cationic Polymerization by Addition–Fragmentation Reactions: Bifunctional Addition–Fragmentation Agents as Photoinitiators for Cationic Polymerization

Yusuf Yagci and Aysen Onen

Istanbul Technical University, Science Faculty, Department of Chemistry,
Maslak 80626, Istanbul, Turkey

Specially designed allylic salts (addition-fragmentation agents, AFA) in conjunction with conventional radical initiators are shown to initiate cationic polymerization. The initiation mechanism involves addition of photochemically or thermally produced radicals to an AFA and subsequent fragmentation to yield reactive radical cations. For further extension of this new concept, self initiating AFAs were synthesized and used in photoinitiated cationic polymerization. For this purpose long absorbing chromophores (Michler's ketone, benzophenone or morpholino ketone) which gives the possibility of producing radical sites upon irradiation were introduced in the structure of addition fragmentation agents. Thus, this type of initiators function without the requirement of additional free radical sources.

Photoinitiated cationic polymerization is of great scientific and technological interest because of its range of application in coatings, adhesives, inks and resists (1). Photoinitiated polymerization is based on the photogeneration of acids and reactive cations. Diaryliodonium (2), triarylsulfonium (3,4) and mixed-ligand arene cyclopentadienyl metal salts (5) are widely used as powerful photoinitiators for cationic polymerization. The major concern for their practical uses was related to the overlap of their absorbances with the emission spectra of the commercial medium and low-pressure mercury lamps. Since this requirement is not fulfilled for certain easily available cationic photoinitiators, it was tried to extend their photosensitivity to higher wavelengths, e.g., $\lambda > 350$ nm with the aid of appropriate compounds. Free radical photoinitiators (6), photosensitizers (7), or charge transfer complexes (8) have been successfully employed to extend their spectral response to longer wavelengths. In this case electron transfer from the excited photosensitizer or photogenerated electron donor radicals to the onium salts results in the formation of reactive species which are capable of initiating the cationic polymerization of related monomers. Another method to overcome this problem is to introduce long absorbing chromophores in the structure of the photoinitiator.

We have recently developed an elegant and flexible way of initiating cationic polymerization by the use of specially designed allylic addition fragmentation agents (AFA) in conjunction with free radical sources (9-20). The obvious advantage of using AFAs is that initiation can be triggered by either heat or light. Moreover, as far as photopolymerization is concerned, it is extremely easy to tune a desired wavelengths' range (the emission band of the light source used) by choosing appropriate radical initiators. The system takes the advantage of the availability of the numerous radical initiators with excellent yields and good storage stability. Moreover, it is not limited to electron donor radicals, i.e. any radicals which are capable of adding double bonds may be employed. This possibility is not offered by any other existing salts, including iodonium salts which are known to be the strongest oxidants. Allylic salts with various substituents in the allylic moiety were shown to be very efficient AFAs for the initiation of cationic polymerization.

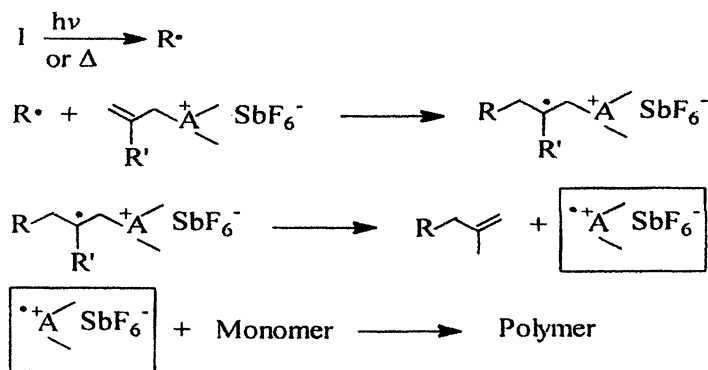
General Aspects on Addition Fragmentation Reactions

The use of addition fragmentation type reactions for cationic polymerization has been studied in detail. In this system various radical sources can be employed to activate the addition fragmentation agent. Table I gives an information on the structure of addition fragmentation agents synthesized so far and their mode of activation. Outlined in Scheme 1 is the mechanism which we propose for the addition-fragmentation type initiation. In the first step, radicals generated either by heat or light add to the double bond of the allylic salt producing a radical in the β position to the heteroatom of the onium salt cation. Consequently, the

Table I. Addition- Fragmentation Agents and Their Mode of Activation

AFA	Structure	<u>Direct</u>		<u>Radical Induced</u>	
		Thermal	Photo	Thermal	Photo
AFA1	$\text{CH}_2=\underset{\text{R}'}{\text{C}}-\text{CH}_2-\text{S}^+\text{[]} \text{SbF}_6^-$	Yes	No	Yes	Yes
AFA2	$\text{CH}_2=\underset{\text{R}'}{\text{C}}-\text{CH}_2-\text{N}^+(\text{C}_6\text{H}_5) \text{SbF}_6^-$	Yes	Yes	Yes	Yes
AFA3	$\text{CH}_2=\underset{\text{R}'}{\text{C}}-\text{CH}_2-\text{O}-\text{N}^+(\text{C}_6\text{H}_5) \text{SbF}_6^-$	Yes	Yes	Yes	Yes
AFA4	$\text{CH}_2=\underset{\text{R}'}{\text{C}}-\text{CH}_2-\text{O}-\text{N}^+(\text{C}_{10}\text{H}_7) \text{SbF}_6^-$	Yes	Yes	Yes	Yes
AFA5	$\text{CH}_2=\underset{\text{R}'}{\text{C}}-\text{CH}_2-\text{N}^+(\text{C}_6\text{H}_5)(\text{CH}_3)_2 \text{SbF}_6^-$	Yes	Yes	Yes	Yes
AFA6	$\text{CH}_2=\underset{\text{R}'}{\text{C}}-\text{CH}_2-\text{P}^+(\text{C}_6\text{H}_5)_3 \text{SbF}_6^-$	Yes	No	Yes	Yes

molecule undergoes fragmentation yielding radical cations which with high rates initiate the polymerization of cationically polymerizable monomers.



Scheme 1. Mechanism of addition-fragmentation type initiation

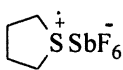
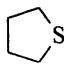
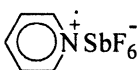
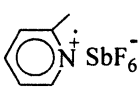
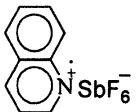
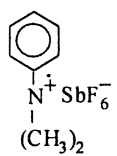
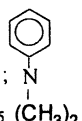

Fragmentation brings about the elimination of the substituents that formerly prevented the cationic center from reacting with monomer. The allylic moiety represents the reactive site for the addition step whereas the charged onium cation is a latent initiating species which is released by fragmentation. Chromatographic analysis of remaining polymerization mixtures shows that depending on the structure of the AFA, various olefinic, hydroxyl and aldehyde compounds, and epoxides are also formed in the course of fragmentation (Table II). The analytical detection of these side products is taken as another proof that the initiation mechanism indeed involves addition-fragmentation.

It should also be pointed out that in some cases favourable redox potentials allows the salts (allylsulphonium and allyloxy pyridinium salts) to participate in electron transfer reactions, thus initiating polymerization. For this reaction to occur, the radicals should be nucleophilic. Carbon centered radicals with electron donating substituents are more easily oxidized by AFA. Thus, depending on the type of radical source employed only addition-fragmentation or both addition-fragmentation and electron transfer mechanisms may be operative (Table III).

Bifunctional Addition-Fragmentation Agents

In our recent studies we synthesized bifunctional photoactive AFAs (16,17,18). These types of initiators include an intrinsic chromophoric group for radical generation and an allylic salt structure for the addition fragmentation scheme in the same structure. In this case the system takes the advantage of generating free radicals without any additional radical sources by irradiating the initiator itself at wavelengths where commercial light sources emit.

Table II. Initiating Species and By-Products Resulting From Addition Fragmentation Mechanism

<i>AFA</i>	<i>Ionic Species</i>	<i>By Products</i> ^a	<i>Reference</i>
AFA1		$\text{R-CH}_2\text{-C} \begin{array}{l} \text{CH}_2 \\ \parallel \\ \text{COOC}_2\text{H}_5 \end{array}$; 	9
AFA2		$\text{R-CH}_2\text{-C} \begin{array}{l} \text{CH}_2 \\ \parallel \\ \text{COOC}_2\text{H}_5 \end{array}$	10
AFA3		$\text{R-CH}_2\text{-C} \begin{array}{l} \text{O} \\ \diagup \quad \diagdown \\ \text{CH}_2 \quad \text{CH}_2 \\ \parallel \\ \text{COOC}_2\text{H}_5 \end{array}$; $\text{R-CH}_2\text{-C} \begin{array}{l} \text{HC=O} \\ \parallel \\ \text{COOC}_2\text{H}_5 \end{array}$	12
AFA4		$\text{R-CH}_2\text{-C} \begin{array}{l} \text{O} \\ \diagup \quad \diagdown \\ \text{CH}_2 \quad \text{CH}_2 \\ \parallel \\ \text{COOC}_2\text{H}_5 \end{array}$	14
AFA5		$\text{C}_6\text{H}_5\text{-C(=O)-CH}_2\text{-C} \begin{array}{l} \parallel \\ \text{COOC}_2\text{H}_5 \end{array} \text{=CH}_2$; 	20
AFA6		$\text{R-CH}_2\text{-C} \begin{array}{l} \parallel \\ \text{COOC}_2\text{H}_5 \end{array} \text{=CH}_2$	13

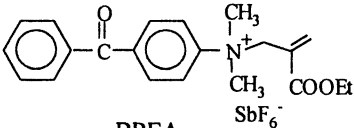
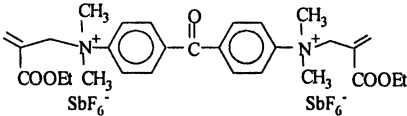
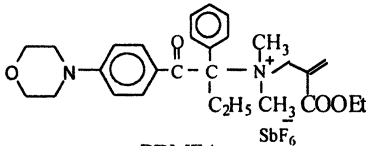
^aDetected by GC-MS

Table III. Radical Sources Used in Addition Fragmentation Type Initiation

Radical Source	Radicals participating in Electron transfer	Radicals participating in Addition fragmentation
4,4'-Azobisisobutyronitrile (AIBN)	--	
Dibenzoylperoxide (BPO)	--	
Phenylazotriphenylmethane (PAT)		
Benzoin (B)		
2,4,6-Trimethylbenzoyl diphenylphosphonyl oxide (TMDPO)	--	
Benzophenone + Hydrogen Donor (BP+RH)		R·

Bifunctional photoactive AFAs have been synthesized by the reaction of ethyl α -(bromomethyl)acrylate with Michler's ketone, N,N-dimethylamino-benzophenone or morpholino ketone. The structure and absorption characteristics of these AFAs were summarized in Table IV. As can be seen from Table IV, bifunctional AFAs may be placed in two classes: (1) those which undergo intramolecular bond cleavage, such as morpholino derivative (BDMEA), and (2) those which undergo intermolecular H-abstraction, notably benzophenone and Michler's ketone derivatives (BPEA and MKEA, respectively).

Table IV. Structure and Characteristics of Photoactive Addition Fragmentation Agents

<i>AFA</i>	<i>Absorption Characteristics</i>		<i>The Mode of Radical Generation</i>
	λ_{max} (nm)	ϵ ($l\ mol^{-1}\ cm^{-1}$)	
 <p>BPEA</p>	347	24032	Hydrogen abstraction
 <p>MKEA</p>	361	43076	Hydrogen abstraction
 <p>BDMEA</p>	365	19600	α -cleavage

Intramolecular Bond Cleavage Type AFA

Polymerization initiated by Morpholino Ketone ethyl acrylate salt (BDMEA) .

Photoinitiated cationic polymerization of CHO was carried out with BDMEA . As can be seen from Table V, CHO can be polymerized quite effectively upon irradiation at rather long wavelenghts. Upon absorption of light, this compound undergoes α -cleavage analogous to the precursor photoinitiator 2-benzyl-2-(N,N-dimethylamino)-1-(4-morpholinophenyl)-butane-1-one (BDM) and forms radicals which may then add to another molecule (Scheme 2). In this case the addition fragmentation mechanism operates in the usual manner.

In order to gain more insight to the mechanism of initiation, CHO was polymerized with the combination BDM and a simple allyl ammonium salt namely, N,N-dimethylanilinium ethyl acrylate (DMEA) under the same experimental conditions. Although at lower rate, the combined system also initiated the polymerization via an addition-fragmentation scheme. In this case radicals are formed independently and subsequently added to the free salt for the generation of reactive cations.

Intermolecular Hydrogen Abstraction Type AFAs

Polymerization initiated by benzophenone ethyl acrylate salt (BPEA).

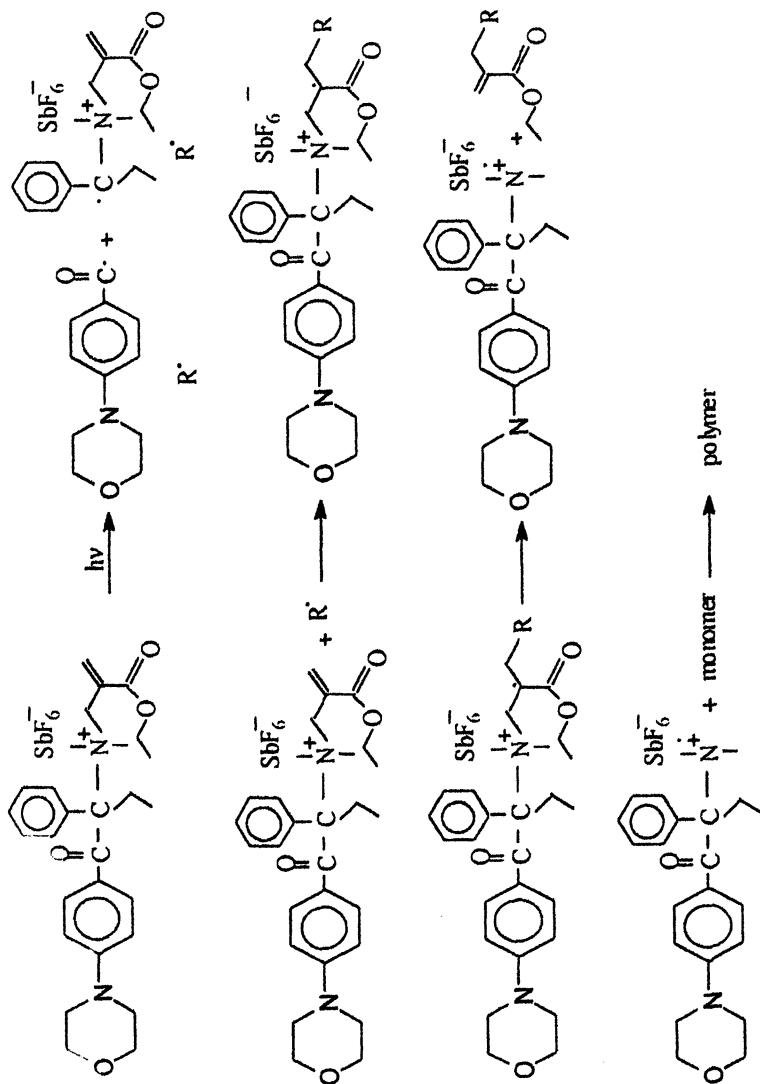
Benzophenone and derivatives are known to initiate radical polymerization via the hydrogen abstraction mechanism as shown below in Scheme 3.

Table V. Polymerization of CHO^a in the Presence of Allylic Salt BDMEA at Different Wavelengths

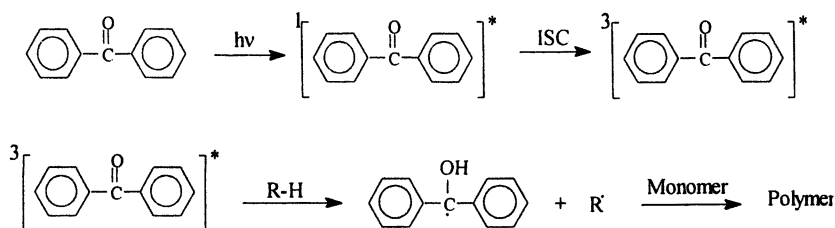
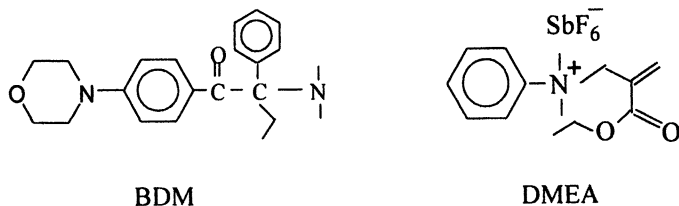
<i>Wavelength</i> $\lambda(\text{nm})$	<i>Conversion</i> (%)	<i>Mn</i> (g mol^{-1})
350	5.58	1300
380	21.46	6845
400	11.47	1300

^a[CHO] = 9.88 mol/L, [I1] = 5×10^{-3} mol/L, Time= 6 min.

SOURCE: Reproduced with the permission from reference 16. Copyright 2002 Wiley-VCH .



Scheme 2. Initiation of cationic polymerization by BDMEA

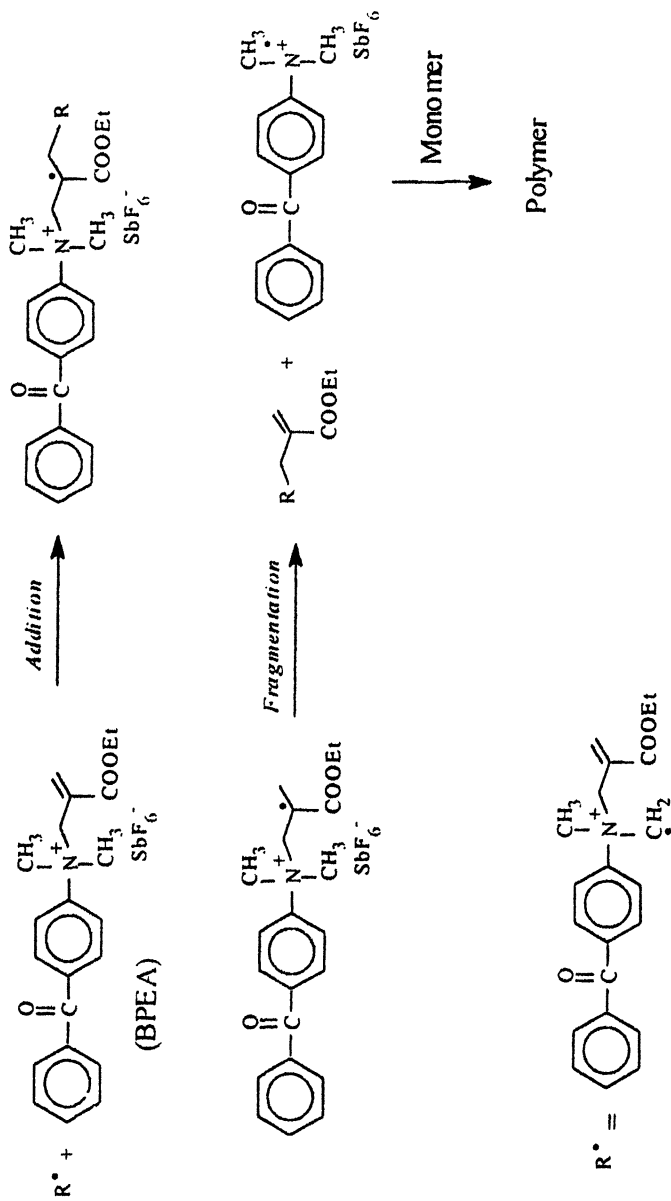


Scheme 3. Photoinitiated free radical polymerization by using benzophenone

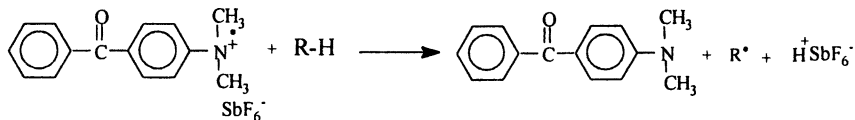
In our case upon irradiation of benzophenone-allyl salt (BPEA), the precursor benzophenone group produces the radical species by hydrogen abstraction from ground state BPEA in a mechanism similar to that described above for benzophenone. These radicals add to the allylic double bond and subsequently the ammonium radical cation is released which initiates polymerization (Scheme 4). Additional support for the initiation by radical addition fragmentation processes was obtained by irradiating a methanol solution of $5 \times 10^{-3} \text{ mol.L}^{-1}$ BPEA in the absence of monomer and analysing the photolysis products by GC-MS. Notably, GC-MS detection of the unsaturated addition and fragmentation product ($m-1 = 449$) confirms the proposed mechanism.

The resulting ammonium radical cations are potentially able to initiate cationic polymerization. Spectral investigation of the polymers obtained with BPEA was also studied to understand the initiating species. UV spectrum of the polymer isolated by precipitation with MeOH shows an absorption maxima at 341 nm attributable to the end benzophenone moiety. However, this absorption may be due to the termination of the propagating ends by the liberated N,N-dimethylaminobenzophenone as was proposed for benzylic ammonium salts (23).

Besides the direct initiation by radical cations, the initiation by a Brønsted acid generated after H abstraction must also be considered (Scheme 5). In this case the radical cations may abstract a hydrogen atom from the solvent, monomer or ground state allylic salt, and the resulting intermediate dissociates to liberate a strong acid.



Scheme 4. Initiation of cationic polymerization by BPEA



Scheme 5. Brønsted acid generation by hydrogen abstraction

Support for the proposed mechanism was readily obtained by studying the effect of BPEA concentration on the CHO polymerization. The results apparently show that conversions to poly(cyclohexene oxide) increased rapidly with increasing concentration of BPEA as the probability of hydrogen donation is increased. According to these investigations it is not easy to determine which mechanism is operative for the initiation step.

As can be seen from Figure 1, CHO can be polymerized effectively in the presence of BPEA. In Fig.1-A BPEA concentration was adjusted as $\text{OD}_{347\text{nm}} = 0.95$. In this case the conversion to poly(cyclohexene oxide) increases with time and reaches 55% in 20 min. By considering the effect of BPEA concentration on the conversion, time-conversion behaviour of CHO polymerization was also examined at a higher concentration of BPEA. As shown in Fig.1-B CHO conversion reaches to limiting value of 73% in 2 min. time and remains in the same order.

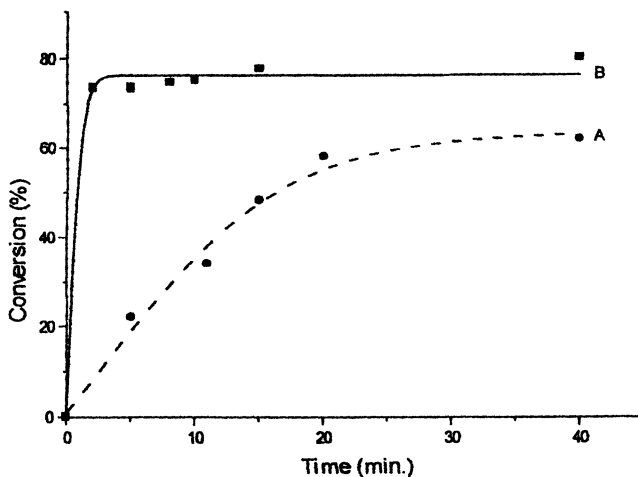


Figure 1. Photopolymerization of CHO in the presence of BPEA. $[\text{CHO}] = 9.88 \text{ mol.L}^{-1}$, $\lambda > 300 \text{ nm}$, 20°C , (A) $\text{OD}_{347\text{nm}} = 0.95$, $[\text{BPEA}] = 4.17 \times 10^5 \text{ mol.L}^{-1}$ (B) $[\text{BPEA}] = 5 \times 10^3 \text{ mol.L}^{-1}$

For comparison with allylic type ammonium salts, the benzyl salt of 4-N,N-dimethylamino benzophenone (BPB) was also synthesized and used as an initiator for CHO polymerization resulting in no polymer. These experiments were performed at a concentration providing the same absorbance at the irradiation wavelength.

Polymerization initiated by Michler's Ketone ethyl acrylate salt (MKEA)

Photoinitiated cationic polymerization of cyclohexene oxide (CHO) was carried out with MKEA (Figure 2). The polymerization did not take place up to 1 min irradiation probably owing to the trace impurities present in the system, but the reaction reached 60 % conversion immediately thereafter. Strong electron donating monomers such as N-vinyl carbazole, isobutyl vinyl ether and n-butyl vinyl ether undergo explosive polymerization upon illumination with light.

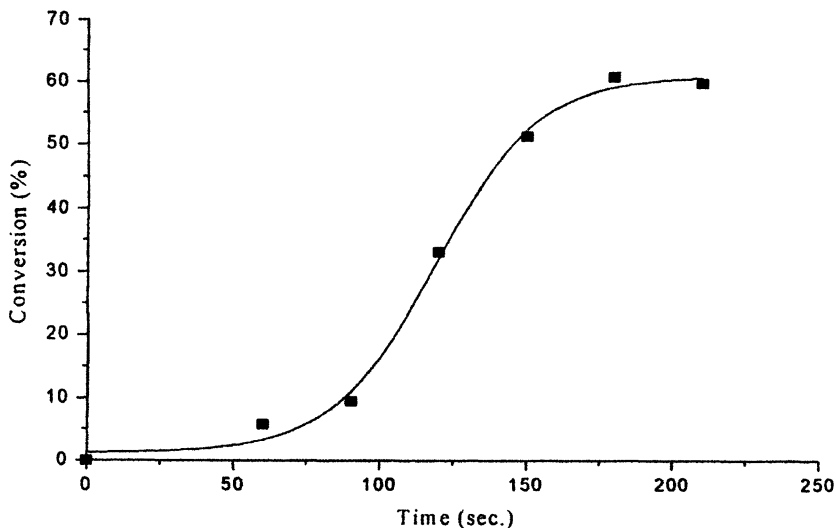
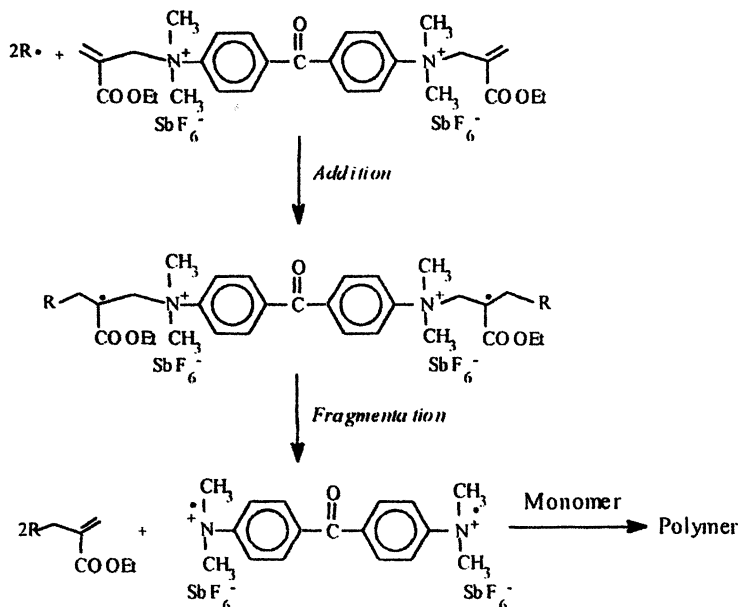


Figure 2. Photopolymerization of CHO in the presence of MKEA, $[CHO] = 9.88 \text{ mol.l}^{-1}$, $[MKEA] = 2.2 \times 10^{-5} \text{ mol.l}^{-1}$, $\lambda_{inc} = 350 \text{ nm}$ (Reproduced with permission from reference 17. Copyright 2001 Elsevier.)



Scheme 6. Initiation of cationic polymerization by MKEA

On the basis of photochemistry of MK and the previous discussions on polymerization with AFAs, the initiating species generated from MKEA in this cationic polymerization could be considered to be again ammonium radical cations (Scheme 6). Accordingly, radicals formed by hydrogen abstraction mechanism adds to the double bond, and subsequently ammonium radical cation is released which either directly initiates the polymerization or participates in further hydrogen abstraction reactions to generate reactive Bronsted acids as discussed above for benzophenone type salts.

Further support for the initiation mechanism was obtained by polymerizing CHO with an initiating system consisting of radical generating and addition fragmentation components independently. Using combination of MK and N,N dimethyl anilinium ethyl acrylate salt (DMEA) at a concentration providing the same absorbance at the irradiation wavelength produced polymers with similar yields.

References

1. *Chemistry and Technology of UV&EB Formulation for Coatings, Inks&Paints*; Dietliker, K.; SITA Technology Ltd.: London, 1991; Vol.III
2. Crivello, J.V.; ..Lam, J.H.W. *J. Polym.Sci. Polym.Chem.Ed.* **1980.**, 18, 2677.

3. Crivello, J.V.; Lam, J.H.W. *J.Polym.Sci., Polym.Chem.Ed.* **1980**, *18*, 2967.
4. Crivello, J.V. ;Lam, J.H.W. *Macromolecules*, **1979**, *10*, 1307 .
5. Meier, K.; Zweifel H.J. *J.Radiat.Curing*, **1986**, *13*, 26.
6. Ledwith, A. *Polymer*, **1978**, *19*,1217.
7. Pappas, S.P.; Pappas, B.C.; Gatechair, L.R.; Jilek, J.H.; Schnabel , W. *Polym.Photochem.* **1984**, *5*, 1.
8. Yagci, Y.; .Lukac, I.; Schnabel, W. *Polymer*, **1993**, *34*, 1130 .
9. Denizligil, S.; Yagci, Y.; .McArdle, C. *Polymer*, **1995**, *36*, 16, 3093.
10. Yagci, Y.; Onen, A. *J.Polym.Sci., Polym.Chem.Ed.*, **1996**, *34*, 3621.
11. Bacak, V.; Reetz, I.; Yagci, Y.; Schnabel, W. *Polym.Int.*, **1998**, *47*, 345.
12. Yagci, Y.; Reetz, I. *Macromol.Symp.*, **1998**, *132*, 153 .
13. Atmaca, L.; Kayihan, I.; Yagci, Y. *Polymer*, **2000**, *41*, 6035.
14. Atmaca, L.; Onen,A.; Yagci,Y. *Eur.Polym.J.* **2001**, *37*, 677.
15. Onciu, M.; Onen,A.; Yagci,Y. *Polym.Int.* **2001**, *50*, 144.
16. Yagci,Y.; Yildirim.S.; Onen,A. *Macromol.Chem.Phys.*, **2001**, *202*, 527.
17. Onen, A.; Yagci,Y. *Polymer*, **2001**, *42*, 6681.
18. Yurteri,S.; Onen, A.;Yagci, Y. *Eur.Polym.J.*, **2002**, *38*, 1845.
19. Onen, A.;Yagci, Y. *Macromol.Chem.* **2001**, *202*, 1950.
20. Yagci, Y.; Onen, A.; Reetz,I. *Macromol.Symp.* **2001**, *174*, 255.
21. Onen, A.;Yagci, Y. *Macromolecules*, **2001**, *34*, 7608.
22. Bayramoglu, F.; Onen, A.; Yagci, Y. *e-Polymers*, **2001**, *10*.
23. Lee, S.; Takata, T.; Endo,T. *Macromolecules*, **1991**, *24*, 2689.

Chapter 17

Diazonium Salts as Cationic Photoinitiators: Radical and Cationic Aspects

U. Müller^{1,5}, A. Utterodt^{2,5}, W. Mörke³, B. Deubzer⁴,
and Ch. Herzig⁴

¹Kompetenzzentrum Holz GmbH, St.-Peter-Strasse 25,
A-4021 Linz, Austria

²DETAX GmbH and Company KG, Carl-Zeiss-Strasse 4,
D-76275 Ettlingen, Germany

³Institut für Analytik und Umweltchemie der Martin-Luther-Universität
Halle-Wittenberg, Geusaer Strasse, D-06217 Merseburg, Germany

⁴Wacker-Chemie GmbH, Johannes-Hess-Strasse 24,
D-84489 Burghausen, Germany

⁵Former address: Institut für Organische Chemie der Martin-Luther-
Universität Halle-Wittenberg, Geusaer Strasse,
D-06217 Merseburg, Germany

4-Hexyloxysubstituted diazonium salts with complex anions are thermostable compounds in several solvents (dioxane: 12 d; 1,2-dichloroethane: 410 d; 40°C; salt as hexafluoroantimonate).

These salts efficiently initiate the photocrosslinking of vinyl ethers and epoxides. Interestingly, oxygen influences the efficiency of this cationic process. EPR-experiments prove that radicals possess a key function for the production of the initiating species. α -Ether radicals induce a secondary radical induced cation formation. Such reactions are always possible if E_{red} of the onium salt is lower than -1V. Oxygen inhibits this radical induced cation formation. On the other hand, the decay of peroxides results in a branched radical reaction. The reaction rate is faster under air with respect to inert conditions.

The high thermostability of the used salt decreases by addition of a small amount of monomer. A bimolecular dediazonation

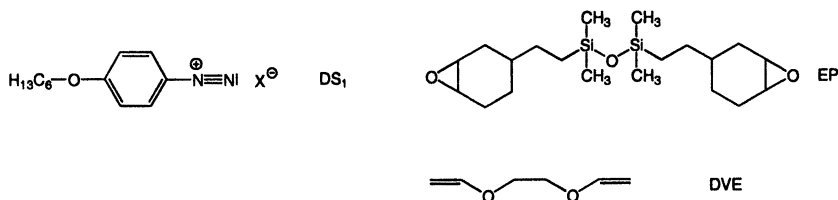
mechanism explains the observed effects. This mechanism produces directly initiating cationic species, which start the cationic polymerization.

The monomer and its by-products are the cause of the poor thermal stability of the diazonium salts and not the inherent thermal instability of the salt used.

Introduction

Aromatic diazonium salts with anions of low nucleophilicity (1) have received remarkable attention as the first efficient photoinitiators for cationic polymerization. However, the poor thermal stability of diazonium salts often limits their use as photoinitiators for cationic systems. Interestingly, diazonium salts possess sufficient thermal stability in diazomicro films and printing plates (2) over several months or years.

The 4-hexyloxysubstituted diazonium salt (see Scheme 1) with complex anions like BF_4^- , PF_6^- , SbF_6^- and $\text{B}(\text{C}_6\text{F}_5)_4^-$ is a thermostable compound in several solvents. The measured half-lives of the SbF_6^- -salt in solution is greater than 12 d at 40°C and depend strongly on the solvent used (dioxane: 12 d; dichlorethane: 410 d). Moreover, the UV-absorption of these salts ($\lambda_{\text{max}} \approx 315 \text{ nm}$; $\epsilon \approx 27000 \text{ l}\cdot\text{mol}^{-1}\cdot\text{cm}^{-1}$) overlaps very well with the emission of excimer lamps ($\lambda = 308 \text{ nm}$). Additionally, no absorption of diffuse daylight and a high photosensitivity ($\Phi \approx 0,4$) characterize this onium salt.



Scheme 1. Used compounds

Both photosensitivity and the match between absorption maxima and emission line of excimer lamps argue for the use of diazonium salts as photoinitiators. Nevertheless, diazonium salts are known as relative unstable compounds. The contradiction in the thermal stability in several applications was the purpose to reexamine again the cationic photopolymerization of epoxides and vinyl ether derivatives using diazonium salts as photoinitiators; see Scheme 1.

Results and Discussion

Kinetics of Photocrosslinking

General crosslinking kinetics

The rate of polymerization (R_P) and the conversion (x) can be obtained at selected reaction times from the heat flow value if the standard reaction heat is known for the system used, see Eq. (1).

$$R_P = -\frac{d[M]}{dt} = -\frac{dx}{dt} \cdot [M]_0 = -\frac{dH}{dt} \cdot \frac{[M]_0}{\Delta_R H^\circ} \quad (1)$$

where $[M]$ is the molar concentration of polymerizable functional groups, t is the time, x is the conversion, dH/dt is the heat flow of the reaction, and $\Delta_R H^\circ$ is the standard reaction enthalpy of the crosslinking.

Using Eq. (2) one can describe the rate of the photocrosslinking process (R_P) in bulk under stationary irradiation conditions,

$$R_P = k(x) \cdot [M]^\alpha \cdot I_0^\beta \quad (2)$$

where $k(x)$ is a conversion (x) dependent quantity, I_0 is the intensity of the incident light, α and β are exponents.

The exponent β gives information about termination mechanisms. The following relationships can be outlined for β (4, 5):

- $\beta = 1$, first-order termination,
- $0.5 < \beta < 1$, mixed first- and second-order termination,
- $\beta = 0.5$, second-order termination.

The photoinduced crosslinking allows one to stop the initiation of the crosslinking reaction at a defined time (t_{ex}). The kinetics of the crosslinking is simplified to propagation and termination steps. The conversion of the monomer in the dark period (x_D) after initiation corresponds to Eq. (3); see (4):

$$-\ln(1-x_D) = k_p/k_t [P^*]_0 (1-\exp(-k_t \cdot t)) \quad (3)$$

where x_D is the double bond conversion in the dark period, $[P^+]_0$ is the polymer cation concentration at beginning of postpolymerization, k_p is the polymerization rate constant, k_t is the termination rate constant.

Crosslinking using diazonium salts

The used salt efficiently initiates the photocrosslinking of vinyl ethers and epoxides, (Figure 1). The plot R_p vs. I_0 shows linear behavior, which stands in agreement with ideal cationic polymerizations ($\beta = 1$). Therefore, the cationic polymerization should occur independently of atmospheric conditions. Surprisingly, the measured reaction rate differs under air and inert conditions. A second maximum in the reaction rate can be observed under air. The reaction rate is faster under air than under inert conditions, see Figure 1. Nevertheless, in comparison to crosslinking under inert conditions, the time to reach the maximum value of R_p is delayed under air.

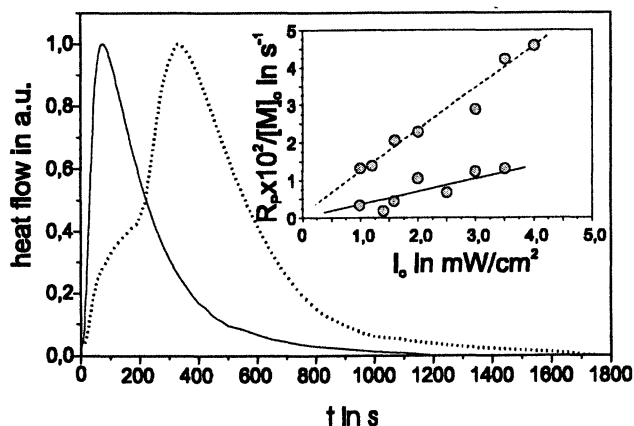


Figure 1. Measured heat flow in the crosslinking of the system EP/DS₁ under air (dotted line) and under reduced pressure (14 mbar; full line). Insert: R_p as function of the incident light ($[DS_1] = 2 \cdot 10^{-2}$ mol/l; DS₁ as SbF₆⁻, $I_0 = 2$ mW/cm²).

Modified reprint from Ref. 3 by permission of ELSEVIER SCIENCE.

Postpolymerization experiments were made to study the effect of oxygen on the propagation and termination step. The results of this study are summarized in Figure 2.

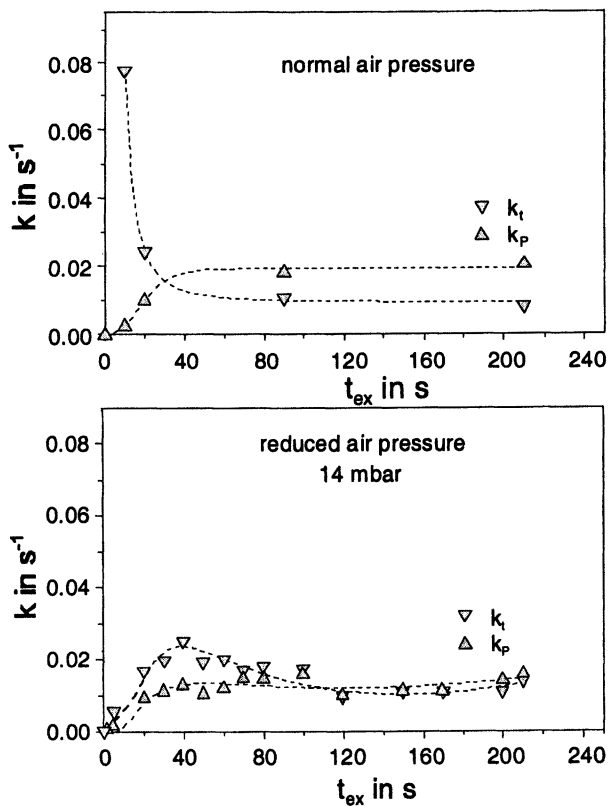


Figure 2. Rate constants of propagation (k_p) and termination (k_t) as a function of the irradiation time t_{ex} (system EP/DS₁; [DS₁] = $2 \cdot 10^{-2}$ mol/l; DS₁ as SbF₆⁻; $I_0 = 3$ mW/cm², top: under air, bottom: reduced pressure). Reprinted from Ref. 3 by permission of ELSEVIER SCIENCE.

As expected, k_p is nearly independent of the atmospheric conditions. The k_p -value increases asymptotically with increasing irradiation time t_{ex} . Surprisingly, our results show a strong dependence of the termination step on the atmospheric conditions. Under inert conditions, the k_t -value is small, increases, reaches a maximum and approaches a constant value at prolonged irradiation time. Such behavior suggests that only a small amount of inhibitor is present in the formulation. Moreover, the increasing k_t could be caused by immobilization of the reactive chain end.

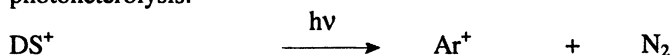
However, a very effective inhibition was found under air; k_t starts at a high level and decreases with increasing irradiation time t_{ex} . These facts show that

oxygen influences the termination reaction. This effect is surprising since k_t is a function of a cationic process and should not show any interaction with oxygen.

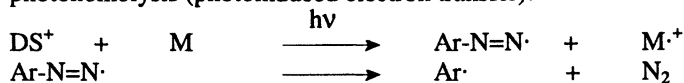
EPR-experiments — Electron transfer

The photolysis of the diazonium salts is independent of oxygen in several organic solvents (acetonitrile, 1,2-dichloroethane, 1,2-dimethoxyethane) (3). These results show that the salts decompose by photoinduced heterolysis, (Scheme 2).

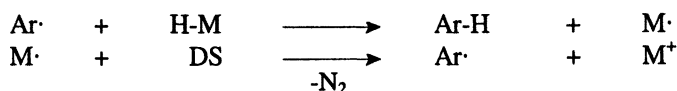
photoheterolysis:



photohomolysis (photoinduced electron transfer):



MEERWEIN-reduction:



Scheme 2. Photolysis and MEERWEIN-reduction of diazonium salts.

Nevertheless, the oxygen influence on the cationic crosslinking shows that radical reactions play a key role in the crosslinking process. The EPR-experiments show that radicals were formed during the photolysis; (Figure 3). The photolysis of the diazonium salt in the different monomer systems results in similarly shaped EPR-signals. The independence of the monomer's signal shape shows that the observed radical is a photoproduct of the diazonium salt, which can be interpreted as superposition of an aryl radical signal and an another unstructured broad paramagnetic signal. The position of the signal corresponds to literature values with a typical g -factor of 2.003 (6).

These experiments show that the mechanism of the cation formation strongly differs in an inert solution (photoinduced heterolysis) and in a reactive system (photoinduced electron transfer). The EPR-study show that the photocrosslinking starts with a photoinduced electron transfer from the monomer to the diazonium salt. Radical cations originating from the monomer are formed. These species can initiate the cationic crosslinking of the monomer themselves or by their

consecutive products. Moreover, the aryl radicals induced a secondary thermally initiated cation formation, by the Meerwein reduction of the diazonium salt, (Scheme 2). This free radical reduction of onium salts is well known for diazonium (7, 8), iodonium (8-12) and sulfonium salts (8, 11, 12).

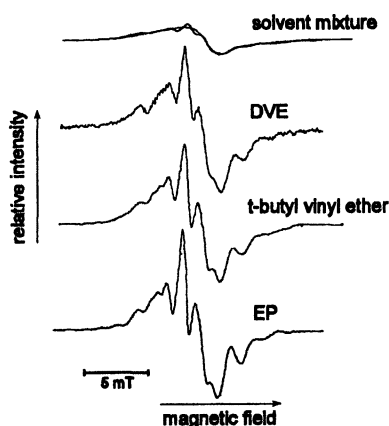


Figure 3. EPR-signals obtained under irradiation of the diazonium salt DS_1 without (top) and with monomer (bottom) in a solution of 1,2-dichloroethane/methylene chloride (1:3) at 77K (DS_1 as PF_6^- , $\lambda = 313$ nm, $[DS_1]$: saturated, $[monomer] \approx 0.5$ mol/l). Reprinted from Ref. 3 by permission of ELSEVIER SCIENCE.

These transfer reactions are thermodynamically possible, if the conditions of Eq. (4) are fulfilled.

$$\Delta G = E_{ox} - E_{red}(onium) < 0 \quad (4)$$

$$\Delta G = E_{ox} - E_{red}(onium) - *E < 0 \quad (5)$$

ΔG is free energy of electron transfer, E_{ox} is the oxidation potential of the reaction partner (monomer, radical etc.), $E_{red}(onium)$ is the half-wave reduction potential of the onium salt used, and $*E$ is the energy of the excited state of the onium salt.

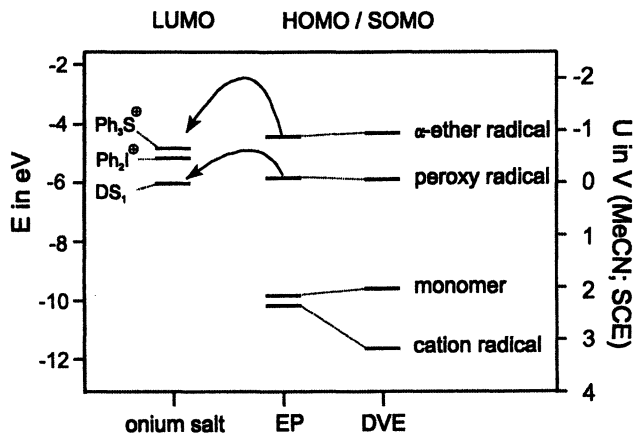


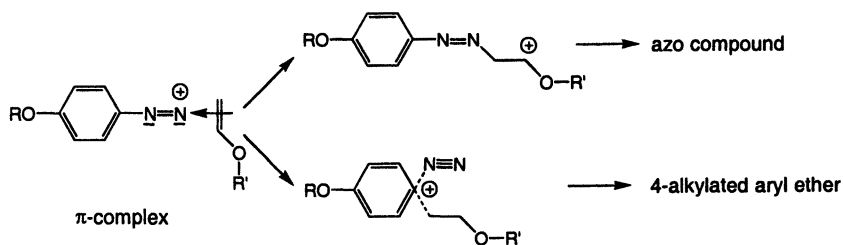
Figure 4. Calculated oxidation and reduction potentials of several onium salts as e^- -acceptors and monomers and radicals as e^- -donors.

The energetics given in Figure 4 show that the thermodynamic conditions of Eq. (4) become a reality for several radicals and onium salts. Thermodynamics also show that an electron transfer between the monomer and onium salt is forbidden in the ground state. The electron transfer is allowed only after excitation of the onium salt; see Eq. (5). Furthermore, thermodynamics show that oxy radicals, which were formed during radical scavenging by oxygen, cannot reduce onium salts in the dark. Nevertheless, the potential of the peroxy radicals lies in a critical range where an electron transfer to the diazonium salt is possible.

The electron transfer mechanism explains the influence of oxygen on the cationic crosslinking kinetics. Formation of the initiating species occurs by a photoinduced electron transfer reaction. That reaction is independent of the oxygen concentration. Consequently, one observes the same inhibition time for crosslinking in air as well as under inert conditions. Oxygen inhibits the chain growth process. Furthermore, some reaction steps produce water and alcohol, which retard the cationic crosslinking. On the other hand, the decomposition of thermally unstable peroxides resulting in a branched radical reaction. Finally, the reaction rate becomes faster under air than under inert conditions.

Thermostability

The high thermostability of the salt in 1,2-dichloroethane ($k(40^\circ\text{C}) = 7 \cdot 10^{-5} \pm 3 \cdot 10^{-5} \text{ h}^{-1}$) drops down by addition of a small amount of monomer. The decomposition of the diazonium salt increases in a solution that contains 0.2 mol/l divinyl ether 400 times faster ($k(40^\circ\text{C}) = 0.030 \pm 6 \cdot 10^{-5} \text{ h}^{-1}$) than in pure 1,2-dichloroethane and it is even 18 times faster than in pure dimethoxyethane. Absence of EPR-signals shows that thermolysis of the diazonium salt occurs according to nonradical pathway.



Scheme 3. Bimolecular dediazonation.

This behavior corresponds to the findings of Zollinger (7), who proposed a bimolecular dediazonation (see Scheme 3). Because vinyl ether derivatives act as nucleophilic compounds, the initiating cation of the cationic polymerization is directly produced without an intermediate aryl cation. Catalytic amounts of that intermediate catalyze the monomer decay. Therefore, dediazonation products cannot be observed in nonpolar solvents (see Figure 5). Moreover, in polar medium, which inhibits the polymerization, one can observe a simultaneous conversion of both the monomer and the diazonium salt. Dediazonation products are detectable.

Our results show the reason for the poor thermal stability of the diazonium salts: a) peroxy content of the monomer and, b) nucleophilicity of the monomer. Both effects demand a thermal formation of cations, which initiate the crosslinking reaction. The monomer and its by-products are even the reason of the poor thermal stability of the diazonium salts and not as the assumed thermal instability of the salt used. Traces of radicals can initiate the cationic polymerization. Moreover, one can deduce that only onium salts with $E_{\text{red}} < -1\text{V}$ (SCE) prevent the thermal radical induced formation of an initiating species from the level of the reduction potential of several onium salts, see (3, 13).

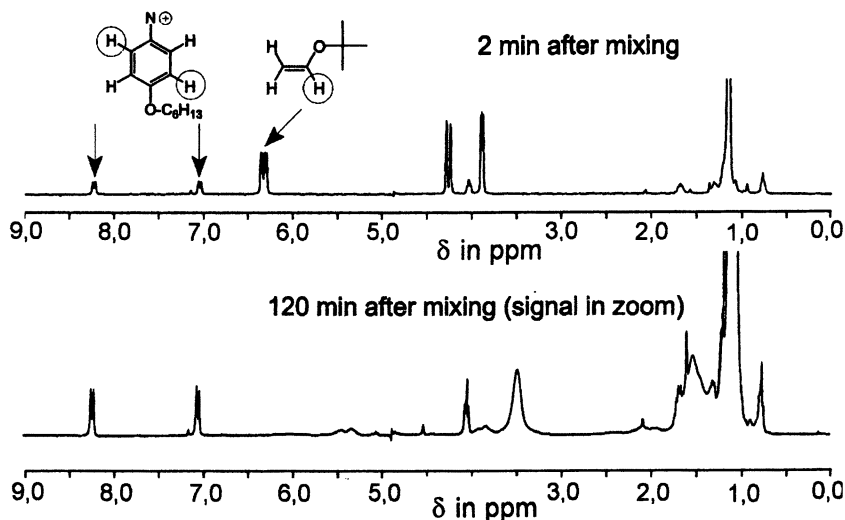


Figure 5. $^1\text{H-NMR}$ -spectra of the reaction of DS_1 with *t*-butyl vinyl ether in chloroform- d at room temperature 2 and 120 minutes after mixing ($[\text{DS}_1] = \text{saturated}$; DS_1 as SbF_6^- ; $[\text{vinyl ether}] / [\text{DS}_1] \approx 10$). Reprinted from Ref. 3 by permission of ELSEVIER SCIENCE.

Acknowledgement

The authors are grateful to Wacker-Chemie GmbH for financial and material support and thank Wacker-Chemie GmbH for the permission to present these new findings.

The paper is based on material published on Ref. 3. The partial reprint from J. Photochem. Photobiol. A: Chem. 140, U. Müller, A. Utterodt, W. Mörke, B. Deubzer, and Ch. Herzig "New insight about diazonium salts as cationic photoinitiators" pp. 53-66, copyright 2001, takes place with permission from ELSEVIER SCIENCE.

References

1. Lohse, F.; Zweifel, H. *Advances in Polymer Science* **1987**, *78*, 61.
2. Baumann, H.; Timpe, H.-J. *J. Prakt. Chem.* **1994**, *336*, 377.
3. Müller, U.; Utterodt, A.; Mörke, W.; Deubzer, B.; Herzig, Ch.; J. *Photochem. Photobiol. A: Chem.* **2001**, *140*, 53.

4. Müller, U.; Jockusch, S.; Timpe, H.-J.; *J. Polym. Sci. Polym. Chem.* **1992**, *30*, 2755.
5. Timpe, H.-J.; Strehmel, B. *Makromol. Chem.* **1991**, *192*, 779.
6. *Landolt-Börnstein, Zahlenwerte und Funktionen*, Berndt, A.; Fischer, H.; Paul, H., Eds.; Springer-Verlag: Berlin, Heidelberg, New York, 1977, NS II/9b p. 310.; *Landolt-Börnstein, Zahlenwerte und Funktionen*, Fischer, H., Ed.; Springer-Verlag: Berlin, Heidelberg, New York, 1965, NS II/1, p. 21.
7. Zollinger, H.; *Diazo Chemistry I*, VCH Verlagsgesellschaft mbH: Weinheim, 1994.
8. Ledwith, A.; *Polymer* **1978**, *19*, 1217.
9. Timpe, H.-J.; Schikowsky, V.; *J. Prakt. Chem.* **1989**, *331*, 447.
10. Bi, Y.; Neckers, D. C.; *Macromolecules* **1994**, *27*, 3683.
11. Sundell, P.-E.; Jönsson, S.; Hult, A.; *J. Polym. Sci. Polym. Chem.* **1991**, *29*, 1525.
12. Sundell, P.-E.; Jönsson, S.; Hult, A.; *J. Polym. Sci. Polym. Chem.* **1991**, *29*, 1535.
13. Müller, U.; *Trends in Photochemistry & Photobiology* **1999**, *5*, 117.

Chapter 18

2,3-Dihydrofuran: A Special Vinyl Ether for Cationic Photopolymerization

Oskar Nuyken and Harald Braun

Lehrstuhl für Makromolekulare Stoffe, Technische Universität München,
Lichtenbergstrasse 4, D-85748 Garching, Germany

Mono- and bifunctional monomers with 2,3-dihydrofuran moieties were synthesized by the Heck reaction of 2,5-dihydrofuran and various arylbromides. The synthesized monomers were polymerized by typical cationic photoinitiators. Depending upon the type of monomers used, soluble and insoluble polymers were formed and the thermal properties were studied.

Homo- and copolymers of vinyl ethers are used in many commercial products. Reason for the great interest in new polymers with vinyl ether moieties, are their cheap synthesis and their excellent adhesion properties. Vinyl ethers possess double bonds with high electron densities due to their strong electron-donating alkoxy substituent. Consequently, they can not be polymerized by anionic or radical routes, but polymerize via a cationic mechanism. However, a common problem in the application of all linear vinyl ethers, is that they form small amounts of aldehyde during the polymerization (1). This can be avoided using 2,3-dihydrofuran, because of its ring structure. **Figure 1** shows the possible formation of acetaldehyde by the cationic polymerization of ethyl vinyl ether.

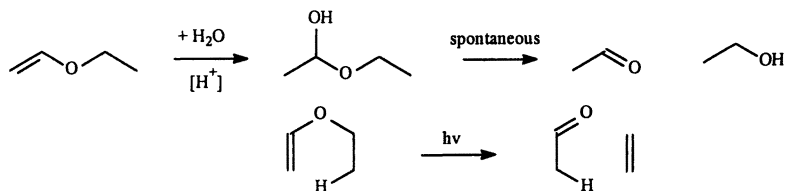


Figure 1. Two possibilities for the formation of acetaldehyde by the cationic polymerization of ethyl vinyl ether.

In the family of vinyl ethers, 2,3-dihydrofuran is known to be most reactive (2). Poly(2,3-dihydrofuran) was first synthesized by Barr et al. with boron trifluoride as initiator (3). The polymerization can also be carried out with other cationic initiators (4,5). An interesting alternative is the photoinduced cationic homopolymerization of 2,3-dihydrofuran initiated by $(\eta^5\text{-cyclopentadienyl})\text{-Fe(II)}\text{-}(\eta^6\text{-isopropylbenzene})$ hexafluorophosphate showing the high reactivity of 2,3-dihydrofuran towards cationic photoinitiators. The driving force of the polymerization of 2,3-dihydrofuran is its ring strain and cis-conformation at the double bond⁶. The synthesis of unsubstituted 2,3-dihydrofuran is easy (7-11). The main synthetic routes are presented in the following scheme.

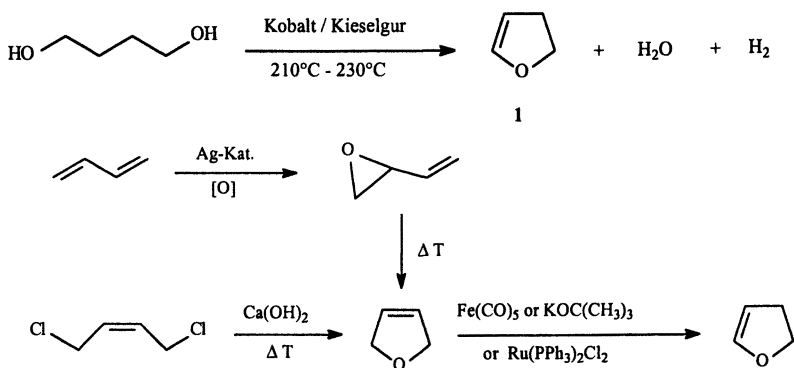


Figure 2. Different synthetic methods for 2,3-dihydrofuran.

Poly(2,3-dihydrofuran) showed excellent film forming properties and adhesion. 2,3-dihydrofuran type monomers were synthesized and examined with respect to their reactivity towards photochemically generated acids, since this is prerequisite for e.g. using such monomers in UV curable coatings. The synthesized compounds fulfill demands for practical applications since they undergo rapid polymerization which is finished within 2 minutes (100% conversion) upon photolysis. However, for application of those monomers to coatings it is essential to crosslink the organic layer, meaning a certain amount of bifunctional monomers must be added. Unfortunately, only a rather complicated synthesis for monomers with two 2,3-dihydrofuran moieties per molecule was available (12). Therefore, we had to look for an alternative route, which we found by reacting aryl dibromides with 2,5-dihydrofuran in the presence of a palladium catalyst (Heck reaction) (13).

A series of mono and bifunctional 2,3-dihydrofuran compounds were synthesized using the Heck reaction. Analogous reaction conditions were applied. A typical reaction mixture contained 1 eq. arylbromide, 2 eq. 2,5-dihydrofuran, 0.5 eq. tetrabutylammonium bromide, 1.2 eq. base: sodium acetate, and 0.01 eq. palladium catalyst, as depicted in **Figure 3**.

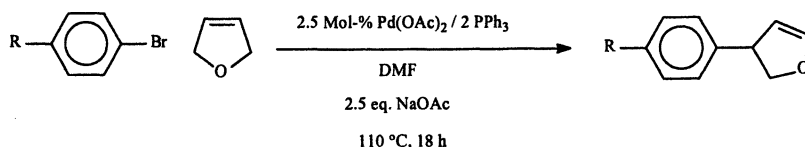


Figure 3. Heck reaction of 2,5-dihydrofuran with different arylbromides.

Nearly complete conversion based on arylbromide was achieved after 18h. The reaction offers a simple route to prepare 2,3-dihydrofuran derivatives in one step. The method can also be applied to the synthesis of monomers with two 2,3-dihydrofuran moieties, that can be used as crosslinkers. Different synthesized monomers are shown in **Figure 4**. The pure monomers could be obtained only by several successive column chromatography steps.

Photopolymerization of 2,3-dihydrofuran derivatives

10 mmol of the monomer and 0.4 mmol of the photoinitiator contained in a quartz flask were dissolved in 5ml methylene chloride at roomtemperature and irradiated from an Ushio UXM 200H Hg-Xe high pressure lamp with a light intensity of 200 mW cm^{-2} . At the end of irradiation, the solution was poured into ten-fold excess of methanol and filtered off. The polymers were then dried

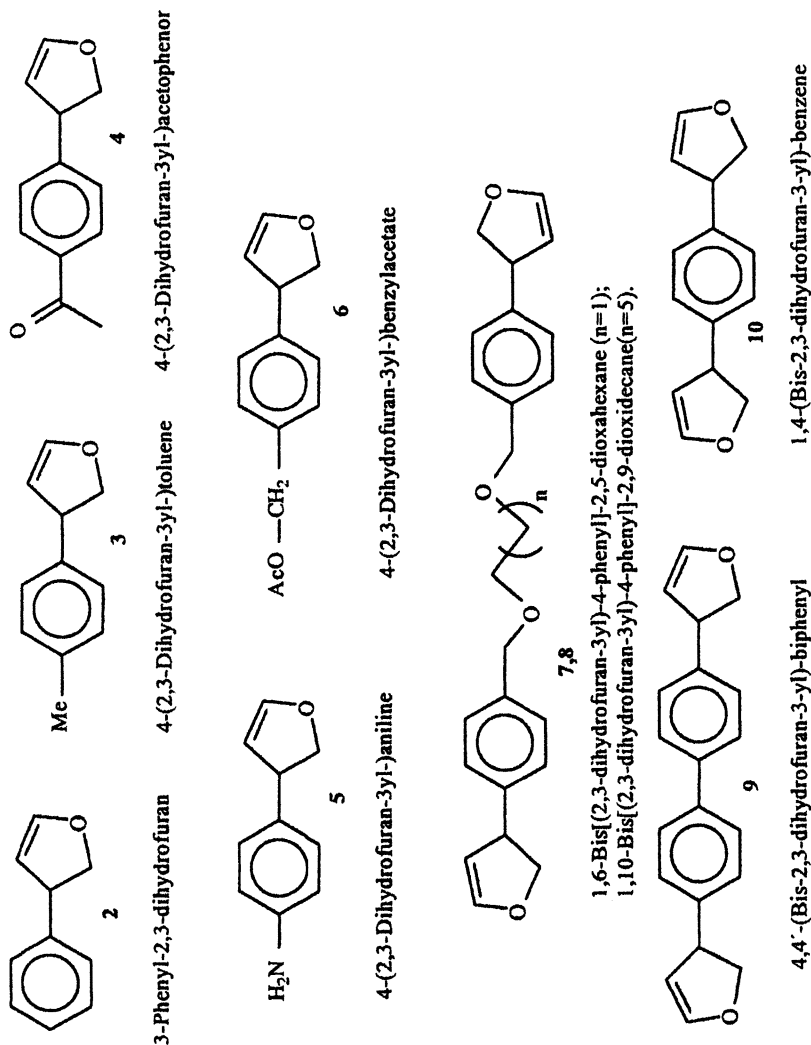


Figure 4. Synthesized 2,3-dihydrofuran derivatives.

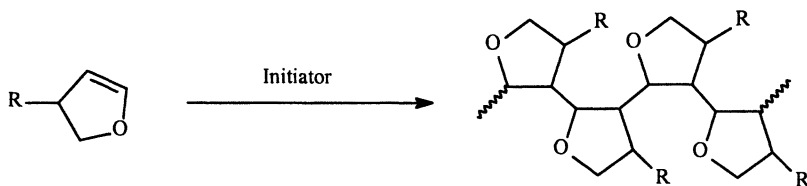


Figure 5. Cationic polymerization of 2,3-dihydrofuran derivatives

at 60°C for 24 h at 10 mbar. In case of bifunctional monomers, a mixture of 9 parts 2,3-dihydrofuran and one part of the bifunctional monomer is used. At the end of irradiation insoluble networks are formed.

Regardless of their functionality, photoinitiated cationic polymerization of all monomers, was completed within 2 min by using a triphenylsulphonium salt (14). The typical cationic formation of poly-2,3-dihydrofuran is shown in **Figure 5**.

Insoluble network polymers were formed when the formulations contained bifunctional monomers (7-10). Molecular weights, molecular weight distributions and glass transition and decomposition temperatures of the monofunctional polymers obtained, are summarized in **Table I**. Although the molecular weights of the polymers were rather low, free standing films from these polymers could easily be formed by solvent casting. Moreover, their adhesion on glass and metal is a good indication for their possible application in coatings. Glass transition temperatures of the polymers were in the range between 124°C and 157°C depending on the substituent of the 2,3-dihydrofuran derivative. As expected, better thermal stabilities were obtained with the crosslinked polymers ($T_d = 341\text{--}391^\circ\text{C}$) compared to that of poly-2,3-dihydrofuran 1 ($T_d = 311^\circ\text{C}$)¹⁴.

Table I. The glass transition and decomposition temperatures, and molecular weights of the uncrosslinked polymers.

Polymer	$T_g / ^\circ\text{C}$	$T_d / ^\circ\text{C}$	M_n	PDI
Poly-2,3-dihydrofuran	311	143	17 100	2.1
Poly(3-Phenyl-2,3-dihydrofuran)	326	124	2 970	1.3
Poly[4-(2,3-dihydrofuran-3-yl)-toluene]	248	145	1 080	1.0
Poly[4-(2,3-dihydrofuran-3-yl)-benzylacetate]	277	139	2 280	1.3
Poly[4-(2,3-dihydrofuran-3-yl)-acetophenone]	317	157	2030	1.5

Source: Reproduced with permission from *Polym. Prepr.* **2001**, 42(2), 779–780. Copyright 2001 Oskar Nuyken.)

Conclusions

2,3-Dihydrofuran type monomers can be prepared by a versatile synthetic procedure in a one-step reaction (Heck reaction) and the monomers were shown to be polymerizable by photoinduced cationic polymerization.

References

1. Murad E. *J. Am. Chem. Soc.* **1961**, *83*, 1327.
2. Nuyken, O.; Raether, R.B.; Spindler C.E. *Des. Monomers Polym.* **1998**, *1*(1), 97.
3. Barr D.A.; Rose J.B. *J. Chem. Soc.*; **1954**, 3766.
4. Kim J.B.; Cho I. *J. Polym. Sci., Part A: Polym. Chem.*, **1989**, *27*, 3733.
5. Sanda F.; Matsumoto M. *Macromolecules*, **1995**, *28*, 6911.
6. Nuyken O.; Aechtner S. *Polym. Bull.*, **1992**, *28*, 117.
7. Dimroth P.; Pasedach H. *Angew. Chem.* **1960**, *72*, 865.
8. Eliel E.L.; Nowak B.E.; Daignault R.H.; Badding V.G. *J. Org. Chem.* **1965**, *30*, 2441.
9. Havel J.J.; Chan K.H. *J. Org. Chem.* **1976**, *41*, 513.
10. Vogel E.; Gunther H. *Angew. Chem.* **1967**, *79*, 429.
11. Eberbach W.; Buchhardt B. *Chem. Ber.* **1978**, *11*, 3665.
12. Nuyken O.; Spindler C.; Raether R.B. *J. M. S.- Pure Appl. Chem.*, **1997**, *A34*(12), 2389.
13. Jeffery T.; David M. *Tetrahedron Let.*, **1998**, *39*, 5751.
14. Nuyken O.; Braun H. *Des. Monomers Polym.*, **2001**, *4*(1), 19.

Chapter 19

Photosensitization of Onium Salt Initiated Cationic Photopolymerizations by Carbazole Monomers, Polymers, and Oligomers

Yujing Hua and James V. Crivello

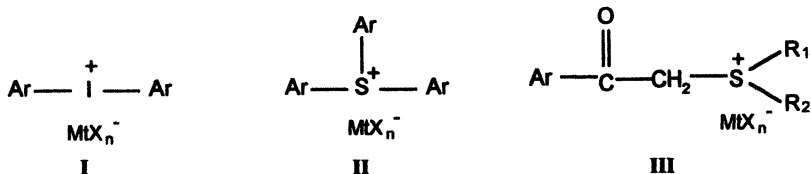
Department of Chemistry, New York Center for Polymer Synthesis,
Rensselaer Polytechnic Institute, 110 8th Street, Troy, NY 12180

Carbazole compounds are efficient electron-transfer photosensitizers for onium salt photoinitiated cationic polymerizations of vinyl and heterocyclic monomers. Oligomers and polymers containing carbazole groups are especially attractive as photosensitizers. Copolymers of N-vinylcarbazole (NVK) with vinyl monomers and a dimeric photosensitizer were also synthesized and shown to be efficient onium salt photosensitizers.

Introduction

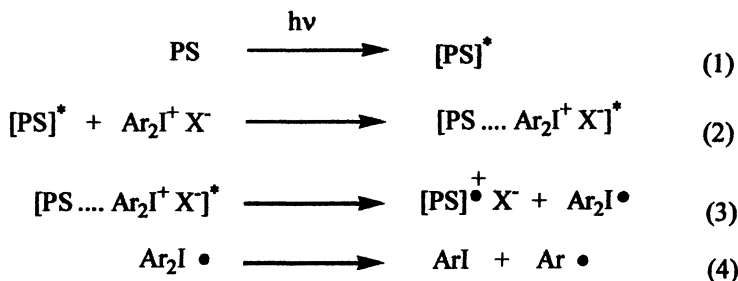
Photoinitiated cationic polymerizations are receiving considerable attention as these reactions are finding an increasing number of commercial uses. Currently, the most commonly used photoinitiators employed for photoinduced cationic vinyl and ring-opening polymerizations are diaryliodonium, I, and

triarylsulfonium salts, **II**, with the general structures shown below in which MtX_n^- represents a weakly nucleophilic counterion. Another class of photoinitiators that show considerable promise is dialkylphenacylsulfonium salts, **III**



Photosensitizers are often included in many applications in which onium salt photoinitiators are employed to improve their overall performance by broadening their spectral sensitivity.¹ In addition, photosensitizers are often employed to “tune” the absorption of a photopolymerization when narrow wavelength emission or monochromatic light sources such as lasers or light emitting diodes are used. However, this aspect of onium salt photochemistry has received little attention and, consequently, the number of known photosensitizers is quite limited. Accordingly, recent work in this laboratory has focused on the development of novel and practical photosensitizer systems.

There are several mechanisms by which the photosensitization of onium salts take place, however, electron-transfer photosensitization appears to be the most efficient and generally applicable process.¹ A generalized mechanism for the electron-transfer photosensitization of diaryliodonium salts is shown in Scheme 1.² Similar mechanisms can be written for the photosensitization of triarylsulfonium and dialkylphenacylsulfonium salts.



Scheme 1

Absorption of light by the photosensitizer, PS, results in its excitation (eq. 1). This species interacts with the diaryliodonium salt (eq. 2) to generate an excited state complex (exciplex) that decays by the formal transfer of an

electron from the photosensitizer to the onium salt (eq. 3). In subsequent reactions, the resulting photosensitizer cation radical can initiate the cationic polymerization of both vinyl and heterocyclic monomers by a number of different mechanisms. Very importantly, the diaryliodonium free radical undergoes facile fragmentation (eq. 4) which prevents back electron-transfer thereby rendering the entire mechanistic sequence irreversible.

Among the best electron-transfer photosensitizers for onium salts are electron-rich polynuclear aromatic hydrocarbons.³ However, these photosensitizers have several disadvantages including a high vapor pressure, toxicity and poor solubility in most monomers. In this article, we report the discovery that low molar mass carbazole compounds, carbazole containing monomers and polymers are excellent photosensitizers for all three types of onium salts shown above.

Experimental

Materials

All monomers, carbazole derivatives and other reagents used were obtained from commercial sources. The photoinitiators, (4-n-decyloxyphenyl)phenyliodonium SbF_6^- (IOC10), (4-n-decyloxyphenyl)diphenylsulfonium SbF_6^- (SOC10) and S-dodecyl-S-methyl-S-phenacylsulfonium hexafluorophosphate ($\text{DSP-C}_{12}\text{PF}_6^-$) were prepared as described previously.⁴

Molecular weights of polymers were determined using a HP-1090M HPLC equipped with a refractive index detector and μ -styragel columns. NMR spectra were obtained using a Varian, Inova 300 MHz Spectrometer. UV spectra were recorded on a Hitachi U-2000 UV-Vis Spectrometer.

Synthesis of Copolymers of NVK⁵

An equimolar mixture of NVK and diethyl fumarate (DEF) was copolymerized under a nitrogen atmosphere in a sealed tube with 2.0 mol% AIBN and different amounts of the chain transfer agent, lauryl mercaptan. The same procedure was followed in the copolymerization of NVK and n-butyl acrylate (BA).

Synthesis of 1,3-Bis(2-carbazoloethyl)-1,1,3,3-tetramethyl-disiloxane (IV)

Into a 25 mL round bottom flask equipped with a magnetic stirrer and reflux condenser were placed 5.1 g (0.026 mol) of N-vinyl carbazole, 10 mL of toluene that was freshly distilled from sodium metal, 1.8 g (0.013 mol) of 1,1,3,3-tetramethyldisiloxane and 3 mg of polymer-bound Wilkinson's catalyst. The reaction mixture was heated to 80 °C and maintained at that temperature for 24 hours. During reaction, the reaction mixture became increasingly more viscous as reaction proceeded. Upon cooling to room temperature, the product solidified. The crude product was purified by dissolving it in a small amount of THF and slowly adding the resulting solution to cold methanol. The product, IV, was obtained as a colorless powder and was recovered by filtration. After drying under vacuum, there were obtained 3.5 g (51% yield) of pure IV. The $^1\text{H-NMR}$ spectrum recorded in CDCl_3 was in accord with the structure.

Photopolymerization Studies Using Fourier Transform Real-Time Infrared Spectroscopy (FT-RTIR)

Photopolymerizations of all monomers were monitored by FT-RTIR. A Midac M-1300 FTIR spectrometer equipped with a liquid nitrogen cooled MCT detector was used. Photopolymerizations were carried out at 25°C in solutions of monomers containing various concentrations of the photoinitiator. All concentrations are given in units of mol% with respect to the epoxide or vinyl ether monomers. The solutions were sandwiched between two identical polypropylene films and then mounted in 5x5 cm slide frames. Infrared spectra were collected at a rate of 1 spectrum per second using LabCalc data acquisition software and were processed using GRAMS-386 software. During irradiation, the decrease of the IR band due to either epoxy ($790\text{-}930\text{ cm}^{-1}$) or vinyl double bond (1641.5 cm^{-1}) of NVK was monitored.

Results and Discussion

Onium Salt Photosensitization by Low Molar Mass Carbazole Compounds

Recently, Chen, et al.⁶ and ourselves⁷ have reported that carbazoles are efficient photosensitizers for both diaryliodonium and triarylsulfonium salts. The rates of iodonium and triarylsulfonium salt cationic photopolymerization of various epoxide and vinyl ether monomers are essentially identical in the presence of 2.0 mol% of simple N-substituted carbazoles. An example of the

iodonium salt photosensitized polymerization of cyclohexene oxide (CHO) using N-vinylcarbazole (NVK) and N-ethylcarbazole (NEK) is depicted in Figure 1. Included in this figure for comparison is a study in which no photosensitizer was used.

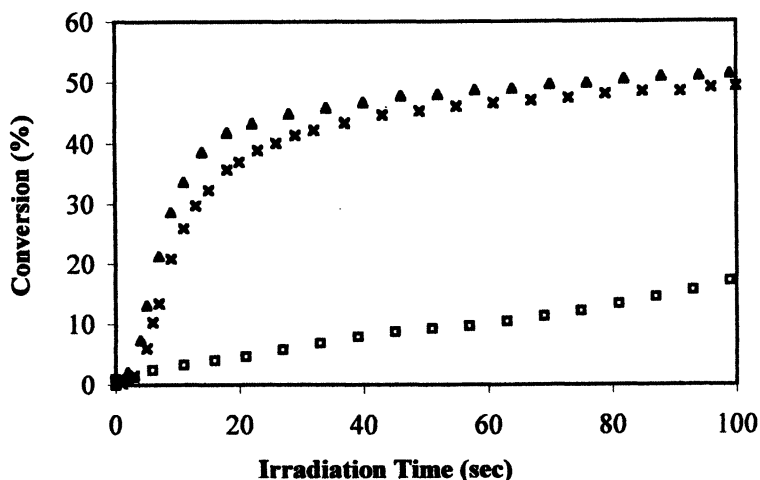
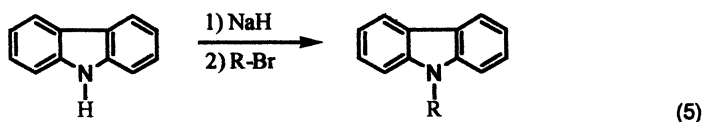


Figure 1. FT-RTIR study of epoxide polymerization of CHO alone (□) and in the presence of 2.0% NVK (Δ) and 2.0% NEK (×). The light intensity was $138 \text{ mJ/cm}^2\text{-min}$, photoinitiator was 0.01% IOC10.

As the results show, the rate of the epoxide polymerization of CHO was significantly enhanced by the addition of NVK and NEK as compared to when no photosensitizer was used. Similar results were observed when these same low molar mass carbazole compounds were employed as photosensitizers for both triarylsulfonium and dialkylphenacylsulfonium salts. The electron-transfer photosensitization mechanism depicted in Scheme 1 is essentially a photoinduced redox reaction. This was confirmed by calculations using the Rehm-Weller equation⁸ that showed that the free energy of electron-transfer is negative for all carbazole compounds and onium salts I-II. The magnitude of the free energy of electron-transfer for diaryliodonium salts was greater than dialkylphenacylsulfonium and triarylsulfonium salts due to the higher redox potentials of the latter class of onium salts. It was found that carbazole cation-radicals can be independently generated by the photolysis of onium salts in the presence of a carbazole photosensitizer in an inert solvent. The ability of carbazole compounds to photosensitize a wide range of onium salts is

extraordinary and this makes them particularly valuable as a class of universal photosensitizers.

N-Substituted carbazoles are interesting as photosensitizers since they can be readily prepared (eq. 5) by the direct treatment of the readily available parent carbazole compound with a strong base followed by alkylation with an alkyl halide.



Investigation of Photopolymerizations of Monomers in Presence of Oligomeric and Polymeric Cabazoles

NVK was of special interest as a photosensitizer since this compound exhibits high reactivity in cationic polymerization and can potentially interact to form polymers with other monomers. In addition, this compound is readily available and inexpensive. Accordingly, a study of the photopolymerization of CHO was carried out in the presence of a larger amount of NVK and the results are given in Figure 2.

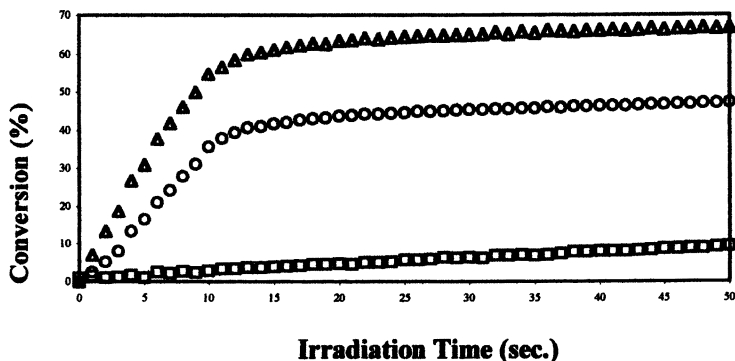
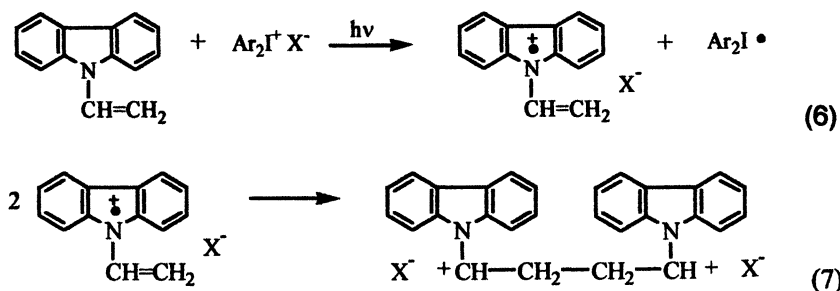


Figure 2. FT-RTIR study of epoxide polymerization of CHO alone (□) and in the presence of 29% NVK (Δ). The rate of conversion of vinyl groups of NVK (○). The light intensity was 138 mJ/cm²·min, photoinitiator was 0.01% IOC10.

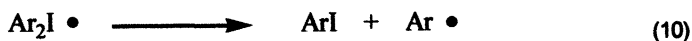
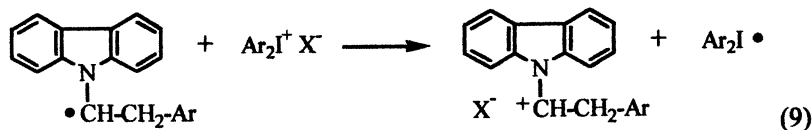
Using FT-RTIR it was possible to simultaneously follow the ring-opening photopolymerizations of the epoxy monomer and the vinyl group of NVK. Again, a large increase in the polymerization rate of CHO was observed in the presence of NVK. It is also worth noting that the rates of the CHO and NVK photopolymerizations are similar. This suggests considerable interaction between the two monomers. There are two potential mechanisms that may account for these results. These are illustrated below using a diaryliodonium salt as an example. First, as noted in Scheme 2, the formation of cation-radical species by electron-transfer photosensitization of the onium salt (eq. 6) results in dimerization (eq. 7). The resulting dication initiates the ring-opening epoxide polymerization.



Scheme 2

A second possible mechanism is depicted in Scheme 3. Aryl radicals generated on photolysis of the onium salt can add to the vinyl double bond of NVK (eq. 8). The resulting radical can be oxidized by an onium salt (eq. 9) to give the corresponding resonance stabilized cation. Thereafter, the cation can initiate ring-opening or vinyl polymerization while the diaryliodonine free radical irreversibly dissociates as noted before to generate an aryl radical and an aryl iodide (eq. 10).

The sequence of equations shown in Scheme 3 constitute a chain reaction in which the onium salt is rapidly converted to cationic species that serve to initiate polymerization. Since the overall process involves free radicals as the chain carriers, it was found to be markedly suppressed by the inclusion of radical retarders and inhibitors. At the same time, the reduction of the induction period that is observed when substantial quantities of NVK are added to the photopolymerization of various monomers is in agreement with the generation of an increased number of initiating species predicted by this mechanism.



Scheme 3

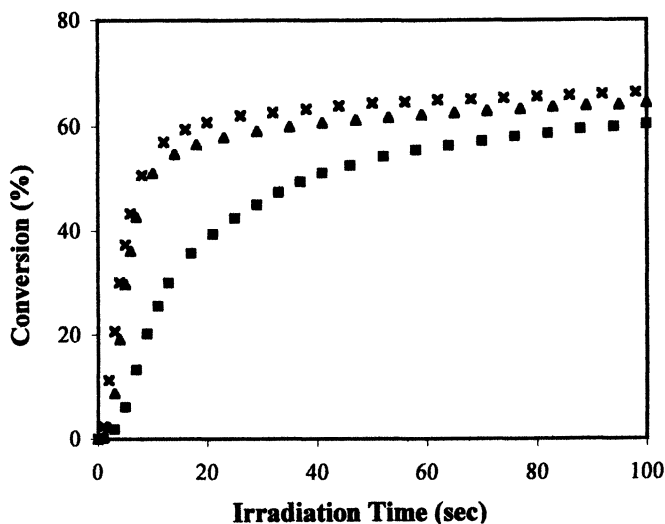
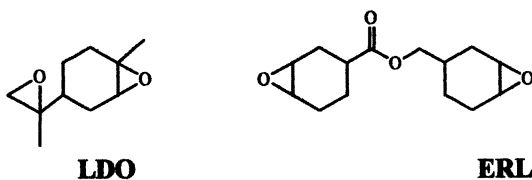


Figure 3. Photopolymerization of CHO in the presence of 0.5 % IOC10 alone (■) and using 0.2 % PVK (×) and 0.2 % NEK (▲). Light intensity 103 mJ/cm²·min

When NVK is photopolymerized, polymers and copolymers containing the carbazole nucleus are generated. Such polymers could also serve as photosensitizers for onium salt photolyses. To examine whether this hypothesis is correct, the study shown in Figure 3 was carried out.

In Figure 3 poly(*N*-vinylcarbazole) PVK ($M_w = 256700$ g/mol) was compared with *N*-ethylcarbazole (NEK) which is a model for the repeating unit of PVK as photosensitizers in the photopolymerization of CHO. Equimolar concentrations of carbazole units were employed in both cases and the diaryliodonium salt, IOC10 was used. The results in Figure 3 show that the polymer and low molar mass carbazole compounds possess essentially the same photosensitizing activity.

Unfortunately, PVK has rather poor solubility in most monomers of interest. For this reason, the free radical alternating copolymerizations of NVK with diethylfumarate (DEF) and butyl acrylate (BA) were carried out. The resulting copolymers showed greatly improved solubility in such epoxy monomers as limonene dioxide (LDO) and 3,4-epoxycyclohexylmethyl 3',4'-epoxycyclohexanecarboxylate (ERL). Figure 4 shows a study in which the latter monomer was photopolymerized in the presence of the two copolymers using NEK as a control. Excellent photosensitizing activity is observed for both copolymers. The use of polymeric photosensitizers is of considerable practical interest since these materials would be expected to possess essentially no toxicity, or vapor pressure.



Electronic energy migration is known to occur from one carbazole group to another along the polymer backbone in solid PVK films.⁸ If such an “antenna effect”⁹⁻¹¹ were to take place with PVK in solution, it should improve the efficiency of PVK as compared to monomolecular photosensitizers. However, as Figure 2 shows, at low concentration of PVK accelerates the photopolymerization of CHO to the same extent as NEK. We, therefore, conclude that the “antenna effect” for this polymer is either absent or very inefficient in the solution. Instead, each repeating unit within the polymer chain behaves independently with respect to its photosensitizing activity. Further, confirmation of this hypothesis was realized by observing that when PVK was compared on an equimolar carbazole unit basis with NEK and with the two copolymers mentioned above, identical rates of polymerization of LDO were observed.

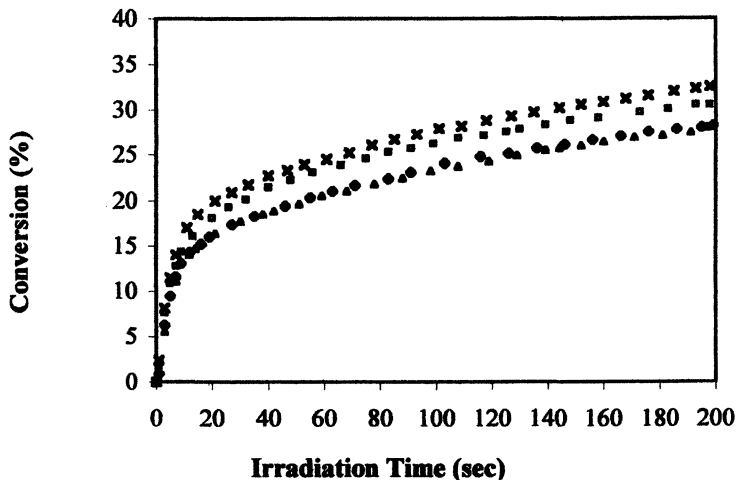
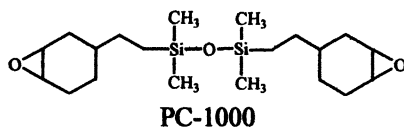


Figure 4. Comparison of the polymerization of ERL in the presence of copolymer NVK/DEF (X) ($M_w = 42400$ g/mol) (▲) ($M_w = 11500$ g/mol), copolymer NVK/BA (◇) ($M_w = 17000$ g/mol) (1.0 % carbazole repeat units) and with 1.0 % NEK (□). The light intensity 2200 mJ/cm²·min, photoinitiator 1.0 % DPS-C₁C₁₂ PF₆⁻

PVK as well as neither of the two BA or DEF copolymers were found to dissolve in the highly reactive nonpolar silicon containing monomer, bis-2(3,4-epoxycyclohexylethyl)-1,3-tetramethyldisiloxane (PC-1000).



Accordingly, we deliberately designed the biscarbazole photosensitizer IV to be used with this monomer and with other types of epoxy-silicone monomers, polymers and oligomers. The simple synthetic route that was employed is depicted in equation 11.

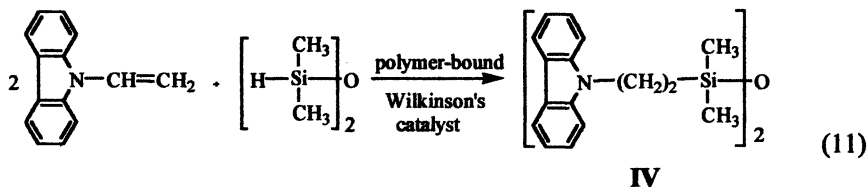


Figure 5 shows that both the dimeric photosensitizer IV and NEK accelerated the polymerization of PC-1000 significantly and to the same extent.

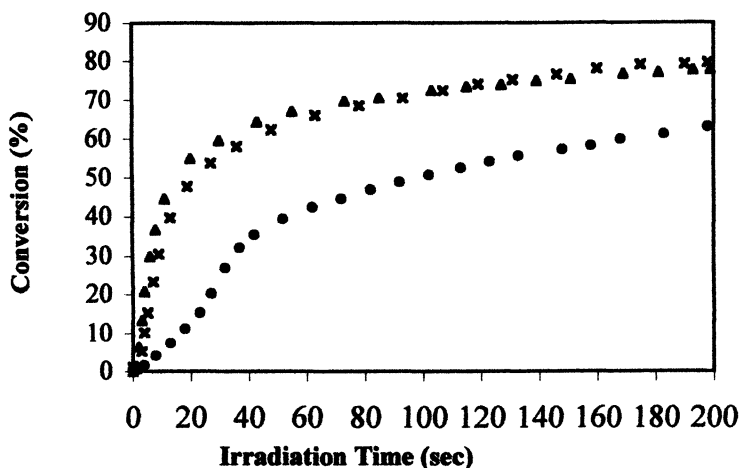


Figure 5. Photopolymerization of PC-1000 with 0.5% IOC alone (●) and in the presence of IV (×) (2.0% carbazole units) and 2.0% NEK (▲) as photosensitizers. Light intensity $374 \text{ mJ/cm}^2 \cdot \text{min}$

Conclusions

A wide variety of low molar mass carbazole compounds exhibit excellent photosensitizing ability for the photolyses of onium salt cationic photoinitiators. At high concentrations, NVK is an especially active photosensitizer that appears to copolymerize with epoxide monomers. Carbazole-containing polymers and copolymers have similar activity to low molar mass compounds as photosensitizers.

Polymeric photosensitizers are especially attractive since they are effective for all types of onium salt cationic photoinitiators, have low volatility and are expected to display a low order of toxicity.

References

1. Crivello J.V.; Dietliker, K. *Chemistry & Technology of UV and EB Formulation for Coatings, Inks & Paints, Vol. III*, Bradley, G., Ed.; SITA Technology Ltd. London, 1998, p. 420.
2. Crivello, J.V. *Ring-Opening Polymerization*, Brunelle, D.J. Ed.; Hanser, Munich, 1993 p. 157.

3. Crivello, J.V.; Lam, J.H.W. *J. Polym. Sci. Part A: Polym. Chem. Ed.* **1979**, 17, 1059.
4. Crivello, J.V.; Lee, J.L. *J. Polym. Sci. Part A: Polym. Chem. Ed.* **1989**, 27, 3951; Akhtar, S.R.; Crivello, J.V.; Lee, J.L. *J. Org. Chem.* **1990**, 55, 4222; Crivello, J.V.; Kong, S. *Macromolecules*, **2000**, 33, 833.
5. Pearson, J.M.; Stolka, M. *Poly(N-vinylcarbazole)* Gordon and Breach Science Pub. New York 1981.
6. Chen, Y.; Yamamura, T.; Igarashi, K. *J. Polym. Sci. Part A: Polym. Chem. Ed.*, **2000**, 38, 90.
7. Hua, Y.; Crivello, J.V. *J. Polym. Sci. Part A: Polym. Chem. Ed.*, **2000**, 38, 3697.
8. Bradley, G.; Davidson, R.S.; Howgate, G.J.; Mouillat, C.G.J.; Turner, P. *J. Photochem. Photobiol. A: Chem.*, **1996**, 100, 109.
9. Klöpffer, W. *J. Chem. Phys.*, **1969**, 50, 2337.
10. Guillette, J.E.; Randall, W.A. *Macromolecules*, **1986**, 19, 224 and references therein.
11. Klöpffer, W.; Fisher, D. *J. Polym. Sci. Part C: Polym. Lett. Ed.* **1973**, 40, 43.

Chapter 20

Phenothiazine Photosensitizers for Onium Salt Photoinitiated Cationic Polymerization

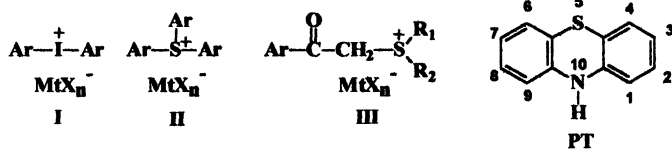
Zaza Gomurashvili and James V. Crivello*

Department of Chemistry, New York Center for Polymer Synthesis,
Rensselaer Polytechnic Institute, 110 8th Street, Troy, NY 12180

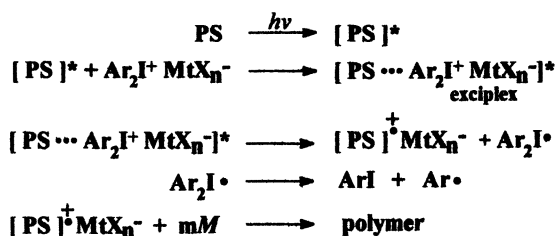
The syntheses of several different substituted phenothiazines are described and the ability of these compounds to photosensitize the photolysis of different onium salt cationic photoinitiators is described. These photosensitizers (PS) are generally operative in the mid- and long-range regions of the UV spectrum. The efficiencies of photosensitization of the cationic photopolymerizations of several typical epoxide and vinyl ether monomers by different substituted phenothiazine compounds were evaluated and compared. In addition, a phenothiazine-containing monomer and polymer were prepared and were shown to be effective photosensitizers.

Introduction

Currently, the most commonly used photoinitiators employed for photoinduced cationic polymerizations are diaryliodonium, **I**, and triarylsulfonium salts, **II**, with the general structures shown below in which MtX_n^- represents a weakly nucleophilic counterion. Another promising class of photoinitiators is dialkylphenacylsulfonium salts, **III**.



Although considerable synthetic efforts have been made to extend the spectral sensitivity of onium salt photoinitiators by substitution of appropriate chromophores onto the aromatic rings of these compounds, it has not been possible to significantly shift their sensitivity beyond the middle range of the UV spectrum.¹ Fortunately, it is possible to photosensitize the decomposition of diaryliodonium and triarylsulfonium salts photoinitiators with electron-transfer photosensitizers. We have reported extensively on our studies in this area^{2,3,4} and other investigators have also been active in this field.^{5,6,7,8} There are several mechanisms by which the photosensitization of onium salts take place, however, electron-transfer photosensitization appears to be the most efficient and generally applicable process.⁹ A generalized mechanism for the electron-transfer photosensitization of diaryliodonium salts is shown in Scheme I.¹⁰



Scheme I

Unfortunately, at the present time, the number of electron-transfer photosensitizers operative in the mid- and long wavelength UV and visible regions are very limited. Many of these photosensitizers suffer from various disadvantages, including toxicity and limited solubility in a wide variety of monomers. For these reasons, we have been conducting investigations directed toward the development of novel classes photosensitizers that mitigate the disadvantages of the former compounds.

The photosensitizing effects of 10H-phenothiazine (PT) for onium salt types II and III were reported and studied by several research groups.^{11,12,13} This compound is potentially useful for applications that require photosensitization in the middle region (300-400 nm) of the UV spectrum. This communication describes the discovery, that a wide variety of substituted phenothiazines are efficient photosensitizers for the photolysis of onium salts. Attempts were made to correlate the structure and spectral characteristics of the phenothiazines with their efficiency of sensitization in the cationic photopolymerizations of several typical epoxide and vinyl ether monomers. In addition, monomers and polymers containing phenothiazine moieties were prepared and evaluated as photosensitizers for onium salt photoinitiators.

Experimental

Materials

All organic starting materials, monomers and reagents, 10H-phenothiazine (PT), 10-methylphenothiazine, 2-chlorophenothiazine, 2-trifluoromethylphenothiazine and 2-acetylphenothiazine were obtained from commercial sources. The photoinitiators, (4-n-decyloxyphenyl) phenyliodonium hexafluoroantimonate (IOC10),¹⁴ (4-n-decyloxyphenyl)-diphenylsulfonium hexafluoroantimonate (SOC10)¹⁵ and S-dodecyl-S-methyl-S-phenacylsulfonium hexafluorophosphate (DPS-C₁₂ PF₆)¹⁶ were prepared as described previously.

Preparation of 10-Decylphenothiazine

A mixture of 20 g. (0.1 mol) of phenothiazine, 35 mL (~0.15 mol) of 1-bromodecane, 9.0 g (~0.15 mol) of potassium hydroxide and 0.48g. (1% w/w) of tetra-n-butylammonium bromide in 300 mL dry toluene was stirred and refluxed for 12 h. The cooled reaction mixture was filtered, washed thoroughly with water, dried over anhydrous sodium sulfate and the solvent removed by evaporative distillation. The residue was fractionally distilled at 0.15 mm Hg. 10-Decylphenothiazine was obtained (yield: 27.5 g, 81%) as a pale yellow oil with a b.p. of 196-201°C (lit.¹⁷ b.p. 183-185°C at 0.5 mm).

¹H NMR (300 MHz, CDCl₃): δ (ppm) 7.17 – 6.86 (m; Ar), 3.86 (t, N-CH₂), 1.81(q, N-CH₂-CH₂), 1.44 - 1.26 (q,m; (CH₂)₇), 0.90 (t, CH₃)

Preparation of 10-Methylphenothiazine-5-oxide

The method of Schmalz and Burger¹⁸ was used for the synthesis of 10-methylphenothiazine-5-oxide from 10-methylphenothiazine. An 85% yield of colorless crystalline 10-methylphenothiazine-5-oxide with a m.p. of 193-194°C (lit.¹⁸ m.p. 193-194°C) was obtained.

¹H NMR (300 MHz, DMSO-d₆): δ (ppm) 7.94 – 7.23 (m; Ar), 3.73 (s, N-CH₃)

Preparation of 10-Methylphenothiazine-5,5-dioxide

10-Methylphenothiazine (1.5 g., 0.7 mmol) was dissolved in 40 mL of glacial acetic acid at 80°C to give a yellow solution. To the solution, 5.0 mL (4.8 mmol) of 30% hydrogen peroxide was added, causing the formation of deep red color. Stirring was continued for 1.5 h at 80°C. After evaporating the solvent, an impure red crystalline product was obtained. Recrystallization from 96% ethanol produced 1.2 g (68%) of orange colored crystals of 10-methylphenothiazine-5,5-dioxide having a m.p. of 221-222°C (decomp.) (lit.¹⁹ m.p. 220-221°C, dec.). The infrared spectrum showed characteristic sulfone bands at 1165 and 1126 cm⁻¹.

^1H NMR (300 MHz, DMSO- d_6): δ (ppm) 7.98 – 7.33 (m; Ar), 3.71 (s, N- CH_3)

In the same way, 10-decylphenothiazine-5,5-dioxide, m.p 95-96°C, was prepared.

Preparation of 10-(2-Vinyloxyethyl)phenothiazine (VPT)

Combined into a 500 mL round bottom flask fitted with a magnetic stirrer, reflux condenser and nitrogen inlet were 5.2 g (0.13 mol) of NaH (60% dispersion in mineral oil), and 350 mL dry tetrahydrofuran. To this solution were added portion-wise 16 g (0.08 mol) of 10H-phenothiazine. The mixture was slowly heated and refluxed for 30 min. After cooling to room temperature, 16.8 mL (0.15 mol) of 2-chloroethyl vinyl ether and 0.40 g tetra-*n*-butylammonium bromide was added and refluxing continued for 30 h. The cooled reaction mixture was filtered and the solvent and excess vinyl ether evaporated under reduced pressure. Toluene was added to the residue and the precipitated unreacted 10H-phenothiazine was removed by filtration. Evaporation of the toluene and distillation of the resulting oil at 170-175°C (0.01T) afforded 5.4 g of VPT as a pale yellow oil. (lit.²⁰ b.p._{0.1T} 150-170 °C).

^1H NMR (500 MHz, CDCl_3): δ (ppm) 7.29 – 6.92 (m; aromatic protons), 6.48 (q, $-\text{CH}=\text{CH}_2$), 4.26-4.20 (m, N- $\text{CH}_2-\text{CH}_2-\text{N}$), 4.08 (m; $\text{CH}=\text{CH}_2$).

Elemental analysis for $\text{C}_{16}\text{H}_{15}\text{NOS}$. Calc.: %C, 71.34; %H, 5.61; %N, 5.20; %S, 11.90. Found: %C, 71.69; %H, 5.64; %N, 5.23; %S, 11.88.

Polymerization of VPT

The polymerization of VPT was carried out at -45°C by injecting boron trifluoride etherate through a rubber septum into a flask that had been charged with a solution of 2.0 g. of the monomer and 25 mL dry dichloromethane. After stirring for 45 min., reaction was quenched by the addition of 3 mL of cold pyridine and then poured into cold ether. The precipitated polymer (PVPT) was collected by filtration, washed with ether and dried overnight in a vacuum oven at 45°C .

Photopolymerization Studies Using Fourier Transform Real-Time Infrared Spectroscopy (FT-RTIR).

Photopolymerizations of the monomers were monitored by FT-RTIR. A Midac M-1300 FTIR spectrometer equipped with a liquid nitrogen cooled MCT detector was used. Experiments were performed at room temperature using broadband UV light from an Hg arc source with a light intensity of $200\text{ mJ}/\text{cm}^2$ min. Photopolymerizations were carried out in monomer solutions containing 1.0 mol% of the photoinitiator. Thin films of the liquid monomer were sandwiched between two identical polypropylene films and then mounted in 5×5 cm slide frames. Infrared spectra were collected at a rate of 1 spectrum per

second using LabCalc data acquisition software and were processed using GRAMS-386 software. During irradiation, the decrease of the IR band due to either epoxy group ($780\text{--}915\text{ cm}^{-1}$) or vinyl ether double bond (1620 cm^{-1}) of the monomers was monitored.

Results and Discussion

Synthesis and UV Characterization of Phenothiazine Compounds.

PT has major UV absorption bands at 253 and 318 nm. A series of substituted phenothiazines bearing different alkyl, acyl and aryl substituents at both the nitrogen atom (10-position) and on the aromatic rings (2-position) were either synthesized or obtained from commercial sources. Comparison of their UV-VIS data showed several general trends. The introduction of electron-withdrawing groups (particularly effective was the acyl group) onto the aromatic rings shifts the λ_{max} absorption to longer wavelengths (281, 397nm). Substitution of PT at the nitrogen atom (10 position) with alkyl or aryl groups produces little change in the absorption characteristics. Oxidation of the phenothiazine sulfur shifts the longest wavelength-absorption maximum to longer wavelengths (λ_{max} 10-n-decylphenothiazine, 297, 336 nm). However, the introduction of an acyl group (10-acetylphenothiazine) shifts the longest absorption to band shorter wavelengths.

Photosensitized Cationic Polymerizations Using Phenothiazines

The ability of phenothiazine, low molar mass compounds, monomers and polymers to photosensitize the cationic photopolymerization of various monomers was evaluated using Fourier transform real-time infrared spectroscopy (FT-RTIR). RTIR has been proven to be an extremely useful method for monitoring the kinetics of very rapid photopolymerization reactions and for that reason, has been used in this laboratory as well as by many other investigators to probe these types of reactions.^{21,22,23,24}

Cyclohexene oxide (CHO) was polymerized in the presence of 0.5% of PT, 10-methylphenothiazine and 10-n-decylphenothiazine. All three compounds display excellent activity as photosensitizers for onium salts. An acceleration of the rate of photoinitiated cationic ring-opening polymerization of the epoxide monomer was observed in all cases. A second, and more important effect is the considerable reduction in the induction period. Figure 1 shows the acceleration effect when the initiator DPS-C₁C₁₂ was used.

Whereas the two 10-alkyl substituted phenothiazines are essentially identical in their influence on the photopolymerizations of CHO, PT is clearly less effective as a photosensitizer for onium salts. An analogous comparison of 10-methyl and 10-phenylphenothiazine with 10-acetylphenothiazine in the IOC10 photoinitiated photopolymerization of CHO is portrayed in Figure 2. While 10-methyl and 10-phenylphenothiazines exhibit essentially the same activity as photosensitizers, as may be predicted from the similarity of their UV absorption spectra, 10-acetylphenothiazine appears to be an inhibitor. The reduced electron density on the acetylated nitrogen atom results in an increase in the oxidation potential of the compound, making it less likely to undergo photoinduced oxidation potential by onium salt photoinitiator.

The introduction of the electron-withdrawing substituents into the 2-position of the aromatic rings of PT produces a shift in the UV absorption bands to longer wavelengths. Figure 3 illustrates a study of the use of 2-acetyl-, 2-chloro- and 2-trifluoromethylphenothiazines in the IOC10 photosensitized polymerizations of CHO. All three phenothiazine compounds display good photosensitizing activity. Oxidizing the sulfur atom of 10-methylphenothiazine also effects the photosensitization of the polymerization of CHO (Figure 4). Surprisingly, 10-methylphenothiazine-5-oxide appears to inhibit the polymerization. In contrast, the corresponding sulfone, 10-methylphenothiazine-5,5-dioxide displays excellent response as a photosensitizer. In further experiments, 10-n-decylphenothiazine-5,5-dioxide exhibited similarly efficient behavior as 10-methylphenothiazine-5,5-dioxide, when used as a photosensitizer

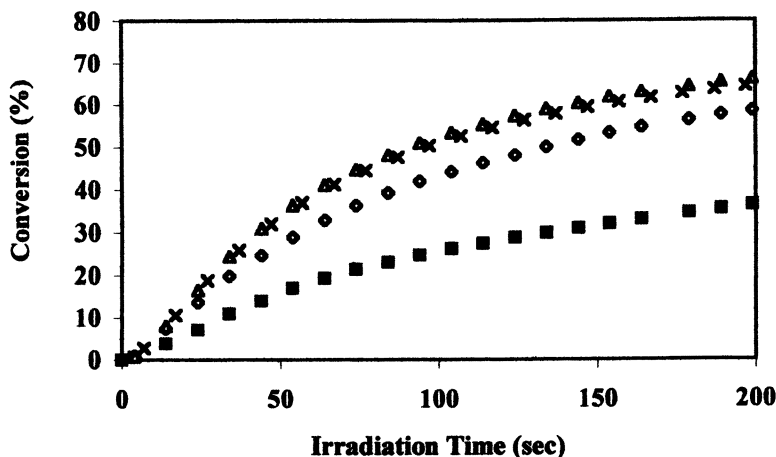


Figure 1. FT-RTIR study of cationic polymerization of CHO (cyclohexene oxide) using DPS-C₁₂ alone (■) and in the presence of 0.5% PT (◇), 10-methylphenothiazine (Δ), and 10-n-decylphenothiazine (×).

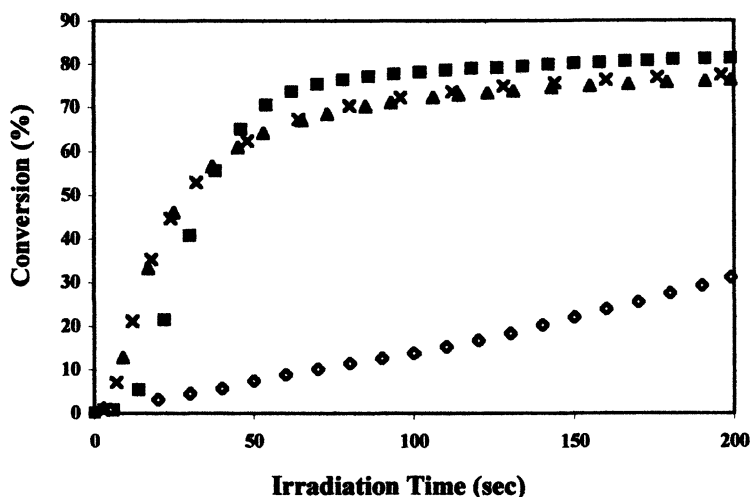


Figure 2. Photopolymerization of CHO in the presence of IOC10 alone (■) and using 0.5 % of 10-acetylphenothiazine (◇), 10-phenylphenothiazine (▲) and 10-methylphenothiazine (×).

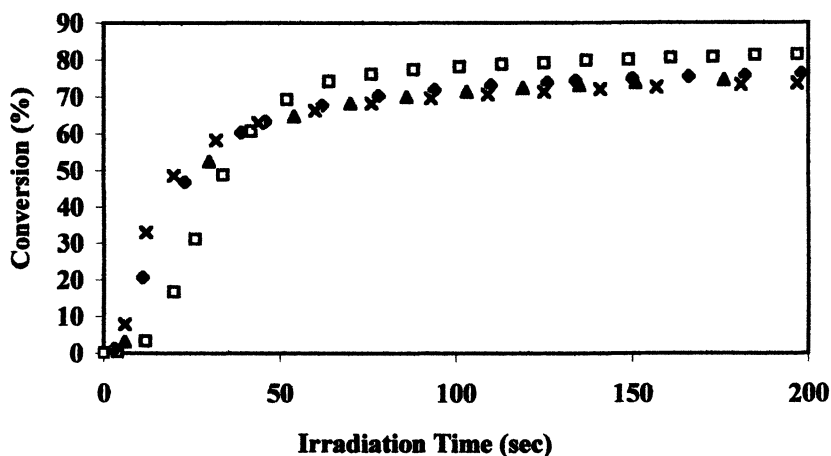


Figure 3. Study of the photopolymerization of CHO with IOC10 alone (□), and with 0.5% 2-acetylphenothiazine (◆), 2-chlorophenothiazine (▲) and 2-trifluoromethylphenothiazine (×) as photosensitizers.

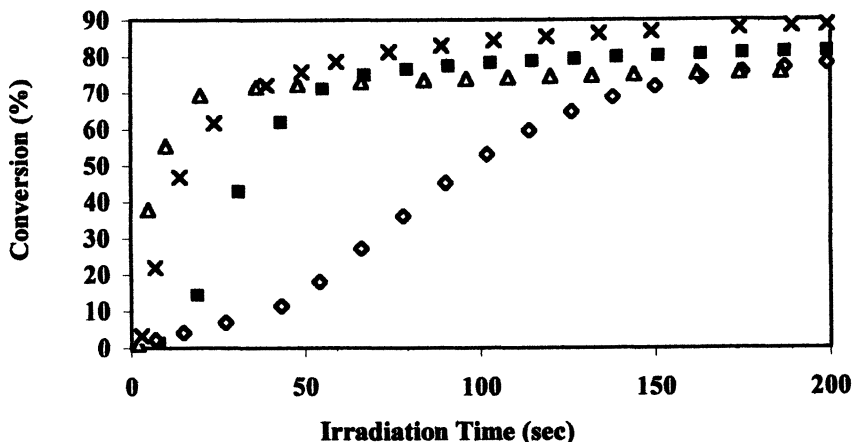


Figure 4. Photopolymerization of CHO with IOC alone (■) and in presence of 0.5% 10-methylphenothiazine (×), 10-methylphenothiazine-5-oxide (◇) and 10-methylphenothiazine-5,5-dioxide (△).

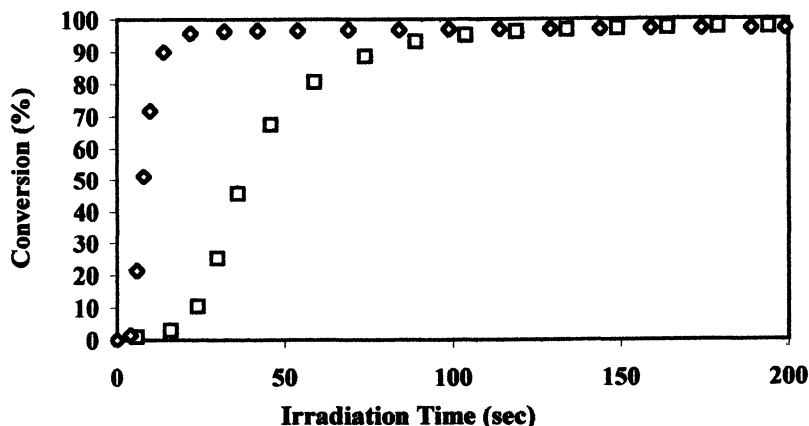


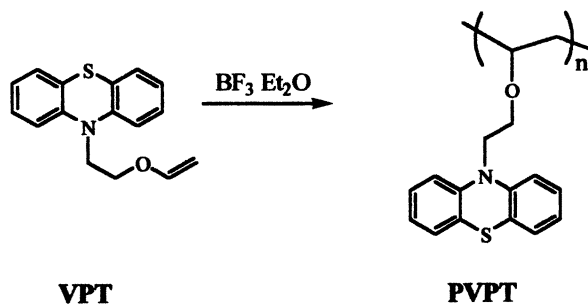
Figure 5. Study of the photopolymerization of 2-chloroethyl vinyl ether in the presence (◇) and absence (□) of 0.5% 10-decylphenothiazine-5,5-dioxide using IOC10 as the initiator.

for CHO or limonene dioxide as well as for vinyl ether monomers (2-chloroethyl vinyl ether; Figure 5).

10-Alkylphenothiazine-5,5-dioxides exhibit extraordinarily photosensitive efficiency not only for diaryliodonium salt photoinitiators as well as for triarylsulfonium and dialkylphenacylsulfonium salts. On the other hand, oxidizing 10-acetylphenothiazine to the corresponding sulfone did not improve the efficiency of this compound as a photosensitizer, indicating that the electron-withdrawing effect of the 10-acyl group is the major effect in the determination of the photosensitizing ability of these two compounds.

To establish whether the primary effect of photosensitization with phenothiazines results from their long wavelength absorption, a study was conducted in which filtered UV light was used. Using glass filter, wavelengths below 300 nm were removed from the irradiation source. As the results show, the rate and extent of the photopolymerization of CHO using 10-alkylphenothiazine-5,5-dioxides are unchanged in the presence and absence of the filter. Thus, the photoactive bands of this photosensitizer can be said to lie primarily at wavelengths greater than 300 nm.

We have also prepared the monomer, 10-(2-vinyloxyethyl)phenothiazine (VPT) as shown in the following equation by the alkylation of PT with 2-chloroethyl vinyl ether. This monomer was readily polymerized (PVPT) in the presence of BF_3 etherate. Figure 6 shows the effect of VPT and PVPT on the photopolymerization of 4-vinylcyclohexene dioxide. The epoxide band at 794 cm^{-1} was monitored for this monomer. Again, both monomer and polymeric phenothiazines display very similar and excellent behavior as photosensitizers in the polymerization of this difunctional epoxide monomer.



Conclusions

Marked acceleration of the onium-salt induced photopolymerizations of epoxides and vinyl ether monomers were noted in the presence of small quantities of low molar mass phenothiazine compounds bearing a wide variety of types of functional groups. Particularly efficient photosensitizers are 10-alkylphenothiazine-5,5-dioxides. Moreover, the ability to readily change the wavelength of absorption of these compounds in a very predictable manner

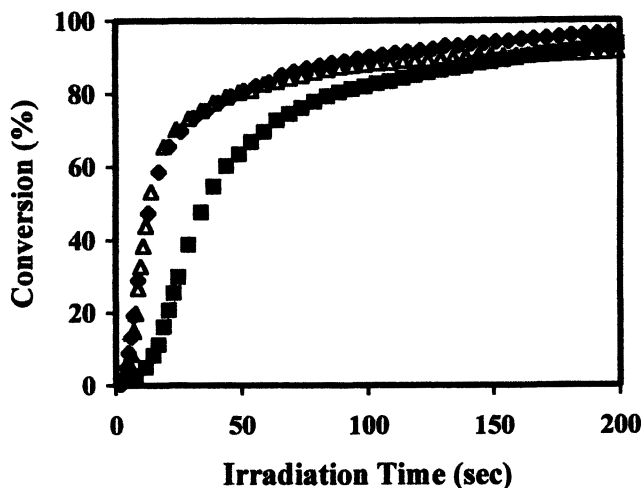


Figure 6. Comparison of the photosensitized polymerization of 4-vinylcyclohexene dioxide carried out with 1.0 % IOC-10 alone (■), in the presence of 0.5 % 10-(2-vinyloxyethyl)phenothiazine (◆) and poly(10-(2-vinyloxyethyl)-phenothiazine) (Δ). (Light intensity 400 mJ/cm²·min.)

makes this new class of onium salt photoinitiators potentially very valuable for photosensitization in the long wavelength UV-VIS regions of the spectrum. The discovery that monomers and polymers containing phenothiazine groups are also excellent photosensitizers for onium salt photoinitiators is also of considerable academic and industrial interest.

References

1. Crivello, J.V. *Photoinitiators for Free Radical Cationic and Anionic Photopolymerization*, Wiley: New York, 1998; p.329.
2. Crivello, J.V.; Lam, J.H.W. *J. Polym. Sci. Part A: Polym. Chem.* **1976**, *16*, 2441.
3. Crivello, J.V.; Lam, J.H.W. *J. Polym. Sci. Part A: Polym. Chem.* **1979**, *17*, 1059.
4. Crivello, J.V.; Lee, J.L. *Macromolecules* **1981**, *14*, 1141.
5. Gu, H.; Zhang, W.; Feng, K.; Neckers, D.C. *J. Org. Chem.* **2000**, *65*, 3484.
6. Chen, Y.; Yamamura, T.; Igarashi, K. *J. Polym. Sci. Part A: Polym. Chem.* **2000**, *38*, 90.

7. Nelson, E.W.; Carter, T.P.; Scranton, A.B. *J. Polym. Sci. Part A: Polym. Chem.* **1995**, *33*, 247.
8. Kampmeier, J.A.; Nalli, T.W. *Macromolecules* **1994**, *59*, 1381.
9. Crivello, J.V. and K. Dietliker, in: *Chemistry & Technology of UV and EB Formulation for Coatings, Inks & Paints*, Vol. III; Bradley, G. Ed.; SITA Technology Ltd.: London, 1998; p.420.
10. Crivello, J.V. in: *Ring-Opening Polymerization*; Brunelle, D.J. Ed.; Hanser: Munich, 1993; p. 157.
11. Crivello, J.V.; Lee, J. L. *Macromolecules* **1983**, *16*, 864.
12. Kunze, A.; Müller, U.; Tittes, K.; Fouassier, J.-P.; Morlet-Savary, F.J. *J. Photochem. Photobiol. A* **1997**, *110*, 115.
13. Neumann, M.G.; Rodrigues, M. R. *J. Polym. Sci. Part A: Polym. Chem.* **2001**, *39*, 46.
14. Crivello; J.V.; Lee, J.L. *J. Polym. Sci. Part A: Polym. Chem.* **1989**, *27*, 3951.
15. Akhtar, S.R.; Crivello; J.V.; Lee, J.L. *J. Org. Chem.* **1990**, *55*, 4222.
16. Crivello, J.V.; Kong, S. *Macromolecules* **2000**, *33*, 833.
17. Gillman, H.; Shirley, D.A. *J. Am. Chem. Soc.* **1944**, *66*, 888.
18. Schmalz, A.C.; Burger, A. *J. Am. Chem. Soc.* **1954**, *76*, 5455.
19. Gilman, H.; Nelson, D.R. *J. Am. Chem. Soc.* **1953**, *75*, 5422.
20. Kamogawa, H. Japanese Patent 73 33,756, Oct 16, 1973; *Chem. Abstr.* **1974**, *81*, 26182h; *J. Polym. Sci. Part A-1* **1972**, *10*, 95.
21. Decker, C.; Moussa, K. *Makromol. Chem.* **1990**, *191*, 963.
22. Decker, C. *J. Polym. Sci.: Part A: Polym. Chem.* **1992**, *30*, 913.
23. Müller, U. *J. Macromol. Sci.; Pure and Appl. Chem.* **1996**, *A33*, 33.
24. Bradley, G.; Davidson, R.S.; Howgate, G.J.; Mouillat, C.G.J.; Turner, P. *J. Photochem. Photobiol. A: Chem.* **1996**, *100*, 109.

Chapter 21

Visible and Long-Wavelength Cationic Photopolymerization

Marco Sangermano¹ and James V. Crivello^{2,*}

¹Dipartimento di Scienza dei Materiali e Ingegneria Chimica, Politecnico di Torino, C.so Duca degli Abruzzi 24, Torino, Italy

²Department of Chemistry, New York Center for Polymer Synthesis, Rensselaer Polytechnic Institute, 110 8th Street, Troy, NY 12180

A new photosensitizing system for efficiently carrying out cationic photopolymerization with visible and long-wavelength UV light is described. This system is based on the principle that certain onium salt cationic photoinitiators can be reduced by free radicals produced by the hydrogen abstraction reactions of photoexcited aryl ketones. The proposed mechanism was confirmed by the experimental results obtained and the effects of different photoinitiators, photosensitizers and the monomer structure were investigated.

Introduction

In recent years, the use of onium salt initiated cationic photopolymerization has reached commercial significance as a wide variety of uses have emerged and the benefits of this technology have been realized. The advantages afforded by photopolymerization processes have led to their rapid growth in applications in different fields such as films, inks and coatings on a variety of substrates, including paper, metal and wood. In addition, a variety of high-tech and electronic applications of this technology, such as coatings for optical fibers and the fabrication of printed circuit boards have emerged. The most important current developments in the field of UV-curing have been summarized in two recent reviews.^{1,2}

Photoinitiated cationic polymerization has found its greatest application in

the ring-opening polymerizations of epoxy monomers and other strained ring systems such as lactones and cyclic acetals. More recently, cationic UV curing technology has also been applied with considerable success to vinyl ether monomers and oligomers.³⁻⁵ Unfortunately, aryl onium salt photoinitiators suffer from the disadvantage that they have their principal absorption bands in the short wavelength region of the UV spectrum. This has placed some limitations on the potential uses of cationic photopolymerization. For example, cationic UV curing is not widely used in reprographic, printing or dental applications that rely on the use of visible light emitting sources, such as laser, quartz halogen lamps and light emitting diodes.

Photosensitization of Onium Salts

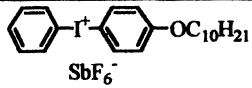
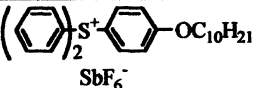
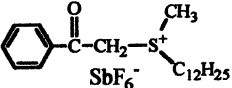
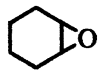
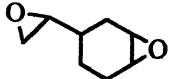
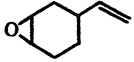
Although considerable synthetic efforts have been made to extend the spectral sensitivity of onium salts photoinitiators by substitution of appropriate chromophores onto the aromatic rings of these compounds, it has not been possible to significantly shift their sensitivity beyond the middle range of the UV spectrum.⁶ Fortunately, it is possible to photosensitize the decomposition of diaryliodonium and triarylsulfonium salts photoinitiators with electron-transfer photosensitizers. We have reported extensively on our studies in this area⁷⁻⁹ and other investigators have also been active in this field.¹⁰⁻¹³ However, the number of photosensitizers operative in the long wavelength UV and visible regions are very limited. Many of these photosensitizers suffer from various disadvantages, including toxicity and limited solubility in a wide variety of monomers. For these reasons, we have been conducting an investigation directed toward the development of novel methods of broadening the spectral sensitivity of onium salt photoinitiators into the long wavelength UV and visible regions, using alternative photosensitization techniques.

Experimental

Materials

Given in Table I are the structures and abbreviations for the monomers and photoinitiators used during the course of this work. The synthesis of diaryliodonium,¹⁴ triarylsulfonium,¹⁵ and dialkylphenacylsulfonium salts have been reported previously.¹⁶ A description of the apparatus and technique of Fourier Transform real-time infrared spectroscopy used to monitor the photopolymerizations has been reported in recent publications from this laboratory.¹⁵

Table I. Structures of Photoinitiators and Monomers

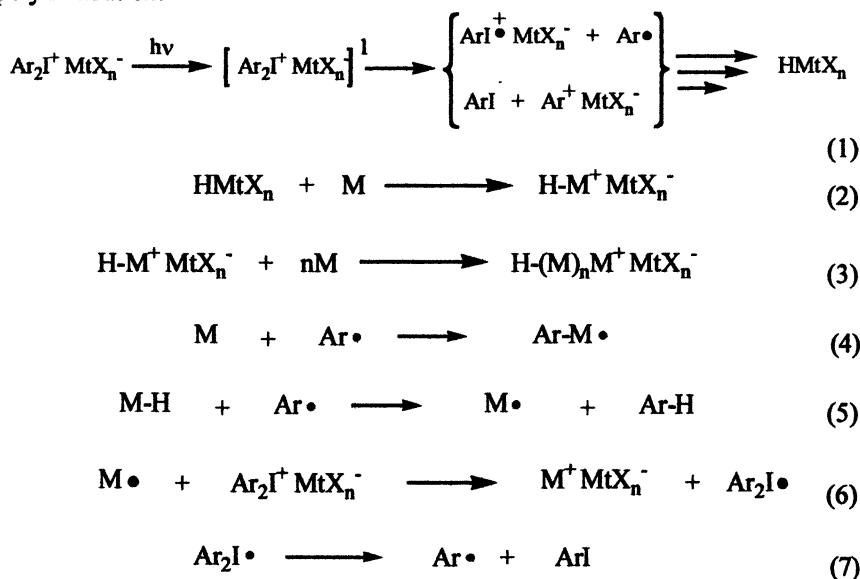
Photoinitiators		
 <p>IOC10 (4-n-decyloxyphenyl)phenyl-iodonium SbF₆⁻</p>	 <p>SOC10 (4-n-decyloxyphenyl)diphenyl-sulfonium SbF₆⁻</p>	 <p>DPS-C₁C₁₂ (S-methy-S-docecyl-S-phenacyl-sulfonium SbF₆⁻</p>
Monomers		
 <p>CHO cyclohexene oxide</p>	 <p>VCHDO 4-vinylcyclohexene dioxide</p>	 <p>VCHO 4-vinyl-1,2-epoxycyclohexane</p>

Results and Discussion

Development of Long-Wavelength Photosensitizers for Cationic Photopolymerization

Mechanistic investigations of the UV induced photolysis of diaryliodonium and triarylsulfonium salts were carried out in this laboratory¹⁷ as well as in several others.^{18,19} The mechanism involves first the photoexcitation of the onium salt and then the decay of the resulting excited singlet state with both heterolytic and homolytic cleavages of the C-I or C-S bonds. Thus, free radical, cation and cation-radical fragments are simultaneously formed. This is depicted for diaryliodonium salts in equation 1 of Scheme 1. The cationic species interact with a proton source, usually the monomer (M), to generate the strong Brønsted acid, HMtX_n. Initiation of polymerization takes place by protonation of the monomer (eq. 2) and this is followed by addition of additional monomer molecules resulting in chain growth (eq. 3). The aryl radicals interact with monomers via the pathways shown in equations 4 and 5. These species can either add to an unsaturated monomer (eq. 4) or alternatively, abstract a hydrogen atom from the monomer (eq. 5). In these reactions, secondary radical species are generated. Redox interaction of these radical species with the diaryliodonium salts gives rise to carbocations and the unstable diaryliodine radical (eq. 6). In a subsequent reaction (eq 7), the diaryliodine radical decays irreversibly to generate an aryl iodide and an aryl free radical. The reactions shown in equations 1-7 constitute a free radical chain reaction in which the

diaryliodonium salt photoinitiator is consumed by a nonphotochemical process. At the same time carbocations are generated that ultimately initiate cationic polymerization.



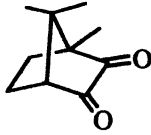
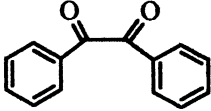
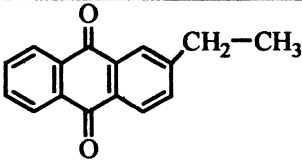
Scheme 1

From Scheme 1 it may be concluded that the photochemically induced decomposition of the diaryliodonium salt photoinitiator can be greatly amplified by the redox cycle of equations 1-7. This results in the very rapid and efficient generation of a large number of initiating cationic species by a nonphotochemical process, which further produces an apparent increase in the rate of consumption of the monomer.^{20,21} This mechanism has considerable precedence in the literature.²²⁻²⁸ In principle, any photochemical source of free radicals can serve to start the above chain of reactions. It follows directly; therefore, that spectral broadening of an onium salt could be achieved if a chemical species is present in the photopolymerizable mixture that is able to generate radicals by absorption at long-wavelength light. It is also necessary that the radicals that are produced be capable of oxidation by the diaryliodonium salt photoinitiator.

Aryl Ketone-Sensitized Cationic Photopolymerization

We decided to investigate the possibility of aryl and other types of ketones

Table II. UV Absorption Spectra of Photosensitizers

Photosensitizer	λ_{max} ($\log_{10}\epsilon$)	Reference
 CQ camphorquinone	478 nm (4)	30
 BZ benzil	260 nm (4.3) 480-486.5 nm (4)	31
 EAQ 2-ethylanthraquinone	256 nm (4.7) 325 nm (3.7)	32

as photosensitizers for onium salts photoinitiators. Table II shows the absorption characteristics of the ketones employed as photosensitizers in this work.

Our initial work has focused on the use of camphorquinone (CQ) as a 1,2-diketone photosensitizer. The choice of this compound was made on the basis of its high molar absorption coefficient and long-wavelength absorption as well as its excellent solubility and low toxicity. Furthermore, CQ is widely used, together with various amines, as a visible-light free radical photoinitiator in dental applications.²⁹ Benzil (BZ), a 1,2-aromatic diketone, and 2-ethylanthraquinone (EAQ) were also employed as photosensitizers and compared with CQ. Initial photopolymerization studies were conducted in the presence of IOC10 as the photoinitiator. Homogeneous liquid samples of the mixtures of the monomer containing the photoinitiator and a photosensitizer were sandwiched between two layers of 12- μm oriented and corona-treated polypropylene film and then irradiated with light to initiate polymerization. A polymer film filter with a cutoff of 290 nm was interposed between the sample and the light source. The decrease in the absorbance of the epoxy IR band (750 cm^{-1}) was monitored using FT-RTIR during the polymerization. Compared, in Figure 1, are the photopolymerization curves for VCHDO in the presence and absence of CQ.

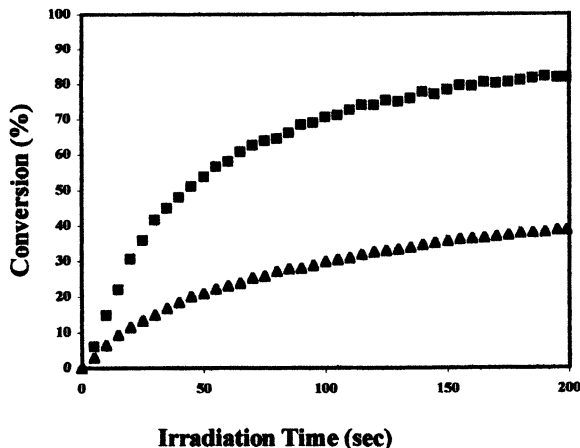
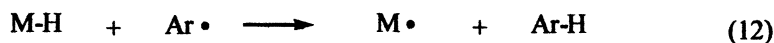
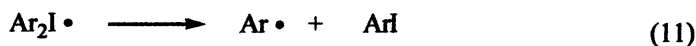
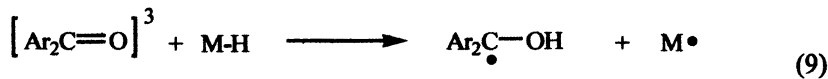
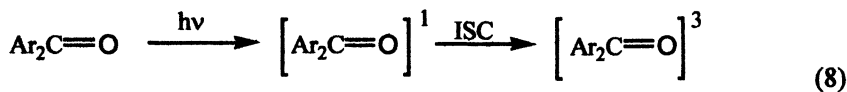


Figure 1. RTIR study of the photopolymerization of VCHDO with 4.0 mol% IOC10 alone (▲) and in the presence of 4.0 mol% CQ (■). (Reproduced with permission from *J. Polym. Sci. Polym. Chem.* 2001, 39, 343–356. Copyright 2001 Wiley.)

Over the course of a 200 second irradiation period, no polymerization was observed in the absence of CQ. It is evident that the presence of the diketone is essential for the photosensitization of the iodonium salt. In contrast, polymerization proceeds rapidly and readily in the presence of the diketone. The proposed mechanism³³ of photosensitization based on hydrogen abstraction by photoexcited ketones is shown in Scheme 2.



Scheme 2

Aryl ketones are well known to undergo $n-\pi^*$ excitation on irradiation to initially generate the excited singlet state that rapidly undergoes efficient intersystem crossing to the excited triplet (eq. 8).³⁴ Due to the diradical character of the excited triplet carbonyl, there is a strong tendency of these species to abstract hydrogen atoms from an appropriate donor. In equation 9, the indicated donor is the monomer in which a weak carbon-hydrogen bond is broken. The usual fate of the resulting benzophenone ketyl radical is to dimerize. However, the onium salt can also oxidize this radical. The carbon-centered monomer radical, M^* , can interact, as shown in Scheme 1 of the previous section, with the onium salt to induce its reduction (eq. 10). The generation of an aryl radical by the decomposition of the diaryliodonide free radical (eq. 11) closes the cycle by providing a species that again can abstract a hydrogen atom from the monomer (eq. 12). To obtain further evidence of the free-radical induced decomposition of the onium salt during long-wavelength photopolymerization, the addition of nitrobenzene as radical retarder was investigated. In the presence of the radical retarder a marked suppression of the rate of the photopolymerization of VCHDO was observed, indicating that the cycle of the radical induced chain mechanism is disrupted in the presence of nitrobenzene. A similar observation was made when a FT-RTIR study was conducted with samples containing CQ with and without a polypropylene cover film. With limited oxygen present (covered sample), the polymerization proceeded readily, but when the sample was run uncovered, polymerization was noticeably retarded.

The effect of the concentration of the photosensitizer and photoinitiator was also investigated. There is a little change in either the rate of photopolymerization or its extent, with an increase in the concentration of CQ by a factor of 2 or 4. Similarly, an increase in the concentration of IOC10 from 4.0 to 12.0 mol% had little effect on the rate of conversion of VCHDO sensitized with 4.0 mol% CQ. Different aryl ketones were employed as photosensitizers and compared with CQ. At the same molar concentration of IOC10 as photoinitiator, CQ was the most efficient photosensitizer, whereas benzophenone (BZ) was only slightly less reactive. 2-Ethylanthraquinone (EAQ) was substantially less active as a photosensitizer than either BZ or CQ.

Effects of Photoinitiator Structure

Three different types of onium salt photoinitiators, IOC10, SOC10 and DPS-C₁₂, were investigated in the CQ photosensitized ring-opening polymerization of VCHDO and the results are shown in Figure 2. A comparison of the principal characteristics of these onium salts is reported in Table III.

Table III: Absorption characteristics and reduction potentials of onium salt photoinitiators

Photoinitiator	λ_{\max}	ϵ	$E_{1/2}$	Ref.
IOC10	247 nm	15,000	- 0.2 V	34
SOC10	262 nm	17,600	- 1.0 to -1.46 V	34
DPS-C ₁ C ₁₂	--	--	- 0.7 V	35

While the diaryliodonium salt is effective in the polymerization of this monomer, the triarylsulfonium salt is not. Although the structure of SOC10 closely resembles that of IOC10, the reduction potential of the sulfonium salt is considerably higher than that of IOC10.³⁶ As a result, SOC10 is not easily reduced by free radical species and consequently, does not undergo free-radical induced decomposition reactions. The reduction potential of DPS-C₁C₁₂ lies between IOC10 and SOC10.³⁷ Although DPS-C₁C₁₂ is not as efficient as photoinitiator as the iodonium salt, it is much more active than the SOC10 in the CQ photosensitized polymerization of VCHDO.

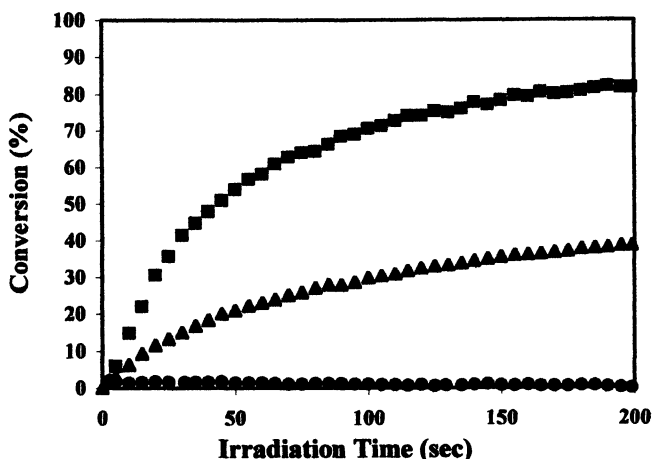
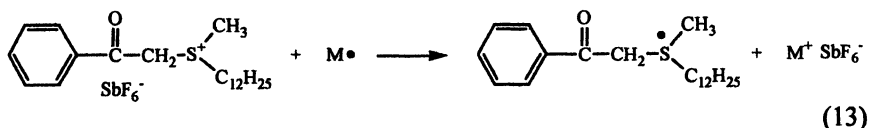
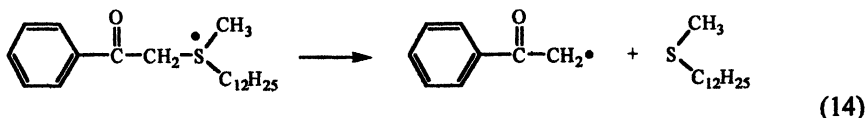


Figure 2. Comparison of VCHDO photopolymerization with 4.0 mol% CQ and 2.0 mol% photoinitiator: IOC10 (■), SOC10 (●) and DPS-C₁C₁₂ (▲)
(Reproduced with permission from *J. Polym. Sci. Polym. Chem.* 2001, 39, 343–356. Copyright 2001 Wiley.)

Equations 13 and 14 show the proposed pathway for the reduction of DPS-C₁C₁₂ by free radicals and the irreversible fragmentation of the resulting free radical species.





Influence of the Structure of the Monomer

Since the above photopolymerizations were carried out in the absence of a solvent, the monomer provides the abstractable hydrogen. For this reason according to the proposed mechanism, the structure of the monomer should play an important role in the efficiency of the photosensitization and subsequent photopolymerization process. To test this conclusion, we compared the CQ-photosensitized photopolymerization of three different epoxide monomers; CHO, VCHDO and VCHO. The results are shown in Figure 3. From this study one can observe that VCHO is by far the more reactive monomer and that VCHDO is considerably more reactive than CHO.

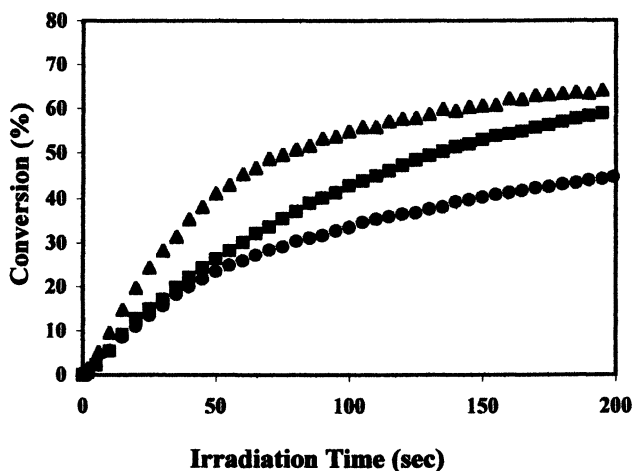


Figure 3. Comparison of the photosensitized polymerization of VCHDO (■), CHO (●) and VCHO (▲) with 2.0 mol% IOC10 and 4.0 mol% CQ. (Reproduced with permission from *J. Polym. Sci. Polym. Chem.* 2001, 39, 343–356 Copyright 2001 Wiley.)

The results can be explained by taking into account that VCHDO is difunctional. In addition, VCHDO has a readily abstractable tertiary proton located at the juncture of the cyclohexane ring and the side chain, while CHO has only less reactive secondary protons. The monomer VCHO bears a labile hydrogen at the juncture of the ring and a vinyl group that is both tertiary and

allylic. On the basis of this analysis, VCHO would be expected to participate most efficiently in mechanism of Scheme 2 resulting in a higher polymerization rate and conversion. This is what was observed.

Conclusions

When ketone photosensitizers such as camphorquinone, benzil and 2-ethylanthraquinone are irradiated with long-wavelength UV light, in the presence of a monomer that can serve as a hydrogen donor, the resulting monomer-bound radicals rapidly reduce diaryliodonium or dialkylphenacylsulfonium salts. The monomer-centered cations that are formed initiate the polymerization of epoxides. Camphorquinone was the most efficient photosensitizer and onium salts with higher reduction potentials, such as triarylsulfonium salts, do not undergo photosensitization by this new pathway. We have further demonstrated that the structure of the monomer as a hydrogen donor plays a key role in the photosensitization process.

References

1. Fouassier, J.P.; Rabek, J.C. *Radiation Curing in Polymer Science and Technology*, Elsevier, London 1993.
2. Pappas, S.P. *Radiation Curing Science and Technology*, Plenum Press, New York 1992.
3. Crivello, J.V. *UV Curing Science and Technology*, Stamford, CT USA, 1985, p. 24.
4. Watt, W.R. *UV Curing Science and Technology*, Stamford, CT USA, 1985, p. 247.
5. Roffey C.G. *Photopolymerization of Surface Coatings*, John Wiley, New York, 1982, p.74.
6. Crivello, J.V. *Photoinitiators for Free Radical Cationic and Anionic Photopolymerization*, Wiley, New York, 1998, p.329.
7. Crivello, J.V.; Lam, J.H.W. *J. Polym. Sci. Part A: Polym. Chem.* **1976**, *16*, 2441.
8. Crivello, J.V.; Lam, J.H.W. *J. Polym. Sci. Part A: Polym. Chem.* **1979**, *17*, 1059.
9. Crivello, J.V.; Lee, J.L. *Macromolecules* **1981**, *14*, 1141.
10. Gu, H.; Zhang, W.; Feng, K.; Neckers, D.C. *J. Org. Chem.* **2000**, *65*, 3484.
11. Chen, Y.; Yamamura, T.; Igarashi, K. *J. Polym. Sci. Part A: Polym. Chem.* **2000**, *38*, 90.
12. Nelson, E.W.; Carter, T.P.; Scranton, A.B. *J. Polym. Sci. Part A: Polym. Chem.* **1995**, *33*, 247.

13. Kampmeier, J.A.; Nalli, T.W. *Macromolecules* **1994**, *59*, 1381.
14. Crivello, J.V.; Lee, J.L. *J. Polym. Sci. Part A: Polym. Chem.* **1989**, *27*, 3951.
15. Akhtar, S.R.; Crivello, J.V.; Lee, J.L. *J. Org. Chem.* **1990**, *55*, 4222
16. Crivello, J.V.; Kong, S.; *Macromolecules* **2000**, *33*, 825.
17. Crivello, J.V. *Makromol. Chem. Macromol. Symp.* **1998**, *13/14*, 15.
18. Devoe, R.J.; Sahyum, M.R.V.; Serpone, N.; Sharma, D.K. *Can. J. Chem.* **1987**, *65*, 2342.
19. Dektar, J.L.; Hacker, N.P. *J. Org. Chem.* **1991**, *56*, 1838.
20. Rajaraman, S.K.; Mowers, W.A.; Crivello, J.V. *J. Polym. Sci. Part A: Polym. Chem.* **1999**, *37*, 4007.
21. Crivello, J.V.; Liu, S.S. *J. Polym. Sci. Part A: Polym. Chem.* **1999**, *37*, 1199.
22. Ledwith, A. *Polymer*, **1978**, *19*, 1217.
23. Abdoul-Rasoul, F.A.; Ledwith, A.; Yagci, Y. *Polymer* **1978**, *19*, 1219.
24. Bi, Y.; Neckers, D.C. *Macromolecules* **1994**, *27*, 3633.
25. Crivello, J.V.; Bratslavsky, S.A. *J. Polym. Sci. Part A: Polym. Chem.* **1994**, *32*, 2755.
26. Muneer, R.; Nalli, T.W. *Macromolecules* **1998**, *31*, 7976.
27. Jönsson, S.; Sundell, P.-E.; Skolling, O.; Williamson, S.E.; Hoyle, C.E. *Aspects of Photoinitiation, Radcure Coat. Inks*, **1993**, *79*, 81.
28. Pappas, S.P. *Prog. Org. Coat.* **1985**, *13*, 35.
29. Crivello, J.V.; Dietliker, K. *Chemistry and Technology of UV & EB Formulation for Coatings, Inks & Paints*, Wiley, New York, **1998**, Vol. III, p. 266.
30. Cook, W.D. *J. Dent. Res. B* **1982**, *1*, 1438.
31. Hulme, B.E.; Marron, J. *J. Paint Resin* **1984**, *1*, 31.
32. *Sadler Standard Spectra* Spectrum No. 4588, Sadler Research Labs., Philadelphia, **1970**, Vol. 19.
33. Fouassier, J.P.; Rabek, J.F. *Radiation Curing in Polymer Science and Technology*, Elsevier, New York, **1993**, Vol. II, p. 181.
34. Gilbert, A.; Baggot, J. *Essentials of Molecular Photochemistry*, Blackwell Science, London, **1995**, p. 177.
35. Pappas, S.P.; Gatechair, L.R.; Jilek, J.H. *J. Polym. Sci. Part A: Polym. Chem.* **1984**, *22*, 77.
36. Kunze, A.; Müller, U.; Tittes, K.; Fouassier, J.-P.; Morlet-Savary, F.J. *J. Photochem. Photobiol. A: Chem.* **1997**, *110*, 115.
37. Sundell, P.E.; Jönsson, S.; Hult, A.; *J. Polym. Sci., Part A: Polym. Chem. Ed.*, **1991**, *29*, 1535.

Chapter 22

Synthesis and Photoinitiated Cationic Polymerization of Organic–Inorganic Hybrid Resins

Ki Yong Song¹, Ramakrishna Ghoshal², and James V. Crivello³

¹Semiconductor R&D Center, SEC, Samsung Electronics Company, Ltd., San #24 Nongseo-Ri, Kiheung-Eup, Yongin-City, Kyungki-Do, Korea

²Polyset Company, P.O. Box 111, Mechanicville, NY 12118

³Department of Chemistry, New York Center for Polymer Synthesis, Rensselaer Polytechnic Institute, 110 8th Street, Troy, NY 12180

A streamlined synthetic scheme was developed for the preparation of a novel series of cationically polymerizable epoxy-functional organic-inorganic hybrid resins. The reaction sequence consisted first, of the regioselective rhodium catalyzed monoaddition of an α,ω -Si-H difunctional siloxane to a vinyl epoxide. The second step involves the addition of the remaining Si-H bond of the latter adduct to vinyl trimethoxysilane. Finally, an ion exchange catalyzed sol-gel hydrolysis of the resulting trialkoxysilane functional epoxide yields the desired silicone-epoxy resins bearing pendant epoxy groups. These resins undergo facile UV and thermally induced cationic photopolymerization in the presence of onium salt photoinitiators to give crosslinked organic-inorganic hybrid glassy matrices. The mechanical and thermal properties of polymerized resins were determined and were correlated with the structures of the resins.

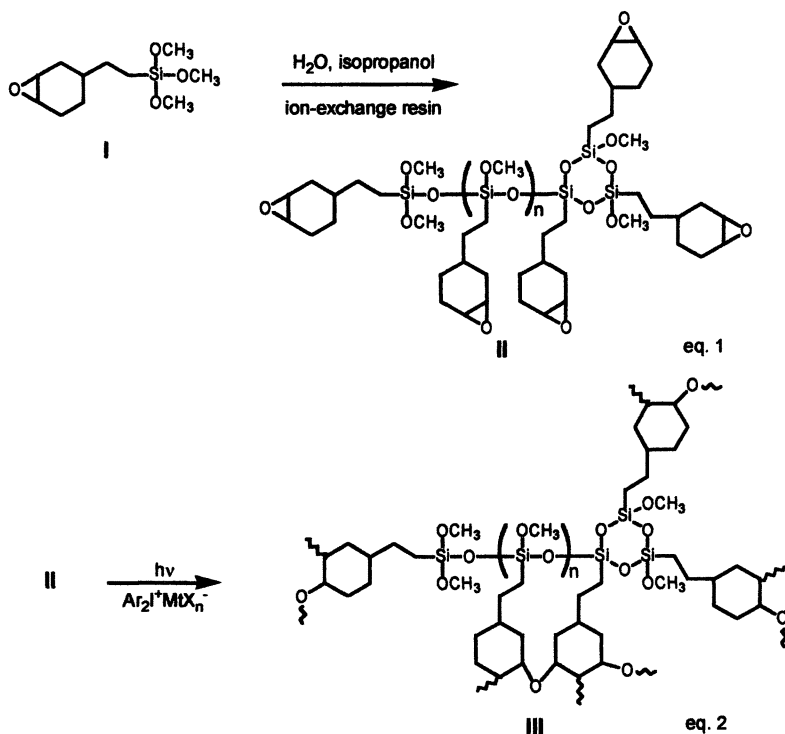
Introduction

In recent years, organic-inorganic hybrid resins have received much attention in the literature due to their unique electrical, optoelectronic and mechanical properties. Much work is currently focused on the synthesis of crosslinked glass-like matrices composed of Si-O-Si linkages employing sol-gel techniques that involve the acid or base catalysed hydrolysis of tri- or tetraalkoxysilanes (1-3). Despite the many potential applications of organic-inorganic hybrid resins, traditional sol-gel techniques for their synthesis have a number of drawbacks which have limited their use. First, sol-gel chemistry is slow, often days and weeks are required for the hydrolysis of the alkoxy silane to proceed to completion. During hydrolysis and subsequent condensation of the resulting silanols, a highly porous, crosslinked matrix resin is formed. If the hydrolysis is carried out too rapidly, fracture of the fragile matrix often occurs. Due to the loss of the alkyl groups as alcohols during hydrolysis, there is always considerable shrinkage of the resin matrix. Densification of the initially formed porous matrix by calcination is often required to produce specimens with good cohesion and mechanical strength. Lastly, the modification of sol-gel matrices through the incorporation of functionalized alkoxy silane precursors is sometimes difficult due to difference in the hydrolysis rates of the components or to their phase separation during the cohydrolysis step.

In this laboratory, we have been addressing some of the problems outlined above by exploring several new approaches to the synthesis of siloxane-based hybrid organic-inorganic resins. Previously (4) we have employed the two-step methodology depicted in Scheme 1 for the preparation of these resins.

First, the sol-gel condensation of a precursor such as **I** containing both a trialkoxysilane and an epoxy functional group (eq. 1) was carried out using an ion exchange resin as a catalyst. The resulting product **II** is an oligomer with a backbone composed of both cyclic and linear siloxane groups and bearing pendant epoxy groups. The structure of the resin shown in equation 1 is idealized. Typically, oligomers with up to 12-15 repeat units can be prepared in which greater than 85% hydrolysis of the alkoxy groups has taken place. Despite the fact that a trialkoxysilane is employed in this reaction, the simultaneous hydrolysis and condensation reactions can be carried out in a controlled manner such that no crosslinking or gel formation takes place. Termination of the reaction can be achieved by simply removing the catalyst by filtration. In a subsequent step, these oligomers can be polymerized via a ring-opening polymerization of the pendant epoxy groups. For example as shown in equation 2, the oligomers undergo very rapid crosslinking with formation of organic-inorganic hybrid networks **III** when irradiated with UV light in the presence of an onium salt photoinitiator.

Scheme 1



The above synthetic approach has the advantage that the normally slow sol-gel hydrolysis condensation can be carried out in a rapid but controlled fashion using the ion-exchange catalyst. In addition, the strategy of initially carrying out the sol-gel reaction removes most of the shrinkage in the first step. The crosslinking photopolymerization of the pendant epoxy functional oligomer II takes place rapidly with rather small shrinkage. No further densification of the polymerized specimen is required.

The present paper describes the development of a new, generally applicable synthetic approach that can be employed to prepare a family of silicone-epoxy resins using simple, readily available precursors. These resins undergo facile cationic photopolymerization to yield organic-inorganic hybrid resins with a wide range of properties.

Experimental

General Synthesis of α -Epoxy- ω -Trialkoxysiloxanes and oligomers

The synthetic procedures given below are typical of those used for the preparation of the α -epoxy- ω -trialkoxysiloxanes and the silicone epoxy oligomers shown in Table 1.

Preparation of 1-[2-(3{7-Oxabicyclo[4.1.0]heptyl}ethyl)-3-[2-trimethoxysilyl-ethyl]-1,1,3,3-tetramethyldisiloxane (VIIIa)

A mixture of 20.0g (0.15 mol) of distilled 1,1,3,3-tetramethyldisiloxane, 18.5g (0.15 mol) of 3-vinyl-7-oxabicyclo[4.1.0]heptane, 20mL of dry toluene were charged into a 250-mL round bottom flask fitted with a reflux condenser and thermometer. There were added 30 mg of Wilkinson's catalyst, and the reaction mixture was heated at 60°C for 4 h in an oil bath. After this time, the ¹H-NMR spectrum showed that the vinyl peaks at 5.5 ppm had disappeared. Next, there were added 22.2g (0.15 mol) of distilled vinyltrimethoxysilane. After 6 hours at 90°C, the infrared absorption at 2160cm⁻¹ (Si-H group) had completely disappeared. Removal of the solvent under reduced pressure gave the desired product, (54.6g, 90% yield) of colorless oil, which was characterized by ¹H-NMR and confirmed to be monomer **VIIIa**.

Sol-Gel Condensation of 2-(3,4-Epoxy-cyclohexylethyl)trimethoxysilane

A mixture of 20g (0.081mol) of **Ia**, 4.4g (0.24 mol) of deionized water, 0.8g of Amberlite IRA-400 ion exchange resin and 10g of isopropanol were placed in a 100 mL round-bottom flask equipped with a magnetic stirrer and a reflux condenser. The condensation reaction was carried out at the reflux temperature, 82°C, for 6 hours. Thereafter, the solution was cooled, filtered and passed through a silica gel column using ethyl acetate as the eluent. The solvent was removed under vacuum, and a viscous liquid oligomer (16.3g) **Ib** was obtained. ¹H-NMR (CDCl₃) δ (ppm) 0.5, CH₂-Si; 1.2-2.2, aliphatic protons; 3.1, epoxy CH; 3.48, OCH₃.

Sol-Gel Condensation of 2-(3{7-Oxabicyclo[4.1.0]heptyl}ethyl)-[2-trimethoxysilylethyl]-methylphenylsilane

A mixture of 6.0g (0.015mol) of **VIIa**, 0.82g (0.0456 mol) of deionized water, 0.24g of Amberlite IRA-400 ion exchange resin and 3.0g of n-propanol were placed in a 100 mL round-bottom flask equipped with a magnetic stirrer

and a reflux condenser. The hydrolysis-condensation reaction was carried out at the reflux temperature, 97°C, for 24 hours. After the solution was filtered, it was passed through a silica gel column using ethyl acetate as the eluent. The ethyl acetate was removed in vacuum and a viscous liquid oligomer (4.9g) **VIIIb** was obtained. ¹H-NMR (CDCl₃) δ(ppm) 0.2-2.2, CH₂-Si and CH₃-Si and aliphatic protons; 3.1, epoxy CH; 3.48, OCH₃; 7.4, aromatic protons.

Sol-Gel Condensation of 1-[2-(3{7-Oxabicyclo[4.1.0]heptyl}ethyl)-3-[2-trimethoxysilylethyl]-1,1,3,3-tetramethyldisiloxane

To a 75mL pressure vessel fitted with a magnetic stirrer were charged 10g (24.6mmol) of **VIIIa**, 1.33g (73.8mmol) of deionized water, 0.4g of Amberlite IRA-400 ion-exchange resin, and 5.0g of isopropanol. The reaction mixture was stirred and heated at 150°C for 12 hours under pressure. After the solution was filtered and passed through a silica gel column using ethyl acetate as the eluent, the solvent was removed in vacuum to give a viscous liquid oligomer **VIIIb** (8.4g). ¹H-NMR (CDCl₃) δ(ppm) 0-0.1, CH₃-Si; 0.5, CH₂-Si; 1.2-2.2, aliphatic protons; 3.1, epoxy CH; 3.4-3.8, OCH₃.

Results and Discussion

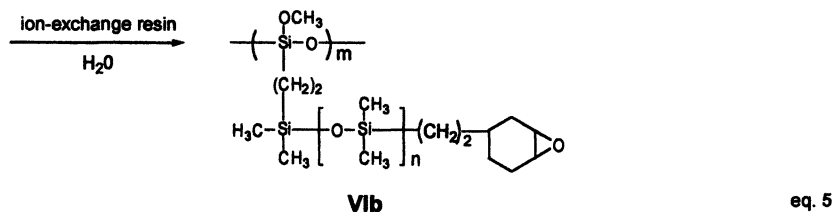
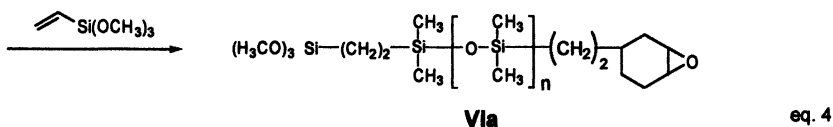
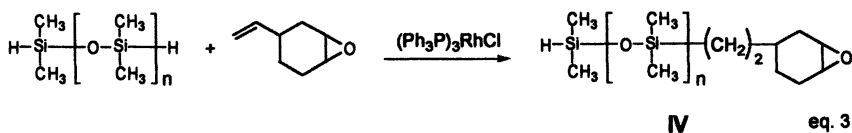
Synthesis of Epoxy-Siloxane Oligomers

In Scheme 1 is described the synthesis and photopolymerization of silicone-epoxide resins that we have previously prepared. This method requires epoxy compounds bearing trialkoxysilane groups as precursors for the sol-gel condensation. There is a dearth of such compounds available from commercial sources and also few compounds of this type have been reported in the literature. Accordingly, we have been seeking alternative techniques for the synthesis of epoxy functional sol-gel resins. A novel series of silicon-containing epoxy resins has been prepared by a streamlined three-step process as depicted in equations 3-5 of Scheme 2 that makes use of readily available and inexpensive substrates.

The discovery that it is possible to carry out a regioselective monohydrosilation addition of a vinyl epoxide at only one of the two Si-H groups an α,ω -Si-H terminated polydimethylsiloxane ($n = 1,2,3$) and methylphenylsilane was made in this laboratory (6, 7). This reaction was employed as shown in equation 3 to prepare monoadducts with the general structure **IV** and also **V** shown below.

In the present case, these monoadducts were not isolated, but were directly carried forward into the next step of the reaction sequence (eq. 4) wherein vinyltrimethoxysilane was added and subjected to further hydrosilylation with the remaining Si-H groups to yield **VIa** and **VIIa** respectively (8). Thus, in a simplified, two-step, one-pot process these and other such compounds bearing both trialkoxysilyl and epoxy groups in the same molecule can be readily prepared in high yields.

Scheme 2



The sol-gel condensations of ambifunctional adducts **Ia** and **VIIa-Xa** (eq. 5) proceed smoothly in the presence of water and a weakly acidic ion-exchange resin. Typically, the condensations were carried out in solution in either hot isopropanol or n-propanol. The reactions were usually terminated when greater than 85% of the methoxy groups (3.55 ppm) had undergone reaction as determined by $^1\text{H-NMR}$. It was found that as the siloxane chain of the spacer is lengthened, increasingly more vigorous conditions for the sol-gel reaction were required. Thus, while **Ia** undergoes sol-gel condensation in 6 h in isopropanol at 82 °C, **Xa**, required 12 h heating at 150 °C under pressure in a sealed vessel.

The desired silicone-epoxy oligomers were obtained as colorless viscous oils by filtering the reaction mixture to remove the ion-exchange resin and then stripping off the solvent under reduced pressure. Under these conditions ring-opening of the epoxy groups was not observed. The resulting silicone-epoxy oligomers were colorless to very pale yellow viscous liquids that displayed high reactivity in photo- and thermally initiated cationic polymerization. Both ^1H -

NMR and ^{29}Si -NMR spectra of **VIIIb** suggest a structure analogous to the proposed structure for oligomer **II** in which various degrees of hydrolysis of the trialkoxysilyl groups has taken place. Collected in Table 1 are the structures of the oligomers together with the conditions of their sol-gel condensations as well as the molecular weight and viscosity data. Again, it should be noted that the structures of the oligomers shown in Table 1 are idealized and that, in fact, the actual structure is much more complex with both cyclic and linear siloxane repeat units in the backbone. The approximate degree of polymerization (DP) is also given in Table 1. The oligomers range from hexamers to undecamers implying that they correspondingly possess on the average from six to eleven reactive epoxy-cyclohexyl groups per molecule. It is interesting to note that the viscosity of the oligomers appears to be closely related to the structure of the oligomers. Oligomer **VIIIb** with aromatic groups has an anomalously high viscosity although the molecular weight is comparatively low. As one increases the length of the dimethylsiloxane spacer in the resin, the viscosity decreases.

Table 1. Epoxy-Functional Silicone Resins

Notation	Ib	VIIb	VIIIb	IXb	Xb
Structure					
Reaction Conditions	IPA*, 82°C, 6 h	NPA#, 91°C, 24 h	IPA, 150°C, 12 h [†]	IPA, 150°C, 12 h [†]	IPA, 150°C, 12 h [†]
Yield (%)	100	92	98	95	93
Viscosity(cP)	2506	33260	2929	648	249
Mw (g/mol)	2430	2381	4186	6440	8135
MWD	1.3	1.1	1.3	1.4	1.7
DP	9	6	9	11	9

*Isopropyl alcohol, #n-propyl alcohol, †under pressure

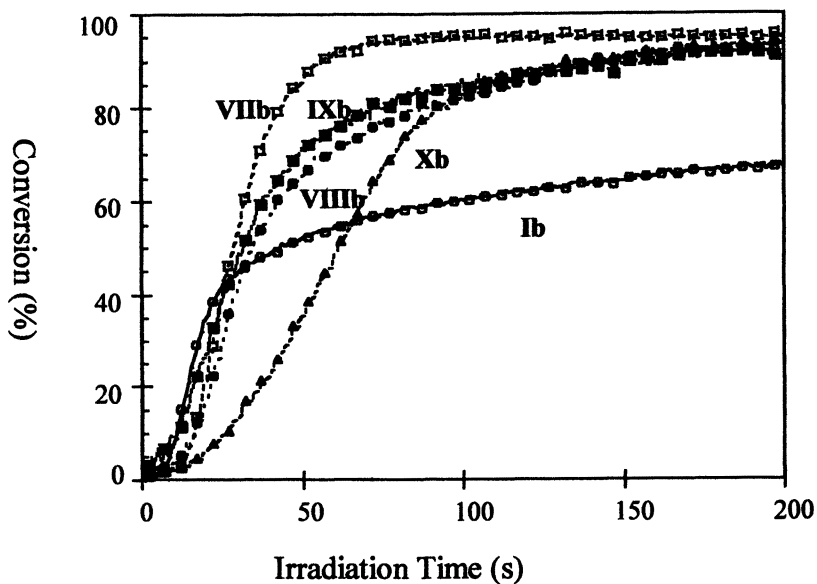
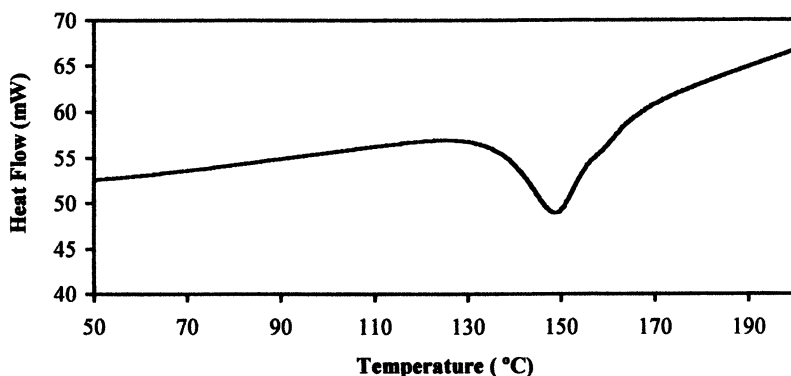


Figure 1. Real-time infrared study of the cationic photopolymerization of silicone-epoxy oligomeric resins using 2.0 mol% of IOC10 as photoinitiator.

Photo- and Thermally Initiated Cationic Polymerization

In previous papers from this laboratory it was reported that monomers bearing epoxycyclohexyl groups in general (9) and silicone-epoxy monomers (10) containing these groups in particular display high reactivity in photoinitiated cationic polymerization. The multifunctional sol-gel silicone-epoxy oligomers prepared in this investigation similarly undergo facile photo- and thermally induced cationic ring-opening polymerization in the presence of photosensitive onium salts. In this study we have employed (4-n-decyloxyphenyl)phenyl- iodonium hexafluoroantimonate (IOC10) as both the thermal and photoinitiator for the cationic ring-opening polymerization of the epoxide groups. This compound was selected for its high solubility in all the silicone-epoxy oligomeric resins and because this onium salt has a high quantum yield (~ 0.7) and is a very efficient photoinitiator for the cationic ring-opening polymerization of epoxides (11). Employing the neat resins containing 2.0 mol% of IOC10, the photopolymerizations were monitored using real-time infrared spectroscopy (RTIR) (12, 13). Using this technique, the disappearance of the infrared band at 886 cm^{-1} due to the epoxy groups was followed as a

function of time. Shown in Figure 1 are the conversion versus time curves obtained from these studies. Included in this figure for comparison is the kinetic curve for the photopolymerization of oligomer **Ib** that was prepared using the process described in Scheme 1. All the epoxy functional oligomers display excellent reactivity in cationic epoxide ring-opening photopolymerization. Some structurally dependant trends can be distinguished in this study. **Ib** shows high reactivity as indicated by the initial portion of the kinetic curve, however, the conversion of epoxy groups reached after 200 seconds irradiation was only approximately 60%. In contrast, the photopolymerizations of all the other resins proceed to nearly quantitative conversions. It may be noted that **Ib** has the shortest and stiffest spacer linking the epoxycyclohexyl group with the siloxane main chain of all the resins. As a consequence, **Ib** would be expected to give the most highly crosslinked polymer. Diffusion and mobility of the bulky epoxycyclohexyl groups in this polymer would be expected to be restricted. This results in vitrification of the polymer during polymerization at low conversions. In contrast, the high mobility of the other resins with flexible siloxane groups in the spacers gives rise to much higher conversions due to suppression of the onset of vitrification.



*Figure 2. DSC scan of the thermally initiated cationic polymerization of silicone-epoxy oligomer **VIIIb** in the presence of 2.0 mol% IOC10 as initiator.*

In Figure 2 is shown the differential scanning calorimetry (DSC) curve for the thermal polymerization of oligomer **VIIIb** in the presence of 2.0 mol% IOC10. The onset of thermal decomposition of IOC10 takes place at 148 °C. Polymerization of this oligomer is very rapid as indicated by the sharpness of the exothermic peak in the DSC curve.

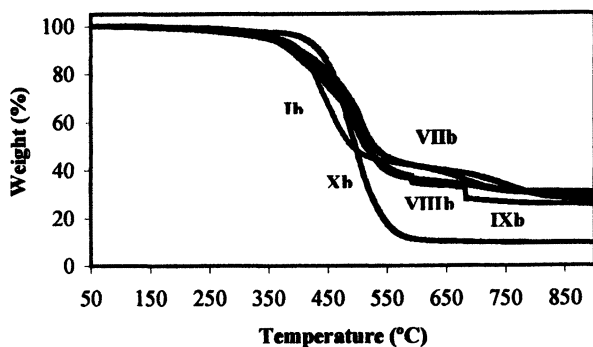


Figure 3. Thermogravimetric analysis study of crosslinked silicone-epoxy resins carried out at a heating rate of 20 °C/min in nitrogen.

Thermal Stability of Epoxy Functional Organic-Inorganic Hybrid Polymers

The thermogravimetric analysis (TGA) curves for thermally cured samples of the silicone-epoxy oligomers are given in Figure 3. The TGA study was carried out in nitrogen at a heating rate of 20°C/min. The polymers display excellent stability with the onset of thermal decomposition at approximately 350–400°C. In contrast, most common epoxy resins decompose below 200°C and this severely limits their utility in many applications.

Mechanical Properties of Epoxy Functional Organic-Inorganic Hybrid Polymers

The mechanical properties of the organic-inorganic hybrid polymers produced by thermal polymerization of the corresponding epoxy functional sol-gel oligomers were determined using dynamic mechanical analysis (DMA). The results are shown in Figures 4 and 5. Again, the polymer derived from Ib was included in this study for comparison. The mechanical properties of the resins are directly related to the length and type of spacer group separating the epoxycyclohexyl groups from the siloxane main chain. Accordingly, Ib would be expected to be the stiffest and highest glass transition polymer. In Figure 4 it can be seen that this polymer exhibits no decrease in the storage modulus at temperatures up to 180°C. In fact, there is no decrease in the modulus or evidence of a glass transition at temperatures below 300°C. As the length of the spacer is increased and flexible siloxane linkages are introduced, one sees a

progressive decrease in the temperature of the fall off of the storage modulus that corresponds to a decrease in the glass transition temperature (Figure 5). Polymer Xb displays the lowest glass transition temperature (-6.5°C) while the T_g s for IXb and VIIIb are respectively, 33°C and 80°C . A similar observation was made for photo-polymerized thin films of these oligomers. While the film derived from Ib was brittle and could not be handled, the films from VIIIb, IXb and Xb were increasingly more flexible and tough.

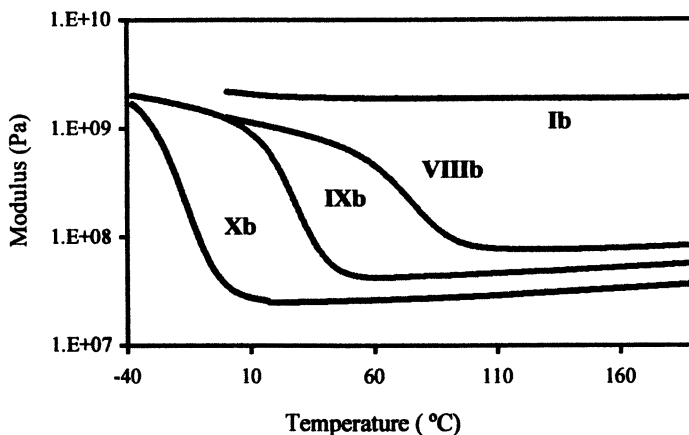


Figure 4. Comparison of the storage moduli as determined by dynamic mechanical testing for thermally crosslinked silicone-epoxy resins Temperature scan rate $10^{\circ}\text{C}/\text{min}$ in nitrogen.

Conclusions

A convenient and high yield method for the synthesis of novel silicone-epoxy resins has been developed. This method takes advantage of several new reactions discovered in this laboratory. First, the regioselective hydrosilation addition of a vinyl epoxide at only one end of an α,ω -Si-H difunctional siloxane or silane provides an intermediate bearing one epoxy and one Si-H group. Further hydrosilation with vinyltrimethoxysilane leads to ambifunctional molecules bearing both trimethoxysilyl and epoxy groups that may be employed as substrates in the sol-gel condensation. In this work, we have utilized acidic ion-exchange catalysts to catalyze this latter reaction. The resulting silicone-epoxide oligomers can be readily converted by either photo- or thermally induced cationic ring-opening polymerization to crosslinked organic-inorganic hybrid resins. The properties of the crosslinked resins depend on the length of the spacer group between the siloxane backbone and the pendant epoxy groups. Short spacer groups lead to highly rigid, glass-like matrices, while longer spacer groups produce more flexible materials with considerable elongation. Many novel applications for these novel resins are anticipated including

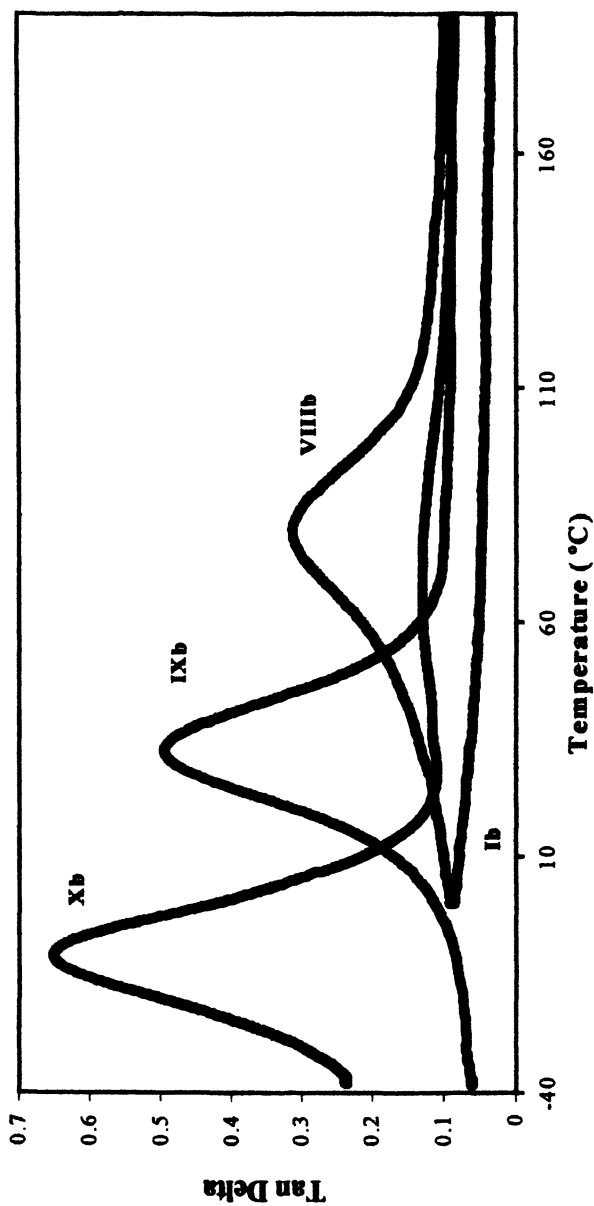


Figure 5. Comparison of the tan delta plots for thermally crosslinked silicone-epoxy resins as determined by dynamic mechanical testing. Temperature scan rate 10 °C/min in nitrogen.

composites, optical adhesives and coatings, wave guides and electronic potting and encapsulating resins.

References

1. Brinker, C.J.; Scherer, G.W. *Sol-Gel Science*, Academic Press, Inc, New York, 1990.
2. Wenzel, J. *J. Noncryst. Solids* **1985**, *73*, 693.
3. Schubert, U.; Hüsing, N.; Lorenz, A. *Chem. Mater.* **1995**, *7*, 2010.
4. Crivello, J.V.; Mao, Z. *Chem. Mater.* **1997**, *9*, 1554.
5. Crivello, J.V.; Lee, J.L. *J. Polym. Sci. Part A: Polym. Chem.* **1989**, *27*, 3951.
6. Crivello, J.V.; Bi, D. *J. Polym. Sci., Polym. Chem. Ed.* **1993**, *31*, 2563.
7. Crivello, J.V.; Bi, D. *J. Polym. Sci., Polym. Chem. Ed.* **1993**, *31*, 2729.
8. Crivello, J.V.; Bi, D. *J. Polym. Sci., Polym. Chem. Ed.* **1993**, *31*, 3121.
9. Crivello, J.V.; Linzer, V. *Polimery* **1998**, *68*, 661.
10. Crivello, J.V.; Lee, J.L. *J. Polym. Sci., Polym. Chem. Ed.* **1990**, *28*, 479.
11. Crivello, J.V. *Ring-Opening Polymerization*, Brunelle, D.J. editor, Hanser Pub., Munich, 1993, p. 157.
12. Decker, C.; Moussa, K. *J. Polymer Sci.: Part A: Polym. Chem.* **1990**, *28*, 3429.
13. Decker, C.; Moussa, K. *Makromol. Chem.* **1990**, *191*, 963.

Chapter 23

The Photoinitiated Cationic Polymerization of 3,4-Epoxy-1-butene

Marco Sangermano¹, Stephen N. Falling², and James V. Crivello^{1,*}

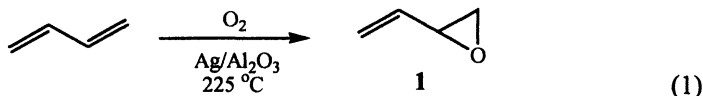
¹Department of Chemistry, New York Center for Polymer Synthesis,
Rensselaer Polytechnic Institute, 110 8th Street, Troy, NY 12180

²Research Laboratories, Eastman Chemical Company, P.O. Box 1972,
Kingsport, TN 37662

The photopolymerization of 3,4-epoxy-1-butene (**1**) was investigated using Fourier transform real-time infrared spectroscopy. The effects of photoinitiator structure and concentration and light intensity on the photopolymerization were investigated. Monomer **1** was found to be more reactive than its saturated analog, 1,2-epoxybutene, and its halogenated derivatives, 3,4-dibromo-1,2-epoxybutane and 3,4-dichloro-1,2-epoxybutane.

Introduction

3,4-Epoxy-1-butene (vinyl oxirane, **1**) is a molecule with considerable potential for the production of new monomers and polymers as well as fine, specialty and commodity chemicals (*1*). An efficient, continuous process for **1** by the selective, vapor-phase oxidation of 1,3-butadiene (equation 1) has been developed by Monnier and co-workers (*2-5*). This development has renewed interest in **1** as a difunctional monomer with reactive epoxy and vinyl groups.



One rapidly emerging technology upon which this monomer may have an impact is cationic UV curing, a process which involves the rapid, photoinduced polymerization of liquid, multifunctional monomers to give solid, crosslinked films useful for coatings, printing inks and adhesives. Typically, onium salt photoinitiators such as diaryliodonium and triarylsulfonium salts are employed in this process (6). Polymerization of the monomer results from attack by a strong protic acid which is generated during photolysis. Monomers containing the epoxide group undergo facile ring-opening polymerization by this process. In the case of **1**, polyethers bearing pendant vinyl groups may result by simple ring-opening polymerization. In addition, there was the possibility that the double bond could also interact with the neighboring epoxy group during polymerization to produce polymers in which all four-carbon atoms of the monomer are incorporated into the polymer backbone (7,8).

Experimental

3,4-Epoxy-1-butene (**1**), 3,4-dibromo-1,2-epoxybutane (**3**) and 3,4-dichloro-1,2-epoxybutane (**4**) were used as received from Eastman Chemical Company (Kingsport, TN). 1,2-Epoxybutane was used as received from Aldrich Chemical Company (Milwaukee, WI). The diaryliodonium salt photoinitiators employed in this investigation were prepared as described previously (9). ¹H-NMR spectra were obtained using a Varian, Inova 500 MHz Spectrometer.

Bulk Photopolymerization of 3,4-Epoxy-1-butene (**1**)

A 3 mL solution of **1** containing 1.0 mol% (4-n-decyloxyphenyl)phenyliodonium hexafluoroantimonate (IOC10) was prepared. The solution was transferred to a 15 mm diameter quartz reaction tube, sealed with a rubber cap then placed in an ice bath and irradiated for two minutes in a Rayonet Photochemical Reactor. Chloroform was added to the reaction mixture and the polymer solution poured into methanol. The precipitated polymer was isolated by filtration then dissolved in chloroform and reprecipitated into methanol. This process was repeated once more. The resulting polymer was dried in a vacuum oven at 50°C then the ¹H-NMR spectrum recorded in CDCl₃.

Photopolymerization Studies

The thin film photopolymerizations were monitored using Fourier transform real-time infrared spectroscopy (FT-RTIR). A Midac M-1300 FTIR spectrometer equipped with a liquid nitrogen-cooled mercury-cadmium-telluride detector was used. The instrument was fitted with a UVEXS Model SCU-110 mercury arc lamp equipped with a flexible liquid optic wand. The end of this wand was placed at a distance of 4-20 cm and directed at an incident angle of 45° onto the sample window. UV light intensities were measured with the aid of a UV radiometer at the sample window.

Photopolymerizations were carried out at room temperature using unfiltered UV light from a Hg arc source with bulk monomers containing various concentrations of the indicated photoinitiator. The monomer/photoinitiator solutions were coated onto 12 μm oriented and corona-treated polypropylene films, covered with identical polypropylene films, then mounted in 5 cm x 5 cm slide frames. The thickness of the liquid monomer films was estimated at 10-25 μm. Infrared spectra were collected at a rate of one spectrum per second using LabCalc data acquisition software and processed using GRAMS-386 software (Galactic Industries Corp.). During irradiation, the decrease of the IR absorbance due to the vinyl group at 1640 cm⁻¹ and/or the epoxy group at 820 cm⁻¹ was monitored. In all cases, 3 to 5 runs were recorded and the results averaged. The kinetic parameter, $R_p/[M_0]$, was determined from the initial slopes of the irradiation time-conversion curves according to equation 2, where R_p and $[M_0]$ are respectively the rate of polymerization and the initial monomer concentration and the conversions are as determined from the curves at irradiation times t_1 and t_2 .

$$R_p/[M_0] = ([\text{conversion}]_{t_2} - [\text{conversion}]_{t_1}) / (t_2 - t_1) \quad (2)$$

Results and Discussion

The diaryliodonium salt photoinitiators selected for this study are (4-alkoxyphenyl)phenyliodonium salts **2**. These were selected for their good solubility in **1** and other epoxide monomers. Furthermore, it has been previously shown that these photoinitiators possess high quantum yields of photolysis and are extraordinarily efficient photoinitiators of both vinyl ether and epoxide cationic polymerizations (10,11). On photolysis (equation 3), diaryliodonium salts **2** undergo irreversible fragmentation to give a variety of organic products together with a protic acid, HMtX_m , derived by hydrogen abstraction reaction from the monomer or solvent (ϕ). The strong acid HMtX_m then catalyzes ring opening polymerization of the epoxide.

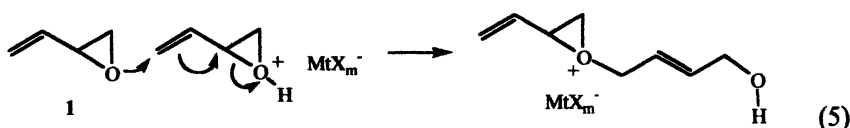
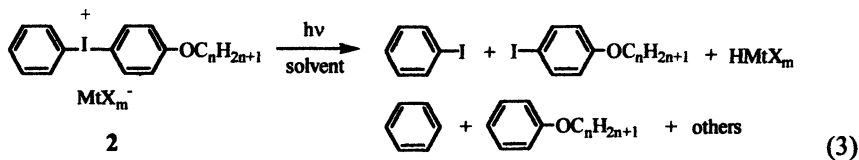


Figure 1 shows the $^1\text{H-NMR}$ spectrum of the polymer of **1** prepared by bulk cationic photopolymerization using (4-*n*-decyloxyphenyl)phenyliodonium hexafluoroantimonate (IOC10, **2** where $\text{C}_n\text{H}_{2n+1} = \text{C}_{10}\text{H}_{21}$ and $\text{MtX}_m^- = \text{SbF}_6^-$) as the photoinitiator. The $^1\text{H-NMR}$ assignments were made on the basis of model compounds (**12**) and published spectra of structurally similar polymers (**13**). The spectrum indicates that about 80% of the repeat units are derived from direct epoxide ring-opening polymerization. Equation 4 illustrates an example of such a direct epoxide ring-opening step. The spectrum also indicates the incorporated into the polymer backbone. Equation 5 illustrates an example of this mode of addition which can be rationalized as proceeding via an $\text{S}_\text{N}2'$ conjugate addition mechanism. Previous work with alcohol-initiated, acid-catalyzed polymerizations of **1** gave polymers with similar compositions (**7,8**).

The polymer formed in this polymerization was also found to be lightly crosslinked. Crosslinking took place whether the polymerization was carried out in air or nitrogen. In contrast, the alcohol-initiated, cationic polymerization of **1** with catalytic trifluoromethanesulfonic acid yields soluble, uncrosslinked polymers (**7**). Photolysis of diaryliodonium salt photoinitiators also yields free radicals that can lead to crosslinking either by hydrogen abstraction-coupling reactions or by direct addition polymerization of the pendant double bonds. The aliphatic absorbance in the $^1\text{H-NMR}$ spectrum is evidence of such crosslinking.

A brief, systematic investigation of the effects of various experimental parameters on the rate of the photoinitiated cationic polymerization of **1** was carried out. In this study we employed FT-RTIR (**14,15**) to monitor the rates of

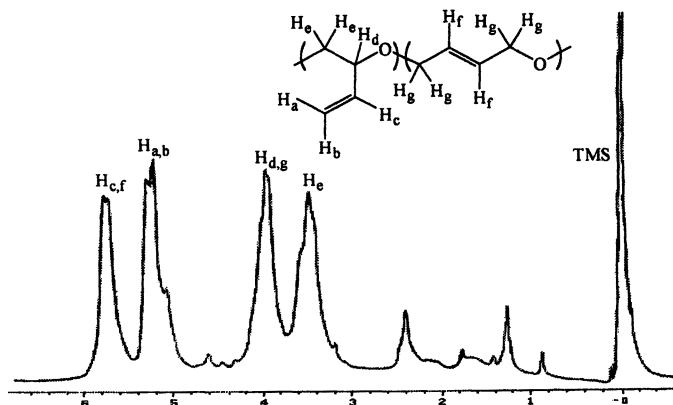


Figure 1. $^1\text{H-NMR}$ spectrum of poly(3,4-epoxy-1-butene) produced by bulk photopolymerization of 1 using 1 mol% IOC10 as photoinitiator.

the photopolymerization. We have described the technique and the configuration of our apparatus in previous publications from this laboratory (10,16). Figure 2 shows an FT-RTIR study of the polymerization of bulk 1 containing 2.0 mol% of IOC10 as photoinitiator. Depicted in this figure are two conversion versus time curves: the epoxy group at 820 cm^{-1} and the vinyl group at 1640 cm^{-1} . These results support the conclusion drawn from the $^1\text{H-NMR}$ spectrum (Figure 1) concerning crosslinking. While the conversion of the epoxy two conversion versus time curves: the epoxy group at 820 cm^{-1} and the vinyl group at 1640 cm^{-1} . These results support the conclusion drawn from the $^1\text{H-NMR}$ spectrum (Figure 1) concerning crosslinking. While the conversion of the epoxy groups is nearly quantitative, only about 30% of the vinyl groups are consumed during the course of the polymerization reaction (250 seconds irradiation).

Effect of Light Intensity

The effect of light intensity on the photopolymerization of bulk 1 containing 1.0 mol% of IOC10 as photoinitiator was investigated using FT-RTIR. The kinetic curves (Figure 3) were obtained at UV light intensities of 10 and 5 mW/cm^2 . The kinetic parameters $R_p/[M_0]$ taken from the initial slopes of these two curves are respectively, $12 \times 10^2\text{ s}^{-1}$ and $1.1 \times 10^2\text{ s}^{-1}$. A considerably faster polymerization rate was observed at the higher light intensity. These results suggest that at the lower light intensity, the rate of polymerization is light limited.

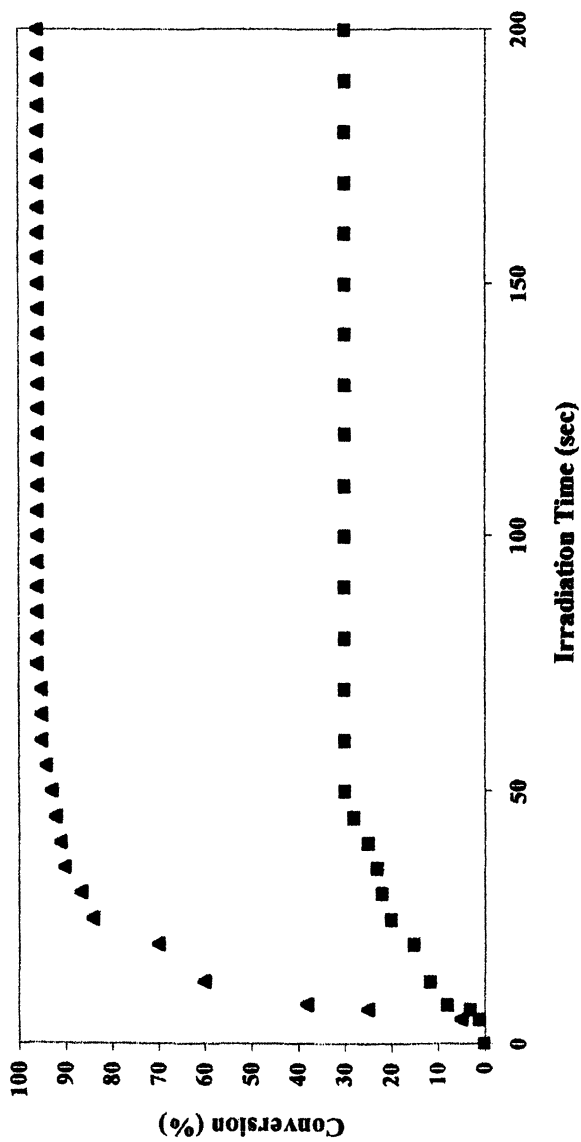


Figure 2. FT-RTIR study of the photopolymerization of 1 with 2 mol% IOC10. Epoxy groups (\blacktriangle); vinyl groups (\blacksquare). Light intensity 15 mW/cm².

Photoinitiator Concentration

The effect of the photoinitiator concentration on the rate of the cationic ring-opening polymerization of **1** was investigated at a UV light intensity of 5 mW/cm² using FT-RTIR (Figure 4). The photopolymerizations were carried out in bulk **1** containing 1.0 mol% or 2.0 mol% of IOC10. A higher polymerization rate was obtained at the higher photoinitiator concentration. Previously (17), we have observed that the maximum rate of epoxide ring-opening photopolymerization was generally achieved at a photoinitiator concentration of 2-3 mol%.

Comparison of Cationic Photoinitiators on **1** Photopolymerization

Several different diaryliodonium salts **2** were employed as cationic photoinitiators for the polymerization of **1**. In each case, the concentration of the photoinitiator was 2.0 mol% with respect to the monomer. Initially, three related hexafluoroantimonate salts were employed, with different length alkoxy groups. Using IOC8, IOC10 and IOC11 (C_nH_{2n+1} = C₈H₁₇, C₁₀H₂₁, C₁₁H₂₃ respectively), no difference in the kinetic behavior of the **1** photopolymerization was observed. However, major differences were observed when the counterion of IOC10 was varied as shown in Figure 5. As expected (18), the polymerization rate decreases according to the sequence: SbF₆⁻ > AsF₆⁻ > PF₆⁻.

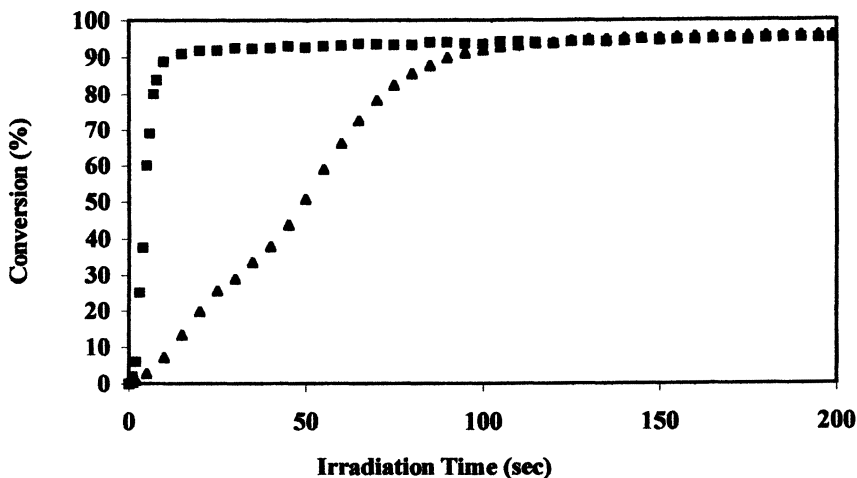


Figure 3. Study of the effect of UV light intensity on the rate of photopolymerization of **1** in the presence of 1.0 mol% IOC10: 5 mW/cm² (▲); 10 mW/cm² (■).

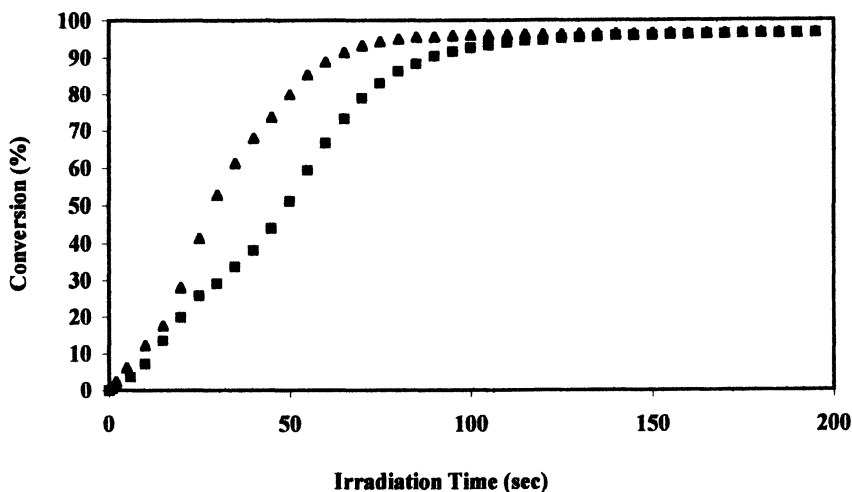


Figure 4. Study of the effect of concentration of IOC10 on the rate of photopolymerization of 1: 1.0 mol% (■); 2.0 mol% (▲). Light intensity 5 mW/cm².

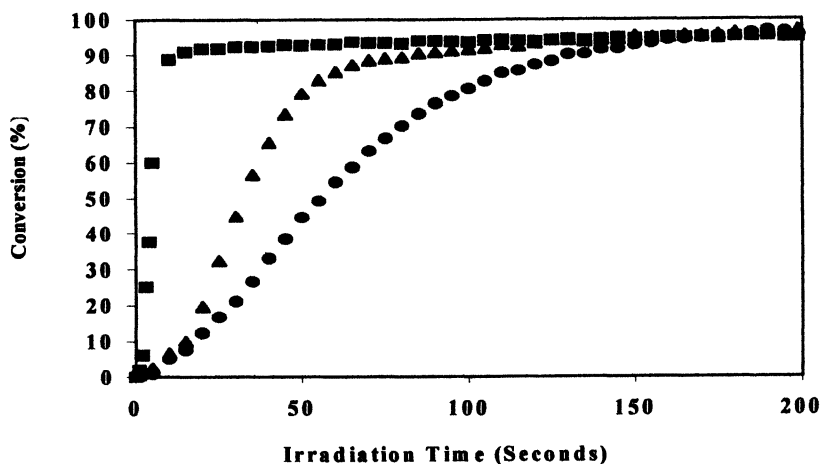


Figure 5. FT-RTIR study of the influence of (4-*n*-decyloxyphenyl)phenyl-*iodonium* counterions on the rate of 1 photopolymerization: SbF₆⁻ (■); AsF₆⁻ (▲); and PF₆⁻ (●). Light intensity 10 mW/cm².

Photopolymerization of Related Monomers

Monomer **1** is also a useful intermediate for the production of a variety of epoxide and vinyl monomers. Olefin hydrogenation of **1** (**19**) gives its saturated analog, 1,2-epoxybutane (**3**), while olefin halogenation (**20**) produces 3,4-dibromo-1,2-epoxybutane (**4**) or 3,4-dichloro-1,2-epoxybutane (**5**) (equation 6).

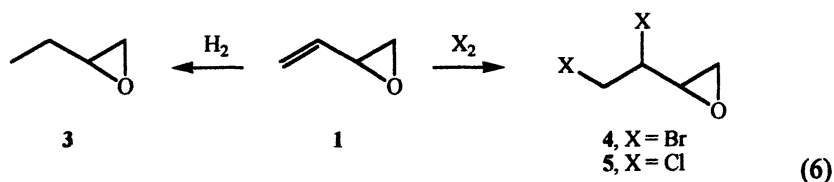
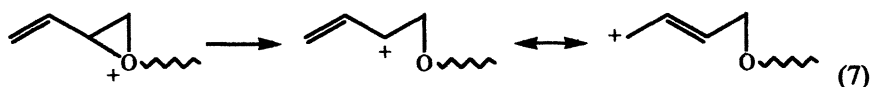


Figure 6 shows a comparison of the photopolymerizations of **1** and derivatives **3-5**. Monomer **1** exhibits considerably higher reactivity in cationic photopolymerization than its saturated analog **3**. This suggests that the neighboring vinyl group of **1** exerts an activating influence on the epoxide group. One way in which this may occur is through resonance stabilization of the propagating oxonium ion end group of the polymer chain as depicted in equation 7.



As shown in Figure 6, monomer **1** is also more reactive than its brominated and chlorinated derivatives: **4** and **5**. These monomers can be viewed as analogs of the industrially-important monomer—epichlorohydrin. Additionally, due to the high reactivity of monomer **1**, it may have utility as a reactive diluent for less reactive epoxide monomers (**21**). However the low molecular weight, volatility and toxicity of epoxide **1** may greatly limit its applications in this regard.

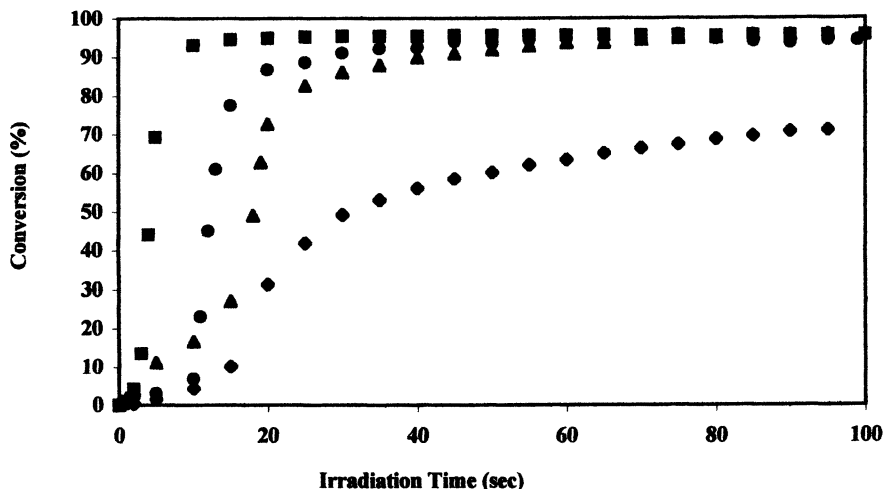


Figure 6. Comparison of the reactivity of 3,4-epoxy-1-butene (1, ■) with 1,2-epoxybutane (3, ◆); 3,4-dibromo-1,2-epoxybutane (4, ▲); and 3,4-dichloro-1,2-epoxybutane (5, ●). Light intensity 10 mW/cm², photoinitiator 2.0 mol% IOC10.

Conclusions

3,4-Epoxy-1-butene (1) is a very reactive monomer in photoinitiated cationic polymerization. Using typical diaryliodonium salt cationic photoinitiators, rapid ring-opening epoxide polymerization of 1 takes place. We have observed that the polymerization of this monomer is subject to the same experimental parameters as other epoxy monomers and that there is an optimum light intensity and photoinitiator concentration necessary to achieve the highest rate. Diaryliodonium salt photoinitiators bearing the hexafluoroantimonate anion are the most reactive for the photopolymerization of 1.

Acknowledgement

Financial support of this work was gratefully received from Eastman Chemical Company, Kingsport, Tennessee.

References

1. Denton, D.; Falling, S.; Monnier, J.; Stavinoha, Jr., J.; Watkins, W. *Chemica Oggi* May 1996, p 17.
2. Monnier, J. R. *Applied Catalysis A: General* **2001**, *221*, 73.
3. Monnier, J. R.; Muehlbauer, P. J. U.S. Patent 4,897,498, 1990.
4. Monnier, J. R.; Muehlbauer, P. J. U.S. Patent 4,950,773, 1990.
5. Stavinoha, J. L.; Tolleson, J. D. U.S. Patent 5,117,012, 1992.
6. Crivello, J. V. In *Ring-Opening Polymerization*, Brunelle, D. J., Ed., Hanser, Munich, 1993, p 157.
7. Matayabas, Jr., J. C.; Falling, S. N. U.S. Patent 5,434,314, 1995.
8. Matayabas, Jr., J. C.; Falling, S. N. U.S. Patent 5,393,867, 1995.
9. Crivello, J. V.; Lee, J. L. *J. Polym. Sci., Polym. Polym. Part A: Chem. Ed.* **1989**, *27*, 3951.
10. Rajaraman, S. K.; Mowers, W. A.; Crivello, J. V. *J. Polym. Sci., Part A: Polym., Part A: Polym. Chem. Ed.* **1999**, *37*, 4007.
11. Mowers, W. A.; Crivello, J. V.; Rajaraman, S. K. *RadTech Report*, March/April, 2000.
12. Godleski, S. A. U.S. Patent 5,189,199, 1993.
13. Wagener, K. B.; Brzezinska, K.; Bauch, C. G. *Makromol. Chem., Rapid Commun.* **1992**, *13*, 75.
14. Decker, C.; Moussa, K. *Makromol. Chem.*, **1990**, *191*, 963.

Chapter 24

Synthesis and Photoinitiated Cationic Polymerization of Fluoroalkyl Propenyl Ethers

Sang-Yeon Shim¹ and Dong Hack Suh²

¹Department of Industrial Chemistry, College of Engineering, Kangnung National University, 123 Chibyeon-dong, Kangnung, Kangwondo 210–702, Korea

²Department of Chemical Engineering, College of Engineering, Hanyang University, 17 Haengdang-dong, Seongdong-gu, Seoul 133–791, Korea

The synthesis of several novel mono- and di-propenyl ethers has been achieved in high yields by the condensation of the perfluoroalkyl alcohol with allyl bromide followed by the ruthenium-catalyzed isomerization of the corresponding allyl ethers. These fluorinated propenyl ethers undergo rapid photoinitiated cationic polymerization using a triarylsulfonium salt bearing a long alkoxy group. UV curing make these monomers highly attractive for a variety of applications.

Introduction

Photoinitiated polymerization of multifunctional monomers is one of the most effective methods for producing rapidly cured network polymers. Owing to its distinct advantages, solvent-free operation, low energy usage, and small floor space requirements, this technology has found a large number of industrial

applications, inks, coatings, and adhesives.ⁱ Photoinduced cationic polymerization has the advantage that it is not inhibited by oxygen and a wide variety of different monomers can be used compare with a radical system. Many different types of mono-, di-, and multifunctional vinyl and propenyl ether monomers have been reported in photoinduced cationic polymerization on the use of onium salt photoinitiators such as diaryliodonium and triarylsulfonium salts.^{ii,iii} While fluorinated polymers have much attention due to their high thermal stability, excellent chemical resistance, low dielectric constant and refractive index.^{iv} Many fluorinated polymers have been reported, but the major products are prepared by radical polymerization of a few fluorinated acryl monomers.^v In this article, we report the syntheses of a new series of mono- and difunctional fluorinated propenyl ether monomers and determine the relative order of reactivity in photoinitiated cationic polymerization.

Experimental

General. All reagents were used as purchased from the Aldrich Chemical Co. without additional purification.; Allyl bromide, 2,2,3,3,3-pentafluoro-1-propanol, 2,2,3,3,4,4-hexafluoro-1,5-pentanediol, 2,2,3,3,4,4,5,5-octafluoro-1,6-hexanediol, 2,2,3,3,4,4,5,5,6,6,7,7,8,8,9,9-hexadecafluoro-1,10-decanediol, sodium hydroxide, diethyl ether, and tris(triphenylphosphine)ruthenium(II) dichloride. The photoinitiator (4-*n*-decyloxyphenyl)diphenylsulfonium triflate was prepared as described previously.^{vi} ¹H-NMR data were recorded with a Jeol Lamda 300 spectrometer using CDCl₃ as a solvent. Routine infrared spectra were obtained using a Jasco Corp. Model 460 Fourier transform infrared spectrometer.

Preparation of 2,2,3,3,3-Pentafluoropropyl Allyl Ether [PAE].

Into a 50 ml round-bottom flask fitted with a magnetic stirrer, a reflux condenser, and a nitrogen inlet were placed 2,2,3,3,3-pentafluoro propanol (5 g, 0.033 mol), allyl bromide (4.83 g, 0.040 mol), tetra-*n*-butylammonium bromide (0.32 g, 0.001 mol), NaOH (1.6 g, 0.040 mol), and ether (10 mL). The reaction mixture was heated at 50°C, overnight and then poured onto water (30mL), the mixture was extracted with ether (3x30 mL), and the organic layer was dried over sodium sulfate. The solution was purified by fractional distillation to afford the pure compound (4.5 g, 71 %). Bp : 78–80 °C.

Preparation of 2,2,3,3,4,4-Hexafluoropentyl Diallyl Ether [HDE]. A solution of 2,2,3,3,4,4-hexafluoro pentanediol (3 g, 0.014 mol), allyl bromide (8.55 g, 0.071 mol), tetra-*n*-butylammonium bromide (0.27 g, 0.85 mmol), NaOH (1.7 g, 0.042 mol), and ether (10 mL) was heated at 50°C overnight. The solution was poured onto water, extracted with ether, and dried over sodium sulfate. After filtration, the solvent was evaporated and concentrated in a vacuum to give the pure product (4.1 g, 99%).

Preparation of 2,2,3,3,4,4,5,5-Octafluorohexyl Diallyl Ether [ODE].

A solution of 2,2,3,3,4,4,5,5-octafluoro hexanediol (3 g, 0.011 mol), allyl bromide (6.92 g, 0.057 mol), tetra-*n*-butylammonium bromide (0.22 g, 0.69 mmol), NaOH (1.4 g, 0.034 mol), and ether (10 mL) was heated at 50°C overnight. The solution was poured onto water, extracted with ether, and dried over sodium sulfate. After filtration, the solvent was evaporated and concentrated in a vacuum to give the pure product (3.9 g, 99%).

Preparation of 2,2,3,3,4,4,5,5,6,6,7,7,8,8,9,9-Hexadecafluorodecyl Diallyl Ether [HDDE]. A solution of 2,2,3,3,4,4,5,5,6,6,7,7,8,8,9,9-hexadecafluoro decanediol (3 g, 6.49 mmol), allyl bromide (3.93 g, 0.032 mol), tetra-*n*-butylammonium bromide (0.13 g, 0.39 mmol), NaOH (0.78 g, 0.019 mol), and ether (10 mL) was heated at 50°C overnight. The solution was poured onto water, extracted with ether, and dried over sodium sulfate. After filtration, the solvent was evaporated and concentrated in vacuum to give the pure product (2.9 g, 95%).

Preparation of 2,2,3,3,3-Pentafluoropropyl Propenyl Ether [PPE].

Into a 50 mL round-bottom flask fitted with a magnetic stirrer, a reflux condenser, and a nitrogen inlet were placed 2,2,3,3,3-pentafluoropropyl allyl ether (2.5 g, 0.013 mol), tris(triphenylphosphine) ruthenium(II) dichloride (13 mg, 0.013 mmol). The reaction mixture was heated at 90°C overnight. The mixture was filtered through a column of silica gel to give the pure product (1.47 g, 59%).

Preparation of 2,2,3,3,4,4-Hexafluoropentyl Dipropenyl Ether [HDPE]. A solution of 2,2,3,3,4,4-hexafluoropentyl diallyl ether (4.1 g, 0.014 mol) and tris(triphenyl phosphine)ruthenium(II) dichloride (27 mg, 0.028 mmol) was heated at 140°C overnight. The residue was diluted with ether (20 mL) and filtered through a column of silica gel to give the pure product (3.82 g, 93%).

Preparation of 2,2,3,3,4,4,5,5-Octafluorohexyl Dipropenyl Ether [ODPE]. A solution of 2,2,3,3,4,4,5,5-octafluorohexyl diallyl ether (3.9 g, 0.011 mol) and tris(triphenyl phosphine)ruthenium(II) dichloride (22 mg, 0.022 mmol) was heated at 150°C overnight. The residue was diluted with ether (20 mL) and filtered through a column of silica gel to give the pure product (3.57 g, 92%).

Preparation of 2,2,3,3,4,4,5,5,6,6,7,7,8,8,9,9-Hexadecafluorodecyl Dipropenyl Ether [HDDPE]. A solution of 2,2,3,3,4,4,5,5,6,6,7,7,8,8,9,9-hexadecafluorodecyl diallyl ether (2.9 g, 0.005 mol) and tris(triphenylphosphine)ruthenium(II) dichloride (10 mg, 0.011 mmol) was heated at 160°C overnight. The residue was diluted with ether (20 mL) and filtered through a column of silica gel to give the pure product (2.58 g, 89%).

The Photopolymerization and Fourier Transform Real-Time Infrared (FT-RTIR) Measurements: Photoinitiated cationic polymerizations were studied by real-time infrared spectroscopy using the method described by Decker.^{vii} Samples were prepared by placing liquid monomers with 0.3 - 0.7

mol % (4-n-decyloxyphenyl)diphenylsulfonium triflate between two 14 μm polyethylene films and then mounting the sandwich in 5 x 5 cm slide frames. The RTIR measurements were performed on a Jasco Corp. Model 460 Fourier transform infrared spectrometer equipped with a Spectral Energy Co. LPS251SR 200W Hg-Xe lamp. All studies were conducted using a broad band and unfiltered UV light at an intensity of 15 mJ/cm^2 min. Light intensity measurements were made with an International Light Co. Model L290 Radiometer. The progress of polymerizations was quantitatively evaluated by monitoring the decrease of the double bond absorption band in the range of 1650 - 1700 cm^{-1} (1-propenyl ether).

Results and Discussion

Synthesis of Mono- and Dipropenyl Ether Monomers. Figure 1 shows the synthesis of fluorinated propenyl ethers. Allyl ether precursors were first synthesized in high yields by the condensation of alcohols with allyl bromide in the presence of NaOH and tetra-*n*-butylammonium bromide in diethyl ether at 50 $^{\circ}\text{C}$. Then, isomerization of allyl ether to the corresponding propenyl ether groups was carried out using tris(triphenylphosphine)ruthenium(II) dichloride as a catalyst.

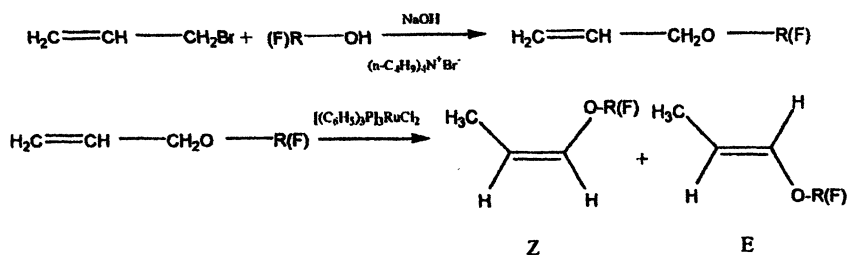


Figure 1. Synthetic scheme of propenyl ether monomers

All the propenyl ethers described above were characterized by $^1\text{H-NMR}$. Typical $^1\text{H-NMR}$ spectra are shown in Figure 2. The peaks at 4.5 - 6.5 ppm are assigned to the protons of the propenyl ether double bonds in the spectrum, and the E : Z ratio in the isomeric mixture was 40 : 60.

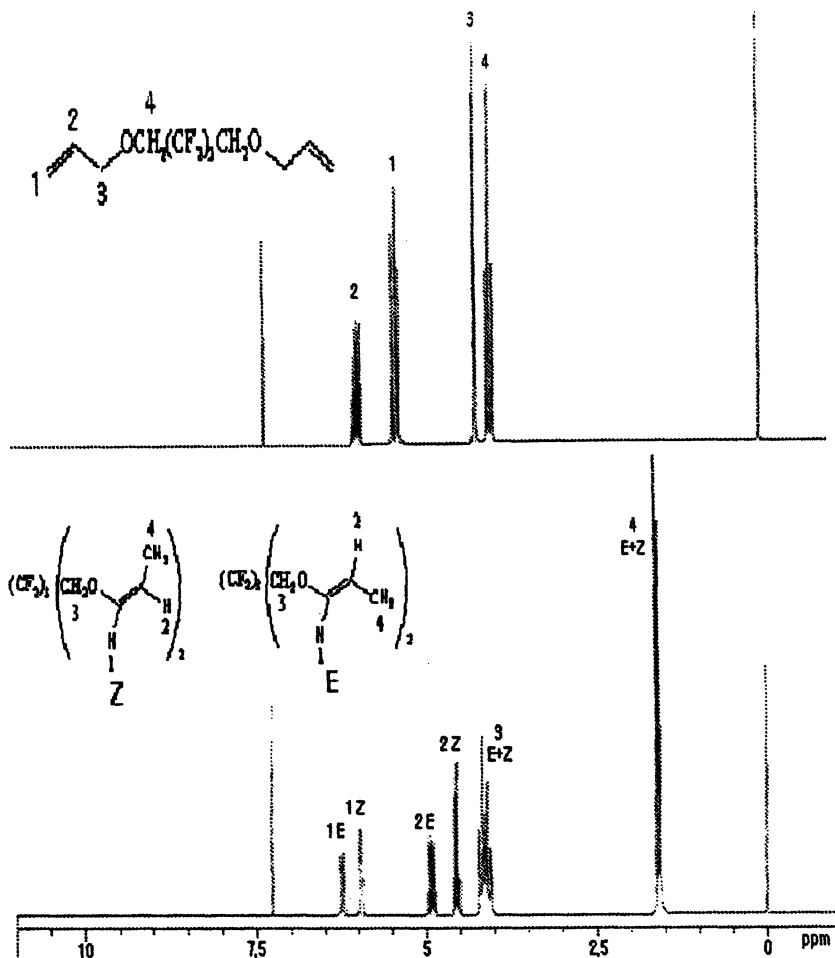


Figure 2. ¹H-NMR spectra (A) before and (B) after the isomerization of 2,2,3,3,4,4-hexafluoropentyl dipropenyl ether.

Photopolymerization Studies. Photopolymerization of mono- and dipropenyl ether monomers was undertaken using the cationic photoinitiator, (4-n-decyloxyphenyl)diphenylsulfonium triflate [DDST], at concentration of 0.3–0.7 mol % to the monomers. Owing to a long alkoxy group, this photoinitiator was quite soluble in all the monomers prepared and showed the high efficiency in cationic polymerization. Figure 3 presents a RTIR study of the cationic photopolymerization of a monomer [HDDPE]. As the Figure shows, the rate of polymerization and conversions to polymer for monomer [HDDPE] are increased slightly as the increase in concentration of the photoinitiator. Figure 4

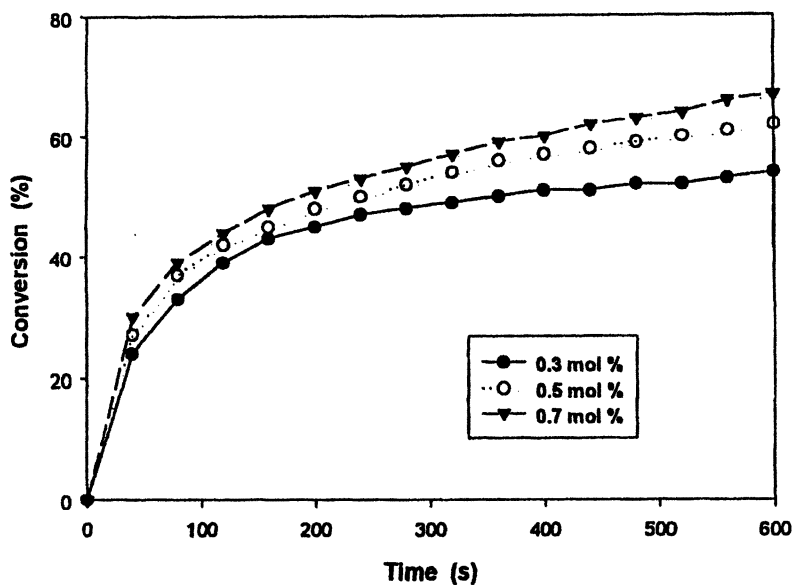


Figure 3. RTIR curves for the cationic polymerization of HDDPE in the presence of 0.3 (●), 0.5 (○), and 0.7 (▼) mol % DDST.

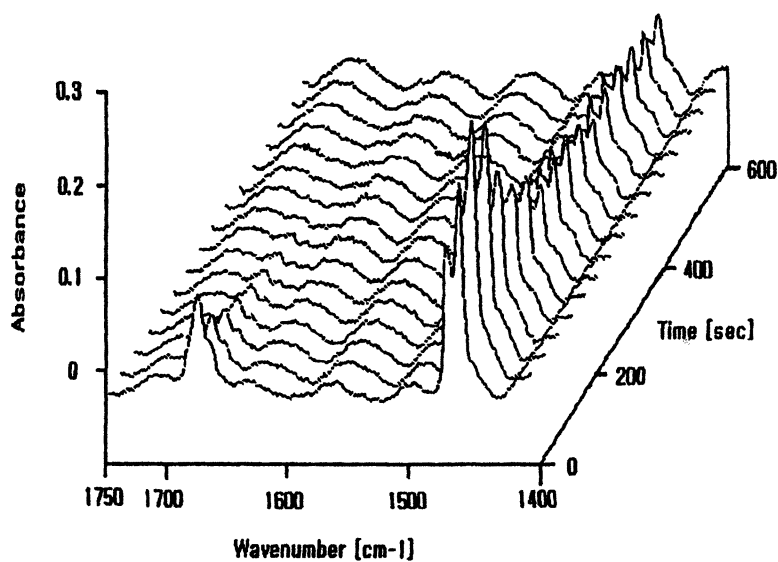


Figure 4. FTIR study of the cationic polymerization of PPE

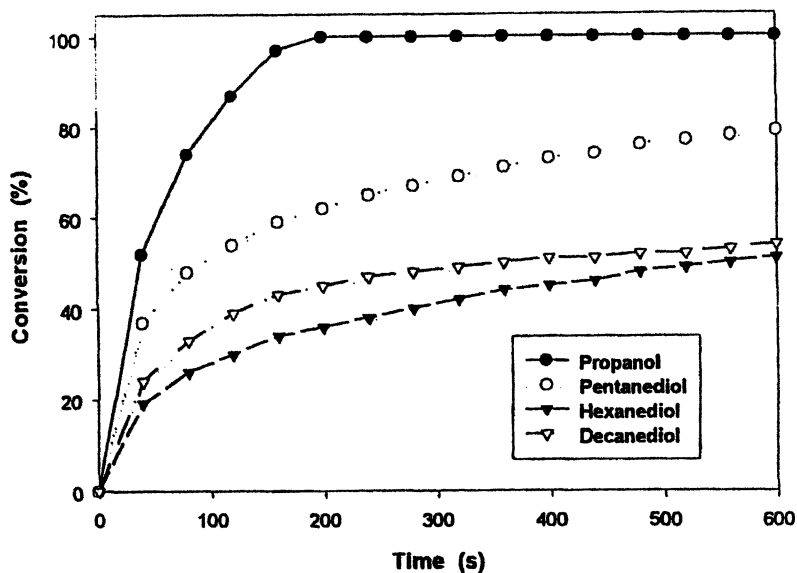


Figure 5. FT-RTIR study of the cationic photopolymerization of monomers in the presence of 0.3 mol % DDST. ●, PPE; ○, HDPE; ▼, ODPE; ▽, HDDPE.

depicts a three-dimensional spectral profile of decrease in the propenyl ether (1680 cm^{-1}) of a monomer [PPE] in the presence of 0.3 mol % DDST. This Figure shows a rapid decrease in the propenyl ether band, indicating that this monomer is highly reactive toward cationic polymerization. In Figure 5, the RTIR curves for the polymerizations of mono- and difunctional propenyl ether monomers show that the reactivities of all these monomers are similar, judged by the initial slopes of the conversion versus time.

Conclusions.

A new series of mono- and difunctional propenyl ethers was prepared in high yields by straightforward methods using mono- and difunctional fluorinated alcohols as starting materials. These monomers exhibit high reactivity in cationic photopolymerization in the presence of a triarylsulfonium salt bearing a long alkoxy group which enhance its solubility in these monomers.

References

- (i) Decker, C.; Moussa, K. J. *Coating Tech.* 1993, 65(819), 49.
- (ii) Crivello, J. V.; Jo, K. D. *J. Polym. Sci., Poly. Chem.* 1993, 31, 1473.
- (iii) Crivello, J. V.; Liu, S. *Chem. Mater.* 1998, 10, 3724.
- (iv) Feiring, A. E. *J. Macromol. Sci.- pure appl. Chem.* 1994, A31(11), 1657.
- (v) Takezawa, Y.; Tanno, S.; Taketani, N.; Ohara S.; Asano, H. J. *Appl. Poly. Sci.* 1991, 42, 3195.
- (vi) Crivello, J. V.; Lee, J. L. *J. Polym. Sci., Poly. Chem.* 1989, 27, 3951.
- (vii) Decker, C. J. *polym. Sci., Poly. Chem.* 1992, 30, 913.

Chapter 25

Cationic Photopolymerization of 2-Phenyloxetanes

Hisao Kato and Hiroshi Sasaki*

Corporate Research Lab, Toagosei Company Ltd., 1-1 Funami-cho,
Minato-ku, Nagoya-shi, Aichi, Japan 455-0027

In cationic polymerization, the polymerizability of oxetanes are known to be high, while the initiation is rather slow, which can be explained by the high-energy barrier for the first ring opening. Due to the stabilizing effect of benzyl groups, the introduction of a phenyl group into the 2-position of the oxetane ring might enhance the stability of intermediate in the initiation. Based on this idea, the reactivity of 2-phenyl-oxetanes (2-phenyl-3, 3-dimethyl-oxetane (HPO) and 2-(4-methoxyphenyl)-3, 3-dimethyl-oxetane (MPO)) was studied using photo-DSC techniques. MPO, possessing an electron donating p-methoxyphenyl group, exhibited faster initiation and higher reactivity compared with 3-ethyl-3-phenoxy-methyloxetane (POX) with no substituent on the ring. MPO was also proved to serve as good accelerator in copolymerizations with other oxetane monomers. Computational calculations also indicated the higher reactivity of MPO.

Introduction

Cationic photopolymerization based on the photogeneration of acid from onium salts induced by UV light and consecutive cationic polymerization initiated by the generated acid was first proposed in 1970's (1). Since then, photocurable materials, using cationically polymerizable monomers such as epoxides and vinyl ether derivatives, have been widely investigated (2). Among these, epoxides are known to give cured coatings with high thermal capability, excellent adhesion and good chemical resistance, however, the curing speed of commercially available epoxides, such as glycidyl ether derivatives, are rather slow. This low reactivity of epoxides has proved to be a considerable drawback to their use in some industrial applications (3). Thus, it is desirable to develop novel monomers that have the same performance capabilities as epoxides, while at the same time possess higher reactivity.

Three major factors, basicity, the ring strain and steric hindrance, contribute to the reactivity of cyclic ethers in the cationic ring-opening polymerization (4). Oxetane, a four membered cyclic ether, possesses rather high ring strain energy (107 kJ/mol) and basicity ($\text{pK}_a = 2.02$) (5). These properties of the oxetane ring should make oxetanes more reactive than epoxides. Previously, the cationic photopolymerization of oxetanes was investigated and these monomers were found to possess quite different polymerization characteristics than epoxides (6). Although the initiation of oxetane polymerization was rather slow, polymerization proceeded smoothly until high conversion of monomer and gave high molecular weight polymer. The slow rate of initiation of oxetanes was explained by the high-energy barrier for the ring opening of the protonated oxetane and high polymerizability results from the high nucleophilicity of oxygen on the ring (6).

It was our interest to investigate a cyclic ether monomer possessing high nucleophilicity as oxetanes and the low energy barrier for the first ring opening as well, which should exhibit fast initiation and high polymerizability. Due to the stabilizing effects of benzyl type structures, it was proposed that the introduction of a phenyl group on the 2-position of an oxetane ring might enhance the stability of the cationic intermediate in the initiating reaction and contribute to a reduction of the energy barrier, while maintaining the high basicity at the oxygen.

In this paper, based on this idea, the reactivity of 2-phenyl-3, 3-dimethyl-oxetane (HPO) and 2-(4-methoxyphenyl)-3, 3-dimethyl-oxetane (MPO) in the cationic photopolymerization in homopolymerization and copolymerization with oxetanes having no substituent (POX and DOX) were studied using photo-DSC measurements.

Experimental

Materials and procedures including experimental conditions and computational calculations used in this study are listed below.

Materials.

Oxetane monomers, 3-ethyl-3-phenoxyethyl-oxetane (POX) and bis-[1-ethyl(3-oxetanyl)-methyl] ether (DOX), are available from Toagosei Co. Ltd. (Scheme 1). The sulfonium salt cationic photoinitiator possessing hexafluoro phosphate as the counteranion (UVI-6990: PI-1) used in the formulation was obtained from Union Carbide Co. All other starting materials and solvents were reagent quality and were used as received. Diphenyl-4-thiophenoxyphenyl sulfonium hexafluoro antimonate (PI-2) was prepared using the procedure of Crivello (7). 2-Phenyl-oxetanes, HPO and MPO, were synthesized from isobutyraldehyde and benzaldehyde derivatives according to the previously reported method (8). All the oxetane monomers were distilled over calcium hydride just before use.

Photo-DSC measurements.

The formulations were prepared by mixing the monomers with 1 wt% of PI-1 or PI-2 in an amber vial at 40°C. The heat of polymerization during photocationic polymerizations was measured using a differential scanning calorimeter (DSC220C: Seiko Instruments Inc.) equipped with UV-1 lighting unit (200 W Hg-Xe lamp, Seiko Instruments Inc.). 2 to 3 mg of samples were applied to aluminum pan and irradiated UV light under dry air atmosphere at 40°C. The light intensity was adjusted to 3, 11 or 20 mW/cm² at 365 nm using ND filter.

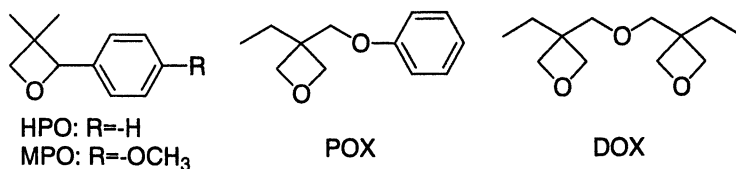
Photopolymerization.

The photopolymerization was carried out under the same conditions as noted above using 20mW/cm² of light intensity. The irradiation time was 2 minutes for full conversion of monomers and the total irradiated energy was 2.4 J/cm². After irradiation, the resulting polymer was dissolved in THF containing small amount of ammonium hydroxide (to neutralize remaining acid) and precipitated from excess amount of methanol. The molecular weight distribution was measured using gel permeation chromatography in THF at 40°C on a TOSOH S8010 GPC system equipped with five polystyrene gel columns (TSK

Gel G-7000HXL, 5000HXL, 4000HXL, MHXL (2 columns)) and a refractive index detector. Glass transition temperature (T_g) was measured using DSC at heating rate of $10^\circ\text{C}/\text{min}$.

Computational Technique.

The *ab initio* theoretical molecular orbital method (RHF/3-21G), which is implemented in the SPARTAN program, was used (9). SPARTAN also served as a graphic user interface to model the structures to run the calculation and to analyze the results. The conformational potential energy surfaces were searched to determine the global energy minimum conformers. The intrinsic reaction coordinate calculations were done to correlate the transition states with the corresponding energy minima.



Scheme 1. Monomers used in this study

Results and Discussion

The photopolymerization results for HPO and MPO containing 1 wt% of onium salt (PI-2: hexafluoro antimonate as counteranion) were summarized in Table I. $^1\text{H-NMR}$ spectra for MPO and its polymer (p-MPO) are shown in Figure 1. The characteristic peaks for the oxetane ring (4.2 and 4.3 ppm for methylene protons and 5.6 ppm for methyne proton on oxetane ring) completely vanished in the spectrum of p-HPO. Under the same conditions, the photopolymerization of MPO, possessing a methoxy group in the para position of the phenyl ring, gave a higher yield. The number average molecular weight (M_n) of the polymers was rather low compared with that for the oxetanes having no substituent on the ring. The T_g for p-MPO was slightly higher than that of p-HPO.

Table I. Photo-Polymerization of HPO and MPO

Monomer	Yield (%)	$M_n^{1)}$	$M_w/M_n^{1)}$	$T_g^{2)}$
HPO	51.5	6450	2.15	72.3
MPO	80.2	7900	2.04	88.8

1) Measured by GPC

2) Measured by DSC

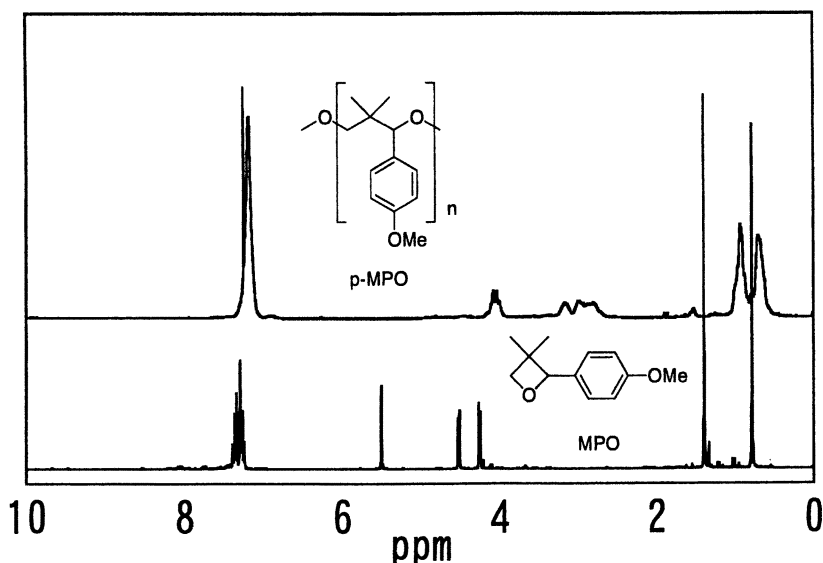
*Figure 1. $^1\text{H-NMR}$ spectrums for MPO and its p-MPO.*

Photo-DSC, which measures the heat of photo-polymerization directly, is an excellent method for the evaluation of monomer reactivity. The heat of polymerization of MPO, PHO and POX with 1 wt% of PI-2 with light intensity of 3 or 20 mW/cm^2 are shown in Figure 2 and 3.

Under both irradiation conditions, quicker generation of the heat, indicating fast initiation, and a sharper exothermal curve, which represents fast propagation, were observed for the cationic photopolymerization of MPO compared with those for POX. On the other hand, a smaller heat generation with a longer induction period was detected for HPO. As the steric conditions around the carbon adjacent to the oxygen atom on the oxetane ring for MPO and HPO should be almost the same, the big difference in the reactivity cannot be explained by steric repulsion during the $\text{S}_{\text{N}}2$ reaction.

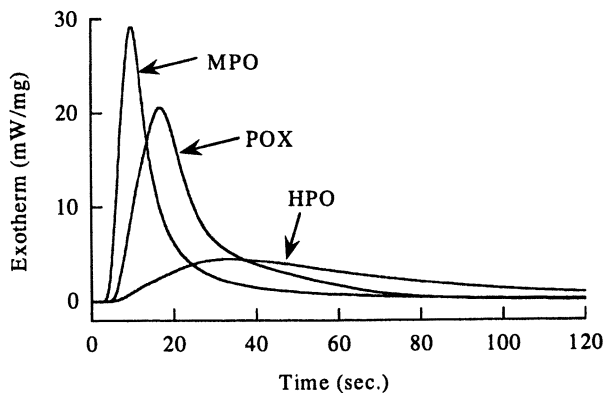


Figure 2. Photo-DSC for HPO, MPO and POX ($I=3 \text{ mW/cm}^2$ at 365 nm) with 1wt% of PI-2

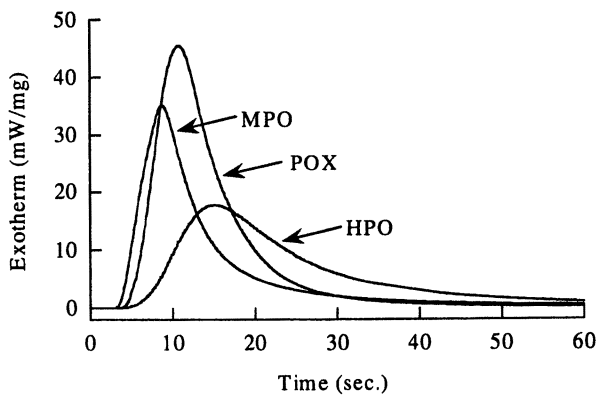


Figure 3. Photo-DSC for HPO, MPO and POX ($I=20 \text{ mW/cm}^2$ at 365nm) with 1wt% of PI-2

To investigate the difference in the reactivity of the two monomers, ring-opening reaction of the protonated monomers in a unimolecular reaction (S_N1) and bimolecular reaction attacked by neutral oxetane (S_N2) were calculated using an *ab initio* theoretical molecular orbital method. The reaction diagrams are exhibited in Figures 4 and 5.

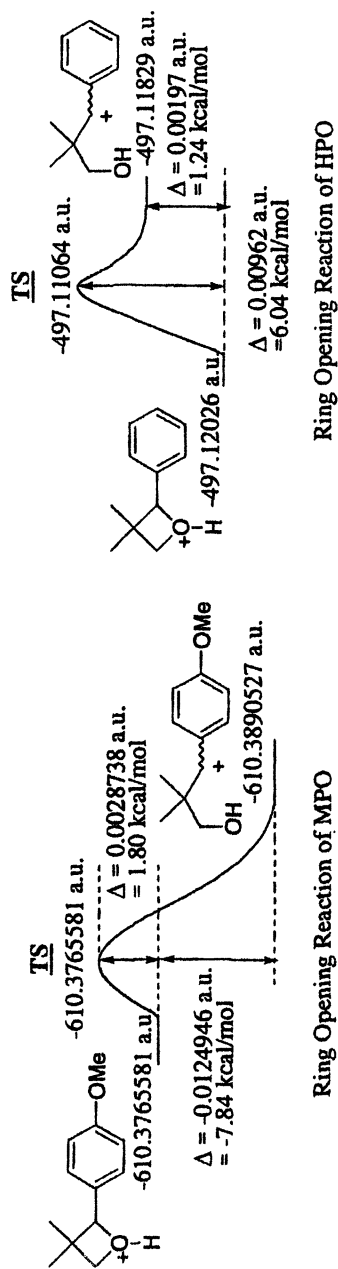


Figure 4. Reaction diagrams of ring-opening reaction of protonated HPO and MPO through a S_N1 reaction

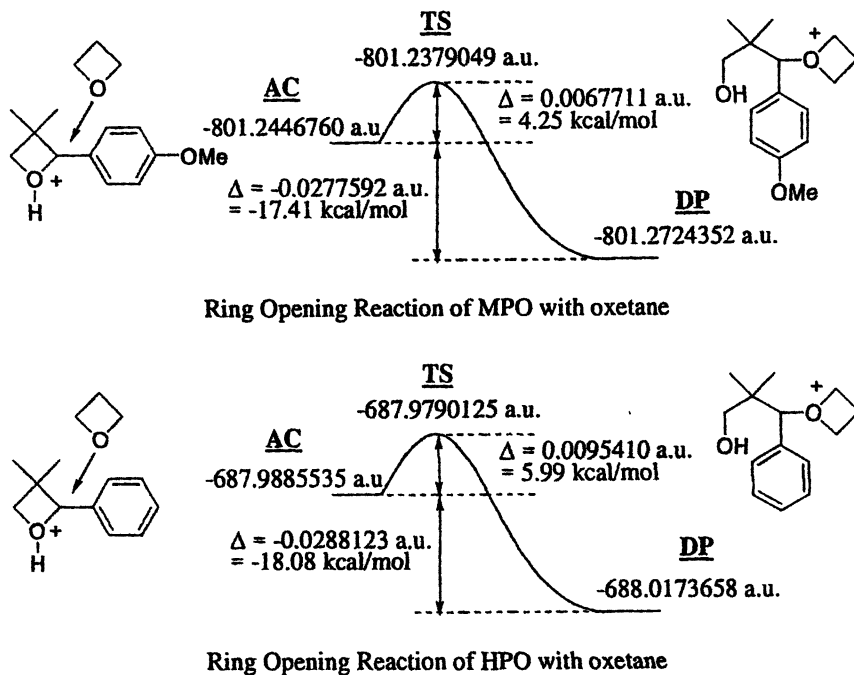


Figure 5. Reaction diagram for the ring-opening reaction of protonated HPO and MPO with oxetane by a S_N2 reaction

Figure 4 shows the reaction diagrams for ring-opening of the protonated monomers by a S_N1 reaction. The formation of carbenium ion for MPO results in the stabilization of the system (by 7.84 kcal/mol), while ring opening of HPO results in the destabilization (by 1.24 kcal/mol). Moreover, the calculated energy barrier for MPO (1.80 kcal/mol) is less than one third of that for HPO (6.04 kcal/mol). These results show that the unimolecular ring opening (S_N1 reaction) of protonated HPO seems difficult both thermodynamically and kinetically.

The energetics of the ring-opening reactions of the protonated monomers and with neutral oxetane by a S_N2 reaction were also calculated (Figure 5). The calculated energy barrier for MPO was slightly lower than that for HPO, which implies that the ring opening of MPO attacked by neutral oxetane seems to occur easily.

Although the detailed mechanism of polymerization of 2-phenyloxetanes are still unclear, the higher reactivity of MPO can be explained by the faster ring-opening reaction during the initiation stage, as indicated by the results of the calculations.

Using the commercially available photoinitiator (PI-1) with a hexafluoro phosphate counteranion, the heat of polymerization of monomers MPO, POX and their formulations with light intensity of 11 mW/cm^2 were measured and the results shown in Figure 6.

Using PI-1, the heat flow for POX during polymerization changed rather slowly, while there was little difference for MPO. With the addition of 10 or 20 wt% of MPO to POX, the exothermic curves were sharper and unimodal. If the polymerization of MPO and POX proceeded separately, the exothermal curve should be bimodal. These unimodal curves indicate that the polymerization of these two monomers underwent co-polymerization and the sharper curves exhibit an accelerated polymerization of the oxetane ring in POX. These acceleration phenomena are likely the result of the fast initiation rate of MPO.

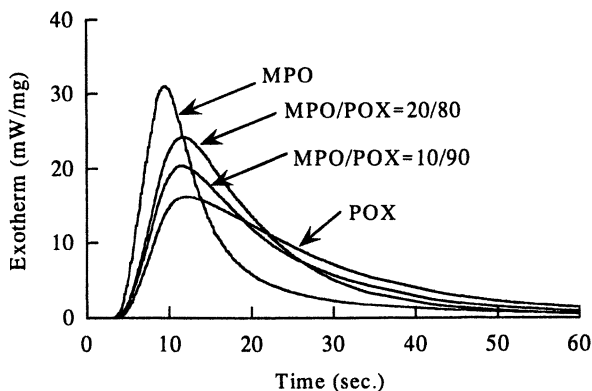


Figure 6. Photo-DSCs for MPO, POX and their formulations (MPO=10 or 20 wt%) with light intensity of 11 mW/cm^2 with 1 wt% of PI-1

The GPC curves of the polymers obtained from above mentioned photo-polymerizations without precipitation are exhibited in Figure 7. The addition of MPO made the molecular weight lower. In the formulated system, the number of active species could be higher due to the fast initiation of MPO. The lower molecular weight of the formulation can be explained by this higher content of active species in the early stages of the polymerization.

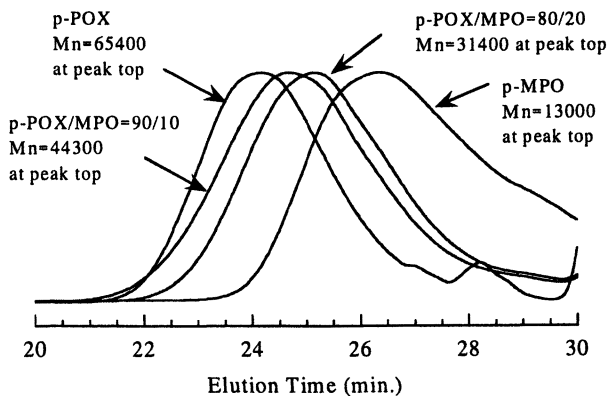


Figure 7. GPC elution curves for polymers of MPO, POX and their formulations photopolymerized under the same conditions as Figure 6.

The heat of polymerization of monomers MPO, DOX and their formulations with 1wt% of PI-1 are shown in Figure 8. Homopolymerization of DOX resulted in a slower polymerization, which is explained by its low mobility. In the same formulation with monofunctional POX, the polymerization of di-functional DOX was also accelerated.

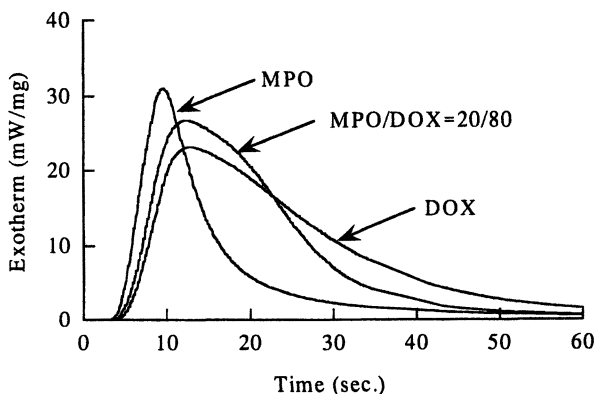


Figure 8. Photo-DSCs for MPO, DOX and their formulation (MPO=20 wt%) with light intensity of 11 mW/cm² with 1wt% of PI-1

Conclusions

The reactivity of 2-phenyloxetanes (MPO and HPO) in the photocationic homo- and copolymerizations with oxetanes were studied using photo-DSC measurements. The photoinitiated cationic polymerization of MPO exhibited a faster initiation and a higher reactivity as compared with POX, having no substituent on the ring. In contrast, HPO resulted in a slow initiation and a low reactivity. The reasons for the difference in the reactivity of the above two monomers were investigated by computational calculations of the energetics of the ring-opening reactions of the protonated monomers. While there were small differences in the energies of bimolecular mechanism in which the protonated monomers were attacked by neutral oxetane, the unimolecular ring opening of MPO was reasonably possible. The higher reactivity of MPO can be explained by a faster ring-opening reaction during the initiation stage. MPO was also shown to work as a good accelerator in the formulation with other oxetane monomers.

References

1. Crivello, J.V.; Lam, J.H.W., *J. Polym. Sci. Polym.: Chem. Ed.*, **1978**, 16, 2441
2. Crivello, J.V.; Lee, J.L.; Conlon, D.A., *J. Radat. Curing*, **1983**, 10(1), 6
3. Sitek, F., *Radcure Europe '87*, **1987**, 274
4. Penczek, S.; Kubisa, P.; Matyjaszewski, K., *Adv. in Polym. Sci.*, **1980**, 37, 5
5. Pell, A.S.; Pilcher, G., *Trans Faraday Soc.*, **1965**, 61, 71
6. Sasaki, H.; Rudzinski, J.M.; Kakuchi, T., *J. Polym. Sci.: Part A*, **1995**, 33, 1807
7. Akhtar, S.R.; Crivello, J.V.; Lee, J.L., *J. Org. Chem.*, **1990**, 55(13), 4222
8. Xianming, H.; Kellogg, R.M., *Synt.* **1995**, 533
9. SPARTAN 4.0, Wavefunction Inc.

Chapter 26

Photocurable Pressure-Sensitive Adhesives Using Alkyl Oxetane

Hiroshi Sasaki

Corporate Research Lab, Toagosei Company Ltd., 1-1 Funami-cho,
Minato-ku, Nagoya-shi, Aichi 455-0027, Japan

As cationically photopolymerizable monomers, oxetanes have been shown to possess many good properties, such as safety (AMES Test negative) and high reactivity. In addition to these properties, alkyl oxetanes, having alkyl side chains, exhibited high compatibility with other monomers and very low viscosities. Using 3-ethyl-3-(2-ethylhexyloxy)methyl oxetane (EHOX), Photocurable PSA formulations in combination with epoxy monomers and a hydrogenated petroleum resin as a tackifier were investigated. The adhesion properties of the cured PSA sheets were evaluated and correlated with the results of viscoelastic measurements. With the aid of EHOX, uniform and clear PSA formulations with low viscosity and high reactivity were achieved. The cured PSA sheets were shown to possess good adhesive properties. Substitution of EHOX with a aliphatic mono-epoxide (UVR-6216) resulted in poorly reactive formulations and poor performance as cured PSA sheets. With aid of a cycloaliphatic diepoxide (UVR-6110), the heat resistance properties of the cured PSA sheets were drastically improved.

Introduction

Pressure sensitive adhesives (PSAs) are widely used not only in industrial applications but also in daily life, such as packaging, tapes, labels and so on, because of their excellent characteristics - easy to stick to many kind of substrates without any activation and easy to peel. Among the many types of PSAs, solvent- or water-borne systems are most popular. With increased environmental pressures, replacement of solvent-borne systems is becoming gradually more important and solvent-free systems are highly desired.

To achieve a solvent-free system, UV-curable PSAs have been proposed as environmental-friendly technologies. UV-curable acrylic monomer systems, that polymerize through radical polymerization has been mainly evaluated (1). As oxygen is known to inhibit the radical polymerization, nitrogen atmosphere or lamination should be applied to complete the radical polymerization of acrylic monomers. At the same time, the residual unreacted monomers are known to cause an odor problem and skin irritation (2). To solve this problem with acrylic radical systems, photoinitiated cationic polymerization systems have been introduced. For example, a cationically curable PSA formulation consisting of a rather low molecular weight heterotelechelic-polymer and a tackifier was introduced (3). Although the UV-cured PSA sheet of this formulation was reported to possess good adhesive properties, some problems seem to remain. The viscosity of the formulation is rather high and temperatures greater than 80°C are required when applying the coating to substrates. The formulation range is also narrow due to the low compatibility of the polymers used. These problems could be a barrier to the industrial applications of this system.

Oxetanes have been shown to possess many good properties, such as safety (AMES Test negative) and high reactivity (4). In addition to these properties, alkyl oxetanes, having alkyl side chains, exhibit high compatibility with other monomers and very low viscosity. Using alkyl oxetanes, low viscosity and highly reactive UV-curable PSA formulation seem to be possible.

In this paper, UV-curable PSA formulations using 3-ethyl-3-(2-ethylhexyloxy)methyl oxetane (EHOX) in combination with the monomers listed on Scheme 1 were investigated and the adhesive properties of the cured PSA sheets correlated with their viscoelastic character.

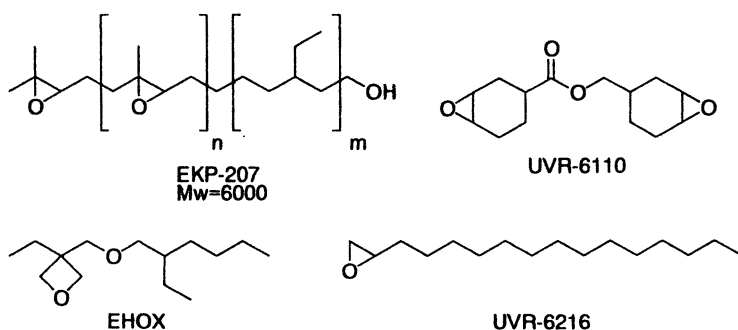
Experimental

Materials and experimental conditions used in this study are listed below.

Materials.

All materials listed below were used as received. Monomers used in this study were shown in Scheme 1.

- EHOX: 3-Ethyl-3-(2-ethylhexyloxymethyl)oxetane from Toagosei Co. Ltd.
- UVR-6216: 1,2-Epoxy-hexadecane from Union Carbide Co.
- EKP-207: Heterotelechelic linear polymer from KRATON Polymers.
- UVR-6110: Cycloaliphatic diepoxide from Union Carbide Co.
- Rhodosil 2074: Iodonium salt cationic photoinitiator from Rhodia Co.
- P-90: Hydrogenated petroleum (C-5) resin (softening point is 90°C) from Arakawa Chemical Ind.



Scheme 1. Monomers used in this study

Sample Formulations.

The PSA formulation was prepared by mixing monomers, photoinitiator, and tackifier in the desired composition at 40°C. The viscosity of formulations was measured by Brookfield viscometer at 25°C.

Photo-DSC measurement.

Heat of polymerization during cationic photopolymerization was measured by DSC220C (Seiko Instruments Inc.) equipped with a UV-1 lighting unit (200 W Hg-Xe lamp, Seiko Instruments Inc.). Samples (2 to 3 mg) were applied to an aluminum pan and irradiated with UV light under an air atmosphere. The light intensity was adjusted to 20 mW/cm² at 365nm using ND filter.

Viscoelasticity Measurements.

A 1mm-thickness PSA formulation was cured using a UV irradiator equipped with 120 w/cm of high pressure Hg lamp for 1 minute. The total irradiated UV energy under this condition was 2.85 J/cm². The viscoelasticity of the cured PSA sample was measured by the parallel plate method using a dynamic mechanical spectrometer (RDS II: Rheometrics Inc.). The modulus dependency versus frequency was measured in the frequency range of 0.1 to 10 rad/sec at 25, 15, 5 and -5°C respectively. A master curve (25°C, 0.1 to 100 rad/sec.) for the modulus versus frequency was made by a horizontal shift of these curves according to the shift factor derived from WLF equation.

Adhesion properties.

The PSA formulation was coated onto 50 µm PET sheet (25 µm thickness) using an applicator. The PSA sheet was prepared by curing the coated liquid formulation using a conveyer type UV irradiator equipped with 120 W/cm of high pressure Hg lamp at a conveyer speed of 10 m/min. The total irradiated UV energy was 135 mJ/cm². The adhesion properties of the PSA sheet, such as peel adhesion (180°) to stainless steel (SUS) or polyethylene (PE) at 25°C and a holding power at 40°C were measured according to JIS-Z0237. The probe tack at 25°C was measured according to ASTM D-2979. Conditions for determination of the shear adhesion failure temperature (SAFT) were: 25mm X 25mm contact area, 500g load, heating rate, 0.4°C/min.

Results and Discussion

The properties of the PSA formulations using EHOX, EKP-207, P-90 (tackifier) and Rhodosil 2074 (photoinitiator) are shown in Table I. The compatibility of each component for these formulations was good and clear solutions were obtained.

The properties of a PSA are known to depend primarily on the viscoelastic nature of the adhesive mass (5). As the rate of deformation of a PSA during bonding is considered to be low, the modulus at low frequencies should be depressed, so that the composition is soft enough to flow and wet the substrate in a short time. On the other hand, during peeling, the deformation rate is high

because the thickness of the adhesive is low. The modulus of a PSA should be elevated to maintain the adhesive layer at a high testing rate. In the formulation of ordinary PSAs, an elastomer or rubbery polymer provides the elastic component, while a tackifier constitutes the viscous component. To function properly, a tackifier must be reasonably compatible with the base polymer. If the compatibility is low, at higher amounts of resin, the modulus of a PSA formulation increases across the entire frequency range of 0.1 to 100 rad/sec. For compatible formulations, as the concentration increases, the modulus is depressed at low frequencies and increases in the higher frequency region.

Table I. PSA Formulations and Their Adhesive Properties

R.N.	1	2	3	4	5	6	7
EHOX	80	80	80	80	60	40	
UVR-6216					20	40	80
EKP-207	20	20	20	20	20	20	20
Rhodorsil 2074	1	1	1	1	1	1	1
P-90	60	80	100	120	120	120	120
Viscosity ¹⁾ (cps)	390	760	1480	2870	2400	2020	1470
180° Peel ²⁾ (g/inch)	SUS	220	620	1050	1210	680	450 ⁻⁶⁾
	PE	40	160	370	618	360	460 ⁻⁶⁾
Holding Power ³⁾ (hrs)	>24	>24	>24	>24	>24	>24	⁻⁶⁾
SAFT ⁴⁾ (°C)	164	126	117	109	91	80	⁻⁶⁾
Probe Tack ⁵⁾ (gf)	579	665	490	371	320	345	⁻⁶⁾

1) Measured at 25°C

2) 25µm coating was cured with 120 W/cm high pressure Hg Lamp at 10 m/min. conveyor speed and measured according to JIS Z-0237

3) Measured at 40°C according to JIS Z-0237

4) 500g of load and heating rate 0.4°C/min.

5) Measured according to ASTM D-2979

6) Not measured due to insufficient cure

(R.N.1 to 4)

The viscosity of the formulations increased with the addition of P-90. Using EHOX, the viscosity of the formulations containing up to 120 phr of P-90 was still low.

The storage modulus (G') and loss modulus (G'') plots against frequency (0.1 to 100 rad/sec.) for the formulations are shown in Figure 1. With higher amounts of P-90, the storage modulus was depressed at low frequencies and increased at high frequencies, which is due to the good compatibility of the tackifier. The loss modulus increased across the entire range. Tan δ versus frequency plots for the formulations are shown in Figure 2. The value of the Tan δ increased with addition of P-90. These high values of Tan δ should contribute to the stress relaxation during bonding and peeling.

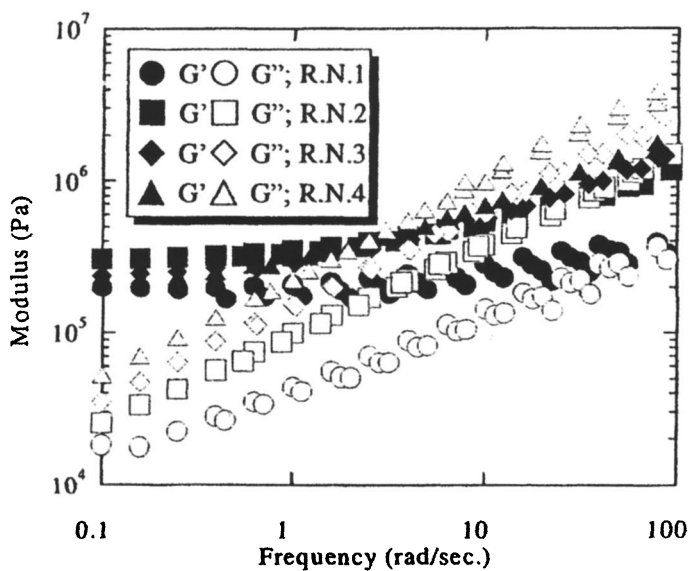


Figure 1. Storage (G') and loss (G'') modulus plot for R.N.1 to 4

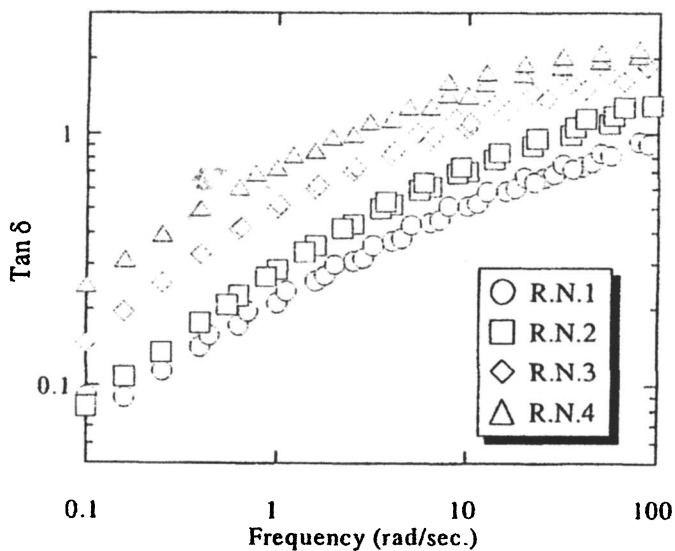


Figure 2. $\text{Tan } \delta$ plot for R.N. 1 to 4

In the formulation of PSAs, the adhesion properties are known to be optimized by the quantity of tackifier used (5). To some extent, the peel strength and tack increases as the content of tackifier is increased, and reaches a maximum. The optimum content of tackifier for tack is lower than that for peel strength.

The peel strength increased with the addition of P-90, and the probe tack reached a maximum at 80 phr. On the other hand, the SAFT was reduced with higher amounts of P-90. This drop can be explained by a decrease in the storage modulus at low frequencies.

(R.N.4 to 7)

With the addition of UVR-6216, the viscosity of the formulations was reduced. Complete substitution of EHOX with UVR-6216 resulted in poor photopolymerization (R.N.7).

The heat of polymerization of formulations was measured using photo-DSC and the results were shown in Figure 3.

In the cationic photopolymerization of R.N.4, a higher exotherm was observed in the early stages of the irradiation and decreased smoothly after the peak. This smooth decrease can be explained by the fast propagation rate

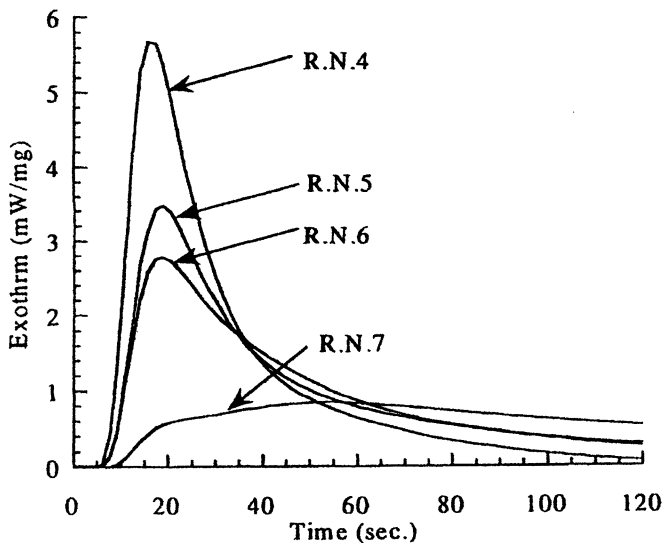


Figure 3. Photo-DSC curves for R.N.4 to 7 ($I=20 \text{ mW/cm}^2$ at 365 nm)

because of the high basicity of oxetane ring. With the addition of UVR-6216 to EHOX, the peak height was reduced (R.N.5 and 6). A smaller exotherm was seen for R.N.7 and the heat generation lasted during the entire period of irradiation. This long heat flow could be explained by the slow polymerization rate of the oxirane ring.

As the content of UVR-6216 is increased, both the storage modulus (G') and loss modulus (G'') was depressed across the entire frequency range (Figure 4). This decrease in modulus could be explained by the presence of residual monomer, which can work as a softener, due to low reactivity of UVR-6216. All the adhesive properties were also depressed with a high content of UVR-6216.

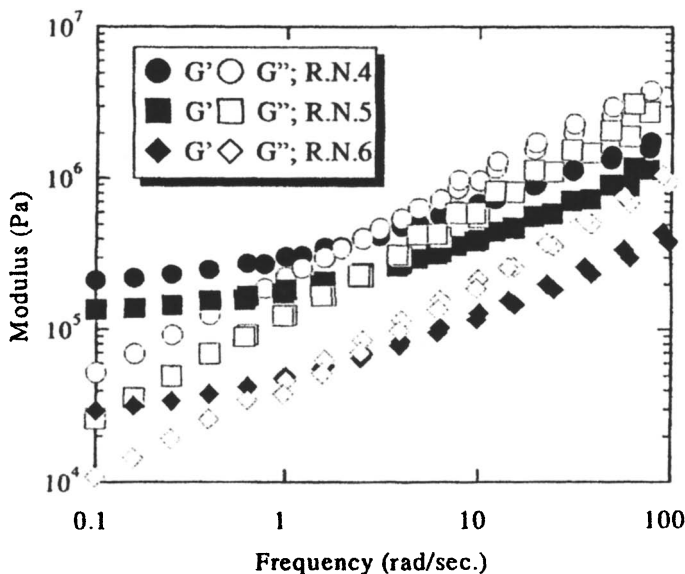


Figure 4. Storage (G') and loss (G'') modulus plot for R.N.4 to 6

Table II shows the formulations with cycloaliphatic diepoxide (UVR-6110) and adhesion properties of the cured PSA sheets. The heat resistance improved remarkably (high SAFT) with the addition of 2 wt% of UVR-6110. On the other hand, the 180° peel strength and probe tack were reduced slightly as the amount of UVR-6110 was increased.

Figure 5 shows the storage modulus (G') of the cured PSA layer with 4% of UVR-6110 and without it as a function of temperature. Without UVR-6110, a steep decrease of the storage modulus around 80°C was observed, while the G' curves for the cured PSA layer with UVR-6110 showed a long plateau zone extending to higher temperatures. The high SAFT value for the PSA layer with UVR-6110 can be explained by this high modulus at elevated temperatures.

Table II. PSA Formulations using UVR-6110 and Their Adhesive Properties ¹⁾

<i>R.N.</i>	8	9	10	11
EHOX	80	78	76	74
EKP-207	20	20	20	20
UVR-6110	-	2	4	6
2074	1	1	1	1
P-90	110	110	110	110
Viscosity ¹⁾ (cps)	2050	2250	2480	2630
180° Peel ²⁾ (g/inch)	SUS	1190	1020	854
	PE	510	464	327
SAFT ³⁾ (°C)	109	202	>205	>205
Probe Tack ⁴⁾ (gf)	510	467	510	570

1) Conditions and procedures are the same as in Table I.

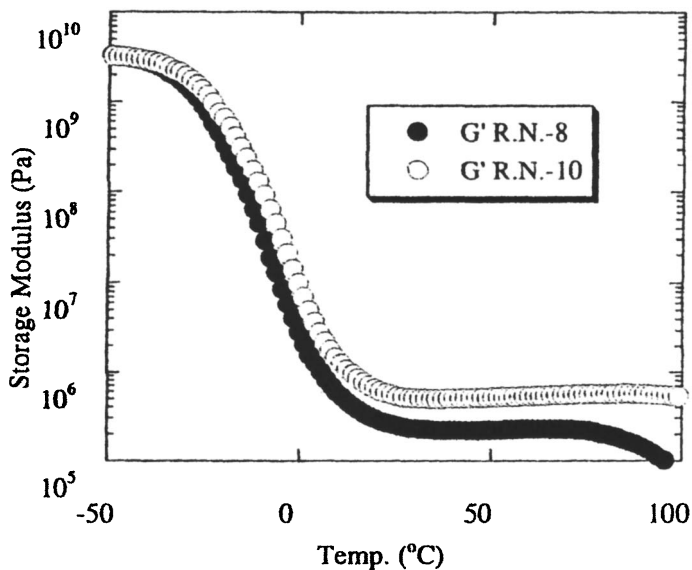


Figure 5. Storage Modulus curves of R.N.-8 and 10

Conclusions

Using the monofunctional alkyl oxetane, EHOX, Photocurable PSA formulations in combination with epoxy monomers and a hydrogenated petroleum resin as tackifier were investigated. The viscoelasticity and adhesion

properties of the cured PSA formulations were also evaluated. The characteristics are listed below.

- A wide variety of formulations was achieved using EHOX possessing an excellent compatibility with other monomers.
- With aid of EHOX, uniform and clear PSA formulations with low viscosity and good reactivity were achieved.
- The cured PSA sheets of the formulation were proved to possess good adhesive properties.
- The use of a cycloaliphatic diepoxide improved the heat resistance properties of the cured PSA sheet.

Due to these superior characteristics, oxetanes should contribute to expand the possibility of UV curable PSAs.

References

1. Zollner, S., RadTech Europe, **1999**, 543
2. Barnes, C.E., J. Am. Chem. Soc., **1945**, 67, 217
3. Erickson, J.; Zimmermann, E.; Southwick, J.; Kiibler, K., Adhesive age, November, **1995**, 18
4. Sasaki, H., RadTech North America, **2000**, 61
5. Butler, G.L., Natural Rubber. Hand book of PSA technology 2nd ed., VAN NOSTRAND RHEINHOLD, 1989, 396 – 456

Chapter 27

Photocationic Curable Silsesquioxanes Having Oxetanyl Group

Hiroshi Suzuki, Seitarou Tajima, and Hiroshi Sasaki

Corporate Research Lab, Toagosei Company Ltd., 1-1 Funami-cho,
Minato-ku, Nagoya-shi, Aichi 455-0027, Japan

Novel oxetanyl-functional silsesquioxanes (SQs) were synthesized and investigated as UV-curable materials. The multi-functional monomer (OX-SQ) was prepared by hydrolytic condensation of 3-ethyl-3-((tri-ethoxysilyl)propoxy)methyloxetane (TESOX). OX-SI-SQ, having a silicone chain partially introduced into SQ skeleton, was also synthesized through polycondensation of TESOX with α , ω -Dihydroxy poly(dimethylsiloxane). OX-SQs (OX-SQ and OX-SI-SQ) were colorless highly viscous liquid and soluble in common solvents. From the ^1H and ^{29}Si -NMR spectra, the SQ unit in OX-SQs was considered to be a mixture of several structures with a random, ladder or cage structure. OX-SQs exhibited good compatibility with cycloaliphatic diepoxide and gave formulations with high reactivity. OX-SQ gave photocured products of high hardness and OX-SI-SQ added silicone characteristics to the surface of the cured products, which showed excellent pollution-free properties. OX-SQs also exhibited high modulus at high temperature and rather high thermal stability.

Introduction

Photo-cationic curable materials, using epoxides and vinyl ether derivatives, have been widely investigated. Among them, oxetanes have been proved to possess many good properties, such as safety (AMES Test negative) and high reactivity (1, 2). Based on this chemistry, application of oxetanes as photo-curable materials are spreading extensively.

In the development of photocurable materials, not only the reactive group but also the structure of the main chain of the oligomer is important. Silicones are very attractive due to their high flexibility and chemical resistance. The introduction of oxetanyl groups into dimethylsiloxane derivatives has already been reported (3, 4). Meanwhile, organic silsesquioxanes (SQ) represented by the formula, $(RSiO_{3/2})_n$, are a well-known class of compounds for the preparation of both nano-composite and nano-structured organic-inorganic hybrid materials, in which the inorganic silica matrix is covalently bound to the organic moiety (5, 6). SQ can be obtained by hydrolytic polycondensation of organic trichlorosilanes or organic trialkoxysilanes. In recent years, there has been a great deal of interest to functionalize SQ with polymerizable groups, for example, vinyl functional-SQ, allyl-SQ, methacryl-SQ, epoxy-SQ and so on (5, 7). It should be interesting to investigate oxetanyl-functional SQ (OX-SQ) which can be considered a novel multifunctional oxetane compounds possessing the SQ backbone.

The present work focuses on the preparation and application of OX-SQ and its derivative having a silicone chain partially introduced into SQ skeleton (OX-SI-SQ). The properties of photocured coatings of OX-SQs (OX-SQ and OX-SI-SQ) were also investigated.

Experimental

Materials and experimental conditions used in this study are listed below.

Materials.

All reagents were used without a further purification. Triethoxysilane (TRIES) and 3-ethyl-3-allyloxymethyloxetane (AOX) were available from Toagosei Co. α , ω -Dihydroxy poly(dimethylsiloxane) (OH-Silicone) was purchased from Shin-etsu Chemical Co. 3, 4-epoxycyclohexylmethyl-3', 4'-epoxycyclohexane carboxylate (UVR-6110) was obtained from Union Carbide

Co. The iodonium salt cationic photoinitiator having hexafluoroantimonate as the counteranion (UV9380C) was available from G.E. Toshiba Silicone Co.

Instrumentation.

Gel permeation chromatography (GPC) analysis was carried out using a TOSOH HLC-802A equipped with two polystyrene gel columns (TSK-GEL, 2500HXL+100HXL) to determine the molecular weight of OX-SQs. ^1H and ^{29}Si -NMR spectra were obtained on a JEOL JNM-400 spectrometer. Photocuring was carried out using an Iwasaki Electric UB062-5B UV processor equipped with a high-pressure mercury lamp (80 W/cm). The viscoelasticity of the cured samples was measured by Dynamic Mechanical Spectrometer (DMS 6100: SEIKO Instruments). TG/DTA320 (SEIKO Instruments) was used for the thermal degradation measurements of cured samples.

Synthesis of 3-ethyl-(tri-ethoxysilylpropoxy)methyl oxetane (TESOX).

Under dry nitrogen, 103.1 g (660 mmol) of AOX and 0.3 mL of $\text{H}_2\text{PtCl}_6 \cdot 6\text{H}_2\text{O}$ in benzonitrile (0.05 mol/L) were introduced into a 500 mL flask fitted with a mechanical stirrer, dropping funnel and a reflux condenser. The mixture was heated to 70°C and 98.6 g (600 mmol) of TRIES was added dropwise. The reaction mixture was maintained at 80°C for 4 hours. After the reaction was completed, the product was isolated by distillation at $130\text{--}140^\circ\text{C}$ under 0.1 mmHg. Yield: 70%.

Preparation of Oxetanyl-functional SQ (OX-SQ).

A 300 mL of flask equipped with magnetic stirrer was charged with 19.2 g (60 mmol) of TESOX and 50 mL of isopropyl alcohol (IPA). To the flask, 3.4 g of an aqueous 5.1% solution of Me_4NOH (Me_4NOH : 2 mmol, H_2O : 180 mmol) was added dropwise. The reaction mixture was left under stirring at room temperature. The reaction process was followed by GPC, and the reaction was over at the time when the TESOX had almost disappeared, i.e., about 20 hours after addition of the mixture. After the reaction was over, the solution was diluted with 200 mL of toluene and washed with an aqueous saturated sodium chloride. The washing was repeated until the aqueous layer became neutral, and the organic layer was fractionated and dehydrated over anhydrous sodium sulfate. Evaporation of the toluene in vacuo gave the desired condensation product (OX-SQ) with quantitative yield.

Preparation of OX-SQ having a partial silicone chain (OX-SI-SQ).

OX-SI-SQ was obtained by hydrolytic co-polycondensation of TESOX with α,ω -dihydroxy poly(dimethylsiloxane) (OH-Silicone). A 300 mL of flask equipped with a magnetic stirrer was charged with 64.1 g (200 mmol) of TESOX, 10.47 g of OH-Silicone ($M_n = 1,000-1,500$) and 100 g of IPA. The mixture was allowed to stir at room temperature, and 21.9 g of an aqueous 1.3% solution of Me_4NOH (Me_4NOH : 3 mmol, H_2O : 1,200 mmol) was added dropwise. The subsequent procedure was the same as OX-SQ and the objective OX-SI-SQ containing 20 wt% silicone chain was obtained with quantitative yield.

Photopolymerization and evaluation methods.

The formulations were prepared by mixing the monomers (OX-SQs and UVR-6110) with UV9380C (2 wt% for film coating and 1 wt% for viscoelastic measurements) as photoinitiator in an amber vial at 40°C.

For film coating evaluations, liquid samples were coated on glass substrate using #5 bar applicator (approximately 10 μm thickness) and irradiated using a conveyor type UV irradiator equipped with 80 w/cm of high pressure Hg lamp at 10 m/min. of conveyor speed.

For viscoelastic measurements, a 1mm-thickness samples were cured using UV irradiator equipped with 80 w/cm of high pressure Hg lamp for 1 minute. The total irradiated UV energy under this condition was 2.85 J/cm². The viscoelasticity of the cured samples was measured using vibration mode (expansion) at 10 Hz. Using a small piece (approximately 10 mg) of the sample used for viscoelastic measurement, thermal degradation of cured samples was measured in air.

Results and Discussion

Synthesis of TESOX.

Hydrosilylation of TRIES with AOX in the presence of $H_2PtCl_6 - 6H_2O$ led to TESOX (Figure 1).

¹H-NMR (in C_6D_6) δ (ppm): 1.21 (t, 9H, $\underline{CH_3}$ -CH₂OSi); 3.84 (q, 6H, CH₃- $\underline{CH_2}$ -OSi); 0.78 (m, 2H, $-\underline{CH_2}$ -Si); 1.88 (m, 2H, CH₂- $\underline{CH_2}$ -CH₂Si); 3.39 (t, 2H, $-O-\underline{CH_2}$ -CH₂); 3.39 (s, 2H, $-\underline{CH_2}$ -O-CH₂CH₂); 0.75 (t, 3H, $\underline{CH_3}$ -CH₂-C); 1.65 (q, 2H, CH₃- $\underline{CH_2}$ -C); 4.37 (2d, 4H, C- $\underline{CH_2}$ -O in oxetane ring).

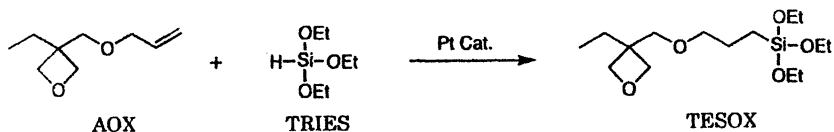


Figure 1. Synthesis of TESOX by hydrosilylation of TRIES with AOX

Preparation of OX-SQ.

The preparation of OX-SQ was carried out by hydrolytic polycondensation of TESOX using an alkaline catalyst (Figure 2).

OX-SQ was colorless highly viscous liquid and soluble in toluene, ether, hexane, acetone and other common solvents in any ratio. The number average molecular weight (M_n) of OX-SQ obtained from GPC measurement was about 2,000. A $^1\text{H-NMR}$ spectrum of OX-SQ is shown in Figure 3.

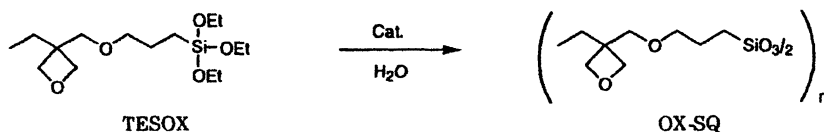


Figure 2. Preparation of OX-SQ by hydrolytic polycondensation of TESOX.

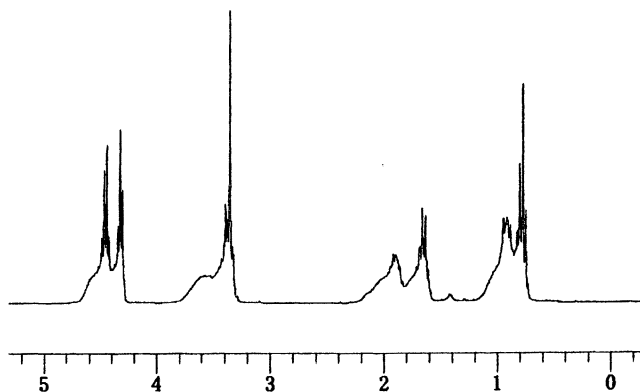


Figure 3. $^1\text{H-NMR}$ spectrum of OX-SQ

The appearance of peaks at 4.3 to 4.5 ppm showed the persistence of oxetane ring and no peak corresponding to the ethoxy group ($\text{Si-O-C}_2\text{H}_5$) was observed. The $^1\text{H-NMR}$ spectrum indicated that substantially all of the ethoxy groups in TESOX were condensed without decomposition of oxetane ring. Since the oxetane ring is stable to water under alkaline conditions, oxetanyl-SQ can be prepared by hydrolysis of the corresponded oxetanyl-alkoxysilanes. On the other hand, unlike oxetane derivatives, it is difficult to prepare of epoxy-functional SQ by hydrolytic condensation of epoxy-alkoxysilanes due to decomposition of epoxy ring. Epoxy-SQ was prepared, for example, by hydrosilylation of allyl-glycidyl ether with hydrogen-functional SQ (7).

As seen in the $^{29}\text{Si-NMR}$ spectrum of OX-SQ (Figure 4), the signals due to the Si-O-Si of SQ structures were observed around -60 to -70 ppm region. The sharp peak at -67.4 ppm showed the existence of a regular SQ structure.

The fact that broad and sharp peaks were concurrently observed in the ^1H and $^{29}\text{Si-NMR}$ chart suggested that OX-SQ consisted of a mixture of several structures with random, ladder and cage structures. Among these peaks, sharp peaks were assumed to be due to a regular cage structure and broad peaks should indicate the existence of ladder or random structures.

Preparation of OX-SI-SQ.

OX-SI-SQ was prepared by the hydrolytic co-polycondensation of TESOX with OH-Silicone according to Figure 5.

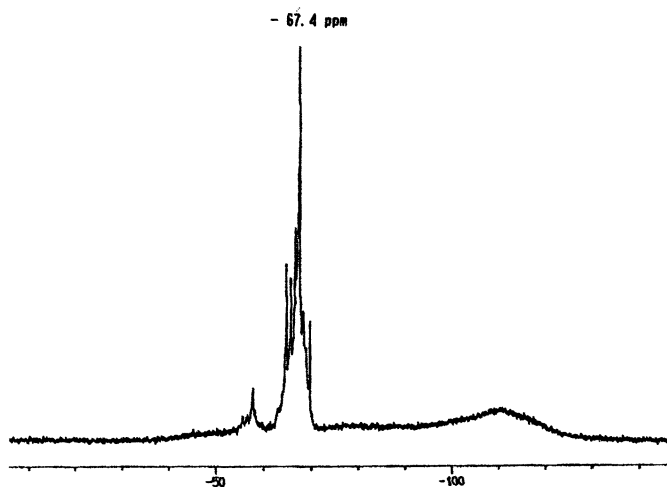


Figure 4. $^{29}\text{Si-NMR}$ spectrum of OX-SQ

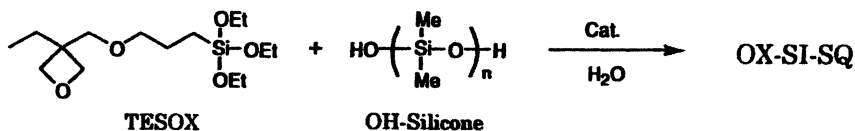


Figure 5. Preparation of OX-SI-SQ by hydrolytic copolycondensation of TESOX with OH-Functional Silicones

OX-SI-SQ was soluble in conventional solvents and had a M_n of about 2,000. In ^{29}Si -NMR spectrum of OX-SI-SQ, the signals due to the silicone and SQ structure were observed at -21.5 ppm and -66 to -68 ppm respectively. The OX-SI-SQ obtained using OH-Silicone was low molecular weight ($M_n < 2,000$) was colorless and clear. On the other hand, the OX-SI-SQ prepared using a higher molecular weight OH-Silicone ($M_n > 4,000$) was turbid in appearance.

Photopolymerization of OX-SQ and OX-SI-SQ

The prepared OX-SQs are a kind of multifunctional oxetane compounds, which can produce photocured products. SQ itself and functionalized SQ are known to be easily used to formulate homogeneous resin compositions due to their high compatibility with organic compounds. OX-SQ and OX-SI-SQ were soluble in various organic compounds and may contain reactive monomers such as typical cycloaliphatic diepoxide monomers (eg. UVR-6110).

As the initiation of oxetane homo-polymerization is known to be slow and accelerated by epoxides (2), the curing properties of OX-SQ were investigated in formulations with UVR-6110 (Table I). With higher amount of OX-SQ, the surface hardness and acetone resistance were improved, owing to the SQ skeleton structure and the high crosslink density. UVR-6110 alone exhibited poor acetone resistance even upon standing for 24 hours after UV exposure. Addition of OX-SQ gave good acetone resistance even after 1 hour standing. The improvement effect could be explained by the fast generation of cross-linked network of oxetanes accelerated by epoxide.

The formulation of OX-SQ and OX-SI-SQ with UVR-6110 are shown in Table II. In spite of the silicone chain, OX-SI-SQ exhibited good compatibility with UVR-6110. Though OX-SQ gave inferior pollution-free properties, all of the cured films from the OX-SI-SQ showed excellent pollution-free properties, i.e. silicone characteristics were given to the surface. These coatings had fairly good surface hardness too. Furthermore, even after wiping 2,000 times under a 500 g load with dry gauze, the ink-repellency was still good. The maintenance of excellent pollution-free properties should be provided by the remaining silicone chain on the coating which is covalently bounded to the SQ structure.

Table I. Formulation of Cycloaliphatic Epoxide (UVR-6110) with or without OX-SQ^{a)}

No.	UVR-6110 ^{b)} (wt%)	OX-SQ (wt%)	Pencil Hardness ^{c)}	Acetone Resistance ^{d)}			
				1 h	2 h	6 h	24 h
Bl	100	-	3H	0	30	50	>200
SQ-1	90	10	3H	40	50	>200	>200
SQ-2	80	20	4H	60	>200	>200	>200
SQ-3	60	40	5H	>200	>200	>200	>200
SQ-4	10	90	6H	>200	>200	>200	>200

a) 2 wt% of UV9380C (GE Toshiba Silicone Corp.) was added and coated on glass substrate to 5 μm thickness with a bar applicator and cured with 80 W/cm of high pressure Hg lamp at 10m/min. conveyor speed

b) Cycloaliphatic epoxy monomer, available from Union Carbide Corp.

c) According to JIS K 5400.

d) Number of rubbing times with a cotton ball wetted with acetone.

Table II. Formulation of OX-SQ and OX-SI-SQ with UVR-6110^{a)}

Sample No.	Exp-1	Exp-2	Exp-3	Exp-4
UVR-6110	100	80	90	80
OX-SQ	-	20	-	-
OX-SI-SQ ^{b)}	-	-	10	20
Transparency of resin	Clear	Clear	Clear	Clear
Pencil hardness ^{c)}	3H	4H	4H	5H
Pollution-free property ^{d)}	initial	NG	NG	OK
	after wiping ^{e)}	NG	NG	OK

a) 2wt% of UV9380C was added and coated on glass substrate to 10 μm thickness with a #5 bar applicator and cured in the same way as Table 1.

b) Containing 20 wt% of silicone.

c) According to JIS K 5400.

d) Lines were drawn using oil marker pen, OK : completely repellent, NG : no repellent.

e) Wiping with dry gauze was performed 2,000 times under a 500 g load.

Thermal properties of photo-cured OX-SQs

The storage modulus (E') and $\tan \delta$ plots against temperature for the photo-cured formulations of SQs with 10 wt% of UVR-6110 and 1 wt% of UV9380C as photoinitiator were shown in Figure 6. The TGA results measured in air for the same materials are exhibited in Figure 7. The formulations and results were summarized in Table III.

Table III. Thermal Properties of OX-SQs Formulated with UVR-6110^{a)}

UVR-6110 (wt%)	OX-SQ (wt%)	OX-SI-SQ (wt%)	E' ^{b)} at 250°C	Thermal Degradation ^{c)}	
				TD5 (°C)	TD10 (°C)
10	90	-	5.45E+8	330	355
10	-	90	4.93E+8	308	341

a) 1 wt% of UV9380C was added and coated to 1 mm thickness on a PTFE plate and cured with 80 W/cm of high pressure Hg lamp for 1 min.

b) Measured by DMS.

c) Measured by TG/DTA, TD5 is 5% and TD10 is 10% weight loss temperature.

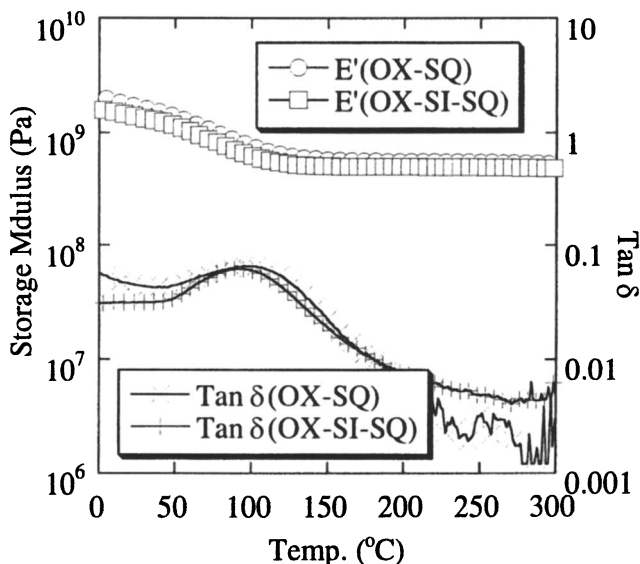


Figure 6. Viscoelastic measurement of OX-SQs at 10Hz

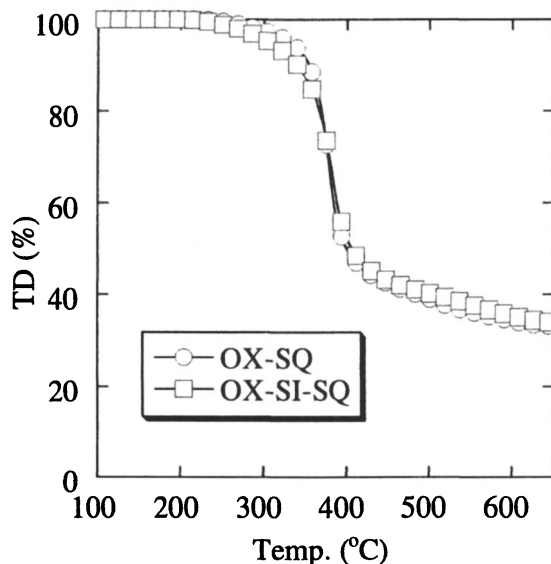


Figure 7. TGA measurement of OX-SQs in air

In spite of introduction of a soft silicone chain, OX-SI-SQ resulted in a similar thermal properties as OX-SQ. Both films exhibited small reduction in the storage modulus around 100°C presumably caused by the relaxation of oxetane polymer main chain and maintained high modulus until 300°C. This high modulus can be explained by the presence of the rigid SQ units.

Conclusions

The preparation of OX-SQs was carried out by hydrolytic condensation of oxetanyl tri-ethoxysilane (TESOX). SQ unit in OX-SQs was considered to be a mixture of several structures with random, ladder or cage structures.

OX-SQ and OX-SI-SQ exhibited high compatibility with UVR-6110. Photocuring of OX-SQ formulation resulted in a coating with high hardness, which can be attributed to the SQ skeleton structure and the presence of multifunctional oxetanyl groups. The OX-SI-SQ possessing a silicone chain gave silicone characteristics to the surface of the cured products. OX-SQs also exhibited high modulus at high temperature and rather high thermal stability. The superior properties make OX-SQ and OX-SI-SQ attractive as novel photocuring materials.

References

1. Sasaki, H.; Crivello, J.V., *J. Macromol. Sci. Part A: Pure Appl. Chem.*, **1992**, A30, 10, 915.
2. Sasaki, H., *RadTech North America*, **2000**, 61
3. Crivello, J.V.; Sasaki, H., *J. Macromol. Sci. Part A: Pure Appl. Chem.*, **1993**, A30, 2&3, 173.
4. Lecamp, L.; Youssef, B.; Lebaudy, P.; Bunel, C., *J. Macromol. Sci. Part A: Pure Appl. Chem.*, **1997**, A34, 11, 2335.
5. Baney, R.H.; Ito, M.; Sakakibara, A.; Suzuki, T., *Chem. Rev.*, **1995**, 95, 1409.
6. Cerveau, G.; Corriu, J.P.R.; Framery, E., *J. Mater. Chem.*, **2000**, 10, 1617.
7. Crivello, J.V.; Malik, R., *J. Polym. Sci. Part A: Polym. Chem.*, **1997**, 35, 407.

Chapter 28

Thermomechanical Studies of Photoinitiated Cationic Polymerization of a Cycloaliphatic Epoxy Resin

R. T. Olsson^{1,2}, H. E. Bair^{1,*}, V. Kuck¹, and A. Hale¹

¹Lucent Technologies, Bell Laboratories, 600 Mountain Avenue, Murray Hill, NJ 07974

²Current address: Royal Institute of Technology, Herserudsv 9A, 18134 Lindingö, Stockholm, Sweden

Thin films of 3,4-epoxycyclohexylmethyl 3',4'-epoxycyclohexane carboxylate were maintained at isothermal temperatures ranging from 0 to 50°C during UV irradiation (1.1 J/cm²). Under those conditions the maximum cure rate was achieved rapidly; however, only a conversion level of less than 10% was obtained before the reaction rate slowed dramatically. This low level of cure is not due to the loss of molecular mobility that is normally associated with a diffusion controlled reaction since the glass transition temperature, T_g , of the epoxide was at least 40°C below its reaction temperature. Raising the sample temperature above 60°C resulted in a sharp increase in the conversion level. Irradiation of films maintained at 100°C yielded a conversion of more than 80%. Using an UV conveyor belt system to expose 1 mm thick films to the same dose of UV irradiation as used with the thin films, the dark reaction effect was observed. After five hours of storage in the dark at ambient temperature, the T_g increased from -20 to 23°C and the modulus rose from 0.2 to 1 GPa. Calorimetric traces taken after various ambient storage times indicated that two major processes were occurring as indicated by the presence of two exothermic maxima in the DSC dynamic curing curves. The maxima were located near 60 and 110°C, when a heating rate of 5°C/min was used. The ultimate T_g for this epoxide is ~190°C.

Introduction

During recent years, there has been a growing interest in UV-light initiated photo-polymerization. The very high rates of polymerization coupled with the low evolution of volatiles have made these polymerizations very attractive for commercial applications. Both radical and cationic polymerizations can be initiated by exposure to UV light. Recently, the latter type has gained much attention due to the development of very efficient cationic initiators and the fact that, unlike radical polymerizations; cationic reactions are not inhibited by oxygen.^{1,2} Among different monomers suitable for cationic initiated UV-polymerization using onium salts, epoxy monomers have been studied extensively.³⁻⁹ In general, radiation produced epoxy polymers are amorphous materials that have good adhesion to a variety of materials, excellent chemical resistance and attractive mechanical properties.¹⁰

In industry, the cyclo-aliphatic epoxide 3,4-epoxycyclohexylmethyl 3',4' epoxycyclohexane carboxylate is one of the more widely used epoxide monomers suitable for photo-initiated cationic polymerization. For the sake of brevity the material will be referred to in the remainder of this paper as epoxy 3,4. Cyclo-aliphatic epoxides with their closed ring configuration have been reported more reactive than their open-chain counterparts and these, in turn, more reactive than glycidyl ethers or glycidyl esters.⁴ Qualitative measurements on the beneficial effect of temperature on cure rate of epoxy 3,4 systems have been reported.³

Using a power compensated, photo-differential scanning calorimeter, PDSC, we have studied the polymerization behavior of epoxy 3,4. With this instrument the sample temperature can be maintained isothermally independent of the heat evolved during polymerization. Hence, in this way one can determine quantitatively the effect of temperature on reaction rate. In addition, we studied the curing behavior of samples of epoxy 3,4 stored in the dark under ambient conditions (typically ~23°C and 35% relative humidity) after UV-irradiation was terminated. The latter process is often referred to as the dark reaction. The development of the glass transition temperature, T_g , and the degree of conversion were determined by temperature modulated DSC methods.^{11,12}

Experimental

The epoxy 3,4 monomer, ERL 4221, was acquired from Union Carbide Chemicals and Plastics Corp. (Danbury, CT) and used as received. The photoinitiator, CyraCure UVI-6974, a triarylsulfonium hexafluoroantimonate, was obtained from Union Carbide and mixed into the epoxy at a concentration of 1 W/W%.

UV-radiation experiments on the curing behavior of epoxy 3,4 were carried out using a differential scanning calorimeter (Perkin-Elmer DSC-7) equipped with an irradiation accessory (DPA7) that was fitted with a 450W high-pressure mercury lamp from Osram (Germany). The sample chamber was swept with helium at a flow rate of 22 cc/min during the testing. The UV light was unfiltered. After calibrating the PDSC for isothermal work using the melting point standards of m-xylene (m.p.= -47.9°C), p-xylene (m.p.= 13.2°C) and indium (m.p.= 156.6°C), the polymerizations were conducted isothermally at temperatures ranging from -40 to 100°C with samples having a weight of 0.7±0.1 mg. To obtain an even distribution of the liquid sample over the bottom of the aluminum sample pans, a disc of transparent polyvinylidene difluoride was placed on top of the liquid sample and left in place during the measurements.¹³ This procedure produced films of relatively uniform thickness that were about 20 μm thick. In addition, the plastic cover diminishes the evolution of volatile products from the liquid epoxy. During the typical period of irradiation the epoxy lost less than 0.10 weight percent until the reaction temperature exceeded 80°C. At temperatures above 80°C a patented, hermetic capsule with a UV transparent lid was used.¹⁴

The power output of the xenon lamp was determined by placing an International Light Corp. Model IL 745A UV Radiometer at position just above the DSC sample holder closure. Most exposures lasted for 7.5 minutes (the shutter opened at 0.5 and closed at 8.0 minutes) and during this exposure period a sample received a dose of approximately 1.1 J/cm². Energy profiles of the Xenon lamp used in these studies revealed a large portion of the light energy lies above 380 nm. This longer wavelength radiation can be absorbed and converted to heat by the epoxy resin inside the DSC pan. Thus, a sample that absorbs radiation in the visible and infrared region can have a large but constant exothermic signal when the lamp is on. This exothermic effect can be easily eliminated when a second run with the same sample is subtracted from the first run.¹³ This difference technique is used in the isothermal DSC experiments shown in this paper. Temperature modulated DSC experiments were carried out in a Perkin-Elmer DSC-7 instrument in an attempt to separate overlapping glass transition endotherms from curing exotherms.

The sample's modulus was determined in a three point bending fixture at frequency of 0.8 Hz and a strain of 0.08% using a dynamic mechanical analyzer (Perkin-Elmer DMA-7e). Each sample's dimensions were approximately 1.0 x 3.4 x 10 mm (HxWxL).

Results and Discussion

A photocalorimetric comparison of the isothermal curing of three 20μm films of epoxy 3,4 maintained at -20, 0 and 30°C during exposure to UV light

($\sim 1.1 \text{ J/cm}^2$) is shown in Figure 1. The peak maximum was found to increase nearly seven-fold from about 0.3 to 2.0 W/g as the reaction temperature was raised from -20 to 30°C , respectively. We assume the exothermic peak is a direct measure of the maximum polymerization rate.¹⁵ In addition, the time to each exothermic peak decreased from 21 to 11 to 6 seconds as temperature was increased from -20 to 0 to 30°C , respectively. Note that at each cure temperature in Figure 1 the fast part of the reaction is over within the first 60 seconds of irradiation. The effect of temperature on these curing rate properties of this photoinitiated cationic polymerization of epoxy 3,4 is similar to that of free radical acrylate polymerizations within the aforementioned temperature range, even though the reaction mechanisms are different.^{13,16}

The apparent heat of reaction, $^*\Delta H_{\text{rxn}}$, was obtained by integrating the exothermic curves in Fig.1 and is equal to -15 , -29 and -46 J/g at -20 , 0 and 30°C , respectively. In this case the degree of conversion, ξ , as a function of time was calculated by dividing $^*\Delta H_{\text{rxn}}$ by the heat of reaction, ΔH_{rxn} . The latter value was -664 J/g based upon a value of -20 kJ/mol per epoxy group polymerized. Note that at curing temperatures of -20 , 0 and 30°C , ξ , multiplied by 100 equals 2, 3 and 7% conversion, respectively. This single digit level of conversion remains until the reaction temperature is raised above 60°C and then the amount of liberated heat begins to increase dramatically (Figure 2). However, from 30 to 80°C the time to the maximum cure rate increased by an order of magnitude and then significantly decreased at 100°C as is shown in

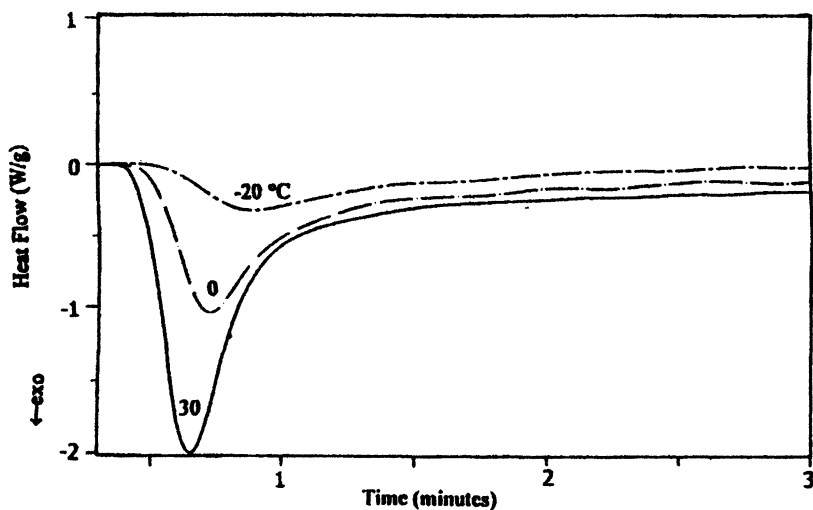


Figure 1. Exothermic reaction of epoxy 3,4 under isothermal conditions.

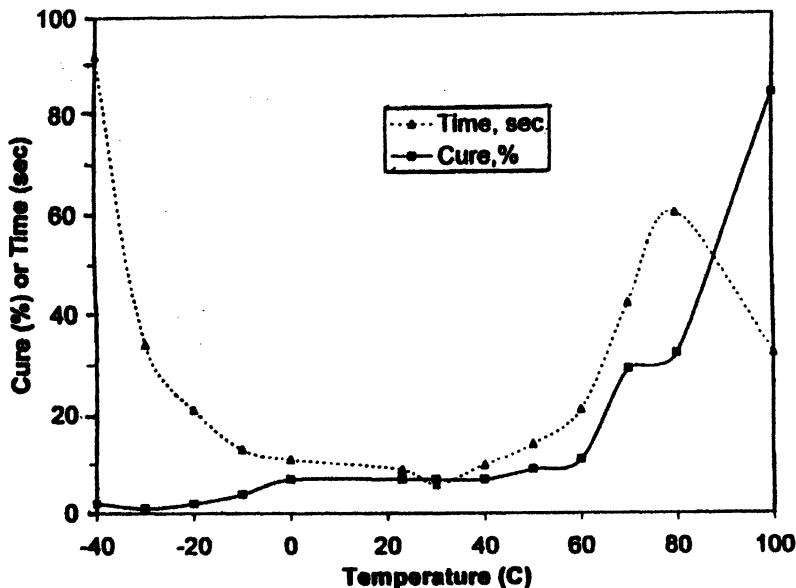


Figure 2. Time to reach the maximum polymerization rate and the extent of conversion during the curing of epoxy 3,4 as a function of temperature.

Figure 2. These findings are in marked contrast to those previously observed with the same monomer and using di(4-t-butylphenyl)iodonium hexafluoroarsenate as the photoinitiator, where the time to reach the maximum cure rate decreased linearly with irradiation time over the temperature range of 25 to 135°C.³

At 70°C the curing exotherm is broadened by a factor of three to four times over that found for the cure at 30°C and consequently $^{\circ}\Delta H_{\text{rxn}}$ equals -192 versus -46 J/g at 70 and 30°C, respectively. This trend continued until at 100°C -560 J/g were liberated (ξ equals 84 %) and the time to the maximum reaction rate decreased to 34 seconds. In earlier work Decker and Moussa determined by IR measurements that 83% of epoxy 3,4 monomer was converted in the presence of 5% of bis [4-(di-phenylsulphonio)phenyl]-bis hexafluorophosphate at 80°C.²

With the absorption of light triarylsulfonium salts form strong protonic acids that remain in epoxy 3,4 until they are neutralized. These strong acids enable the epoxy to react in the absence of UV light. Samples were prepared for dark reaction studies with a dose of 1200 mJ/cm² at ambient temperatures using a Fusion Systems Irradiation Station (Rockville, MD) equipped with a mercury lamp having a D bulb and a conveyor belt for exposing the sample. Note that during irradiation of a 1 mm thick epoxy layer, bounded on both sides by 1 mm

thick microscope cover slides, the temperature of the epoxy rose for a short time to slightly above 50°C during cure. Fifteen minutes after the belt cure at ambient temperature, the T_g was found at -20°C. The unreacted T_g of epoxy 3,4 is -60°C. When a thinner, 0.3 mm thick layer of this epoxy was irradiated to a dose of 3.6 J/cm² without a cover slide its T_g was found near -40°C. However, a similar thin epoxy layer was made under the same experimental conditions but stored at -80°C immediately after irradiation. The latter epoxy had a tough, flexible outer skin that was about 0.1 mm thick with a T_g at -44°C. The liquid inner layer had a T_g of -58°C. These results demonstrate how important the effect of temperature is on the epoxy's curing behavior.

In order to follow the extent of reaction in the dark as the sample ages, ξ can be calculated from

$$\xi = [(1-\xi_0)\Delta H_{rxn} - \Delta H_{res}] / \Delta H_{rxn} + \xi_0 \quad (1)$$

where ΔH_{res} is the residual heat of reaction that is obtained by scanning the partially reacted sample from below T_g to above 230°C. The latter temperature is about 40°C above the ultimate T_g for this epoxy and was selected to enable the material to react as completely as it is possible without causing degradation. ξ_0 is the initial degree of cure that occurs when the epoxy sample is irradiated on the UV conveyor belt, which in this work was found to be 7%.

The determination of T_g and the residual heat of reaction after the belt curing process can be difficult to define because the overlapping endothermic and exothermic processes can offset each other. In addition, the magnitude of the change in C_p at T_g can be diminished due to the restrictions that are imposed on molecular motion as crosslink density increases with the extent of conversion.¹⁷ In order to deconvolute these opposing thermal trends we employed temperature modulated DSC (TMDSC).

The solid line in Figure 3 is the average heat flow for epoxy 3,4 after an initial UV belt cure followed by 4470 minutes of dark reaction at room temperature. It is equivalent to the signal produced in a conventional DSC scan using a linear heating ramp. This average signal is produced from a series of 118 repetitive temperature steps of 2.5 degrees at a rate of 5°C/min with an isothermal hold of 30 seconds between each heating step (broken line with dots, Figure 3). In addition, two exothermic maxima can be seen in the dark aged epoxy 3,4 samples near 60 and 110°C as shown in Figures 3.

In Figure 4 the average heat flow signal from TMDSC experiments for the unreacted epoxy 3,4 and subsequent samples stored in the dark at room temperature for 14, 163 and 4470 minutes are plotted versus temperature from -65 to 230°C. T_g is defined as the temperature at ½ ΔC_p or at -60°C for the unreacted epoxy 3,4. The breadth of the glass transition, ΔT_g, which is determined from the difference in the extrapolated onset and termination of the T_g interval, equals about 6°C for the uncured specimen. The latter value is

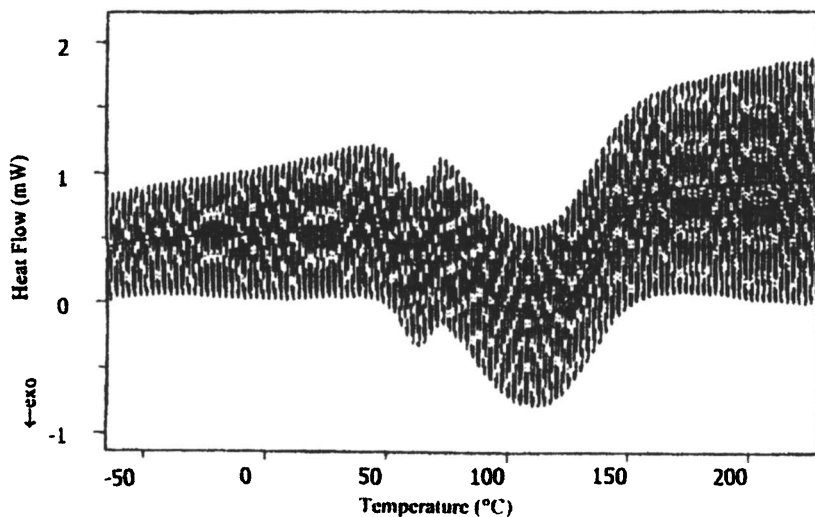


Figure 3. TMDSC experiment of epoxy 3,4 after 470 minutes of dark reaction.

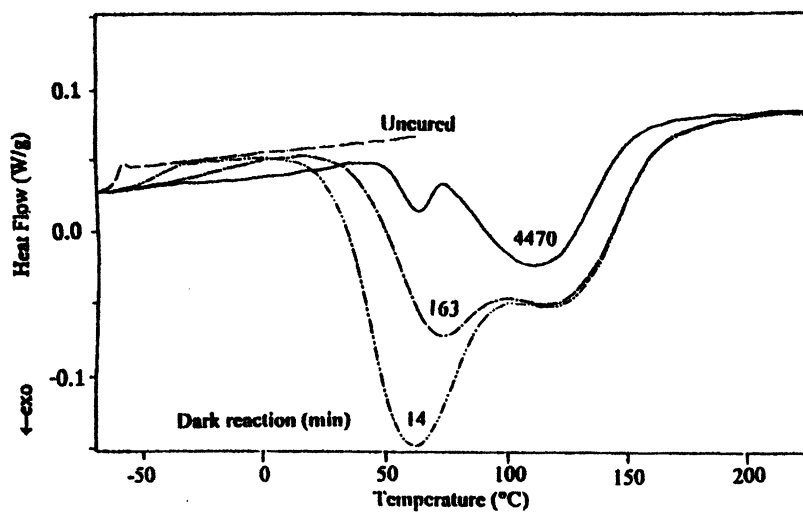


Figure 4. Average heat flow signal from TMDSC experiments on uncured epoxy 3,4 and after 14,163 and 4470 minutes of dark reaction.

typical for a homogenous, single component amorphous material.¹⁸ However, as the epoxy cures in the dark its T_g increases and also broadens. After 14 and 163 minutes of dark reaction T_g occurred at -40 and -16°C and ΔT_g equaled 20 and 35°C , respectively. However, the glass temperature cannot be discerned adequately after 4470 minutes of dark aging as seen in Figure 4 and must be analyzed in a manner that is described below.

The exothermic part of the conventional signal can be eliminated if the thermodynamic part of the DSC signal or storage specific heat, C_p , is plotted (Fig. 5, lower, dashed line). Two T_g s are detected at 52 and 188°C . Note that dashed lines have been extended from below and above each T_g as shown in the C_p versus T plot of Figure 5 to make the two T_g s more visible. The lower T_g is associated with the material that has aged for 4470 minutes but the upper T_g is assumed to be linked to the material after the exothermic cure has been completed during this start and stop TMDSC heating regime. This final T_g is only two degrees lower than if the material is cured by dynamically heating the epoxy to 245°C and repeating the run to find the material's ultimate T_g . ΔC_p is about the same value or $0.19 \text{ J/g}^\circ\text{C}$ for both transitions. Next, one should return to the average heat flow plot (upper, solid line, Figure 5) and place the starting point of the curing reaction at 52°C such that ΔC_p is equal to the value found in the storage C_p plot. A dashed line is cast from this point to end of the reaction exotherm at 175°C . The residual heat is computed from the area under the dashed line and gives a value of -133 J/g . Hence, ξ equals 80%.

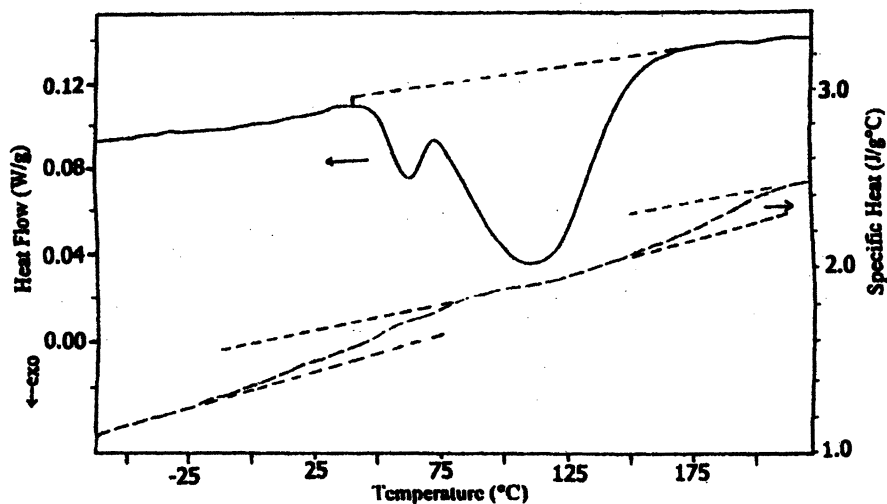


Figure 5. Average heat flow signal and storage C_p versus temperature from TMDSC runs on epoxy 3,4 after 4470 minutes of reacting in the dark.

In Figure 6 the advancement of T_g during the dark reaction is plotted versus the conversion of the epoxy resin using the TMDSC deconvolution scheme. These results show the typical glass transition temperature behavior that has been noted in other thermoset systems where T_g increases linearly with conversion until the latter stages of conversion and then begins to increase abruptly as the crosslinked network develops.^{17,19}

By conventional DSC scans at 15°C/min a series of curves were generated for epoxy 3,4 after ambient storage for 15, 48, 140 and 195 minutes (Figure 7). The lower temperature exotherm near 90°C diminishes with increased aging time but the higher temperature exotherm appears to be unchanged under these aging conditions. In addition, the leading edge of the lower temperature exotherm shifts to higher temperatures with increased aging. When the sample aged for 195 minutes was stopped upon reaching 95°C and quenched and rerun only the high temperature peak was present (solid lines, Figure 5). This latter experiment supports our contention that the lower temperature process is independent of the higher exothermic reaction. Perhaps the epoxide ring opening reaction that is occurring in the lower temperature peak is generating secondary hydroxyl compounds that are free to react at a significant rate at higher temperatures. Spectroscopy measurements are planned in the future to indicate if this hypothesis is correct.

The impact of the dark reaction on the modulus was monitored. Fifteen minutes after a 1 mm thick specimen was belt irradiated its storage modulus equaled 0.2 GPa. During the initial 200 minutes of dark aging the epoxy 3,4's modulus increased rapidly as shown in dash-dot line in Figure 8. Simultaneously the sample's loss modulus showed a maximum after about 200 minutes which indicates that T_g for this material equaled the ambient reaction temperature at this time. This mechanical data supports the DSC results that showed T_g was located at 23°C after 240 minutes of aging in the dark. As the T_g of the material reached the sample temperature, it appears that molecular diffusion became difficult and the reaction rate was reduced significantly.¹⁸⁻²⁰ The glassy epoxy's modulus continued to increase slowly until it reached a value of about 2.8 GPa after 1500 minutes of aging. By heating a second epoxy sample for 20 minutes at 200°C immediately after room temperature irradiation resulted in raising the modulus to the same value obtained by aging at ambient for 1500 minutes or 2.8 GPa (solid line, Figure 8). This latter temperature effect on the sample's modulus could be exploited to rapidly produce fully cured coatings if this type of epoxy is used commercially.

It has been reported that in photoinitiated cationic systems the reaction rate can be accelerated by chain transfer agents, specifically hydroxyl containing compounds such as water and alcohols.³ In these studies the

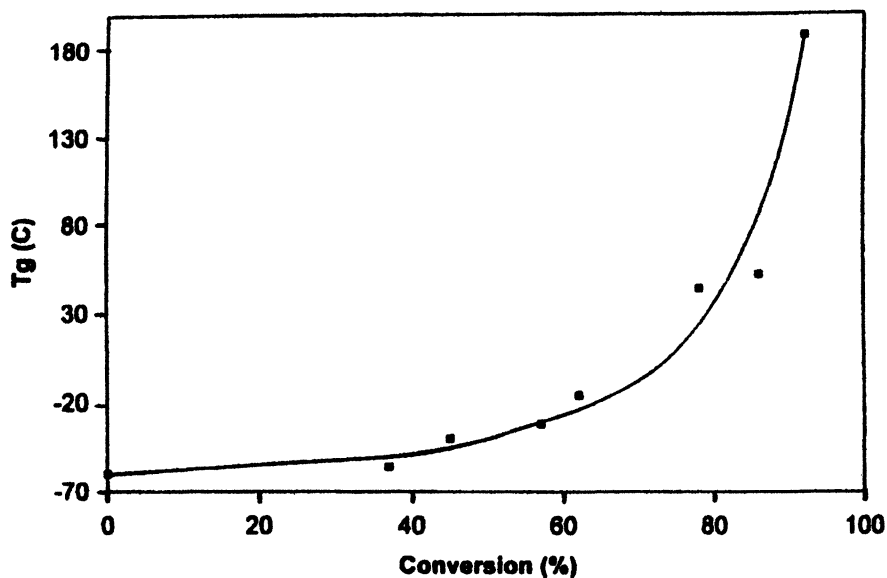


Figure 6. Tg of epoxy 3,4 as a function of conversion.

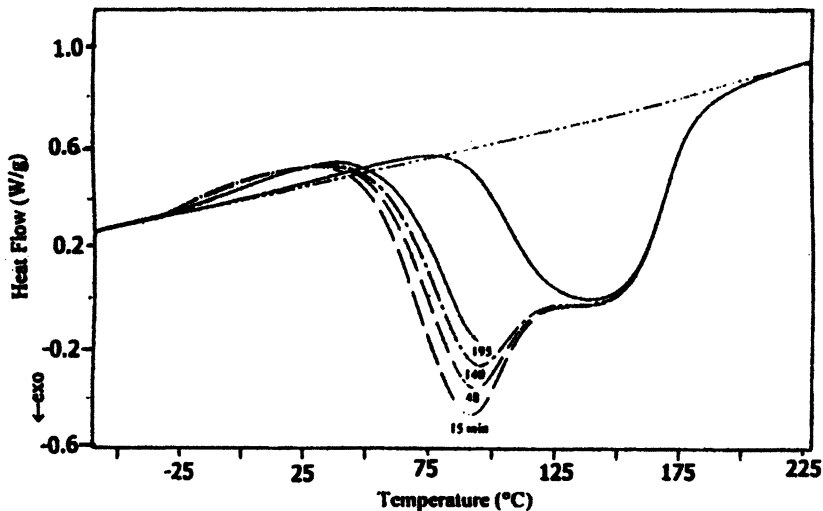


Figure 7. Conventional DSC scans of epoxy 3,4 after dark aging for 15, 48, 140 and 195 minutes. Double dashed line is for fully reacted sample.

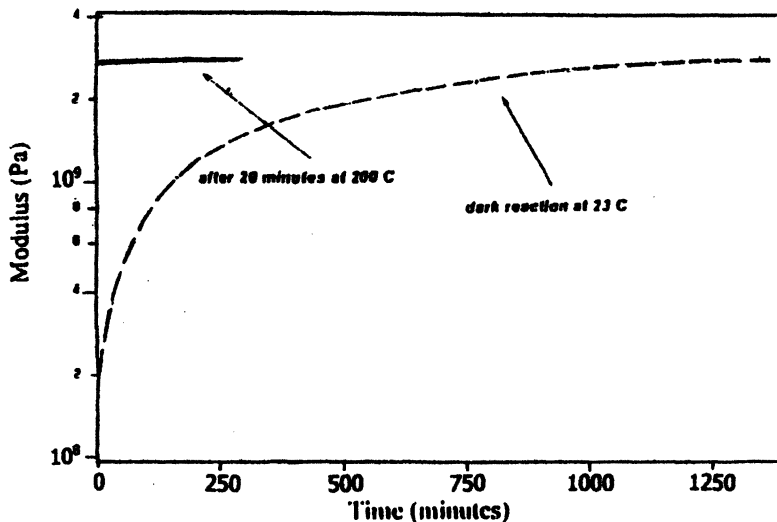


Figure 8. Development of modulus in the epoxy during dark reaction under ambient conditions and after heating to 200°C.

polymerization rate of epoxy 3,4 increased, sometimes markedly, with the use of alcohols but slowed in the presence of water.²¹ For example at 60°C the time to maximum reaction rate occurred in only 19 seconds when the sample was dry but increased to 89 seconds after epoxy 3,4 was equilibrated with 100% relative humidity (~6 weight percent water gain). Also the dry epoxy's heat of reaction is about 20% greater than that found for the wet sample.

Conclusion

Temperature has a profound effect on the photo-initiated cationic polymerization of a cyclo-aliphatic epoxy. In isothermal photocalorimetric measurements from 0 to 50°C the level of epoxy conversion is less than 10% even though the T_g of the partially reacted epoxy is as much as forty degrees below the reaction temperature. However, at temperatures above 50°C the extent of reaction begins to increase significantly until at 100°C the degree of cure exceeds 80%. Samples initially irradiated and stored at room temperature underwent significant dark reaction. In about five hours of dark storage an irradiated epoxy's T_g went from an initial value of -20 to 23°C and its modulus

from 0.2 to 1 GPa. Finally calorimetric scans made after periods of dark storage that ranged from a few minutes to several months showed that two exothermic processes were occurring as indicated by two exothermic maxima in the differential scanning calorimeter (DSC) curing curves. In these latter experiments temperature modulated DSC was found to be able to separate the overlapping thermal processes of the endothermic glass transition and the exothermic curing such that T_g and the residual heat of reaction could be determined accurately. The ultimate T_g of this epoxy is about 190°C.

References

1. Crivello, J. V. *J. Polym. Sci.: Part A: Polym. Chem.* **1999**, *37*, 4241.
2. Decker, C.; Moussa, K. *J. Polym. Sci., Part A, Polym. Chem.* **1990**, *28*, 3429.
3. Crivello, J. V.; Conlon, D. A.; Olson, D. R.; Webb, K. K. *J. Rad. Curing* October **1986**.
4. Crivello, J. V.; Varlemann, U. *J. Polym. Sci.: Part A: Polym. Chem.* **1995**, *33*, 2473.
5. Rajaraman, S. K.; Mowers, W. A.; Crivello, J. V. *Macromolecules* **1999**, *32*, 36.
6. Crivello, J. V.; Liu, S. J. *J. Polym. Sci.: Part A: Polym. Chem.* **1999**, *37*, 1199.
7. Rajaraman, S. K.; Mowers, W. A.; Crivello, J. V. *J. Polym. Sci.: Part A: Polym. Chem.* **1999**, *37*, 4007.
8. Crivello, J. V.; Liu, S. J. *J. Polym. Sci.: Part A: Polym. Chem.* **2000**, *38*, 389.
9. Crivello, J. V.; Mowers, W. A.; Rajaraman, S. K. *Radtech Report* March/April **2000**.
10. Crivello, J. V. In *Developments in Polymer Photochemistry-2*; Allen, N. S., Ed.; Applied Sciences: London, **1981**, Chapter 1.
11. Schawe, J. *Thermochim. Acta* **1995**, *260*, 1; 261, 183.
12. Swier, S.; Van Assche, G.; Van Hemelrijck, A.; Rahier, H.; Verdonck, J.; Van Mele, B. *J. Thermal Analysis* **1998**, *54*, 585.
13. Bair, H. E.; Blyler, L. L. *Proc. 14th NATAS Conference*, September **1985**, p.392.
14. Popielarski, S.; Bair, H. E., Hale, A. patent pending **1998**.
15. Wight, F. J. *J. Polym. Sci. Lett.* **1978**, *16*, 121.
16. Bair, H. E.; Blyler, L. L.; Simoff, D. A. *ACS Polymeric Materials Sci. & Eng.* **1993**, *69*, 268.

17. Hale, A.; Macosko, C. M.; Bair, H. E. *Macromolecules* **1991**, *24*,2610.
18. Bair, H. E., "Glass Transition Measurements by DSC" In *Assignment of the Glass Transition*, ASTM STP 1249, Seyler, R. J., Ed.; American Soc. For Testing and Materials, Philadelphia, PA, **1991**, p 50.
19. Havlicek, I.; Dusek, K. In *Crosslinked Epoxies*; Sedlacek, B.; Kahovec, J., Eds.; Walter de Gruyter & Co.; Berlin **1987**, p. 417.
20. Matsuoka, S.; Quan, X.; Bair, H. E.; Boyle, D. J. *Macromolecules* **1989**, *22*, 4093.
21. Olsson, R. T.; Bair, H. E.; Hale, A.; Kuck, V., to be published.

Chapter 29

Harvesting the Fields of Inorganic and Organometallic Photochemistry for New Photoinitiators

Charles Kotal¹, Yoshikazu Yamaguchi², Wei Ding¹,
Cynthia T. Sanderson¹, Xinyong Li¹, Gary Gamble¹,
and I. Jonathan Amster¹

¹Department of Chemistry, University of Georgia, Field Street,
Athens, GA 30602

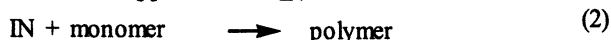
²JSR Corporation, Tsukuba Research Laboratory, 25 Miyukigaoka,
Tsukuba, Ibaraki 305-0841, Japan

Several iron(II) metallocenes are effective photoinitiators for ionic polymerization reactions. Photoexcitation of ferrocene and 1,1'-dibenzoylferrocenes in solutions of ethyl α -cyanoacrylate produces anionic species that initiate polymerization of the electrophilic monomer. Irradiation of $[\text{CpFe}(\eta^6\text{-arene})]^+$ (Cp is $\eta^5\text{-C}_5\text{H}_5$) in epoxide-containing media generates several cationic species capable of initiating ring-opening polymerization. The diversity of photoinitiation mechanisms exhibited by these iron(II) metallocenes is discussed in terms of their electronic structures.

I. Introduction

Photoinitiated polymerization is a process that employs light and a photosensitive compound, termed a photoinitiator, to initiate the production of a polymeric substance from a lower molecular-mass precursor (monomer, oligomer, crosslinkable polymer). While details of the mechanism of photoinitiation will vary from system to system, all processes of this type can be

dissected into two essential steps – one photochemical and the other thermal. In the photochemical step, the absorption of a photon by the photoinitiator, PI, produces one or more reactive species, IN (eq. 1). In some systems, this transformation requires the participation of a second component termed a co-initiator. Following its formation, IN undergoes a thermal reaction with the precursor that initiates the polymerization process (eq. 2). For the majority of reported photoinitiators, IN is a radical or a strong acid (1-4). Common radical-generating photoinitiators include benzoin and its derivatives, benzil ketals, substituted acetophenones, aromatic ketone/amine combinations, acylphosphine oxides, dye-borate systems, and fluorinated titanocene derivatives. Popular acid-generating photoinitiators include 2-nitrobenzyl esters, triazines, cationic iron(II)-sandwich complexes, and onium salts belonging to the diaryliodonium and triarylsulfonium families.



Inspection of the above list reveals that most of the common photoinitiators are organic compounds. The small number of inorganic and organometallic entries is rather surprising, because compounds belonging to these families undergo a fascinating array of photochemical reactions, many of which yield reactive species capable of initiating useful chemistry (2,5,6). Beginning in 1986, we embarked upon a program aimed at expanding the selection of inorganic and organometallic photoinitiators (7). Our primary goals have been to discover new photoinitiators that equal or exceed the performance of their purely organic counterparts, to elucidate the detailed mechanisms by which photoinitiation occurs in these new systems, and to exploit this chemistry in the design of novel photosensitive materials.

This chapter reviews our recent studies of four closely related types of iron(II)-containing metallocene photoinitiators (Figure 1). We begin with a brief discussion of the structures and reactivities of the electronic excited states present in these compounds. We then consider the roles played by the metallocenes in several examples of photoinitiated anionic and cationic

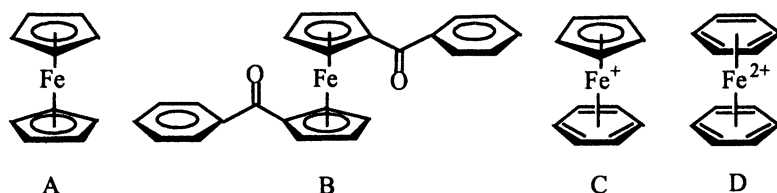


Figure 1. Structures of several types of iron(II) metallocenes.

polymerizations. A particularly intriguing aspect of our results is the change in the mechanism of photoinitiation that follows from variations in metallocene structure.

II. Electronic Excited States of Iron(II) Metallocenes

We shall follow the conventional practice (2,8) of classifying an electronic excited state in terms of its dominant molecular orbital configuration. Transitions between states are then conveniently labeled according to the orbitals that undergo a change in electron occupancy.

Ligand field excited states result from transitions between valence d orbitals primarily localized on the metal. Typically, such a transition involves the promotion of an electron from a d orbital that undergoes a π -bonding (or antibonding) interaction with the attached rings to a higher lying d orbital that is strongly σ -antibonding with respect to the metal-ring bonds. This angular redistribution of electron density does not alter the formal oxidation state of the metal, but it does weaken the metal-ring bonding and thereby enhances the likelihood of ring loss.

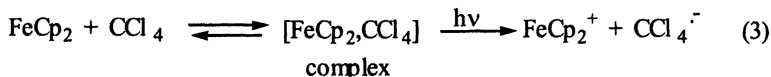
Charge transfer excited states arise from the radial redistribution of electron density between the components (metal and rings) of the metallocene or between the metallocene and the surrounding medium. Transfer of an electron from a ligand-centered orbital to a metal d orbital generates a ligand-to-metal charge transfer (LMCT) excited state. Electron flow in the opposite direction produces a metal-to-ligand charge transfer (MLCT) excited state. A transition that results in the movement of electron density from the metallocene to the surrounding solvent gives rise to a charge-transfer-to-solvent (CTTS) excited state. Each of these transitions occurs with a change in the charge and/or formal oxidation state of the species involved (metal, ligand, solvent). Consequently, charge transfer excited states are susceptible to oxidation-reduction reactions and, in cases where the redox process creates a substitutionally labile metal center, to accompanying ligand dissociation.

III. Photoinitiated Anionic Polymerization

A. Ferrocene

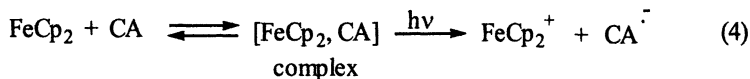
Ferrocene (FeCp_2 , where Cp denotes $\eta^5\text{-C}_5\text{H}_5$; see structure A in Figure 1) is the original and most celebrated metallocene. The compound is photoinert in solvents such as methanol, acetone, and cyclohexane (9). When dissolved in a strong electron-accepting medium such as carbon tetrachloride, however, FeCp_2

forms a ground-state donor-acceptor complex with the solvent that gives rise to a charge-transfer-to-solvent absorption band in the near ultraviolet region. Irradiation into this band induces a redox reaction that yields the ferricenium cation, FeCp_2^+ , and the unstable CCl_4 radical anion, which rapidly dissociates to the CCl_3 radical and chloride ion (eq. 3) (10). This type of chemistry has been used as a source of radicals for the photoinitiated polymerization of vinyl monomers (11).



We have discovered that photooxidation of FeCp_2 also occurs in neat ethyl α -cyanoacrylate (CA) to produce an active initiating species for anionic polymerization of this electrophilic monomer (12). Figure 2 (spectrum a) displays the room-temperature electronic absorption spectrum of the metallocene in tetrahydrofuran (THF). The weak bands above 300 nm correspond to spin-allowed ligand field transitions predominantly localized on the d^6 metal (13,14). Switching the solvent to a 2:3 (v:v) mixture of CA and THF results in the appearance of a band at 355 nm (spectrum b and inset), which is indicative of donor-acceptor complex formation between FeCp_2 and the monomer. Given the ease of oxidizing FeCp_2 and the strong electron-accepting character of CA, we assign this new feature as a CTTS ($\text{Cp}_2\text{Fe} \rightarrow \text{CA}$) transition of the complex.

Solutions of CA containing millimolar concentrations of FeCp_2 undergo no discernible change in viscosity for at least 24 h when stored in the dark at room temperature. Upon exposure to light, however, these solutions polymerize to a hard, plastic-like solid. Neither molecular oxygen nor hydroquinone, known radical scavengers, influences the rate of photoinitiated polymerization. In contrast, methanesulfonic acid exerts a strong inhibiting effect on this process. These findings indicate that polymerization proceeds by an anionic rather than a radical mechanism, with protons serving as an inhibitor by scavenging the photogenerated initiating species and/or reactive anionic sites on growing polymer chains. We propose that photoinduced charge transfer within the metallocene-CA complex leads to the species responsible for initiating CA polymerization. By analogy to the behavior described in eq. 3, irradiation into the CTTS absorption band of this complex (Figures 2) should produce the ferricenium cation and CA radical anion (eq. 4). Attack of the latter species on the monomer then initiates polymerization (eq. 5). Consistent with this charge transfer mechanism, we find that irradiating FeCp_2 in neat CA results in the appearance of the characteristic 617-nm absorption band of FeCp_2^+ (12).



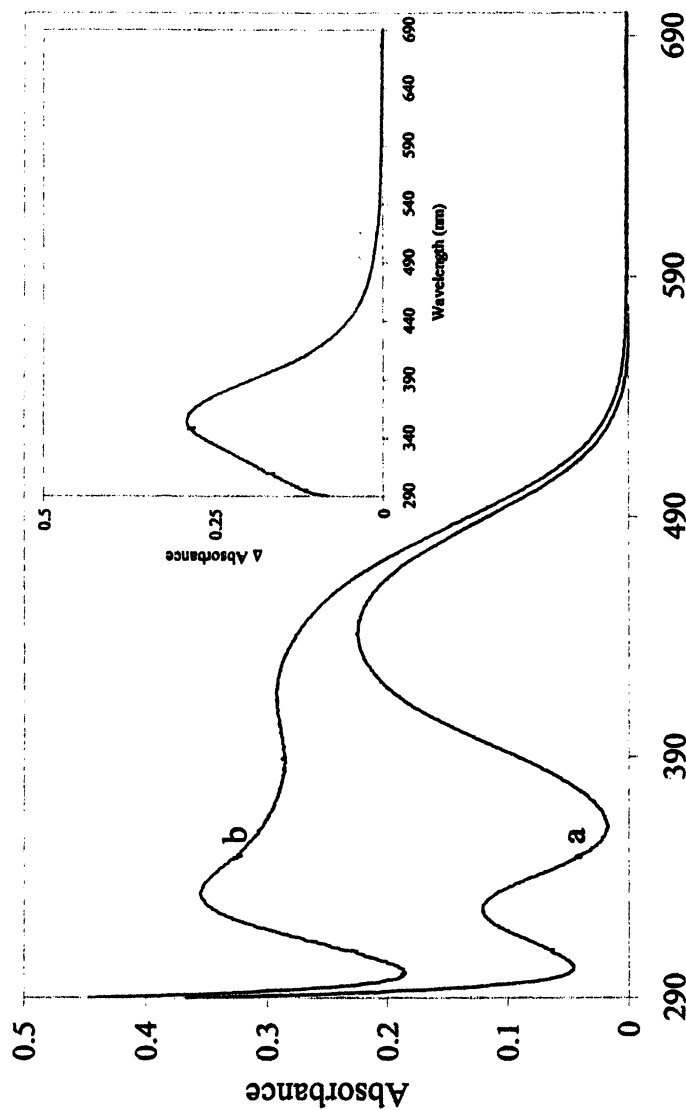


Figure 2. Electronic absorption spectrum of 25 mM ferrocene: (a) in pure THF; (b) in a 2:3 (v:v) mixture of CA and THF. Inset shows the difference spectrum of (a) and (b).

Real-time monitoring of photoinitiated polymerization in CA samples containing FeCp_2 was accomplished with rapid scan Fourier transform infrared spectroscopy. Representative data in Figure 3 reveal that the reaction (plot b) exhibits an induction period, then accelerates rapidly, and finally approaches a plateau at $\sim 90\%$ conversion. We attribute the induction period to the presence in the commercial monomer of 5-10 ppm of strong acid, which serves as a scavenger for adventitious traces of basic impurities. Polymerization is inhibited until sufficient anionic species are photochemically generated to consume this acid, whereupon rapid consumption of monomer commences. As expected, the addition of extra acid to a sample lengthens the induction period and slows the ensuing polymerization process (plot c).

Precedent exists for the involvement of a photosensitive donor-acceptor complex in the generation of an initiator for anionic polymerization (15). In this earlier work, the solvent served as the donor and was present in considerable molar excess over the acceptor monomer. In contrast, our results demonstrate that very low (millimolar) concentrations of FeCp_2 are sufficient for the photoinitiated polymerization of neat CA. The latter type of system is particularly attractive for the increasing number of applications in the coatings, adhesives, and reprographic industries that require solvent-free photosensitive formulations.

B. Benzoyl-Substituted Ferrocenes

Dramatic changes in spectral and photochemical properties result from substituting a benzoyl group for a hydrogen atom on each cyclopentadienyl ring of ferrocene (structure B in Figure 1) (16). As seen in Figure 4, higher intensity bands that extend farther out into the visible region replace the weak ligand field bands appearing in the electronic absorption spectrum of the parent compound. These intense bands arise from transitions to excited states containing appreciable metal-to-ligand charge transfer character. We can represent this MLCT contribution by a resonance structure of the type shown in Figure 5, where the formal charges on iron and oxygen signify a shift of electron density from the metal to the ligand. Conjugation between the π orbitals of the cyclopentadienyl ring and the adjacent carbonyl group allows the transferred charge to be spread over several atoms. Charge delocalization stabilizes the resulting excited states and lowers transition energies (17). Moreover, the mixing of charge transfer character into the transitions relaxes the Laporte selection rule and increases band intensities.

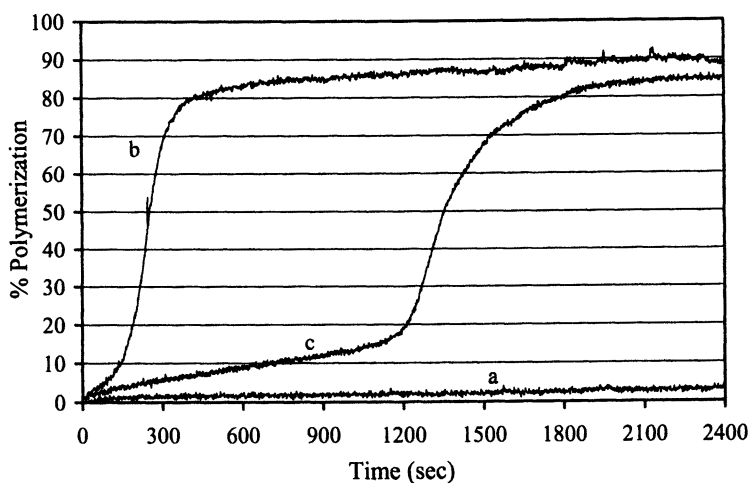


Figure 3. Plots of percentage polymerization vs. time for samples of CA containing 10 mM ferrocene: (a) unirradiated, (b) irradiated, no acid added, (c) irradiated, 150 ppm of methanesulfonic acid added. Samples (b) and (c) were irradiated with 110 mW/cm² of polychromatic light from a 200-W high-pressure mercury lamp.

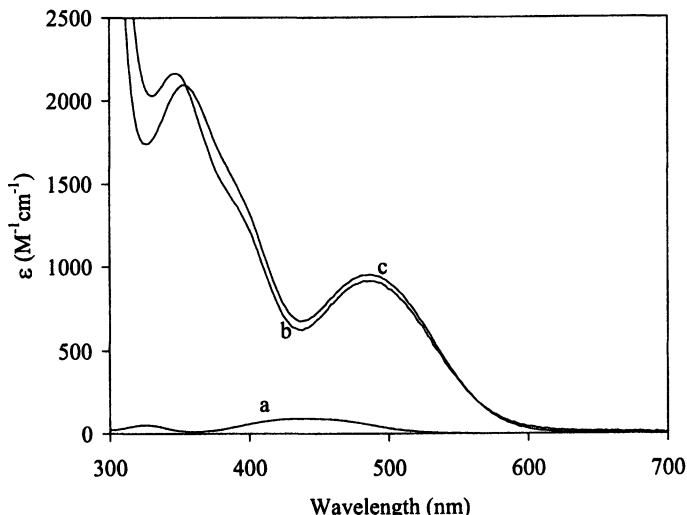


Figure 4. Electronic absorption spectra in room-temperature methanol: (a) ferrocene, (b) 1,1'-bis(*o*-chlorobenzoyl)ferrocene, (c) 1,1'-dibenzoylferrocene.

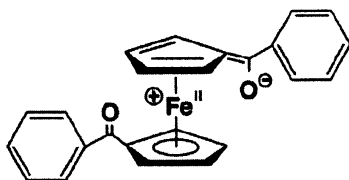


Figure 5. Resonance structure representing the charge transfer character that results from conjugation between the cyclopentadienide ring and the carbonyl group of electronically-excited 1,1'-dibenzoylferrocene. The oxidation state of the metal is indicated by a Roman numeral, while formal charges on atoms are circled.

While ferrocene is photoinert in methanol, 1,1'-dibenzoylferrocene readily undergoes heterolytic metal-ring bond cleavage in this solvent to yield the benzoyl-substituted cyclopentadienide ion and the corresponding half-sandwich cationic complex (eq. 6; S is solvent) (16). This change in photochemical behavior reflects the MLCT character of the low-energy excited states of the benzoyl-containing derivative. Referring again to the resonance structure in Figure 5, we note that these states possess reduced hapticity ($\eta^5 \rightarrow \eta^4$) of a

cyclopentadienyl ring and enhanced susceptibility of the metal center to nucleophilic attack. The first factor weakens ring-metal bonding, while the second assists the formation of bonds to incoming ligands. Collectively, the two factors facilitate the substitution of a cyclopentadienide ligand by the surrounding solvent. Disappearance quantum yield data summarized in Table I reveal that 1,1'-dibenzoylferrocene and several analogues containing substituents on the phenyl ring undergo this process very efficiently. Interestingly, the substituents exert relatively little influence on the quantum efficiency.

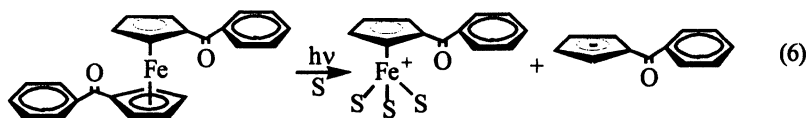
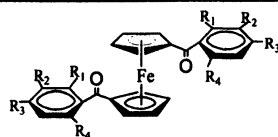


Table I. Photochemical Quantum Yields for the Disappearance of Several 1,1'-Dibenzoyl-ferrocenes (from ref. 16)

Compound ^a	$\phi^{b,c}$
$R_1 = R_2 = R_3 = R_4 = H$	0.45
$R_1 = CH_3; R_2 = R_3 = R_4 = H$	0.41 ± 0.02
$R_1 = R_3 = R_4 = H; R_2 = CH_3$	0.41 ± 0.02
$R_1 = R_3 = R_4 = CH_3; R_2 = H$	0.34 ± 0.00
$R_1 = Cl; R_2 = R_3 = R_4 = H$	0.41 ± 0.01
$R_1 = F; R_2 = R_3 = R_4 = H$	0.47 ± 0.02

^aGeneral structure:



^bExperimental conditions: excitation wavelength, 546 nm; temperature, 22 ± 0.1 °C; solvent is methanol.

^cQuantum yield for disappearance of starting compound; where quoted, error limits denote mean deviation of two or more runs.

Given this efficient photochemical route for generating anions, we decided to test 1,1'-dibenzoylferrocene as a photoinitiator for the polymerization of CA (18,19). The substituted metallocene dissolves readily in the neat monomer to

yield solutions that polymerize rapidly upon exposure to light. Inhibition by strong acid indicates that polymerization proceeds by an anionic mechanism. We have identified the active initiating species as the benzoyl-substituted cyclopentadienide ion that results from photoinduced metal-ring bond cleavage (eq. 6). Kinetic data in Figure 6 demonstrate the effectiveness of 1,1'-dibenzoylferrocene as a photoinitiator even at ppm levels. The trend toward faster polymerization rates at higher photoinitiator concentrations results from the greater fraction of light absorbed by the sample and the corresponding increase in the concentration of the photogenerated anion.

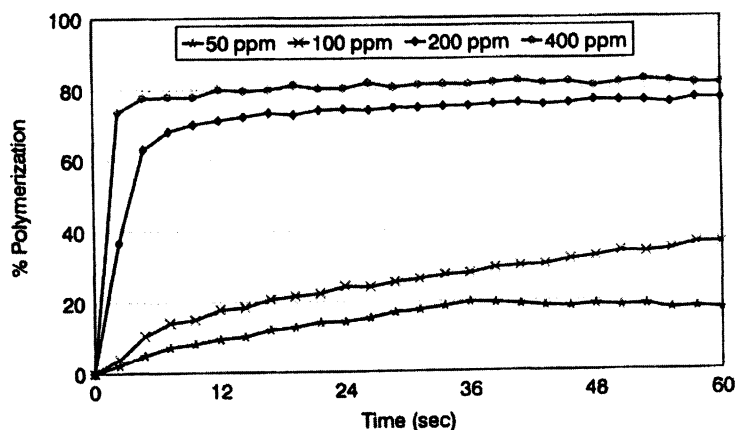


Figure 6. Plots of percentage polymerization vs. time of irradiation for samples of CA containing the indicated amounts of 1,1'-dibenzoylferrocene (400 ppm = 1.1×10^{-3} M). Samples were irradiated with an unfiltered 100-W high-pressure mercury lamp having a power of 27 mW/cm^2 at 366 nm.

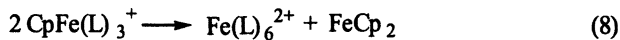
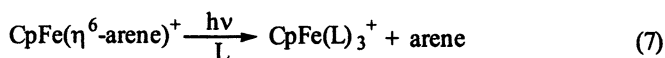
While substituents on the phenyl ring of the benzoyl group have little effect on the quantum efficiency of anion release (Table I), they can dramatically alter the thermal stability of photoinitiator/monomer solutions (19). We discovered that electron-withdrawing *ortho* substituents produce a particularly salutary effect on solution shelf-life (defined as the time required for a sample to undergo a visually noticeable change in viscosity when stored in the dark at room temperature). For example, a CA solution containing 1,1'-bis(*o*-chlorobenzoyl)ferrocene exhibits a much longer shelf-life (86 vs. 16 days) than a comparable sample containing 1,1'-dibenzoylferrocene. In a key experiment, we compared the photosensitivities of two CA solutions containing the former photoinitiator. One solution was irradiated immediately after preparation, while the other was stored for 64 days prior to photolysis. The nearly identical

photosensitivities of the two samples demonstrate that long-term storage does not adversely affect photoinitiator performance. It is thus possible to design photopolymerizable formulations that combine high light-sensitivity and long shelf-life.

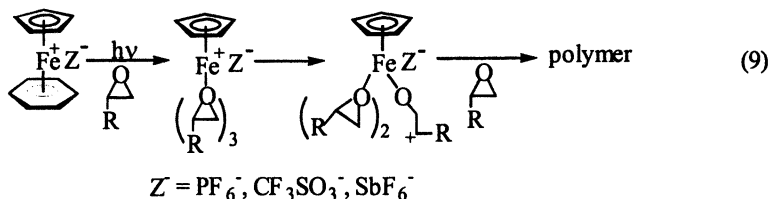
IV. Photoinitiated Cationic Polymerization

A. $[\text{CpFe}(\eta^6\text{-arene})]^+$ Complexes

Replacing one cyclopentadienyl group in ferrocene with an arene molecule yields cationic complexes of general formula $[\text{CpFe}(\eta^6\text{-arene})]^+$ (structure C in Figure 1). Photoexcitation of these mixed-ring sandwich compounds to a ligand field excited state causes efficient photodissociation of the arene to produce $[\text{CpFe}(\text{L})_3]^+$ (eq. 7), where L can be solvent or any Lewis base present in solution (20-23). When L is weakly coordinating, the primary photoproduct is unstable and decomposes in a secondary thermal reaction to yield the dipositive iron cation and ferrocene (eq. 8). Practical interest in the $[\text{CpFe}(\eta^6\text{-arene})]^+$



family centers upon their use as panchromatic photoinitiators for the polymerization of epoxides (24,25) and other monomers (26,27). Despite several mechanistic studies, the identity of the photogenerated species responsible for initiating polymerization remains open to question. Most workers have assigned this role to $[\text{CpFe}(\text{monomer})_3]^+$ (eq. 9, depicted for an epoxide monomer), but neither it nor any polymeric products containing the CpFe^+ unit have been detected. Accordingly, we set out to identify the active initiator(s) formed upon irradiating $[\text{CpFe}(\text{bz})\text{PF}_6]$ (bz is $\eta^6\text{-benzene}$) in the presence of an epoxide, and to monitor the first steps in the ensuing polymerization process.



Because polymerization occurs rapidly in solution, we required a technique that would allow us to trap short-lived photogenerated intermediates and their initially formed products with the monomer. Electrospray ionization mass spectrometry (ESI-MS) has proven to be ideally suited for this task. This soft ionization technique facilitates the transfer of ions from solution to the gas phase with little fragmentation, thus simplifying interpretation of the mass spectrum (28,29). ESI-MS also offers the possibility of trapping and identifying short-lived intermediates, since bimolecular processes involving ionic species in solution are greatly attenuated when the ions pass into the gas phase (30). In our experiments, solutions containing $[\text{CpFebz}]^+$ were irradiated directly in the nanospray tip of the ESI source by an optical fiber that delivered 488-nm light from an argon ion laser (31). The distance, D , between the midpoint of the irradiated zone and the tip end, could be varied by adjusting the position of the fiber with a precision translation stage. With $D = 1.7$ mm and flow rates of 20–80 $\mu\text{L}/\text{h}$, photoproducts required <100 ms to arrive at the tip end for spraying.

Photolysis of $[\text{CpFebz}]^+$ in acetonitrile (AN) solutions containing 0–400 mM cyclohexene oxide (CHO) yielded several series of ionic photoproducts (Figure 7). The major iron-containing products at low CHO concentrations are $[\text{CpFe}(\text{AN})_{1-3}]^+$ and $[\text{Fe}(\text{AN})_{3-6}]^{2+}$. The first series reflects the photodissociation of benzene from the metal center (eq. 7), while the second series arises from the subsequent thermal loss of the cyclopentadienide anion (eq. 8). The coordinatively-unsaturated species observed within each series (e.g. five-coordinate $[\text{CpFe}(\text{AN})_2]^+$ and four-coordinate $[\text{Fe}(\text{AN})_4]^{2+}$) most likely

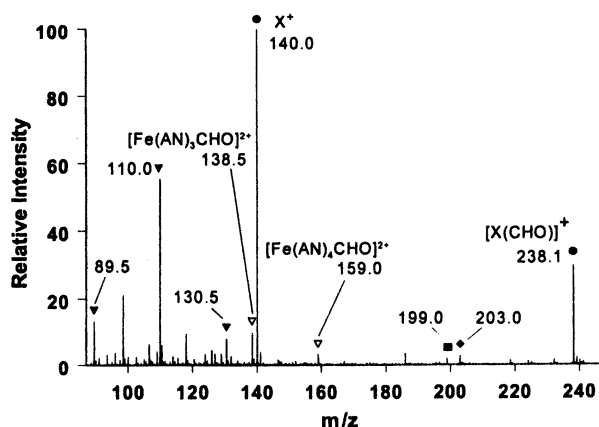


Figure 7. ESI mass spectrum of the products obtained upon irradiating an acetonitrile (AN) solution containing 400 μM $[\text{CpFebz}]^+$ and 400 mM cyclohexene oxide (CHO); $D = 2$ mm.

resulted from collisionally-induced dissociation of AN from $[\text{CpFe}(\text{AN})_3]^+$ and $[\text{Fe}(\text{AN})_6]^{2+}$. High CHO concentrations led to the increased production of $[\text{Fe}(\text{AN})_3(\text{CHO})]^{2+}$ and $[\text{Fe}(\text{AN})_4(\text{CHO})]^{2+}$, but no products containing more than one epoxide molecule were detected in our experiments. The latter result indicates that the poorly coordinating epoxide molecule does not compete effectively with AN for binding sites about Fe(II). Another product, X^+ ($m/z = 140$), has not yet been identified, but an analysis of isotope patterns has established that it does not contain iron. At high CHO concentrations, a species corresponding to $[\text{X}(\text{CHO})]^+$ appeared.

Irradiating $[\text{CpFebz}]^+$ and CHO in the poorly coordinating solvent, 1,2-dichloroethane (DCE), yielded a rich assortment of new products. With $D \geq 1.7$ mm, we observed two main series: $[(\text{H}_2\text{O})\text{Fe}(\text{CHO})_{4-12}]^{2+}$ and $[\text{X}(\text{CHO})_{0-5}]^+$ (Figure 8). A third series, $[(\text{H}_2\text{O})\text{CpFe}(\text{CHO})_{1-4}]^+$ (inset to Figure 8), appeared with $D < 0.5$ mm. This behavior indicates that $[(\text{H}_2\text{O})\text{CpFe}(\text{CHO})_n]^+$ possesses a short lifetime (< 50 ms) in solution and only can be observed when generated near the tip end. The water present in the Fe-containing products most likely originated from traces of moisture introduced to the rigorously dried solvent

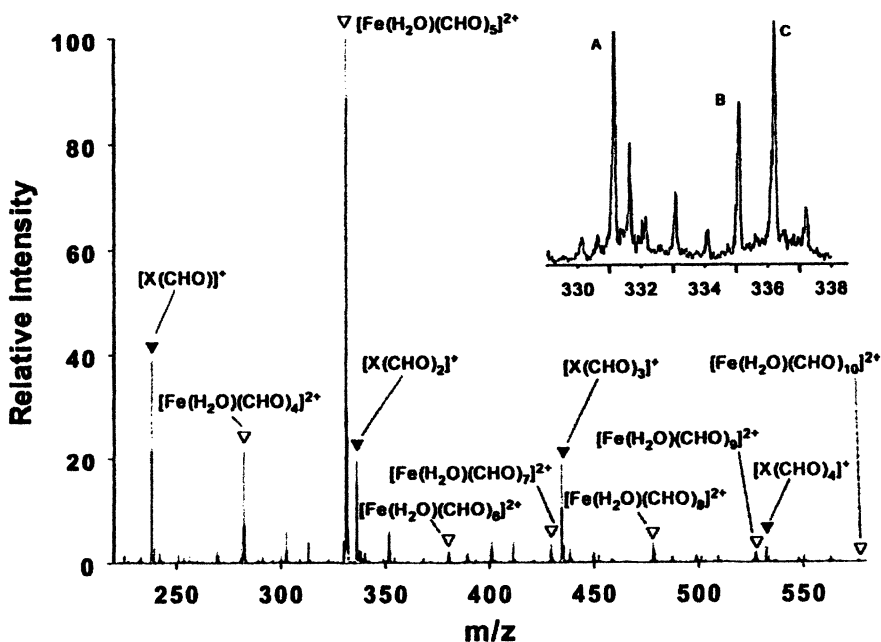
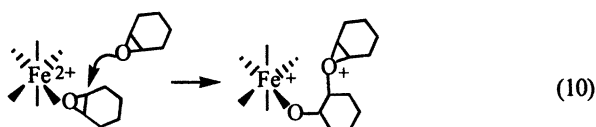


Figure 8. ESI mass spectrum of the products obtained upon irradiating a 1,2-dichloroethane solution containing $60 \mu\text{M}$ $[\text{CpFebz}]^+$ and 70 mM cyclohexene oxide (CHO); $D = 5.8$ mm. Inset: representative members of three product series observed with $D \approx 0.5$ mm: A = $[(\text{H}_2\text{O})\text{Fe}(\text{CHO})_6]^{2+}$, B = $[(\text{H}_2\text{O})\text{CpFe}(\text{CHO})_2]^+$, C = $[\text{X}(\text{CHO})_2]^+$.

during sample preparation and/or present in the ambient atmosphere at the electrospray tip exit. Signals corresponding to the water-free products, $[\text{Fe}(\text{CHO})_{5-8}]^{2+}$ and $[\text{CpFe}(\text{CHO})_{1-5}]^+$ also appeared in the mass spectrum, but with diminished intensities.

Coordination of CHO to a dicationic iron center activates the monomer to nucleophilic attack by the oxygen atom of an uncoordinated CHO molecule (eq. 10). The ensuing C-O bond formation opens the strained three-membered ring and creates another cationic site for continued chain growth. According to this model, which accommodates all of our experimental observations, products such as $[(\text{H}_2\text{O})\text{Fe}(\text{CHO})_{12}]^{2+}$, $[\text{Fe}(\text{CHO})_8]^{2+}$ and $[\text{CpFe}(\text{CHO})_5]^+$ contain a growing polymer chain bound directly to the metal center. The observation that X^+ forms products containing up to five CHO units also is consistent with the polymer-growth model, and we tentatively propose that this non-iron species is an active initiator for epoxide polymerization.



Our results demonstrate the power of the ESI-MS technique for investigating the mechanism of photoinitiated ionic polymerization in solution. By analyzing the sample solution at short times following photolysis, we have detected several cationic species capable of initiating epoxide polymerization. Moreover, we have observed the first few steps in the growth of the polymer chain. Since the ESI-MS technique can be operated in either the positive or negative ion mode, it should be possible to extend the type of detailed mechanistic study reported here to systems undergoing photoinitiated anionic polymerization.

B. $[\text{Fe}(\eta^6\text{-arene})_2]^{2+}$ Complexes

Replacing the Cp ring in $[\text{CpFe}(\eta^6\text{-arene})]^+$ by an arene yields a member of the $[\text{Fe}(\eta^6\text{-arene})_2]^{2+}$ family (structure D in Figure 1; note that the two arenes need not be identical). We were intrigued by reports that these dicationic metallocenes undergo photoinduced loss of both arene ligands. For example, a good electron donor such as ferrocene forms a 1:1 charge-transfer complex with $[\text{Fe}(\eta^6\text{-arene})_2]^{2+}$ in acetonitrile solution (32). Irradiation of this complex induces a redox reaction that initially yields the substitutionally labile Fe(I) species, $[\text{Fe}(\eta^6\text{-arene})_2]^+$ (eq. 11). Rapid loss of both arenes from the metal, followed by back electron transfer to regenerate Fe(II), leads to the observed products. Arene deligation also can occur by a non-redox pathway following direct irradiation of $[\text{Fe}(\eta^6\text{-arene})_2]^{2+}$ (eq. 12) (32). Given our interest in photochemical sources of cationic initiating species, we undertook a detailed study of the spectroscopy, photochemistry, and photoinitiation behavior of one

member of the bis(arene) family, $[\text{Fe}(\text{mes})_2]^{2+}$, where mes is η^6 -mesitylene (1,3,5-trimethylbenzene) (33, 34).

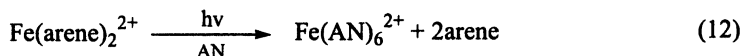
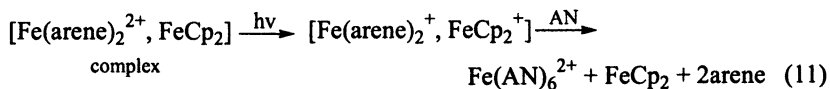


Figure 9 shows the electronic absorption spectrum of $[\text{Fe}(\text{mes})_2]^{2+}$ in acetonitrile solution at room temperature. Low-intensity bands above 320 nm are assigned as ligand field transitions by analogy to the spectrum of ferrocene (13,14). The more intense band at 303 nm arises from a mes \rightarrow Fe charge transfer transition. This LMCT assignment is supported by the observation that replacing mesitylene by the better electron donor hexamethylbenzene lowers the energy of this transition. The very intense band near 250 nm results from a π - π^* transition localized on the mesitylene ligand, although the possibility exists that it may contain some charge transfer character.

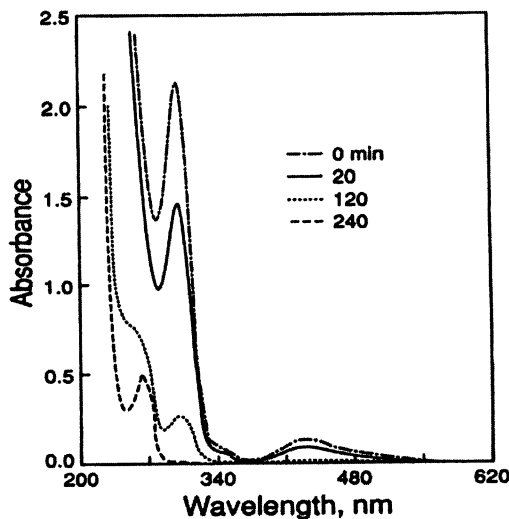


Figure 9. Spectral changes resulting from the 438-nm photolysis of $1.2 \times 10^{-3} \text{ M } [\text{Fe}(\text{mes})_2]^{2+}$ in acetonitrile. Irradiation times are indicated. (Reproduced with permission from reference 34. Copyright 1994 Wiley.)

Figure 9 also depicts the spectral changes that result from the 438-nm photolysis of $[\text{Fe}(\text{mes})_2]^{2+}$ in acetonitrile. The steady bleaching of the absorbance of the metallocene is accompanied by the appearance of a band at 266 nm attributable to free mesitylene and a very weak band at ~ 900 nm due to solvated Fe^{2+} . Quantitative analysis of the photolyte establishes that these photoproducts are formed in a 2:1 stoichiometric ratio, thus confirming that the net photoreaction is substitution of both arene ligands by solvent (eq. 12). Similar results are obtained for photolyses performed at 313 and 254 nm, indicating that arene deligation is a general pathway independent of the type of excited state (ligand field, charge transfer, or $\pi\text{-}\pi^*$) initially populated. Quantum yield data summarized in Table II demonstrate that arene deligation occurs with high efficiency under a variety of experimental conditions. This process is independent of the initial metallocene concentration, oxygen concentration, and the presence of excess counterion.

Table II. Photochemical Quantum Yields for Disappearance of $\text{Fe}(\text{mes})_2^{2+}$ (from ref. 33).

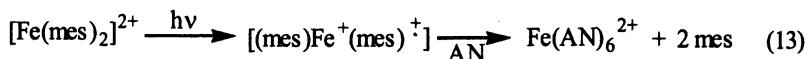
λ_{excit} (nm)	$[\text{Fe}(\text{mes})_2^{2+}]$ (M)	Ar purged	ϕ^a
438	9.51×10^{-4}	Yes	0.97 ± 0.04
	6.02×10^{-3}	Yes	0.90 ± 0.02
	4.80×10^{-4}	No	0.98 ± 0.05
313	1.72×10^{-3}	Yes	0.76 ± 0.02
	$1.88 \times 10^{-3}{}^b$	Yes	0.74 ± 0.01
254	3.15×10^{-4}	Yes	0.72 ± 0.04
	1.96×10^{-3}	Yes	0.64 ± 0.06

^aQuantum yield for disappearance of $\text{Fe}(\text{mes})_2^{2+}$; error limits represent deviation from the mean. Irradiations performed at $20 \pm 1^\circ\text{C}$ in acetonitrile.

^bSolution contains 4×10^{-3} M NH_4PF_6 .

The photochemistry of $[\text{Fe}(\text{mes})_2]^{2+}$ can be explained in terms of the simple structure-reactivity concepts discussed in section II. Irradiation of the metallocene at 438 nm populates a ligand field excited state that, because of weakened metal-ring bonding relative to the ground state, undergoes facile substitution of arene by solvent (eq. 12). Photoexcitation at 313 nm produces a $\text{mes} \rightarrow \text{Fe}$ charge transfer state that can be viewed, in a formal sense, as an

iron(I) center bound to a neutral mesitylene and a mesitylene radical cation. This high-energy species should undergo rapid arene loss and back-electron transfer to yield the observed products (eq. 13) (32). Our results do not establish the nature of the primary photochemical reaction resulting from 254-nm excitation. One possibility is that the initially populated π - π^* excited state relaxes to the mes \rightarrow Fe charge transfer state, which then undergoes the redox-mediated deligation process just described (eq. 13).



Exploratory experiments were conducted to test the behavior of $[\text{Fe}(\text{mes})_2]^{2+}$ as a photoinitiator for the crosslinking of an epoxide-functionalized polymer (34). Even relatively mild processing conditions insolubilized a nonirradiated polymer film containing the metallocene. This result presumably arises from the decomposition of the metallocene with the accompanying formation of an active crosslinking agent. Thus, despite its high photosensitivity, the poor thermal stability of $[\text{Fe}(\text{mes})_2]^{2+}$ precludes its use as a practical photoinitiator. Because methylation of the arene ring generally enhances the stability of $[\text{Fe}(\eta^6\text{-arene})_2]^{2+}$ compounds, it may be possible to ameliorate this problem by replacing mesitylene with durene (1,2,4,5-tetramethylbenzene).

V. Prospectus

Table III summarizes the photochemical behavior of the iron(II) metallocenes considered in this chapter. The profound changes that result from varying the structure of the metallocene can be attributed to the different excited states involved. When dissolved in a good electron-accepting medium such as ethyl α -cyanoacrylate, ferrocene undergoes photooxidation from a CTTS excited state to produce the ferricenium cation and the CA radical anion (eq. 4). Attack of the latter species on the monomer then initiates anionic polymerization. Placing an electron-withdrawing benzoyl group on each Cp ring introduces MLCT character into the low-energy excited states of the resulting 1,1'-dibenzoylferrocene. These states favor heterolytic ring-metal bond cleavage that liberates a benzoyl-substituted cyclopentadienide (eq. 6) capable of initiating anionic polymerization. Replacing one or both Cp rings by an arene yields cationic metallocenes. Populating the ligand field and/or LMCT excited states in these compounds leads to arene dissociation (eq. 7, 12, and 13). The metal-containing photoproducts are good Lewis acids that can initiate polymerization via a cationic pathway.

Table III. Summary of Iron(II) Metallocene Photochemistry

<i>Metallocene</i>	<i>Solvent^a</i>	<i>Excited State^b</i>	<i>Major Photoreaction</i>
ferrocene	CA	CTTS	photooxidation of metallocene
1,1'-dibenzoyl-ferrocene	CA	MLCT	dissociation of benzoyl-substituted cyclopentadienide
CpFe(η^6 -arene) ⁺	CH ₃ CN	LF	dissociation of arene
Fe(η^6 -arene) ₂ ²⁺	CH ₃ CN	LF/LMCT	dissociation of arene

^aCA is ethyl α -cyanoacrylate.

^bPhotoactive excited state: CTTS is charge-transfer-to-solvent; MLCT is metal-to-ligand charge transfer; LF is ligand field; LMCT is ligand-to-metal charge transfer.

Iron(II) metallocenes constitute a versatile class of photoinitiators for ionic polymerization reactions. These organometallic compounds dissolve in a broad selection of nonaqueous solvents (including neat monomer), can be tailored to possess good thermal stability in solution, and absorb strongly in the ultraviolet and visible wavelength regions. Ease of synthesis, modest cost, and low environmental impact are other attractive features. We plan additional studies of these metallocenes with the aims of expanding fundamental knowledge of their spectroscopy and photochemistry, and exploiting their desirable properties in the design of new photosensitive materials.

Acknowledgments

We thank Dr. D. Billy Yang, Dr. Bentley J. Palmer, Dr. Keith A. Johnson, Alan Morgan, Michael Murphy, and Professor Richard A. Dluhy for technical assistance. Financial support for this work was received from the National Science Foundation, JSR Corporation, and the University of Georgia Research Foundation.

References

1. Reichmanis, E.; Houlihan, F. M.; Nalamasu, O.; Neenan, T. X. *Chem. Mater.* **1991**, *3*, 394.
2. Yang, D. B.; Kutal, C. In *Radiation Curing: Science and Technology*; Pappas, S. P., Ed.; Plenum: New York, 1992; Chap. 2.
3. Monroe, B. M. *Chem. Rev.* **1993**, *93*, 435.
4. Davidson, R. S. *J. Photochem. Photobiol A: Chem.* **1993**, *73*, 81.

5. Roloff, A. In *Photosensitive Metal-Organic Systems*; Kutal, C.; Serpone, N., Eds.; American Chemical Society: Washington, DC, 1993; Chap 20.
6. Hendrickson, W. A.; Palazzotto, M. C. In *Photosensitive Metal-Organic Systems*; Kutal, C.; Serpone, N., Eds.; American Chemical Society: Washington, DC, 1993; Chap 21.
7. Kutal, C. *Coord. Chem. Rev.* **2001**, 211, 353.
8. Balzani, V.; Carassiti, V. *Photochemistry of Coordination Compounds*; Academic Press: New York, 1970; Chap. 5.
9. Geoffroy, G. L.; Wrighton, M. S. *Organometallic Photochemistry*; Academic Press: New York, 1979, Chap. 5.
10. Traverso, O.; Scandola, F. *Inorg. Chim. Acta* **1970**, 4, 493.
11. Tsubakiyama, K.; Fujisaki, S. *J. Polym. Sci.* **1972**, B10, 341.
12. Sanderson, C. T.; Palmer, B. J.; Morgan, A.; Murphy, M.; Mize, T.; Dluhy, R. A.; Amster, I. J. Kutal, C. submitted for publication.
13. Warren, K. D. *Struct. Bonding (Berlin)* **1976**, 27, 45.
14. Clack, D. W.; Warren, K. D. *Struct. Bonding (Berlin)* **1980**, 39, 1.
15. Irie, M.; Tomimoto, S.; Hayashi, K. *Polym. Lett.* **1972**, 10, 699.
16. Yamaguchi, Y.; Kutal, C. *Inorg. Chem.* **1999**, 38, 4861.
17. Treadway, J. A.; Loeb, B.; Lopez, R.; Anderson, P. A.; Keene, F. R.; Meyer, T. J. *Inorg. Chem.* **1996**, 35, 2242.
18. Yamaguchi, Y.; Palmer, B. J.; Kutal, C.; Wakamatsu, T.; Yang, D. B. *Macromolecules* **1998**, 31, 5515.
19. Yamaguchi, Y.; Kutal, C. *Macromolecules* **2000**, 33, 1152.
20. Gill, T. P.; Mann, K. R. *Inorg. Chem.* **1983**, 22, 1986.
21. McNair, A. M.; Schrenk, J. L.; Mann, K. R. *Inorg. Chem.* **1984**, 23, 2633.
22. Chrisope, D. R.; Park, K. M.; Schuster, G. B. *J. Am. Chem. Soc.* **1989**, 111, 6195.
23. Rabubek, V.; Lees, A. J. *Inorg. Chem.* **2000**, 39, 5779.
24. Roloff, A.; Meier, K.; Reideker, M. *Pure Appl. Chem.* **1986**, 58, 1267.
25. Lohse, F.; Zweifel, H. *Adv. Polym. Sci.* **1986**, 78, 61.
26. Rabek, J. F.; Lucki, J.; Zuber, M.; Qu, B. J.; Shi, W. F. *J. Macromol. Sci. Appl. Chem.* **1992**, A29, 297.
27. Kotch, T. G.; Lees, A. J.; Fuerniss, S. J.; Papatthomas, K. I. *Chem. Mater.* **1995**, 7, 801.
28. Bakhtiar, R.; Hop, C. E. C. A. *J. Phys. Org. Chem.* **1999**, 12, 511.
29. Griffiths, W. J.; Jonsson, A. P.; Liu, S.; Rai, D. K.; Wang, Y. *Biochem. J.* **2001**, 355, 545.
30. Arakawa, R.; Mimura, S.; Matsubayashi, G.; Matsuo, T. *Inorg. Chem.* **1996**, 35, 5725.
31. Ding, W.; Johnson, K. A.; Amster, I. J.; Kutal, C. *Inorg. Chem.* **2001**, 40, 6865.
32. Lehmann, R. E.; Kochi, J. K. *J. Am. Chem. Soc.* **1991**, 113, 501.
33. Gamble, G.; Grutsch, P. A.; Ferraudi, G.; Kutal, C. *Inorg. Chim. Acta* **1996**, 247, 5.
34. Gamble, G.; Kutal, C. *Polym. Adv. Technol.* **1994**, 5, 63.

Chapter 30

Quaternary Ammonium *N,N*-Dimethyldithiocarbamates as Photobase Generators

Masahiro Tsunooka, Hideki Tachi, Takayuki Yamamoto, and Masamitsu Shirai

Department of Applied Chemistry, Graduate School of Engineering,
Osaka Prefecture University, 1-1 Gakuen-cho, Sakai,
Osaka 599-8531, Japan

Photo-chemical behavior of quaternary ammonium dithiocarbamates (QA salts) as photobase generators (PBGs) and photo-initiated thermal insolubilization of epoxides with the QA salts were investigated. Stability of QA salts in various solutions was also examined. They were stable in acetonitrile, DMF, DMSO and aq. alkaline solution, though their structure affected their stability. QA salts acted as effective photo-initiated thermal crosslinker for poly(glycidyl methacrylate). 4-Chlorothioxanthone, phenanthrene, and benzophenone were found to be sensitizers for the photolysis of QA salts.

Recently, photobase generators (PBGs) which generate basic compounds such as amines upon UV irradiation have become very attractive compounds similar to well accepted photoacid generators (PAGs) in the fields of UV curing and microlithography (1,2). The papers on PBGs are, however, very few compared with those on PAGs (3-7).

Tertiary amines are much stronger bases than primary and secondary amines, and photo-generated tertiary amines are expected to be very promising in their use as catalysts in the above fields. Most papers on PBGs, however, are those on photo-generation of primary or secondary amines from them, and only a few papers on PBGs which generate tertiary amines were published. *N,N,N*-

trimethylbenzhydrylammonium iodide (8), quaternary ammonium carboxylic acid and quaternary ammonium borates (9,10) were reported to generate tertiary amines photochemically.

In previous papers (11-15), we have already reported that the quaternary ammonium *N,N*-dimethyldithiocarbamates (QA salts) act as PBGs which produce tertiary amines such as 1,4-diazabicyclo[2,2,2]octane (DABCO) on UV irradiation. They acted effectively as photo-initiated thermal crosslinkers for poly(glycidyl methacrylate) (PGMA). We have also reported that the bifunctional QA salt having *N,N*-dimethyldithiocarbamate anions, which was derived from *N,N,N',N'*-tetramethyl hexamethylenediamine, acted as an effective photo-initiated thermal crosslinker for epoxy compounds (11). Counter anions of QA salts affected their photolysis and the efficiency of photo-induced thermal crosslinking of PGMA also depended on the anions. In these papers, QA salts bearing dithiocarbamate anions derived from DABCO were mainly examined.

In this chapter, we describe effects of *N*-methylpiperidine or DABCO moieties on photolysis of QA salts and their efficiency as photo-initiated thermal crosslinkers for PGMA films. Furthermore, the effects of photo-sensitizers on their photolysis of QA salts were also investigated

EXPERIMENTAL

Material

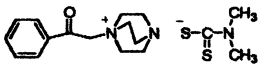
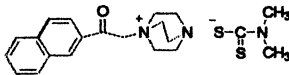
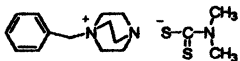
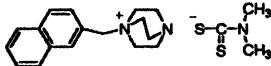
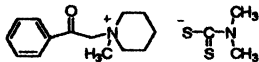
QA salts having dithiocarbamate anions were prepared in a similar manner described in the previous paper (11). That is, QA salts having a bromide anion were prepared by the reaction of phenacylbromide and *N*-methylpiperidine. The anion exchange of the salts was carried out using sodium *N,N*-dimethyldithiocarbamate. Structures and properties of QA salts are summarized in Table 1. Poly(glycidyl methacrylate) (PGMA) ($M_n=104000$, $M_w/M_n=2.04$, $T_g=84.0$ °C) was prepared by solution polymerization of glycidyl methacrylate in benzene using 2,2'-azobisisobutyronitrile as initiator. Benzophenone (Bp), 4-chlorothioxanthone (CTX), phenanthrene (Phn) and anthracene (Ant) were used as sensitizers for photolysis of QA salts after purification.

Instruments

UV spectra were obtained on a Shimadzu UV-2400PC spectrometer. $^1\text{H-NMR}$ spectra were measured on a JEOL GX-270 (270 MHz). Film thickness was determined by two-beam interferometry using a metallurgical microscope (Nikon

OPTIPHOTO XPF-UM), an interference apparatus (Nikon) and a video microscaler (FOR.A IV-550). Thermal gravimetry was conducted on a Rigaku Denki DSC-8230 at a heating rate of 10 °C/min.

Table 1 Structure and Properties of QA Salts

Abbrivation	Structures	m.p. (°C)	Td (°C)*	λ max(ϵ) in acetonitrile
QA salt I		—	125	$\epsilon_{251}=21700$, $\epsilon_{295}=11900$
QA salt II		112	116	$\epsilon_{252}=48300$, $\epsilon_{294}=19100$, $\epsilon_{340}=2200$
QA salt III		131	149	$\epsilon_{256}=15200$, $\epsilon_{296}=16200$
QA salt IV		119	131	$\epsilon_{259}=15800$, $\epsilon_{295}=19600$
QA salt V		—	108	$\epsilon_{251}=25000$, $\epsilon_{295}=14700$

* Measured by TGA

Photo-irradiation method and Photo-initiated thermal insolubilization of PGMA films

The polymer thin films (ca. 0.3 μm or 0.5 μm) with 5 mol % of QA salt were prepared by casting tetrahydrofuran (THF) or chloroform solutions of polymers and salts on a glass plate. UV irradiation was carried out with a low-pressure mercury lamp (Ushio Denki ULO-6DQ, 6W) (light intensity : 1.0 mW/cm^2 at 254 nm) or a medium-pressure mercury lamp (Ushio Denki UM-102, 100W) in air or under N_2 at room temperature. The light at 366 nm from the medium-pressure mercury lamp was selected by the use of glass filter (Toshiba glass, UV-36B). The light intensity was determined by the light illuminometer (ORC UV-M02). If necessary, the irradiated films were followed by baking at a given temperature on a hot plate. After the irradiation or baking, the films were soaked in THF for 10 min at room temperature. The insoluble fraction of irradiated polymer films with QA

salts was calculated from the ratio of the film thickness determined by the interference microscope before and after the soaking.

Analysis of the photo-products of QA salt having N-methylpiperidine moiety by $^1\text{H-NMR}$ spectroscopy

$^1\text{H-NMR}$ spectra were measured in CDCl_3 in a similar manner as described in the previous paper (11). The photolysis of the QA salt was monitored as a decrease at 4.40 ppm due to methylene protons of the QA salt. *N*-methylpiperidine and the *N,N*-dimethyldithiocarbamate derivative as photo-products were detected by the appearance of signals at 2.18 ppm and 4.82 ppm, respectively.

Estimation of half-life of QA salts in solvents

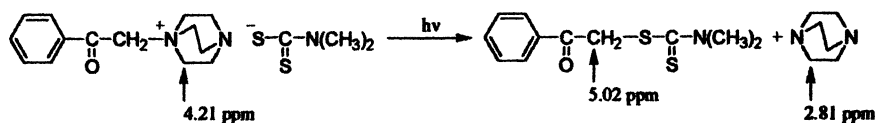
QA salts were dissolved in various solvents such as water, methanol, acetonitrile, DMF, DMSO and chloroform. UV spectra of the solution (1.0×10^{-4} M) were measured after a given time. The half-life of the QA salts was determined by a decrease of absorption band at around 290 nm due to the *N,N*-dimethyldithiocarbamate anions.

RESULTS AND DISCUSSION

Photo-chemical behavior of QA salts

In previous papers (11,12), we have already reported that QA salts I and II acted as PBGs which generate tertiary amines. The formation of basic compounds in the photolysis of QA salt I was ascertained by a color change of Phenol Red from yellow to red. $^1\text{H-NMR}$ spectral changes of QA salt I on UV irradiation showed a decrease in a peak at 4.21 ppm due to QA salts and an increase of peaks at 2.81 ppm due to DABCO and at 5.02 ppm due to phenacyl *N,N*-dimethyldithiocarbamate. These facts show that the photolysis of QA salt I results in the formation of DABCO and phenacyl *N,N*-dimethyldithiocarbamate as shown in the next equation.

QA salts I and II have an unblocked tertiary amino group. However, the effect of the unblocked amino groups on their photolysis was not investigated in the previous paper. Thus, in this chapter, photolysis of QA salt V which was derived from a mono-functional amine was examined.



Analysis of photo-products of QA salt V

Fig. 1 shows $^1\text{H-NMR}$ spectral changes of QA salt V on irradiation at 366 nm under N_2 . A decrease of peak at 4.40 ppm due to methylene protons shows the photolysis of QA salt V, and the peaks at 2.18 ppm due to *N*-methylpiperidine and 4.82 ppm due to *N,N*-dimethyldithiocarbamate derivatives increased with irradiation. The amounts of photolyzed QA salt V and photo-products were calculated from the NMR data. As shown in Table 2, the amounts of the resulting *N*-methylpiperidine and *N,N*-dimethyldithiocarbamate derivatives agreed approximately with the amount of decomposed QA salt V. These facts show that QA salt V quantitatively generated *N*-methylpiperidine and *N,N*-dimethyldithiocarbamate derivatives as photo-products. These results also agreed with those of QA salt I (11), and it can be concluded that the photolysis of these onium salts did not depend on their onium structure.

Table 2. Photolysis of QA Salt V in CDCl_3 and Yields of Photo-Products ^{a)}

Irradiation energy (mJ/cm^2)	Conversion of QA salt V (%)	Photo-Products (%)	
		A ^{b)}	B ^{b)}
1000	40	36	40
2000	74	65	73

a) NMR analysis

b) A : *N*-methylpiperidine,

B : phenacyl *N,N*-dimethyldithiocarbamate

Thermal stability of QA salts and their stability in various solvents

QA salts I-V are thermally stable to 110-150 $^\circ\text{C}$ depending on their structures as shown in Table 1. However, as they were unstable in some solvents, their stability in solvents was investigated. UV spectral changes of QA salt I kept in methanol at room temperature were very similar as those of its photolysis, though the rate was very slow compared with that of its photolysis. The decomposition of QA salt I in chloroform was followed by $^1\text{H-NMR}$. Products were the same as photo-products reported previously (11).

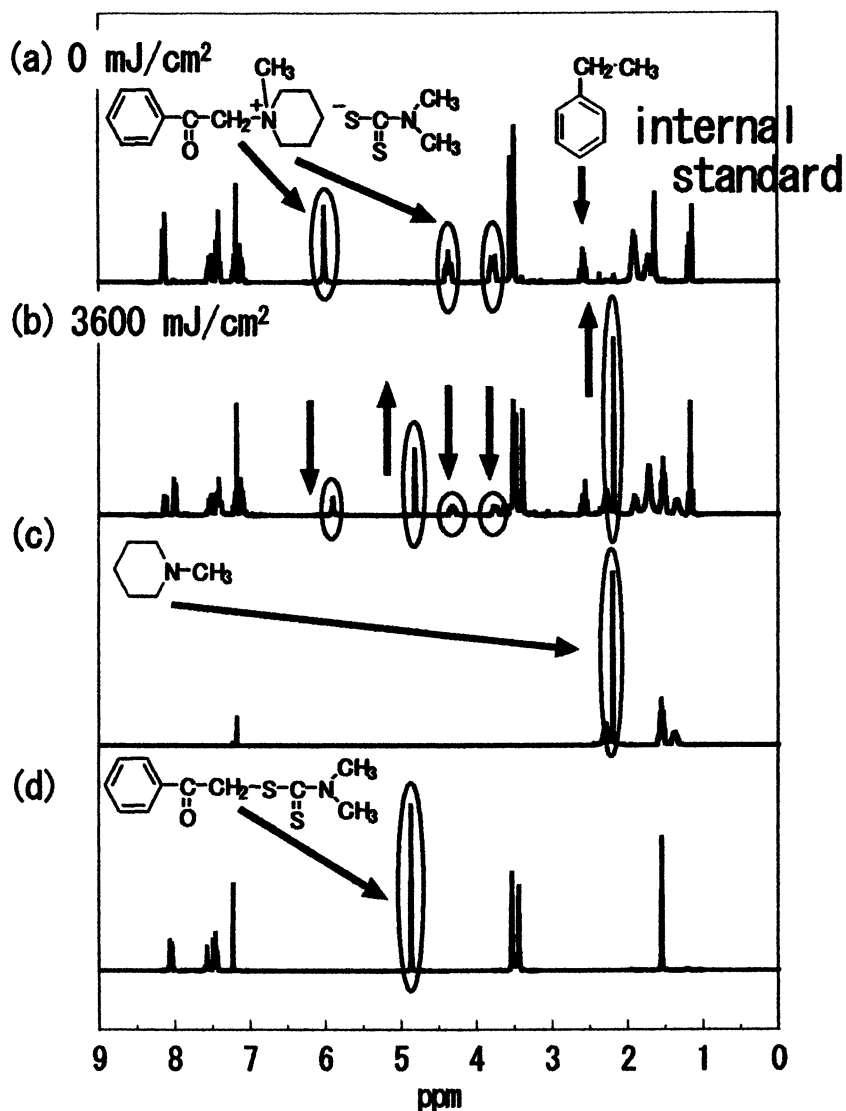


Figure 1. ¹H-NMR spectral changes of QA salt V in CDCl₃. Irradiation at 366 nm under N₂. [QA salt] = 1.88 × 10⁻² (mol/l). (Reproduced with permission from reference 34. Copyright 1994 Wiley.)

Table 3 shows the half-life of QA salts determined from a decrease of the absorption at around 290 nm in various solvents. Although QA salts were stable in polar solvents such as acetonitrile, water, DMF, and DMSO, they were unstable in MeOH and chloroform. In water, they were unstable under pH=7 and the presence of a base such as amines increased their stability. The effect of substituent groups such as phenacyl and benzyl in QA salts on their half-life was also observed. QA salt V derived *N*-methylpiperidine was unstable compared with QA salt I having a DABCO moiety in solution except for DMSO.

Table 3. Half-Life of QA Salts in Solution ^{a)}

	<i>Half-life (hour)</i>					
	<i>water</i>	<i>methanol</i>	<i>acetonitrile</i>	<i>DMF</i>	<i>DMSO</i>	<i>chloroform</i>
QA salt I	39.0	1.4	38.2	22.6	38.7	2.2
QA salt II	4.1	1.2	21.0	14.5	60.8	7.2
QA salt III	12.0	4.2	34.0	— ^{b)}	— ^{b)}	7.2
QA salt IV	22.0	2.1	35.0	— ^{b)}	— ^{b)}	11.0
QA salt V	7.4	2.2	19.3	16.9	49.4	4.1

a) [Salt] = 1.0×10^{-4} (mol/l)

b) no data.

Photo-initiated thermal insolubilization of PGMA films

Photo-initiated thermal insolubilization of PGMA films with 5 mol% of QA salts I-IV was investigated (Table 4). The films with QA salts I and II turned insoluble with only irradiation at 254 nm, but the photo-insolubilization of the films with other QA salts were not observed even at 60 mJ/cm². The degree of insoluble fraction of the irradiated films was increased by post-baking at 80 °C as shown in Table 4. The photolysis rate of QA salt I was faster than that of other QA salts, and the efficiency of photo-initiated thermal insolubilization of PGMA films decreased in the order of QA salt I > QA salt II > QA salt III > QA salt IV. The photolysis of QA salt I was fastest among them. However, not much difference in their photolysis rate except QA salt I was observed. Thus, further studies on the quantitative yields of products in their photolysis are required for an understanding of the crosslinking rate.

The effect of ammonio groups of QA salts on photo-initiated thermal insolubilization of PGMA films was investigated. Fig.2 shows photo-initiated insolubilization of PGMA films with QA salts I or V. The efficiency of photo- and post-thermal insolubilization of PGMA films with QA salt I was higher than that with QA salt V. It is apparent that QA salt I worked more effectively than QA salt V in the insolubilization. As there is no difference in their photolysis rate, the

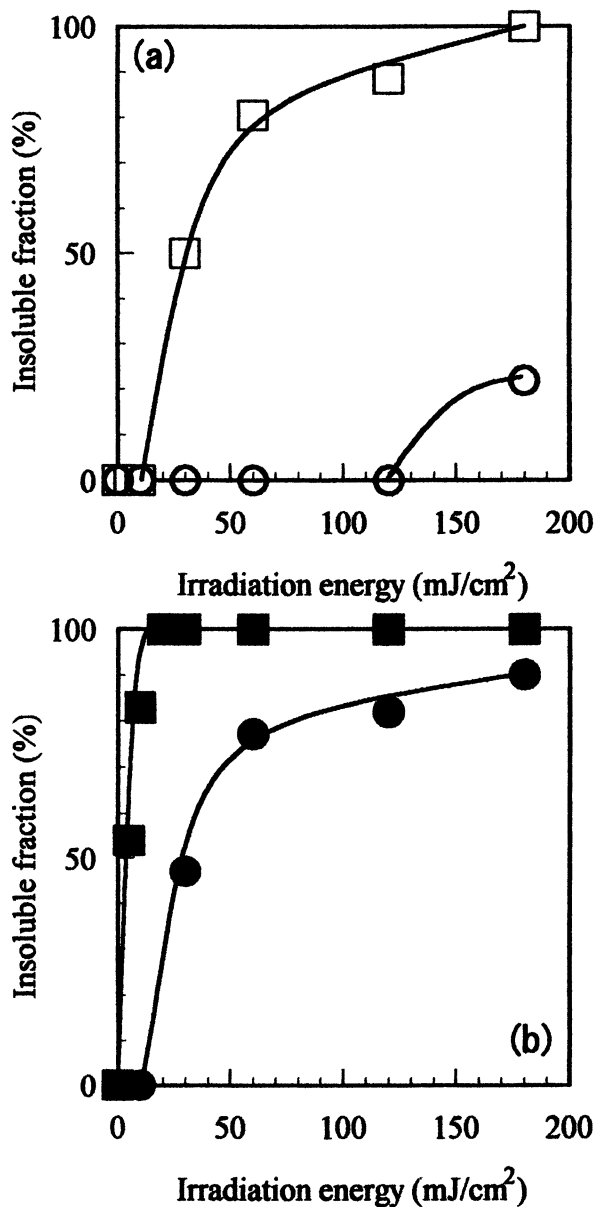


Figure 2. Effect of ammonio groups on (a) photo-insolubilization and (b) post-thermal insolubilization of PGMA films. (□, ■) QA salt I, (○, ●) QA salt V.

above result is thought to be due to the difference in basicity and nucleophilicity of resulting amines. The pKa of *N*-methylpiperidine is 10.1 and that of DABCO 8.7 and 3.0, and this result was not explained by the difference in their basicity. Imidazole is known as a good curing reagent irrespective of its low basicity (pKa=6.92). Thus, bifunctionality of DABCO and two lone pairs on nitrogen without steric hindrance are thought to be more effective for the crosslinking.

Table 4. Photo-Initiated Thermal Insolubilization of PGMA Films with QA Salts

QA salt	Irradiation Energy (mJ/cm ²) at 254 nm	% Insolubilization	
		Only Irradiation	Post-Baking at 80 °C for 5 min
I	30	60	95
	60	60	100
II	30	30	80
	60	35	80
III	30	0	65
	60	0	80
IV	30	0	60
	60	0	70

[Salt] = 5 (mol%).

Effects of sensitizers on the photolysis of QA salts

From the viewpoint of effective use of energy, the efficient use of UV light at 366 nm emitted from the medium-pressure mercury lamp is very attractive. Fig.3 shows the relationship between the photolysis of QA salt I in CDCl₃ under N₂. The presence of CTX, BP, and Phn promoted the photolysis of QA salt I, though the effect of Ant was not observed. The activity of photosensitizers in the photolysis decreased in the order of CTX > BP > Phn. The yield of DABCO depended on the degree of the photolysis of QA salt I. On the basis of their excited triplet energy levels: E_T(BP)=69.0, E_T(CTX)=65.5, E_T(Phn)=62.0 and E_T(Ant)=42.0 (kJ/mol), and the order of their molecular absorption coefficient at 366nm: CTX>BP>Phn, it is thought that the sensitization was induced by those QA salts which have triplet energy higher than about 60 kJ/mol and that the apparent order of their sensitization depended on the order of their absorption coefficient. Furthermore, the photolysis of QA salt I was depressed in air. These results suggest that the photosensitization occurs by triplet-triplet energy transfer.

Fig.4 shows photo-initiated thermal insolubilization of PGMA films with QA salts and photo-sensitizers at 366 nm irradiation. In this experiment, post-baking

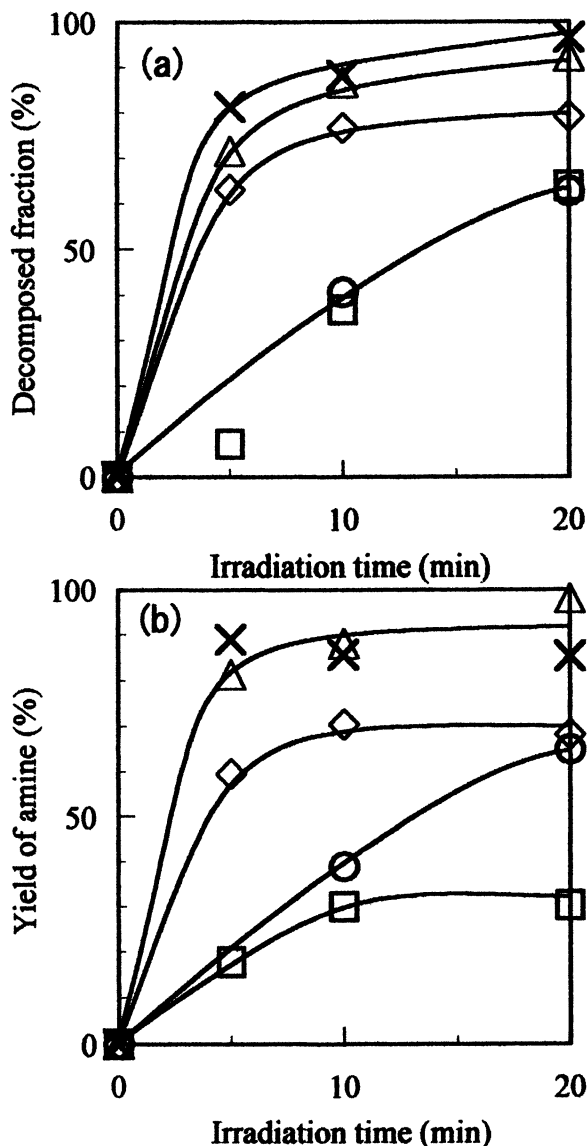


Figure 3. Photolysis of QA salt I in the presence of sensitizers under N_2 . (a) Decomposed fraction of QA salt I with photo-sensitizers. (b) Yield of amine detected from irradiated solution of QA salt I. (X) with CTX, (Δ) with Bp, (\square) with Ant, (\diamond) with Phn, (\circ) without sensitizer. $[QA\ salt\ I] = [sensitizer] = 3 \times 10^{-2}$ (mol/l).

was not carried out. CTX was effective for insolubilization of PGMA films. On the other hand, the films with BP and Phn were not insolubilized at this irradiation energy, because their absorption coefficient at 366 nm was very small or zero, respectively.

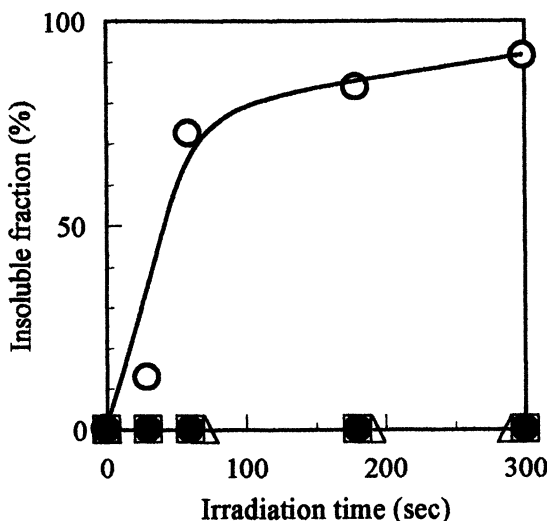


Figure 4. Photo-insolubilization of PGMA films with 5 mol% of QA salt I at 366 nm. (□) without sensitizer, (○) with CTX, (△) with Phn, (●) BP.

CONCLUSIONS

We have investigated the photolysis of QA salts bearing onium moieties derived N-methylpiperidine or DABCO and an N,N-dimethyldithiocarbamate anion. They were thermally stable under 100 °C. They were also stable in acetonitrile, DMF, DMSO and H₂O, though their stability depended on their structure. QA salt I having DABCO moiety was more stable than QA salt V having N-methylpiperidine moiety in the solvents except DMSO. All QA salts became stable at pH>7 in aq. alkaline solution.

Photolysis of QA salt I was sensitized by CTX, BP and Phn. The presence of CTX made it possible for PGMA films with QA salt I to become insoluble at 366 nm irradiation.

The QA salts were proved to be useful PBGs in photo-initiated thermal insolubilization of epoxides.

Acknowledgement : This work was supported by a Grant-in-Aid for Scientific Research (c) (10650870) from the Japan Society of the Promotion of Science.

REFERENCES

1. Fouassier, J. P. *Photoinitiation, Photopolymerization and Photocuring: Fundamentals and Applications*; Hanser: Munich, 1995; pp 102-245.
2. Fouassier, J. P.; Rabek, J. F. *Radiation Curing in Polymer Science and Technology*; Elsevier Applied Science: London, 1993; Vol. 2, pp 435-554.
3. Crivello, J. V.; Dietliker, K. *Photoinitiators for Free Radical, Cationic & Anionic Photopolymerization*; Bradley, G., Ed.; Wiley: New York, 1999; pp 329-566.
4. Frechet, J. M. J. *Pure Appl. Chem.* **1992**, *64*, 1239.
5. Shirai, M.; Tsunooka, M. *Prog. Polym. Sci.* **1996**, *21*, 1.
6. Shirai, M.; Tsunooka, M. *Bull. Chem. Soc. Jpn.* **1998**, *71*, 2483.
7. Shirai, M.; Suyama, K.; Tsunooka, M. *Trends Photochem. Photobiol.* **1999**, *5*, 169.
8. Hanson, J. E.; Jensen, K. H.; Gargiulo, N.; Motta, D.; Pingor, D. A.; November, A. E.; Mixon, D. A.; Kometani, J. M.; Knurek, C. *Polym. Mater. Sci.* **1995**, *72*, 201.
9. Kaneko, Y.; Sarker, A. M.; Neckers, D. C. *Chem. Mater.* **1999**, *11*, 170.
10. Sarker, A. M.; Kaneko, Y.; Neckers, D. C. *J. Photochem. Photobiol. A Chem.* **1999**, *121*, 83.
11. Tachi, H.; Yamamoto, T.; Shirai, M.; Tsunooka, M. *J. Polym. Sci. Part A Polym. Chem.* **2001**, *39*, 1329.
12. Tsunooka, M.; Tachi, H.; Yamamoto, T.; Akitomo, K.; Shirai, M. *J. Photopolym. Sci. Technol.* **2001**, *14*, 153.
13. Tachi, H.; Tsunooka, M. *J. Photopolym. Sci. Technol.* **2000**, *13*, 153.
14. Tsunooka, M.; Tachi, H.; Shirai, M. *Proc. RadTech 2000 North America, Baltimore, 2000*, p 358.
15. Tachi, H.; Tsunooka, M. *J. Photopolym. Sci. Technol.* **1999**, *12*, 313.

Chapter 31

Synthesis and Photochemical Reaction of High-Performance UV-Curing Oligomers

T. Nishikubo¹, A. Kameyama², and H. Kudo¹

Departments of ¹Applied Chemistry and ²Chemistry,
Faculty of Engineering, Kanagawa University, Rokkakubashi,
Kanagawa-ku, Yokohama 221-8686, Japan

As high performance UV-curing oligomers, certain calixarenes derivatives containing (meth)acrylate, vinyl ether, propargyl ether, oxetane, oxirane, or spiro ortho ester groups were synthesized by the reactions of calixarenes with (meth)acrylic acid derivatives, vinyl ether compounds, propargyl bromide, oxetane derivatives, epibromohydrin, and spiro ortho ester derivatives. It was found that most of the obtained calixarene derivatives containing polymerizable groups had excellent thermal stability and high photochemical reactivity.

Over the last 20 years, UV and EB curing systems have been of great interest¹, and have been introduced in the fields of coatings, printing inks, photofabrications, adhesives, and solder masks. These systems are also important methods in various industries for reducing the use of harmful organic solvents, carbon dioxide due to the combustion of fuels, and fossil energy. Recently, these UV and EB curing systems have been further extended²⁻⁴ in the new technology fields such as microelectronics, micromachines, three-dimensional fabrications, liquid crystal displays, insulating materials for multiple print-circuit board, optical media, optoelectronic materials, and so on. In these curing systems, radically polymerizable acrylate monomers and oligomers have been widely used, because these polyfunctional acrylates have high photochemical reactivity to produce the crosslinked insoluble masses or films

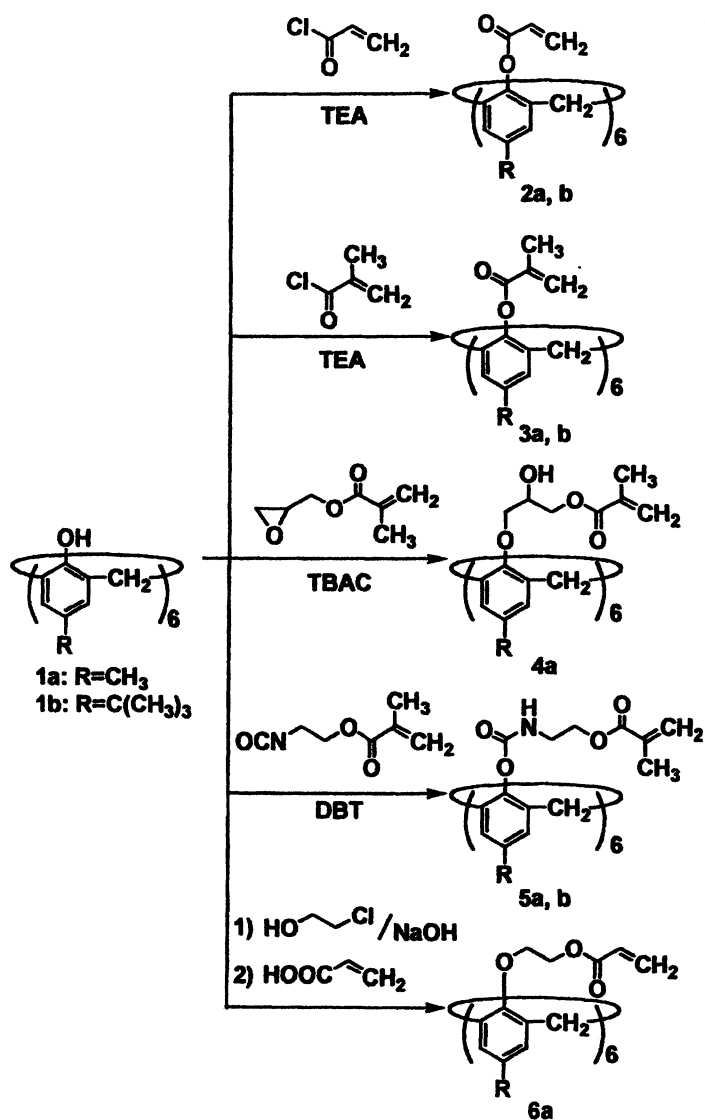
with excellent mechanical and physical properties. However, the thermal stability and glass transition temperature (T_g) of commercially available acrylate oligomers such as epoxy-acrylate⁵, urethane-acrylate⁶, polyester-acrylate⁷, and polyether-acrylate are too low for new application fields to achieve high-performance. The same UV and EB curing systems using cationically polymerizable monomers and oligomers³ such as vinyl ethers, oxiranes, and oxetanes have also been developed; however, these cationically polymerizable monomers and oligomers could not achieve enough thermal stability and high T_g . Recently, Teramoto et al⁸ have synthesized new types of epoxy-acrylates with relatively good thermal stability. However, the thermal stability of this monomer is not enough. Our research group⁹ also synthesized new imide-type photo-curable polyfunctional acrylates. Although these oligomers have higher thermal stability than 500 °C, the miscibility of these oligomers with reactive diluent is not good enough. Meanwhile, calixarenes are cyclic oligomers with many hydroxyl groups in the benzene rings, which are easily prepared from the reaction of phenols with aldehydes. Calixarenes have been studied¹⁰ as the third host-molecule following crown-ethers and cyclodextrins in the field of host-guest chemistry, and the synthesis¹¹ of various calixarene derivatives and chemical modification¹² of calixarenes have been investigated in an attempt to induce the targeted character. Recently, it was also found that calixarenes have many other unique characteristics as follows: 1) Calixarenes have many reactive groups in small size molecules. 2) Calixarenes have excellent thermal stability¹³. 3) Calixarenes have high T_g and high T_m ¹³. 4) Although the characters of calixarenes are affected by the structure of each molecule, certain calixarenes are amorphous in solid state. 5) Calixarenes are synthesized by the reaction of commercial phenols with aldehydes. Therefore, these compounds will be obtained commercially at reasonable prices in the near future.

From these backgrounds, calixarenes will possibly be considered to be used in such new application fields as; A) High-resolution photo-resists¹⁴⁻¹⁶. B) High performance photo-curable oligomers¹³. C) New crosslinking reagents for epoxy resins¹⁷. D) Starting materials for star polymers¹⁸.

In this paper, the authors report on the synthesis of various photo-curable calixarene derivatives containing radical polymerizable (meth)acrylate groups¹³, and cationically polymerizable vinyl ether¹⁴, propargyl ether¹⁴, oxetane¹⁵, oxirane¹⁵ and spiro ortho ester¹⁶ groups. Furthermore, thermal properties and photochemical reactivity of the obtained calixarene derivatives are also examined.

Synthesis of Calixarene Derivatives Containing (Meth)acrylate Groups and Their Thermal and Photochemical Properties

Calixarene derivatives containing radically polymerizable (meth)acrylate groups were synthesized by the reaction of certain calixarenes such as *p*-methylcalix[6]arene (**1a**) and *p*-*tert*-butylcalix[6]arene (**1b**) with (meth)acrylate derivatives (Scheme 1). That is, calix[6]arenes **2a** and **2b** containing acrylate groups



Scheme 1

were prepared by the condensation reaction of **1a** and **1b** with acryloyl chloride in *N*-methylpyrrolidone (NMP) using triethylamine (TEA) as a base. Calix[6]arene **3a** and **3b** containing methacrylate groups were also obtained by the reaction of **1a** and **1b** with methacryloyl chloride under the same conditions. Calix[6]arene **4a** containing methacrylate groups and alkyl spacer chains was synthesized by the addition reaction of **1a** with glycidyl methacrylate (GMA) in NMP using tetrabutylammonium chloride (TBAC) as a catalyst. Calix[6]arenes **5a** and **5b** containing methacrylate groups and alkyl spacer chains were prepared by the addition reaction of **1a** and **1b** with (2-methacryloxy)ethyl isocyanate (MOI) in NMP using dibutyltin dilaurate as a catalyst. Calix[6]arene **6a** containing acrylate groups and oxyethylene spacer chains between **1a** and acrylate groups was also synthesized by the condensation reaction of the oxyethylene modified **1a** with acrylic acid. Calixarene derivatives **2a**, **2b**, **3a**, **3b**, **4a**, **5a**, and **5b** containing (meth)acrylate groups were solid at room temperature; however, calixarene derivative **6a** containing acrylate group and oxyethylene spacer was liquid at room temperature. All reactions proceeded very smoothly to give the corresponding products in 100 mol-% conversions in good yields, and the structures of these obtained calixarene derivatives containing (meth)acrylate groups were confirmed by IR and ¹H NMR spectra.

10 wt-% loss temperatures of the calixarene acrylate **2a** and calixarene methacrylate **2b** were measured by the thermogravimetric analysis to evaluate the thermal stability, and it was found those of **2a** and **2b** were 434 and 406 °C, respectively. This means that calixarene acrylate **2a** and calixarene methacrylate **2b** had excellent thermal stability. The other calixarene derivatives containing (meth)acrylate groups also showed good thermal stability; however, the stability of these oligomers decreased with the introduction of spacer chains between calixarene molecules and (meth)acrylate groups. The photopolymerization of calixarene derivatives **2a**, **3a**, **4a**, and **5a** was examined using (2-phenyloxy)ethyl acrylate as a reactive diluent (50 wt-%) and benzyl dimethyl ketal (Irgacure 651, Chiba-Geigy) (1 wt-%) as a photoinitiator upon irradiation with UV light. As shown in Figure 1, calixarene derivative **2a** containing acryloyl groups showed higher photochemical reactivity than other calixarene derivatives **3a**, **4a**, and **5a** containing methacryloyl groups. Furthermore, calixarenes **4a** and **5a** with alkyl spacer chains showed higher photochemical reactivity than calixarene **3a**. From these photochemical data, the authors consider that polyfunctional (meth)acrylates with calixarene backbones can be expected to be novel and thermally stable photoreactive acrylate oligomers.

Synthesis of Calixarene Derivatives Containing Propargyl Ether or Vinyl Ether Groups and Their Thermal and Photochemical Properties

p-Methylcalix[6]arene derivatives containing cationically polymerizable propargyl ether (**7a**) and allyl ether (**8a**) groups were synthesized by the substitution reaction of potassium salt of **1a** with propargyl bromide and allyl

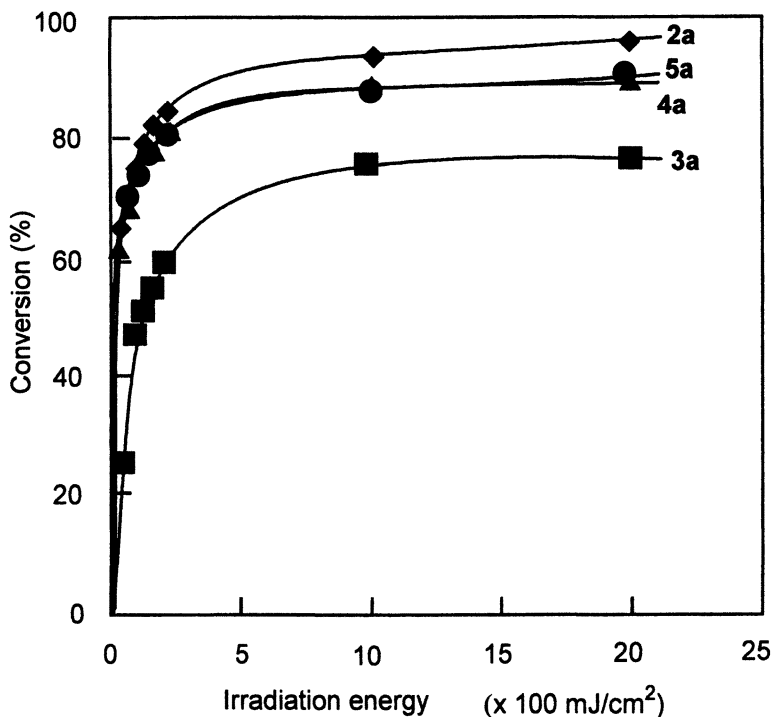


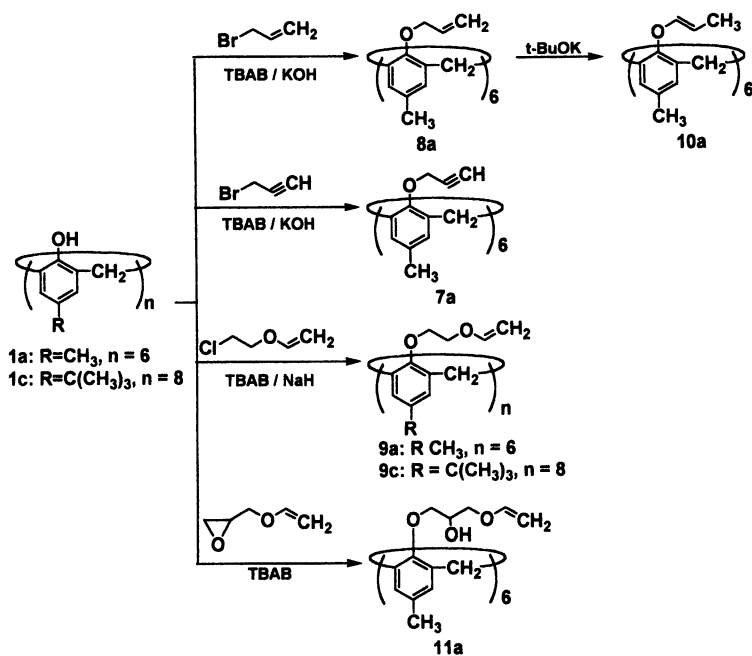
Figure 1. Rates of the photoinitiated radical polymerization of calixarenes 2a – 5a containing (meth)acrylate groups with (2-phenyloxy)ethyl acrylate (50 wt-%) and Irgacure 651 (1 wt-%) upon UV irradiation: (◆) calixarene 2a; (●) calixarene 5a; (▲) calixarene 4a; (■) calixarene 3a.

bromide, respectively, using tetrabutylammonium bromide (TBAB) as a phase-transfer catalyst (PTC) at 50 °C for 24 h in NMP. *p*-Methylcalix[6]arene and *p*-*tert*-butylcalix[8]arene derivatives **9a** and **9c** containing 2-ethoxy vinyl ether groups were prepared by the same reaction of sodium salts of **1a** and *p*-*tert*-butylcalix[8]arene (**1c**) with 2-chloroethyl vinyl ether (CEVE), respectively, using TBAB as a PTC at 80 °C for 24 h in NMP. *p*-Methylcalix[6]arene derivative **10a** containing 1-propenyl ether was obtained by the isomerization of **8a** using potassium *tert*-butoxide as a catalyst at 80 °C for 24 h in NMP according to the reported method by Crivello et al.¹⁹ *p*-Methylcalix[6]arene derivative **11a** containing pendant hydroxyl groups and vinyl ether groups was prepared by the addition reaction of **1a** with glycidyl vinyl ether (GVE) using TBAB as a catalyst at 110 °C for 48 h in NMP (Scheme 2).

All reactions proceeded very smoothly to give the corresponding products in 100 mol-% conversions in good yields, and the structures of the synthesized cationically polymerizable calix[n]arene derivatives were confirmed by IR and ¹H NMR spectra, and elemental analysis. λ max of UV spectra of the calixarene derivatives **7a**-**11a** was observed in the range of 272-280 nm. Further, glass transition temperatures (T_g) and 10 wt%-loss temperature (T_{d10}) were measured at a heating rate of 10 °C/min under nitrogen atmosphere by differential scanning calorimetry (DSC) and thermogravimetric analysis (TGA). It was found that all the calixarene derivatives had high T_g s = 148-314 °C and very good thermal stabilities, T_{d10} s = 349-412 °C, respectively. The photochemical reactions of calixarene **7a**, **9a**, **9c**, **10a**, and **11a** were examined with the photoacid generator in the film state under the same irradiation conditions. As shown in Figure 2, when bis[4-(diphenylsulfonio)phenyl]sulfide bis(hexafluorophosphate) (DPSP) was used as a photoacid generator, calixarenes **9a** and **9c** containing ethoxy vinyl ether groups showed very high photochemical reactivity. On the other hand, although it has been reported¹⁹ that 1-propenyl ether compounds showed similar or slightly higher photochemical reactivity than vinyl ether compounds, the reactivity of calixarene **10a** containing 1-propenyl ether groups was lower than those of calixarene **9a** and **9c** containing ethoxy vinyl ether groups. It seems that molecular motion of 1-propenyl ether groups bonded directly to calixarene was inhibited strongly in the film state. Lower photochemical reactivity of calixarene **10a** containing vinyl ether groups may be due to the pendant hydroxyl groups.

Synthesis of Calixarene Derivatives Containing Cyclic Ether Groups and Their Thermal and Photochemical Properties

p-Methylcalix[6]arene, *p*-*tert*-butylcalix[8]arene and C-methylcalix[4]resorcinarene derivatives **12a**, **12c**, **12d** containing oxetane groups were synthesized by the reaction of **1a**, **1c** and **1d** with (3-methyl-3-oxetanyl methoxy) tosylate (MOMT), which was prepared by the reaction of (3-methyl-3-hydroxymethyl) oxetane with *p*-toluenesulfonyl chloride using KOH as a base and TBAB as a PTC at 70 °C for 24 h in NMP (Scheme 3, (a) and (b)). Each reaction proceeded smoothly to produce targeted products in good yields, and



Scheme 2

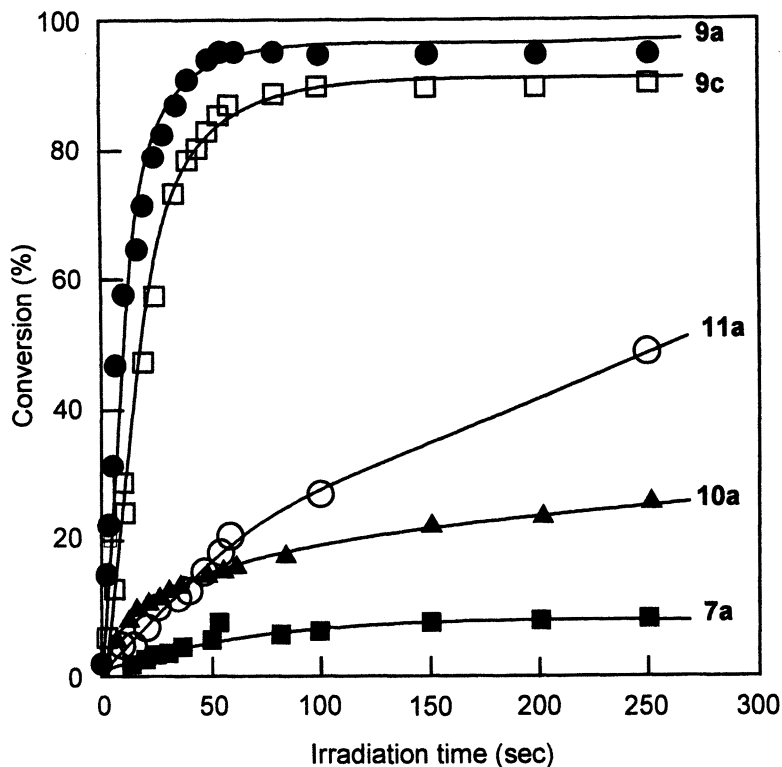
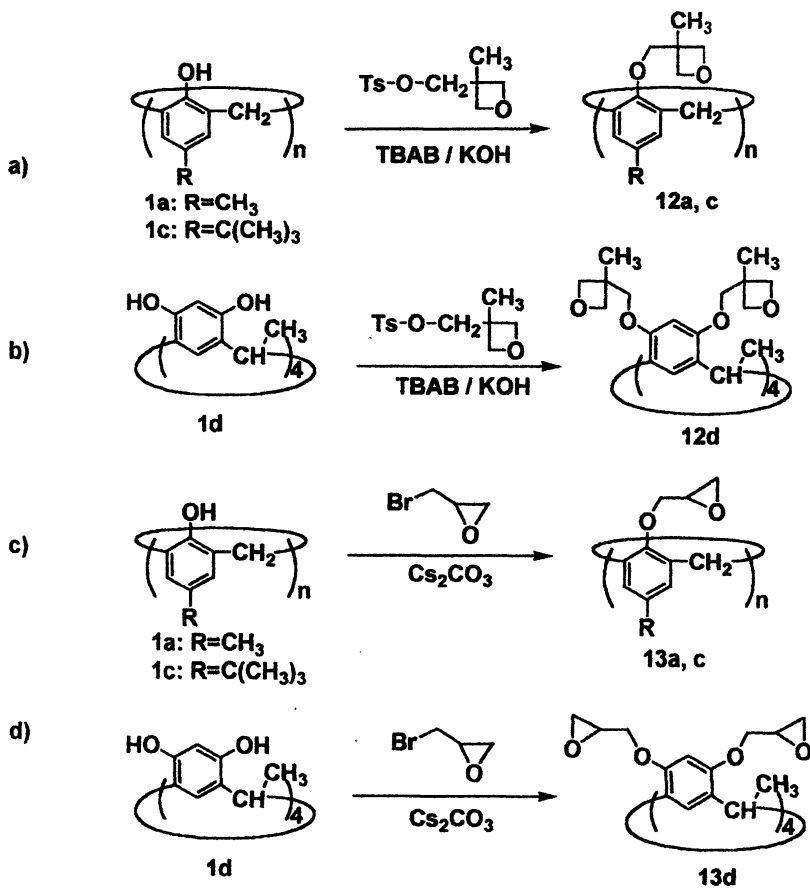


Figure 2. Rates of the photoinitiated cationic polymerization of calixarenes 7a-11a containing propargyl ether, vinyl ether, or 1-propenyl ether groups with DPSP (5 mol-%) upon UV irradiation: (●) calixarene 9a; (□) calixarene 9c; (○) calixarene 11a; (▲) calixarene 10a; (■) calixarene 7a.

the structures of the obtained calixarene derivatives containing oxetane groups were confirmed by IR and ^1H NMR spectra, and elemental analysis. These results suggested that the reactions of calixarene **1a**, **1c** and **1d** with MOMT proceeded quantitatively. *p*-Methylcalix[6]arene, *p*-*tert*-butylcalix[8]arene and *C*-methylcalix[4]resorcinarene derivatives **13a**, **13c**, **13d** containing oxirane groups were also prepared by the reaction of **1a**, **1c** and **1d** with epibromohydrin (EBH) in NMP at 50 °C for 48 h in NMP (Scheme 3, (c) and (d)). The reaction proceeded smoothly to produce calixarene derivatives in good yields, when Cs_2CO_3 was used as a base, and the structures of the obtained calixarene derivatives containing oxirane groups were confirmed by IR and ^1H NMR spectra, and elemental analysis. On the other hand, when the reaction was performed using pyridine, triethylamine, 1,8-diazabicyclo[5.4.0]undecene-7 (DBU), potassium hydroxide, or sodium as base, only insoluble gel products were obtained. When Na_2CO_3 or K_2CO_3 were used as base, degrees of etherification of the calixarene derivatives were lower than that with Cs_2CO_3 under the same reaction conditions.

$T_{\text{d}10\%}$ of **12a**, **12c**, **12d**, **13a**, **13c**, and **13d** were 367, 394, 414, 357, 366, and 396 °C, respectively. This means that the obtained calixarenes containing oxetane groups or oxirane groups had good thermal stability. Especially, calixarene derivatives composed of calix[4]resorcinarene structure showed higher thermal stability than those composed of calix[n]arene structures. The photochemical reaction of calixarene derivative **12d** containing pendant oxetane groups was examined in the film state with 5 mol-% of DPSP under UV irradiation. As shown in Figure 3, the reaction proceeded rapidly and the conversion reached 81 mol-% in 360 sec., and the photo-irradiated calixarene film became insoluble in all organic solvents. This means that photocrosslinking reaction of calixarene derivative **12d** containing oxetane groups occurred in the film state at room temperature. The photochemical reactions of other calixarenes **12a** and **12c** containing oxetane groups were also examined with 5 mol-% of DPSP under the same irradiation conditions, and it was found that although the photo-initiated cationic polymerization of calixarenes **12a** and **12c** proceeded smoothly, the rate of the photochemical reaction of these compounds composed of calix[n]arene structures were lower than that of calixarene **12d** composed of calix[4]resorcinarene structure (Figure 3).

The photochemical reactions of calixarenes **13a**, **13c** and **13d** containing oxirane groups were also examined with 5 mol-% of DPSP under the same irradiation conditions, and it was found that although the photo-initiated cationic polymerization of calixarenes **13a** and **13c** proceeded smoothly, the rates of the photochemical reactions of these compounds were lower than that of calixarene **13d** composed of calix[4]resorcinarene structure (Figure 4). These results also showed that the rates of photochemical reaction of the pendant oxetane groups in calixarenes were higher than those of the pendant oxirane groups in the corresponding calixarenes in the film state under the same conditions.



Scheme 3

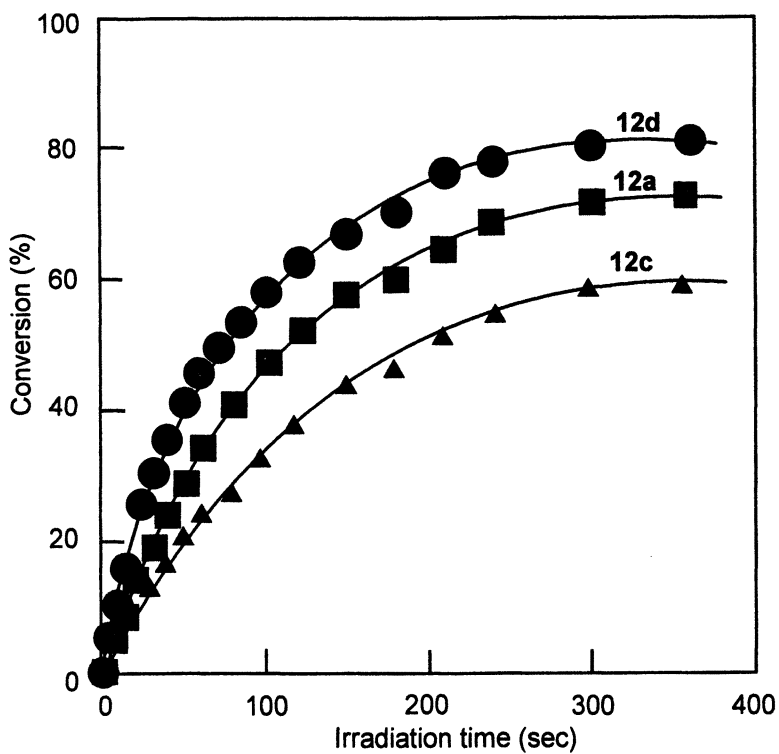


Figure 3. Rates of the photoinitiated cationic polymerization of calixarenes 12a, 12c, and 12d containing pendant oxetane groups with DPSP (5 mol-%) upon UV irradiation: (●) calixarene 12d; (■) calixarene 12a; (▲) calixarene 12c.

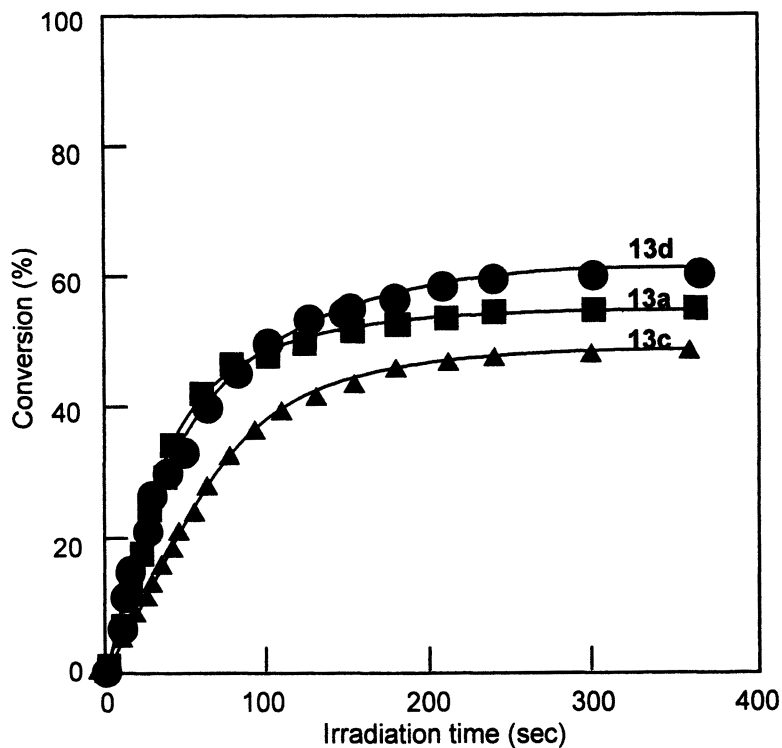


Figure 4. Rates of the photoinitiated cationic polymerization of calixarenes **13a**, **13c**, and **13d** containing pendant oxirane groups with DPSP (5 mol-%) upon UV irradiation: (●) calixarene **13d**; (■) calixarene **13a**; (▲) calixarene **13c**.

Calixarene Derivatives Containing Spiro Ortho Ether Groups

p-Methylcalix[6]arene, *p*-*tert*-butylcalix[8]arene and C-methylcalix[4]resorcinarene derivatives **14a**, **14c**, and **14d** containing spiro ortho ester groups were synthesized¹¹ by the reaction of **MCA-2**, **BCA-2** and **CRA-2** derivatives containing carboxyl groups, which were prepared by the reaction of calixarene **1a**, **1c**, and **1d** with methyl α -bromoacetate followed by hydrolysis, with 2-bromoethyl-1,4,6-trioxaspiro[4.4]nonane (BMTSN) using DBU as a base. The reaction proceeded smoothly in NMP 90 °C for 48 h. The structures of these synthesized calix[n]arene derivatives were confirmed by IR and ¹H NMR spectra, and elemental analysis (Scheme 4). However, the reaction of calixarenes **1a**, **1b**, and **1d** with BMTSN using KOH and TBAB as did not proceed due to their steric hindrance.

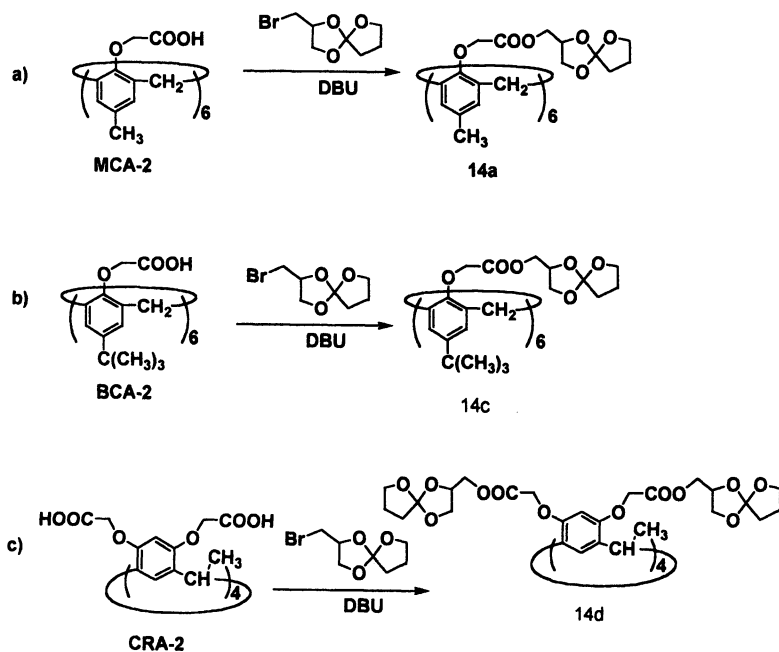
When the photochemical reactions of **14a**, **14c**, and **14d** were examined with 5-mol% of DPSP in the film state under the same irradiation conditions, interestingly enough the reaction of pendant spiro ortho ester groups in calixarenes did not proceed. However, when the films were irradiated for 5 min followed by heating at 150 °C, the reaction proceeded smoothly with 50 - 80% conversions.

CONCLUSION

From all these results, following conclusions can be drawn: 1. Certain new calixarene derivatives containing radically polymerizable (meth)acrylate groups or cationically polymerizable propargyl ether, vinyl ether, oxirane, oxetane or spiro ortho ester groups were synthesized in good yields. 2. These synthesized calixarene derivatives had good thermal stability. 3. These calixarene derivatives had good photochemical reactivity excepting calixarenes **14a**, **14c**, and **14d** containing pendant spiro ortho ester groups.

REFERENCES

1. Nishikubo, T., Ed. *Synthesis and Application of Photosensitive Polymers*; CMC; Tokyo, **1979**.
2. Holman, R.; Oldring, P.; Eds., *UV and EB Curing Formulation for Printing Inks, Coatings and Paints*; International Training Associates Limited: London, **1988**.
3. Tabata, Y.; Takimoto, Y.; Tominaga, Y.; Nakamoto, H.; Nishikubo, T.; Eds. *Ultraviolet and Electron Beam Curable Materials*; CMC, Tokyo, **1989**.
4. Tabata, Y.; Isobe, T.; Otaka, T.; Sato, M.; Takayama, M.; Tominaga, Y.; Nishikubo, T.; Eds. *Technology & Application of UV/EB Curing*; CMC, Tokyo, **1997**.
5. Nishikubo, T.; Imaura, M.; Mizuko, T.; Takaoka, T. *J. Appl. Polym. Sci.*, **1974**, *18*, 3445.



Scheme 4

6. Labana, S. S. *J. Polym. Sci. A-1*, **1968**, *6*, 3283.
7. Tatemichi, H.; Ogasawara, T. *Chem. Economy & Eng. Rev.*, **1978**, *10*, 37.
8. Endo, T.; Masuda, T. Nishikubo, T.; Eds. *Polymer Design for the Next Generation*, IPC, Tokyo, **2000**, pp. 169-186.
9. Nishiyama, Y.; Kameyama, A.; Nishikubo, T.; *Polym. Preprints, Jpn.*, **1994**, *43*, 1103.
10. For example; Gutsche, C. D. *Calixarenes*; Royal Society of Chemistry, Cambridge, **1989**.
11. For example; Arimura, T.; Shinkai, S.; Matuda, T. *J. Syn. Org. Chem. Jpn.*, **1989**, *47*, 523.
12. For example; a) Takeshita, M.; Shinkai, S. *Bull. Chem. Soc. Jpn.*, **1995**, *68*, 1088. b) Lhotak P.; Shinkai, S. *J. Syn. Org. Chem. Jpn.*, **1995**, *53*, 523.
13. a) Iyo, M.; Tsutsui, K.; Kameyama, A.; Nishikubo, T. *J. Polym. Sci. Part A. Polym. Chem.*, **1999**, *37*, 3071. b) Nishikubo, T.; Kameyama, A.; Tsutsui, K.; Iyo, M. *J. Polym. Sci. Part A. Polym. Chem.*, **1999**, *37*, 1805. c) Nishikubo, T.; Kameyama, A.; Tsutsui, K. *J. Polym. Sci. Part A. Polym. Chem.*, **2001**, *39*, 1169. d) Tsutui, k.; Kameyama, A.; Nishikubo, T. Preprints of the 76th Annual Meeting of Chemical Society, Japan, II, 1999, p.1319.
14. a) Fujita, j.; Onishi, Y.; Ochiai, Y.; Matsui, S. *Appl. Phys. Lett.*, **1996**, *68*, 1297. b) Ochiai, Y.; Manako, S.; Yamamoto, H.; Teshima, T.; Fujita, J.; Nomura, E. *J. Photopolymer. Sci. Tech.* **2000**, *13*, 413.
15. a) Nakayama, T.; Haga, K.; Haba, O.; Ueda, M. *Chem. Lett.*, **1997**, 265. b) Ueda, M.; Takahashi, D.; Nakamura, T.; Haba, O. *Chem. Mater.*, **1998**, *10*, 2230. c) Takeshi, K.; Nakayama, R.; Ueda, M. *Chem. Lett.*, **1998**, 865. d) Nakayama, T.; Nomura, M.; Haga, K.; Ueda, M. *Bull. Chem. Soc., Jpn.*, **1998**, *71*, 2979.
16. Nishikubo, T.; Kameyama, A.; Kudo, H.; Tsutsui, K. *J. Polym. Sci. Part A. Polym. Chem.* **2002**, *40*, 1293.
17. Adachi, T.; Kameyama, A.; Nakamura, S.; Nishikubo, T. *Abstracts of 76th Annual Meeting of Chemical Society of Japan*, **1999**, Part II, p. 1351.
18. a) Jacob, S.; Majoros, Kennedy, J. P. *Macromolecules*, **1996**, *29*, 8631. b) Ueda, J.; Kamigaito, M.; Sawamoto, M. *Macromolecules*, **1998**, *31*, 6762.
19. a) Crivello, J. V.; Yang, B. *J. Polym. Sci. Part A. Polym. Chem.*, **1995**, *33*, 1381. b) J. V. Crivello, J. V.; Yang, B. *J. Polym. Sci. Part A. Polym. Chem.*, **1996**, *34*, 2051.

Chapter 32

Photopolymerization Kinetics of Nanostructured Polymers Templated by Lyotropic Liquid Crystals

C. Allan Guymon and Christopher L. Lester

Department of Polymer Science, University of Southern Mississippi,
2609 West 4th Street, Hattiesburg, MS 39406-0076

Nanostructured materials have been the focus of much attention due to their applicability in nanocomposites, separations media, drug delivery devices, and many other applications requiring a nanometer size scale. Recently, using lyotropic liquid crystalline (LLC) phases to template their unique nanostructure onto organic polymers has been proposed. This work details the photopolymerization of acrylamide in various phases of LLC systems. The photopolymerization kinetics are correlated to monomer organization for different phases at a variety of concentrations and temperatures. The photopolymerization kinetics of acrylamide in the LLC phases depend strongly on the LLC morphology. The polymerization rates are significantly faster in compositions of surfactant resulting in a hexagonal geometry as the acrylamide monomer is preferentially oriented. These results indicate that acrylamide is strongly associated with the LLC interface and the surfactant. Photopolymerization of these templated systems results in structure retention of the parent LLC phase.

Introduction

In recent years the synthesis of nanostructured materials has become the focus of much research. Lyotropic liquid crystal (LLC) phases possess a wide range of controllable nanometer morphologies that are formed with mixtures of amphiphile and water. When amphiphiles are solvated in water at sufficient concentrations, a variety of ordered phases may form. At concentrations above the critical micelle concentration, micelles will form. At higher concentrations of amphiphile, these micelles may pack into discontinuous cubic arrays. At successively higher concentrations of amphiphiles, hexagonally packed rod-like aggregates and bilayer lamellar phases may form as shown in Figure 1.¹ These phases, however, are not robust and therefore not useful from a materials standpoint. If the nanostructure of the LLC phases could be templated onto the polymer, a wide variety of applications could benefit including ultrafiltration membranes, catalytic media, and drug delivery devices.

Using LLC phases as templates for the synthesis of nanostructured materials has been attempted, but with mixed results. Typically, the polymer morphologies reported are a result of phase separation during polymerization as it is thermodynamically unfavorable for polymer chains to adopt such constrained conformations.² In some cases the successful templating of LLC phase structure onto polymers has been reported,³ but these studies do little to detail what mechanisms allow phase retention versus phase separation. Some studies have alluded to kinetic trapping of the otherwise thermodynamically unfavorable state as a possible mechanism to control structure. Polymerization kinetics, therefore, are important to consider when attempting to retain the original LLC phase structure of templated systems. Conversely, it is also

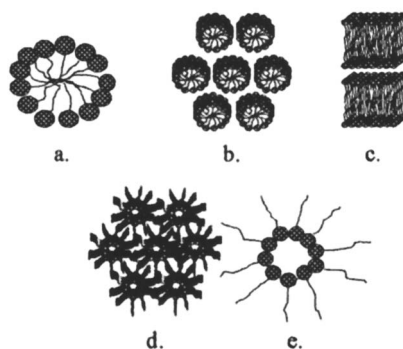


Figure 1. Schematic of selected lyotropic liquid crystalline phases. Shown in order of increasing amphiphile concentration are the a) micellar, b) hexagonal, c) lamellar, d) inverse hexagonal, and e) inverse micellar phases.

important to understand how the nanostructure of the LLC template impacts the polymerization mechanism and how the monomers are organized prior to polymerization.

Recently, photopolymerization has been utilized as a means to develop controlled LLC nanostructures.⁴ Photopolymerization is not only extremely rapid, which may allow kinetic trapping, but also allows facile examination of the polymerization kinetics. Previous studies have shown that the final properties of analogous thermotropic systems are greatly dependent on the polymerization kinetics for a variety of monomers/LC systems.⁵⁻⁷ Other results indicate that the photopolymerization kinetics and structure retention of monomeric LLC amphiphiles are influenced by the type and degree of LLC order.⁸⁻¹⁰ Additionally, the polymerization kinetics of a variety of monomers templated in LLC phases are quite dependent on the original LLC morphology.¹¹ These studies illustrate the importance of understanding the polymerization kinetics of LLC systems and the relationship of the polymerization to structure retention. It is therefore extremely important to correlate the photopolymerization kinetics to the original LLC morphology as well as to the degree of structure retention.

The goal of this work is to further elucidate the details of templated polymerization in LLC phases to allow the development of nanostructured polymers that can be reliably and controllably synthesized. Specifically, the polymerization kinetics of an acrylamide will be correlated to the organization of the monomer in an LLC template. The local mobility and environment of the monomer will be examined and the resulting polymeric materials will be characterized to determine phase retention. The results of this study will aid in optimizing templated LLC materials for applications requiring controlled polymeric nanostructures.

Experimental

Materials

The monomer examined in this study was acrylamide, while the LLC template was formed by the nonionic surfactants Brij 56 and Brij 58 with deionized water. Figure 2 depicts the chemical structures of the monomer and surfactant. The photoinitiator used was Irgacure® 2959.

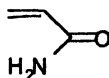
Methods

Small angle x-ray scattering (SAXS) was used to characterize the phase behavior using a Siemens XPD 700P WAXD/SAXS with a $\text{CuK}\alpha$ line of 1.54 Å. A polarized light microscope (Nikon) equipped with a hot stage was utilized to corroborate data collected with SAXS by looking for characteristic textures of the various mesophases. Reaction profiles were monitored in real time with a differential scanning calorimeter (Perkin-Elmer DSC-7) modified with a medium pressure UV arc lamp and quartz windows. Samples were covered with a thin film of FEP (DuPont fluorinated copolymer) to prevent evaporation of water. The samples were heated to 60 °C at 20 °C/min after which they were held isothermally for one minute to allow the samples to flow and level to ensure good thermal contact. The samples were then allowed to cool at 10 °C/min to the desired polymerization temperature. The polymerizations were initiated with monochromatic 365 nm light at an intensity of 4.5 mW/cm². The heat of polymerization was utilized to directly calculate the rate of polymerization. For these studies the theoretical values of 18.5 kcal/mol was used as the heat evolved per acrylamide double bond reacted. The kinetic parameters, k_p and k_t , were determined from after effect experiments as described elsewhere.¹¹

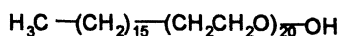
NMR spectra were acquired using a Bruker MSL-400 NMR spectrometer operating at a frequency of 28.9 MHz for ¹⁴N. A standard 10mm probe was used. Spectra were obtained using the DEPTH sequence to suppress ¹⁴N background due to the probe.¹² The 90° pulse width was 22 μs, the probe dead time was 10 μs, and the acquisition time was 131 ms. The recycle delay was 600 ms, and no proton decoupling scheme was implemented. Samples were typically acquired without spinning.

Results and Discussion

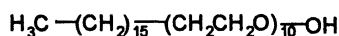
Previous work indicates that the polymerization kinetics is of utmost importance in structure retention of the original LLC phase. Interestingly, the



a.



b.



c.

Figure 2. Chemical structures of a) acrylamide, b) Brij 58, and c) Brij 56.

polymerization rate of acrylamide in various LLC phases of Brij 56 exhibits considerable differences depending on the morphology of the system. In Figure 3 the polymerization rate is plotted as a function of double bond conversion for 25% acrylamide with increasing concentration of surfactant at 35°C. By increasing the surfactant over this range, discontinuous cubic, hexagonal, and inverse micellar phases are observed. Also shown is a profile of an isotropic solution polymerization of the same concentration of acrylamide in water at the same conditions. An extraordinarily slow photopolymerization rate is observed in the isotropic sample. The rate is so slow, in fact, that it is difficult to obtain consistent results due to the small exotherm. On the other hand, with addition of an appropriate amount of surfactant to reach the discontinuous cubic phase the polymerization rate is more than six times faster than that observed in the isotropic system. Further increases are observed in hexagonal samples with 50% and 60% surfactant that yield a polymerization rate more than ten times that of the isotropic phase and also considerably faster than that of the cubic phase. Interestingly, with further increases in surfactant concentration to 70% an inverse micellar phase is formed that exhibits a polymerization rate less than the other ordered LLC phases with lower surfactant concentrations. This further substantiates that changes in polymerization kinetics are strongly dictated by the LLC morphology and not inherently by the surfactant concentration.

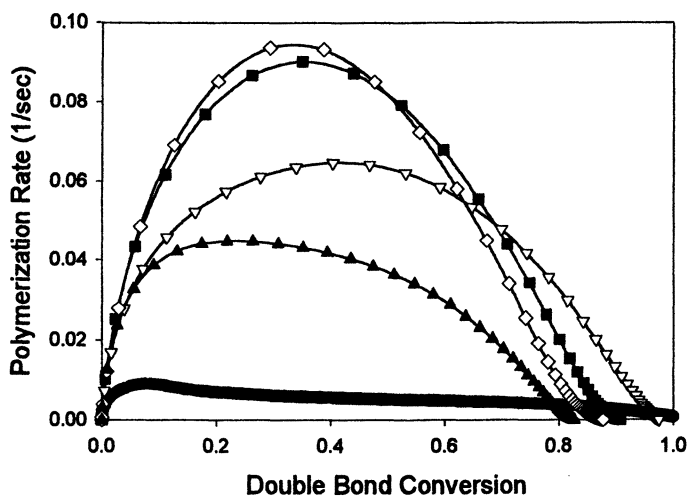


Figure 3. Polymerization rate versus double bond conversion for 25 wt% acrylamide in the LLC phases of Brij 56/water with increasing Brij 56 concentration. Shown are 0% (Isotropic- ●), 40% (Cubic- ▽), 50% (Hexagonal- ■), 60% (Hexagonal- ◇), and 70% (Inverse Micellar, ▲) surfactant.

To understand the kinetic mechanism driving these striking increases in rate, it is valuable to determine the apparent rate parameters of propagation (k_p) and termination (k_t). Figure 4 gives k_p and k_t for the isotropic acrylamide solution as well as a solution of acrylamide in the micellar phase of Brij 58, a closely related surfactant to Brij 56. Rate increases in this system are virtually identical to those described for the Brij 56 system.¹³ The parameters k_p and k_t for both the isotropic and micellar solutions remain fairly constant as the reaction proceeds. Additionally, k_p appears to be approximately the same for both systems over the range of conversions studied. On the other hand, a large change is observed in k_t . The values decrease almost an order of magnitude when comparing the isotropic to the micellar system. Such a decrease is indicative of decreased mobility of the growing polymer chains which leads to an increase in the radical concentration and thus a higher rate. Similar decreases in termination have been observed for polymerizations in thermotropic LCs,⁶ as well as the polymerization of reactive lyotropic LC.^{8,9}

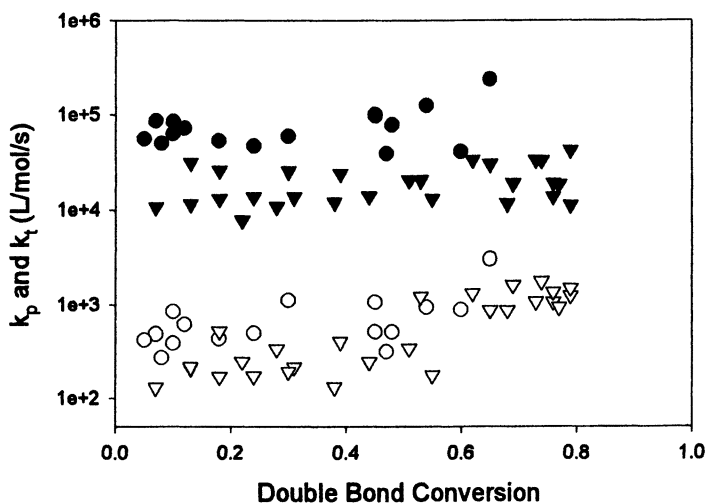


Figure 4. Termination (k_t) and propagation (k_p) rate parameters of 25% acrylamide in LLC phases of Brij 58/water as a function of double bond conversion. Given are k_t for 30% Brij 58- Micellar (▼), k_t for 0% Brij 58- Isotropic (●), k_p for 30% Brij 58 Micellar (▽), and k_p for 0% Brij® 58- Isotropic (○).

From these results, it is logical to conclude that the order inherent in these templated lyotropic systems leads to dramatic changes in polymer evolution and kinetics. A valuable technique to provide direct information about the reaction environment and local ordering is ^{14}N NMR. ^{14}N is a quadrupolar nuclei that yields a splitting pattern indicative of the degree of order in an anisotropic environment. To determine the ordering of the amide nitrogen in the acrylamide as a function of global lyotropic order, spectra were obtained in the various LLC phases of the Brij 56 system. In Figure 5 the ^{14}N spectra from the acrylamide before polymerization are plotted for three different concentrations of Brij 56. These three concentrations correspond to the hexagonal, cubic, and isotropic phases. The isotropic solution of acrylamide and water exhibits a relatively sharp peak with no splitting pattern indicating no anisotropy and therefore no organization of the monomer. The cubic LLC with 40% surfactant yields a broader peak with shoulders at the base of the peak at approximately 4 and 8 kHz. This broadening of the peak indicates a less mobile environment, which could account for the increase in polymerization rate through inducing an early onset of the gel effect that lowers the termination rate. Also, the presence of the shoulders on the base of the peak at this composition indicates some preferential orientation of the acrylamide. When increasing the

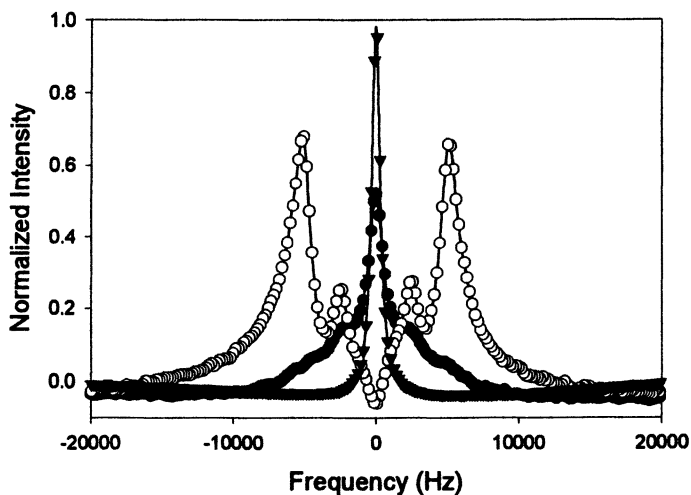


Figure 5. ^{14}N NMR spectra of 25% acrylamide in the various LLC phases of Brij 56/water with increasing concentration of surfactant in water. Shown are spectra with 0% (Isotropic- \blacktriangledown), 40% (Cubic- \bullet), and 50% (Hexagonal-O) surfactant.

concentration further to 50% surfactant, a hexagonal LLC phase is present. As stated previously this composition yielded a tenfold increase in the polymerization rate. The ^{14}N spectra of this sample exhibits two splitting patterns with relatively broad peaks. The broadening certainly could be due to a decrease in mobility of the monomer which may account for some of the increase in polymerization rate. The splitting patterns are also an indication that the LLC phase is inducing ordering on the acrylamide and that it possesses a preferred orientation within the LLC system. This behavior shows that the acrylamide is strongly associated with the surfactant and the increase in rate may be due both to decreased termination,⁸ resulting from less mobility, and an increased local concentration of double bonds.¹¹ The orientation of monomer may also enhance the polymerization rate by causing polymerization to occur topologically along the LLC phase interface.

Although, the phase and ordering of lyotropic LCs is typically modulated by composition, they are also inherently thermotropic as well in that they exhibit changes in phases with increase in temperature. In fact, the polymerization of the Brij 56/acrylamide/water system exhibits a distinct dependence on temperature. Figure 6 shows the polymerization rate as a function of conversion for polymerizations of 25% acrylamide in 40% Brij 56 at 25, 30 and 50°C. Interestingly, a relatively slow polymerization rate is

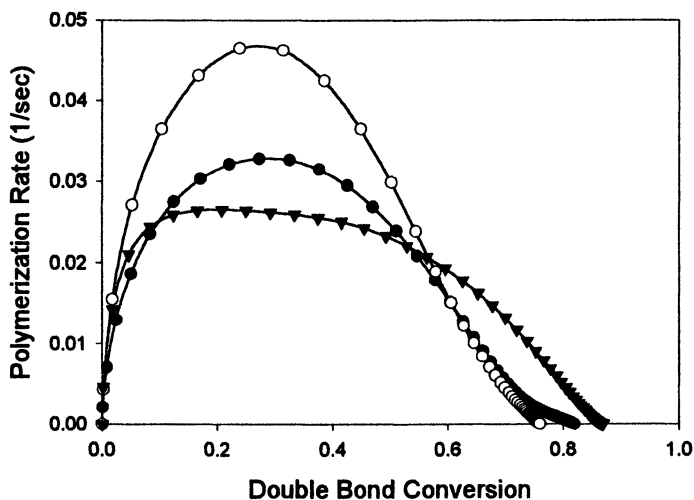


Figure 6. Polymerization rate as a function of conversion for 25 wt% acrylamide in 40% Brij/ 35% water with increasing temperature. Shown are polymerizations at 25°C (Isotropic/Crystalline- ▼), 35°C (Cubic- O), and 45°C (Isotropic- ●).

observed for the system at 25°C. At this temperature a biphasic system is observed using polarized microscopy with crystallites and isotropic micellar regimes. When the temperature is increased to 30°C, which corresponds to a completely homogeneous hexagonal phase, the polymerization rate almost doubles. This large increase cannot be accounted for simply by the increase in temperature alone. This significant increase in polymerization rate is due to the increased organization of the monomer in the LLC phase that may enhance the propagation rate and potentially lower the termination rate due to the high degree of order imposed on the propagating chains. Additionally, the sample at 25°C possesses crystalline domains that would not readily polymerize and therefore decrease overall rate. Further evidence of the dependence of the polymerization rate on the LLC phase morphology is given when the polymerization takes place at 50°C. At this temperature the polymerization rate actually decreases substantially. One might expect that the polymerization rate should increase with increasing temperature. Again, the ordering of the system yields a logical answer. With an increase in temperature to about 40°C, the sample changes to a micellar system. The decrease in order from the hexagonal to micellar phase appears to be directly responsible for the decrease in rate.¹⁴

While the kinetic results and ordering of the system before polymerization are important to develop controlled nanostructured LLC systems, it is also critical to look at structure retention after polymerization. Figure 7 shows the small angle X-ray scattering (SAXS) profile of both polymerized and unpolymerized samples with 25% acrylamide in 40% Brij 58 surfactant. The unpolymerized sample shows the strong primary reflection as well as the secondary reflections of the bicontinuous cubic phase. After polymerization very little change is seen. Both primary and secondary reflections are evident and a large degree of structure retention is observed. Such behavior is in great contrast to thermally polymerized samples¹⁴ in which very little if any structure retention is observed. By retaining these LLC nanostructures, the physical properties of the polymer can also be dramatically altered.¹⁵ These results also show the importance of understanding polymerization kinetics and the potential of photopolymerization for nanostructure development and retention in templated lyotropic LC systems.

Conclusions

This work presents the photopolymerization kinetics of acrylamide correlated with monomer organization in various phases of an LLC system. The photopolymerization kinetics of acrylamide depend strongly on the LLC morphology. The polymerization rates are enhanced in the more ordered LLC phases as a result of the preferential orientation of the acrylamide monomer.

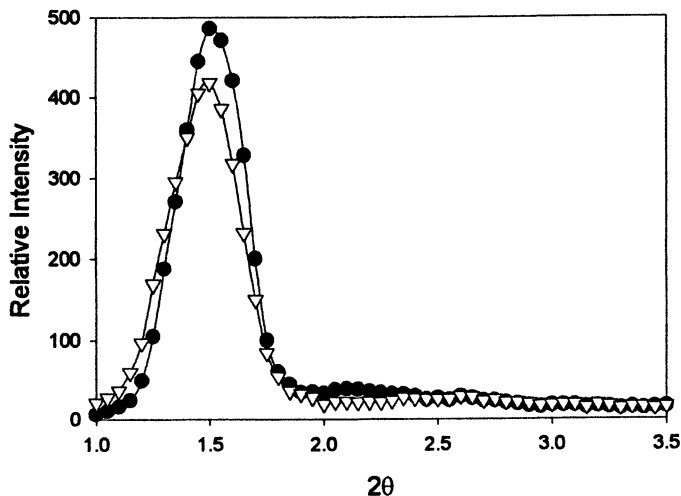


Figure 7. SAXS profiles of 25% acrylamide in the bicontinuous cubic phase formed with 40% Brij 58 and water before (●) and after (▽) polymerization.

The effect is observed both with changing temperature and changing composition. These results indicate that acrylamide is strongly associated with the LLC interface and coaggregates with the surfactant. LLC order strongly influences photopolymerization behavior and consequently the polymer structure. Photopolymerization under appropriate conditions also allows successful templating of the LLC nanostructure onto the acrylamide polymer.

Acknowledgements

The authors thank the University of Southern Mississippi, the Petroleum Research Fund, and the National Science Foundation (CTS-0093911) for financial support of this project. Also Dr. Bill Jarrett is gratefully acknowledged for obtaining the ^{14}N spectra.

References

1. Gray, G. W.; Winsor, P. A. *Liquid Crystals & Plastic Crystals*, 1st ed.; Gray, G. W.; Winsor, P. A., Ed.; John Wiley & Sons, Inc.: New York, 1974; Vol. 1, pp 314.
2. Göltner, C. G.; Antonietti, M. *Adv. Mater.* **1997**, *9*, 431.
3. Anderson, D. M.; Strom, P. *Physica A* **1991**, *176*, 151.

4. Gray, D. H.; Gin, D. L. *Chem. Mater.* **1998**, *10*, 1827.
5. Guymon, C. A.; Hoggan, N. A.; Rieker, T. P.; Walba, D. M.; Bowman, C. N. *Science* **1997**, *275*, 57.
6. Guymon, C. A.; Bowman, C. N. *Macromolecules* **1997**, *30*, 5271.
7. Guymon, C. A.; Dougan, L. A.; Martens, P. J.; Clark, N. A.; Walba, D. M.; Bowman, C. N. *Chem. Mater.* **1998**, *10*, 2378.
8. Lester, C. L.; Guymon, C. A. *Macromolecules* **2000**, *33*, 5448.
9. Lester, C. L.; Guymon, C. A. *Polymer* **2002**, *43*, 3707.
10. Fendler, J. H.; Tundo, P. *Acc. Chem. Res.* **1984**, *17*, 3.
11. Lester, C. L.; Colson, C.; Guymon, C. A. *Macromolecules* **2001**, *34*, 4430.
12. Cory, D. G.; Ritchey, W. M. *J. Magn. Reson.* **1988**, *80*, 128.
13. Lester, C. L.; Smith, S. W.; Guymon, C. A. *Macromolecules* **2001**, *34*, 8587.
14. Lester, C. L.; Guymon, C. A. *Langmuir* (submitted).
15. Lester, C. L.; Guymon, C. A. *Chem. Mater.* (submitted).

Chapter 33

Photopolymerization of Silica-Filled Composites: Encapsulants for Microelectronic Devices

Kiran K. Baikerikar¹, Vishal Sipani², Chris N. Coretsopoulos²,
and Alec B. Scranton²

¹The Dow Chemical Company, Building 1776, Office F33,
Midland, MI 48674

²Department of Chemical and Biochemical Engineering, University of Iowa,
4133 SC, Iowa City, IA 52242

Encapsulation of microelectronic devices is typically accomplished using a transfer molding process in which the molding compound is cured by heat. Most transfer molding processes suffer from significant problems due to the high operating temperatures and high pressures required to fill the mold. Photopolymerizable liquid encapsulants (PLEs) offer important advantages over the conventional encapsulants such as reduced in-mold cure times, lower thermal stresses, and reduced wire sweep. In this contribution, we discuss a new strategy for encapsulating microelectronic devices based upon a low viscosity, epoxy novolac-based vinyl ester resin, with highly filled fused silica fillers, that cures rapidly upon exposure to UV light. For these PLEs, the viscosity, flexural strength and modulus, coefficient of thermal expansion, glass transition temperature, initiation scheme, and illumination time for systems containing 70.0 – 74.0 wt% fused silica have been characterized. A photocurable encapsulant containing 74.0 wt% fused silica was found to be very promising for microelectronic encapsulation. These liquid encapsulants cure (to an ejectable hardness) in less than two minutes for an initiating light intensity of 200 mW/cm² and exhibit appropriate the thermal and mechanical properties.

Introduction

The microelectronics, communications, and computers industries have undergone a major shift from highly sophisticated and expensive mainframe systems to small-scale systems such as personal computers and communication devices. This trend arises from the continuous push for the integration of many functions on a single chip. Very large scale integration (VLSI) and ultra large scale integration (ULSI) are made possible by the ability to fabricate devices with smaller and smaller feature sizes. However, as the feature sizes on a semiconductor chip are reduced, the probability of contamination or damage is dramatically increased. For this reason microelectronic devices are typically encapsulated in a plastic package to protect the silicon chip from adverse mechanical, thermal, chemical, and electrical environments, and also from physical and chemical damage.

Traditionally, this encapsulation is done by using a transfer molding process. This process, however, suffers from significant problems due to the high operating temperatures and high pressures required to fill the mold. These aspects of the current process can lead to incomplete mold filling, thermal stresses (since the reaction temperature is much higher than the final use temperature), and wire sweep (deformation or displacement of the wires that provide electrical interconnection between the silicon chip and the leadframe as a result of flow stresses imparted by the encapsulation material). As the size of the encapsulant and the associated wires shrink to smaller and smaller dimensions, so does the operating window for transfer molding; hence, it is difficult to control wire sweep in the high pin count, fine pitch packages.

In order to minimize these problems, current encapsulation materials must possess appropriate values for a number of critical parameters, such as viscosity, flexural strength and modulus, coefficient of thermal expansion, and glass transition temperature. Photopolymerizable liquid encapsulants (PLEs) appear to satisfy these requirements. The use of light rather than heat to initiate the polymerization allows precise control over when the reaction starts, and therefore completely decouples the mold filling and the cure. In this contribution, we discuss an encapsulation process based upon a low viscosity, epoxy novolac-based vinyl ester resin that cures rapidly upon exposure to UV light. Specifically, we have characterized the viscosity, flexural strength and modulus, coefficient of thermal expansion, glass transition temperature, and initiation scheme of PLEs containing 70.0-74.0 wt.% fused silica. We have also investigated the effects of illumination time and the postcure time, fused silica loading, and the inclusion of a thermal initiator, on the thermal and mechanical properties of the final cured encapsulants.

Experimental

Materials

The photopolymerizable liquid encapsulant in this study is comprised of a base resin, fused silica filler, photoinitiator, silane coupling agent, and in some cases a thermal initiator (1,2). The base resin used in these studies was an epoxy novolac-based vinyl ester resin (DERAKANE 470-45, Dow Chemical) that was chosen for its low initial viscosity (40-80 cP at 25 °C), as well as, its appropriate thermal and mechanical properties upon cure. The photoinitiator used was bis(2,4,6-trimethylbenzoyl) phenylphosphine oxide (IRGACURE 819, Ciba). This photoinitiator, which we will henceforth denote as BAPO, has been shown to be especially appropriate for curing relatively thick polymers and composites due to its efficient photobleaching (3,4). In some systems, the thermal initiator, benzoyl peroxide (Aldrich), was used in order to investigate the effects of a dual photo/thermal initiation scheme on the resulting material properties of the encapsulant. The fillers used were crushed (angular), untreated fused silica obtained from MINCO, Inc. A silane coupling agent, 3-methacryloxypropyltrimethoxysilane (Dow Corning), was used to provide a stable bond between the base resin and the fused silica filler, and to improve the processability of the liquid encapsulant formation. For the viscosity studies, three different fused silica products, each with its own continuous particle size distribution, were used. The broadest distribution of particles (which also contained the largest particles), MIN-SIL 40 (henceforth referred to as particle size distribution A, or PSD-A) had a volume average particle size = 32.42 μm , and a median particle size = 22.11 μm . The second distribution of particles, MIN-SIL 20, (henceforth referred to as PSD-B) had a volume average particle size = 19.37 μm and a median particle size = 13.17 μm . The narrowest distribution of particles (which contained the largest fraction of small particles), MIN-SIL 550 (henceforth referred to as PSD-C) had a volume average particle size = 10.37 μm and a median particle size = 6.03 μm . For the thermal and mechanical property characterization studies, only a 50:50 mixture of PSD-A and PSD-C was used.

Sample Preparation and Characterization Methods for Cured Encapsulants

To determine the effect of blending two different fused silica particle size distributions on the viscosity of the PLE, the DERAKANE 470-45 resin was mixed with 70.0 wt.% fused silica, 0.20 wt.% BAPO photoinitiator (based on resin weight), and 1.43 wt.% of the silane coupling agent (based on filler weight). In some cases, the thermal initiator, benzoyl peroxide, was also added in the amount of 1.2 wt.% (based on resin weight). In this study, all samples contained 70.0 wt.% (0.526 volume fraction) fused silica. The fused silica particle size distribution was varied by preparing binary mixtures of the

individual distributions, PSD-A, PSD-B, and PSD-C. Viscosities were measured using a Brookfield DV I+ Viscometer equipped with the Small Sample Adapter (SC4-34 spindle and 13R chamber) at 30°C and a shear rate of 0.56 sec⁻¹.

Specimens for flexural testing and thermal conductivity measurements were prepared by photopolymerizing the liquid encapsulant in rectangular silicone molds with unfiltered UV light (200 mW/cm² UVA intensity) from a 3000 W arcless mercury vapor lamp (Fusion UV Systems, model F450T). Light intensities were measured (over the 320-390 nm range) using a UVICURE Plus high energy UV integrating radiometer. The specimens were 76.2 mm long, 12.7 mm wide, and 3.2 mm deep. To investigate the effect of illumination time, the samples were illuminated for 60.0, 90.0, 120.0, 150.0, and 180.0 seconds. The degree of cure was determined using differential scanning calorimetry (DSC). The instrument used was a Perkin Elmer DSC 7 Differential Scanning Calorimeter interfaced with computer via the TAC 7/DX Thermal Analysis Instrument Controller. In these experiments, cure was monitored by measuring the heat released by the sample as the reaction proceeded. To determine the effect of thermal postcure (after UV illumination) on the resulting thermal and mechanical properties, some specimens were postcured at 170°C in a laboratory oven for 2, 4, 6, and 8 hours. The flexural strength and modulus of the photocured samples were determined using a United SFM-20 instrument in accordance with the ASTM D 790 method. The flexural properties were measured using the three point flexural test with a span length of 50.8 mm, a span-to-depth ratio of 16:1, a 454 kg load cell, and a downdrive rate of 1.7 mm/min. Flexural strength and modulus values were calculated using DATUM 97 software (United Testing Systems).

Specimens for the coefficient of thermal expansion (CTE) testing were 11.0 mm length x 8.0 mm width x 3.2 mm thickness. The CTE below glass transition (α_1) and CTE above glass transition (α_2) were both measured using a DuPont 943 thermomechanical analyzer (TMA) interfaced with a DuPont model 9900 thermal analyzer controller. The samples were heated from room temperature (23°C) to 234°C at a constant rate of 3°C/min. The change in the sample thickness during heating was recorded in the personal computer and α_1 was obtained from the inclined line connecting two points on the TMA curve, 50°C and 70°C. To determine α_2 , the inclined line connecting 200°C and 230°C was used. The glass transition temperature was taken to be the temperature at the intersection of these two lines.

Thermal conductivity measurements were performed by Holometrix, Inc. (Bedford, MA) using the Holometrix Thermaflash 2200 Laser Flash system and in accordance with the ASTM E1461-92 method. In this technique, the measurement of the thermal diffusivity of a material is carried out by rapidly heating one side of the flat disk sample and measuring the temperature as a function of time (the temperature rise curve) on the opposite side. Based upon this temperature profile, the through-plane diffusivity is measured, and the thermal conductivity is calculated using the known values of the specific heat

and bulk density. The dimensions of the cured specimens were 76.2 mm length \times 25.4 mm width \times 3.2 mm thickness, which were then machined into disks with diameter of 12.7mm and a thickness of 1.0 mm for the thermal conductivity testing.

Results and Discussion

Effect of Fused Silica Particle Size Distribution on Viscosity

For encapsulating microelectronic devices, it is desirable to achieve a low enough viscosity to allow the molding compound to easily flow over the chip, wirebond, and lead frame assembly to avoid problems associated with incomplete mold filling, lead frame displacement, and wire sweep. We have characterized the viscosity of PLEs containing 70.0, 72.0, and 74.0 wt.% silica, and found that a blend of particle size distributions with a particle size ratio of 3.13 (PSD-A and PSD-C) resulted in the best viscosity reduction (5). For example, in experiments performed for a constant filler loading of 0.526 volume fraction (70.0 wt.%), the particle size distribution had a marked effect on the viscosity of the PLE. A 50:50 mixture of PSD-A and PSD-C resulted in a PLE viscosity three times lower than that obtained using only the PSD-A filler, and four times lower than a PLE prepared using a 50:50 mixture of PSD-A and PSD-B. In addition, the 50:50 mixture of PSD-A and PSD-C resulted in a PLE viscosity 40% lower than that obtained using a 50:50 mixture of PSD-B and PSD-C. The experimental results for the effect of the particle size distribution on the PLE viscosity were well correlated by the Krieger-Dougherty equation to account for the blending of two particle size distributions. Experiments performed to investigate the effect of the silane coupling agent on the viscosity of the PLE revealed that the viscosity decreased slightly with increasing concentration of the coupling agent.

As the fused silica loading was increased from 70.0 to 74.0 wt.%, the PLE viscosity increased markedly. This apparently small increase in the fused silica loading can be important for microelectronic encapsulants because it can lead to a lower coefficient of thermal expansion and an enhanced thermal conductivity. As the amount of fused silica was increased from 70.0 to 72.0 wt.%, the viscosity increased by a factor of 2.3, and as the fused silica loading was increased from 70.0 to 74.0 wt.%, the viscosity increased more than five-fold. The current epoxy molding compounds are solid at room temperature, therefore even the PLE containing 74.0 wt.% fused silica has a much lower viscosity at ambient temperature than the traditional molding compounds. Thus, the resulting PLEs exhibit low viscosities at ambient temperature while maintaining desirable material properties for microelectronic applications.

Flexural Strength and Modulus

Encapsulants must have excellent mechanical properties in order to withstand mechanical shock, vibration, and handling during assembly. An important mechanical property for microelectronic encapsulants is the flexural modulus, which characterizes the stiffness of a material under an applied load. The optimal value of the flexural modulus provides a balance between two conflicting requirements. A high value of the flexural modulus is desired to maximize the protection of the chip from an applied load; however, lower values of the flexural modulus lead to lower thermal stresses. Thermal stresses associated with high modulus encapsulants can lead to failure of the microelectronic device. In particular, this stress has been reported to cause interfacial cracking and breakage of the wirebond leads, as well as passivation layer cracking and aluminum pattern deformation. To reduce the thermal shrinkage stresses, while maintaining appropriate protection against mechanical shock, vibration, *etc.*, a flexural modulus near $1000 \text{ kg}_f/\text{mm}^2$ (9800 MPa) is recommended (6).

The effects of filler loading (three different compositions, 70, 72, and 74 wt% silica) and UV illumination time (60, 90, 120, 150, and 180 seconds) on the flexural modulus and strength of the photocured encapsulants were studied. As expected, the flexural modulus and flexural strength increase with fused silica content. In addition, the flexural properties do not change significantly as the illumination time is increased beyond 120 seconds. Therefore, 120 seconds was chosen for the in-mold illumination time for subsequent experiments. In all these cases, except for the illumination time of 60 seconds, values of the flexural modulus are found to be near the desired value of $1000 \text{ kg}_f/\text{mm}^2$. These results suggest that the PLEs could allow the in-mold cure time to be reduced significantly below 120 seconds (which is the typical in-mold cure time for transfer molding compounds). For example, the mechanical properties observed after 90 seconds are essentially equivalent to those after 120 seconds, and an ejectable hardness is certainly achieved even earlier. This result is significant because the in-mold cure time consumes approximately 70% of the overall cycle time and an in-mold cure time reduction of even 15 seconds can translate to a productivity increase of about 10% (6).

The flexural strength of the samples as they are taken from the mold, immediately after the illumination, ranges from 3 to $4.5 \text{ kg}_f/\text{mm}^2$ (~ 30 to 45 MPa). Current microelectronic encapsulants exhibit a flexural strength of at least $9 \text{ kg}_f/\text{mm}^2$ (after being postcured); therefore, the strength of the PLEs immediately after illumination is below the range of desired values. To address this point, we investigated the effect of a 6 hour postcure step (after photocuring the samples for 120 seconds) and the inclusion of a thermal initiator, benzoyl peroxide (1.2 wt% based on resin weight) on the flexural strength. This result is shown in Figure 1.

Figure 1 illustrates that postcure and the thermal initiator both have a significant impact on the flexural strength of the specimens, resulting in values which are in the necessary range for microelectronic encapsulants. For example, the samples filled with 74.0 wt.% fused silica exhibit an increase in the flexural strength from a value of 4 kg/mm² with no postcure to more than 9 kg/mm² after a 6 hour postcure. Addition of thermal initiator had no effect on the flexural modulus values, as shown in Table 1.

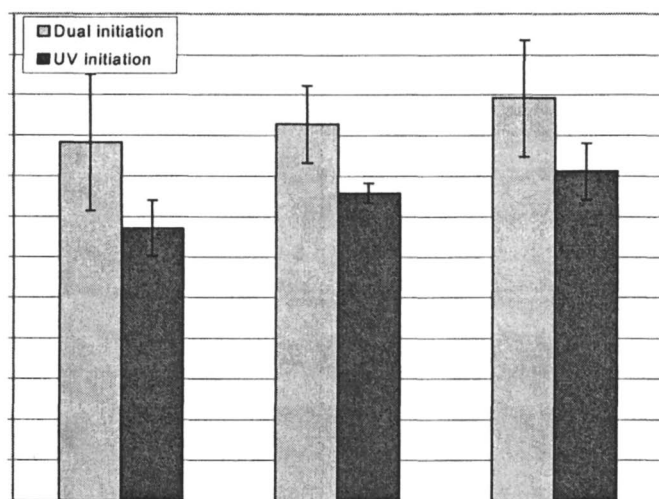


Figure 1. Effect of the thermal initiator, benzoyl peroxide(1.2 wt% based on resin weight), on the flexural strength.

Table 1. Effect of Thermal Initiator on Flexural Modulus for Samples that were postcured for 6 hours at 170°C

<i>Wt% Fused Silica</i>	<i>Flexural Modulus (kg/mm²) Without Thermal Initiator</i>	<i>Flexural Modulus (kg/mm²) With Thermal Initiator</i>
70.0	1059.24±111.18	973.40±89.13
72.0	1160.11±62.23	1139.05±123.83
74.0	1240.38±96.62	1206.61±116.55

Coefficient of Thermal Expansion and Glass Transition Temperature

The coefficient of thermal expansion (CTE) is an important parameter in semiconductor encapsulation because a significant CTE mismatch between the encapsulant, lead frame, and the silicon chip can lead to the build up of internal stresses in the semiconductor device, and could lead to cracking of the chip or encapsulant. Current encapsulants exhibit α_1 values (CTE below the glass transition temperature) in the range of 15-30 $\mu\text{m}/\text{m}^\circ\text{C}$. The α_1 values for the copper lead frame is 16-17 $\mu\text{m}/\text{m}^\circ\text{C}$, and that for silicon is 3-4 $\mu\text{m}/\text{m}^\circ\text{C}$. For the microelectronic encapsulants the value of the CTE above the glass transition temperature, α_2 , is not as important as the CTE below glass transition temperature, α_1 , because the service temperature is typically between 75 and 85°C, which is well below the T_g of the encapsulant.

The experiments for the coefficient of thermal expansion below glass transition were done for postcure time of 0, 2, 4, 6, and 8 hours after irradiation with UV light of 200 mW/cm^2 UVA intensity for 120 seconds. It was found that for all three filler loadings, a significant reduction in α_1 was observed after just 2 hours of postcure. This reduced value of the CTE may be attributed to the enhanced cure, approx. 8% additional cure, associated with the postcure step. Most of this additional cure occurs within the first two hours of postcure. After a two-hour postcure, all of the photocured samples exhibit α_1 values well within the range required for current encapsulants. As expected, α_1 decreased as the fused silica loading was increased from 70.0 to 74.0 wt.%. The 74.0 wt.% silica system looks especially promising for microelectronic encapsulants because of its low α_1 value, approx. 20 $\mu\text{m}/\text{m}^\circ\text{C}$). The presence of the thermal initiator was found to have no appreciable effect on the value of α_1 for all the three fused silica loading.

The CTE above the glass transition temperature, α_2 , was also measured as a function of filler loading and postcure time for systems containing only the photoinitiator, and also for the systems containing both the photoinitiator and the thermal initiator. It was found that α_2 decreases with an increase in the fused silica content, and it is essentially independent of the postcure time and the presence of the thermal initiator.

Encapsulants must be in the glassy state to be able to provide effective protection of the microelectronic device. Commercial encapsulants typically exhibit glass transition temperatures in the range of 140 to 180°C. Glass transition temperatures for all of the PLE samples in this study were found to increase with postcure time and were all in the range of 145 to 155°C, well within the range required for microelectronic encapsulants.

Thermal Stress Parameter

Thermal stress parameter is important because lowering the stress parameter results in improved device reliability. Conventional microelectronic encapsulants typically exhibit thermal stress parameters anywhere between 0.50 and 1.50 kg_f/mm². For example, a typical epoxy encapsulant has thermal stress parameter of ~1.3 kg_f/mm². Effect of reduced UV illumination times (for 60, 90, and 120 seconds) on thermal stress parameter, for samples that were photocured with UV light of 200 mW/cm² UVA intensity and then postcured for 6 hours at 170°C, were studied. These samples generally exhibited stress parameter ranging from 0.6 to 1.3 kg_f/mm², and are therefore within the range exhibited by the current encapsulants. The thermal stress parameter for a PLE sample containing 74.0 wt% fused silica was found to be between 0.8 and 1.2 kg_f/mm².

Thermal Conductivity

Microelectronic devices generate a significant amount of heat during their use, and from performance point of view it is important that the silicon chip does not overheat during its operation. The thermal conductivity determines the amount of heat that can be removed from the device, and thus affects the operating temperatures of electronic components. The thermal conductivity of a molding compound is highly dependent on the filler used. Conventional microelectronic encapsulants based upon fused silica typically exhibit thermal conductivities between 0.5 to 0.7 W/m·K.

Samples used for this study were photocured for 90 seconds from the 3000W arcless mercury vapor lamp UV light of 200 mW/cm² UVA intensity and then postcured in a laboratory oven for 6 hours at 170°C. All the samples contained 70.0 to 74.0 wt% fused silica, 1.0 wt% silane coupling agent (based on filler weight), 0.2 wt% BAPO (based on resin weight), 1.2 wt% benzoyl peroxide (based on resin weight), and the balance epoxy novolac-based vinyl ester resin. The thermal conductivity of the cured resin, with no filler, is approx. 0.182 W/m·K, and that for fused silica is 1.5 W/m·K. The thermal conductivity of the PLEs increases as the fused silica content is increased and the values range between 0.56 and 0.62 W/m·K. Hence they are more suitable for applications with low stress requirements, rather than devices with high heat outputs (which require high thermal conductivity fillers such as silicon carbide, $k = 85$ W/m·K; aluminum nitride, $k = 150$ -220 W/m·K; or boron nitride, $k = 250$ -300 W/m·K).

Specific Heat and Thermal Diffusivity

Specific heat is a measure of the quantity of heat a material must absorb to raise its temperature a specified increment. It was found that the specific heat

for the PLEs ranges from 0.83 and 0.87 J/g·K. The specific heat decreases when the weight content of the fused silica increases. Similarly, the thermal diffusivity was found to increase as the fused silica content is increased, with values ranging between 3.7×10^{-3} and 4.2×10^{-3} cm²/s.

Conclusions

This research has demonstrated the tremendous potential of highly filled photopolymerizable liquid encapsulants (PLEs) for microelectronic devices. The PLEs in this study are comprised of an epoxy novolac-based vinyl ester resin (~25 wt.%), fused silica filler (70-74 wt.%), and small amounts of a photoinitiator, silane coupling agent, and a thermal initiator. These PLEs have the material properties required by the microelectronic industry, (*i.e.* flexural modulus and strength, coefficient of thermal expansion, glass transition temperature, thermal conductivity and adhesion). In addition, there PLEs exhibit much lower viscosity than other transfer molding compounds and allow shorter in-mold cure times. PLEs will allow the in-mold cure time to be reduced from 120 seconds to 60-90 seconds, while simultaneously offering important advantages such as, lower thermal stresses, and reduced wire sweep. Table 2 provides a head-to-head comparison of the material properties between the PLEs and conventional transfer molding compounds.

Table 2. Comparison of material properties between PLEs and conventional molding compounds

	<i>PLE</i>	<i>Molding Compound (6)</i>
Viscosity (cP)	5,000 – 30,000 @ 30°C	1,5000 – 100,000 @ 170°C
Flexural Modulus (kg _f /mm ²)	1,000 – 1,200	1,000 – 1,500
Flexural Strength (kg _f /mm ²)	9 – 11	9 – 15
CTE (μm/m°C)	19 – 22	16 – 25
T _g (°C)	145 – 155	140 – 180
Thermal Stress Parameter (kg _f /mm ²)	0.6 – 1.3	0.5 – 1.5
Thermal Conductivity (W/m·K)	0.56 – 0.62	0.50 – 0.70

References

1. Baikerikar, K.K.; Scranton, A.B. *Polymer* **2000**, *42*, 431.
2. Baikerikar, K.K.; Scranton, A.B. *J. Appl. Polym. Sci.* **2001**, *81*, 3449.
3. Narayanan, V.; Scranton, A.B. *TRIP* **1997**, *5*, 415.
4. Narayanan, V.; Baikerikar, K.K.; Scranton, A.B. *RadTech '98 North America UV/EB Conf. Proc.* **1998**, 31.
5. Baikerikar, K.K.; Scranton, A.B. *Polym. Compos.* **2000**, *21*, 297.
6. *Plastic Packaging of Microelectronic Devices*; Manzione, L.T.; Van Nostrand Reinhold, New York, 1990.

Chapter 34

Photocurable, Hydrophobic Oligomers Based on Liquid Polybutadienes

Bo Yang and Bill Schaeffer

Sartomer Company, 502 Thomas Jones Way, Exton, PA 19341

Abstract

A series of photocurable, hydrophobic oligomers have been synthesized based on liquid polybutadiene prepolymers. The unique polybutadiene backbone chemistry provides films cured from these oligomers with inherent hydrolytic stability, resistance to aqueous acids and bases, low temperature flexibility, low moisture permeability, and dielectric properties. The base prepolymers are functionalized with either (meth)acrylate or epoxy groups making these new oligomers undergo facile photo-induced polymerization by either free radical or cationic mechanism. Basic photocuring behaviors of these oligomers and physical properties of cured films are investigated and reported.

Introduction

In recent years, photocuring technology has experienced rapid growth in coatings, inks, adhesives, and photolithography. While formulators now make their oligomer choice among commercially available acrylated epoxies, urethanes, polyesters, or polyethers, however, it was well recognized that the range of chemical and mechanical properties obtainable with these conventional materials is limited. For example, because these oligomers are generally hydrophilic in nature, it is difficult to obtain films having high degree of flexibility (especially at low temperature), hydrolytic stability, and dielectric properties. At the same time, functionalized elastomeric polybutadiene resins have been available for a number of years but are usually limited in their functionality to hydroxyl, vinyl, or carboxyl groups.

One feasible approach is to incorporate (meth) acrylic ester or epoxy functionality into the elastomeric liquid polybutadiene which then can be photo crosslinked to produce networks which combines the properties of rubbers and (meth)acrylic/epoxy resins. Further, these oligomers are liquid at room temperature and thus can be easily handled by conventional application processes. Similar considerations have led Decker and his coworkers¹ to modify diene polymers by attaching acrylic ester groups and Kennedy et. al.² to prepare epoxy techellic poly(isobutylenes). Both of these groups studied the UV induced crosslinking of the functionalized elastomers.

In this paper, we describe the basic chemistry of these liquid polybutadiene based elastomeric oligomers. Reactivity of these oligomers under photocuring condition was examined. Difference in photocuring responses between (meth)acrylate and 1, 2 vinyl/1, 4 double bonds was studied. Glass transition temperature, tensile properties, surface hardness, and resistance to acids and bases were measured and discussed.

Experimental

Materials

All liquid polybutadiene oligomers were from Sartomer Company: (meth)acrylated liquid polybutadiene (Ricacryl[®] 3801); epoxidized liquid polybutadiene (Poly BD[®] 600E and 605E); liquid polybutadiene dimethacrylate (CN301 and CN303); liquid polybutadiene urethane diacrylate (CN302). Both Ricacryl[®] and Poly BD[®] are trademarks of Sartomer Company. Specialty

photoinitiator Esacure KIP-100F and cycloaliphatic epoxy SarCat®K126 were also from Sartomer Company. ITX was provided by First Chemical Corporation. Irgacure 651 was supplied by Ciba Specialty Chemicals.

Wet film preparation

For standard film testing, a 5 mil wet films was cast on mill finished aluminum Q-Panels by using zero drawdown rods with double tapes. Great care was taken to obtain films with uniform thickness. This is very important because film thickness is a critical factor in determining a coating's performance.

Measurement of double bonds conversion

Conversion of double bonds from both the (meth)acrylic esters and polybutadiene unsaturation were measured by Fourier Transform Infrared Spectroscopy (FTIR) technique. A MIDAC FTIR spectrometer Model 1012801 was used. An UVEXS Model CCU-A conveyORIZED unit equipped with a single medium mercury vapor lamp was used to UV cure the samples. The UV dosage was measured using UVPS CON-TROL-CURE Model M007-008 compact radiometer. A detailed description of the technique and experimental results can be found from Estrin's original work³.

UV curing system (for studies other than FTIR)

An Asheed UV curing system was used. For physical properties testing, the films were passed four times under two 300W/in Hg lamps.

Prior to testing, all the coated panels were stored in the dark after curing for three days. This was done to ensure a uniform environmental history of the samples.

Test for acid and base resistance

The test procedure followed ASTM method D 1308-79. 50% sulfuric acid (H_2SO_4) was used. For tensile measurement, filmstrips were fully immersed in the testing reagents in an amber bottle. The strips were exposed using the same intervals as those for the covered spot test. The strips were washed and dried before testing.

Mechanical Properties Test

Tensile strength, elongation, and tensile modulus were determined with a Thwing-Albert tensile tester with a strain rate of 0.5 in/min. For each sample, at least 5 specimens were tested and an average value was reported.

Results and Discussion

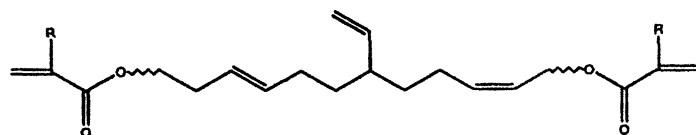
1. Basic Chemistry

a. (Meth)acrylated Liquid Polybutadiene Oligomers

Ricacryl[®]3801, CN301, CN302, and CN303 are (meth)acrylated liquid polybutadienes. As depicted in Scheme 1, the (meth)acrylate groups are located either terminally or along its linear backbone. For Ricacryl[®]3801, the oligomeric backbone was further functionalized with amines to render the oligomer adhesion promoting characteristic and aqueous dispersible.

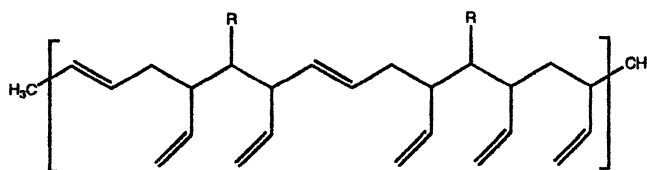
General physical properties of these liquid oligomers are described in Table 1.

Scheme 1: Chemical structures of (meth)acrylated liquid polybutadienes



R = H for CN302 (acrylate)

R = CH₃ for CN301 and CN303 (methacrylates)

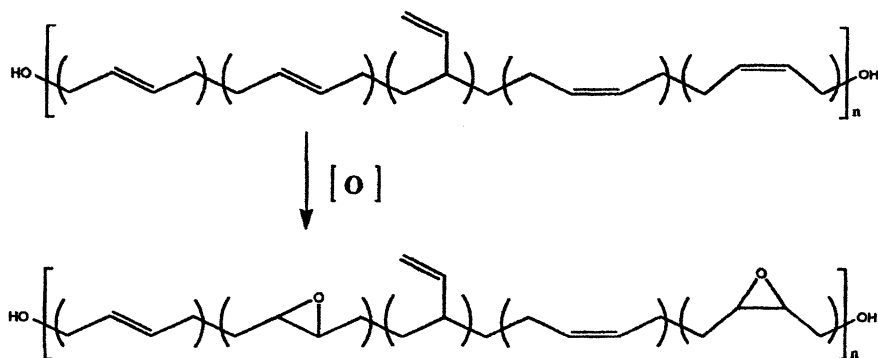


R = acrylate, methacrylate, or amine group Ricacryl[®]3801

Table 1: General physical properties of the (meth)acrylated liquid polybutadiene oligomers

Oligomers		Ricacryl ®3801	CN301	CN302	CN303
MW		3200	3000	3000	3000
Function ality	Acrylate	2	-	2	-
	Methacrylate	6	2	-	2
	1,2 Vinyl	26	-	-	-
	Trans 1,4-	10	-	-	-
Viscosity		25,000 @45°C	970 @60°C	17,000 @60°C	4,125 @60°C

Scheme 2. Epoxidation of Polybutadiene



b. Epoxidized Liquid Polybutadiene Oligomers

As shown in Scheme 2, Poly BD® E600 and E605 were obtained by epoxidation of liquid polybutadienes, mainly through 1, 4 double bounds. An earlier investigation by Crivello et. al.⁴ on a similar epoxidation experiment shown that 1, 4 double bonds are much more reactive than 1,2 vinyl double bonds towards epoxidation, mainly due to the higher electronic density associated with the 1,4 double bond. Basic properties of these two oligomers are described in Table 2.

2. Photo Reactivity and Properties of Cured Films of (Meth)acrylated Liquid Polybutadiene Oligomers

The photo reactivity of the four (meth)acrylated liquid polybutadiene oligomers were first compared (see Table 3). The order of reactivity is ranked as following: Ricacryl®3801 > CN301 ~ CN303 > CN302.

Table 2 Basic properties of Poly BD® E600 and E605

	E600	E605
Epoxy Value, meq/g	2-2.5	3-4
Epoxy Equivalent Weight	500-400	260-330
Oxirane Oxygen%	3.4	4.8-6.2
Viscosity mPas @30°C maximum	7000	22,000
Water, Wt., %, maximum	0.10	0.10
Specific Gravity	1.01	1.01
Hydroxyl value (meq/g)	1.70	1.74
Approximate microstructure (mol.)		
Epoxy cis	7 to 10	
Epoxy trans	8 to 12	
Vinyl double bonds	22	
1,4 – double bonds	53 to 60	
Opened Epoxy	3 to 4	

With eight pendant (meth)acrylate groups, Ricacryl®3801 possesses the highest reactivity under photo-induced polymerization. The high functionality also contributes to high tensile and modulus but an accordingly lower elongation. It is interesting to note that a glass transition temperature of -18.2°C was recorded with such a highly crosslinked polymeric network. Overall, Ricacryl®3801 is a unique building block for formulations where hydrophobicity, high photo speed, and high crosslink density are desirable. The less functionalized CN300 series produced films more or less resembling the elastomeric polybutadiene backbone: low tensile and modulus and high elongation. The photo-induced crosslinking only brought the glass transition temperature (T_g) from polybutadiene's intrinsic value of -75°C up to around -40°C . This low temperature transition is critical for delivery of film flexibility desired by electronics and specialty coating applications.

3. Ricacryl®3801: Influence of Photoinitiators and UV Dosage on Photo Reactivity and Film Properties

As indicated in Table 1, Ricacryl®3801 contains 44 potentially photochemically reactive double bonds among which are: 2 acrylates, 6 methacrylates, 26 1,2 vinyls, and 10 1,4 trans.

FTIR was utilized to monitor degree of conversion of different double bonds. Peaks at three distinct wavenumbers, 812 cm^{-1} , 910 cm^{-1} , and 968 cm^{-1} were used for (meth)acrylic, 1,2 vinyl, and 1,4 trans double bonds, respectively.

As one can see from Figure 1, over eighty percent of the (meth)acrylic double bonds were converted during photopolymerization while only twenty seven percent of 1,4 trans and fourteen percent of 1,2 vinyl double bonds participated in the free radical chain polymerization. Although the 1,4 and 1,2

Table 3. Photo curing speed and physical properties of cured films of (meth)acrylated polybutadiene oligomers

	<i>Ricacryl</i> ® <i>3801</i>	<i>CN301</i>	<i>CN303</i>	<i>CN302</i>
Rate of surface cure, FPM *	50	20	20	10
Tensile strength, psi **	1,659	639	166	235
Elong. @ break % **	6.6	15.2	36.2	35.2
Modulus psi**	52,846	6,979	724	1,185
Reverse impact, in/lbs**	<2	48	75	28
Tg (°C) **	-18.02	-44.45	-39.83	-38.93

*One 300W/in. Hg lamp; Film thickness: 5 mils; 5% KIP-100F as photoinitiator

** Two 300W/in. Hg lamps, four passes, 50 feet per minute (FPM)

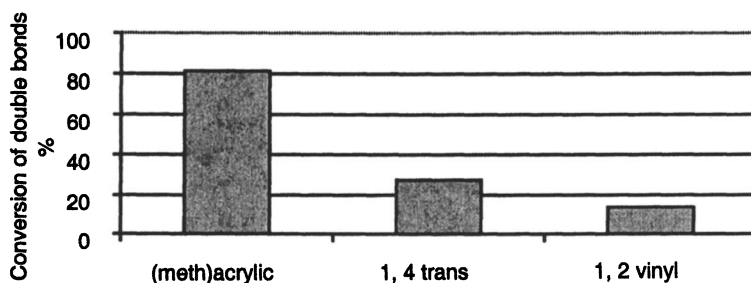


Figure 1. Conversion of double bonds in Ricacryl®3801: 3% KIP-100F, 5J/cm²

vinyl double bonds are much less reactive photochemically, their contribution to the final crosslink density of the polymeric network are significant due to their large initial population (36 Vs 8 for (meth)acrylate per molecule). Figure 2 provides the number of crosslinks (number of initial double bonds * % conversion) produced by different double bonds per molecule of Ricacryl[®]3801. The combined 1,2 vinyl and 1,4 double bonds produced almost equivalent amount of crosslinks as the (meth) acrylate did.

The conversions of double bonds were also found to differ greatly with the choice and level of photoinitiators.. Figure 3 illustrates the effects of three photoinitiators, ITX, KIP-100F, and Irg651, on the conversion of polybutadiene

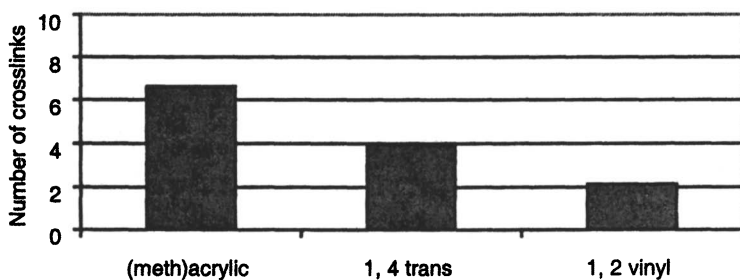


Figure 2. Number of crosslinks formed per molecule of Ricacryl[®]3801: 3% KIP-100F, 5J/cm²

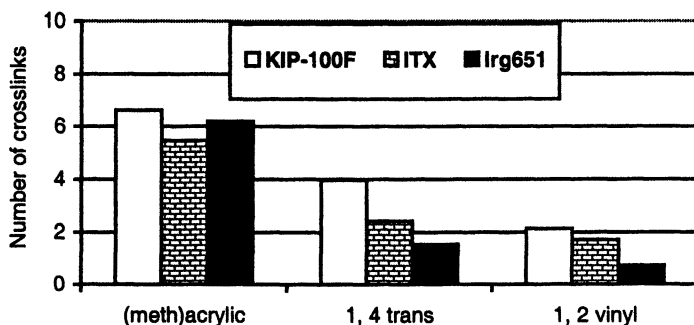


Figure 3. Influence of photoinitiator on the number of crosslinks for each double bond type Ricacryl[®]3801: 3% photoinitiator, 5J/cm²

and acrylic double bonds. While both ITX and KIP-100F were highly efficient towards the polybutadiene double bonds, Irg651 exhibited only half of the reactivity. All three photoinitiators seemed to be equally reactive to the (meth)acrylic double bonds. Again, 1, 4 was more reactive than 1,2 vinyl.

In general, double bond conversion increased as more photoinitiator was used. Again, this concentration effect was more effective for polybutadiene double bonds (Figure 4).

As with other photocuring system, UV dosage was observed greatly altering crosslink density of the polymeric network. This was demonstrated in Figure 5 where UV dosage was increased from 3 to 11 joules/cm². While the conversion of (meth)acrylic double bond reached a slightly higher conversion with

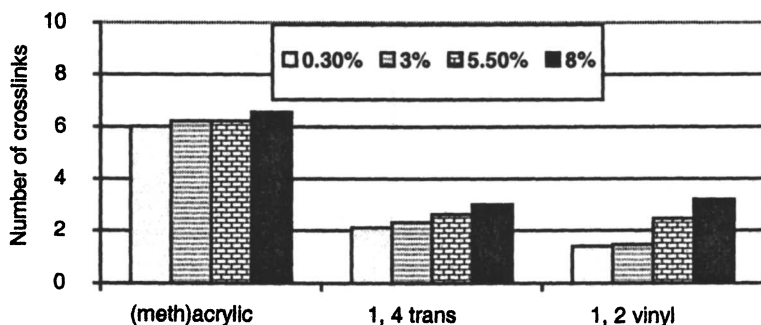


Figure 4. Effect of photoinitiator concentration on number of crosslinks for each double bond type. Ricacryl[®]3801: ITX, 8 J/cm²

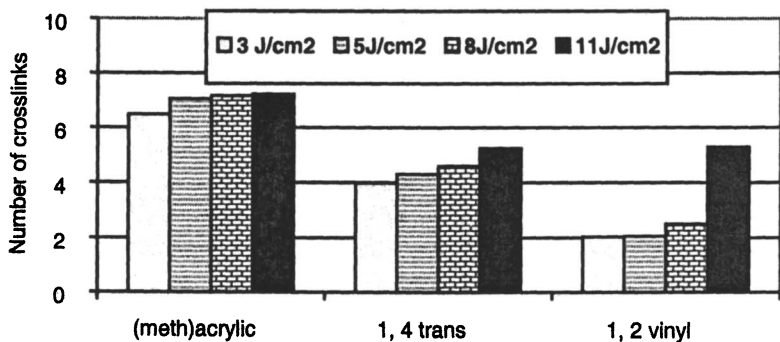


Figure 5. Effect of UV dosage on number of crosslinks for each double bond type. Ricacryl[®]3801: 8% KIP-100F

increasing UV dosage, the polybutadiene double bonds were much more responsive to the change in UV dosage.

The change in double bond conversion, regardless of its causes, should be reflected on the properties of the final films. Surface properties, measured by pencil hardness, were found to vary greatly with UV dosages, choice and level of photoinitiators. This was depicted in Figure 6.

More extensive data on this subject can be found from Estrin's original work³ from which this entire section is based on.

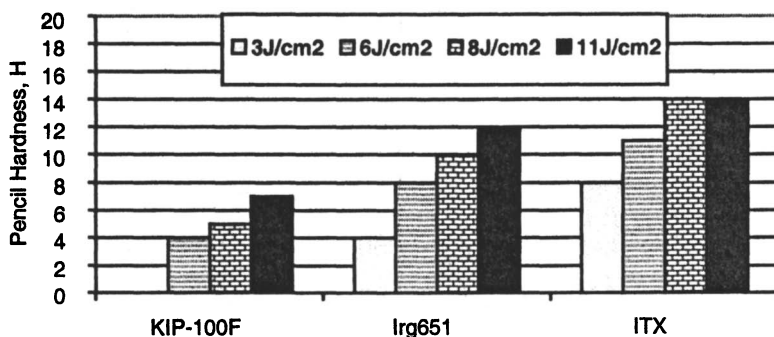


Figure 6. Effect of double bond conversion on surface hardness. Ricacryl[®]3801: 3% photoinitiator

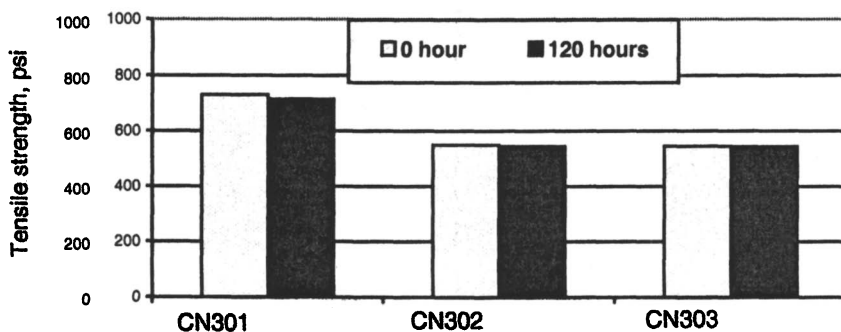


Figure 7. Effect of 50% sulfuric acid on tensile strength, room temperature

4. Chemical Resistance of (Meth)acrylated Liquid Polybutadienes

Polybutadiene are well known for its superior hydrolytic stability, low moisture permeability, and excellent resistance to aqueous acids and bases. The additional crosslinks from the photopolymerization should make the films even more resistant to attacks by chemicals, especially aqueous acids and bases. Here,

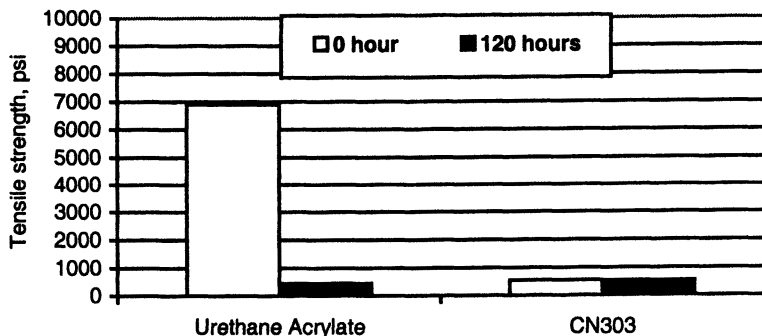


Figure 8. Effect of 50% sulfuric acid on tensile strength at elevated temperature (60°C)

films cured from CN301 and CN302 were exposed in 50% sulfuric acid and changes in physical properties with time were monitored. As evident in Figure 7, after 120 hours immersion at room temperature, the tensile strength of the CN300 series remained essentially unchanged. The crosslinked network and polybutadiene's hydrophobic domain effectively protects the films from water penetration and subsequent degradation by the strong oxidizing sulfuric acid.

In a related experiment, the immersion temperature was raised to 60°C . A polyester based urethane acrylate was also included for comparison (Figure 8).

Again, after 120 hours, the films made of CN302 experienced little change in tensile properties. Meanwhile, the film made of urethane acrylate suffered significant reduction in tensile strength, retained less than ten percent of its initial value. For the latter, the photo-chemically formed network along was simply not strong enough to withstand the 50% sulfuric acid at elevated temperature (60°C). Hydrolysis of the ester linkage and subsequent damage to the polymeric network were inevitable in this case. A similar experiment with 50% NaOH resulted in similar outcomes.

Conclusion

Both (meth)acrylated and epoxidized liquid polybutadienes undergo photo-chemically induced polymerization. 1,2 vinyl and 1,4 trans double bonds react slowly compared to its (meth)acrylic counterpart but significantly contribute to final conversion and film properties. Films with varied degree of flexibility can be obtained with proper choice of oligomers. All oligomers exhibited glass transition temperatures well below zero degree after curing. The polybutadiene backbone combined with the crosslink generated from the photopolymerization of the (meth)acrylic or polybutadienes double bonds produced hydrolytically stable films with superior resistance to aqueous acids and bases.

References

- [1] H. L. Xuan and C. J. Decker, *J. Polym. Sci., Polym. Chem. Ed.*, **31**, 769, 1993
- [2] J. A. Puskas, G. Kaszas, and J. P. Kennedy, *J. P., J. Macromol. Sci. Chem.*, **A28(1)**, 6, 1991
- [3] T. Estrin, *International Coatings Exposition, Dallas, Texas*, 1999
- [4] J. V. Crivello and B. Yang, *J. M. S. - Pure Appl. Chem.*, **A31(5)**, pp.517-533, 1994

Chapter 35

UV-Curable Acrylated Oligomers: Effect of Structural Variation on Liquid and Cured Film Properties

A. J. Tortorello

DSM Desotech, Inc., 1122 St. Charles Street, Elgin, IL 60120

Unique acrylate functional oligomers have been developed with the concept of versatile property selection in mind. Spectroscopic structural confirmation using model compounds has demonstrated that synthesis of the desired compositions has been achieved. A variety of oligomeric compositions have been synthesized and characterized. When formulated into typical UV curable coatings, a range of liquid and film properties become attainable depending upon the oligomer being used. Cured films covering the spectrum from soft and flexible to hard and brittle have been made. This study will focus on the range of properties achievable using these oligomers. Selection of a suitable oligomer composition required to attain desired film properties has become apparent. In certain cases, a sufficiently wide range of properties has been found to suggest the use of a single oligomer for multiple applications.

Introduction

Polymers of acrylic acid and methacrylic acid esters are well known and find widespread use in commerce (*1a*). In coatings applications, they have found use in architectural, appliance, furniture, automotive, and aerospace finishes. Their general attraction stems from many factors including ready commercial availability and a wide variety of applied film properties (*1b*). Acrylic coatings are typically provided in the form of solutions in volatile organic solvents or aqueous dispersion.

Acrylics are also widely used in the radiation cured coatings industry as well (*2a*). Here lower molecular weight polymers (oligomers) containing acrylic or methacrylic ester functional groups are polymerized, usually with monomers, and crosslinked through the action of a source of radiation, usually ultraviolet light (*2b*). One of the main attractions of radiation cured coatings is the lack of significant volatile byproducts emitted after application and curing.

High molecular weight acrylic copolymers containing acrylate ester functional groups are not widely available, presumably because of the unique challenge required of the synthesis. The functional groups reacted during the polymerization are the same as those which must be preserved for functionalizing the resulting polymer. Free-radical polymerization is not sufficiently selective to preserve one functional group in the presence of the same functional group located elsewhere in the same monomer molecule.

We have recently applied the concept of latent functionality to introduce the acrylate ester functional group into higher molecular weight acrylic copolymers (*3*). Structural confirmation has been demonstrated using spectroscopic studies on model compounds (*4*). This report summarizes the characterization of liquid oligomers and cured films and the effect of structural variation on the respective properties.

Experimental

Random acrylic copolymers were prepared by preheating suitable hydroxy-functional prepolymers to reaction temperature (usually 80°C) under nitrogen atmosphere in a 4-neck reaction flask. A mixture of monomers, (usually methyl methacrylate, 2-ethylhexyl acrylate and 2-hydroxyethyl acrylate), and thermal initiator (t-butylperoxy 2-ethylhexanoate) was added to the flask contents over three hours. After addition, the resulting polymer solution was heated to 105°C

for three hours, then cooled, isolated, and characterized for molecular weight, viscosity, and hydroxyl content. Molecular weight was determined by GPC comparison to polystyrene standards using a Waters Associates model 2690 chromatograph with 5 micron TSK-GEL packing and THF eluent at 1 mL/min flow. Viscosity was recorded on a Physica Rheolab MC10 viscometer using a Z4 bob and cup assembly at 10.3 (sec)^{-1} rate of shear.

The resulting hydroxy-functional acrylic copolymer solutions were converted to urethane-acrylate oligomers by first reacting 2 equivalents of a desired isocyanate (usually isophorone diisocyanate, IPDI) with one equivalent of a hydroxy-functional acrylate ester (usually 2-hydroxyethyl acrylate, HEA) in the presence of catalyst (dibutyltin dilaurate) and inhibitor (2,6-di-*t*-butyl-4-methylphenol). The reaction was conducted in a 4-neck reaction flask under dry air atmosphere. The flask contents were then heated to 80°C followed by addition of one equivalent of acrylic copolymer solution and suitable acrylate ester monomer to control viscosity as needed. The reaction temperature was maintained until completion of reaction as indicated by measurement of residual isocyanate. The resulting product was then characterized for viscosity, oligomer concentration, and residual isocyanate.

UV curable coatings were formed by blending oligomer with suitable acrylate ester monomer and photoinitiator until uniform mixtures were obtained. Coating viscosity was recorded on a Brookfield Model RVT viscometer using a no. 15 spindle at 20 or 50 rpm. The coatings were applied to glass plates as 75 micron liquid films and cured under nitrogen atmosphere using a medium pressure mercury lamp at a dosage of 1 joule(cm)^{-2} (Fusion Systems D lamp). Mechanical film properties were then recoded by carefully removing 1.25X11.25 cm film strips. The specimens were analyzed using an Instron model 4201 tensile tester with System 9 software, and secant modulus at 2.5% elongation was reported as an average of 5 samples. Dynamic mechanical analysis results were recorded on a Rheometrics RSA II Analyzer at a frequency of 1 radian/sec. with values taken at 2°C intervals.

Results and Discussion

Acrylate functional acrylic copolymers can be prepared in a two step sequence as outlined in Scheme I. In the first step, acrylic monomers, one of which is hydroxy-functional, are polymerized by thermal initiation in the presence of a hydroxy-terminated prepolymer, resulting in a random copolymer “solution” (1). In the second step, this product is converted to an acrylate composition (3)

through urethane formation by reaction of the hydroxyl groups with an isocyanate containing acrylate. The critical material for this conversion is depicted in Scheme I as the 1:1 molar addition product (2) of isophorone diisocyanate and 2-hydroxyethyl acrylate which is made *in-situ*. The conversion is completed by monitoring the loss of isocyanate functionality and may be conducted in the presence of acrylate containing ester monomer to control viscosity, if needed.

Vinyl/Acrylic Copolymer (1) Solution Properties

The solution properties of the copolymer have been shown to be affected by several factors including the calculated copolymer glass transition temperature, the concentration of hydroxyl groups in the copolymer, and the type of diluent used in the synthesis of the copolymer. Each of these factors adds a degree of versatility to the design of features for selected properties and highlights the advantage of acrylic copolymers.

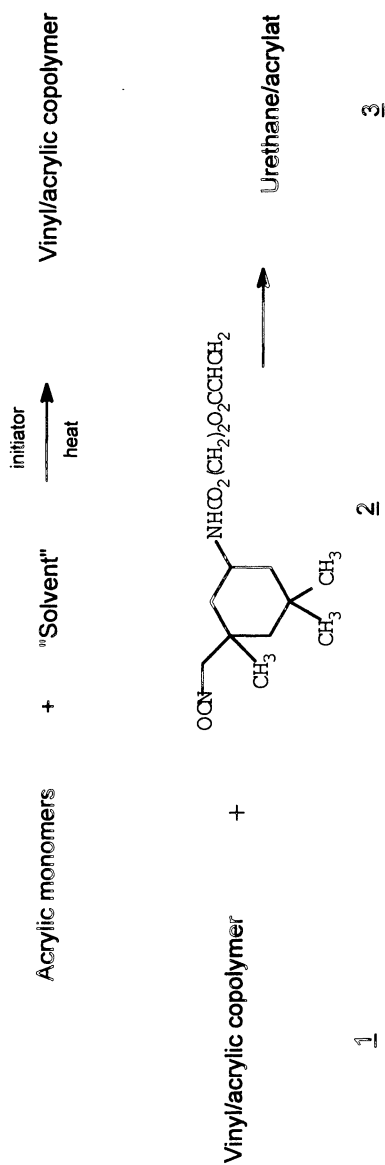
Effect of Diluent Polyol Molecular Weight on Solution Viscosity

A series of copolymers having the same monomer composition, glass transition temperature, and weight percent concentration were synthesized in hydroxy-terminated poly(propylene glycol)s of varying molecular weight. The results of the viscosity of each composition as a function of diluent molecular weight are depicted in figure 1 for the series of copolymers containing 5 weight percent of hydroxyl monomer. These results are typical of compositions containing varying levels of hydroxyl monomer and indicate a trend toward increasing solution viscosity with diluent molecular weight. This effect can be attributed to a reduction in solvent molar concentration for the same solvent mass as molecular weight increases.

Urethane/Acrylate Oligomer (3) Solution Properties

Since diluent molecular weight, copolymer hydroxyl content, and copolymer T_g have been found to have dramatic effects on the solution properties of the copolymer (1), it is reasonable to expect similar effects for the urethane acrylate oligomer (3). However, these effects may be compounded by the effect of hydrogen bonding attributed to the urethane which results from the reaction. Typically, one sees a reduction in solution viscosity for a series of urethanes made from hydroxy-terminated prepolymers of increasing molecular weight.

SCHEME I: ACRYLATED ACRYLIC SYNTHESIS



Effect of Diluent Molecular Weight on Acrylic Solution Viscosity

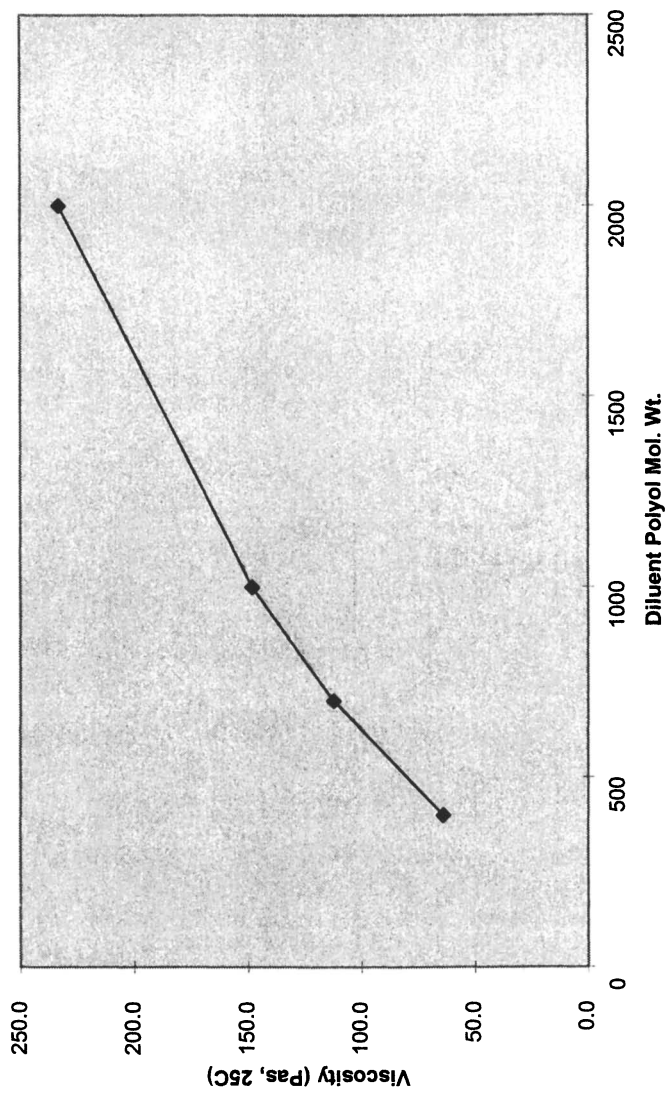


Figure 1: Effect of Polyol Molecular Weight on Viscosity

This is a direct consequence of dilution of hydrogen bonding by the molecular size of the prepolymer. Thus the solution properties of the urethane acrylates were of interest.

Effect of Diluent Monomer Glass Transition Temperature on Urethane Viscosity.

A series of acrylic copolymer solutions having the same monomer composition, calculated glass transition temperature, hydroxyl content, and weight concentration in 400 molecular weight poly(propylene glycol) were converted to urethane acrylate in the presence of varying diluent monomers. The effect of the glass transition temperature of the diluent monomer's homopolymer is depicted in figure 2. The results indicate a trend toward dramatic viscosity increase within the series of isodecyl acrylate, 2-phenoxyethyl acrylate, and isobornyl acrylate. Since each of these monomers is approximately the same in molecular weight, variation in molar concentration should be minimal. Thus the effect seems to be consistent with previously reported effects for high solids solutions (5).

Effect of Acrylic Hydroxyl Content on Urethane Viscosity

Solutions of copolymers (1) having identical calculated glass transition temperature and weight concentration in hydroxy-terminated poly(propylene glycol) but varying in polyol molecular weight and acrylic hydroxyl content, were converted to urethane acrylate by the reaction with adduct (2). Each product was prepared in constant concentration of isobornyl acrylate as the diluent monomer of choice. The effect of acrylic hydroxyl content on each series is shown in figure 3. Within each series of polyol molecular weights, urethane viscosity is found to increase with acrylic hydroxy content. Presumably this is due to the effect of increasing urethane formation and hydrogen bonding. However, one cannot determine from this study alone that the polyol molecular weight has no contribution to the effect.

Effect of Prepolymer Molecular Weight on Urethane Viscosity

Figure 4 demonstrates the effect of poly(propylene glycol) molecular weight on urethane viscosity for each series with the same acrylic hydroxyl content. Polyol molecular weight seems to have the most dramatic effect. As expected, viscosity is seen to decrease with increasing molecular weight, but this appears to be true

Effect of Diluent Monomer Tg on UA Viscosity

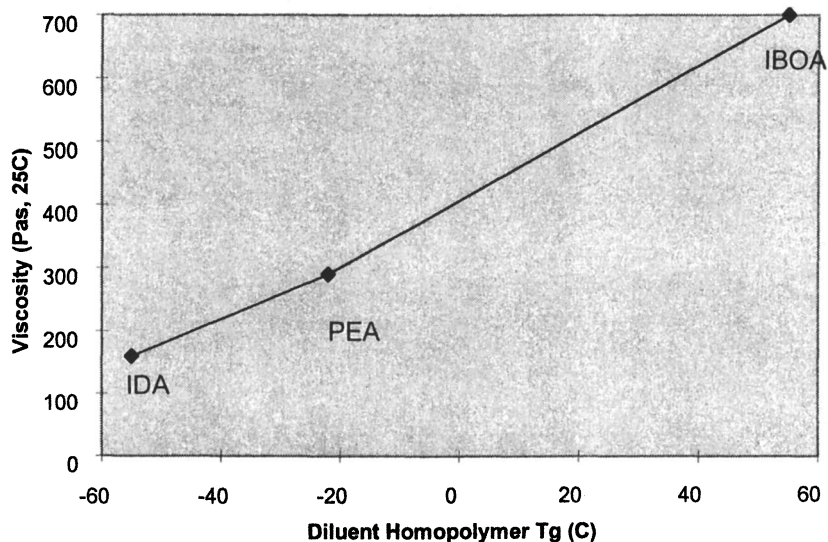


Figure 2: Effect of Diluent Tg on Urethane Viscosity

Effect of Acrylic Hydroxyl Content on Urethane Viscosity

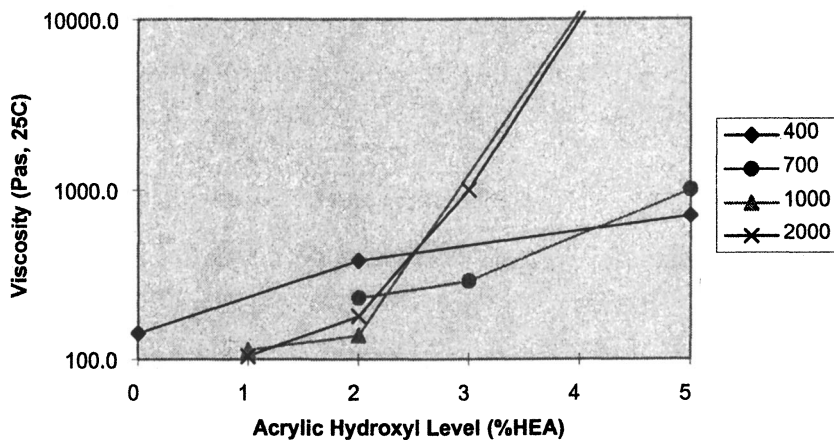


Figure 3: Effect of Acrylic Hydroxyl Content on Urethane Viscosity

only for acrylics with lower hydroxyl contents. For those with higher hydroxyl concentrations, the trend is reversed. Furthermore, the series at 5 weight percent hydroxyl produced gelled urethanes when the polyol molecular weight exceeded 700 g/mole. This phenomenon could be rationalized by considering that the higher hydroxyl series likely contains a small concentration of molecules of very high functionality sufficient to exceed the gel point during urethane formation.

Cured Film Mechanical Properties

The urethane acrylate oligomers (3) prepared from acrylic copolymer solutions (2) were blended into simple UV curable coatings by mixing with diluent monomer and photoinitiator. The oligomer was dissolved in either isobornyl acrylate, 2-(2-ethoxyethoxy)ethyl acrylate, or isodecyl acrylate at a weight ratio of 1:1 followed by 2-hydroxy-2-methyl-1-phenyl propane-1-one (Darocure[®] 1173) photoinitiator at 3 pph based on total composition. The resulting coatings were cast as thin films onto glass plates and cured at 1 joule/sq.cm. under nitrogen atmosphere. Mechanical properties of each film were then recorded.

Effect of Structural Design Features on Cured Film Modulus

Figure 5 represents a response surface plot of how cured film modulus is affected by the combined features of hydroxy-terminated prepolymer molecular weight used in the acrylic solution and Tg of the acrylate ester monomer used as the coating diluent. The plot displays the results for the series of acrylic copolymers with 1% hydroxyl content but is representative of the higher hydroxyl content compositions as well. The plot indicates a general decrease in cured film modulus as polyol molecular weight increases and as diluent Tg decreases. These results do not seem to be surprising and reflect typical effects of reduced crosslink density and film softening, respectively.

Effect of Structural Features on Cured Film Elongation

Figure 6 depicts the response of cured film elongation as affected by the same design features. Elongation is seen to increase with polyol molecular weight and diluent Tg. This response is expected for polyol molecular weight and is typical of all the series examined. However, the effect of diluent Tg is surprising. One would expect an embrittlement and reduction in elongation with increasing Tg. Furthermore, the effect is typical only of the acrylics with lower hydroxyl

Effect of Polyol Mol Wt on Urethane Visc

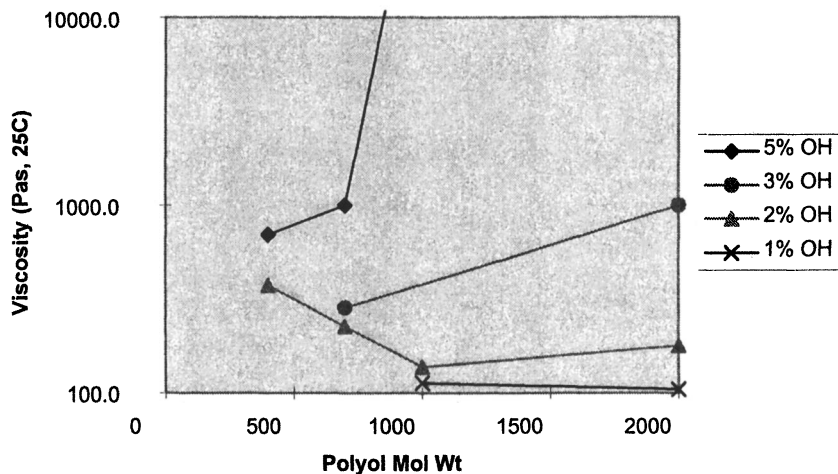


Figure 4: Effect of Polyol MW on Urethane Viscosity

Modulus of 1% HEA Acrylated Acrylics

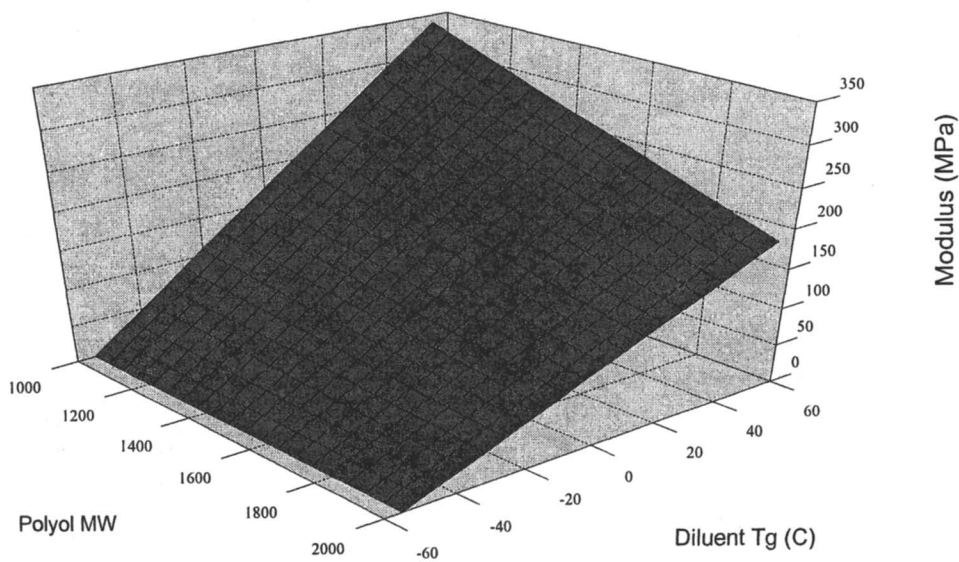


Figure 5: Combined Structural Feature Effects on Cured Film Modulus

Elongation of 1% HEA Acrylated Acrylics

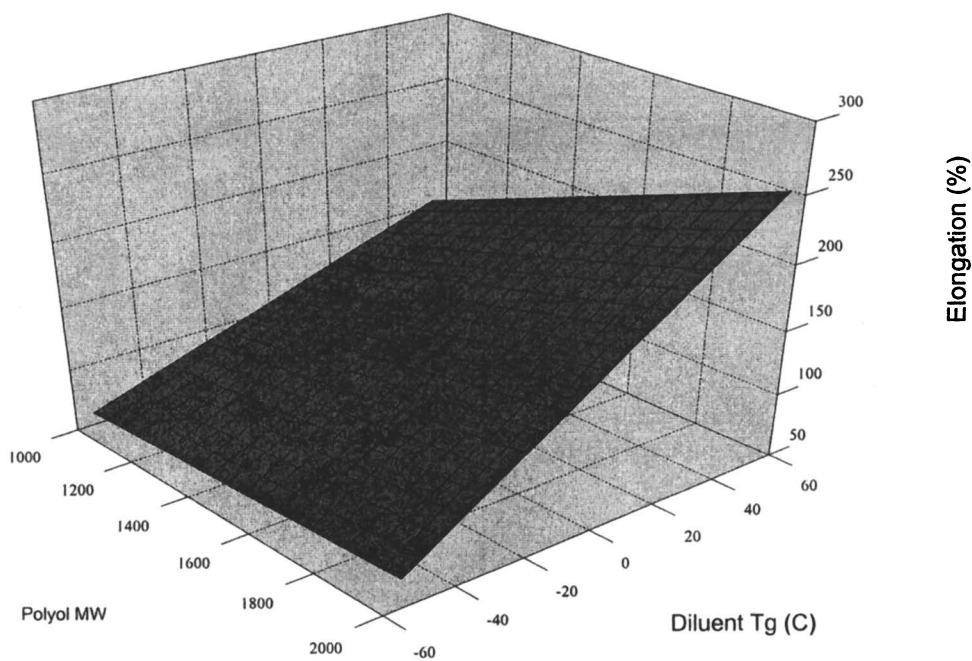


Figure 6: Combined Structural Effects on Film Elongation

content (1 and 2 percent) and seems to indicate an overall toughening of these lightly crosslinked films by the higher T_g diluents.

Mixture Design Studies

Preliminary coating design studies were begun in order to determine whether a single oligomer could be used for separate coating types. The oligomer was selected based on desirable mechanical properties demonstrated in the previous structure/property studies. The acrylic copolymer (1) was based on methyl methacrylate, 2-ethylhexyl acrylate, and 2-hydroxyethyl acrylate (2% by weight) synthesized in 1000 molecular weight poly(propylene glycol). The urethane acrylate (3) was the addition product of the acrylic copolymer with adduct (2) as described in Scheme I, and the reaction was conducted in the presence of 20 weight percent isobornyl acrylate diluent. Coating was prepared by dissolving the urethane oligomer in suitable acrylate monomers along with photoinitiator, and viscosity stabilizer. Coatings were cast as thin films onto glass plates and cured under nitrogen atmosphere with a medium pressure mercury lamp (Fusion Systems D) at 1 joule/cm².

Table 1 summarizes the composition and properties of the coatings prepared. Coatings designated as L were intended for low crosslink density applications while those with H designations were intended for higher crosslink density applications. The results indicate that the L series coatings are fairly consistent with respect to mechanical properties. However, the H series coatings demonstrate a much wider range in both secant modulus and elongation values. This result offers the hope that a single oligomer may indeed be useful for separate applications.

Conclusions

The synthesis of urethane acrylate oligomers bearing acrylate functional groups from acrylic copolymers has been demonstrated. The effects of structural composition variation on liquid properties of both the acrylic copolymer and the resulting urethane acrylate have been determined. The urethane acrylates have been formulated into simplified UV curable coating compositions by blending with suitable acrylate ester monomer diluents and photoinitiator. Cured films of the coatings have been examined for the effects of structural variation in the oligomer and diluent composition on mechanical properties of tensile strength,

Table 1. Preliminary Coating Design Studies

	L1	L2	L3	L4	H1	H2	H3	H4
Oligomer	80.0	50.0	50.0	60.0	70.0	40.0	40.0	50.0
Isodecyl acrylate	20.0	50.0	20.0	30.0			30.0	40.0
2-Phenoxyethyl acrylate			30.0	10.0				
Isobornyl acrylate					30.0	60.0		
Hexanediol diacrylate							30.0	10.0
Irgacure [®] 184 (pph)	3.0	3.0	3.0	3.0	3.0	3.0	3.0	3.0
Irganox [®] 1035 (pph)	0.5	0.5	0.5	0.5	0.5	0.5	0.5	0.5
Cyagard [®] UV416 (pph)	0.5	0.5	0.5	0.5	0.5	0.5	0.5	0.5
Properties								
Viscosity (mPa·s, 25°C)	9625	385	640	1230	46750	1300	790	3200
Tensile str. (MPa)	0.5	0.2	0.3	0.3	2.1	14.0	17.0	10.0
Elongation (%)	50	54	45	44	138	215	17	65
Modulus (MPa)	1.4	0.6	0.9	1.0	2.8	190.0	358.0	111.0

modulus, and elongation. Preliminary mixture design studies have suggested the possible use of a single oligomer for various application needs.

References

- 1a) Howe-Grant, M., ed. in "Encyclopedia of Chemical Technology," vol.1, John Wiley & Sons, New York, 1991, pp. 314-338; b) Brendley, W.H., *Paint and Varnish Prodn.*, 1973, July, 19-27.
- 2a) Kroschwitz, J.I., ed. in "Encyclopedia of Polymer Science and Engineering," vol.1, John Wiley & Sons, New York, 1985, p. 274; b) Pappas, S.P., ed. in "UV Curing: Science & Technology," vol.2, Technology Marketing Corp., Norwalk, Conn., 1985, ch.4.
- 3a) Tortorello, A.J.; Murphy, E.J. US 5847021, December 8, 1998; (DSM, N.V.); b) Tortorello, A.J.; Murphy, E.J. US 6107361, August 22, 2000; (DSM N.V.).
- 4) Tortorello, A.J. *Polymer Preprints*, 1999, 40(2), 1273.
- 5) Hill, L.W.; Kozłowski, K.; Sholes, R.L. *J. Coatings Technol.*, 1982, 54(692), 67-75.

Chapter 36

Real-Time Fluorescence for Determining the Relative Sensitivities of Reactive and Non-Reactive Fluorescent Probes

Wolter F. Jager and Otto van den Berg

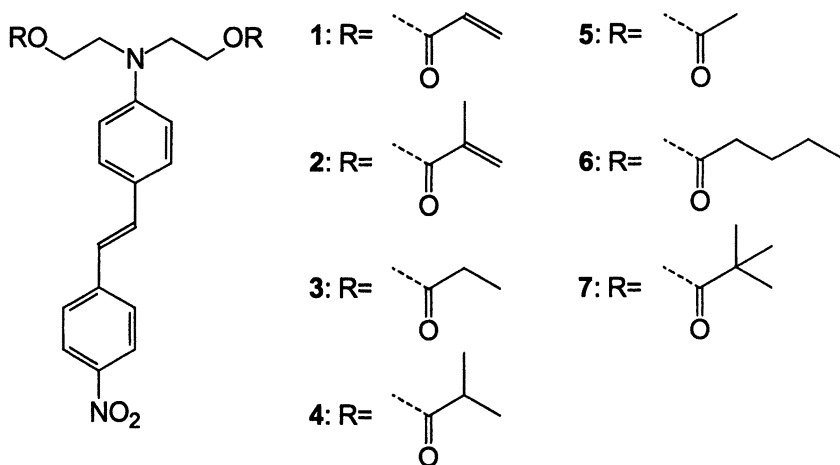
Department of Polymer Materials and Polymer Engineering, Delft University of Technology, Julianalaan 136, 2628 BL, Delft, The Netherlands

The relative sensitivities of structurally similar nitrostilbene based fluorescent probes, bearing substituents of different sizes and reactivities, were determined during the photoinitiated polymerization of HEXDMA by real-time fluorescence spectroscopy. Reactive probes are significantly more sensitive than corresponding non-reactive probes, up to conversions of 78-87%, and the reactivity of the substituent, has a very pronounced effect on the probe sensitivity. Increasing the probe size resulted in a small decrease in probe sensitivity at all stages of the reaction. These findings can be utilized for tuning the sensitivity of fluorescent probes for specific applications.

Introduction

Fluorescent probes, molecules whose emission responds to changes in their direct environment, are frequently used as analytical tools for monitoring photoinitiated polymerization processes. Fluorescent probe technology is non-destructive and often employed in real-time, and since fluorescence spectra can be recorded for samples of different sizes and geometries, fluorescent probe technology is suitable for on-line monitoring of photocured products.

During a polymerization process, the anisotropy, the wavelength λ_{\max} , the intensity I_{\max} , and the half width of emission of the added fluorescent probe may change. Our research is focused on charge transfer probes (1,2) whose wavelength λ_{\max} strongly shifts to the blue due to increases in microviscosity as the medium polymerizes. These probes are very sensitive, and their application requires no calibration of individual samples. Monitoring a photoinitiated polymerization by real-time fluorescence, using the excitation light for simultaneous excitation of probe and photoinitiator molecules, is easily automated by recording an intensity ratio $R = I_{\lambda_1}/I_{\lambda_2}$ instead of λ_{\max} , and this procedure has been used for determining photoinitiator efficiencies. (3,4)



Scheme 1. Fluorescent probes 1-7.

Until recently, developing more sensitive fluorescent probes usually came down to finding more sensitive chromophores. However, we have demonstrated that strong increases in probe sensitivity can be obtained by attaching reactive groups to the chromophore, i.e. by making *reactive* fluorescent probes. (5,6) The

increase in sensitivity is very pronounced in network forming di(meth)acrylates and is clearly linked to the distribution of chromophores throughout a highly inhomogeneous polymerizing medium.⁽⁶⁾ In this process diffusion of *non-reacted* probe molecules out of cross-linking regions is of paramount importance. Therefore, it is anticipated that, apart from the reactivity, which governs the rate of probe incorporation in the network, the size of the moiety attached to the chromophore will affect the sensitivity of a fluorescent probe as well.

Here we report the effects of reactivity and size of a substituent on the sensitivity of fluorescent probes during all stages of the reaction, as determined by real-time fluorescence during the photoinitiated polymerization of HEXDMA. We have employed a series of structurally similar disubstituted nitrostilbenes 1-7, bearing ester functionalities that vary in reactivity (1 versus 2) and size (7) (3-7), see Scheme 1. It should be emphasized that 1-7 are spectroscopically virtually identical, implying that:

- 1: Photoinitiated polymerizations take place at the same rate, providing [photoinitiator] and [probe] are identical.
 - 2: Differences in probe response are caused by differences in probe distribution.
- (8)

Experimental

HEXDMA (1,6-hexanediol dimethacrylate) and the starting materials for the synthesis of 1-7 were purchased from Aldrich and used as received. The fluorescent probes 1-7 were synthesized by esterification of the corresponding diol, as described earlier for 2 and 4. (5) The photoinitiator Irgacure 907 (2-methyl-1-[4-(methylthio)phenyl]-2-morpholinopropanone-1) was a gift from Ciba-Geigy.

Stock solutions containing 1.00% of photoinitiator in HEXDMA were prepared. To each of these solutions fluorescent probe was added to make 3.0×10^{-4} mol kg⁻¹ solutions. A few drops of these formulations were squeezed between microscope slides held apart by 75 μ m polypropylene spacers, with 50*15 mm windows, while clamps on both edges held the slides together. The surface of the top slide was made hydrophobic by treatment with hexamethyldisilazane, to ensure a reproducible detachment of the shrinking polymer from the top slide. (9) Samples were placed directly on the head of a CM 1000 cure monitor (3,4) and small spots (≈ 3 mm in diameter) on the layer were cured by the excitation beam. Plots of the intensity ratio $R = I_{614}/I_{654}$, versus the irradiation time t , were constructed by averaging 3-4 consecutive real-time measurements performed on the same sample. Double bond conversions were determined by IR measurements on 15 μ m films between NaCl plates using a Mattson 6020 Galaxy Series FT-IR spectrometer. First derivatives of the intensity

ratio R versus the conversion C , (dR/dC) , were determined numerically employing the software package Table curve from Jandel.

Results and Discussion

Comparing Reactive and Corresponding Non-reactive Probes.

Real-time fluorescence performed on formulations containing added fluorescent probes results in plots of an intensity ratio R versus the irradiation time t . At low and equal [probe] the rate of the polymerization is identical for all formulations and therefore one can directly compare the overall sensitivities of all probes. The normalized intensity ratios $R_{\text{norm}} = (I_{614}/I_{654})_t - (I_{614}/I_{654})_{t=0}$ for 1-4 are depicted in Figure 1.

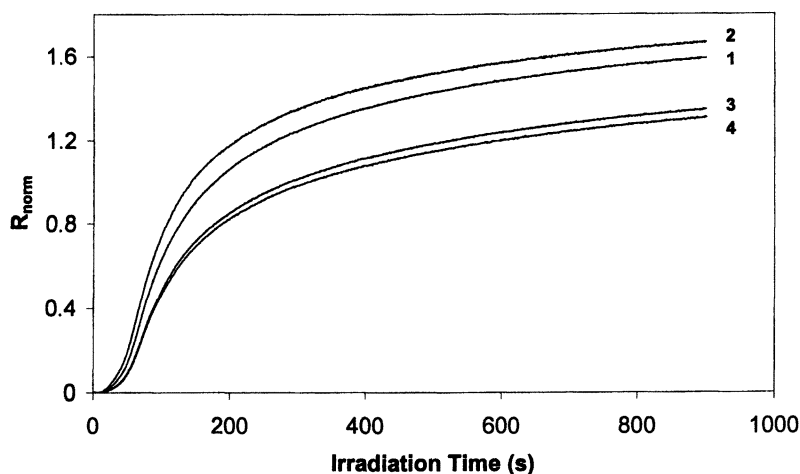


Figure 1. Normalized intensity ratio $R_{\text{norm}} = (I_{614}/I_{654})_t - (I_{614}/I_{654})_{t=0}$ for 1-4 in HEXDMA, versus the irradiation time t .

From Figure 1, the overall sensitivities are determined: $2 > 1 \gg 3 > 4$. It is obvious that the reactive probes 1 and 2 are far more sensitive than the non-reactive probes 3 and 4. However, within each class differences in sensitivity are observed; 2 is significantly more sensitive than 1, whereas 3 is slightly more sensitive than 4.

The curves in Figure 1 are a product of the rate of the polymerization, C versus t , times the responses of the individual probes, R versus C . As the rate of polymerization largely determines the shape of the curves in Figure 1, and since we are interested in the probe sensitivity primarily, we have plotted R as a function of C for 1-4 in Figure 2. For all probes the gradient of the curves in Figure 2 increase monotonically as the reaction proceeds, indicating that the probe sensitivity, defined as (dR/dC) , increases at higher conversions. This effect is most pronounced for the non-reactive probes 3 and 4, primarily because they are relatively insensitive at low conversions.

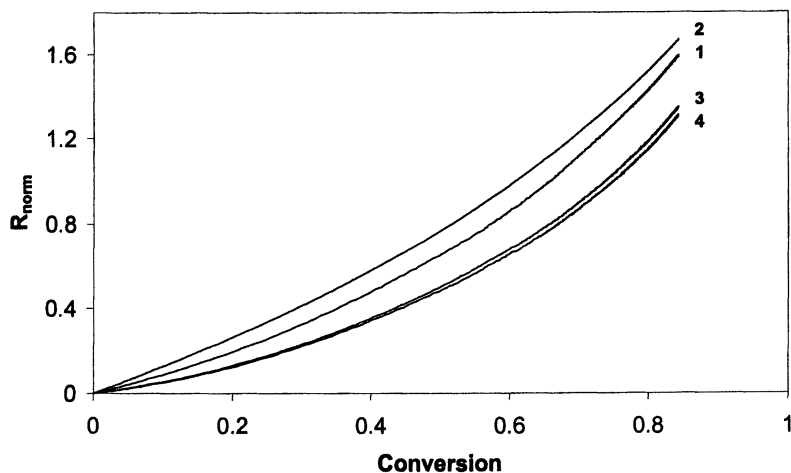


Figure 2. Normalized intensity ratio $R_{\text{norm}} = (I_{614}/I_{654})_t - (I_{614}/I_{654})_{t=0}$ of 1-4 in HEXDMA, versus the conversion C .

In Figure 3, the sensitivity (dR/dC) for 1-4, obtained by numerical differentiation, is plotted as a function of the conversion C . From figure 3, the order of sensitivity of 1-4 at all stages of the reaction is determined.

For all probes, the sensitivity increases strongly throughout the reaction; by a factor 3-5 for reactive probes, and by a factor 12-14 for non-reactive probes. Differences in sensitivity between the non-reactive probes 3 and 4 are very small, and 3 is slightly more sensitive than 4 at all stages of the reaction. For the reactive probes 1 and 2, differences in sensitivity are more pronounced. At the beginning of the reaction 2 is significantly more sensitive than 1. A reversal of sensitivity is observed at 59% conversion, and above that conversion 1 is more sensitive than 2. It should be noted that differences in sensitivity are particularly large at low conversions, with 2 being twice as sensitive as 3 and 4 at conversions below 10%.

From Figure 3 we can determine which probe is the most sensitive at all stages of the reaction. Up to a conversion of 59% **2** is the most sensitive probe. Above 59% conversion **1** takes over, up to a conversion of 87%, above which **3** is the most sensitive probe. It should be noted that at high conversions differences in sensitivity between **3** and **4** appear to be negligible, and that for HEXDMA conversions above 90% are not likely to be achieved.

An alternative method for determining the relative sensitivities of 1-4, at all stages of the reaction is by plotting the difference of intensity ratios ΔR of two selected probes as a function of the conversion C , see Figure 4. From the gradient of these curves one can determine which probe is the most sensitive. Since this method does not require any data manipulation, apart from transforming the X-axis from time to conversion, it is preferred for cases in which differences in probe sensitivity approach the limits of detection.

From Figure 4, one can deduce that **2** is more sensitive than **1** up to a conversion of 62%, more sensitive than **4** up to a conversion of 78%, and that **3** is more sensitive than **4** at all stages of the reaction. Furthermore **1** is more sensitive than **3** throughout the entire reaction, but it appears that a reversal of sensitivity will occur around an 85% conversions. Clearly these observations are in agreement with those extracted from Figure 3, indicating that identical results are obtained by both procedures.

The relative sensitivities of 1-4 are explained in a straightforward manner by taking into account the reactivities and the sizes of the substituents attached to these probes. Comparing the sensitivity of the non-reactive probes **3** and **4**, only size can play a role. (7) Probe **3**, the smaller probe, is found to be slightly more sensitive throughout the reaction, indicating that decreasing the size of a probe increases its sensitivity.

The larger sensitivity of **2** over **1** during the first 60% of the polymerization is explained by taking into account the reactivities, and the sizes of methacrylates and acrylates. Based on reactivity ratios (11) it is expected that methacrylates will be incorporated in the network at higher rates during the initial stages of the reaction. (12) This will result in a higher sensitivity of **2** at low conversions. Differences in size will play an opposite role, increasing the sensitivity of unreacted **1**. Since **2** is the more sensitive probe at low conversions, we conclude that differences in reactivity have the largest effect on the sensitivity of both reactive probes. This consistent with the small differences in sensitivity between **3** and **4**, the compounds that mimic the behavior of unreacted **1** and **2**.

When comparing reactive and corresponding non-reactive probes, **1** versus **3** and **2** versus **4**, the largest differences in sensitivity are observed. Covalent attachment of reactive probes to the polymer network, increasing the rate of probe incorporation in rigid highly cross-linked areas, explains the large increase in sensitivity of the reactive probes over the non-reactive probes. The increase in sensitivity of **2** compared to **4** is much larger than the increase in sensitivity of **1**

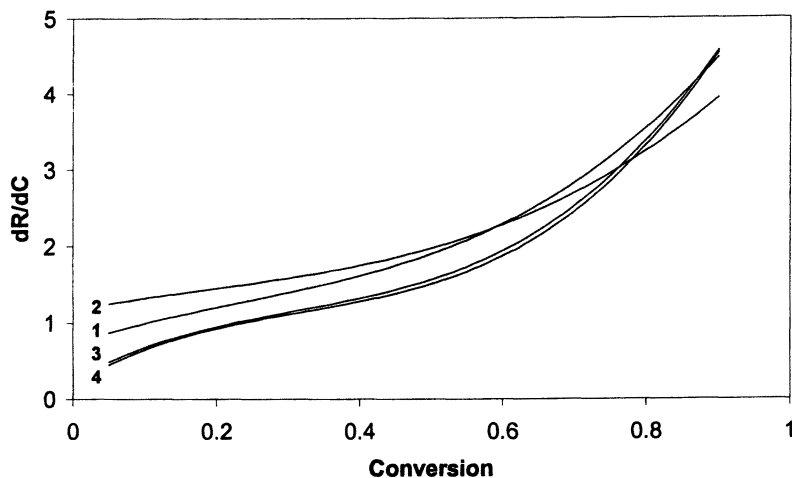


Figure 3. First derivative of the intensity ratio R versus the conversion C , (dR/dC), plotted against the conversion C .

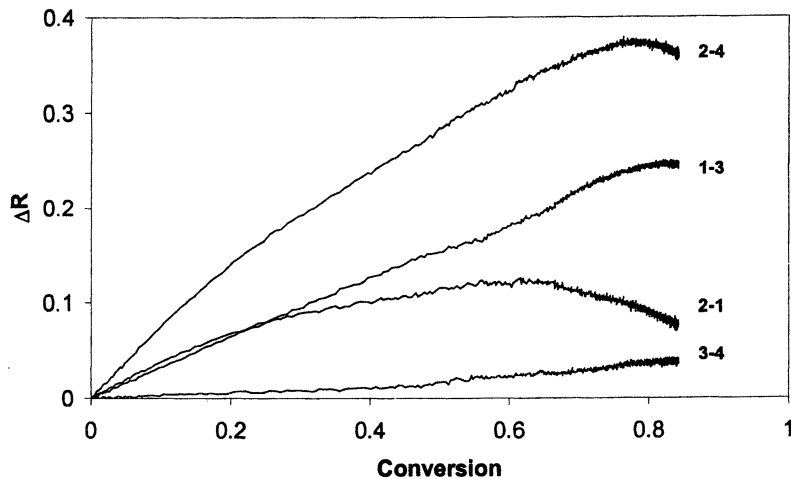


Figure 4. Differences in intensity ratio $\Delta R = R_{\text{probe 1}} - R_{\text{probe 2}}$ for selected probes versus the conversion C .

over **3**. This is explained by taking into account the effects of reactivity, favoring **2** over **1**, and size, favoring **3** over **4**, although the magnitude of the last effect is expected to be negligible. At very high conversions non-reactive probes are more sensitive than their non-reactive counterparts. This might be due to a higher concentration of non-reactive probes in the few remaining mobile monomer rich regions, resulting in a higher rate of probe incorporation in the network as these regions finally polymerize.

Comparing Non-reactive Probes with Substituents of Different Sizes. (7)

From the results presented in the previous section it was concluded that not only the reactivity, but also the size of the substituents effect the sensitivity of structurally similar probes. In order to investigate the effect of probe size in more detail we have employed **3** and **5-7**. In this series **3**, **5,6** the ester is linear and extended by methylene groups, and the weight of the probe increases while the polarity decreases. The pivaloyl ester **7** is the branched analogue of the valerate **6**. The molecular weights of **6** and **7** are identical, but the mobility of **7** might be reduced due to steric hindrance.

Plots of R versus t and C for **3** and **5-7** in HEXDMA are depicted in Figures 5 and 6. Obviously the differences in sensitivity between these non-reactive probes are small, compared to those between reactive and non-reactive probes. Based on the order of the overall sensitivity, $5 > 3 > 6 > 7$, it is concluded that the sensitivity decreases as the size of the substituent increases. The effect of branching on probe sensitivity is very small, and it appears that branching decreases probe sensitivity since **6**, is slightly more sensitive than **7**.

By subtracting selected curves the order of sensitivity throughout the polymerization is determined, see Figure 7. It is concluded that larger probes are less sensitive at all stages of the polymerization reaction. Figure 7 also shows that the decrease in sensitivity due to branching occurs at high conversions only.

This brings us to the conclusion that the size of a probe influences the probe distribution during the photoinitiated polymerization. Larger probes are less sensitive, and therefore enriched in mobile monomer rich regions to a larger extent. This may be caused by a more effective exclusion of larger probe molecules from cross-linking regions, a process known as photodiffusion. In addition diffusion of probe and monomer molecules back into cross-linked regions, a swelling process, may occur and this process is expected to be faster and occurring to a larger extent for smaller molecules, due to steric constraints imposed by the network. It is expected that for both processes the *relative* size of the probe compared to the mesh size of the network will be a decisive factor.

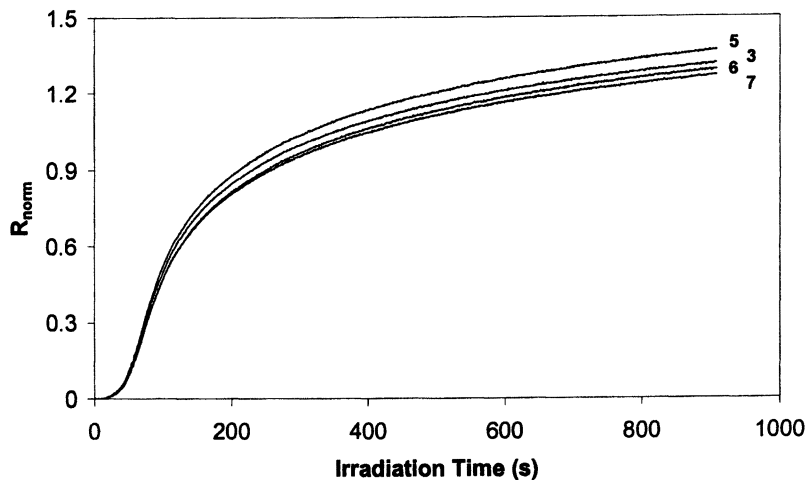


Figure 5. Normalized intensity ratio $R_{\text{norm}} = (I_{614}/I_{654})_t - (I_{614}/I_{654})_{t=0}$ of 3 and 5-7 in HEXDMA, versus the irradiation time.

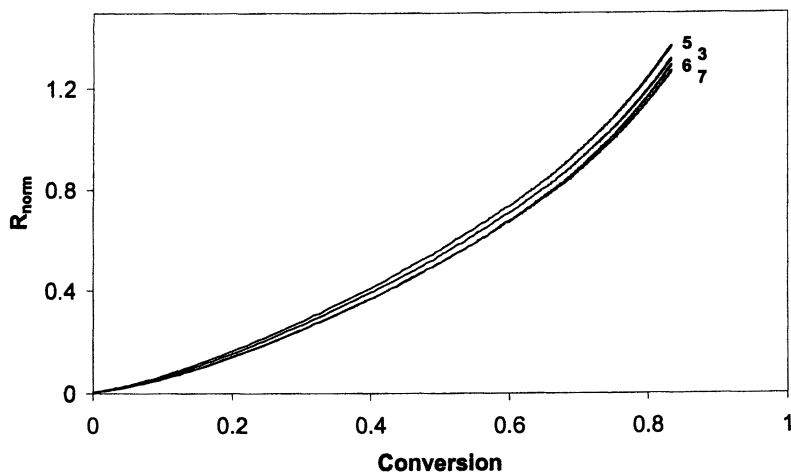


Figure 6. Normalized intensity ratio $R_{\text{norm}} = (I_{614}/I_{654})_t - (I_{614}/I_{654})_{t=0}$ of 3 and 5-7 in HEXDMA, versus the conversion C .

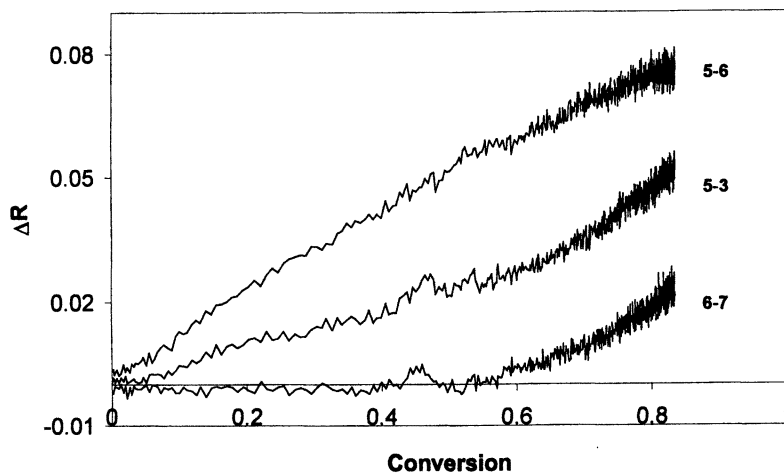


Figure 7. Differences in intensity ratio $\Delta R = R_{\text{probe 1}} - R_{\text{probe 2}}$ for selected probes versus the conversion C .

Conclusions

The sensitivity of fluorescent probes bearing the same chromophore can be altered by substitution, and subtle changes in probe structure may cause significant differences in probe sensitivity. Large increases in sensitivity, in particular at low conversions, can be obtained by making reactive probes, i.e. by attaching reactive moieties to a chromophore. The reactivity of this moiety has a large effect on probe sensitivity, in particular at low conversions. The size of the substituents also plays a role; larger substituents result in probes that are less sensitive throughout the reaction.

Real-time fluorescence, employing the intensity ratio method, is an excellent technique for detecting even the slightest differences in probe sensitivity at all stages of the reaction. Based on the findings of this research we are able to tune the sensitivity of structurally similar probes for specific applications.

Acknowledgements. The Royal Netherlands Academy for Arts and Sciences (KNAW) is gratefully acknowledged for funding part of this research.

References and notes

1. Jager, W.F.; Volkers, A.A.; Neckers, D.C. *Macromolecules* **1995**, *28*, 8153.
2. van Ramensdonk, H.J.; Vos, M.; Verhoeven, J.W.; Möhlmann, G.R.; Tissink, N.A.; Meesen, A. *Polymer* **1987**, *28*, 951.
3. Hu, S.; Polpielarz, R.; Neckers, D. C. *Macromolecules* **1998**, *31*, 4107.
4. Paczkowski, J.; Neckers, D. C. *Macromolecules* **1992**, *25*, 548.
5. Jager, W. F.; Sarker, A. M.; Neckers, D. C. *Macromolecules* **1999**, *32*, 8791.
6. Jager, W. F.; Norder, B. *Macromolecules* **2000**, *33*, 8576.
7. It should be noted that in the series 3-7, the size of the probe increases, while the polarity decreases. In this paper we ascribe differences in probe sensitivity to differences in size, but it should be taken into account that we cannot a priori exclude that polarity might play a role as well.
8. For reactive probes this is true only if emission spectra do not undergo significant shifts upon covalent attachment to a polymer backbone. The results presented in references 5 and 6, indicate that this assumption is valid for dimethacrylate systems.
9. Detachment from the top glass layer does not influence the polymerization process, whereas detachment from the bottom glass layer results in reflections that cause loss of excitation light, and therefore a decrease in the rate of polymerizations.
10. The choice of λ_1 and λ_2 is a compromise between obtaining a large signal by increasing $\Delta\lambda = \lambda_1 - \lambda_2$, and eliminating noise by choosing a lower value of $\Delta\lambda$ around the emission maximum of both monomer and polymer.
11. The reactivity ratios for the acrylate/methacrylate A/MA system are: $r_1 = k_{A-A}/k_{A-MA} = 0.4$; $r_2 = k_{MA-MA}/k_{MA-A} = 2$. Data taken from: Polymer Handbook 3rd Ed; Brandrup, J.; Immergut, E. H., Eds.; John Wiley and Sons: New York, 1989.
12. Since the rate of incorporation is defined as $-d[\text{probe}]/dt = k[\text{probe}]$ a higher k value will lead to a faster decrease in $[\text{probe}]$ and therefore a lower rate of incorporation at high conversions.

Chapter 37

Continuous Photopolymerization in a Novel Thin Film Spinning Disc Reactor

**Kamelia V. K. Boodhoo, William A. E. Dunk,
and Roshan J. Jachuck**

**Process Intensification and Innovation Centre (PIIC), Department of
Chemical and Process Engineering, University of Newcastle Upon Tyne,
Newcastle Upon Tyne NE1 7RU, United Kingdom**

n-Butyl acrylate has been polymerized in bulk by UV initiation using a novel spinning disc reactor (SDR). Very high conversions were achieved in seconds, whilst the polymer so produced was unbranched. This observation contradicts the accepted view that acrylates give insoluble network polymers even at low conversions when bulk polymerization is attempted. We present here the principles underlying the development of the SDR, and its application to photopolymerization. The results of our work with *n*-butyl acrylate and the effects of disc rotational speed, monomer feed rate, and UV radiation intensity are presented and qualitatively discussed. Application of the SDR to continuous polymerization processes, and its potential in reducing plant space i.e. process intensification will also be discussed briefly in this chapter.

Introduction

The observation that certain compounds could be affected by sunlight to give materials having the same chemical composition but very different physical properties was made as long ago as 1845. Blyth and Hofmann (1) noted that styrene was converted from a liquid to a glassy solid when exposed to sunlight and it was shown by Kopp (2) that the two materials were chemically the same. Similar observations were reported for other vinyl compounds, but it was not until 1910 that the chain reaction nature of the process was shown (3).

In 1912 Ciamician reviewed the field of photochemistry and foresaw possible applications in the chemical industry (4). However the potential was never exploited in any significant way for the large scale production of liner soluble polymers although in the 1920s I.G.Farben used sunlight to polymerize vinyl chloride and vinyl acetate. Inability to scale up laboratory light sources and the seasonable uncertainties of sunshine presence led to abandonment of these plans (5). Subsequently photopolymerization was confined to laboratory studies and no viable industrial process has emerged although the patent literature discloses ideas for reactors. Many of these are based on having films of monomer on a moving belt that passes under a bank of UV lamps (6,7). Since there is no agitation, mixing is minimal thus the polymerization proceeds in what is essentially a static film. In addition, the removal of the heat of polymerization is limited to the dimensions of the belt.

Photochemical initiation has several advantages over initiation by free-radicals obtained by the thermal dissociation of chemical initiators:

- Polymerization may be carried out over a very wide range of temperatures, even as low as -100°C .
- Production of primary radicals is essentially independent of temperature.
- Rate of polymerization is much less affected by temperature than when thermal initiators are used.
- Polymerization of monomers having low ceiling temperatures becomes feasible.
- Compared to redox initiator systems that exhibit low activation energy, photo-initiation may be finely tuned.

With these advantages it seems surprising that no real progress has been made in the industrial utilization of photopolymerization since the abortive attempts at IG Farben. Of course the problems of radiation penetration and uniformity in bulk reactions is not trivial, whilst reactor design and development have done little to address these issues.

Novel Spinning Disc Photopolymerizer

The novel spinning disc reactor (SDR) has previously been shown to dramatically increase the rates of step-growth (8) and radical chain (9) polymerizations. The ability of the SDR to continuously generate thin, sustainable films under the action of the centrifugal field represents an important advancement towards the design of a viable continuous reactor system applicable to bulk photopolymerization reactions. Not only would the thin film (50-300 μm) allow efficient penetration of UV light used to initiate the polymerization, but the shear forces developed within the film would also promote excellent mixing conditions. The intense fluid dynamics environment on the rotating disc is expected to enhance initiation and propagation steps. We believe that the applied centrifugal field extends polymer chains that have been disentangled by shear, causing them to grow radially. Translation diffusion of the active chain ends may then be restricted so that bimolecular termination reactions are reduced (10). In this event, we feel that there may be tendency towards a "living" mechanism of propagation. A study of the kinetics involved in polymerizations on the spinning disc is currently underway in our laboratory to elucidate the mechanism of chain formation and growth.

Bulk polymerization of monomers by the free radical mechanism has the advantage that only the monomer and an initiator are involved, thus the polymer produced will be free of contaminants. However the highly exothermic nature and rapid rates of many monomers, combined with the high viscosities at high monomer conversion, severely limit the use of this technique in conventional polymer reactors. These problems are particularly relevant to the esters of acrylic acid, and to a lesser extent to methacrylates, both of which find wide industrial application. These issues are addressed in the SDR by the greatly enhanced heat transfer characteristics achievable on the rotating disc (11) and the intense mixing levels generated within the film even at high viscosities. These SDR features would allow a good control over the reaction exotherm so that the bulk polymerization process proceeds safely in the SDR to yield polymer with tightly controlled molecular weight distribution (MWD).

n-Butyl acrylate was chosen as the test monomer to evaluate the performance of the SDR for photopolymerization since, with a propagation rate constant of ca 16,000 L/(mol.sec) at 30°C (12) and a heat of polymerization of 77.4 kJ/mol (13), the bulk polymerization of n-butyl acrylate presents significant challenges as a fast, highly exothermic reaction system. Furthermore, n-butyl acrylate polymerization is normally complicated by the ease in which branching occurs by tertiary hydrogen abstraction, resulting in insoluble polymer networks. This is common to most acrylic esters but particularly so for the n-butyl ester. This problem has recently been suggested to be at the root of the inability to determine by extrapolation accurate k_p values above 30°C by pulsed laser

techniques (14). The high intensity mixing in the SDR offers the potential to control the extent of such transfer reactions and therefore reduce polymer network formation.

Experimental

Materials

n-Butyl acrylate (care: lachrymator) was obtained from Aldrich and freed from inhibitor by washing with 0.5% chilled sodium hydroxide solution, then with distilled water. The monomer was dried over-night with anhydrous magnesium sulfate and filtered before use. The photo-initiator Irgacure 651 (2,2-dimethoxy-2-phenyl acetophenone) was obtained from Ciba Speciality Chemicals and used as received. The monomer was de-aerated and polymerizations performed using oxygen free grade nitrogen from BOC Gases.

Equipment

A schematic of the SDR is shown in Figure 1. The reaction surface is a 200 mm diameter stainless steel smooth disc which is supported on an internal cooling chamber mounted on the rotating shaft. Water from a thermostatically controlled bath circulates in this chamber to maintain the disc temperature. The monomer/photo-initiator mixture was fed to the centre of the disc by means of a Watson Marlow 505S/RL peristaltic pump. The UV source (1000 W metal halide flood lamp from UV Light Technology Ltd) was clamped over the disc surface with the beam directed towards the centre of the disc. The UV lamp and the top section of the SDR were enclosed in box made of UV absorbing acrylic sheets to contain the UV radiation when the lamp was in operation. Suitable eye and skin protection gear were also used. The intensity of the lamp was measured by a UV-A meter (from UV Light Technology Ltd). A flat glass plate transparent to 365 nm wavelength of the UV spectrum separates the disc surface and the UV lamp to contain any splashing of the monomer/initiator mixture.

Procedure

Inhibitor-free n-butyl acrylate containing the desired concentration of photo-initiator was placed in a flask protected from light by a black shield, then

sparged with nitrogen using a sintered glass distributor for 30 minutes. The SDR was flushed with nitrogen prior to and throughout the polymerization. The UV lamp was allowed to warm up for 5 minutes before commencing the disc irradiation. The intensity of the UV radiation was controlled by adjusting the distance of the lamp from the surface of the disc. When the chosen disc temperature and disc speed had been set the monomer/photo-initiator mixture was pumped onto the disc under the UV radiation. On completion of the run the lamp was switched off, the disc stopped and polymer collected from the reactor housing and, where possible, the disc surface.

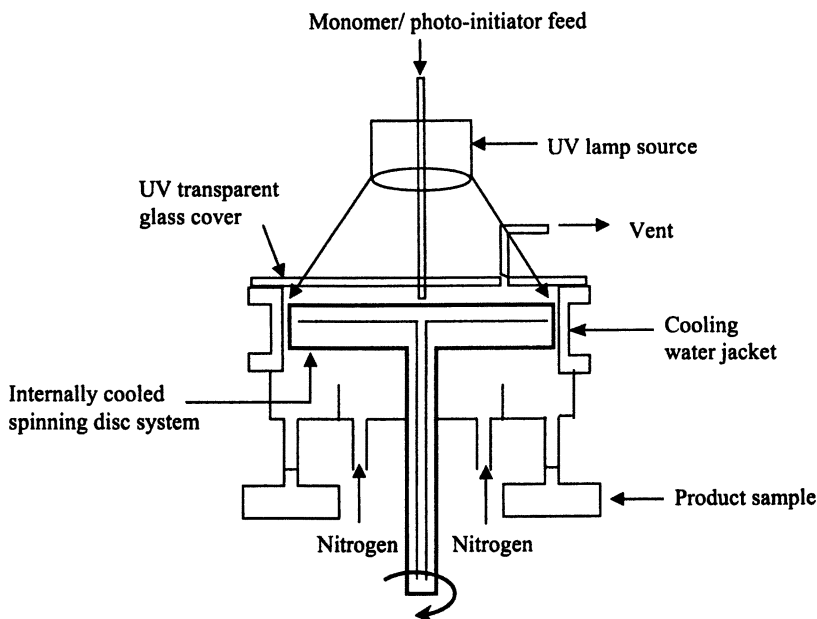


Figure 1. Schematic of spinning disc reactor for photopolymerization

Characterization

Molecular weights, polydispersities and monomer conversions were obtained by gel permeation chromatography using two PL gel 5 m Mixed-C columns (Polymer Laboratories), each of dimensions 300mm x 7.5mm, set at 30°C. Tetrahydrofuran was used as solvent at a flowrate of 1.0 ml/min. An RI

detector was used to detect polymer and monomer peaks. Molecular weight data were calibrated against Easi-Cal polystyrene standards whilst conversion was measured against calibration samples of pure n-butyl acrylate and pure poly(n-butyl acrylate). The conversion and molecular weight analyses were performed by PL Caliber LC-GC and GPC/SEC softwares respectively. Branching in the polymer formed in the SDR was assessed by analysis of ^{13}C NMR spectra obtained using a Varian Associates Unity 500 spectrometer operating at 125.8 MHz.

Results and Discussion

The two most important variables affecting the performance of the SDR are the disc residence time (t_{res}) and the film thickness (δ) which are governed by operational parameters such as the rotational speed (N) of the disc and the feed flowrate (Q). For a smooth disc (θ),

$$t_{\text{res}} = \left(\frac{81 \pi^2 \nu}{16 \omega^2 Q^2} \right)^{1/3} \left(r_o^{4/3} - r_i^{4/3} \right) \quad (1)$$

$$\delta = \left(\frac{3}{2} \frac{\nu Q}{\pi \omega^2 r^2} \right)^{1/3} \quad (2)$$

where ν is the kinematic viscosity of the liquid, $\omega = 2\pi N/60$ and r is the radial distance from the centre of the disc, with subscripts o and i representing outer and inner respectively.

Plots showing the effect of disc rotational speed and feed flowrate on the mean residence time in the SDR and mean film thickness across the disc, based on equations (1) and (2) above respectively, are presented in Figure 2. Changes in the two variables will have a direct influence on the extent of n-butyl acrylate photopolymerization in the SDR as will be demonstrated by the findings of the present study.

Influence of disc rotational speed and feed flowrate

As the rate of rotation of the disc is increased from 200 to 1000 rpm at constant flowrate of 1 ml/s of monomer/initiator feed mixture, conversion of n-butyl acrylate falls quite sharply from about 90% ($t_{\text{res}} = 2.1$ s) to about 30% ($t_{\text{res}} = 0.7$ s) as shown in Figure 3 below. This may be explained by a decreasing

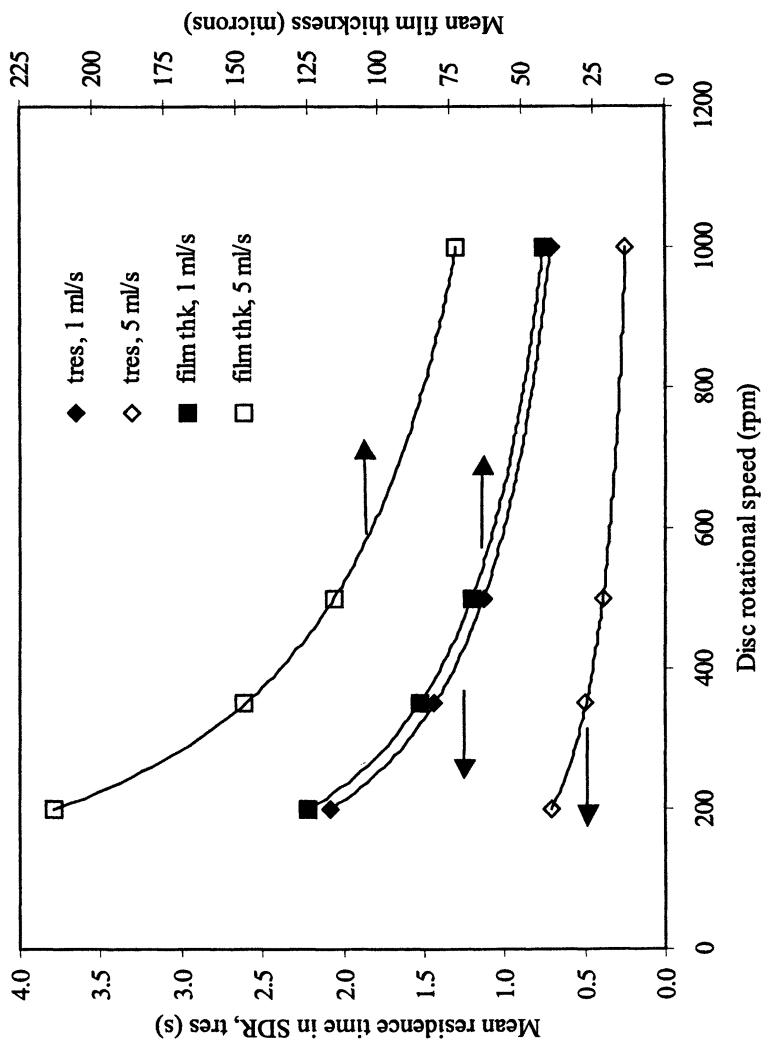


Figure 2. Theoretical profiles of mean residence time and film thickness across a smooth disc surface at various rotational speeds and feed flowrates

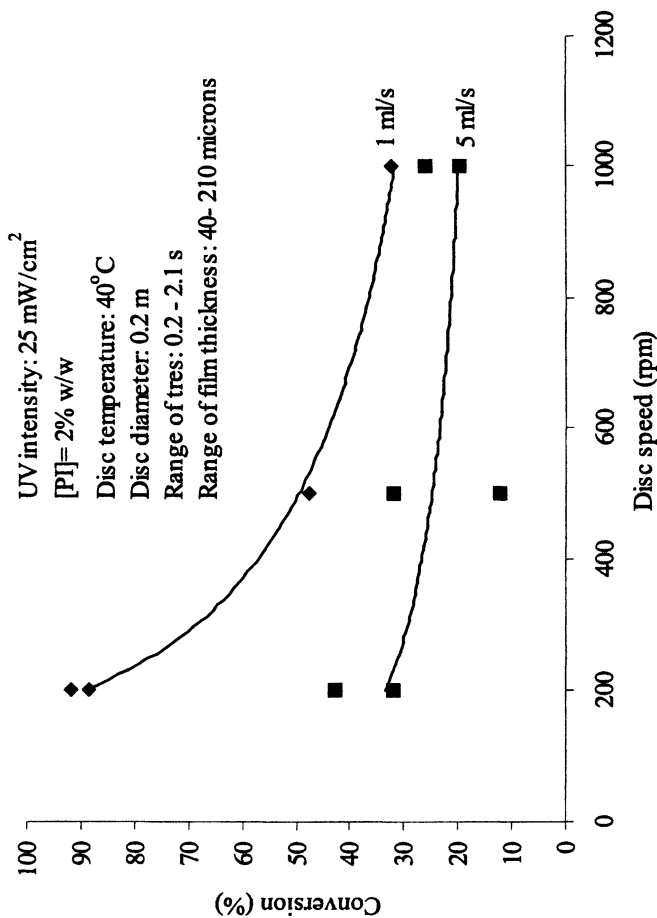


Figure 3. Effect of disc rotational speed on conversion of *n*-butyl acrylate in the SDR at different feed flowrates

residence time on the disc with rotational speed which results in reduced exposure to the UV illumination. It would seem that the decrease in film thickness (from 125 μm at 200 rpm to 43 μm at 1000 rpm), which would tend to encourage more efficient UV penetration into the film, has less of an influence on the conversion achieved than the residence time. Therefore residence time is the controlling factor for this particular set of operating conditions. The drop in conversion with rotational speed is less significant at the higher flowrate of 5 ml/s. A comparison between Figures 2 and 3 reveals that the trend in conversion at different flowrates follows closely the corresponding residence time profiles. This is further indication that residence time is more influential on the conversion achieved in the SDR than film thickness.

Influence of UV intensity

Within the range of UV intensities tested (11-125 mW/cm^2), the results show that the extent of photopolymerization in the SDR is significantly enhanced as UV intensity is increased from 11 mW/cm^2 to about 30-40 mW/cm^2 for all the rotational speeds studied (Figure 4). Beyond the 30-40 mW/cm^2 UV intensity range, conversion drops sharply in all cases. These results suggest that an optimum UV intensity exists for each rotational speed at which conversion is highest, as shown in Figure 4. In contrast, Decker and co-workers (15) found that increasing the light intensity from 10 to 600 mW/cm^2 in the UV curing of multi-functional acrylates caused the final conversion to rise from 80% to nearly 100%. This was attributed, in part, to increased sample temperature at high UV intensity which promoted molecular mobility of reacting species. However, in the SDR, the temperature of the polymerizing film flowing across the disc is maintained at the set value of 40°C by the highly efficient heat removal system. It would seem therefore that temperature effects are minimized in the SDR.

The trend in Figure 4 may be explained as follows. As intensity is increased, a larger number of initiator radicals is generated in the flowing film which allows more monomer molecules to be consumed, resulting in a rise in conversion. However, beyond a certain optimum intensity, the number of radicals is so exceedingly high that they are more likely to terminate growing chains rather than initiate new chains so that, overall, there are less active chain ends available for addition of monomer molecules.

Molecular weight properties and branching effects

The average molecular weights (M_n , M_w) and the polydispersity (PDI) of the poly(butyl acrylate) formed in the SDR are presented in Table I below. It is

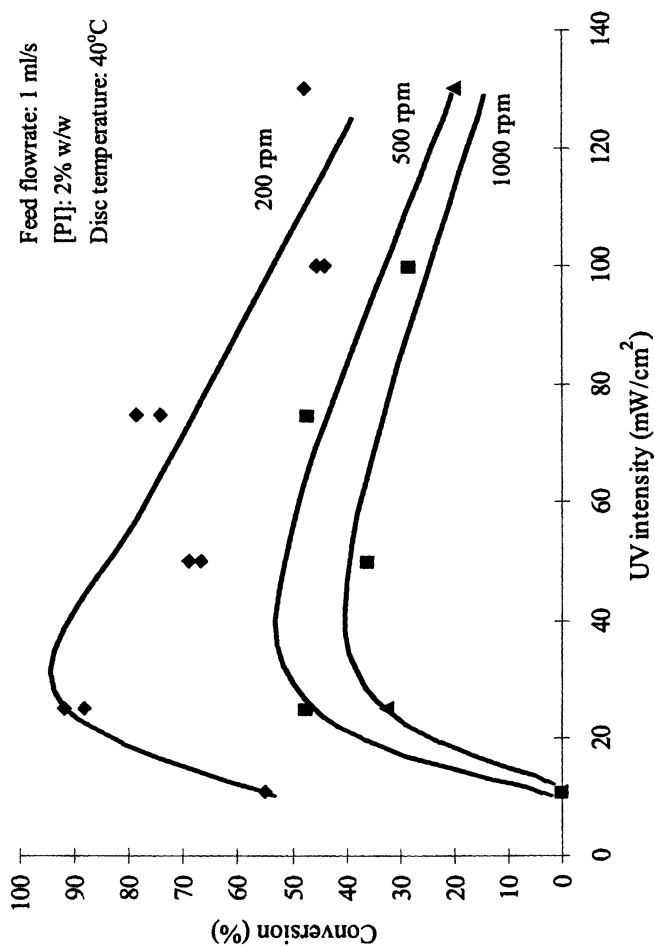


Figure 4. Effect of UV intensity on conversion of *n*-butyl acrylate in SDR for a range of disc rotational speeds

clearly seen that as intensity is increased from 11 mW/cm² to 125 mW/cm², there is a significant drop in both M_n and M_w values for 200 and 500 rpm. This predictable effect can be attributed to the large number of initiator radicals formed at more intense UV irradiation which increases the probability of termination reaction reactions and hence shorter chains being formed. This observation fits in with the explanation offered in the previous section whereby conversion drops at the highest intensity due to increased chain termination in the presence of increased number of radicals.

Table I. Molecular weight properties of poly(butyl acrylate) in SDR

Disc speed (rpm)	Feed flowrate = 1 ml/s			
	UV intensity (mW/cm ²)	M_n	M_w	PDI
200	11	140000	300000	2.14
300	11	260000	490000	1.88
200	25	33761	68725	2.03
500	25	31005	58626	1.89
1000*	25	67807	238696	3.55
200	125	25394	50529	1.99
500	125	20900	41735	2.00
1000*	125	73803	198376	2.69

Polymer from the SDR at 200 and 500 rpm has narrow molecular weight distribution (MWD) as indicated by the polydispersity index (PDI) in the range of 1.8 to 2.1 (Table I). This observation indicates that a rapid rate of initiation can be sustained in the SDR which is comparable to the rate of propagation. Also, under the influence of intense mixing in the film on the disc, the propagation rate constant is likely to remain as high as it was in the initial stages of the polymerization.

It is to be noted, however, that molecular weight properties (M_n , M_w and PDI) at 1000 rpm (*) are higher than expected. The data presented are for samples taken from the walls rather than from the disc as virtually no polymer was left on the disc surface. The growing chains may be joining up in bimolecular termination reactions in the film flowing down the wall. In sharp contrast, we believe that disentangled, extended growing chains in the SDR flow environment (10) would be less likely to combine and hence molecular weights of polymer on the disc would be lower.

The extent of branching in the polymer formed in the SDR was also of significant interest. It is well known that when acrylate monomers are polymerized in bulk, extensive branching occurs even at low conversions due to transfer reactions resulting in highly branched, insoluble polymer networks (13).

However, much to our surprise, ^{13}C NMR spectra analysis (16) revealed that poly(butyl acrylate) formed by bulk polymerization on the rotating disc was entirely linear. The absence of branching may be linked to the extensional flow regime in the high centrifugal fields of the rotating disc which somehow suppresses any transfer reactions in the film.

In using the SDR for bulk polymerization the auto-acceleration effect, arising as a result of the inability of active polymer chains to terminate thus allowing uncontrolled monomer addition, appears to be eliminated. It is our belief that conditions on the spinning disc lead to a controlled addition of monomer, rather similar to that which is observed in anionic and cationic polymerizations i.e. molecular weight increases linearly with conversion.

Static film vs. SDR film

The effect of mixing in the highly sheared thin film in the SDR is better understood by comparing the SDR performance data with static film data at comparable film thicknesses. Measured data for an average SDR film thickness of about 125 μm (from equation 2 above, with disc speed of 200 rpm, feed flowrate of 1 ml/s and n-butyl acrylate viscosity of 7.0×10^{-4} Pa.s at 40°C) are compared against those for a 200 μm static film at 25 mW/cm^2 UV intensity as shown in Table II below.

Table II. Comparison of static film and SDR film at 25 mW/cm^2

<i>Film type</i>	<i>Exposure time (s)</i>	<i>Conversion (%)</i>	<i>M_w</i>	<i>M_n</i>	<i>PDI</i>
Static	10	30	52,000	28,000	1.8
SDR (dynamic)	2.1	90	70,000	33,000	2.1

From Table II, it is observed that the photopolymerization proceeds at a much faster rate in the dynamic SDR film as a result of the enhanced mixing levels promoted by the shear forces. The concentration of primary radicals at the same UV intensity would be similar in both the static and the SDR film but it is likely that the efficiency factor f of these radicals in initiating polymer chains is greater in the SDR film due to the increased mixing. Thus more polymer chains are generated in the SDR film, which consume more monomer molecules in the propagation reactions to give a higher conversion in a shorter exposure time. We have also noted that in order to achieve comparable conversions of ~90% in the static film, it needs to be exposed for 40 s to a UV intensity of 75 mW/cm^2 .

However, due to the higher UV intensity and exposure times, the resulting molecular weights ($M_w \sim 35,000$ and $M_n \sim 18,000$) are far less than those in the SDR film. Hence, the SDR is a more efficient reactor system at moderate UV intensities.

Opportunity for process intensification

The thin film spinning disc reactor is an example of a compact, intensified reactor which uses the centrifugal forces to promote mixing and transport properties (heat and mass transfer) in the polymerizing film. The fluid dynamics generated in the fluid film provide the ideal environment for inherently fast reactions such as photopolymerization to take place in a controlled manner. Also, with the use of thin films and therefore reduced amount of inventory in the reactor at any one time, the intrinsic safety of processes requiring the handling of hazardous materials is greatly improved. The safety of polymerization processes is largely dependent on the extent to which the exotherm of the reaction can be controlled, which has a direct influence on the molecular weight distribution. With its enhanced heat transfer rates, the SDR has the ability to closely control reaction temperature in the film thus preventing runaway reactions and producing polymer with a narrow distribution. The compactness of the SDR combined with the additional benefits offered by the use of the spinning disc technology highlight the potential for achieving intensification of photopolymerization processes.

Conclusions

The novel thin film spinning disc reactor presents a tremendous opportunity for performing continuous photopolymerization of monomers in bulk. With its enhanced mixing, high heat removal capabilities, sustainable thin film flow for efficient UV penetration and short, controllable residence time, the SDR has the potential of producing high conversion, high molecular weight polymers with narrow MWD and hence improved product quality. The SDR also appears to have the ability to control the gel effect thus giving tighter control over polydispersity.

References

1. Blyth, J.; Hoffmann, A.W. *Ann.* **1845**, *53*, 292.
2. Kopp, E.; *Compt. Rend.* **1845**, *21*, 1378.

3. Ostromislensky, I.; *J. Russ. Phys. Chem. Soc.* **1911**, *44*, 204.
4. Ciamician, G., *Science* **1911**, *36*, 385.
5. Morawetz, H. *Polymers: The Origins and Growth of a Science*; John Wiley & Sons: New York, 1985; p.95.
6. Boutin, J.; Neel, J. German Patent 2,716,606, 1977.
7. Arndt, P.J. et al. German Patent, 3,208,369, 1983.
8. Boodhoo, K.V.K.; Jachuck, R.J.J. *Green Chem.* **2000**, *2*, 235.
9. Boodhoo, K.V.K.; Jachuck, R.J.J. *Appl. Therm. Eng.* **2000**, *20*, 1127.
10. Boodhoo, K.V.K.; Dunk, W.A.E.; Jachuck, R.J.J. *J. Appl. Polym. Sci.* **2001**, *in press*.
11. Jachuck, R.J.J.; Ramshaw, C. *Heat Rec. Sys. & CHP.* **1994**, *14(5)*, 475.
12. Beuermann, S.; Paquet, D.A. (Jr); McMinn, J.H.; Hutchinson, R.A. *Macromolecules* **1996**, *29*, 4206.
13. *Concise Encyclopedia of Polymer Science and Engineering*; Kroschwitz, J.I., Ed.; Wiley-Interscience: New York, 1990, p.16-20.
14. Van Herk, A.M. *Macromol. Rapid Commun.* **2001**, *22(9)*, 687.
15. Decker, C. *Polym. Internat.* **1998**, *45(2)*, 133 and references therein.
16. Ahmad, N.M.; Heatley, F.; Lovell, P.A. *Macromolecules* **1998**, *31*, 2822.

Chapter 38

Pulsed Laser Polymerization of Methyl Methacrylate Using Wilkinson's Catalyst as a Photoinitiator

M. Sakhawat Hussain¹, Shafique Ahmad Awan¹, M. A. Khan²,
and Haleem Hamid³

¹Department of Chemistry, ²Center for Applied Physical Sciences, and
³Research Institute, King Fahd University of Petroleum & Minerals,
Dhahran 31261, Saudi Arabia

Pulsed laser polymerization (PLP) of methyl methacrylate (MMA) with $[(C_6H_5)_3P]_3RhCl$ (Wilkinson's catalyst), with and without AIBN was investigated at room temperature. PLP of a MMA sample without Wilkinson's catalyst produced 0.107% PMMA, while the sample having 1.3 millimolar Wilkinson's's catalyst yielded 0.565%. The Wilkinson's catalyst was found to act as a mild photoinitiator promoting the process. The GPC revealed that the values of the polydispersity index became narrower in the presence of Wilkinson's catalyst. The ¹H NMR spectra indicated the atactic nature of the resulting PMMA.

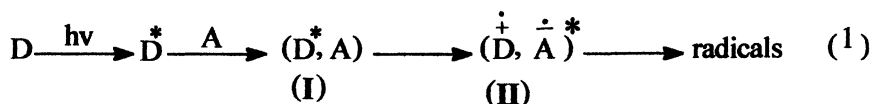
Introduction

Photoinitiated polymerization occurs when radicals are produced by ultraviolet and visible light irradiation of a reaction system (1). Photoinitiated polymerization offers significant practical advantages such as control of the initiation rates by a combination of the source of radicals, light intensity and temperature. Extensive use of these advantages has been made in the printing and coating industries (2,3). Photopolymerizations are of special interest in applications where economic and/or environmental considerations require the use of solvent-free systems. Due to the assiduous work of Olaj and co-workers (4-6) a technique has developed which utilizes a pulsed laser light source to evaluate the individual kinetic rate constants in free-radical polymerization.

Controlled synthesis of low molecular weight polymers is assuming great importance as their applications in the detergents, coatings, and water treatment industries continue to develop. Poly(methyl methacrylate) (PMMA) and its copolymers have found a great range of applications because of their good thermo-mechanical and chemical properties in addition to their excellent weatherability, unique transparency and biocompatibility (7). Catalytic chain transfer polymerization was discovered in 1975 but reported in the literature in early 1980s (8). The use of metal-chelates in catalytic chain transfer polymerization is now well known and is considered as a very highly effective method for producing oligomers (9). The chelates of cobalt(II) have been reported as catalytic chain transfer agents (CCTAs) for the controlled thermal polymerization of MMA, styrene, and other monomers (10, 11).

Some transition metal complexes have also been used as catalysts for the polymerization of MMA and styrene. Kato (12) and coworkers achieved well-controlled polymerization of MMA using a ternary initiating system consisting of CCl_4 , $\text{RuCl}_2(\text{PPh}_3)_3$, and $\text{MeAl}(\text{ODBP})_2$. In 1997, Sawamoto and coworkers reported two new catalysts, $\text{FeCl}_2(\text{PPh}_3)_3$ (13) and $\text{NiBr}_2(\text{PPh}_3)_2$ (14) for the atom transfer radical polymerization (ATRP) of MMA. Percec and coworkers (15) reported the ATRP of styrene by using Wilkinson's catalyst but no rigorous treatment of the role of Wilkinson's catalyst in the polymerization was given.

Similarly, Jerome and coworkers (16) reported the polymerization of MMA initiated by 2,2'-dichloroacetophenone in the presence of Wilkinson's catalyst plus 7 equivalent of PPh_3 , in THF at 60 °C. They concluded that Wilkinson's catalyst indeed facilitates MMA polymerization initiated by 2,2'-



dichloroacetophenone at a temperature as low as 60 °C. In the PLP of MMA, the role of Wilkinson's catalyst can be summarized by the formation of exciplex (17) as shown in Equation 1 where D is the donor specie (Wilkinson's catalyst) and "A" is an acceptor, which is MMA (monomer) and/or AIBN (initiator). In (I) the excited donor and acceptor atoms come close to each other providing free radicals via intermediate (II).

In the present paper we report, the bulk polymerization of MMA using an excimer laser (XeCl @ 308 nm) in the presence of Wilkinson's catalyst with and without AIBN. The role of Wilkinson's catalyst as a CCTA or photoinitiator has been investigated. To the best of our knowledge, the PLP of MMA with Wilkinson's catalyst has not so far been reported.

Experimental

Materials

The MMA (>99 %) obtained from Fluka was mixed with 10% NaOH to remove inhibitor. It was then washed with distilled water. And the residual water was removed by adding anhydrous sodium sulfate. The monomer was distilled under dry nitrogen at 58-60 torr and 33-35 °C (18). AIBN was recrystallized from CH₂Cl₂. *Since MMA is harmful to respiratory system and skin and can also cause irritation to eyes, all these steps need to be performed under a fume hood.* Wilkinson's catalyst from Fluka and methanol from BDH were used as received from the manufacturer.

Gel Permeation Chromatography

The PMMA samples were analyzed on WATERS GPC 150C plus. The 1,2,4-Trichlorobenzene was used as solvent with PL Gel 10 μm column. The flow rate was 1.0 ml/min and temperature was 150°C. Polystyrene standards were used for determining molecular weights and polydispersity of PMMA prepared in this study.

¹H NMR.

The ¹H NMR spectra were recorded on Jeol JNM-LA 500 NMR spectrometer at 500 MHz frequency at 297⁰ K in CDCl₃. The spectra were

recorded with the following instrumental conditions: points = 32768, frequency = 10000.0 Hz, pulse delay = 5.361 sec, resolution = 0.31 Hz, scans = 16, Solvent = CDCl_3 , temperature = 298 $^\circ\text{K}$.

UV LASER.

A Lambda Physik Model EMG 203 MSC with XeCl Excimer laser giving 308 nm input at 10 Hz was used. The pulse duration was about 20 ns.

UV/Vis Spectrophotometer.

A Perkin Elmer Lambda 5 UV/Vis spectrophotometer was used to record the UV spectra. using quartz cells with the following conditions: slit = 2 nm, response = 0.2 sec, lamp = 332.8 nm, solvent = chloroform.

Pulsed Laser Polymerization

Wilkinson's catalyst (2.0 mg) was dissolved by slight warming in 10.0 ml of freshly distilled MMA. Four Schlenk tubes containing 20.0 mg of AIBN were labeled as A, B, C, and D. To the tube A, were added 1.0 ml of Wilkinson's catalyst solution and 5.0 ml of MMA; to tube B, 3.0 ml Wilkinson's catalyst solution and 3.0 ml MMA; to tube C, 5.0 ml of Wilkinson's catalyst solution and 1.0 ml of MMA; while to tube D (control sample) only 6.0 ml of pure MMA (without any Wilkinson's catalyst). The dissolved O_2 was removed by repeated freeze-thaw technique and the tubes were sealed. Just prior to PLP, the seal was broken and the contents of the tube was transferred to a 4.0 ml capacity quartz cell under dry nitrogen atmosphere. Thus, each sample in the quartz cell contained 13.8 mg (2.03×10^{-2} M) of AIBN, with different concentrations of Wilkinson's catalyst.

A Lambda Physik Model EMG 203 MSC was used for excimer laser (XeCl) irradiation (45 minutes for each of the sample) at 308 nm, using the system shown in Figure 1 (19). Typical laser energy per pulse was 150 mJ with a repetition rate of 10 Hz. The laser beam spot size was 10 mm x 30 mm which covered most of the volume of the sample cell. No focusing or beam expansion was needed in this system.

Laser energy was continuously monitored using a Moleclectron J-50 probe. The discharge voltage on the laser tube was increased in a controlled manner to maintain a constant energy output. The resulting polymer was added to 40 ml of methanol with constant stirring. Subsequently, all methanol and residual MMA was evaporated. For removing any traces of residual MMA, a vacuum drying procedure was applied.

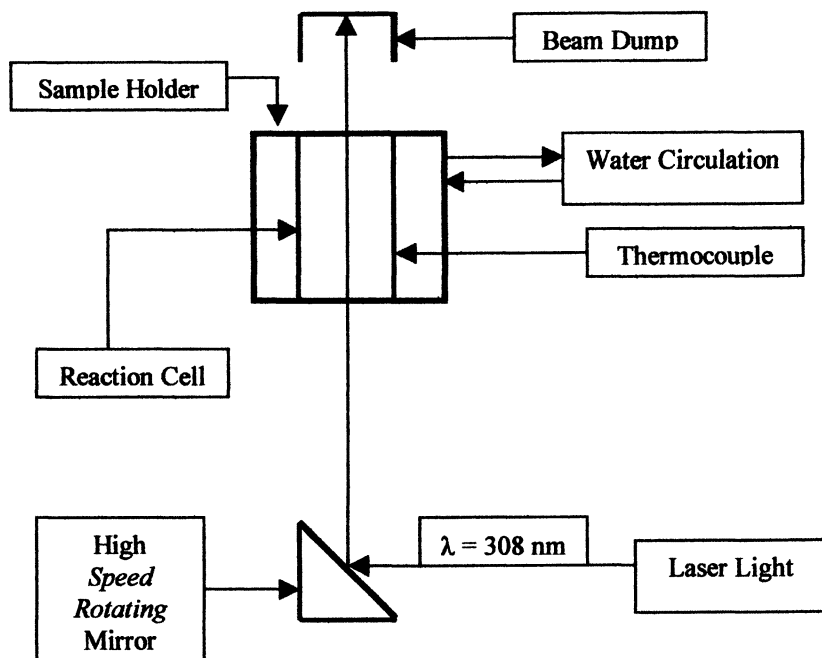


Figure 1. Schematic diagram showing PLP of MMA at 25 °C.

Results and Discussion

Initially, both AIBN and Wilkinson's catalyst were used on the assumption that the latter will act as a catalytic chain transfer agent and restrict further growth of polymer chains. The data to investigate the effects of the concentration of Wilkinson's catalyst on the molecular weights and polydispersity of PMMA using 2.03×10^{-2} M AIBN as initiator in the pulsed laser polymerization of MMA are shown in Table I.

Table I. Effect of the Concentration of Wilkinson's catalyst on the Molecular Weights and Polydispersity of PMMA using 2.03×10^{-2} M AIBN as Initiator in Pulsed Laser Polymerization of MMA.

Run #	Conc. (mM)	Conversion (%)	M_n	M_w	PDI
Reference	0	12.72	14030	26570	1.89
A	0.0361	15.05	6330	9830	1.52
B	0.1083	15.71	10490	16350	1.56
C	0.1805	17.26	13150	24290	1.85

Table I indicates that the polydispersity of the PMMA samples is less than 1.89 which is most likely due to a termination process, that under the prevailing conditions is mainly by disproportionation. There is decrease of the PDI values from 1.89 in the reference sample to 1.52 in the presence of 0.0361 mM solution (Sample A) of Wilkinson's catalyst. The polydispersity index (PDI) increases for sample B and sample C. that is apparently due to the increase in percent conversion of MMA resulting in an increase in the molecular weights. It looks as though the autoacceleration is due to a gel effect that might be operating to some extent. Actually, the polymer weight depends on the ratio $[M]/[I]^{1/2}$. Normally, the initiator concentration $[I]$ decreases faster than $[M]$ and the molecular weight of the polymer produced at any instant increases with conversion. As a result, the molecular weight distribution increases with percent conversion. But it is worthwhile to note that PDI for sample C in which 0.1805 mM Wilkinson's catalyst was used is still less (1.85 with a percent conversion of 17.26 %) as compared to control sample for which PDI is also 1.89 with percent conversion 12.72 %. Therefore, it can be concluded that though the Wilkinson's catalyst does not inhibit polymerization (rather promote it), it still narrows the MWD.

The GPC chromatograms are shown in Figure 2. It is clear from these chromatograms that the shape of the chromatogram C is similar to that of the reference sample R. The difference between chromatogram A and reference

samples indicates that there is some change in the termination process in the presence of Wilkinson's catalyst, indicating that Wilkinson's catalyst might be responsible for the increase in the percent conversion.

Figure 3 shows that percent conversion of MMA increases as a function of the amount of Wilkinson's catalyst used. Since the amount of AIBN is constant in each sample, it is concluded that Wilkinson's catalyst is responsible for the increase in the percent conversion of PMMA.

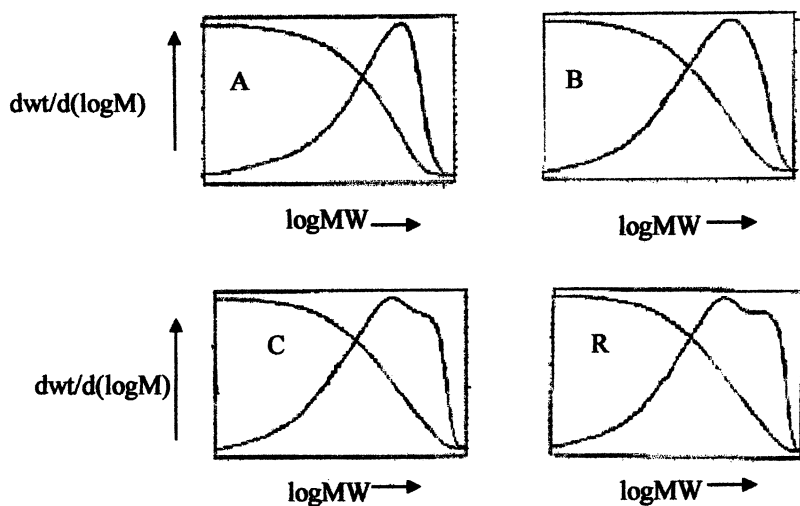


Figure 2. Molecular weight distribution Curves for different samples determined by GPC. A, B, C and R have the same meaning as in Table I.

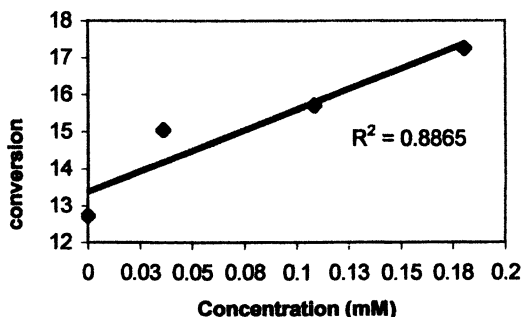


Figure 3: Dependence of the PMMA conversion (%) on the concentration (millimoles per liter) of Wilkinson's catalyst using AIBN as initiator.

In order to verify that Wilkinson's catalyst can act as mild photoinitiator, the effect of irradiation time on PLP of MMA at a constant concentration of Wilkinson's catalyst without adding AIBN, was investigated. The results are presented in Table II.

Table II. Effect of the irradiation time on Pulsed Laser Polymerization of MMA at constant concentration (1.3mM) of Wilkinson's catalyst without AIBN.

<i>Sample #</i>	<i>Time (min.)</i>	<i>Conversion (%)</i>
1	25	0.122
2	35	0.565
3	45	0.710
Control	35	0.107

A control experiment (having no Wilkinson's catalyst) was irradiated by the laser for 35 minutes, the percent conversion was found to be 0.107 %, while for sample #2 having Wilkinson's catalyst for the same duration of laser irradiation, the percent conversion was higher (0.565 %).

The UV/Vis spectrum for Wilkinson's catalyst indicates strong absorption bands at 276, 268, and 260 nm. There is also significant absorption around 308 nm for Wilkinson's catalyst, while for AIBN and MMA there is no significant absorption at this wavelength. All these observations suggest that Wilkinson's catalyst either dissociates to give free radicals, which in turn produce free radicals of MMA directly or enhances the total number of free radicals of AIBN when it is present. In this case, photochemical activation has accelerated the ligand dissociation from Wilkinson's catalyst. Absorption of UV photons of the proper wavelength can excite an electron which is due to a strong δ -anti-bonding effect would favor the loss of the more strongly δ -donating ligand (20). In the present case, P(Ph)₃ is a stronger sigma donating ligand (21) compared to Cl⁻, therefore, the Rh-P(Ph)₃ bond is most probably broken. Another possibility is that Wilkinson's catalyst absorbs energy generates an excited state and from this excited state it loses its extra energy to AIBN or directly to the MMA monomer, and thus helps to form free radicals as indicated in equation

1. Thus, Wilkinson's catalyst behaves like a photoinitiator or photosensitizer under excimer laser irradiation.

The ^1H NMR spectra of PMMA formed in our study are shown in Figure 4. The peaks around 3.60 ppm are due to OCH_3 , whereas the peak around 3.76

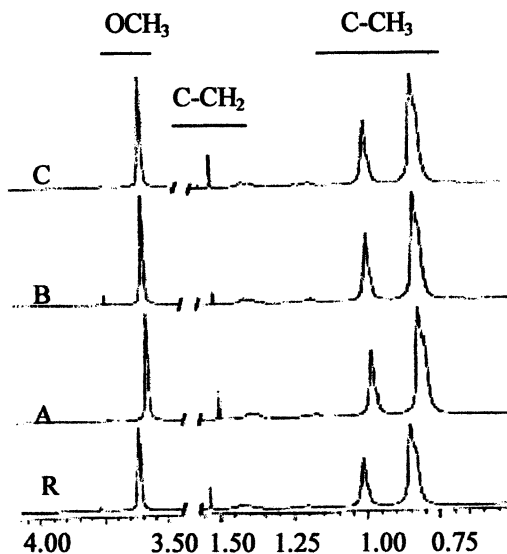


Figure 4. 500MHZ ^1H NMR of PMMA in CDCl_3 at room temperature. The A, B, C and R have the same meaning as in Table I.

ppm is either from unreacted residual monomer or due to the terminal ester group, which is adjacent to a chlorine atom (16). Unfortunately, the CH_2 signals can not be analyzed unambiguously. Figure 4 suggests that in all cases in our experiments, atactic PMMA was formed *i.e.* polymer incorporates simultaneously both type of C-CH_3 groups *i.e.* syndiotactic and isotactic. Both C-CH_3 and O-CH_3 peaks for the samples C, B, and A are shifted to some extent with respect to C-CH_3 and OCH_3 peaks in the reference sample. For the analysis of tacticity by ^1H NMR spectroscopy, not only the nearest, but also the next nearest neighbors, should also be included *i.e.* we usually need to look at the triad, tetrad sequences as compared to diad sequence (22).

The atactic PMMA formed in this work (Figure 4), is similar to this polymer prepared by other methods where C-CH_3 groups produce three signals of very different intensities in the region 0.80-1.18 ppm. The signal at 0.80

ppm indicates syndiotactic arrangement of C-CH₃ groups in the atactic PMMA sample, while the signal around 0.98 ppm corresponds to an isotactic arrangement of C-CH₃ groups in the same atactic PMMA sample. The signal at 1.18 ppm belongs to methyl groups at changeover positions between isotactic and syndiotactic C-CH₃ groups in the atactic PMMA sample. Integration ratios for syndiotactic to isotactic C-CH₃ groups are shown in Table III.

Table III. Intensity Ratios of Syndiotactic to Isotactic C-CH₃ groups in ¹H NMR of atactic PMMA

<i>Sample #</i>	<i>Intensity ratio</i>
Ref.	2.495
A	2.522
B	2.474
C	2.416

The intensity ratio is around 2.5, which indicates that the number of syndiotactic type C-CH₃ groups are approximately 2.5 times greater than the isotactic C-CH₃ groups in the experimentally formed atactic PMMA in this study.

Conclusion

Our results indicate that Wilkinson's catalyst allows MMA to be polymerized at room temperature using excimer laser irradiation in the presence as well as absence of AIBN as initiator acting as a mild photoinitiator. The PDI values become narrower in the presence of Wilkinson's catalyst, but on the other hand there is increase of PDI values with percent conversion. The resulting PMMA is atactic in nature. The mechanism by which Wilkinson's catalyst takes part in the polymerization process needs further investigation.

Acknowledgement.

This research was supported by KFUPM through SABIC grant (Project # SABIC/1999-5). We are also grateful to the Research Institute KFUPM for GPC analysis.

References

1. Oster, G.; Yang, N. L. *Chem. Rev.* **1968**, *68*, 125.
2. Pappas, S. P.; "Photopolymerization," in *Encyclopedia of Polymer Science and Engineering*, Wiley Interscience, New York, **1988**, *11*, 186-212.
3. Pelgrims, J. J. *Oil Col. Chem. Assoc.* **1978**, *61*, 114.
4. Olaj, O. F.; Bitai, I.; Gleixner, G. *Makromol. Chem.* **1985**, *186*, 2569.
5. Olaj, O. F.; Bitai, I.; Hinkelmann, F. *Makromol. Chem.* **1987**, *188*, 1689.
6. Olaj, O. F.; Bitai, I. *Angew. Makromol. Chem.* **1987**, *155*, 117.
7. Janeczek, H.; Jedlinski, Z.; Bosek, I. *Macromolecules*, **1999**, *32*, 4503.
8. Gridnev, A. J. *Polymer Science, Part A, Polymer Chemistry*, **2000**, *38*(10), 1753.
9. Suddaby, K. G.; Sanayei, R. Amin; Rudin, R.; O'Driscoll, K.F., *J. Applied Polymer Science*, **1991**, *43*, 1565.
10. Burczyk, A. F.; O'Driscoll, K. F.; Rempel, G. L. *Journal of Polymer Science. Polymer Chemistry Edition*, **1984**, *22*, 3255-3262.
11. Sanayei, R. A.; O'Driscoll, K. F. *J. Macromol. Sci.-Chem.* **1989**, *A 26*(8), 1137-1149.
12. Kato, M.; Kamigaito, M.; Sawamoto, M.; Higashimura, T. *Macromolecules*, **1995**, *28*, 1721-1723.
13. Ando, T. ; Kamigaito, M.; Sawamoto, M. *Macromolecule*, **1997**, *30*, 16, 4507.
14. Uegaki, H.; Kotani, Y.; Kamigaito, M.; Sawamoto, M. *Macromolecules*, **1997**, *30*, 2249.
15. Percec, V.; Marboiu, B.; Neumann, A.; Ronda, J. C.; Zhao, M. *Macromolecules*, **1996**, *29*, 3665.
16. Moineau, G.; Granel, C.; Dubois, Ph.; Jerome, R.; Teyssie, Ph. *Macromolecules*, **1998**, *31*, 542-544.
17. Odian, G. *Principles of Polymerization*, Third Edition, A Wiley-Interscience Publication, **1991**, 222-226.
18. Billmeyer, F. W.; Collins, E. A.; Bares, J. *Experiments in Polymer Science*, John Wiley & Sons, **1973**, 333-335.
19. Davis, T. P.; O'Driscoll, K. F.; Piton, M. C.; Winnik, M. A. *Macromolecules*, **1989**, *22*, 2785-2788.
20. Lukehart, C. M. *Fundamental Transition Metal Organometallic Chemistry*, Brooks/ Cole Publishing Company, California, **1985**, 67.
21. Miessler G. L.; Tarr, D. A. *Inorganic Chemistry*, Second Edition, Prentice- Hall, Inc. **1999**, 408.
22. Friebolin, H. *Basic One and Two – Dimensional NMR Spectroscopy*, New York : VCH, **1991**, 305-307

Chapter 39

Two-Photon Photoinitiated Polymerization

Kevin D. Belfield and Katherine J. Schafer

Department of Chemistry and School of Optics, University of Central
Florida, P.O. Box 162366, Orlando, FL 32816-2366

The three-dimensional (3-D) spatial resolution of the two-photon absorption (2PA) process is being harnessed for 3-D microstructure fabrication and microlithography. In addition to the inherent spatial resolution of the two-photon excitation process, two-photon absorption can occur in certain materials at wavelengths well beyond that which monomers, polymers, and most organic substances absorb (one-photon), affording a greater depth of penetration and, in principle, creating little or no damage to the host. The near-IR two-photon induced free radical polymerization of (meth)acrylate monomers and the near-IR two-photon induced cationic polymerization of epoxide monomers using commercially available photoinitiator systems is described. We report the two-photon induced polymerization of a thiol-ene resin system utilizing near-IR radiation and a commercially available photoinitiator, isopropylthioxanthone (ITX). Polymerization depths of over 2 cm were achieved, demonstrating a new paradigm for deep curing of adhesives.

Introduction

The past 50 years has witnessed wide spread adoption of UV and visible photoinitiated polymerization for a variety of applications in coatings, inks, photolithography, dental materials, to name just a few. The desire to create three-dimensional objects has resulted in adopting UV laser curing monomers in stereolithography in which free-radical and cationic photoinitiated processes have been employed. Stereolithography involves a layer-by-layer build up of polymerized resin to create the final structure. In this technique, a laser is scanned in the X and Y dimensions over a thin film of photoinitiator-containing monomer to create a solidified pattern. Recoating to form another thin film over top of the polymerized layer then rescanning creates the next solidified layer. Repeating this two-dimensional polymerization procedure results in building up a layered structure in the third dimension (Z), hence stereolithography. Miniaturization of this technology has resulted in the microfabrication of relatively complex three-dimensional (3-D) structures. Both conventional and stereolithographic UV-visible curing are single-photon absorption-based processes, in which the initiator undergoes excitation to an electronically excited state via absorption of a single photon (UV or visible).

Recently, two-photon induced organic photochemical transformations have been reported. Two-photon absorption can be defined as simultaneous absorption of two photons via virtual states in a medium (Figure 1) (*I*). This is distinct from sequential absorption of two or more photons in which each absorption is governed by the same single-photon selection rules. The simultaneous absorption of two or more photons requires high peak power, which is available from pulsed lasers. Since the photon energy is essentially summed, the photons can be of much longer wavelength than required for single-photon absorption, typically in the near-IR. Even though multiphoton processes have been known for some time, materials that exhibit multiphoton absorption have yet to find widespread application. This may likely be due to the interdisciplinary nature of developing multiphoton-based techniques and processes, i.e., an understanding of photophysics, photochemistry, polymer science, and optics.

Why two-photon photochemistry? Let's consider a major feature that distinguishes single-photon absorption (IPA) from two-photon absorption (2PA); the rate of energy (light) absorption as a function of incident intensity. In single-photon absorption, the rate of light absorption is directly proportional to the incident intensity ($dw/dt \propto I$), i.e., as the incident intensity is increased, the rate of photon absorption increases linearly for the molecule in question. By contrast, in simultaneous two-photon absorption, the rate of energy absorption is proportional to the square of the incident intensity ($dw/dt \propto I^2$) (*I*). This quadratic, or nonlinear, dependence has substantial implications. For example, in a medium containing one-photon absorbing chromophores,

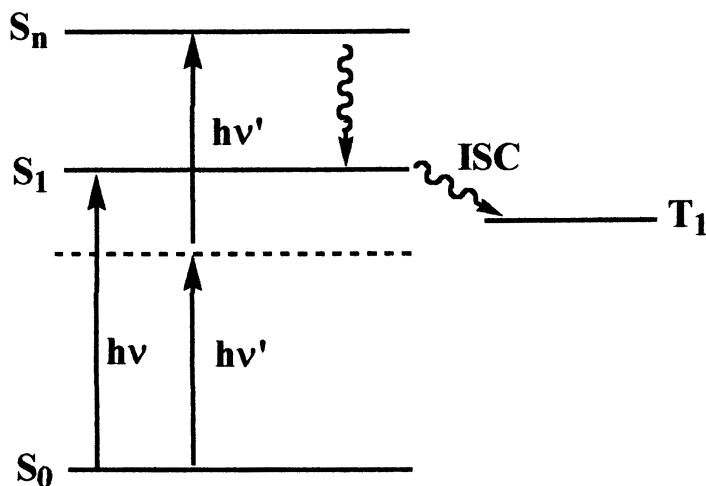


Figure 1. Simplified Jablonski energy level illustration of single-photon and two-photon absorption. Excitation of a molecule from the ground state (S_0) to an excited state (S_1) can occur through single-photon absorption (1 photon of wavelength $h\nu$) or to an excited state (S_n) via two-photon absorption (2 photons of wavelength $h\nu'$). Intersystem crossing can produce a long-lived reactive excited state.

significant absorption occurs all along the path of a focused beam of suitable wavelength light. This can lead to, e.g., photodegradation or photobleaching. In 2PA, negligible absorption occurs except in the immediate vicinity of the focal point of a light beam of appropriate energy. This allows spatial resolution about the beam axis as well as radially, and is the principle basis for two-photon fluorescence imaging. In 2PA, two long wavelength photons can be absorbed simultaneously by a material at the focal point of a light beam where the intensity is highest, e.g., at 800 nm. Thus, certain materials can undergo nonresonant two-photon absorption at wavelengths far beyond their linear absorption spectrum.

Let's examine nonresonant two-photon absorption further. Normally, molecules are promoted from the ground state to an excited state through resonant single-photon absorption. However, under appropriate conditions, this excitation can be accomplished by two-photon absorption (2PA). In this process, two longer wavelength photons undergo simultaneous absorption via a so-called virtual state V. Since this virtual state is quantum mechanically disallowed, both photons must interact simultaneously with the absorbing molecule to promote it to an electronically excited state. The physics of this

interaction is best thought of in a perturbation theory analysis (2). Here, the intermediate state (or states) is a real state that is occupied for a time determined by the energy mismatch between the level splitting and the photon energy, and the uncertainty principle $\Delta E \Delta t > \hbar$. The Δt determines the degree of “simultaneity” which is usually subfemtosecond. The intermediate states are all the states reached by dipole allowed single-photon transitions. As any intermediate state becomes resonant, this time becomes the level decay time and then the process is referred to as sequential absorption or excited state absorption. It is also important to note that the parity of the energy levels reached by 2PA and linear absorption are different so that two-photon spectra can be quite different from linear spectra depending on the structure of the molecule. In 2PA, the final state reached has the same parity as the initial state, while in single-photon absorption the parity is opposite as given by dipole selection rules. However, in most solids and complex molecules, the parity can become mixed in “bands”.

Two-Photon Polymerization

Although several reports of two or multiphoton induced polymerization have appeared in the literature as early as 1971 (3), most of these involve two or more sequential, resonant single-photon excitation processes at single or multiple wavelengths (i.e., excited state absorption) (4, 5). The resonant processes must be distinguished from the simultaneous two-photon excitation process of concern in this proposal due to the fundamental differences in achieving spatially-resolved polymerization, i.e., a much higher degree of inherent 3-D spatial resolution in the simultaneous process. There are a limited number of accounts of apparent two-photon induced polymerization in the gas phase (6-9).

A number of research groups have reported two-photon induced polymerization in the condensed phase. Strickler and Webb conducted polymerization of a commercial acrylate monomer/oligomer mixture at 620 nm using a colliding-pulse mode-locked dye laser (100 fs pulses) fitted to a laser scanning confocal microscope (10). This report was followed by another in which the same researchers utilized the same resin and laser system to create a record-once, read-many optical data storage medium by two-photon point by point excitation/polymerization (11). In order to achieve relatively high resolution, the resin was subjected to single-photon prepolymerization (gelation), followed by two-photon exposure to form small dots. Maruo,

Nakamura, and Kawata reported a second account of two-photon induced polymerization for microfabrication (12). This work was similar to that of Strickler and Webb in that a commercial acrylate monomer/oligomer system was employed along with a fs light source. A relatively well-defined three-dimensional helical structure was formed upon scanning exposure to 200 fs pulses from a Ti:sapphire laser tuned to 790 nm. The diameter of the helical structure was 7 μm with a strand width of 1.3 – 2.2 μm . This was followed up by a demonstration of fabricating more intricate structures with subdiffraction limit resolution, including a bull figure, and micro-oscillator (13). The same group also created fluorescent microstructures by conducting two-photon polymerization of a monomer system that contained a fluorescent dye (14)

A further example of two-photon induced polymerization of an acrylate resin was reported by Zheltikov *et al.*, using a fs Ti:sapphire laser tuned to 810 nm (200 fs pulses) (15, 16). A periodic structure was obtained with point by point photopolymerization. The authors also pointed out the need for more efficient two-photon photoinitiators. Prasad and coworkers reported two-photon induced polymerization of an "epoxy" resin to form optical circuits (17). While a very nice example of two-photon polymerization was provided by Cumpston *et al.* in which a number of 3-D microstructures (photonic bandgap structure, waveguide structure, and an array of cantilevers) were fabricated in 120 – 150 μm thick films of acrylate mixtures (18). Other examples include two-photon polymerization for holographic recording by Fouassier *et al.* (19), Kirkpatrick *et al.* (20), and Diamond *et al.* (21), polymerization of acylamide and fabrication of protein-based microstructures by Campagnola *et al.* (22, 23), and holographic nanopatterning of biocatalytically formed silica by Brott *et al.* (24).

Recently, we reported the near-IR two-photon induced polymerization of (meth)acrylate monomers using a commercially available photoinitiator system based on a visible light absorbing dye (25, 26). Two-photon initiated polymerization was conducted at 775 nm via direct excitation of a commercially available dye (5,7-diiodo-3-butoxy-6-fluorone, H-Nu 470) in the presence of an arylamine, and (meth)acrylate monomer, resulting in an electron-transfer free radical initiation process. The excitation wavelength was well beyond the linear absorption spectrum for 5,7-diiodo-3-butoxy-6-fluorone (strong and weak absorption maxima at 330 and 470 nm, respectively). Four commercial acrylate or methacrylate monomer systems were used: ethoxylated bisphenol A diacrylate (SR349, Sartomer), pentaacrylate ester (SR9041, Sartomer), aromatic urethane acrylate blended with tripropylene glycol diacrylate (CN973A80, Sartomer), and 2-methyl-2-propenoic acid (1-methylethylidene)-bis(1,4-phenyleneoxy-2-hydroxy-1,3-propanediyl)ester (BisGMAx950, Esschem). A number of commercial free radical photoinitiators, representing a number of different mechanistic types, were employed with several depicted in Figure 2. Their corresponding UV-visible spectra are presented in Figure 2 where one can observe no linear absorption beyond 500 nm.

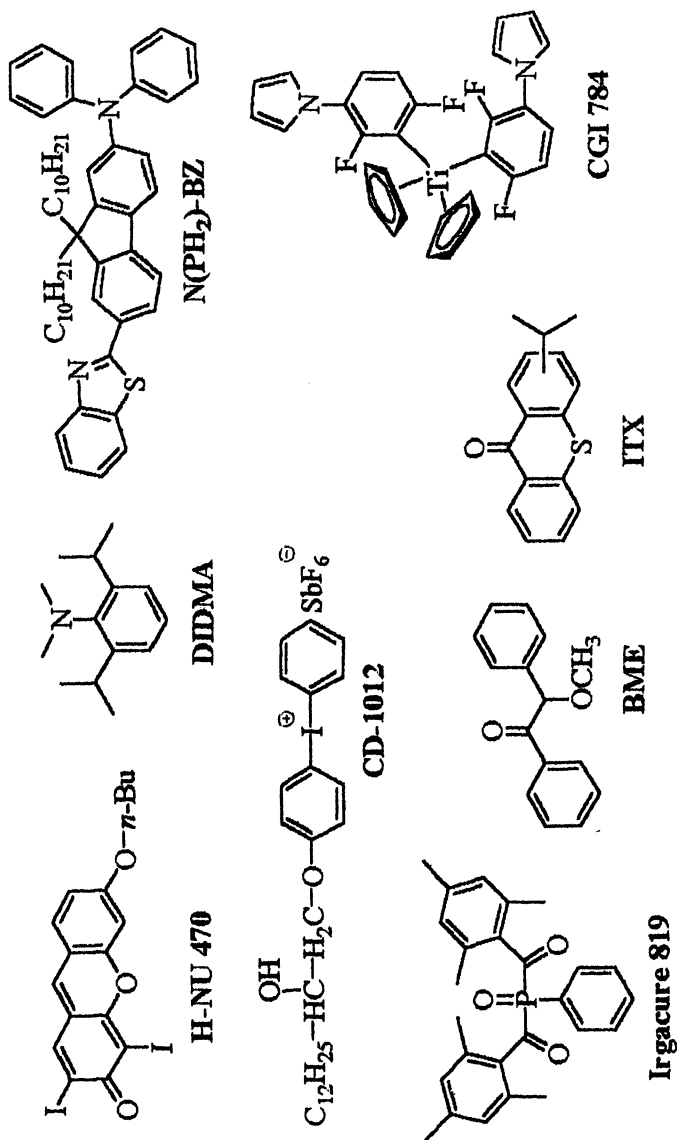


Figure 2. Structures of free-radical photoinitiators.

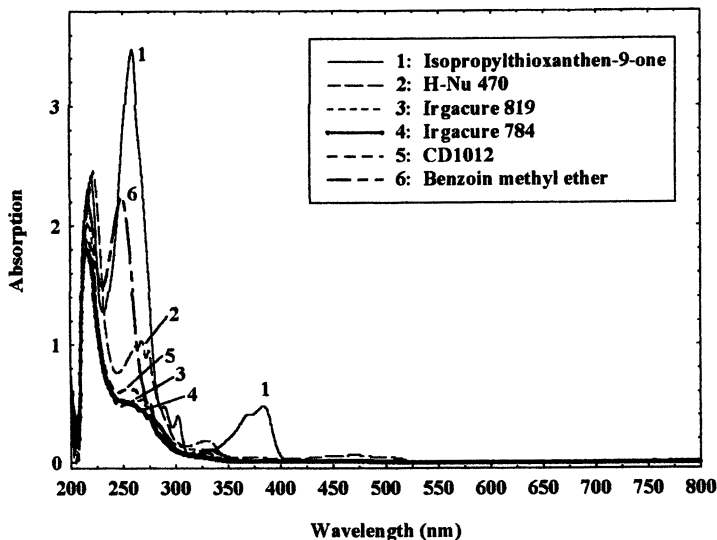


Figure 3. UV-visible spectra of free-radical photoinitiators.

The experimental exposure apparatus and set up are illustrated in Figure 4. A number of control experiments were performed to support a two-photon based excitation process. First, experiments were performed using a Ti:sapphire laser in continuous wave (CW) vs. mode-locked (80 fs pulse width). Polymerization was not observed in CW mode, while polymerization occurred only when the laser was mode-locked. Next, experiments were performed on monomer alone (no initiator), in which no polymerization was observed upon exposure to near-IR fs radiation. Furthermore, an initiator system comprised of isopropylthioxanthone (ITX) and DIDMA (monomer:ITX:DIDMA mole ratio $1:1.4 \times 10^{-3}:5.4 \times 10^{-3}$) also afforded polymer in the presence of an acrylate monomer under near-IR fs irradiation, attesting to the generality of the electron transfer polymerization discussed above. Similarly, no polymer was produced when the ITX/DIDMA/acrylate mixture was exposed to the same wavelength in CW mode.

The formation of polymeric microstructures with a variety of dimensions was accomplished with the H-NU 470 initiator/acrylate monomer system (Figure 5a). Similar 2-D microstructures were obtained via two-photon polymerization of acrylate monomers using commercial photoinitiators and a 775 nm fs laser. In particular, arylketone photoinitiators such as

isopropylthioxanthone (ITX), benzoin methyl ether (BME), and an acylphosphine oxide (Irgacure 819, CIBA) were found to be effective initiators (all have $\lambda_{\text{max}} < 400$ nm), resulting in well-defined microstructures. Typical monomer:initiator molar ratios were $1:3.5 \times 10^{-4}$ (ITX), $1:7.5 \times 10^{-3}$ (BME), $1:1.1 \times 10^{-3}$ (Irgacure 819), $1:1.9 \times 10^{-3}$ (a fluorenyl derivative (27), Figure 5b). In addition, compositions comprised of acrylate monomer SR349, ITX, and N-ethyl-diethanolamine, or SR349, H-NU 470, and N-ethyl-diethanolamine in $1:3.2 \times 10^{-3}:0.36$ or $1:7.2 \times 10^{-4}:0.32$ molar ratios, respectively, were effective in forming microstructures upon two-photon excitation (2PE).

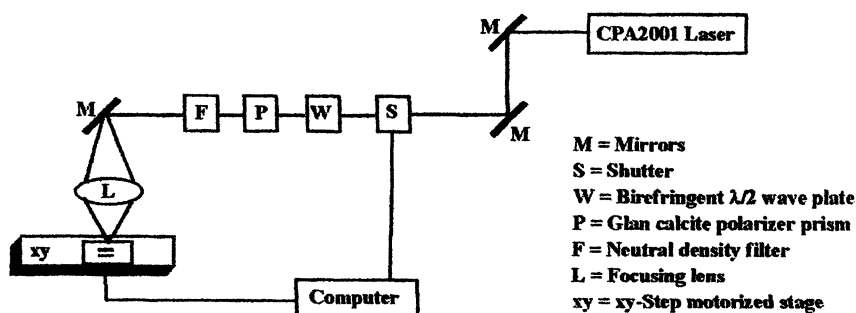


Figure 4. Schematic representation of two-photon polymerization experimental set up.

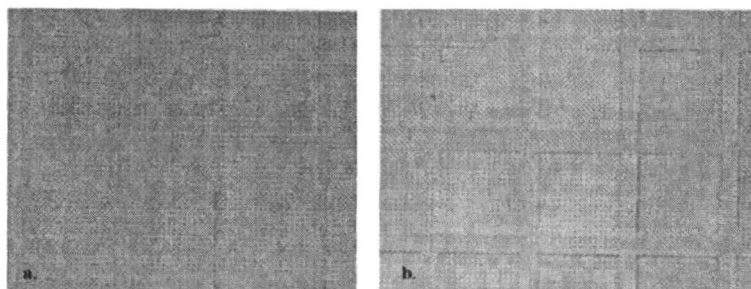


Figure 5. Optical micrographs of grid-type microstructures created via two-photon polymerization of an acrylate monomer (SR349) (a) using the H-NU 470 initiating system ($9 \mu\text{m}$ line width, $100 \mu\text{m}$ line spacing) and (b) using a fluorenyl derivative as initiator ($18 \mu\text{m}$ line width, $\sim 100 \mu\text{m}$ line spacing).

Cationic photoinitiated polymerization of epoxides, vinyl ethers, and methylenedioxylenes have received increasing attention, due in large part to the oxygen insensitivity of the cationic process (28, 29). Commercially available diaryliodonium (CD-1012, Sartomer) and triarylsulfonium (CD-1010, Sartomer) salts, and to a lesser extent a ferrocenium-type initiator, (Figure 6) were found to initiate polymerization of multifunctional epoxide and vinyl ether monomers, affording well-defined microstructures (26). As can be seen in Figure 7, the initiators have no appreciable single-photon (linear) absorption beyond 400 nm. Typical multifunctional epoxide monomers investigated were a mixture of poly(bisphenol A-co-epichlorohydrin, glycidyl end-capped and 3,4-epoxycyclohexylmethyl 3,4-epoxy-cyclohexanecarboxylate (K126, Sartomer) or Epon SU-8 (Shell) and K126 in 1:4 weight ratios, respectively, with 1 wt% of either the sulfonium or iodonium initiators. In Figure 8a, the line width is 18 μm with progressively increasing line spacing, from bottom to top, beginning at 72 μm (as programmed with the computer-controlled scanner). The microstructure in Figure 8b has 18 μm line widths with 72 μm line spacing.

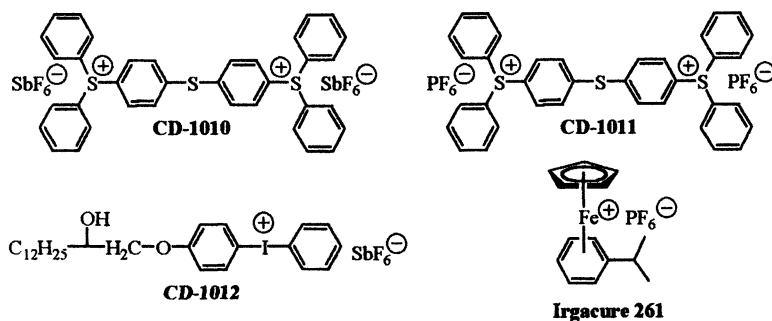


Figure 6. Structures of cationic photoinitiators.

Results of Thiol-Ene Two-Photon Polymerization

In addition to the inherent spatial resolution of the two-photon excitation process, two-photon absorption can occur in certain materials at wavelengths well beyond that which monomers, polymers, and most organic substances absorb (one-photon), affording a greater depth of penetration and, in principle, creating little or no damage to the host. Deep curing of adhesives continues to be a challenge, as typical UV curing is accompanied by limited depth of light penetration (and curing). Near-IR induced two-photon

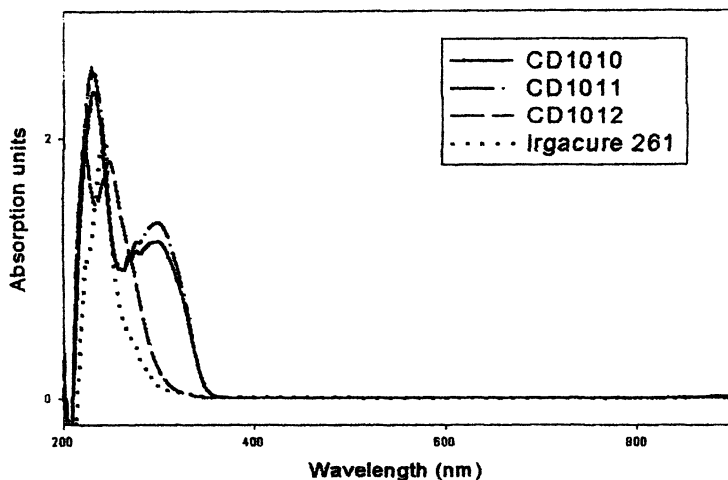


Figure 7. UV-visible absorption spectra of cationic photoinitiators.

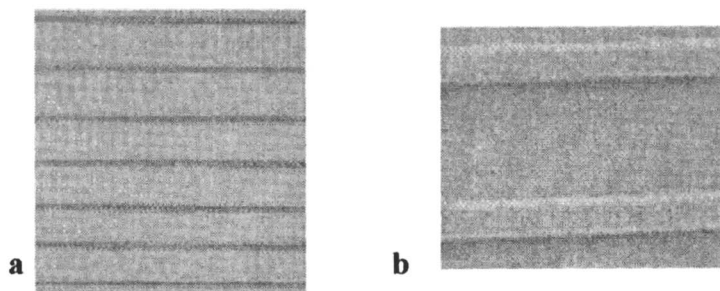


Figure 8. (a) Optical microscopy image of microstructures (18 μm line width, progressively increasing line spacing beginning with 72 μm , from bottom to top) formed via the two-photon cationic polymerization of a mixture of poly(bisphenol A-co-epichlorohydrin, glycidyl end-capped and 3,4-epoxycyclohexylmethyl 3,4-epoxy-cyclohexanecarboxylate (K126, Sartomer) using CD-1012. (b) SEM image (250x magnification) of microstructure (18 μm line width, 72 μm line spacing) formed via the two-photon cationic polymerization of Epon SU-8 (Shell) and K126 with CD-1010.

polymerization represents a unique strategy to afford curing deep in materials. Thiol-ene resins systems have found application in a number of areas including UV-curable coatings and adhesives, in large part due to their flexibility and adhesive energy properties (30, 31). We wish to report two-photon induced polymerization of a thiol-ene resin system utilizing near-IR radiation and commercially available photoinitiators, isopropylthioxanthone (ITX) and N-methylmaleimide (NMM). Polymerization depths of over 2 cm were readily obtained upon exposure to 775 nm radiation (120 fs, 1 kHz repetition rate). Combined with our previous demonstrations of near-IR two-photon induced polymerization of acrylates and epoxides (25, 26), a new paradigm for deep curing of adhesives has been realized.

The absorption spectrum of ITX in acetonitrile (ACN) is shown in Figure 9a. Two major absorption bands were observed, with λ_{maxima} at 257 and 383 nm. As can be seen, there is no linear absorption in the near-IR region where the two-photon excitation was performed. Figure 9b displays the single-photon fluorescence spectrum for ITX upon excitation at 381 nm (QY = 0.009), no fluorescence was observed upon excitation at wavelengths less than 300 nm. Also shown in Figure 9b is the two-photon upconverted fluorescence spectrum of ITX upon excitation at 790 nm. The red shift of the two-photon fluorescence spectrum is simply due to a concentration effect, i.e., the concentration of the solution used for two-photon upconverted fluorescence must be relatively high due to the low intensity of the signal (in this case, over four orders of magnitude greater than the concentration used for single-photon fluorescence measurements). The fluorescence spectrum was recorded for ITX to enable determination of its two-photon absorptivity (two-photon absorption cross-section, $\delta = 2 \text{ GM}$ at 790 nm in ACN).

To confirm that ITX indeed undergoes two-photon absorption in the near-IR, the total integrated upconverted fluorescence was measured as a function of incident intensity at two different wavelengths. A two-photon absorption process will exhibit a quadratic dependence of fluorescence intensity on the incident intensity (pump intensity). As shown in Figure 10a, ITX exhibits such a quadratic dependence, a characteristic hallmark of simultaneous two-photon absorption. An important parameter for molecules to be used in two-photon absorption based processes is their two-photon absorption cross-section (δ), expressed in Goepfert-Mayer units (GM). The two-photon absorption cross-sections were determined for ITX at a number of fs pump wavelengths, as illustrated in Figure 10b. The maximum two-photon absorption cross-section for ITX was ca. 2 GM at 790 nm.

The thiol-ene/initiator mixtures were placed into glass vials and irradiated with 775 nm, 120 fs, near-IR radiation, with the beam focused below

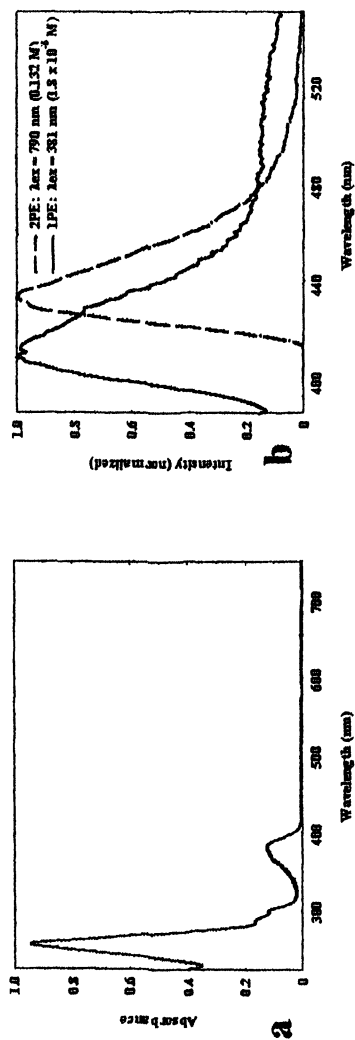


Figure 9. (a) Absorption spectrum of ITX in ACN ($2.0 \times 10^{-5} M$). (b) Single photon and two-photon upconverted fluorescence spectra of ITX in ACN.

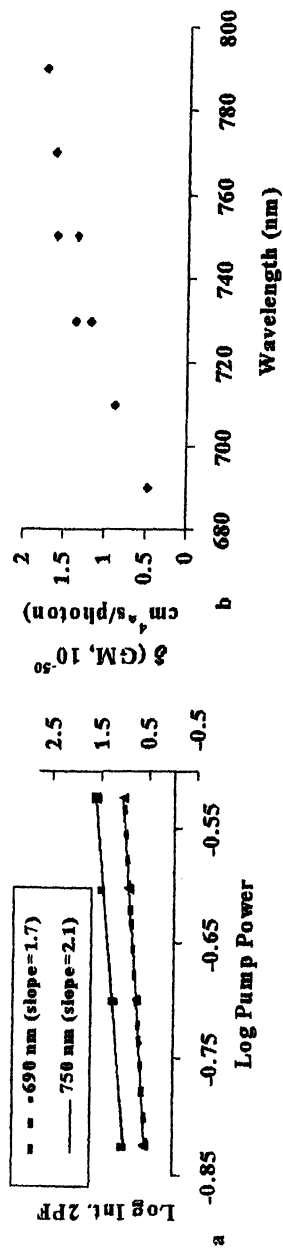


Figure 10. (a) Quadratic dependence of fluorescence intensity of ITX on the incident intensity (pump intensity). (b) Two-photon absorption cross-section of ITX as a function of fs pump wavelength.

the bottom of the vial. Both mixtures containing ITX alone and the coinitiator system of ITX and NMM resulted in polymer formation (Figure 11). However, the combination of ITX with NMM resulted in the observation of faster cure times and more complete curing. With the ITX/NMM initiator system, curing depths in excess of 2 cm were realized.



Figure 11. Two-photon induced polymerization of a thiol-ene monomer mixture using ITX and NMM. The polymeric material formed are the two-vertical strips contained within the glass vial (2.2 cm height).

Experimental

Instrumentation

UV-visible absorption and fluorescence emission spectra from solutions were recorded with a Varian Cary 3 spectrophotometer and a Photon Technologies International (PTI) Quantamaster spectrofluorimeter fitted with

one excitation monochromator (Xe lamp) and two emission monochromators (PMT detectors), respectively. Two-photon upconverted fluorescence emission spectra were recorded with the PTI spectrofluorimeter using a Clark-MXR CPA-2001 laser system. Femtosecond (fs) pulses from a frequency-doubled erbium-doped fiber ring oscillator were stretched to about 200 ps, then passed through a Ti:Sapphire regenerative amplifier and compressed down to 160 fs. The energy of the output single pulse (centered at $\lambda = 775$ nm) was 137 nJ at a 1 kHz repetition rate. This pumped a Quantronix OPO/OPA, producing fs pulsed output, tunable from 550 nm to 1.6 μm . The two-photon induced cross-linking of the thiol-ene system was performed using the same Clark-MXR CPA-2001 laser system.

General Procedures for Thiol-Ene Polymerization

ITX was recrystallized twice (MeOH and CH_2Cl_2) prior to spectroscopic studies performed in ACN deaerated with N_2 gas. The fluorescence quantum yield of ITX was estimated using rhodamine 6G in ethanol as the standard. Two-photon induced cross-linking of the thiol-ene systems was performed in glass vials containing dissolved initiators in neat monomer mixtures. ITX (1.5 mmol) was dissolved into a thiol-ene mixture (10.2 and 14.6 mmol, respectively) for one sample. Another sample consisted of ITX (0.908 mmol) and NMM (1.4 mmol) dissolved in the thiol-ene mixture (10.2 and 14.6 mmol, respectively). The fs, near-IR laser light (775 nm, 100 mW average power, 120 fs, 1 mm beam diameter) was passed through a 1 m focusing lens, such that a defocused beam penetrated through the sample from the top. The thiol-ene mixtures were exposed for various durations and the resultant polymers isolated by removing unreacted monomer mixture followed by acetone washing (4x).

Conclusions

The near-IR two-photon induced free radical polymerization of (meth)acrylate monomers and the near-IR two-photon induced cationic

polymerization of epoxide and vinyl ether monomers using commercially available photoinitiator systems were demonstrated. Single-photon visible photoinitiators and chromophores synthesized in our laboratory possessing high 2PA cross sections were used. The effectiveness of commercially available photoinitiators lends credence to the practical applications of two-photon induced polymerizations, positioning this as a technology of the future with broad implications for microfabrication and microlithography.

Critical two-photon absorption properties for an important photoinitiator, ITX, were measured at a number of significant near-IR pump wavelengths using a laser producing output of 120 fs at a repetition rate of 1 kHz. For the first time, near-IR two-photon induced polymerization of a thiol-ene monomer system was demonstrated. The use of near-IR radiation afforded practically unprecedented deep curing, in excess of 2 cm thick, validating the potential of two-photon polymerization for deep curing of coatings and adhesives. The versatility of two-photon polymerization is now well-positioned to enable to fabrication of complex three-dimensional microstructures and to be used where deep curing of materials is necessary, prospects we are continuing to pursue.

Acknowledgments

The National Science Foundation (ECS-9970078, DMR9975773), the National Research Council (COBASE), the Research Corporation, and the donors of The Petroleum Research Fund of the American Chemical Society are gratefully acknowledged for support of this work. Profs. Eric W. Van Stryland, David J. Hagan, and Mr. Joel M. Hales are acknowledged for providing assistance in two-photon absorption measurements.

References

1. Goepfert-Mayer, M. *Ann. Physik* **1931**, *9*, 273-294.
2. Kershaw, S. In *Characterization Techniques and Tabulations for Organic Nonlinear Optical Materials*; Kuzyk, M. G.; Dirk, C. W. Eds.; Marcel Dekker: New York, 1998, Chapter 7.
3. Chin, S. L.; Bedard, G. *Phys. Lett.* **1971**, *36A*, 271-272.
4. Ichimura, K.; Sakuragi, M. *J. Polym. Sci., Part C: Polym. Lett.* **1988**, *26*, 185-189

5. Jent, F.; Paul, H.; Fischer, H. *Chem. Phys. Lett.* **1988**, *146*, 315-319.
6. Papouskova, Z.; Pola, J.; Bastl, Z.; Tlaskal, J. *J. Macromol. Sci. – Chem.* **1990**, *A27*, 1015-1028.
7. Morita, H.; Sadakiyo, T. *J. Photochem. Photobiol. A* **1995**, *87*, 163-167.
8. Morita, H.; Semba, K.; Bastl, Z.; Pola, J. *J. Photochem. Photobiol. A* **1998**, *116*, 91-95.
9. El-Shall, M. S.; Daly, G. M.; Yu, Z.; Meot-Ner, M. *J. Am. Chem. Soc.* **1995**, *117*, 7744-7752.
10. Strickler, J. H.; Webb, W. W. *Proc. SPIE – Int. Soc. Opt. Eng.* **1991**, *1398*, 107-118.
11. Strickler, J. H.; Webb, W. W. *Opt. Lett.* **1991**, *16*, 1780-1782
12. Maruo, S.; Nakamura, O.; Kawata, S. *Opt. Lett.* **1997**, *22*, 132-134.
13. Kawata, S.; Hong-Bo, S.; Tanaka, T.; Takada, K. *Nature* **2001**, *412*, 697-698.
14. Hong-Bo, S.; Tanaka, T.; Tadada, K.; Kawata, S. *Appl. Phys. Lett.* **2001**, *79*, 1411-1413.
15. Borisov, R. A.; Dorojkina, G. N.; Koroteev, N. I.; Kozenkov, V. M.; Magnitskii, S. A.; Malakhov, D. V.; Tarasishin, A. V.; Zheltikov, A. M. *Appl. Phys. B* **1998**, *67*, 765-767.
16. Borisov, R. A.; Dorojkina, G. N.; Koroteev, N. I.; Kozenkov, V. M.; Magnitskii, S. A.; Malakhov, D. V.; Tarasishin, A. V.; Zheltikov, A. M. *Laser Phys.* **1998**, *8*, 1105-1108.
17. Joshi, M. P.; Pudavar, H. E.; Swiatkiewicz, J.; Prasad, P. N.; Reinhardt, B. A. *Appl. Phys. Lett.* **1999**, *74*, 170-172.
18. Cumpston, B. H.; Ananthavel, S. P.; Barlow, S.; Dyer, D. L.; Ehrlich, J. E.; Erskine, L. L.; Heikal, A. A.; Kueblern, S. M.; Sandy Lee, I.-Y.; McCord-Maughon, D.; Qin, J.; Rockel, H.; Rumi, M.; Wu, X.-L.; Marder, S. R.; Perry, J. W. *Nature* **1999**, *398*, 51-54.
19. Lougnot, D. J.; Fouassier, J. P.; Carre, C.; Van de Walle, P. *Proc. SPIE-Int. Soc. Opt. Eng.* **1989**, *1026*, 22-28.
20. Kirkpatrick, S. M.; Baur, J. W.; Clark, C. M.; Denny, L. R.; Tomlin, D. W.; Reinhardt, B. R.; Kannan, R.; Stone, M. O. *Appl. Phys. A: Mater. Sci. Process* **1999**, *69*, 461-464.
21. Diamond, C.; Boiko, Y.; Esener, S. *Opt. Exp.* **2000**, *6*, 64-68.
22. Campagnola, P. J.; Delguidice, D. M.; Epling, G. A.; Hoffacker, K. D.; Howell, A. R.; Pitts, J. D.; Goodman, S. L. *Macromolecules* **2000**, *33*, 1511-1513.
23. Pitts, J. D.; Campagnola, P. J.; Epling, G. A.; Goodman, S. L. *Macromolecules* **2000**, *33*, 1514-1523.
24. Brott, L. L.; Naik, R. R.; Pikas, D. J.; Kirkpatrick, S. M.; Tomlin, D. W.; Whitlock, P. W.; Clarson, S. J.; Stone, M. O. *Nature* **2001**, *413*, 291-293.
25. Belfield, K. D.; Ren, X.; Van Stryland, E. W.; Hagan, D. J.; Dubikovski, V.; Meisak, E. J. *J. Am. Chem. Soc.* **2000**, *122*, 1217-1218.

26. Belfield, K. D.; Schafer, K. J.; Liu, Y.; Liu, J.; Ren, X.; Van Stryland, E. *W. J. Phys. Org. Chem.* **2000**, *13*, 837-849.
27. Belfield, K. D.; Schafer, K. J.; Mourad, W. *J. Org. Chem.* **2000**, *65*, 4475-4481.
28. Belfield, K. D.; Abdelrazzaq, F. B. *J. Polym. Sci.: Part A: Polym. Chem.* **1997**, *35*, 2207-2219.
29. Belfield, K. D.; Abdelrazzaq, F. B. *Macromolecules* **1997**, *30*, 6985-6988.
30. Jacobine, A. F. In *Radiation Curing in Polymer Science and Technology*, Vol. III; Fouassier, J. P.; Rabek, J. F., Eds.; Elsevier: London, 1993, Ch. 7.
31. Lecamp, L.; Houllier, B.; Youssef, B.; Bunel, C. *Polymer* **2001**, *42*, 2727.

Chapter 40

Fluorinated Distyrylbenzene Containing Copolymers for Photoinduced Formation of Anisotropic Materials as Photoalignment Layers for Liquid Crystals

Veronika Strehmel^{1,2,*}, Burkhard Stiller⁴, Bernd Strehmel^{5,*},
Ananda M. Sarker^{5,6}, and Douglas C. Neckers⁶

¹Institute of Chemistry, ²Applied Polymer Chemistry, and ³Physical Chemistry, University of Potsdam, Karl-Liebknecht Strasse 24/25, D-14476 Golm, Germany

⁴Institute of Physics, University of Potsdam, Am Neuen Palais 10, D-14415 Potsdam, Germany

⁵Department of Polymer Science and Engineering, University of Massachusetts at Amherst, Amherst, MA 01003-4510

⁶Center for Photochemical Sciences, Bowling Green State University, Bowling Green, OH 43403

New fluorine containing photoactive polymers that contain the distyrylbenzene chromophore in the main chain have been investigated for use as photoalignment layers. Both photoisomerization and [2+2] photocycloaddition can occur competitively depending on the substitution pattern. The latter in particular results in anisotropic properties if the polymer film is irradiated with linearly polarized light. [2+2] photocycloaddition results in an insoluble material that is useful for efficient alignment of liquid crystals. Extinction difference (ED) diagrams support the result that mainly the [2+2] photocycloaddition is responsible for an increase of dichroism. Particularly the fluorine substitution in the chromophore influences both the photoreactivity of the polymer and the alignment of a liquid crystal in a manufactured cell. The results are compared with a distyrylbenzene copolymer with no fluorine. The dichroism of the liquid crystal obtained using a photoalignment layer with a particular substitution pattern

is comparable with that of a commercial cell made of a rubbed polyimide film. AFM measurements of fluorine containing polymers indicate a significant increase of surface roughness after irradiation. In addition, AFM figures show a nanostructural pattern. The results should give new impetus for development of photoalignment layers that could be used to substitute classical rubbed polyimide films in LC devices.

Introduction

Photooriented polymer films have become of increased interest for the alignment of liquid crystalline compounds¹ despite the broad distribution of mechanically rubbed polyimide surfaces², and materials that can be aligned either by electric³ or magnetic fields⁴ used commercially. Alignment of liquid crystals has been an important technological problem for the development of flat panel displays. Despite their widely known disadvantages, rubbed polyimide films have been generally used in commercial display applications. These disadvantages include dust formation and static electricity build-up during the rubbing process. Photoalignment layers obtained by photochemical reactions reduce the problems of the commercially rubbed polyimide films. Furthermore, photoalignment layers include the possibility of using light to locally control the orientational direction of liquid crystals. Surface effects are particularly crucial for the alignment of liquid crystals controlled by photoactive polymeric films.

Polymers containing side chains of azobenzene, coumarin and cinnamate have been investigated in detail for their use as photoalignment layers^{1a}. In the case of polymers containing azobenzene chromophores *trans-cis* photoisomerization is significant for photoorientation. The dichroism of the materials formed after irradiation with linearly polarized light is quite high. However, the thermal stability is often not sufficient enough because the *cis*-isomer formed thermally reverts to the *trans*-isomer without light. Coumarins and cinnamates are alternative materials because they can form a polymer with anisotropic structures after irradiation with linearly polarized light that does not lose its dichroism due to the formation of crosslinked structures by means of a [2+2] photocycloaddition reaction. It is assumed that the *trans-cis* photoisomerization contributes to the formation of anisotropic structures in the case of cinnamates and the [2+2] photocycloaddition finally freezes the anisotropy. Coumarins cannot undergo an isomerization reaction but they are useful for the generation of anisotropic structures by means of a [2+2] photocycloaddition by irradiation with linearly polarized light. [2+2] Photocycloaddition has had a long tradition in photoinduced crosslinking⁵ in solid materials. Thus it may be attractive for some applications because no additional photoinitiator is

necessary to start this reaction. However, such materials mostly absorb light (<350 nm), where exposure is becoming increasingly problematic. Our polymers are bathochromically shifted allowing illumination with common mercury lamps at either 365 or 405 nm.

Commercially rubbed polyimides orient liquid crystals although the general alignment mechanism and the molecular function of the material used is not generally understood in detail. Microgroove formation and alignment of near-surface polyimide chains are thought to be the main factors controlling the alignment process². However, the disadvantages of rubbed polyimides that we have mentioned above have encouraged many groups to focus their research on the substitution of rubbed polyimide films by photoalignment layers. Macroscopic topography and anisotropy of photoalignment layers are prerequisites in order to orient liquid crystals. The generation of anisotropy occurs at the nanometer scale by irradiation with linearly polarized light. Anisotropic structures can be analyzed by polarized UV-spectroscopy. Macroscopic topography has been examined using atomic force microscopy (AFM).

In this work, new fluorine containing photoactive polymers that contain the distyrylbenzene chromophore within the main chain have been investigated. π -Stacking between tetrafluorinated benzene rings and benzenes without fluorine was previously reported.^{6,7} This resulted in a prealignment of our polymers. Both photoisomerization and [2+2] photocycloaddition can competitively occur in these compounds. Because formation of π -stacked structures should favor the occurrence of [2+2] photocycloaddition, *trans-cis* photoisomerization is of minor importance. Both photoreactions are responsible for the generation of nanostructures. The copolymers used in this work show a particular influence of fluorine substitution on the chromophore on both the photoreactivity of the polymer and the alignment capability of the anisotropic polymer film.

Experimental Part

Materials. The copolymers described previously⁸ were used for film preparation. All solvents were spectroscopic grade. The films were spin-coated on quartz substrates and on ITO covered glass substrates (used for AFM) from stock solutions of the polymer dissolved in chloroform. Depending on the solubility of the polymer, concentrations between 10-20 g/l were used for preparing stock solutions. Film thickness was determined by AFM.

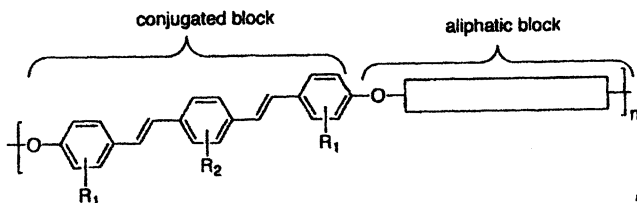
LC cells were manufactured from quartz substrates that were covered with a polymer film irradiated with linearly polarized light. Spacers (Spectro-Film, thickness 3.8 μm) were used in order to achieve similar film thickness for all measurements. The manufactured cell was filled with the liquid crystal ZLI 2293 (donated by MERCK), tempered 30° K above its clearing point (85°C) for 30 min and finally cooled to room temperature.

Techniques. Linearly polarized light (mercury lamp, 365 nm interference filter) was used for irradiation experiments. UV spectra were measured using Perkin Elmer $\lambda 2$ and a diode-array spectrometer (Polytec XDAP V2.3). The latter was taken for anisotropy measurements in order to determine spectroscopically the dichroism D ($D = (E_{||} - E_{\perp}) / (E_{||} + E_{\perp})$, E corresponds to the extinction either at parallel (\parallel) or perpendicular (\perp) position of the analyzer). AFM (AUTOPROBE CP, Park Scientific) was employed for investigation of the film topography (working in contact mode, silicon nitride tips, forces about 10 nN). Polarized FTIR measurements (Perkin Elmer) were carried out in order to determine the liquid crystal dichroism (integration of the CN-stretching vibration at 2225 cm^{-1}). Quantum yields (Φ_{-A}) of the photoreactions of the copolymers were determined by UV spectroscopy using a standard irradiation setup (mercury lamp, 365 nm interference filter). This was calibrated with a thermocouple and the calibration reliability checked using 4-dimethylaminobenzenediazonium hexafluorophosphate ($\Phi_{-A} = 0.72$ in acetonitrile⁹, $\Phi_{-A} = 0.39$ in cellulose diacetate¹⁰). The quantum yield was determined from the initial slope ($\Delta E / (\Delta t \cdot I_{\text{abs}}$); (E : extinction at the irradiation wavelength, t : irradiation time, I_{abs} : absorbed light intensity).

Results and Discussion

Polymers 1-4 are copolymers bearing the rigid distyrylbenzene chromophore and a flexible aliphatic chain (Scheme 1). Distyrylbenzenes are chromophores with a well defined structure that usually exhibit large emission yields^{7c,8a;11}. The chromophore, i.e. the distyrylbenzene unit, is connected by either an oligoethyleneoxide or oligomethylene chain. Thus, the solubility of the chromophore in ordinary organic solvents is improved and films can be easily spin-coated. The incorporation of a tetrafluorobenzene unit in 1-3 results in materials bearing an electron deficient unit. However, electron-donating substituents, such as methyl or methoxy groups yield chromophores that bear a donor-acceptor-donor substitution pattern. Previously, we showed enhanced formation of intramolecular charge transfer (ICT) even by the substitution of alkoxy groups on the distyrylbenzenes bearing the tetrafluorobenzene ring in the chromophore unit⁷.

Polymers 1 and 2 were investigated in order to examine the influence of ring substitution on photoalignment. Both polymers are of similar structure



Scheme 1

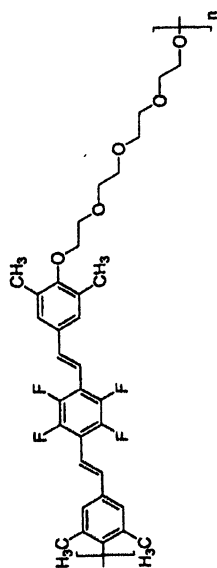
with distinct substituents at both terminal benzene rings of the distyrylbenzene chromophore. This structural pattern should, in general, influence the electronic properties of the distyrylbenzene chromophore and the packing of polymer chains in the spin-coated film. π -Stacking can occur between fluorinated benzene rings and benzenes with no fluorine. It has been previously shown through the use of similar distyrylbenzenes⁶ and *Y*-enynes¹² that, in particular, tetrafluorobenzene derivatives and benzene rings with no fluorine form well aligned disc shape structures.

Alternatively, **3** possesses a similar distyrylbenzene unit in comparison with **1** but the aliphatic chain differs. The oligoethyleneoxide chain in both **1** and **2** is expected to be of higher flexibility in comparison with the oligomethylene chain in **3**. One might therefore expect distinct packing of the spin-coated material resulting in different photophysical and photochemical behavior of the polymer upon irradiation.

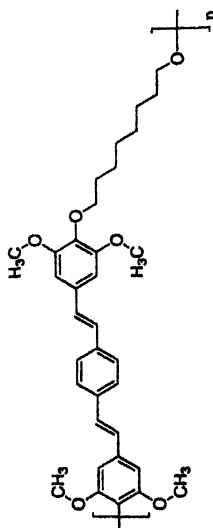
Polymer **4** is without fluorine. It was chosen in order to examine the influence of fluorine on the photochemical properties of the copolymers of the general structure in Scheme 1. π -Stacking should be of minor importance in **4**.

The photochemical processes observed in fluorine containing distyrylbenzenes are described generally by the reactions depicted in Scheme 2. *trans-cis*-Photoisomerization and [2+2] photocycloaddition can occur competitively. The preponderance of each reaction may depend on the substituents found at the terminal benzene rings. π -Stacking may favor the fluorinated material in [2+2] photocycloaddition because the chromophore is prealigned in solid film due to a planar disc-like structural pattern. Each distyrylbenzene unit possesses two double bonds that can either isomerize or form cyclic structures resulting in formation of insoluble crosslinked material.

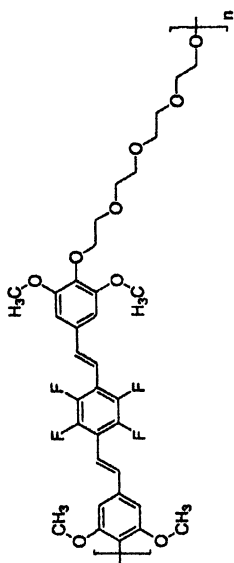
Irradiation of **3** in solution results in a decrease of absorption at 372 nm. An isosbestic point is observed at 337 nm for the first irradiation cycles. This disappears and a significant hypsochromic shift is observed after



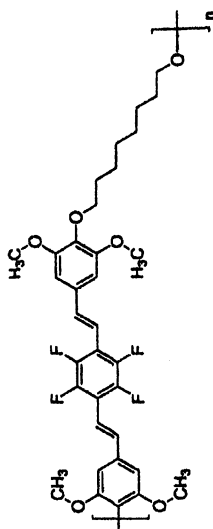
2



4

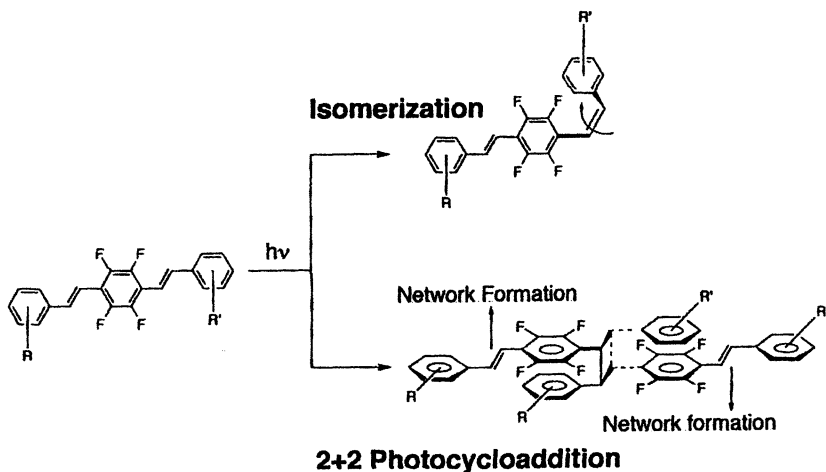


1



3

prolonged irradiation time. The absorption at 352 nm decreases faster in comparison to the absorption at 372 nm. This is caused by the competitive photochemistry shown in Scheme 2. A plot of absorption decrease (ΔOD) at 372 nm normalized to absorbed light intensity results in a curved line (Figure 1- right half). This shows again that at least two photochemical reactions with distinct rates are competing because one photoreaction would yield a straight line.



Quantum yields for the decrease of absorption (Φ_A) are compiled in Table I. Polymer **4**, which is without fluorine, gives the lowest value while all polymers with fluorine (**1-3**) have significant higher values. The larger Φ_A for the three fluorine-containing polymers results because of π -stacking between fluorinated and non-fluorinated benzene rings. The distinctly smaller values measured in films can be explained by the reduced reactivity when the reaction medium is changed from a dilute solution to a solid film. Each of the copolymers investigated in the current work evidence reasonable efficiencies for fluorescence^{8a}. Therefore, fluorescence occurs in a competitive pathway to photochemical reaction. The efficiency for fluorescence in solution depends on substitution and was determined for **1-3** between 30-50%.

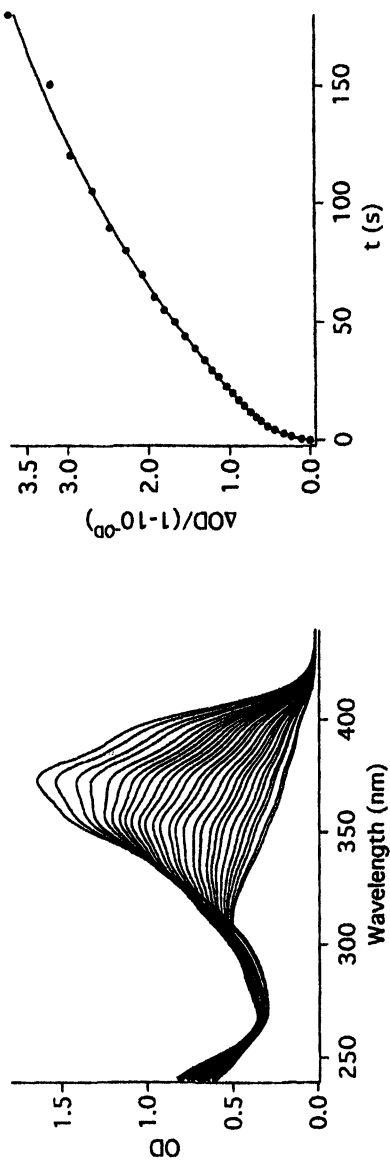


Figure 1. Irradiation of 3 in chloroform at 365 nm at different irradiation times (left) and changes of optical density (ΔOD) at 373 nm (absorption maximum at $t = 0$) as a function of irradiation time (right), data are normalized to absorbed light ($1-10^{-06}$)

Table I. Quantum yields (Φ_{-A}) for the copolymers in solution (CHCl_3) and spin-coated film

<i>polymer</i>	λ_{max} (nm) (CHCl_3)	Φ_{-A} (CHCl_3)	λ_{max} (nm) <i>film</i>	Φ_{-A} (<i>film</i>)
1	372	0.25	366	0.09
	392 (shoulder)		406 (shoulder)	
2	363	0.71	346	0.08
	384 (shoulder)		370 (shoulder)	
			395 (shoulder)	
3	372	0.19	372	0.04
	394 (shoulder)		405 (shoulder)	
4	371	0.09	363	0.003
	390 (shoulder)		374	
			398 (shoulder)	

Similar patterns for the decrease of absorption were obtained if linearly polarized light was used, Figure 2. After many irradiation cycles, the spin-coated polymer was rendered insoluble in common organic solvents indicating the formation of network structures (Scheme 2). Spectra obtained after several irradiation cycles are shown for polymers 1 and 2 (Figure 2). Polymer 1 shows again an isosbestic point for the first irradiation cycles that disappears after prolonged irradiation. Similar patterns in regards to the occurrence of an isosbestic point in the absorption spectra were obtained for the polymers 3 and 4 as well. However, only photobleaching was observed for 2, which bears methyl substituents instead of the methoxy groups at the terminal benzene rings, Figure 2. Although the difference between electron donating properties of the methyl and the methoxy group is significant, we do not believe that this alone results in such a significant change in reaction mechanism. Thus the molecular packing of the film should be more important and the data suggests it has the strongest influence in the case of polymer 2. Therefore, the packing of the polymer chains in the film determines whether or not *trans-cis*-photoisomerization can compete with [2+2] photocycloaddition. The better the packing, the higher the efficiency for photocycloaddition. The latter dominates in the case of 2 if it is irradiated as a spin-coated film. Again, the [2+2] photocycloaddition is the main source for the formation of crosslinked products particular for all fluorine containing copolymers investigated.

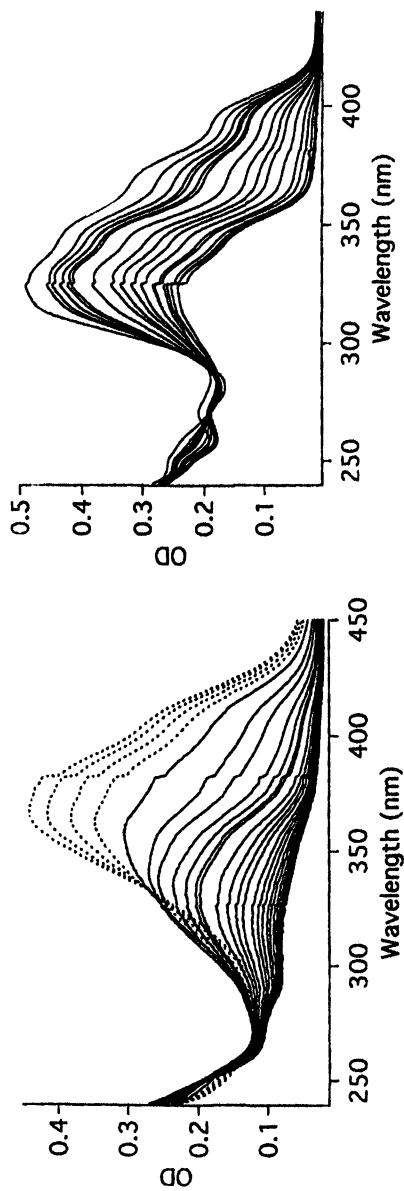


Figure 2. Absorption spectra of the films obtained after several irradiation cycles for the polymers **1** (left) and **2** (right) at 365 nm, $P=1.5 \text{ mW/cm}^2$

The data obtained from the spectra in Figure 2 were used to construct the extinction differences (ED) diagrams¹³, Figure 3. One can extract from the ED-diagram for polymer 1 that two main photoprocesses with distinct reaction rates occur. We assign the first reaction to photoisomerization and the latter to photobleaching. Polymers 3 and 4 show similar behavior as compared to 1. The dichroism D , which was measured in parallel for each irradiation cycle, indicates that no significant increase of this quantity can be observed for the period where photoisomerization dominates. However, an increase of dichroism can be seen for the part of irradiation where photocycloaddition dominates. This result stands in contrast to what is observed with azobenzenes and poly(vinyl cinnamates)^{1a}. In the case of these materials only *trans-cis* photoisomerization contributes for the increase of dichroism. Our results indicate that [2+2] photocycloaddition is responsible for an increase in the dichroism of the material irradiated with linearly polarized light. Therefore, *trans-cis* photoisomerization is of minor importance for an increase of dichroism in our compounds after irradiation with linearly polarized light. We can prove this by the fact that polymer 2 shows a clear increase of D after several irradiation cycles. Polymer 2 does not isomerize in a spin-coated film.

AFM of polymers 1, 2 and 3 indicates a significant change of surface morphology after irradiation with linearly polarized light. A nanostructural pattern with microgrooves is formed for all fluorine containing polymers 1-3. One quantity describing the change of surface morphology is the surface roughness ($\text{RMS}_{10\mu\text{m}}$). This significantly increases with irradiation with linearly polarized light for all fluorine containing polymers, Figure 4 and Table II. No increase of surface roughness was observed for polymer 4, which is without fluorine, after irradiation with linearly polarized light. Its roughness remains approximately constant after irradiation. The increase of $\text{RMS}_{10\mu\text{m}}$, which is related to the formation of microgrooves, can be considered as one crucial point for the alignment of liquid crystals in LC-cells, where our films can function as a photoalignment layer.

Table II. Surface roughness ($\text{RMS}_{10\mu\text{m}}$) of the copolymers (spin-coated film) before and after irradiation with linearly polarized light

<i>Polymer</i>	1	2	3	4
film thickness (nm)	50	140	<50	60
$\text{RMS}_{10\mu\text{m}}$ (without irradiation)	6	3.5	3	2.5
$\text{RMS}_{10\mu\text{m}}$ (irradiated film)	11	18	5	1.5

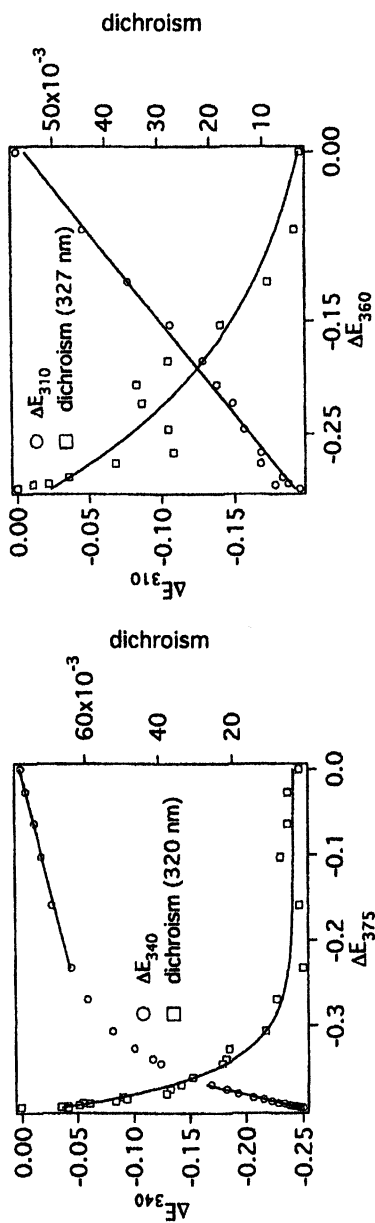
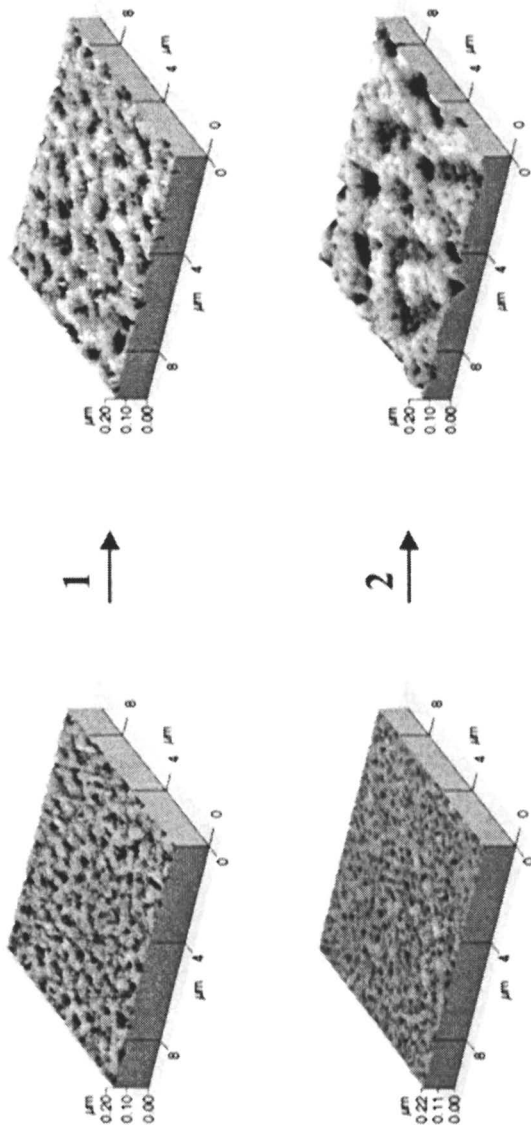


Figure 3. ED-diagrams ($\Delta E_{340}=E_{365}-E_{340}$ and $\Delta E_{375}=E_{365}-E_{375}$) for **1** (left) and **2** (right) obtained by analysis the corresponding spectra from Figure 2



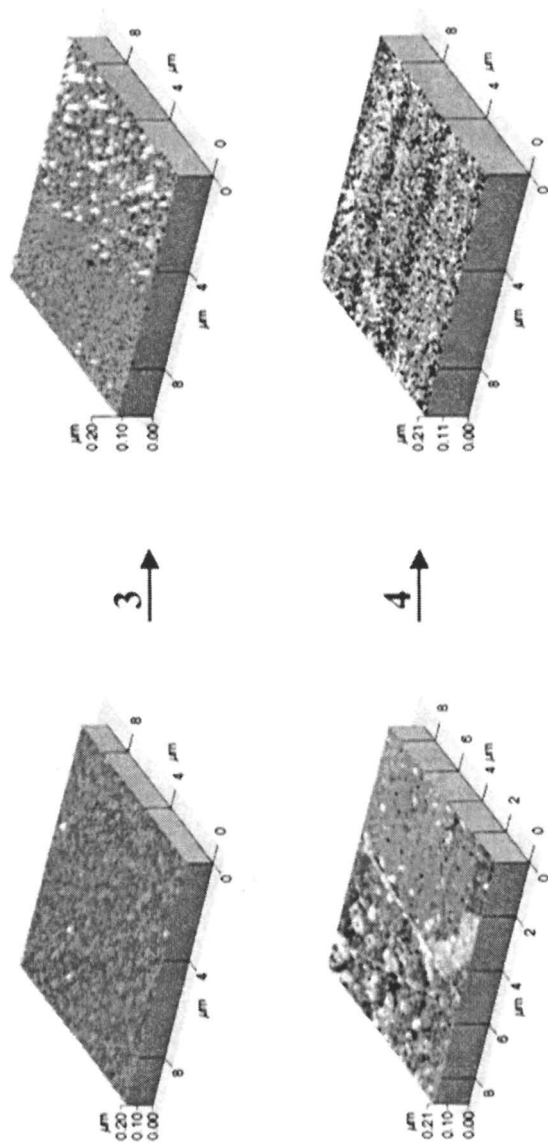


Figure 4. AFM of the Polymers 1-4 without irradiation (left) and after irradiation (right) with linearly polarized light ($\lambda_{irr} = 365\text{ nm}$)

In order to manufacture a LC cell with photoalignment layers, films of the polymers 1-4 were irradiated with linearly polarized light. In this procedure, a quartz plate, which was spin-coated with the corresponding polymer, was irradiated with linearly polarized light. The polarizer position was 0° . After completing the irradiation, the procedure was repeated with a second plate and then both irradiated plates were connected by a spacer and filled with the liquid crystal. The device obtained was tempered at 120°C for about 1/2 h and finally cooled to room temperature. A second device was produced by the same procedure except the polarizer position was switched from 0 to 90° . The ability of the photoalignment layer to align the liquid crystal was analyzed by polarized FTIR-spectroscopy using the CN-stretching vibration as a function of the rotation angle. FTIR-measurements show a maximum at 0° for the sample irradiated with 0° polarizer position during irradiation with linearly polarized light, Figure 5. In other words, the liquid crystal is aligned in the direction of the polarization plane of the linearly polarized light. The validity of this result is proven by a second device made by using a 90° polarizer position for irradiation. We found that with this device both the orientation of the liquid crystal and the polarization plane of the linearly polarized light have the same orientation, Figure 5. It has previously been reported that *trans-cis* photoisomerization results in a perpendicular alignment of the liquid crystal with respect to the orientation vector of the linearly polarized light. However, our results indicate the opposite behavior. Therefore, *trans-cis* photoisomerization must be of minor importance and does not therefore contribute to the alignment of the liquid crystal when our materials were used as photoalignment layers. Furthermore, no isomerization is necessary for the alignment procedure. This is confirmed by polymer 2, which shows no *trans-cis* photoisomerization. Polymer 2 possesses the best capacity for the alignment of the liquid crystal.

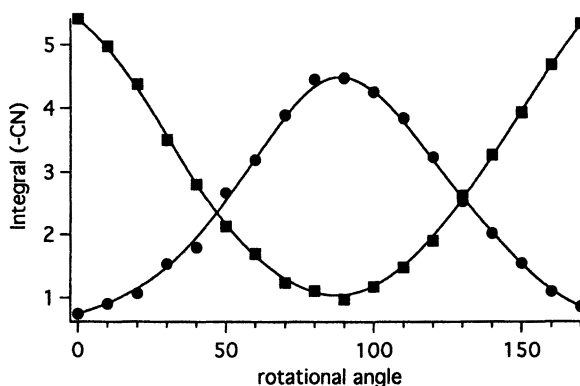


Figure 5. Orientation of the liquid crystal ZLI 2293 on photoalignment layers made of polymer 2 by irradiation with linearly polarized light using a polarizer position of 0° (●) and 90° (■), respectively

The dichroism of the oriented liquid crystal is considerably higher when compared to that of the photoalignment layer used for its orientation, Table III. Therefore, the photoinduced anisotropy of the film holds a key role in the manufacture of LC cells based on photoalignment layers. Furthermore, we found the largest dichroism for the polymer **2** film. The dichroism of the liquid crystal obtained is comparable with that of a commercial cell made of a rubbed polyimide film, Table III. Moreover, each of the fluorine containing polymers **1**, **2** and **3** results in a significantly higher dichroism for the aligned liquid crystal when compared with polymer **4**, which has no fluorine. A system favored to give [2+2] photocycloaddition (i.e. polymer **2**) possesses the highest capacity to orient the liquid crystal in a manufactured cell. The photoinduced anisotropy of the film formed is stable over a broad temperature region because it is a crosslinked material. However, photoalignment layers based on a material made by a *trans-cis* photoisomerization possess less thermal stability because the photochemically produced *cis*-isomer can thermally revert to the *trans* isomer. The copolymers investigated in this work are, to our knowledge, the first photoalignment layers that have been made according to a photocrosslinking procedure via [2+2] photocycloaddition using light at either 365 or 405 nm for irradiation.

Table III. Dichroism of the polymers D_m and the liquid crystal in the manufactured cell D_{LC} in comparison with the dichroism of the liquid crystal aligned in a commercial cell

<i>material</i>	1	2	3	4	<i>commercial cell</i>
D_m	0.053	0.18	0.06	0.046	
D_{LC}	0.46	0.71	0.61	0.2	0.71

Conclusions

The results shown above should give new impetus to further development of photoalignment layers that could be used to substitute classical rubbed polyimide films in LC devices. Tetrafluoro substitution of the benzene ring in either **1**, **2** or **3** enhances the photoreactivity of the distyrylbenzene chromophore in comparison to cinnamates. Furthermore, [2+2] photocycloaddition is the key reaction for an efficient alignment of liquid crystals oriented by using of main chain photochromic polymers, which were irradiated with linearly polarized light. Further developments of photoalignment layers should focus on a material that can be (1) easily crosslinked according to a [2+2] photocycloaddition, (2) possesses an absorption that favors the use of common mercury illuminators (i.e. 365 or 405 nm) and (3) finally possesses a sufficient solubility in order to spin-coat a high quality film. The latter can be accomplished by combination of a chromophore block and an aliphatic chain, Scheme 1.

Acknowledgement

The authors in Germany gratefully acknowledge MERCK for the liquid crystal mixture ZLI-2293 and the Deutsche Forschungsgemeinschaft for financial support. The work at Bowling Green was supported by the National Science Foundation (DMR-9526755), and the Office of Naval Research (Navy N00014-97-1-0834). Additionally, the authors acknowledge Ms. D. Stabenow, Institute of Physics at the University of Potsdam, for the AFM measurements.

References

- (1) a) Ichimura, K. *Chem. Rev.* **2000**, *100*, 1847. b) Kawanishi, Y.; Tamaki, T.; Ichimura, K. *ACS Symp. Ser.* **1994**, *537*, 453.
- (2) Stöhr, J.; Samant, M. G.; Cossy-Favre, A.; Diaz, J.; Momoi, Y.; Odahara, S.; Nagata, T. *Macromolecules* **1998**, *31*, 1942.
- (3) Körner, H.; Shiota, A.; Bunning, T. J.; Ober, C. K. *Science* **1996**, *272*, 252.
- (4) Hoyle, C. E.; Watanabe, T.; Whitehead, J. B. *Macromolecules* **1994**, *27*, 6581. b) Barclay, G. G.; McNamee, S. G.; Ober, C. K.; Papatomas, K. I.; Wang, D. W. *J. Polym. Sci. Polym. Chem. Ed.* **1992**, *30*, 1845.
- (5) Wegner, G. in *Methoden der organischen Chemie (Houben Weyl): Photochemie*; Thieme Verlag: Stuttgart, 1975; Vol. 6, p 1499.
- (6) Coates, G. W.; Dunn, A. R.; Henling, M. L.; Ziller, J. W.; Lobkovsky, E. B.; Grubbs, R. H. *J. Am. Chem. Soc.* **1998**, *120*, 3641.
- (7) a) Strehmel, B.; Sarker, A. M.; Malpert, J. H.; Strehmel, V.; Seifert, H.; Neckers, D. C. *J. Am. Chem. Soc.* **1999**, *121*, 1226. b) Strehmel, B.; Sarker, A. M.; Malpert, J. H.; Neckers, D. C. *Macromolecules* **1999**, *32*, 7476. c) Strehmel, B.; Henbest, K. B.; Sarker, A. M.; Malpert, J. H.; Chen, D. Y.; Rodgers, M. A. J.; Neckers, D. C. *J. Nanosc. Nanotechn.* **2001**, *1*, 107.
- (8) a) Sarker, A. M.; Strehmel, B.; Neckers, D. C. *Macromolecules* **1999**, *32*, 7409. b) Yang, Z.; Sokolik, I.; Karasz, F. E. *Macromolecules* **1993**, *26*, 1188.
- (9) Utterodt, A. PhD Thesis; Martin-Luther University Halle-Wittenberg: Halle, 1999.
- (10) Cox, A.; Kemp, T. J.; Rayne, D. R.; Pinot de Moira, P. In *RPS Unconventional Photographic Systems*; Oxford, 1977.
- (11) a) Bush, T. E.; Scott, G. W. *J. Phys. Chem.* **1981**, *85*, 144. b) Erckel, R.; Fruehbeis, H. *Z. Naturforsch., B: Anorg. Chem., Org. Chem.* **1982**, *37B*, 1472. c) Oelkrug, D.; Rempfer, K.; Prass, E.; Meier, H. *Z. Naturforsch., A: Phys. Sci.* **1988**, *43*, 583.
- (12) Kaafarani, B. R.; Pinkerton, A. A.; Neckers, D. C. *Tetrahedron Lett.* **2001**, *42*, 8137.
- (13) Mauser, H.; Gauglitz, G. *Photokinetics: Theoretical Fundamentals and Applications*; Elsevier: Amsterdam, 1998; Vol. 36.

Chapter 41

UV-Curing of Fluorinated Systems: Synthesis and Properties

Roberta Bongiovanni, Giulio Malucelli, and Aldo Priola

Dipartimento di Scienza dei Materiali ed Ingegneria Chimica, Politecnico di Torino, C.so Duca degli Abruzzi 24, 10129 Torino, Italy

The study concerns the UV-curing of systems containing fluorinated products. New difunctional and monofunctional acrylic and methacrylic monomers bearing either a perfluoroalkyl chain or a perfluoropolyether structure were synthesized. The properties of the films obtained were investigated. By copolymerizing a small amount of the fluorinated acrylates with acrylic resins, while the bulk properties of the films were not changed, the surface properties were deeply modified and became highly hydrophobic. This behaviour was due to a selective enrichment of the fluorinated monomer at the film surface. The dependence of the surface properties on the monomer structure, on its concentration and on the type of substrate was studied.

Introduction

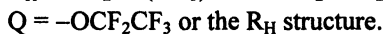
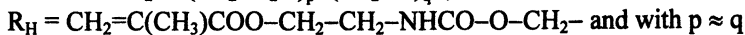
Perfluorinated polymers show outstanding properties such as low surface tension, chemical inertness, thermal stability, together with a peculiar frictional, optical and electrical behavior (1-3). As the copolymerization of fluorinated with hydrogenated monomers improves the processability and reduces the cost of the products, several researches have focused on new fluorinated copolymers (4-8). Recently some authors showed that a small amount of the perfluoroalkylethylmethacrylate monomer introduced in the chain is enough to lower the surface tension (7). Others obtained good results from a series of methacrylates with oligohexafluoropropeneoxide side groups having different length (6).

Due to the outstanding properties of fluorine derivatives described briefly above, the use of fluorinated monomers in UV-curable systems seemed very promising topic to obtain films having particular characteristics (9), through a simple and fast polymerization technique (10,11). In this context we obtained interesting results curing new difunctional and monofunctional acrylic and methacrylic monomers bearing either a perfluoroalkyl chain or a perfluoropolyether structure (12-14). These products, when used as comonomers with hydrogenated acrylic systems, preferentially concentrate in the outermost layers of the films and strongly improve their hydrophobicity even when the amount of the fluorinated comonomer is very low (< 0.5% w/w). Pursuing this work we are performing a systematic investigation on fluorine-containing systems in order to get relationships between the structure of the fluorinated comonomer and the properties of the UV-cured films. In this paper we present the latest developments in this field and compare the behavior of different types of reactive comonomers in the modification of the surface properties of the cured films.

Materials and methods

Fluorinated monomers

Two types of fluorinated derivatives have been investigated. Type A products are perfluoropolyether urethane methacrylates (PFEUMA) which can be mono or bifunctional. Their general structure is R_H -PFPE-Q where



The synthesis of bifunctional monomers is reported elsewhere (15). The monofunctional derivative was synthesized through a series of complex reactions, which gave rise to a mixture of alcohol, diol, and non-functionalized molecules (16). The mixture was subjected to a chromatographic separation, obtaining a middle fraction having OH functionality equal to 1.02, as reported in Ref.17. The fluorinated alcohol was reacted with isocyanatoethyl methacrylate (EIM). The full characterization of the final product is reported in (18).

Type B monomers are perfluorinated acrylates having general structure $R_f - R - \text{OCO} - \text{CH} = \text{CH}_2$ where

R = spacer group, i.e. $-(\text{CH}_2)_2-$ (Et), $-(\text{CH}_2)_3-$ (Pr) or $-(\text{CH}_2)_{11}-$ (Un);

$R_f = -\text{C}_n\text{F}_{2n+1}$

The $\text{C}_n\text{F}_{2n+1}\text{Et}$ derivatives were investigated previously (12). The synthesis and characterisation of $\text{C}_8\text{F}_{17}\text{Pr}$ and $\text{C}_8\text{F}_{17}\text{Un}$ is in ref.19.

Other materials

The fluorinated monomers were UV-cured either as pure products or in mixture with a typical UV-curable resin (Bisphenol-A-dihydroxyethylether diacrylate, BHEDA, kindly supplied by UCB Belgium), in the presence of 2-hydroxy-2-methyl-1-phenylpropan-1-one (Darocure 1173, from Ciba Geigy) as photoinitiator.

Curing reaction

The films were obtained by coating the photopolymerizable mixtures on glass. First, solutions of the monomers of accurate concentration were prepared. Accurate volumes of them were added to BHEDA together with the photoinitiator (4 % w/w): this procedure permitted the control of the final concentration of the fluorinated comonomer and insured a better homogeneity of the mixtures after a careful stirring. The mixtures were spread on a glass slide with a calibrated wire-wound applicator to obtain a thickness of about 100 μm . The solvent was left to evaporate in air. Then, the curing reaction was performed under a N_2 atmosphere (O_2 content < 20 ppm) by UV irradiation with a 500 W medium pressure Hg lamp (light intensity = 12 mW/cm² on the film surface), equipped with a water jacket for IR radiation screening and a camera shutter to control the UV exposure time. The overall time of exposure to the UV light was 45 s, alternating 15 s of irradiation and 15 s of dark. The irradiation was

monitored by FTIR measurements and a constant double bond conversion was found at the end of the curing reaction. The films were peeled away from the substrate and the surface in contact with the substrate was labeled as the glass side, the other one as the air side.

Films characterization methods

The film thickness was measured using a Minitest 3000 Instr. (Elektrophysik Koln, Germany). The double-bond conversion was determined by Fourier Transform Infra-Red spectroscopy (FTIR) by measuring the change of the area of the absorption band at 1640 cm^{-1} . The FTIR measurements were performed by using a ATI Mattson Genesis spectrometer, computer controlled. The gel content was determined by measuring the weight decrease after 24 hour-treatment at room temperature with chloroform.

The amount of the unreacted monomer in the cured films was evaluated by gel permeation chromatography (GPC) after extraction with hot THF. GPC analyses were performed on a Varian 5020 Instruments, in THF solutions at 25°C with a series of Styragel columns (Polymer Laboratories) and a Hewlett-Packard UV-detector. Polystyrene was used as standard.

DSC analyses were performed by means of a Mettler DSC 20 instrument (Initial $T = -50^\circ\text{C}$, final $T = 150^\circ\text{C}$, heating rate $10^\circ\text{C}/\text{sec}$).

Contact angle measurements were performed with a Kruss DSA10 instrument, equipped with a camera and an image processing system. The measurements were made at room temperature (20°C). At least 6 measurements were performed on every sample; the difference from the average value was no more than 2° for the advancing angle, 4° for the receding angle. The measuring liquid was doubly distilled water whose surface tension at 20°C was $72.1\text{ mN}/\text{m}$.

XPS measurements were carried out on the films containing 0.8% w/w of the fluorinated additives by a VG Instrument electron spectrometer using a $\text{Mg K}_{\alpha,1,2}$ X-ray source (1253.6 eV). The X-ray source in the standard conditions had been working at 100 W , 10 KV and 10 mA . The base pressure of the instrument was 5×10^{-10} Torr and an operating pressure of 2×10^{-8} Torr typically. A pass energy of 100 eV and 50 eV was used for widescans and narrowscans respectively. The take-off angle of the electrons was 90° with respect to the surface of the sample. Depth profile informations were obtained running measurements on electrons taking-off from sample surface with angles of 45° and 25° . All data analysis (linear background subtraction and peak integration) were accomplished using a VGX900x (version 6) software. Binding energies were referenced to the C-H level at 285.0 eV .

Results and discussion

Characterization of PFEUMA-BHEDA UV-cured mixtures

The UV-cured coatings obtained from the monofunctional PFEUMA-BHEDA mixtures were homogeneous and transparent when a maximum amount of 1.2% w/w of the fluorinated monomer was present. For higher amounts of PFEUMA, the films became hazy and then opaque.

As far as the bulk properties are concerned, due to its low concentration, the perfluoropolyether monomer did not change the double bond conversion of the BHEDA resin, which was almost quantitative under the adopted irradiation conditions. Moreover the gel percentage of the UV cured mixtures was higher than 96% in all the cases. To check the effective copolymerisation of the fluorinated additive, selective extractions were performed: the amount of the extracted monomer, determined after pre-concentration, was always found negligible (around 1/100 of the original content in the mixture).

The Tg values of the films, assessed by DSC and DMTA analyses (60°C and 70°C respectively), were the same as the pure BHEDA resin.

On the contrary, the surface properties of the films were deeply modified in the presence of the fluorinated comonomer. In Figure 1 the wettability of the UV-cured films as a function of the PFEUMA comonomer content is reported: it is clear that the films gain a high hydrophobicity only on their air side (i.e. the side in contact with air), while on the glass side (i.e. the side in contact with the substrate), the measured value (66°) is independent of the type of formulation. Moreover the asymptotic value of the curve (116°) is reached at a very low concentration of the fluorinated monomer (0.7% w/w).

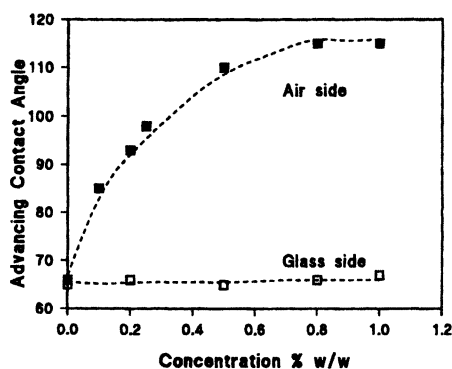


Figure 1. Contact angle vs. concentration of PFEUMA for UV-cured BHEDA-PFEUMA films (Data from reference 18)

The fluorine concentration determined through XPS analysis on the air side of the films is very different from the calculated one (two order of magnitude) and confirms the migration of the fluorinated chains on the outermost layers of the films, as reported in Table I.

When the t.o.a. is 10° , i.e. the thickness of the investigated layer is minimal (very surface), the fluorine concentration is higher than before and even higher than the value calculated for the PFEUMA monomer itself (i.e. the fluorinated chain alone). Therefore, the surface of the copolymeric network can be considered as though it were mainly composed of the fluorinated monomer.

Table I: XPS data for the fluorinated film of a typical BHEDA-mono PFEUMA copolymer (0.8% PFEUMA w/w)

	F_{1s}/C_{1s}
<i>Calculated value of the copolymer</i>	0.012
<i>Calculated value of the PFEUMA monomer</i>	1.43
<i>Experimental value at t.o.a. = 45°</i>	1.11
<i>Experimental value at t.o.a. = 10°</i>	1.70

Data are from reference 13.

In the case of bifunctional PFEUMA oligomers (Figure 2) the same migration phenomenon occurs.

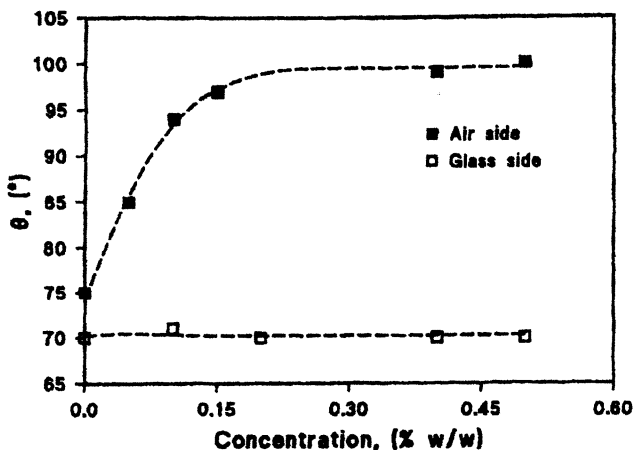


Figure 2. Contact angle vs. concentration for a bifunctional PFEUMA monomer (Data from reference 14)

However, at the same concentration, the enrichment in fluorine on the air side of the film is lower with respect to the monofunctional monomer, giving rise to lower contact angle values. Therefore, the monofunctional monomer, whose fluorinated chain is free to move outside the surface, allows to reach higher contact angle values (about 116°), which are typical of fully fluorinated surfaces.

Films containing the PFEUMA monomers were prepared on a polyethylene substrate. Comparing the contact angle values of films coating either glass or polyethylene slides, as reported in Table II, a different wettability is found. It is evident that the character of the substrate effects the surface properties of the copolymers and their surface compositions (the XPS measurements were discussed in a previous paper) (14). In fact, when the substrate is polar there is a selective migration of the fluorinated molecules towards the apolar phase (which is air). On the contrary, when the substrate is apolar such as polyethylene, the surface enrichment can concern both sides of the film. As a consequence, the substrate side becomes hydrophobic.

The PFEUMA systems, both mono and bifunctional, when cured as pure products, frequently show a biphasic structure as revealed by DSC and DMTA analyses. A typical DMTA spectrum is reported in Figure 3, where two maxima of the $\tan \delta$ curve are recognizable at -90°C and $+70^\circ\text{C}$.

The first transition is very close to the one revealed in the DSC thermogram of the diol from which the methacrylate was obtained by esterification: it clearly corresponds to the glass transition temperature of a soft fluorinated moiety.

The transition at higher temperature concerns the hard hydrogenated part of the network.

Although the fluorinated structure has a refractive index very different from that of the hydrogenated one, i.e. 1.31 and 1.50 respectively, the biphasic nature of the films does not modify the light transmittance of the coatings, which are perfectly transparent.

Table II: Dependence of the wettability of the cured films on the type of coated substrate (additive = bifunctional PFPE monomer)

% w/w	0	0.05	0.1	0.2	0.5
<i>Film coated on glass</i>					
<i>Air side</i>	75	85	93	99	101
<i>Glass side</i>	70	68	69	70	70
<i>Film coated on polyethylene</i>					
<i>Air side</i>	75	103	103	103	104
<i>PE side</i>	70	61	65	69	86

Some data are from reference 14.

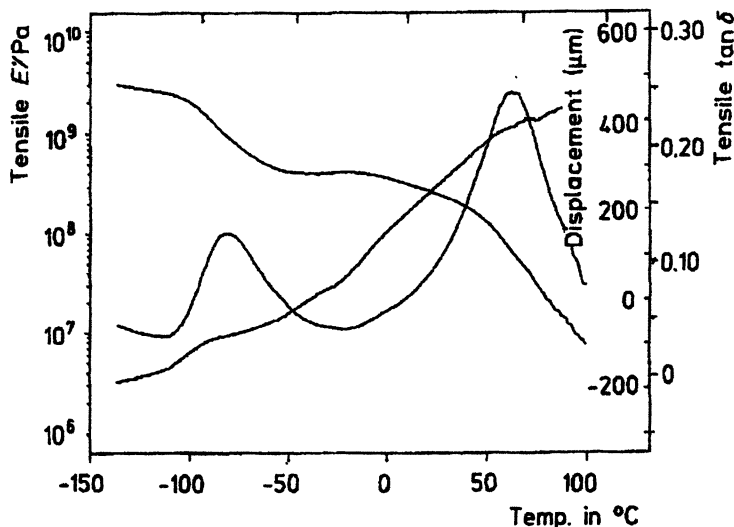


Figure 3. DMTA spectrum of a cured film based on a bifunctional PFPE monomer (Reproduced with permission from reference 15 Copyright 1997 Wiley)

The transparency must be attributed to the small dimensions of the domains: therefore we can conclude that nanophases are dispersed into the system. TEM analyses (Figure 4) confirm the inhomogeneous structure of the cured networks, evidencing clusters (20 - 200 nm) dispersed in the matrix and connected with each other, forming a sort of spider's web (20).

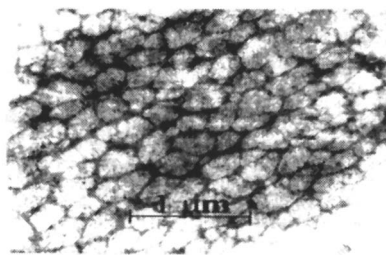


Figure 4. TEM micrograph of a UV-cured bifunctional PFEUMA film

Characterization of fluoroacrylates-BHEDA UV-cured mixtures.

The UV-cured films obtained from BHEDA and $\text{CH}_2=\text{CHCOO-R-R}_f$ mixtures were homogeneous and transparent when a maximum amount of 0.8% w/w of the fluorinated monomer was present; for higher amounts of fluorinated monomer they became hazy and then opaque. As for Type A monomers, the bulk

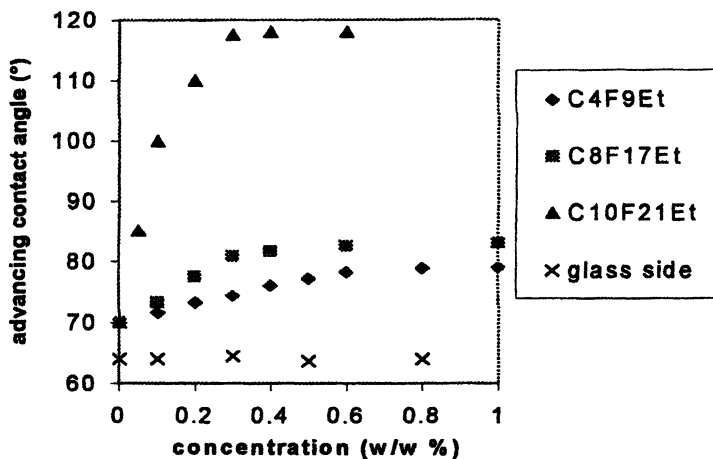


Figure 5. Advancing contact angles of UV-cured films (air side) containing fluoromonomers with different fluorine content (Data from reference 12)

properties of these mixtures were unchanged with respect to those of pure BHEDA resin. On the contrary, the presence of the fluorinated monomer changed the wettability of the air side of the UV-cured films, while the glass side maintained the same wettability of the pure BHEDA resin. In Figure 5 the advancing contact angle values, measured on the air side of UV-cured films containing fluoroacrylates having a different length of the fluorinated chain are plotted as a function of the concentration of the fluorinated additive.

The contact angle measured on the air side clearly depends on the fluorinated monomer concentration. The behavior of C4F9Et, C8F17Et and C10F21Et is asymptotic and shows a plateau value which is reached at a concentration called the critical value. Comparing the three plots, one sees that the longer the fluorinated chain, i.e. the higher the fluorine content, the lower the critical value. The same dependence links the plateau value to the type of monomer employed. The highest contact angle, which is around 120° and is typical of a complete hydrophobic surface such as PTFE, is obtained with C10F21Et.

If one compares comonomers having the same fluorinated chain, a clear effect of the spacing group R becomes evident. In Figure 6 it is shown that the amount of comonomer able to make the surface hydrophobic is extremely low for C8F17Un: interestingly at around 0.1 % w/w, the contact angle is higher than 90°. For the perfluorooctylacrylate with the lowest M.W., i.e. C₈F₁₇Et, the solubility limit is reached without obtaining the same effect. The lowest concentration for overcoming the hydrophobicity threshold, i.e. the critical value of the monomer concentration, decreases by increasing the M.W. of the perfluorooctylacrylates. At the same time, the longer the spacer, the higher the advancing contact angle.

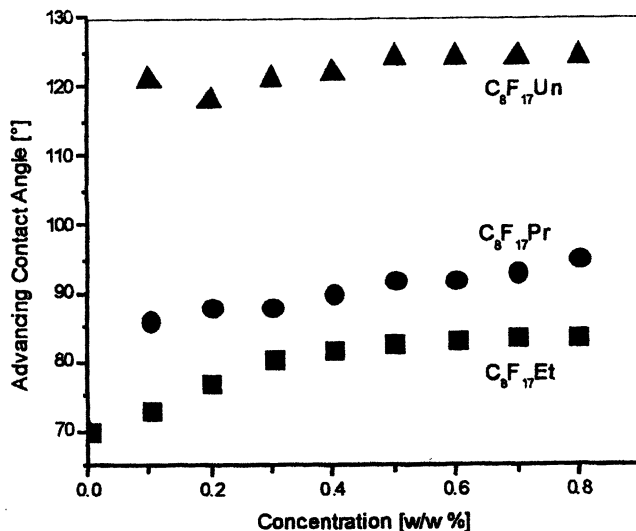


Figure 6 Advancing contact angles measured on the air side of UV-cured films containing fluoro-octyl monomers with different spacer length (Data from reference 19)

These results are in agreement with those of Pospiech and coworkers (21), who showed that semifluorinated alkyl groups linked as side chains to polyester backbone can self-organize at the polymer surface when a critical M.W. is reached.

In Table II the XPS data related to the BHEDA-fluoroacrylated UV-cured films are collected: they indicate that at the air side of the films, the fluorine is in large excess with respect to its bulk concentration (the theoretical F_{1s}/C_{1s} ratio on the basis of the bulk composition is 0.0043 ± 0.0003 for all the systems). On the contrary, the glass sides of the films always showed a negligible or undetectable fluorine concentration. The data of Table II obtained at different t.o.a. evidence the existence of a fluorine concentration gradient, from the inner (higher t.o.a.) to the very external surface (according with the equation $d = 3\lambda \sin\theta$, sample depths are lower when the t.o.a. is smaller). Therefore, it is clear that the fluorinated comonomers selectively migrate towards the air side of the films. Finally, the surface composition depends on the length of the fluorinate chain. Moreover, a key factor is the spacer group of the additive used. Considering the F_{1s}/C_{1s} ratios obtained for t.o.a. of 25° (indicative of the mean composition of the outer layers) it is evident that, being the same the fluorine content of the monomer, the longer the alkyl spacer, the higher the fluorine concentration at the surface.

Table II. XPS results at different take-off angles (concentration of the fluorinated comonomer = 0.8% w/w)*

Fluorinated Comonomer	Air surface F_{1s}/C_{1s}		
	t.o.a = 90°	t.o.a = 45°	t.o.a = 25°
C_4F_9Et	0.01	-	0.02
$C_{10}F_{21}Et$	0.54	-	1.01
$C_8F_{17}Et$	0.13	0.17	0.18
$C_8F_{17}Pr$	0.13	0.19	0.31
$C_8F_{17}Un$	0.56	0.68	1.05

*Some data from reference 19

Conclusions

Acrylic and methacrylic fluorinated monomers can be UV-cured in the bulk, giving rise to films with a biphasic structure where the domains are at a nanometric level. The use of these monomers in UV-curable formulations allows obtaining interesting modifications as far as the surface properties are concerned.

The film surface can be modified deeply also in the presence of very low amounts of the fluorinated monomers.

Selective enrichment of the fluorinated monomers at the film surface can be obtained as confirmed by XPS analysis depending on the monomer structure and its concentration. The key factors are the length of the fluorinated chain and the length of the spacer group present in the monomer. Thus highly hydrophobic surfaces containing practically pure fluorinated monomer can be obtained by using mixtures with very low amounts of additive.

Acknowledgements

The authors would like to thank Dr. B.Ameduri (CNRS, Montpellier) for the synthesis of some fluoroacrylates and Dr. C.Tonelli (Ausimont, Milano) for the synthesis of PFEUMA. Prof. A. Pollicino is acknowledged for the XPS analyses. UCB, Atochem, and Ciba Specialties are acknowledged for supplying monomers and photoinitiators.

References

1. Feiring A. Fluoroplastics in Organofluorine Chemistry: Principles and Commercial Applications Banks R.E, Smart B.E., tatlow J.C. Eds. Plenum Publishing, New York, 1994, chapter 15;
2. Hung M.H. in Fluoropolymers 1: Synthesis Hougham G., Johns K., Cassidy P.E., Davidson T. Eds. Plenum Publishing, New York, 1999, chapter 4;
3. Thomas R. in Fluoropolymers 2: Properties Hougham G., Johns K., Cassidy P.E., Davidson T. Eds. Plenum Press, New York, 1999, chapter 4
4. Yoon S.C., Sung Y.K., Ratner B.D. *Macromolecules* 1990, **23**, 4351
5. McLain S.J., Sauer, B.B., Firment, L.E. *Macromolecules* 1996, **29**, 8211
6. Thomas R.R., Douglas R.A., Graham W.F., Darmon M.J., Sauer B.B., Stika K.M., Swartzfager D.G., *Macromolecules* 1997, **30**, 2883
7. Morita M., Ogisu H., Kubo M., *J.Appl.Polym.Sci.* 1999, **73** (9), 1741
8. Krupers M., Slagen P., Moller M., *Macromolecules* 1998, **31**, 2552
9. Torsterson M., Ranby B., Hult A. *Macromolecules* 1990, **23**, 126
10. Pappas S.P. (Ed.), *Radiation Curing, Science and Technology*, Plenum Press, New York, 1992
11. Fouassier J.P., Rabek, J.C. (Eds.), *Radiation Curing in Polymer Science and Tecnology*, Vol. 1-4, Elsevier, London, 1993
12. Ameduri B., Bongiovanni R., Malucelli G., Pollicino A., Priola A., *J. Pol. Sci.: Part A: Polymer Chem.*, 1999, **37**, 77
13. Bongiovanni R., Beamson G., Mamo A., Priola A., Recca A., Tonelli C., *Polymer*, 2000, **41**, 409
14. Bongiovanni R., Malucelli G., Pollicino A., Tonelli C., Priola A., *Macromol. Chem. Phys.*, 1998, **199**, 1099
15. Priola A., Bongiovanni R., Malucelli G., Pollicino A., Tonelli C., *Macromol. Chem. Phys.*, 1997, **198**, 1893
16. Tonelli C., Gavezzotti P., Strepparola E.J., *Fluorine Chem.*, 1999, **95**, 51
17. Tonelli C., Turri S., Gianotti G., Levi M., USP 5,262,057 to Ausimont (1993)
18. Bongiovanni R., Lombardi V., Malucelli G., Priola A., Tonelli C., Di Meo A., Fluorine in Coatings IV Brussels March 2001 Proceeding Paper 14
19. Ameduri B., Bongiovanni R., Malucelli G., Priola A., *J. Pol. Sci.: Part A: Polymer Chem.*, 2001, **39**, 4227
20. Bongiovanni R., Malucelli G., Gerard J.F., Nonnis C., Priola A., manuscript in preparation
21. Pospiech D., Jehnichen D., Haubler I., Voigt D., Grundke K., Ober C.K., Korner H., Wang J., *Polymer Prepr. Am.Chem.Soc. Div.polym.Chem.* 1998, **39**(2), 882

Chapter 42

Autohesion of Polyethylene Plates by the Photoinduced Grafting of Methacrylamide

Kazunori Yamada, Shigeki Takeda, and Mitsuo Hirata

Department of Applied Molecular Chemistry, College of Industrial Technology, Nihon University, Narashino, Chiba 275-8575, Japan

In an attempt to provide the low- and high-density polyethylene (LDPE and HDPE) plates with the autohesive and adhesive properties at lower grafted amounts, methacrylamide (MAAm) was photografted onto their surfaces. The surfaces of the LDPE and HDPE plates were made highly hydrophilic by the photografting of MAAm, and their wettabilities leveled off when the substrate surfaces were wholly covered with grafted PMAAm chains. The water-absorptivities of the grafted layers formed on the substrate surfaces increased with an increase in the grafted amount. The enhancement in the hydrophilicities of the LDPE and HDPE plates by the photografting of MAAm led to the development of autohesion strength as well as adhesion strength. The substrate breaking occurred at lower grafted amounts for the MAAm-grafted plates than for the plates photografted with methacrylic acid (MAA), acrylic acid (AA), and 2-(dimethylamino)ethyl methacrylate (DMAEMA).

For most of the dielectric polymers such as polyolefins, the characteristic low surface energy and the resulting poor adhesion between polymer materials or to other materials have created numerous technical challenges, while they exhibit a wide range of outstanding properties including excellent chemical resistance and low water adsorption. Therefore, the physical and chemical inertness of the polyolefins have accelerated the use of various methods for achieving the required surface modification [1, 2]. For the last two decades, a number of techniques have been devoted directly to the surface modification of polyolefins for adhesion improvement. They have reported the surface modification of polyolefins through plasma treatment, plasma polymerization, UV irradiation, grafting with the use of glow discharge, corona discharge, and irradiation with UV or Co⁶⁰ radiation [3-7]. Among these techniques, the plasma treatment and UV irradiation are of increasing importance. However, a main drawback is that the physicochemical characteristics of the modified polymer surfaces, including surface compositions, are time-dependent. Chain and polar group reorientation in the surface region can result in gradual deterioration of the surface reactivity and wettability [8]. On the other hand, photografting, due to its low cost and ease of continuous processing, is also one of the more favored techniques to overcome the time-dependent surface characteristics. Since the radicals formed during UV-irradiation are restricted to the surface of the used polymer substrate, the location of grafting is limited to the surface regions. The key advantage of this technique is, moreover, that the substrate surfaces subjected to surface modification can possess different properties through the choice of different monomers, leaving the bulk properties of the polymer substrate intact [9].

We have investigated the surface modification of PE and poly(tetrafluoroethylene) (PTFE) plates by the photografting technique [10-12]. The surface properties such as wettability and adhesivity of low-density PE (LDPE) plates were considerably improved by the photograftings of hydrophilic monomers. In addition, the grafted polymer chains would have high mobility in the water-swollen state because the grafted layers consisting of grafted polymer chains formed on the substrate surfaces possess high water-absorptivity [11, 12].

Pioneering studies on autohesion referred to self-adhesion or adhesive-free adhesion were widely carried out by Voyutskii and his co-workers [13, 14]. They concluded that autohesion was caused by self-diffusion of polymer segments from one into another layer across the interface. The migrated polymer segments entangle with other ones, thus enhancing fracture resistance. Therefore, grafted polymer chains in the water-swollen grafted layers can be entangled through their self-diffusion, when the two grafted plates are brought close contact by heat pressing. In our previous studies, autohesion strength was markedly enhanced without any adhesives by swelling the PE plates photografted with methacrylic acid (MAA), acrylic acid (AA), and 2-(dimethylamino)ethyl methacrylate (DMAEMA) in water, and then heat-pressing at 80 °C under a constant load of 2.0 kg/cm² [15, 16].

We follow up the surface modification of the LDPE and HDPE plates and the enhancement of adhesion and autohesion strength at lower grafted amounts by the photografting of methacrylamide (MAAm). Moreover, the increased adhesion and autohesion properties are discussed from the surface compositions determined by ESCA, wettability, and water-absorptivity.

Experimental Section

Photografting: The LDPE and HDPE plates were used as a polymer substrate for the photografting (Table 1). These polymer plates of 6 cm length and 3 cm width were washed with methanol and acetone, and then dried under reduced pressure. MAAm was recrystallized from benzene at 80 °C. The LDPE and HDPE plates coated with benzophenone (BP) as a photo-sensitizer were immersed in an aqueous MAAm solution at 1.0 M. The photografting was carried out at 60 °C by applying UV-rays emitted from a 400 W high-pressure mercury lamp to the aqueous MAAm solutions in which the BP-coated LDPE and HDPE plates were immersed with a Pyrex glass tube [10, 11, 17]. After photografting, the grafted amount was calculated in $\mu\text{mol}/\text{cm}^2$ from the weight increase in the LDPE and HDPE plates.

Surface compositions and hydrophilic properties: The photoelectron spectra for MAAm-grafted plates were recorded on a Shimadzu ESCA 750 type spectrometer with $\text{MgK}\alpha$ (1253.6 eV) operating at 8kV and 30 mA, and the intensity ratios, O1s/C1s and N1s/C1s, were calculated from the individual peak areas determined. The contact angles for water were estimated with a sessile drop method at 25 °C under an atmosphere of saturated vapor water using a Kyowa Kagaku TYP-QI type goniometer. The amount of absorbed water was measured from the weight increase in the MAAm-grafted plates immersed and equilibrated in distilled water at 25 °C [12]. The n_{water} value defined here as the number of water molecules assigned to a MAAm segment was calculated from the amounts of grafted MAAm and absorbed water [10, 11].

Autohesion and adhesion strength: The-MAAm-grafted plates of the same grafted amount (10×30 mm) immersed in water at 25 °C for 24 h were put together with their grafted surfaces facing each other with a 10 by 10 mm overlap. The overlapped samples were heat-pressed by adding the load of 2.0 kg/cm^2 at 80 °C for 24 hr. For adhesion strength measurements, a commercial two-component type epoxy adhesive, "Araldite", was applied to the surfaces of the MAAm-grafted plates to provide a 10 by 10 mm overlap. The adhesives applied were cured at 60 °C for 24 hr while the load of 0.5 kg/cm^2 was kept on the bonded grafted plates. The tensile shear strength was measured with a strain rate of 3 mm/s at 25 °C [15, 16].

Results and Discussion

Surface properties. The MAAm-grafted plates with different grafted amounts were prepared by varying the UV irradiation time for the preparation of the MAAm-grafted plates. Surface analysis by ESCA and contact angle measurements were carried out to estimate the increased hydrophilicity of the LDPE and HDPE surfaces by the photografting of MAAm and to discuss the correlation between the chemical compositions as an indication of the coverage of the substrate surfaces with grafted PMAAm chains and the surface wettability. Figure 1 shows the changes in the intensity ratios, O1s/C1s and N1s/C1s, and $\cos \theta$ value with the grafted amount for the MAAm-grafted plates. The intensity ratios increased with the grafted amount, and then leveled off for both grafted plates. The constant intensity ratios mean that the chemical compositions of the outer surface regions of the grafted layers remained unchanged after the whole coverage of the LDPE and HDPE surfaces with grafted PMAAm chains. The $\cos \theta$ values increased with an increase in the grafted amount, and then stayed constant around the grafted amounts at which the intensity ratios became constant. These results indicate that the photografting of MAAm leads to the hydrophilization of the LDPE and HDPE surfaces.

The constant intensity ratios and $\cos \theta$ values and the grafted amounts at which they become constant for the MAAm-grafted plates are summarized in Table 2 together with the values for the LDPE and HDPE plates photografted with MAA, AA, and DMAEMA [17]. The constant $\cos \theta$ value for the HDPE-g-PMAAm plates was obtained at lower grafted amount than that for the LDPE-g-PMAAm plates. Although the internal grafting in general occurs concurrently with the surface grafting for the photografting of any hydrophilic monomers onto the polyolefin substrates, the location of the photografting onto the HDPE plates is more restricted to the surface region than that of the LDPE plates due to higher crystallinity of the HDPE plate for the photografting of MAAm. In addition, it is apparent from Table 2 that the MAAm-grafted plates possessed much more hydrophilic surfaces of any other grafted plate prepared in our study because the grafted layers enriched with grafted PMAAm chains were formed.

Water-absorptivity. Figure 2 shows the changes in the amount of absorbed water with the grafted amount for the MAAm-grafted plates. The amount of absorbed water increased with an increase in the grafted amount. The grafted layers formed on the HDPE plates have a little higher water-absorptivity than those formed on the LDPE plates because the location of the photografting of MAAm was restricted the surface regions for the HDPE plates probably due to their high crystallinity. The water-absorptivities of the grafted layers was explicated in terms of the n_{water} values as well as the amount of absorbed water.

Table 1 Determination of the degrees of crystallinity and the ultimate strengths of the LDPE and HDPE plates used in this study.

Substrate	Density (g/cm ³)	Crystallinity (%)	Ultimate strength (kgf/cm ²)
LDPE	0.924	46	14.1
HDPE	0.958	70	24.2

Table 2 Surface compositions and wettabilities of the LDPE and HDPE plates photografted with hydrophilic monomers.

Sample	Grafted amount (mmol/cm ²)	Constant intensity ratio		cos θ
		O1s/C1s	N1s/C1s	
LDPE				-0.120
HDPE				-0.230
PMAAm		0.253	0.153	0.98
PMAA		0.384		0.74
PAA		0.518		0.19
PDMAEMA		0.253	0.142	0.49
LDPE-g-PMAAm	1.2	0.25	0.15	0.95
HDPE-g-PMAAm	0.8	0.2	0.14	0.95
LDPE-g-PMAA	25	0.30		0.45
LDPE-g-PAA	8	0.37		0.50
LDPE-g-PDMAEMA	7	0.22	0.11	0.10
HDPE-g-PMAA	10	0.31		0.40
HDPE-g-PAA	5	0.37		0.25
HDPE-g-PDMAEMA	2	0.24	0.08	0.10

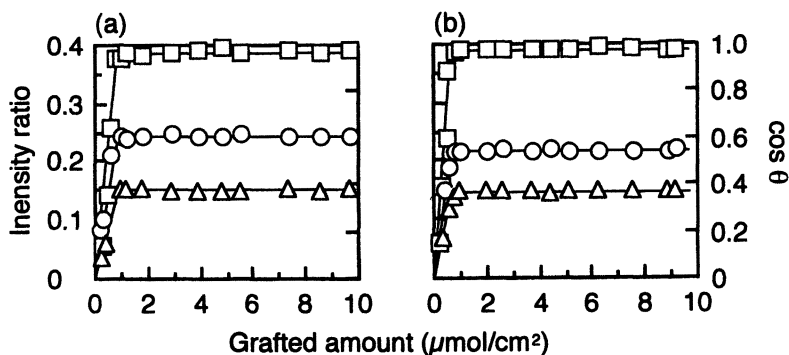


Figure 1 Changes in the intensity ratios, O1s/C1s (\circ) and N1s C1s (\triangle), and $\cos \theta$ value (\square) with the grafted amount for (a) LDPE-g-PMAAm and (b) HDPE-g-PMAAm plates.

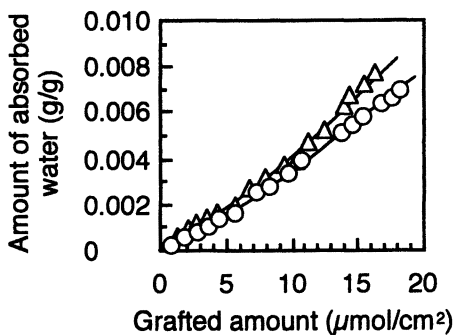


Figure 2 Changes in the amount of absorbed water with the grafted amount for the LDPE-g-PMAAm (\circ) and HDPE-g-PMAAm (\triangle) plates.

Figure 3 shows the changes in the n_{water} value with the grafted amount for the MAAM-grafted plates. The n_{water} values tended to level off around the grafted amounts of 0.8 and 1.2 mmol/cm² for the LDPE-g-PMAAm and HDPE-g-PMAAm plates, respectively. This means, taking into consideration the surface analysis by ESCA, that the thickness for the MAAM-grafted layers continues to increase without a considerable change in the chemical compositions in the range where the n_{water} values stayed constant. However, the n_{water} values for the MAAM-grafted plates were lower than those for other three kinds of grafted plates prepared in our previous papers [16, 18], although the MAAM-grafted plates possessed the most hydrophilic surfaces of them as shown in Table 2. The surface wettability is considered to be influenced by the location of the photografting (the surface and internal graftings), the chemical structure of the used monomers (presence of α -methyl group and the kind of functional groups), and the configuration of grafted polymer chains (the linearity and branching). However, it is difficult to control these factors by our grafting conditions and closely correlate them with the water-absorptivity.

Autohesion strength. The MAAM-grafted plates with water-swollen grafted layers were heat-pressed at 80 °C under a constant load of 2.0 kg/cm² in this study. These experimental conditions were determined on the basis of the experimental results obtained by the measurement of autohesion strength as a function of the temperature and the load on heat-pressing [16, 18]. Figure 4 shows the changes in autohesion strength with the grafted amount for the MAAM-grafted plates. In addition, the grafted amounts at which the substrate breaking occurred are summarized in Table 3.

The substrate was broken above the grafted amounts of 1.5 and 2 $\mu\text{mol}/\text{cm}^2$ for the LDPE-g-PMAAm and HDPE-g-PMAAm plates, respectively. The values of autohesion strength at the substrate breaking were almost equivalent to the ultimate tensile strength of the substrates used (14.1 kgf/cm² for LDPE plate and 24.2 kgf/cm² for HDPE plate). This indicates that the LDPE and HDPE plates can be surface-modified by photografting of MAAM without interfering with the bulk properties. The grafted layers of the MAAM-grafted plates possessed much more hydrophilic surfaces and less water-absorptivities than those of any other grafted plate prepared in our previous study [16]. The increased wettability for the MAAM-grafted plates would lead to an increase in autohesion strength in the range of a low grafted amount. It was also understandable from Tables 2 and 3 that the grafted amounts at the substrate breaking are higher than those at which the substrate surfaces were covered with grafted PMAAm chains in analogy with other three kinds of grafted plates. It can be considered that the autohesion is caused by the intermolecular interactions such as hydrogen bonding between –CONH₂ groups and the entanglement of grafted PMAAm chains. The grafted amounts at the substrate breaking for the MAAM-grafted plates were much lower

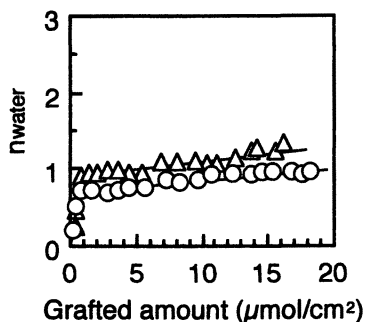


Figure 3 Changes in the n_{water} value with the grafted amount for the LDPE-g-PMAAm (\circ) and HDPE-g-PMAAm (\triangle) plates.

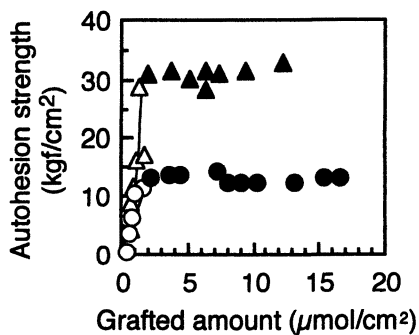


Figure 4 Changes in tensile shear autohesion strength with the grafted amount for the LDPE-g-PMAAm (\circ) and HDPE-g-PMAAm (\triangle) plates heat-pressed at 80 °C under the load of 2.0 kg/cm².

Failure-

(open) : cohesive failure, (shaded) : substrate breaking

than those for the other grafted plates. It can be considered from this result that the increase in adhesion strength is caused rather by the hydrogen-bonding between $-\text{CONH}_2$ groups affixed to the grafted PMAAm chains than by the entanglement of grafted PMAAm chains as the intermolecular interactions. The formation of the grafted layers enriched with grafted PMAAm chains can facilitate the self-diffusion of grafted PMAAm chains across the interfaces of the grafted layers. It is of much great interest that autohesion strength of the LDPE and HDPE plates can be markedly improved by heat-pressing the MAAm-grafted plates with water-swollen grafted layers without any adhesives.

Adhesion strength. Figure 5 shows the adhesion strength for the MAAm-grafted plates using a commercial two-component type epoxy adhesive "Araldite". The grafted amounts at the substrate breaking are also summarized in Table 4. The adhesive properties of the LDPE and HDPE plates were considerably enhanced in the range of lower grafted amounts mainly due to highly improved hydrophilicity by the photografting of MAAm. At higher grafted amounts, the adhesion strength increased beyond the ultimate strength of the original substrates so that the MAAm-grafted plates were broken. It can be understood from Figure 3 and Table 4 that the grafted amounts at which the substrate breakings in autohesion strength occur are 2 to 3 times as high as those in adhesion strength, as expected. In addition to autohesive properties, adhesive properties were also effectively enhanced at lower grafted amounts compared with LDPE and HDPE plates photografted with MAA, AA, and DMAEMA.

Conclusions

We have pursued the enhancement of the autohesive and adhesive properties of the LDPE and HDPE plates by the photografting of MAAm in relation to the wettability and water-absorptivity of the grafted MAAm plates.

The grafted amounts at which the wettabilities become constant almost agree with those at which the surface compositions become constant, and the surfaces of the LDPE and HDPE plates are made highly hydrophilic by the photografting of MAAm. The water-absorptivities of the MAAm-grafted plates increase with an increase in the grafted amount. Both autohesion and adhesion strengths exceed the ultimate strength of the original substrates, and the failure of the MAAm grafted plates occurs at lower grafted amounts than that of the substrate plates photografted with other hydrophilic monomers such as MAA, AA, and DMAEMA.

Literature Cited

1. Kaur, I., Kumar, S.; Chauhan, G. S.; Misra, B. N. *J. Appl. Polym. Sci.* **1999**, *73*, 2959-2969.

Table 3 The grafted amounts at which the substrate breaking occurs on the autohesion strength measurements for the LDPE and HDPE plates photografted with hydrophilic monomers.

Sample	Grafted amount ($\mu\text{mol}/\text{cm}^2$)
LDPE-g-PMAAm	1.5
HDPE-g-PMAAm	2
LDPE-g-PMAA	60
LDPE-g-PAA	20
LDPE-g-PDMAEMA	15
HDPE-g-PMAA	30
HDPE-g-PAA	15
HDPE-g-PDMAEMA	20

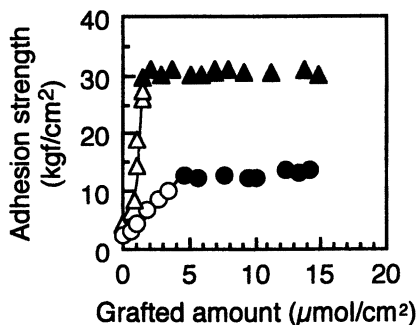


Figure 5 Changes in tensile shear adhesion strength with the grafted amount for the LDPE-g-PMAAm (○) and HDPE-g-PMAAm (△) plates cured at 60 °C under the load of 0.5 kg/cm².

Failure-

(open) : cohesive failure, (shaded) : substrate breaking

Table 4 The grafted amounts at which the substrate breaking occurs on the adhesion strength measurements for the LDPE and HDPE plates photografted with hydrophilic monomers.

Sample	Grafted amount ($\mu\text{mol}/\text{cm}^2$)
LDPE-g-PMAAm	2
HDPE-g-PMAAm	3
HDPE-g-PMAA	12
HDPE-g-PAA	3
HDPE-g-PDMAEMA	10

2. Liu, Y. X.; Kang, E. T.; Neoh, K. G.; Tan, K. L. *J. Polym. Sci. Polym. Chem.* **2000**, *38*, 80-89.
3. Zhang, J.; Kato, K.; Uyama, Y.; Ikada, Y. *J. Polym. Sci. Polym. Chem.* **1995**, *33*, 2629-2638.
4. Dessouki, A. M.; Taher, N. H.; El-Arnaouty, M. B. *Polym. Int.* **1998**, *45*, 67-76.
5. Seto, F.; Muraoka, Y.; Sakamoto, N.; Kishida, A.; Akashi, M. *Angew. Makromol. Chem.* **1999**, *266*, 56-62.
6. Novak, I.; Chodak, I. *Macromol. Symp.* **2001**, *170*, 341-348.
7. Simon, D.; Liesegang, J.; Pigram, P. J.; Brack, N.; Pura, J. L. *Surface Interface Anal.* **2001**, *32*, 148-153.
8. Kang, M. S.; Chun, B.; Kim, S. O. *J. Appl. Polym. Sci.* **2001**, *81*, 1555-1566.
9. Shukla, S. R.; Athalye, A. R. *J. Appl. Polym. Sci.* **1994**, *51*, 1567-1574.
10. Yamada, K.; Kimura, T.; Tsutaya, H.; Hirata, M. *J. Appl. Polym. Sci.* **1992**, *44*, 993-1001.
11. Yamada, K.; Tsutaya, H.; Tatekawa, S.; Hirata, M. *J. Appl. Polym. Sci.* **1992**, *46*, 1065-1085.
12. Yamada, K.; Ebihara, T.; Gondo, T.; Sakasegawa, K.; Hirata, M. *J. Appl. Polym. Sci.* **1996**, *61*, 1899-1912.
13. Voyutskii, S. S.; Zamazii, V. M. *Rubber Chem. Technol.* **1957**, *30*, 544-547.
14. Voyutskii, S. S.; Shtarkh, B. V. *Rubber Chem. Technol.* **1957**, *30*, 548-554.
15. Yamada, K.; Isoda, J.; Ebihara, T.; Hirata, M. In *Interfacial Aspects of Multicomponent Polymer Materials*; Sperling, L. H.; Plenum: New York, 1998; pp173-194.
16. Yamada, K.; Kimura, J.; Hirata, M. *J. Appl. Polym. Sci.* submitted for publication.
17. Yamada, K.; Tatekawa, S.; Hirata, M. *J. Colloid Interface Sci.* **1994**, *164*, 144-150.
18. Yamada, K.; Kimura, J.; Hirata, M. *J. Photopolym. Sci. Technol.* **1998**, *11* 263-270.

Author Index

- Allonas, Xavier, 140
Amster, I. Jonathan, 332
Awan, Shafique Ahmad, 451
Bachemin, M., 52
Baikerikar, Kiran K., 389
Bair, H. E., 317
Belfield, Kevin D., 76, 464
Bongiovanni, Roberta, 499
Boodhoo, Kamelia V. K., 437
Braun, Harald, 213
Cao, H., 152
Carlsson, Ingemar, 65
Cavitt, T. Brian, 27, 41
Chawla, Chander P., 165
Cole, M., 52
Coretsopoulos, Chris N., 389
Coussens, Betty, 127
Crivello, James V., 178, 219, 231,
242, 253, 266
Currie, E., 152
Decker, Christian, 92
Deubzer, B., 202
Dias, Aylvin A., 127
Ding, Wei, 332
Dorschu, Marko, 127
Dunk, William A. E., 437
Dupre, Juliette, 165
El-Maazawi, Mohamed, 15
Falling, Stephen N., 266
Fouassier, Jean-Pierre, 140
Gamble, Gary, 332
Ghoshal, Ramakrishna, 253
Gomurashvili, Zaza, 231
Guymon, C. Allan, 378
Hale, A., 317
Hamid, Haleem, 451
Harden, Adrian, 65
Herzig, Ch., 202
Hirata, Mitsuo, 511
Hoyle, Charles E., 2, 27, 41, 52, 76
Hua, Yujing, 219
Hussain, M. Sakhawat, 451
Jachuck, Roshan J., 437
Jager, Wolter F., 426
Jansen, Johan F. G. A., 127
Jean, Y. C., 152
Jönsson, Sonny, 2, 27, 41, 52, 76
Kalyanaraman, Viswanathan, 27,
41, 52
Kameyama, A., 363
Kato, Hisao, 285
Khan, M. A., 451
Khudyakov, Igor V., 113
Kim, Dongkwan, 15
Krongauz, Vadim V., 165
Kuang, W. F., 2, 52
Kuck, V., 317
Kudo, H., 363
Kutal, Charles, 332
Lalevée, Jacques, 140
Lee, T. Y., 2
Lester, Christopher L., 378
Li, Xinyong, 332
Lindgren, K., 76
Liu, Zhiqiang, 105
Lundmark, Stefan, 65
Malucelli, Giulio, 499
Manea, Ana, 65

- Miller, Chris W., 2
Mörke, W., 202
Müller, U., 202
Nason, C., 2
Neckers, Douglas C., 482
Nguyen, Chau K., 27, 41
Nishikubo, T., 363
Nuyken, Oskar, 213
O'Shaughnessy, Ben, 105
Olsson, R. T., 317
Onen, Aysen, 187
Padon, Kathryn Sirovatka, 15
Phillips, Brian, 41
Priola, Aldo, 499
Purvis, Michael B., 113
Rehnberg, Nicola, 65
Sanderson, Cynthia T., 332
Sangermano, Marco, 242, 266
Sarker, Ananda M., 482
Sasaki, Hiroshi, 285, 296, 306
Schaeffer, Bill, 400
Schafer, Katherine J., 464
Scranton, Alec B., 15, 389
Shier, E., 76
Shim, Sang-Yeon, 277
Shirai, Masamitsu, 351
Sipani, Vishal, 389
Song, Ki Yong, 253
Stiller, Burkhard, 482
Strehmel, Bernd, 482
Strehmel, Veronika, 482
Suh, Dong Hack, 277
Suzuki, Hiroshi, 306
Svensson, Lennart, 65
Tachi, Hideki, 351
Tajima, Seitarou, 306
Takeda, Shigeki, 511
Tilley, M., 152
Tortorello, A. J., 412
Tsunooka, Masahiro, 351
Turro, Nicholas J., 105, 113
Utterodt, A., 202
van den Berg, Otto, 426
Viswanathan, K., 2, 76
Weber, Matthias, 105
Yagci, Yusuf, 187
Yamada, Kazunori, 511
Yamaguchi, Yoshikazu, 332
Yamamoto, Takayuki, 351
Yang, Bo, 400
Yang, D., 76

Subject Index

A

Acids, photoinitiators generating, 333

Acrylamide. *See* Lyotropic liquid crystals (LLC)

Acrylate formulations. *See* Hexanedioldiacrylate (HDDA) formulations

Acrylate photopolymerization consequences of pre-organization via

hydrogen bonding, 131

effect of bridge length, 132

effect of tacticity, 133, 135

effect of temperature, 132–133

effect of temperature on infrared

shifts of amide moiety, 134*f*

elucidation of reactivities, 128

experimental, 136–138

hydrogen bonding and reactivity, 128–129

maximum rates of polymerization of monomers capable of hydrogen bonding and counterparts, 131*t*

measuring reactivity of system, 128

monomers capable of hydrogen bonding vs. non-hydrogen bonding analogues, 129, 131

photodifferential scanning calorimetry (photo-DSC), 128

proposed mechanism of pre-organization via hydrogen bonding, 135*f*

reactive monomers, 129*f*

experimental, 413–414

formation of UV curable coatings, 414

mixture design studies, 423

real-time infrared spectroscopy (RTIR), 128–129, 136–137

synthesis of ethyl-*O*-urethane-*N*-ethyl acrylate, 137–138

synthetic routes to various acrylates, 130*f*

tacticity data of poly(methacrylates), 136*t*

undecyl amide *N*-ethyl-acrylate, 132–133

See also Kinetics of acrylate photopolymerization

Acrylated oligomers

combined structural effects on film elongation, 422*f*

combined structural feature effects on cured film modulus, 421*f*

cured film mechanical properties, 420, 423

effect of acrylic hydroxyl content on urethane viscosity, 418, 419*f*

effect of diluent monomer glass transition temperature on urethane viscosity, 418, 419*f*

effect of diluent polyol molecular weight on solution viscosity, 415, 417*f*

effect of prepolymer molecular weight on urethane viscosity, 418, 420, 421*f*

effect of structural design features on cured film modulus, 420, 421*f*

effect of structural features on cured film elongation, 420, 422*f*, 423

preliminary coating design studies, 424*t*

preparation in two-step sequence, 414–415

- radiation cured coatings industry, 413
- random acrylic copolymer
 - preparation, 413–414
 - synthetic scheme, 416
- urethane acrylate oligomers, 416, 423
- urethane/acrylate oligomer solution
 - properties, 415, 418, 420
- vinyl/acrylic copolymer solution
 - properties, 415
- Acrylates
 - calixarene derivatives, 364, 366
 - two-photon induced polymerization, 468
 - See also* Fluorinated systems; Hexanedioldiacrylate (HDDA) formulations; Kinetics of acrylate photopolymerization; Liquid polybutadienes; Monomer blends, photopolymerization; Phthalimide derivatives, sensitized; Radical photopolymerization
- Addition-fragmentation reactions
 - addition-fragmentation agents (AFAs), 188
 - AFAs and mode of activation, 189*t*
 - bifunctional AFAs, 190, 193
 - Brønsted acid generation by hydrogen abstraction, 196, 198
 - cationic photopolymerization
 - photoinitiators, 188
 - electron transfer reactions, 190
 - fragmentation, 190
 - general aspects, 188, 190
 - initiating species and by-products
 - from addition-fragmentation mechanism, 191*t*
 - initiation of cationic polymerization
 - by morpholino ketone ethyl acrylate salt (BDMEA), 195
 - initiation of cationic polymerization
 - by benzophenone ethyl acrylate salt (BPEA), 197
 - initiation of cationic polymerization
 - by Michler's ketone ethyl acrylate salt (MKEA), 200
 - intermolecular hydrogen abstraction
 - type AFAs, 194, 196–200
 - intramolecular bond cleavage
 - type AFA, 194
 - mechanism of addition-fragmentation
 - type initiation, 190
 - mechanism of initiation, 194
 - photoinitiated free radical
 - polymerization using benzophenone, 196
 - photopolymerization of CHO (cyclohexene oxide) in presence of BPEA, 198*f*
 - photopolymerization of CHO in presence of MKEA, 199*f*
 - polymerization by BPEA, 194, 196–199
 - polymerization by MKEA, 199–200
 - polymerization by BDMEA, 194
 - radical sources for initiation, 192*t*
 - structure and characteristics of photoactive AFAs, 193*t*
 - synthesis of bifunctional photoactive AFAs, 193
 - See also* Cationic photopolymerization
- Addition reactions
 - alkyl vinyl ethers, 181
 - vinyl ethers, 184
- Adhesion
 - changes in tensile shear adhesion
 - strength with grafted amount for polyethylene plates, 520*f*
 - grafted amounts at substrate breaking, 519, 521*t*
 - strength for methacrylamide-grafted plates, 519
 - strength measurement method, 513
 - See also* Photoinduced grafting of methacrylamide; Pressure sensitive adhesives

- Aging, dark. *See* Epoxy resin, cycloaliphatic
- Alignment
liquid crystals, 483
See also Photoalignment
- Alkenes, reactivity towards thiyl radicals, 66–67
- N*-Alkylamides
structures, 4*f*
See also Hexanedioldiacrylate (HDDA) formulations
- Alkyl oxetane. *See* Pressure sensitive adhesives
- Alkyl vinyl ethers, addition reactions, 181
- Allyl ethers in thiol-ene reaction
characterization of cured films, 70–73
coating characteristics of formulations with thiols and pentaerythritol triallyl ether (APE), 71*t*
coating characteristics of non-stoichiometric formulations, 72*t*
contact angle, 71*t*
ene, 67–68
ene characteristics, 68*t*
formulations with trimethylolpropane tris(3-mercaptopropanoate) (TMP3MP3), 70
Koenig hardness and glass transition T_g of thiol-ene coatings, 70*f*
non-stoichiometric formulations, 72
reactivity towards thiyl radicals, 66–67
structures of evaluated allyl derivatives, 67*f*
structures of thiols, 69*f*
thermal stability of thiol-ene coatings, 72–73
thermogravimetric analysis of films with various stoichiometric ratios of TMP3MP3 and APE, 73*f*
thiol characteristics, 68*t*
thiols, 68
thiols in formulations with APE, 71
- Anionic photopolymerization
benzoyl-substituted ferrocenes, 337, 339–342
ferrocene, 334–337
- Anthracene, triplet energy, 31*t*
- Aryl ketones, generation of aryl radicals, 248
- Atomic force microscopy (AFM)
copolymers before and after irradiation with linearly polarized light, 492, 494*f*, 495*f*
technique, 485
- Autohesion
grafted amounts at substrate breaking, 517, 520*t*
method for measuring, strength, 513
pioneering studies, 512
strength of methacrylamide-grafted plates, 517, 519
swelling poly(ethylene) plates, 512
See also Photoinduced grafting of methacrylamide
- Azobenzene chromophores,
photoalignment, 483
- 4,4'-Azobisisobutyronitrile (AIBN),
addition-fragmentation type initiation, 192*t*
- B**
- Benzil
structure, 246*t*
UV absorption spectra, 246*t*
- Benzoin, addition-fragmentation type initiation, 192*t*
- Benzophenone
abstraction type photoinitiator, 28
addition-fragmentation type initiation, 192*t*
photoinitiated free radical polymerization, 194, 196
reaction pathways for photolysis, 28*f*
triplet energy, 31*t*

- Benzophenone ethyl acrylate salt (BPEA)**
 initiation of cationic polymerization, 194, 196–199
 structure and characteristics, 193*t*
- 4-Benzoylbiphenyl**, triplet energy, 31*t*
- Benzoyl radicals**, photochemical generation of substituted, 109
- Bis-[1-ethyl(3-oxetanyl)-methyl] ether (DOX)**
 structure, 288
See also 2-Phenylloxetanes
- Blends.** *See* Monomer blends, photopolymerization
- Brønsted acid generation**, hydrogen abstraction, 196, 198
- Bulk photopolymerizations**, 3,4-epoxy-1-butene, 267, 269, 270*f*
- Butyl acrylate**
 evaluating performance of spinning disc reactor, 439–440
 rate constant and enthalpy of reaction for addition of radicals, 148*t*, 149*t*
See also Continuous photopolymerization
- Butyl methacrylate**, rate constant and enthalpy of reaction for addition of radicals, 148*t*, 149*t*
- C**
- Calixarenes**
 applications, 364
 characteristics, 364
 derivatives containing spiro ortho ethers, 375
 host-molecule, 364
 photoinitiated cationic polymerization rates for, containing pendant oxetane groups, 373*f*
 photoinitiated cationic polymerization rates for, containing pendant oxirane groups, 374*f*
- photoinitiated cationic polymerization rates for**, containing propargyl ether, vinyl ether, and 1-propenyl ether groups, 370*f*
- photoinitiated radical polymerization rates for (meth)acrylate derivatives**, 367*f*
- scheme to cyclic ether derivatives**, 372
- scheme to (meth)acrylate derivatives**, 365
- scheme to propargyl ether and vinyl ether derivatives**, 369
- scheme to spiro ortho ether derivatives**, 376
- synthesis of derivatives containing cyclic ether groups**, 368, 371
- synthesis of derivatives containing (meth)acrylate groups**, 364, 366
- synthesis of derivatives containing propargyl ether and vinyl ether groups**, 366, 368
- thermal stability for**, containing oxirane and oxetane groups, 371
- thermal stability for**, containing propargyl and vinyl ethers, 368
- thermogravimetric analysis of acrylate and methacrylate derivatives**, 366
- Camphorquinone**
 photopolymerization of 4-vinylcyclohexene dioxide (VCHDO), 247*f*, 249*f*, 250*f*
 structure, 246*t*
 thermal lens spectroscopy, 143–144
 UV absorption spectra, 246*t*
- Carbazoles.** *See* Photosensitization of onium salts
- Cationic photoinitiators**
 polymerization of epoxides, vinyl ethers, and methylenedioloxanes, 472

- structures, 472*f*
 UV-visible spectra, 473*f*
- Cationic photopolymerization
 acceleration of ring-opening
 polymerization of heterocyclic
 monomers, 184
 alkyl vinyl ethers undergoing
 addition reactions, 181
 application, 242–243
 aryl ketone-sensitized, 245–248
 commercial applications, 179
 comparison of, of various benzyl
 ether containing epoxy monomers,
 182*f*
 comparison of photopolymerizations
 of two epoxy monomers with (4-
 decyloxyphenyl) phenyliodonium
 SbF_6^- (IOC10), 185*f*
 $[\text{CpFe}(\eta^6\text{-arene})]^+$ complexes, 342–
 345
 diazonium salts, 203
 2,3-dihydrofuran, 214
 epoxide monomers undergoing
 hydrogen abstraction reactions,
 181
 experimental, 179
 $[\text{Fe}(\eta^6\text{-arene})_2]^{2+}$ complexes, 345–
 348
 generation of oxidizable free
 radicals, 181
 initiation by benzophenone ethyl
 acrylate salt (BPEA), 194, 196–
 199
 initiation by Michler's ketone ethyl
 acrylate salt (MKEA), 199–200
 IOC10, 181
 mechanism, 180–181
 NVK (*N*-vinylcarbazole) as
 photosensitizer, 184
 onium salt photolysis, 180, 185–186
 photoinitiators, 179, 188, 219–220,
 231–232
 photopolymerization of 3,4-
 epoxycyclohexylmethyl 3',4'-
 epoxycyclohexanecarboxylate
 alone and with *n*-butyl vinyl ether,
 183*f*
 photopolymerization of cyclohexene
 oxide with NVK, 184*f*
 photopolymerization of
 triethyleneglycol divinyl ether,
 182*f*
 photosensitizer for onium salt
 photolysis, 184
 polymerization rate, 180
 proposed mechanism for photolysis
 and initiation, 179–180
 rate equation, 180
 rate of polymerization of epoxide in
 presence of NVK, 184–185
 real time infrared (RTIR) study of
 two epoxy acetal monomers,
 183*f*
 vinyl ethers undergoing hydrogen
 abstraction and addition, 184
See also Addition-fragmentation
 reactions; Calixarenes; 3,4-Epoxy-
 1-butene; Epoxy resin,
 cycloaliphatic; Fluoroalkyl
 propenyl ethers; Organic-inorganic
 hybrid resins; 2-Phenylloxetanes;
 Visible and long-wavelength
 cationic photopolymerization
- Cationic polymerization, photo- and
 thermally initiated, 260–261
- Chain transfer agents,
 photopolymerization, 173
- Charge transfer excited states, iron(II)
 metallocenes, 334
- Charge-transfer-to-solvent (CTTS),
 excited state, 334
- Chemical resistance, (meth)acrylated
 liquid polybutadienes, 409–410
- Chemical sensitization, process, 30
- Chemistry
 epoxidized liquid polybutadiene
 oligomers, 404
 (meth)acrylated liquid polybutadiene
 oligomers, 403–404
- Cinnamates, photoalignment, 483

- Coatings, thermal stability of thiol-ene, 72–73
- Coefficient of thermal expansion, photopolymerizable liquid encapsulants, 396
- Communications industry. *See* Photopolymerizable liquid encapsulants (PLEs)
- Complexes. *See* Metallocene complexes
- Composites. *See* Photopolymerizable liquid encapsulants (PLEs)
- Computer industry. *See* Photopolymerizable liquid encapsulants (PLEs)
- Contact angles
 advancing, of UV-cured films, 507*f*, 508*f*
 components of thiol-ene coatings, 71*t*
 non-stoichiometric formulations, 72*t*
 thiols and pentaerythritol allyl ether formulations, 71*t*
See also Fluorinated systems
- Continuous photopolymerization
 advantages of photochemical initiation, 438
n-butyl acrylate as test monomer, 439–440
 characterization methods, 441–442
 comparison of static and spinning disc reactor (SDR) film, 448*t*
 effect of disc rotational speed and feed flow rate on mean residence time and film thickness, 443*f*
 effect of disc rotational speed on conversion of *n*-butyl acrylate in SDR at different feed flow rates, 444*f*
 equipment, 440, 441*f*
 experimental, 440–442
 film thickness, 442
 influence of disc rotational speed and feed flow rate, 442, 445
 influence of UV intensity, 445, 446*f*
 materials, 440
 molecular weight properties and branching effects, 445, 447–448
 molecular weight properties of poly(butyl acrylate) in SDR, 447*t*
 novel spinning disc photopolymerizer, 439–440
 opportunity for process intensification, 449
 photopolymerization procedure, 440–441
 residence time (t_{res}), 442
 schematic of SDR, 441*f*
 SDR, 439
 static film vs. SDR film, 448–449
 variables affecting performance of SDR, 442
- Copolymerizations. *See* Maleimide/donor photocopolymerizations
- Coumarins, photoalignment, 483
- Crosslinked polymers
 bulk photopolymerization of 3,4-epoxy-1-butene, 269
 evaluating extent, 94
See also Monomer blends, photopolymerization; Photocrosslinking
- Curing behavior
 effect of temperature on epoxy, 321–322, 327–328
See also Epoxy resin, aliphatic
- Cyclic ethers, calixarene derivatives, 368, 371
- Cycloaliphatic diepoxide. *See* Pressure sensitive adhesives; Silsesquioxanes (SQs), oxetanyl-functional
- Cycloaliphatic epoxy resin. *See* Epoxy resin, cycloaliphatic
- Cyclohexene oxide (CHO)
 cationic photopolymerization, 184*f*
 influence of monomer structure, 250–251
 photopolymerization in presence of carbazoles, 224–229

photosensitized polymerization using phenothiazines, 235–239
 polymerization by benzophenone ethyl acrylate salt (BPEA), 194, 196–199
 polymerization by Michler's ketone ethyl acrylate salt (MKEA), 199–200
 polymerization by morpholino ketone ethyl acrylate salt (BDMEA), 194
See also Phenothiazine photosensitizers

D

Dark aging. *See* Epoxy resin, cycloaliphatic
 Decomposition temperatures, poly(2,3-dihydrofuran)s, 217*t*
 Design studies, acrylated oligomers, 423, 424*t*
 Diaryliodonium salt
 cationic photopolymerization, 179–180
 electron-transfer photosensitization, 232
 Diazonium salts
 bimolecular dediazonation, 210
 calculated oxidation and reduction potentials of onium salts, 209*f*
 cationic photopolymerization of epoxides and vinyl ether derivatives, 203
 crosslinking, 205–207
 electron paramagnetic resonance (EPR) signals under irradiation of, without and with monomer, 208*f*
 ¹H NMR spectra of reaction with *t*-butyl vinyl ether, 210, 211*f*
 4-hexyloxysubstituted, with complex anions, 203
 initiating photocrosslinking of vinyl ethers and epoxides, 205*f*

 photoinitiators, 203
 photolysis and MEERWEIN-reduction, 207
 rate constants of propagation and termination vs. irradiation time, 206*f*
 thermostability, 210
 Dibenzoyl peroxide (BPO), addition-fragmentation type initiation, 192*t*
 Dichroism
 fluorinated distyrylbenzene copolymers, 492, 493*f*
 oriented liquid crystal, 497
 Diepoxide, polymerization, 94, 96
 2,3-Dihydrofuran
 cationic polymerization of derivatives, 217*f*
 film forming properties of polymer, 215
 glass transition and decomposition temperatures of uncrosslinked polymers, 217*t*
 Heck reaction with arylbromides, 215*f*
 molecular weights of uncrosslinked polymers, 217*t*
 photopolymerization of derivatives, 215, 217
 polymerization, 214
 synthesized derivatives, 216*f*
 synthetic methods, 214*f*
 2,2-Dimethoxy-2-phenylacetophenone (DMPA)
 photoinitiator, 3
 Type I photoinitiator, 28, 42
 Dioxolanes (DOX). *See* Maleimide/donor photocopolymerizations
 Diphenyliodonium chloride (DPI)
 effect on termination rate, 21
 See also Initiator systems, three-component
 Distyrylbenzene containing copolymers, fluorinated. *See*

Fluorinated distyrylbenzene containing copolymers
 Dodecyl vinyl ether (DDVE) polymerization with difunctional maleimide monomer Q-bond, 79–81, 83
See also Maleimide/donor photocopolymerizations
 Doppler broadening of energy spectrum (DBES), technique, 154
 Dual-cell UV-visible absorption spectroscopy
 eosin Y, *N*-methyldiethanolamine and diphenyliodonium chloride system, 23–24
 experimental for three-component initiator systems, 19

E

Efficiency, photoinitiator, 116–117
 Electron density modeling, maleimide/donor copolymerization, 84–85
 Electron paramagnetic resonance (EPR), initiation rate coefficients, 106–107
 Electron spectroscopy chemical analysis (ESCA) method, 154–155
 urethane–acrylate coatings, 157
 Electron spin echo (ESE) instrumentation, 108
 photoinitiators, 110*f*
 Electronic excited states, iron(II) metallocenes, 334
 Electrospray ionization mass spectrometry (ESI–MS), trapping photogenerated intermediates, 343
 Elongation, cured film from urethane acrylate oligomers, 420, 422*f*, 423
 Encapsulants. *See* Photopolymerizable liquid encapsulants (PLEs)

Encapsulation, transfer molding process, 390
 Energy diagram, benzophenone/amine, 146*f*
 Eosin Y. *See* Initiator systems, three-component
 Eosin Y spirit soluble (EYss). *See* Initiator systems, three-component
 Epoxidation, polybutadiene, 404
 Epoxide monomers
 cationic polymerization, 96
 hydrogen abstraction reactions, 181
 photocrosslinking, 205–207
See also Monomer blends, photopolymerization
 Epoxidized polyisoprene (EPI), UV-irradiation of, and diacrylate, 97, 98*f*
 Epoxy acetal monomers, cationic photopolymerization, 183*f*
 Epoxy–acrylates, thermal stability, 364
 3,4-Epoxy-1-butene
 bulk polymerization, 267
 cationic UV curing, 267
 comparing cationic photoinitiators for photopolymerization, 272
 comparing reactivity of related monomers, 275*f*
 crosslinking, 269
 diaryliodonium salt photoinitiators, 268
 effect of light intensity, 270, 272*f*
 experimental, 267–268
 Fourier transform real-time infrared spectroscopy (FT–RTIR), 268, 269–270, 271*f*
¹H NMR spectrum of polymer by bulk cationic photopolymerization, 270*f*
 influence of (4-*n*-decyloxyphenyl)phenyliodonium counterions on polymerization rate, 273*f*

- monitoring photopolymerization rates, 269–270, 271*f*
- photoinitiator concentration, 272, 273*f*
- photopolymerization of related monomers, 274
- photopolymerization studies, 268
- preparation, 266–267
- ring-opening polymerization of epoxide, 268–269
- structure, 267
- 3,4-Epoxycyclohexylmethyl 3',4'-epoxycyclohexane carboxylate (epoxy 3,4)
- monomer for photoinitiated cationic polymerization, 318
- See also* Epoxy resin, cycloaliphatic
- Epoxy functional silicone resins. *See* Organic-inorganic hybrid resins
- 1,2-Epoxy-hexadecane. *See* Pressure sensitive adhesives
- Epoxy monomers. *See* Cationic photopolymerization; Monomer blends, photopolymerization
- Epoxy resin, cycloaliphatic
- acceleration by chain transfer agents, 325, 327
- apparent heat of reaction, 320
- average heat flow for 3,4-epoxycyclohexylmethyl 3',4'-epoxycyclohexane carboxylate (epoxy 3,4) after initial UV belt cure, 322, 323*f*
- average heat flow signal and storage specific heat (C_p) vs. temperature, 324*f*
- average heat flow signal from temperature modulated differential scanning calorimetry (TMDSC) experiments, 322, 324
- conventional DSC scans of epoxy 3,4 after dark aging, 326*f*
- cycloaliphatic epoxide epoxy 3,4, 318
- degree of conversion as function of time, 320
- effect of temperature on curing behavior, 321–322
- effect of temperature on curing rate properties, 320
- energy profiles of xenon lamp, 319
- exothermic reaction of epoxy 3,4 under isothermal conditions, 320*f*
- experimental, 318–319
- extent of conversion vs. temperature, 321*f*
- extent of reaction in dark with aging, 322
- glass transition, 322, 324
- glass transition temperature and residual heat of reaction after belt curing process, 322
- impact of dark reaction on modulus, 325, 327*f*
- modulus by three point bending, 319
- photocalorimetric comparison of isothermal curing of three epoxy 3,4 films, 319–320
- temperature effects, 327–328
- T_g during dark reaction vs. conversion, 325, 326*f*
- time to maximum polymerization rate vs. temperature, 321*f*
- UV-radiation experiments, 319
- 2-Ethylanthraquinone
- structure, 246*t*
- UV absorption spectra, 246*t*
- N*-Ethylcarbazole (NEK). *See* Photosensitization of onium salts
- 3-Ethyl-3-(2-ethylhexyloxymethyl)oxetane (EHOX)
- pressure sensitive adhesives, 298, 304–305
- See also* Pressure sensitive adhesives
- 3-Ethyl-3-phenoxyethyl-oxetane (POX)
- photodifferential scanning calorimetry, 290*f*

structure, 288

See also 2-Phenyloxetanes

Extinction difference (ED) diagram,
fluorinated distyrylbenzene
copolymers, 492, 493*f*

F

Fast signal S_F

equation, 147

evolution for different monomer
concentration, 148*f*

Ferrocene ($FeCp_2$)

benzoyl-substituted, 337, 339–342

charge transfer mechanism, 335

complexing with solvents, 334–335

concentrations for

photopolymerization of ethyl α -

cyanoacrylate (CA), 337

electronic absorption spectra of, and

benzoyl-substituted, 339*f*

electronic absorption spectrum, 336*f*

metal-to-ligand charge transfer

(MLCT) character, 334, 339–340

photochemical quantum yields for

1,1'-dibenzoyl-ferrocene

disappearance, 340*t*

photochemical route for generating

anions, 340–341

photooxidation in CA, 335

polymerization vs. time for CA

containing, 338*f*

polymerization vs. time for CA

containing 1,1'-

dibenzoylferrocene, 341*f*

quantum efficiency of anion release

and phenyl ring substituents, 341–

342

real-time monitoring of CA

photopolymerization, 337

resonance structure showing charge

transfer character, 339*f*

solution shelf-life, 341–342

structure, 340

viscosity in CA solutions, 335

Fibers, ribbons, 153

Film thickness, performance of

spinning disc reactor, 442, 443*f*

Films. *See* Fluorinated systems

Flexural strength and modulus

effect of filler loading, 394

effect of thermal initiator, 395*f*

photopolymerizable liquid

encapsulants, 394–395

specimens for testing, 392

Fluorenone, triplet energy, 31*t*

Fluorescent probes

comparing non-reactive probes with
substituents of different sizes, 433

comparing reactive and

corresponding non-reactive
probes, 429–433

developing sensitive, 427–428

difference of intensity ratios of two
probes vs. conversion, 432*f*

differences in intensity ratio vs.

conversion, 435*f*

disubstituted nitrostilbenes, 427–428

double bond conversions by IR

measurements, 428–429

experimental, 428–429

1,6-hexanediol dimethacrylate

(HEXDMA) polymerization, 428

intensity ratio R of probes 1–4 in

HEXDMA vs. conversion, 430*f*

intensity ratio R vs. irradiation time,
429*f*

non-destructive and real-time, 427

plots of R vs. irradiation time and

conversion for probes 3 and 5–7 in

HEXDMA, 434*f*

probe sensitivity definition, 430

relative sensitivities, 431, 433

sensitivity for probes 1–4 vs.

conversion, 432*f*

sensitivity vs. reaction, 430

structures for probes 1–7, 427

Fluorinated distyrylbenzene

containing copolymers

- absorption spectra, 490, 491*f*
dichroism by irradiation cycle, 492, 493*f*
dichroism of oriented liquid crystal, 497
extinction differences (ED)
 diagrams, 492, 493*f*
manufacturing liquid crystal cell with photoalignment layers, 496
photoisomerization vs.
 photocycloaddition, 486, 488, 490
quantum yields, 488, 490*t*
 π -stacking between fluorinated and non-fluorinated benzene rings, 484, 486, 488
structure, 485, 486
surface morphology before and after irradiation, 492, 494*f*, 495*f*
surface roughness, 492*t*
See also Photoalignment
- Fluorinated systems
 advancing contact angles of UV-cured films containing monomers with different fluorine content, 507*f*
 advancing contact angles on air side of UV-cured films with monomers of different spacer length, 508*f*
 characterization of fluoroacrylates–bisphenol-A-dihydroxyethylene diacrylate (BHEDA) UV-cured mixtures, 506–508
 characterization of perfluoropolyether urethane methacrylates (PFEUMA)–BHEDA UV-cured mixtures, 503–506
 contact angle measurements, 502
 contact angle vs. concentration for bifunctional PFEUMA monomer, 504*f*
 contact angle vs. PFEUMA concentration, 503*f*
 copolymerization of fluorinated with hydrogenated monomers, 500
 curing reaction, 501–502
 dependence of wettability of cured films on substrate type, 505*t*
 DMTA spectrum of cured film based on bifunctional PFPE monomer, 506*f*
 effect of spacing groups, 507, 508*f*
 film characterization methods, 502
 films containing PFEUMA monomers on polyethylene (PE) substrate, 505
 film thickness measurement, 502
 fluorinated monomers, 500–501
 fluorine concentration on air side vs. glass side of films, 508, 509*t*
 materials and methods, 500–502
 TEM micrograph of UV-cured bifunctional PFEUMA film, 506*f*
 UV-curable, 500
 wettability of UV-cured films vs. PFEUMA comonomer content, 503
 XPS data for fluorinated film of typical BHEDA–mono PFEUMA copolymer, 504*t*
 XPS results at different take-off angles, 509*t*
 X-ray photoelectron spectroscopy measurements, 502
- Fluoroalkyl propenyl ethers
 experimental, 278–280
 Fourier transform real-time infrared (FT–RTIR) study of cationic polymerization of 2,2,3,3,3-pentafluoropropyl propenyl ether, 282*f*
 ¹H NMR spectra before and after isomerization of 2,2,3,3,4,4-hexafluoropentyl dipropenyl ether, 281*f*
 materials, 278
 photopolymerization and FT–RTIR measurements, 279–280

- photopolymerization studies, 281, 283
 - preparation methods for various, 278–279
 - RTIR curves for cationic polymerization of 2,2,3,3,4,4,5,5,6,6,7,7,8,8,9,9-hexadecylfluorodecyl dipropenyl ether, 282*f*
 - synthesis of mono- and dipropenyl ether monomers, 280
 - synthetic scheme of propenyl ether monomers, 280*f*
 - Free radical initiators, thiols, 66
 - Free radical photoinitiators
 - categories, 28
 - structures, 469*f*
 - UV-visible spectra, 470*f*
 - Free radical polymerization (FRP)
 - industrial preparation, 105–106
 - studying competing reactions, 106
 - UV-curable coatings, 114
 - See also* Kinetics of acrylate photopolymerization
- G**
- Gel formation, thiol-ene photopolymerization, 54
 - Glass, wettability of cured films, 505*t*
 - Glass transition temperature, T_g
 - curing process of epoxy resin, 322, 324
 - non-stoichiometric formulations, 72*t*
 - photopolymerizable liquid encapsulants, 396
 - poly(2,3-dihydrofuran)s, 217*t*
 - thiol-ene coatings, 70*f*
 - thiols and pentaerythritol allyl ether formulations, 71*t*
 - Grafting. *See* Photoinduced grafting of methacrylamide

H

- Half-life
 - estimation method, 354
 - quaternary ammonium dithiocarbamates (QA salts) in solution, 357*t*
- Hardness
 - effect of double bond conversion of (meth)acrylated polybutadiene films, 409
 - non-stoichiometric formulations, 72*t*
 - thiol-ene coatings, 70*f*
 - thiols and pentaerythritol allyl ether formulations, 71*t*
- HDDA. *See* Hexanedioldiacrylate (HDDA); Hexanedioldiacrylate (HDDA) formulations
- Heck reaction, 2,3-dihydrofuran and arylbromides, 215*f*
- Helium purging, radical photopolymerization, 170
- Heterocyclic monomers, ring-opening polymerization, 184
- Heterotelechelic linear polymer. *See* Pressure sensitive adhesives
- Hexanedioldiacrylate (HDDA)
 - effect of 2-benzoxazolethiol on photopolymerization, 172*f*
 - oxygen effect on shear modulus of photopolymerizing resin, 174*f*
 - photopolymerization kinetics, 172*f*
 - structure, 56
 - See also* Radical photopolymerization; Thiol-ene systems
- Hexanedioldiacrylate (HDDA) formulations
 - acronyms and structures of *N*-substituted amides, 4*f*
 - amides, *N*-substituted, as additives, 5–7
 - conditions and compounds, 3
 - excitation of complex or formation of exciplex, 11

- hydrogen abstraction process, 12
inhibition, 12
kinetics of difunctional vinyl monomer formulation with added monofunctional vinyl monomer, 10–11
NVP (*N*-vinylpyrrolidinone) enhancing polymerization efficiency, 11
oxygen consumption process, 12
photodifferential scanning calorimetry (photo-DSC) results, 5–7
photo-DSC for *N*-vinylamide/HDDA formulations polymerized in air, 6*f*
photo-DSC for *N*-vinylamide/HDDA formulations polymerized in nitrogen, 6*f*
photoinitiator, 3
real time Fourier transform infrared (RT–FTIR) results, 7, 10
reversible UV-absorption spectral shifts for NVP and *N*-methylpyrrolidinone (NMP), 11
RT–FTIR conversion of HDDA vs. wt% NVP in HDDA in laminate and air, 9*f*
RT–FTIR conversion of NVP vs. wt% NVP in HDDA in laminate and air, 9*f*
RT–FTIR conversion vs. time for 10% NVP in HDDA in laminate and air, 8*f*
RT–FTIR conversion vs. time for 60% NVP in HDDA in laminate and air, 8*f*
UV-visible spectroscopic results, 10
See also Maleimides, *N*-substituted, as photoinitiators
1,6-Hexanediol dimethacrylate (HEXDMA)
photopolymerization by real-time fluorescence spectroscopy, 428–429

See also Fluorescent probes
Hexyl acrylate
photo-DSC exotherm of photopolymerization, 58*f*
structure, 56
High performance UV-curing oligomers. *See* Calixarenes
Hydrogen abstraction
Brønsted acid generation, 198
epoxide monomers, 181
mechanism of photosensitization by photoexcited ketones, 247
N-vinylamide/hexanedioldiacrylate formulation, 12
vinyl ethers, 184
Hydrogen bonding
consequences of pre-organization, 131
effect of bridge length, 132
maximum photopolymerization rates of monomers capable, 131*t*
monomer reactivity, 128–129
monomers capable of, vs. non-hydrogen bonding analogues, 129, 131
proposed mechanism of pre-organization via, to isotactic polymer, 135*f*
See also Acrylate photopolymerization
Hydroxybenzophenone (BPOH), photoacoustic spectroscopy of, and bifunctional initiator, 142–143
- ## I
- Inhibition. *See* Oxygen inhibition
Initiation. *See* Kinetics of acrylate photopolymerization; Mechanisms; Photoinitiators
Initiation rate coefficients, electron paramagnetic resonance (EPR), 106–107
Initiator systems, three-component

- comparison of eosin Y (EY) and EY spirit soluble (EYss)
 photobleaching by DPI, 24*f*
 dark polymerization exotherms for various DPI concentrations, 22*f*
 description, 17–18
 differential scanning calorimetry (DSC) dark-cure experiments, 19
 dual-cell UV-visible absorption spectroscopy, 19
 effect of DPI on rate of termination, 21
 electron transfer/proton transfer reaction, 25
 experimental, 18–19
 flexibility, 17
 free radical photoinitiators, 16
 influence of oxygen on consumption rate of methylene blue, 21–22
 major reaction steps for MB/MDEA/DPI, 21
 materials, 18
 methylene blue, *N*-methyl-diethanolamine and diphenyliodonium chloride system, 20–22
 photo-DSC, 18–19
 role of iodonium salt, 20, 21
 time-resolved steady state fluorescence, 19
 two component systems, 17
 visible light radical photoinitiators, 17
See also Maleimides, *N*-substituted, as photoinitiators
 Inorganic photoinitiators, program expanding, 333
 Insolubilization. *See* Quaternary ammonium dithiocarbamates (QA salts)
 Intermolecular hydrogen abstraction, addition-fragmentation agents, 194, 196–200
 Interpenetrating polymer networks (IPN)
 photoinitiation, 92
 photopolymerization of polymer blends, 92
See also Monomer blends, photopolymerization
 Intramolecular bond cleavage, addition-fragmentation agents, 194, 195
 Intramolecular chain transfer (ICT), formation, 485
 Ionic photopolymerization. *See* Metallocene complexes
 Iron(II) metallocenes
 electronic excited states, 334
 photochemistry summary, 348–349
 structures of types, 333*f*
 Isopropylthioxanthone (ITX)
 absorption spectrum, 474, 475*f*
 confirming two-photon absorption, 474
 initiating acrylate polymerization with phthalimide derivatives and ITX sensitizer, 44–47
 quadratic dependence of fluorescence intensity, 476*f*
 quenching constants, 48*t*
 single- and two-photon upconverted fluorescence spectra, 475*f*
 thiol-ene two-photon polymerization, 472, 474–477
 triplet energy, 31*t*
See also Two-photon photopolymerization
 Isotactic polymer, proposed mechanism by pre-organization via hydrogen bonding, 135*f*
- ## K
- Ketyl radicals, photochemical generation, 109
 Kinetics
 cationic photopolymerization, 180

- cure, dependence on layer thickness, 171*f*
diffusion control, 171
difunctional vinyl monomer with added monofunctional vinyl monomer, 10–11
thiol-ene photopolymerization, 53–54
See also Kinetics of acrylate photopolymerization; Lyotropic liquid crystals (LLC); Radical photopolymerization; Thiol-ene systems
- Kinetics of acrylate photopolymerization
chain free radical reaction with bimolecular chain termination k_t , 114
comparing one pulse and two pulses for polymerization, 119, 122–124
concepts in literature, 114–115
conversion dependent parameters k_p and $2k_t$, 115–117
dependencies of $2k_t/[k_p(1-\xi)]$ vs. ξ (acrylate conversion) for primary and secondary coatings, 122*f*
experimental, 117–118
experimental verification of reaction diffusion, 116
initiation of polymerization, 119, 122–124
kinetic expressions for postpolymerization, 114
kinetics of cure of primary coating under irradiation by one pulse and by two pulses, 123*f*
kinetics of cure of secondary coating under irradiation by one pulse and by two pulses, 124*f*
materials, 117
photodifferential scanning calorimetry (photo-DSC) experiments, 117–118
photo-DSC trace during polymerization of primary coating, 119, 120*f*
photo-DSC trace during polymerization of secondary coating, 119, 121*f*
photoinitiator efficiency, 116–117
polymerization and postpolymerization, 119
primary and secondary coatings, 124–125
real time infrared (RT FTIR) experiments, 118
UV-curable coatings, 114
Koenig hardness. *See* Hardness
- L**
- Laser flash photolysis
establishing mechanism for sensitizer effect, 36–39
experimental for sensitized initiator system, 31–32
interaction between phthalimides and isopropylthioxanthone (ITX), 44, 48
maleimide/donor photocopolymerizations, 83–84
Ligand field excited states, iron(II) metallocenes, 334
Ligand-to-metal charge transfer (LMCT), excited state, 334
Light intensity, bulk photopolymerization of 3,4-epoxy-1-butene, 270, 272*f*
Liquid crystalline phases. *See* Lyotropic liquid crystals (LLC)
Liquid crystals
alignment, 483
analysis of photoalignment by polarized Fourier transform infrared spectroscopy, 496

- dichroism of oriented, 497
 manufacturing cell with photoalignment layers, 496
 orientation of, and polarization plane, 496
 orienting polyimides, 484
See also Fluorinated distyrylbenzene containing copolymers;
 Photoalignment
- Liquid encapsulants. *See* Photopolymerizable liquid encapsulants (PLEs)
- Liquid polybutadienes
 basic chemistry, 403–404
 basic properties, 405*t*
 chemical resistance of (meth)acrylated, 409–410
 chemical structures of (meth)acrylated, 403
 conversion of double bonds, 406*f*
 conversions of double bonds, 407–408
 effect of 50% sulfuric acid on tensile strength at elevated temperatures, 410*f*
 effect of 50% sulfuric acid on tensile strength at room temperature, 409*f*
 effect of double bond conversion on surface hardness, 409*f*
 effect of photoinitiator concentration on number of crosslinks for each double bond type, 408*f*
 effect of UV dosage on number of crosslinks for each double bond type, 408*f*
 epoxidation of polybutadiene, 404
 epoxidized oligomers, 404
 experimental, 401–403
 Fourier transform infrared spectroscopy (FTIR), 402
 incorporating (meth)acrylic ester or epoxy functionality, 401
 influence of photoinitiator on number of crosslinks for each double bond type, 407*f*
 influence of photoinitiators and UV dosage on photoreactivity and film properties, 406–409
 materials, 401–402
 measurement of double bond conversion, 402
 mechanical properties test, 403
 (meth)acrylated oligomers, 403–404
 number of crosslinks formed per molecule, 407*f*
 photocuring speed and physical properties of cured films of (meth)acrylated oligomers, 406*t*
 photoreactivity and properties of cured films of (meth)acrylated oligomers, 405
 physical properties of (meth)acrylated oligomers, 404*t*
 test for acid and base resistance, 402
 UV curing system, 402
 UV dosage, 408–409
 wet film preparation, 402
- Living free radical polymerization, monodisperse polymer samples, 106
- Long-wavelength cationic photopolymerization. *See* Visible and long-wavelength cationic photopolymerization
- Long-wavelength photosensitizers, development for cationic photopolymerization, 244–245
- Lytotropic liquid crystals (LLC)
 apparent rate parameters of propagation and termination, 383
 chemical structures of acrylamide and Brij nonionic surfactants, 381*f*
 materials, 380
 methods, 381
 nanometer morphologies, 379
¹⁴N NMR spectra of 25% acrylamide in LLC phases, 384–385
 phase and ordering, 385–386
 photopolymerization kinetics and structure retention, 380, 381–382

polymerization dependence on temperature, 385–386
 polymerization rate vs. conversion for 25 wt% acrylamide with increasing temperature, 385*f*
 polymerization rate vs. double bond conversion for 25wt% acrylamide, 382*f*
 reaction environment and local ordering, 384–385
 SAXS method (small angle X-ray scattering), 381
 SAXS profiles of 25% acrylamide in bicontinuous cubic phase before and after polymerization, 386, 386*f*
 schematic of selected phases, 379*f*
 structure retention after polymerization, 386
 templates for synthesis of nanostructured materials, 379–380
 termination and propagation rate parameters of 25wt% acrylamide in LLC phases vs. double bond conversion, 383*f*

M

Maleimide/donor

photocopolymerizations
 1,2-addition reaction of 4-methylene-2-phenyl-1,3-dioxolane (MPDOX), 80
 advantages, 77
 quenching of singlet state *N*-alkyl maleimide (MI) by MPDOX, 86
 difunctional maleimide monomer Q-bond, 79
 dioxolanes (DOX), 77
 effect of polymerization temperature on ring opening of MPDOX, 81, 83
 equilibrium constant of charge-transfer complex, 85

equilibrium constants and electron density distributions for *t*-butyl maleimide (*t*-BMI)/dodecyl vinyl ether (DDVE) and *t*-BMI/MPDOX, 87*t*
 experimental, 78
 Hanna–Ashbough equation, 85
 Hanna–Ashbough plot for 2-phenyl-4-methylene-1,3-dioxolane (MPDOX)/*t*-BMI system, 87*f*
¹H NMR and C=C electron density modeling (HMO), 84–85
 laser flash photolysis, 83–84
 laser flash photolysis method, 78
 laser flash quenching rate constants for *N*-methylmaleimide (MMI) triplet state, 84*t*
 maleimides with vinyl ethers, 77
 monitoring with real-time infrared (RTIR) spectroscopy, 77–78
 relative ratio of ring-opening and 1,2-addition reaction in copolymerization of Q-bond/MPDOX vs. temperature, 83*f*
 ring-opening/elimination reaction of MPDOX, 82*f*
 ring-opening reaction of MPDOX, 80
 RTIR method, 78
 RTIR polymerization, 79–83
 RTIR recordings of copolymerization of 1:1 Q-bond/MPDOX and Q-bond/DDVE, 81*f*
 Maleimides
 initiating photopolymerization, 29
See also Maleimides, *N*-substituted, as photoinitiators
 Maleimides, *N*-substituted, as photoinitiators
 amine coinitiator, 29
 chemical sensitization, 30
 efficiency, 29–30
 electron/proton transfer mechanism for maleimide/amine, 29*f*
 electron transfer mechanism, 30*f*
 experimental, 31–32

- laser flash photolysis, 36–39
- laser flash photolysis method, 31–32
- laser flash quenching constants in acetonitrile, 37*t*
- laser flash quenching constants in acetonitrile solutions, 37*t*
- mechanism, 29
- photodifferential scanning calorimetry (photo-DSC), 31
- photo-DSC exotherms, 32–36
- photo-DSC exotherms for 1,6-hexanedioldiacrylate (HDDA) initiated by sensitized *N*-methylmaleimide (MMI), 34*f*, 35*f*
- photo-DSC exotherms for nitrogen-purged HDDA initiated by sensitized MMI, 33*f*
- rate constants for quenching MMI triplet by *N*-methyl-*N,N*-diethanolamine (MDEA), 36–37
- rates with sensitizer/maleimide/amine mixtures, 32–34
- semipinacol reduction mechanism, 38*f*
- Stern–Volmer equation, 36
- triplet sensitizers, 31*t*
- Mechanical properties**
- comparing storage moduli for thermally crosslinked silicone–epoxy resins, 263*f*
- comparing tan delta plots for thermally crosslinked silicone–epoxy resins, 264*f*
- epoxy functional organic-inorganic hybrid polymers, 262–263
- modulus in epoxy resin during dark reaction, 325, 327
- pressure sensitive adhesives, 299, 301*f*, 303*f*, 304*f*
- viscoelastic measurement of oxetanyl-functional silsesquioxanes, 314
- See also* Epoxy resin, cycloaliphatic
- Mechanisms**
- acetaldehyde formation by cationic polymerization of ethyl vinyl ether, 213, 214*f*
- addition-fragmentation type initiation, 190
- cation formation in inert and reactive systems, 207–208
- cationic photopolymerization, 180–181
- electron/proton transfer for maleimide/amine, 29
- electron-transfer photosensitization of diaryliodonium salts, 232
- energy transfer for initiation, 30
- initiating species for cationic polymerization, 225–226
- initiation of cationic photopolymerization, 195, 197, 200
- oxygen scavenging for thiol-enes, 60
- photoinitiated polymerization, 332–333
- photosensitization by hydrogen abstraction by photoexcited ketones, 247
- photosensitization of onium salts, 220–221
- proposed initiation involving phthalimide derivatives and isopropylthioxanthone (ITX), 49–50
- proposed mechanism of pre-organization via hydrogen bonding to isotactic polymer, 135*f*
- semipinacol reduction, 38*f*
- thiol-ene polymerization, 66
- Mercaptans, reactions with oxygen, 172
- Metallocene complexes**
- coordination of CHO to dipositive iron center, 345
- $[\text{CpFe}(\eta^6\text{-arene})]^{2+}$, 342–345
- electronic absorption spectrum of $[\text{Fe}(\text{mes})_2]^{2+}$, 346–347

- electrospray ionization mass spectrometry (ESI-MS) trapping intermediates, 343, 343–344
- $[\text{Fe}(\eta^6\text{-arene})_2]^{2+}$, 345–348
- irradiating $[\text{CpFe}b\text{z}]^+$ and cyclohexene oxide (CHO) in poorly coordinating solvent, 344–345
- mechanism of ionic photopolymerization in solution, 345
- photochemical quantum yields for disappearance of $[\text{Fe}(\text{mes})_2]^{2+}$, 347*t*
- photochemistry of $[\text{Fe}(\text{mes})_2]^{2+}$, 347–348
- photolysis of $[\text{CpFe}b\text{z}]^+$ in acetonitrile (AN), 343–344
- polymerization, 342
- testing behavior of $[\text{Fe}(\text{mes})_2]^{2+}$ as photoinitiator, 348
- Metalloenes**
- electronic excited states of iron(II) metalloenes, 334
- structures of types of iron(II) metalloenes, 333*f*
- See also* Ferrocenes (FeCp_2)
- Metal-to-ligand charge transfer (MLCT), excited state, 334**
- Methacrylamide. *See* Photoinduced grafting of methacrylamide**
- Methacrylates**
- calixarene derivatives, 364, 366
- two-photon induced polymerization, 468
- See also* Fluorinated systems; Liquid polybutadienes; Pulsed laser polymerization (PLP)
- 2-(4-Methoxyphenyl)-3,3-dimethyloxetane (MPO)**
- ^1H NMR spectrum of MPO and its polymer, 289*f*
- photodifferential scanning calorimetry, 290*f*
- photopolymerization, 289*t*
- reaction diagrams, 291*f*, 292*f*
- structure, 288
- See also* 2-Phenyloxetanes
- Methyl methacrylate (MMA)**
- schematic of pulsed laser polymerization, 455*f*
- Wilkinson's catalyst, 452–453
- See also* Pulsed laser polymerization (PLP)
- N*-Methyldiethanolamine (MDEA).**
- See* Initiator systems, three-component; Maleimides, *N*-substituted, as photoinitiators
- Methylene blue. *See* Initiator systems, three-component**
- 4-Methylene-2-phenyl-1,3-dioxolane (MPDOX)**
- 1,2-addition reaction, 80
- polymerization with difunctional maleimide monomer Q-bond, 79–83
- real-time FTIR recordings of copolymerization with Q-bond, 81*f*
- relative ratio of ring-opening and 1,2-addition reaction vs. temperature, 83*f*
- ring-opening/elimination reaction, 82
- ring-opening reaction, 80
- See also* Maleimide/donor photocopolymerizations
- Michler's ketone ethyl acrylate salt (MKEA)**
- initiation of cationic polymerization, 199–200
- structure and characteristics, 193*t*
- Microelectronics. *See* Photopolymerizable liquid encapsulants (PLEs)**
- Mixture design studies, acrylated oligomers, 423, 424*t***
- Modulus, cured film from urethane acrylate oligomers, 420, 421*f***
- Molecular oxygen, inhibiting photopolymerizations, 2–3**

Molecular weights

- poly(2,3-dihydrofuran)s, 217*t*
- poly(butyl acrylate) by spinning disc reactor, 445, 447–448

Monodisperse oligomeric/polymeric photoinitiators

- electron spin polarization (ESP), 110
- end group exchange method, 109
- experimental, 107–109
- instrumentation, 108
- materials, 107
- monodisperse polystyrene with photoinitiator as end label, 109–110
- phase memory time (T_M) and spin-lattice relaxation time (T_1) of substituted benzoyl radicals and ketyl radicals, 110–111
- photochemical generation of substituted benzoyl radicals and ketyl radicals, 109
- preparation of large quantities, 106
- structures for preparation of end-labeled and non-labeled polystyrenes, 107*f*
- studying initiation rate coefficients, 106–107
- synthesis methods, 108–109
- time-resolved continuous wave electron paramagnetic resonance (TR CW EPR), 106–107
- TR FT EPR of four photoinitiators, 110*f*

Monomer blends,

- photopolymerization
- accelerated polymerization of epoxide with photosensitizer, 96, 98*f*
- cationic polymerization of epoxide, 96
- crosslinking polymerization, 97
- evaluating extent of crosslinking reaction, 94
- experimental, 93–94

- influence of diacrylate monomer on photocrosslinking of epoxidized polyisoprene, 97, 98*f*
- influence of triacrylate monomer on photoinduced insolubilization of acrylonitrile–butadiene elastomer, 102, 103*f*
- light-induced crosslinking polymerization, 92–93
- monomers and functionalized oligomers, 93
- photoinitiated cationic polymerization of epoxy monomer, 101, 103*f*
- photopolymerization of epoxy and acrylate monomers, 95*f*
- photopolymerization of vinyl ether/epoxide blend, 100*f*
- polymerization of diepoxide, 94, 96
- real-time infrared (RTIR) spectroscopy, 93–94
- sequential polymerization of polyurethane–acrylate/divinyl ether mixture, 100*f*
- UV-curing of acrylate and vinyl monomer blends, 101–102
- UV-curing of acrylate/epoxide blends, 94–97
- UV-curing of acrylate/vinyl ether blends, 97, 99
- UV-curing of vinyl ether/epoxide, 99, 101
- variation of infrared spectrum of acrylate/epoxide blend, 95*f*
- Morpholino ketone ethyl acrylate salt (BDMEA)
- initiation of cationic polymerization, 194, 195
- structure and characteristics, 193*t*

N

- Nano-indentation method, 155

- tests on urethane–acrylate coatings, 157, 160
- Nanostructured materials. *See* Lyotropic liquid crystals (LLC)
- NEK (*N*-ethylcarbazole). *See* Photosensitization of onium salts
- Nitrogen purging, radical photopolymerization, 169–170
- Nitrostilbenes, disubstituted, fluorescent probes, 427–428
- Nuclear magnetic resonance (NMR), ^{14}N for reaction environment and local ordering, 384–385
- NVCL (*N*-vinylcaprolactam). *See* Hexanedioldiacrylate (HDDA) formulations
- NVF (*N*-vinylformamide). *See* Hexanedioldiacrylate (HDDA) formulations
- NVP (*N*-vinylpyrrolidinone). *See* Hexanedioldiacrylate (HDDA) formulations
- O**
- Oligomeric carbazoles. *See* Photosensitization of onium salts
- Onium salt photoinitiators
absorption characteristics and reduction potentials, 249*t*
broadening spectral sensitivity range, 243
calculated oxidation and reduction potentials, 209*f*
cationic photopolymerization, 180, 185–186, 242
electron-transfer photosensitizers, 221
mechanisms of photosensitization, 220–221
See also Phenothiazine photosensitizers;
Photosensitization of onium salts
- Optical microscopy
grid-type microstructures via two-photon polymerization, 471*f*
microstructures via two-photon polymerization, 473*f*
- Ordering. *See* Lyotropic liquid crystals (LLC)
- Organic-inorganic hybrid resins
comparing tan delta plots for thermally crosslinked silicone–epoxy resins, 264*f*
comparison of storage moduli for thermally crosslinked silicone–epoxy resins, 263*f*
differential scanning calorimetry (DSC) of thermally initiated cationic polymerization of silicone–epoxy oligomer, 261*f*
epoxy-functional silicone resins, 259*t*
experimental, 256–257
general synthesis of α -epoxy- ω -trialkoxysiloxanes and oligomers, 256–257
idealized structure, 254–255
mechanical properties of epoxy functional, 262–263
photo- and thermally initiated cationic polymerization, 260–261
properties, 254
real-time infrared study of cationic photopolymerization of silicone–epoxy oligomeric resins, 260*f*
streamlined three-step process, 258
synthesis of epoxy–siloxane oligomers, 257–259
synthetic approach, 255
thermal stability of epoxy functional, 262
thermogravimetric analysis of crosslinked silicone–epoxy resins, 262*f*
- Organometallic photoinitiators, program expanding, 333
- Orientation
liquid crystal and polarization plane, 496

See also Photoalignment

Oxetanes

calixarene derivatives, 368, 371

cationic photopolymerization of calixarene derivatives, 373*f*

3-ethyl-3-(2-ethylhexyloxymethyl)oxetane, 298, 304–305

properties, 297

See also 2-Phenyloxetanes; Pressure sensitive adhesives; Silsesquioxanes (SQs), oxetanyl-functional

Oxiranes

calixarene derivatives, 368, 371

cationic photopolymerization of calixarene derivatives, 374*f*

Oxygen

effect on propagation and termination steps, 205, 206*f*

effect on shear modulus of photopolymerizing resin, 174*f*

efficiency of removal by helium and nitrogen, 170*f*

influence on rate of methylene blue consumption, 21–22

inhibitor of acrylate photopolymerization, 153

molecular, inhibiting photopolymerizations, 2–3

polymer chain termination, 173

radical photopolymerization, 165–167

reactions with mercaptans, 172

See also Radical photopolymerization

Oxygen consumption, *N*-vinylamide/hexanedioldiacrylate formulation, 12

Oxygen inhibition

acrylate based radical polymerization, 54

coating surface properties, 160–161
degree of curing, 160–161

difference spectra ΔS vs. incident energy and implantation depth, 158*f*

Doppler broadening of energy spectrum (DBES) technique, 154

electron spectroscopy chemical analysis (ESCA) method, 154–155

ESCA for matrix coatings, 157

lacking in thiol-ene reaction, 66

materials and methods, 154–155

micro-TA thermograms for matrix coatings, 157, 158*f*, 159*f*

microthermal analysis (micro-TA) technology, 155

nano-indentation method, 155

nano-indentation on matrix coatings, 157, 160

oxygen concentration gradient near surface, 163

PAS methods (positron annihilation spectroscopy), 154

PAS of ribbon samples, 155, 157

pathways in free radical polymerization, 161

positronium annihilation, 163

predissolved oxygen in liquid coating, 162

ribbon curing process, 160

S-parameter depth profiles of urethane-acrylate matrix coatings A and B, 156*f*

sensitivity, 161–162

surface layer thickness and oxygen diffusion length, 162

UV curing technology, 160

Oxygen scavenging

photopolymerization, 173

thiol-ene mechanism, 60

P

Panchromatic photoinitiators, 342

Pentaerythritol triallyl ether (APE)

- conversion vs. time for 50:50 trimethylolpropane tris(β -mercaptopropionate)/pentaerythritol triallyl ether mixture, 62*f*
- photo-DSC exotherms of 1:1 mixtures of trimethylolpropane tris(β -mercaptopropionate) and APE, 59*f*
- structure, 56
- thermal stability of thiol-ene coatings, 72–73
- thiols in formulations with APE, 71
- See also* Allyl ethers in thiol-ene reaction; Thiol-ene systems
- Perfluorinated polymers
properties, 500
- See also* Fluorinated systems
- Perfluoropolyether urethane methacrylates (PFEUMA). *See* Fluorinated systems
- Perylene, triplet energy, 31*t*
- Phases. *See* Lyotropic liquid crystals (LLC)
- Phenanthrene, triplet energy, 31*t*
- Phenothiazine photosensitizers
10-alkylphenothiazine-5,5-dioxides, 239
- cationic polymerization using, 235–239
- 2-chloroethyl vinyl ether polymerization, 238*f*
- comparing 10-methyl and 10-phenylphenothiazine with 10-acetylphenothiazine, 236, 237*f*
- comparing 10-methylphenothiazine, 10-methylphenothiazine-5-oxide, and 10-methylphenothiazine-5,5-dioxide, 236, 238*f*
- cyclohexene oxide (CHO)
polymerization, 235–239
- effect of 10-(2-vinylxyethyl)phenothiazine (VPT) and poly(VPT) (PVPT) on photopolymerization of 4-vinylcyclohexene dioxide, 239, 240*f*
- electron-withdrawing substituents in 2-position of aromatic rings of PT, 236, 239
- experimental, 233–235
- long wavelength absorption, 239
- materials, 233
- mechanism for electron-transfer photosensitization, 232
- onium salts, 232
- photopolymerization of 4-vinylcyclohexene dioxide, 239, 240*f*
- photopolymerization studies using Fourier transform real-time infrared spectroscopy (FT-RTIR), 234–234
- preparation of 10-decylphenothiazine, 233
- preparation of 10-methylphenothiazine-5,5-dioxide, 233–234
- preparation of 10-methylphenothiazine-5-oxide, 233
- preparation of VPT, 234
- synthesis and UV characterization of phenothiazine compounds, 235
- use of 2-acetyl-, 2-chloro-, and 2-trifluoromethylphenothiazines, 236, 237*f*
- VPT polymerization, 234
- Phenylazotriphenylmethane (PAT),
addition-fragmentation type initiation, 192*t*
- 2-Phenyl-3,3-dimethyl-oxetane (HPO)
photodifferential scanning calorimetry, 290*f*
- photopolymerization, 289*t*
- reaction diagrams, 291*f*, 292*f*
- structure, 288
- See also* 2-Phenylloxetanes
- 2-Phenyl-4-methylene-1,3-dioxolane (MPDOX). *See* Maleimide/donor photocopolymerizations

2-Phenylloxetanes

bis-[1-ethyl(3-oxetanyl)-methyl]
ether (DOX), 287, 288

computational technique, 288

3-ethyl-3-phenoxymethyl-oxetane
(POX), 287, 288

experimental, 287–288

gel permeation chromatography
(GPC) curves of polymers, 293,
294*f*

heat of polymerization of monomers
MPO, DOX and their
formulations, 294

heat of polymerization of monomers
MPO, POX and their formulations,
293

¹H NMR spectrum for MPO and its
polymer, 289*f*

materials, 287

2-(4-methoxyphenyl)-3,3-dimethyl-
oxetane (MPO), 287, 288

monomer structures, 288

photodifferential scanning
calorimetry (photo-DSC)
measurements, 287

photo-DSC evaluating monomer
reactivity, 289, 290*f*

photopolymerization of HPO and
MPO, 288, 289*t*

photopolymerization procedure, 287–
288

reaction diagrams of ring-opening
reaction of protonated HPO and
MPO through SN₁ reaction, 291*f*

reaction diagrams of ring-opening
reaction of protonated HPO and
MPO with oxetane by SN₂
reaction, 292*f*

reactivity differences between
unimolecular and bimolecular
reactions, 290, 292

Phosphorescence, substituted *N*-
phenylphthalimides, 44, 48

Photoacoustic spectroscopy (PAS)
methodology, 142–143

See also Photothermal techniques

Photoalignment

analyzing, by polarized Fourier
transform infrared spectroscopy,
496

atomic force microscopy (AFM) of
polymers before and after
irradiation, 492, 494*f*, 495*f*

azobenzene chromophores, 483

changes in optical density vs.
irradiation time, 489*f*

cinnamates, 483

copolymers bearing rigid
distyrylbenzene chromophore and
flexible aliphatic chain, 485, 486

coumarins, 483

dichroism of oriented liquid crystal,
497

enhancing formation of
intramolecular charge transfer
(ICT), 485

experimental, 484–485

extinction differences (ED)
diagrams, 492, 493*f*

fluorine containing photoactive
polymers, 484

influence of fluorine on
photochemical properties of
copolymers, 486

influence of ring substitution on,
485–486

irradiation of polymer in chloroform
at 365 nm at different irradiation
times, 489*f*

isobestic point in absorption spectra,
490, 491*f*

manufacturing a liquid crystal with,
layers, 496

materials, 484

orientation of liquid crystal and
polarization plane of linearly
polarized light, 496

photoisomerization vs.
photocycloaddition, 486, 488,
490

- quantum yields for copolymers in solution and spin-coated film, 488, 490*t*
- π -stacking between fluorinated and non-fluorinated benzene rings, 486, 488
- surface morphology after irradiation with linearly polarized light, 492, 494*f*, 495*f*
- surface roughness of polymers before and after irradiation, 492*t*
- techniques, 485
- See also* Fluorinated distyrylbenzene containing copolymers
- Photobase generators. *See* Quaternary ammonium dithiocarbamates (QA salts)
- Photochemical initiation, advantages, 438
- Photocrosslinking
- crosslinking using diazonium salts, 205–207
 - electron transfer, 207–209
 - general crosslinking kinetics, 204–205
 - kinetics, 204–210
 - thermostability of diazonium salts, 210
- Photocuring
- thiol-ene, 55, 64
- See also* Liquid polybutadienes; Photopolymerizable liquid encapsulants (PLEs); Pressure sensitive adhesives; Silsesquioxanes (SQs), oxetanyl-functional; Thiol-ene systems
- Photocycloaddition
- anisotropy, 483–484
 - applications, 483–484
 - vs. photoisomerization, 486, 488, 490
- Photodifferential scanning calorimetry (photo-DSC)
- cationic polymerization of 2-phenyloxetanes, 293–294
 - DSC dark-cure experiments, 19
 - eosin Y, *N*-methyldiethanolamine and diphenyliodonium chloride system, 23
 - experimental, 3
 - experimental for sensitized initiator system, 31
 - experimental for three-component initiator systems, 18–19
 - HDDA (hexanedioldiacrylate) formulations, 5, 7
 - HDDA polymerization, 32–36
 - initiating acrylate polymerization with phthalimide derivatives, isopropylthioxanthone (ITX) sensitizer, 44–47
 - isothermal curing of films of cycloaliphatic epoxide, 319–320
 - methylene blue, *N*-methyldiethanolamine and diphenyliodonium chloride system, 20–21
 - N*-vinylamide/HDDA formulations in air, 6*f*
 - N*-vinylamide/HDDA formulations in nitrogen, 6*f*
 - polymerization behavior of cycloaliphatic epoxide, 318–319
 - pressure sensitive adhesives, 298, 302*f*
 - See also* 2-Phenyloxetanes; Thiol-ene systems
- Photoinduced grafting of methacrylamide
- adhesion strength, 519, 520*f*
 - autohesion and adhesion strength, 513
 - autohesion strength, 517, 519
 - changes in amount of absorbed water with grafted amount for low density polyethylene-g-poly(methacrylamide) (LDPE-g-PMAAm) and high density polyethylene (HDPE)-g-PMAAm plates, 516*f*

- changes in intensity ratios and $\cos \theta$ value with grafted amount for LDPE-*g*-PMAAm and HDPE-*g*-PMAAm plates, 516*f*
- changes in n_{water} value with grafted amount for LDPE-*g*-PMAAm and HDPE-*g*-PMAAm plates, 518*f*
- changes in tensile shear adhesion strength with grafted amount for LDPE-*g*-PMAAm and HDPE-*g*-PMAAm plates, 520*f*
- changes in tensile shear autohesion strength with grafted amount for LDPE-*g*-PMAAm and HDPE-*g*-PMAAm plates, 518*f*
- degrees of crystallinity and ultimate strengths of LDPE and HDPE plates, 515*t*
- experimental, 513
- grafted amounts at substrate breaking, 519, 520*t*, 521*t*
- photografting procedure, 513
- surface compositions and hydrophilic properties, 513
- surface compositions and wettability of photografted LDPE and HDPE plates, 515*t*
- surface properties, 514
- water-absorptivity, 514, 517
- Photoinitiators**
- acid-generating, 333
- cationic photopolymerization, 179–180, 188, 219–220, 231–232
- classes, 16, 42
- common radical-generating, 333
- comparison of cationic, for photopolymerization of 3,4-epoxy-1-butene, 272, 273*f*
- concentration for photopolymerization of 3,4-epoxy-1-butene, 272, 273*f*
- effect of structure, 248–249
- efficiency, 116–117
- free radical, 16
- free radical categories, 28
- influence on photoreactivity and cured films of (meth)acrylated polybutadiene oligomers, 406–409
- program expanding inorganic and organometallic, 333
- structures of types of iron(II) metallocenes, 333*f*
- Type I, 42
- Type II, 42
- visible light radical, 17
- See also* Initiator systems, three-component; Maleimides, *N*-substituted, as photoinitiators; Monodisperse oligomeric/polymeric photoinitiators;
- Photoinsolubilization.** *See* Quaternary ammonium dithiocarbamates (QA salts)
- Photoisomerization**
- anisotropy, 483
- vs. photocycloaddition, 486, 488, 490
- Photopolymerizable liquid encapsulants (PLEs)**
- bis(2,4,6-trimethylbenzoyl) phenylphosphine oxide photoinitiator, 391
- coefficient of thermal expansion and glass transition temperature, 396
- comparison of material properties between, and conventional molding compounds, 398*t*
- effect of benzoyl peroxide on flexural strength, 395*f*
- effect of fused silica particle size distribution on viscosity, 393
- effect of thermal initiator on flexural modulus, 395*t*
- effects of filler loading on flexural modulus and strength, 394
- epoxy novolac-based vinyl ester resin, 391
- experimental, 391–393
- fillers, 391

- flexural strength and modulus, 394–395
- impact of postcure and thermal initiator on flexural strength, 395
- materials, 391
- sample preparation and characterization methods for cured encapsulants, 391–393
- satisfying requirements, 390
- specific heat and thermal diffusivity, 397–398
- specimens for coefficient of thermal expansion (CTE) measurements, 392
- specimens for flexural testing, 392
- specimens for thermal conductivity measurements, 392
- thermal conductivity, 397
- thermal conductivity measurements, 392–393
- thermal stress parameter, 397
- Photopolymerization
- kinetics and structure retention of lyotropic liquid crystals, 380
- mechanism, 332–333
- molecular oxygen, 2–3
- thiol-ene process, 53–54
- See also* Acrylate
- photopolymerization; Cationic photopolymerization; Continuous photopolymerization; Hexanedioldiacrylate (HDDA) formulations; Lyotropic liquid crystals (LLC); Radical photopolymerization; Thiol-ene systems
- Photoreactivity
- influence of photoinitiators and UV dosage, 406–409
- (meth)acrylated liquid polybutadiene oligomers, 405
- See also* Liquid polybutadienes
- Photosensitization, mechanism of, by hydrogen abstraction by photoexcited ketones, 247
- Photosensitization of onium salts
- antenna effect, 227
- broadening spectral sensitivity, 243
- chain reaction for onium salt conversion to cationic species, 225–226
- comparison of polymerization of 3,4-epoxycyclohexylmethyl 3',4'-epoxycyclohexanecarboxylate (ERL) in presence of carbazole-containing copolymers, 228*f*
- dimeric 1,3-bis(2-carbazoleethyl)-1,1,3,3-tetramethyl-disiloxane (photosensitizer IV) and *N*-ethylcarbazole (NEK) accelerating polymerization, 229
- electronic energy migration along PVK backbone, 227
- experimental, 221–222
- Fourier transform real-time infrared spectroscopy (FT–RTIR) study of epoxide polymerization of cyclohexene oxide (CHO) alone and with *N*-vinylcarbazole (NVK) and NEK, 223*f*, 224*f*
- investigation of photopolymerization of monomers in presence of oligomeric and polymeric carbazoles, 224–229
- low molar mass carbazole compounds, 222–224
- materials, 221
- mechanism of dication formation, 225
- NVK, 224
- photopolymerization studies using FT–RTIR, 222
- polymers and copolymers containing carbazole nucleus, 226*f*, 227
- poly(NVK) vs. NEK, 227
- potential mechanisms for initiation, 225–226
- preparation of *N*-substituted carbazoles, 224

- rate of epoxide polymerization of
CHO by adding NVK and NEK,
223–224
- synthesis of biscarbazole
photosensitizer, 228
- synthesis of copolymers of NVK,
221
- synthesis of photosensitizer IV, 222
See also Phenothiazine
photosensitizers
- Photosensitizers
2-ethylanthraquinone, 246
benzil, 246
camphorquinone, 246
onium salt photoinitiators, 184–185,
220–221
UV absorption spectra, 246*t*
See also Phenothiazine
photosensitizers;
Photosensitization of onium salts;
Sensitizers
- Photothermal techniques
bond dissociation energy of
coinitiators, 145
experimental, 141
fast signal S_F equation, 147
interaction A^\bullet /monomer, 146–148
interaction R^\bullet /monomer, 149–150
photoacoustic (PAS) methodology,
142–143
rate constant of interaction between
radicals and monomers, 145–150
reactivity of radicals, 144–150
schematic of energy diagram for
different processes, 146*f*
separation between fast and slow
heat deposit processes, 142*f*
Stern–Volmer relationship for
lifetime of A^\bullet , 147
thermal lens (TLS) spectroscopy
methodology, 143–144
TLS signal for camphorquinone, 144*f*
triplet states, 142–144
typical PAS signal for
hydroxybenzophenone (BPOH)
and bifunctional photoinitiator
Esacure 1001, 143*f*
- Phthalimide derivatives, sensitized
electron affinities and reduction
potentials of electron acceptors,
43*t*
experimental, 43–44
initiating acrylate polymerization,
44–47
laser flash photolysis, 48
laser flash photolysis method, 44
materials, 43
phosphorescence method, 44
phosphorescence of substituted PPI
derivatives, 48
photodifferential scanning
calorimetry (photo-DSC) method,
43
photo-DSC, 44–47
photo-DSC exotherms of *N*-(3,4-
dimethoxyphenyl) phthalimide
(DMPPI)/ITX/MDEA in nitrogen
purged HDDA, 47*f*
photo-DSC exotherms of *N*-
phenylphthalimide
(PPI)/ITX/MDEA in nitrogen
purged HDDA, 46*f*
photo-DSC exotherms of
phthalimide/ITX/MDEA in
nitrogen purged HDDA, 45*f*
proposed initiation mechanism, 49–
50
quenching constants of
isopropylthioxanthone (ITX), 48*t*
Type II photoinitiators, 42
- Polarized Fourier transform infrared
spectroscopy, analysis of
photoalignment, 496
- Polybutadienes. *See* Liquid
polybutadienes
- Poly(2,3-dihydrofuran)
film forming properties and
adhesion, 215
See also 2,3-Dyhydrofuran
- Poly(ethylene) (PE)

- density, crystallinity, and ultimate strength of high-density (HDPE) and low-density (LDPE), 515*t*
- photografting procedure, 513
- surface composition and wettabilities of photografted LDPE and HDPE plates, 515*t*
- surface modification, 512
- wettability of cured films, 505
- See also* Photoinduced grafting of methacrylamide
- Poly(glycidyl methacrylate) (PGMA)**
- effect of ammonio groups on photoinsolubilization and post-thermal insolubilization of PGMA films, 358*f*
- photoinitiated thermal insolubilization of, films with QA salts, 359*t*
- photoinitiated thermal insolubilization of PGMA films, 357, 359
- photoinsolubilization of PGMA films with QA salt and sensitizers, 361*f*
- photoirradiation method and photoinitiated thermal insolubilization of PGMA films, 353–354
- See also* Quaternary ammonium dithiocarbamates (QA salts)
- Polymeric carbazoles.** *See* Photosensitization of onium salts
- Polymerization rate, difunctional vinyl monomer with added monofunctional vinyl monomer, 10–11**
- Poly(methyl methacrylate) (PMMA)**
- applications, 452
- dependence of conversion on Wilkinson's catalyst concentration, 457*f*
- effect of Wilkinson's catalyst concentration on molecular weight and polydispersity, 456*t*
- ¹H NMR spectra, 459
- molecular weight distribution curves, 457*f*
- tacticity, 459–460
- Wilkinson's catalyst, 452–453
- See also* Pulsed laser polymerization (PLP)
- Polyolefins**
- properties, 512
- surface modification, 512
- See also* Photoinduced grafting of methacrylamide
- Polystyrene.** *See* Monodisperse oligomeric/polymeric photoinitiators
- Poly(tetrafluoroethylene) (PTFE)**
- surface modification, 512
- See also* Photoinduced grafting of methacrylamide
- Positron annihilation spectroscopy (PAS)**
- method, 154
- urethane–acrylate coatings, 155–157
- Postpolymerization.** *See* Kinetics of acrylate photopolymerization
- Pressure sensitive adhesives**
- adhesion properties, 299
- applications and characteristics, 297
- dependence of properties on viscoelastic nature of adhesive mass, 299–300
- 3-ethyl-3-(2-ethylhexyloxymethyl)oxetane (EHOX), 298, 304–305
- experimental, 297–299
- formulations and adhesive properties, 300*t*
- formulations R.N.1 to 4, 300, 302
- formulations R.N.4 to 7, 302–303
- formulations using cycloaliphatic diepoxide and adhesive properties, 304*t*
- materials, 297–298
- monofunctional alkyl oxetane, EHOX, 304–305
- monomers, 298

photodifferential scanning (photo-DSC) measurement, 298
 photo-DSC curves for R.N.4 to 7, 302*f*
 sample formulations, 298
 storage and loss modulus plot for R.N.1 to 4, 301*f*
 storage and loss modulus plot for R.N.4 to 6, 303*f*
 storage modulus curves of R.N.8 and 10, 304*f*
 tan delta plot for R.N.1 to 4, 301*f*
 UV-curable, 297
 viscoelasticity measurements, 299
 Primary coatings. *See* Kinetics of acrylate photopolymerization
 Probes. *See* Fluorescent probes
 Propagation rate, parameters of 25% acrylamide in lyotropic liquid crystal phases, 383
 Propagation rate coefficients, pulsed-laser polymerization-size exclusion chromatography (PLP-SEC), 106
 Propargyl ether, calixarene derivatives, 366, 368
 Propenyl ethers. *See* Fluoroalkyl propenyl ethers
 Pulsed laser polymerization (PLP)
 catalytic chain transfer agent, 456
 dependence of poly(methyl methacrylate) (PMMA)
 conversion on Wilkinson's catalyst concentration, 457*f*
 effect of irradiation time on PLP of methyl methacrylate (MMA) at constant Wilkinson's catalyst concentration, 458*t*
 effect of Wilkinson's catalyst concentration on molecular weight and polydispersity of PMMA, 456*t*
 experimental, 453–454
 gel permeation chromatography (GPC), 453
¹H NMR method, 453–454
¹H NMR spectra of PMMA, 459*f*

intensity ratios of syndiotactic to isotactic C–CH₃ groups in ¹H NMR of atactic PMMA, 460*t*
 materials, 453
 molecular weight distribution curves, 457*f*
 PLP procedure, 454
 schematic of MMA, 455*f*
 UV laser, 454
 UV/vis spectrophotometer, 454
 UV/vis spectrum for Wilkinson's catalyst, 458
 Wilkinson's catalyst, 452–453
 Pulsed-laser polymerization-size exclusion chromatography (PLP-SEC), propagation rate coefficients, 106
 Pulses. *See* Kinetics of acrylate photopolymerization

Q

Quaternary ammonium dithiocarbamates (QA salts)
 analysis of photoproducts of QA salt V, 355
 effect of ammonio groups on photoinsolubilization and post-thermal insolubilization of poly(glycidyl methacrylate) (PGMA) films, 358*f*
 effects of sensitizers on photolysis, 359, 361
 estimation of half-life in solvents, 354
 experimental, 352–354
 half-life in solution, 357*t*
¹H NMR spectra changes of QA salt V in CDCl₃, 356*f*
¹H NMR spectroscopy, 354
 instruments, 352–353
 material, 352
 photobase generators, 351–352
 photochemical behavior, 354

photoinitiated thermal
 insolubilization of PGMA films,
 357, 359
 photoinitiated thermal
 insolubilization of PGMA films
 with, 359*t*
 photoinitiated thermal
 insolubilization of PGMA films
 with, and photosensitizers, 361*f*
 photoirradiation method and
 photoinitiated thermal
 insolubilization of PGMA films,
 353–354
 photolysis of QA salt I in presence of
 sensitizers, 360*f*
 photolysis of QA salt V in CDCl_3
 and yields of photoproducts, 355*t*
 stability in solvents, 355, 357
 structure and properties, 353*t*
 thermal stability, 355, 357

R

Radiation cured coatings
 acrylics, 413
 See also Acrylated oligomers
 Radical photopolymerization
 addition of chain-transfer agents and
 oxygen scavengers, 173
 anisotropy in films, 166–167
 2-benzoxazolethiol effect on
 hexanediol diacrylate (HDDA)
 polymerization, 172*f*
 computed rate dependence on resin
 layer thickness, 166*f*
 cure kinetics dependence on layer
 thickness, 171*f*
 diagram of anisotropic
 photopolymerization of coating,
 165*f*
 diffusion-controlled kinetics, 171
 effects of aromatic thiols on
 photopolymerization kinetics,
 173

 efficiency of oxygen removal by
 helium and nitrogen, 170*f*
 experimental, 167
 HDDA photopolymerization kinetics,
 172*f*
 helium purging, 170
 integral heat emission dependence on
 nitrogen purge time, 169*f*
 kinetics of mechanical properties
 change vs. time, 174*f*
 mercaptans reacting with oxygen,
 172
 nitrogen purging, 169–170
 one-sided illumination, 166
 oxygen effect on shear modulus of
 photopolymerizing resin, 174*f*
 photopolymerization rate dependence
 on distance from illuminated
 surface, 166
 polymer chain termination in oxygen,
 173
 reactions in presence and absence of
 oxygen, 169
 sample weight dependence on total
 heat of polymerization, 168*f*
 Radicals
 aminoalkyl, 147
 bond dissociation energy of
 coinitiators, 145
 direct cleavage of photoinitiator,
 145–146
 efficient production, 145–146
 evolution of S_F for different
 monomer concentration, 148*f*
 fast signal S_F equation, 147
 generation of aryl radicals, 248
 generation of oxidizable free
 radicals, 181
 interaction of A^{\bullet} /monomer, 146–148
 interaction of R^{\bullet} /monomer, 149–150
 photochemical generation of
 substituted benzoyl and ketyl, 109
 photoinitiators generating, 333
 photoreduction of benzophenone by
 amine, 145

- rate constant and enthalpy of reaction for addition of, on butyl acrylate and butyl methacrylate, 148*t*, 149*t*
- rate constant of interaction between, and monomers, 145–150
- reactivity, 144–150
- schematic of energy diagram for different processes, 146*f*
- Rate of polymerization, difunctional vinyl monomer with added monofunctional vinyl monomer, 10–11
- Reactivity
- radicals, 144–150
- See also* Acrylate
- photopolymerization; Radicals
- Real-time fluorescence. *See* Fluorescent probes
- Real-time Fourier transform infrared spectroscopy (RT–FTIR)
- cationic photopolymerization of fluoroalkyl propenyl ethers, 279–280, 281, 283
- cationic photopolymerization of silicone–epoxy oligomeric resins, 260*f*
- cationic polymerization of cyclohexene oxide (CHO) using phenothiazine photosensitizers, 234–235, 236*f*
- experimental, 3
- maleimide/donor photocopolymerizations, 79–83
- monitoring photopolymerization of monomer blends, 93–94
- N*-vinylamide/hexanedioldiacrylate (HDDA) formulations, 7, 10
- photopolymerization of 3,4-epoxy-1-butene, 269–270, 271*f*
- reactivity and hydrogen bonding, 128–129, 136–137
- RT–FTIR conversion of HDDA vs. wt% *N*-vinylpyrrolidinone (NVP) in HDDA, 9*f*
- RT–FTIR conversion of NVP vs. wt% NVP in HDDA, 9*f*
- RT–FTIR conversion vs. time for 10% NVP in HDDA, 8*f*
- RT–FTIR conversion vs. time for 60% NVP in HDDA, 8*f*
- Residence time, performance of spinning disc reactor, 442, 443*f*
- Ribbon curing process, 160
- illustration of 4-fiber structure, 153*f*
- UV-curable coatings, 153
- Roughness, surface, copolymers before and after irradiation with linearly polarized light, 492*t*
- S**
- Sample size, dependence of total heat of photopolymerization, 167–168
- Scanning electron microscopy, microstructures via two-photon polymerization, 473*f*
- Secondary coatings. *See* Kinetics of acrylate photopolymerization
- Self-adhesion pioneering studies, 512
- See also* Autohesion
- Semipinacol reduction evidence for mechanism, 38–39
- mechanism, 38
- Sensitivity. *See* Fluorescent probes
- Sensitizers accelerated polymerization of epoxide, 96, 98*f*
- chemical sensitization, 30
- effects on photolysis of quaternary ammonium dithiocarbamates (QA salts), 359, 360*f*, 361
- interaction of isopropylthioxanthone (ITX) with phthalimides, 48
- N*-vinylcarbazole (NVK), 184–185
- triplet, 31*t*

- See also* Maleimides, *N*-substituted, as photoinitiators; Phenothiazine photosensitizers; Photosensitization of onium salts; Photosensitizers; Phthalimide derivatives, sensitized; Quaternary ammonium dithiocarbamates (QA salts)
- Shear modulus, oxygen effect on, of photopolymerizing resin, 174*f*
- Shrinkage, thiol-ene photopolymerization, 54
- Silica-filled composites. *See* Photopolymerizable liquid encapsulants (PLEs)
- Silicone resins, epoxy functional. *See* Organic-inorganic hybrid resins
- Silsesquioxanes (SQs), oxetanyl-functional
 experimental, 307–309
 formulation of cycloaliphatic epoxide (UVR-6110) with or without oxetanyl-functional SQ (OX-SQ), 313*t*
 formulation of OX-SQ and OX-SQ having partial silicone chain (OX-SI-SQ) with UVR-6110, 313*t*
 gel permeation chromatography (GPC), 308
¹H NMR spectrum of OX-SQ, 310*f*
 instrumentation, 308
 materials, 307–308
 photocationic curable, 307
 photopolymerization and evaluation methods, 309
 photopolymerization of OX-SQ and OX-SI-SQ, 312
 preparation of OX-SI-SQ, 309, 311–312
 preparation of OX-SQ, 308, 310–311
²⁹Si NMR spectrum of OX-SQ, 311*f*
 synthesis of 3-ethyl-(triethoxysilylpropoxy)methyl oxetane (TESOX), 308
 synthesis of TESOX, 309, 310*f*
 thermal properties of photocured OX-SQ, 314–315
 viscoelastic measurement of OX-SQs at 10 Hz, 314*f*
- Single-photon absorption
 rate of light absorption, 465–466
 simplified Jablonski energy level illustration, 466*f*
- Single-pulse pulsed-laser polymerization (SP-PLP),
 termination rate coefficients, 106
- Small angle X-ray scattering (SAXS)
 phase characterization method, 381
 SAXS profile of polymerized and unpolymerized samples with 25% acrylamide, 386, 387*f*
- Sol-gel condensation
 organic-inorganic hybrid resins, 254–255
 silicone-epoxy resins, 256–257, 258
See also Organic-inorganic hybrid resins
- Specific heat, photopolymerizable liquid encapsulants, 397–398
- Spinning disc reactor (SDR)
 continuous polymerization, 439
 description, 440
 influence of disc rotational speed and feed flow rate, 442, 445
 influence of UV intensity, 445, 446*f*
 opportunity for process intensification, 449
 polymerization procedure, 440–441
 schematic, 441*f*
 variables affecting performance, 442
See also Continuous photopolymerization
- Spiro ortho ether, calixarene derivatives, 375, 376
- Stability, thermal, of thiol-ene coatings, 72–73
- Stereolithography, technique, 465
- Stern-Volmer relationship, radical lifetime, 147

- Storage moduli, thermally crosslinked silicone–epoxy resins, 263*f*
- Sulfuric acid, effect of, on tensile strength of (meth)acrylated polybutadiene films, 409–410
- Surface characterization
- electron spectroscopy chemical analysis (ESCA) of urethane–acrylate coatings, 154–155, 157
 - microthermal analysis (micro-TA) method, 155
 - nano-indentation tests on urethane–acrylate coatings, 155, 157, 160
 - positron annihilation spectroscopy (PAS) method, 154
 - urethane–acrylate coating analysis by micro-TA, 157, 158*f*, 159*f*
 - urethane–acrylate matrix coatings by PAS, 155–157
- See also* Oxygen inhibition
- Surface condition, ribbons, 153
- Surface morphology, copolymers
- before and after irradiation with linearly polarized light, 492, 494*f*, 495*f*
- Surface roughness, copolymers before and after irradiation with linearly polarized light, 492*t*
- T**
- Tacticity
- acrylate photopolymerization, 133, 135
 - poly(methacrylates), 136*t*
 - poly(methyl methacrylate), 459–460
- Tan delta
- oxetanyl-functional silsesquioxanes, 314*f*
 - pressure sensitive adhesive formulations, 301*f*
 - thermally crosslinked silicone–epoxy resins, 264*f*
- See also* Mechanical properties
- Temperature
- acrylate photopolymerization, 132–133
 - dependence of polymerization rate for 25% acrylamide, 385–386
 - effect on curing behavior of epoxy, 321–322
 - effect on IR shifts of amide moiety, 134*f*
 - photoinitiated cationic polymerization of cycloaliphatic epoxy, 327–328
- See also* Epoxy resin, cycloaliphatic
- Tensile strength, effect of 50% sulfuric acid on, of (meth)acrylated polybutadiene films, 409–410
- Termination rate, parameters of 25% acrylamide in lyotropic liquid crystal phases, 383
- Termination rate coefficients, single-pulse pulsed-laser polymerization (SP-PLP), 106
- Thermal conductivity, photopolymerizable liquid encapsulants, 397
- Thermal diffusivity, photopolymerizable liquid encapsulants, 397–398
- Thermal insolubilization. *See* Quaternary ammonium dithiocarbamates (QA salts)
- Thermal lens (TLS) spectroscopy methodology, 143–144
- See also* Photothermal techniques
- Thermal stability
- calixarene acrylate and calixarene methacrylate, 366
 - calixarenes containing oxetane or oxirane groups, 371
 - calixarenes containing propargyl and vinyl ethers, 368
 - epoxy–acrylates, 364
 - epoxy functional organic-inorganic hybrid polymers, 262
 - thiol-ene coatings, 72–73

- Thermal stress parameter,
photopolymerizable liquid
encapsulants, 397
- Thermogravimetric analysis
crosslinked silicone–epoxy resins,
262*f*
oxetanyl-functional silsesquioxanes,
314–315
- Thermomechanical studies. *See* Epoxy
resin, cycloaliphatic
- Thiol-ene reaction
features, 66
propagation steps, 66*f*
step growth addition mechanism, 66
step growth mechanism, 54, 66
See also Allyl ethers in thiol-ene
reaction
- Thiol-ene systems
addition of multifunctional thiols to
multifunctional acrylates, 60–63
basic oxygen scavenging mechanism,
60
conversion vs. time for 50:50
trimethylolpropane tris(β -
mercaptopropionate)/pentaerythritol
triallyl ether mixture, 62*f*
experimental, 55
free-radical curing, 53–54
gel formation, 54
percent allyl ether and thiol
conversion from real time infrared
analysis vs. exposure time, 62*f*
photocuring examples, 64
photo-DSC exotherms for
polymerization of 1,6-
hexanedithiol and
trimethylpropane diallyl ether, 58*f*
photo-DSC exotherms for
polymerization of 1,6-hexanediol
diacrylate (HDDA), 58*f*
photo-DSC exotherms for
polymerization of hexylacrylate,
58*f*
photo-DSC exotherms for
polymerization of
trimethylolpropane triacrylate
(TMPTA), 59*f*
photo-DSC exotherms of 1:1
mixtures of trimethylolpropane
tris(β -mercaptopropionate) and
pentaerythritol triallyl ether, 59*f*
photo-DSC exotherms of 25:75
trimethylolpropane tris(β -
mercaptopropionate):HDDA
mixture, 63*f*
photo-DSC exotherms of 25:75
trimethylolpropane tris(β -
mercaptopropionate) with
triethyleneglycol divinylether, 63*f*
photo-DSC exotherms of HDDA
with added trithiol, 62*f*
photo-DSC exotherms of HDDA
with varying trimethylolpropane
tris(β -mercaptopropionate), 61*f*
photopolymerization process, 53
polymerization rate in nitrogen
compared to acrylate, 57, 58*f*
polymerization rates in air compared
to acrylates, 57–60
procedure for thiol-ene
polymerization, 478
shrinkage, 54
step growth mechanism, 54, 66
structures of monomers, 56
variation in ene structures, 54–55
varying amounts of
trimethylolpropane tris(β -
mercaptopropionate), 61*f*
versatility, 55
See also Two-photon
photopolymerization
- Thiols
alkene reactivity towards thiyl
radicals, 66–67
effects of aromatic, on
photopolymerization kinetics,
173
free radical initiators, 66
- Thioxanthenes, abstraction type
photoinitiator, 28

Three-component initiator systems.

See Initiator systems, three-component

Time-resolved continuous wave electron paramagnetic resonance (TR CW EPR), initiation rate coefficients, 106–107

Time-resolved steady state

fluorescence

eosin Y, *N*-methyl-diethanolamine and diphenyliodonium chloride system, 23

experimental for three-component initiator systems, 19

methylene blue, *N*-methyl-diethanolamine and diphenyliodonium chloride system, 21–22

Transfer molding process

encapsulation, 390

See also Photopolymerizable liquid encapsulants (PLEs)

Transition metal complexes, polymerization catalysts, 452

Triethyleneglycol divinylether cationic photopolymerization, 182*f* photo-DSC exotherms of 25:75

trimethylolpropane tris(β -mercaptopropionate) with, 63*f*

structure, 56

See also Thiol-ene systems

2,4,6-

Trimethylbenzoyldiphenylphosphonyloxide (TMDPO), addition-fragmentation type initiation, 192*t*

Trimethylolpropane diallyl ether

photo-DSC exotherms for polymerization of 1,6-hexanedithiol and, 58*f*

structure, 56

See also Thiol-ene systems

Trimethylolpropane triacrylate (TMPTA)

structure, 56

See also Thiol-ene systems

Trimethylolpropane tris(3-mercaptopropionate) (TMP3MP3) allyl ethers in formulations with, 70

thermal stability of thiol-ene coatings, 72–73

See also Allyl ethers in thiol-ene reaction

Trimethylolpropane tris(β -mercaptopropionate)

conversion vs. time for 50:50

trimethylolpropane tris(β -mercaptopropionate)/pentaerythritol triallyl ether mixture, 62*f*

structure, 56

See also Thiol-ene systems

Triphenylene, triplet energy, 31*t*

Triplet states

separation between fast and slow heat deposit processes, 142*f*

See also Photothermal techniques

Two-photon absorption

definition, 465

isopropylthioxanthone, 474, 476*f* nonresonant, 466–467

rate of energy absorption, 465–466 simplified Jablonski energy level

illustration, 466*f*

Two-photon photopolymerization absorption spectrum of

isopropylthioxanthone (ITX) in acetonitrile, 475*f*

acrylate resin, 468

cationic photoinitiated

polymerization of epoxides, vinyl ethers, and methylenedioxyolanes, 472

condensed phase, 467–468

confirming two-photon absorption of ITX, 474

experimental, 477–478

experimental exposure apparatus, 470, 471*f*

instrumentation, 477–478

- near-infrared, of (meth)acrylate monomers, 468
- optical micrographs of grid-type microstructures, 471*f*
- optical microscopy image of microstructures via, cationic polymerization, 473*f*
- polymeric microstructure formation, 470–471
- procedure for thiol-ene polymerization, 478
- quadratic dependence of fluorescence intensity of ITX, 476*f*
- scanning electron microscopy (SEM) of microstructure via, cationic polymerization, 473*f*
- schematic of experimental setup, 471*f*
- single photon and two-photon upconverted fluorescence spectra of ITX, 475*f*
- structures of cationic photoinitiators, 472*f*
- structures of free-radical photoinitiators, 469*f*
- thiol-ene, 472, 474–477
- thiol-ene monomer mixture using ITX and *N*-methylmaleimide (NMM), 477*f*
- two-photon absorption cross-section of ITX vs. fs pump wavelength, 476*f*
- UV-visible absorption spectra of cationic photoinitiators, 473*f*
- UV-visible spectra of free-radical photoinitiators, 470*f*
- acrylate and vinyl monomer blends, 101–102
- acrylate/epoxide blends, 94–97
- acrylate/vinyl ether blends, 97, 99
- applications, 363
- components, 28
- free radical photopolymerization of acrylates, 114
- photoelectronics industry, 153
- ribbon, 153
- use of fluorinated monomers, 500
- vinyl ether/epoxide, 99, 101
- See also* Acrylated oligomers; Calixarenes; Epoxy resin, cycloaliphatic; Fluorinated systems; Kinetics of acrylate photopolymerization; Liquid polybutadienes; Monomer blends, photopolymerization; Silsesquioxanes (SQs), oxetanyl-functional
- Ultraviolet (UV) intensity, influence on spinning disc reactor, 445, 446*f*
- Ultraviolet-visible curing, stereolithography, 465
- Ultraviolet-visible spectroscopy dual-cell, experimental for three-component initiator systems, 19
- N*-vinylamide/hexanedioldiacrylate (HDDA) formulations, 10
- reversible UV-absorption spectral shifts, 11
- Undecyl amide *N*-ethyl-acrylate, photopolymerization, 132–133
- Urethane–acrylate coatings electron spectroscopy chemical analysis (ESCA), 157
- microthermal analysis, 157, 158*f*, 159*f*
- nano-indentation, 157, 160
- positron annihilation spectroscopy (PAS), 155–157
- See also* Oxygen inhibition
- Urethane/acrylate oligomer

U

- Ultraviolet dosage, influence on photoreactivity and cured films of (meth)acrylated polybutadiene oligomers, 406–409
- Ultraviolet (UV) curing

effect of acrylic hydroxyl content on urethane viscosity, 418, 419*f*
 effect of diluent monomer glass transition temperature on urethane viscosity, 418, 419*f*
 effect of prepolymer molecular weight on urethane viscosity, 418, 420, 421*f*
 solution properties, 415, 418, 420
See also Acrylated oligomers

V

Versatility, thiol-ene photocuring, 55

Vinyl/acrylic copolymers
 solution properties, 415, 417*f*
See also Acrylated oligomers

N-Vinylamides
 structures, 4*f*
See also Hexanedioldiacrylate (HDDA) formulations

N-Vinylcaprolactam (NVCL). *See* Hexanedioldiacrylate (HDDA) formulations

N-Vinylcarbazole (NVK)
 photosensitizer for onium salt photolysis, 184–185, 220–221
 synthesis of copolymers of NVK, 221
See also Photosensitization of onium salts

4-Vinylcyclohexene dioxide (VCHDO)
 camphorquinone as photosensitizer for polymerization, 247*f*, 249*f*, 250*f*
 photosensitized polymerization, 239, 240*f*
 structure, 244*t*

4-Vinyl-1,2-epoxycyclohexane (VCHO)
 influence of structure on photopolymerization, 250–251
 structure, 244*t*

Vinyl ethers
 calixarene derivatives, 366, 368
 homo- and copolymers, 213
 hydrogen abstraction and addition reactions, 184
 photocrosslinking, 205–207
See also Cationic

photopolymerization; Monomer blends, photopolymerization
N-Vinylformamide (NVF). *See* Hexanedioldiacrylate (HDDA) formulations

Vinyl monomers. *See* Monomer blends, photopolymerization

Vinyl oxirane. *See* 3,4-Epoxy-1-butene

10-(2-Vinylloxyethyl)phenothiazine (VPT)
 effect on photopolymerization of 4-vinylcyclohexene dioxide, 239, 240*f*

polymerization, 234
 preparation, 234
 structure of VPT and polymer, 239
See also Phenothiazine

photosensitizers
N-Vinylpyrrolidinone (NVP). *See* Hexanedioldiacrylate (HDDA) formulations

Visible and long-wavelength cationic photopolymerization
 absorption characteristics and reduction potentials of onium salt photosensitizers, 249*t*
 aryl ketone-sensitized, 245–248
 benzil, 246*t*
 camphorquinone, 246*t*
 CHO (cyclohexene oxide), 244*t*, 250
 comparing photosensitized polymerization of 4-vinylcyclohexene dioxide (VCHDO), CHO, and 4-vinyl-1,2-epoxycyclohexane (VCHO), 250*f*
 comparing VCHDO photopolymerization with

camphorquinone and various initiators, 249*f*
development of long-wavelength photosensitizers, 244–245
effects of photoinitiator structure, 248–249
2-ethylanthraquinone, 246*t*
experimental, 243
generation of aryl radical, 248
influence of monomer structure, 250–251
materials, 243
proposed mechanism of photosensitization by hydrogen abstraction by photoexcited ketones, 247
real-time infrared (RTIR) study of VCHDO photopolymerization using camphorquinone sensitizer, 247*f*
structures of photoinitiators and monomers, 244*t*
UV absorption spectra of photosensitizers, 246*t*
VCHDO, 244*t*, 247, 250
VCHO, 244*t*, 250

W

Wettability, dependence on substrate, 505
Wilkinson's catalyst
dependence of poly(methyl methacrylate) (PMMA) conversion on concentration, 457*f*
effect of concentration on molecular weight and dispersity of PMMA, 456*t*
methyl methacrylate polymerization, 452–453
pulsed laser polymerization process, 454
UV/vis spectrum, 458
See also Pulsed laser polymerization (PLP)

X

X-ray photoelectron spectroscopy (XPS). *See* Fluorinated systems